

ELEVENTH INTERNATIONAL WORKSHOP
ON MEASUREMENT AND COMPUTATION
OF TURBULENT (NON) PREMIXED FLAMES



DARMSTADT
GERMANY

WORKSHOP
JULY 26-28, 2012

Conference Location

Address:

WELCOME HOTEL DARMSTADT

Karolinenplatz 4

64289 Darmstadt

T: +49-6151-3914-0

F: +49-6151-3914-444

E: info.dar@welcome-hotels.com



Sponsors



Table of Contents

Cover	1
Location	2
Sponsors page	3
Summary	5
List of Participants	18
Agenda	20

Technical Sessions and Coordinators

Turbulent Stratified Flames and Model Comparisons – <i>B. Fiorina and A. Kempf</i>	
Abstract	22
Presentation	25
Differential Diffusion Effects in Turbulent Flames – <i>S. Hochgreb and L. Vervisch</i>	
Abstract	70
Presentation	75
Lifted Flames in Vitiated Coflow – <i>M. Ihme and E. Richardson</i>	
Abstract	89
Presentation: Modelling and Experiments	95
Presentation: Insight and Challenges from DNS	142
Piloted Premixed Jet Burner – <i>A. Masri, M. Dunn, and H. Pitsch</i>	
Abstract	160
Presentation	162
Chemistry, Complex Fuels, and New Combustion Modes – <i>D. Roekaerts and P. Lindstedt</i>	
Abstract: DME Flames and Chemistry	191
Presentation: DME Flames and Chemistry	193
Abstract: Oxy-fuel and MILD Combustion	209
Presentation: Oxy-fuel and MILD Combustion	212
Interpretation and Utilization of Time Resolved Data – <i>W. Meier and A. Steinberg</i>	
Abstract.....	241
Presentation: Experimental Perspective	242
Presentation: DNS and LES Perspective	255
LES/DNS: Quality and Best Practice – <i>J. Oefelein and S. Pope</i>	
Abstract	268
Presentation	270
Turbulent Opposed Jet Flames – <i>D. Geyer and A. Gomez</i>	
Abstract	301
Presentation	302
Closing Discussion and Action Items – <i>J. Janicka</i>	
Presentation	342
Poster Session	
List of Poster Titles and Authors	348
Poster Abstracts	350

SUMMARY

Eleventh International Workshop on Measurement and Computation of Turbulent Nonpremixed Flames (TNF11)

26-28 July 2012
Darmstadt, Germany

R.S. Barlow, J.-Y. Chen, B. Dally, A. Dreizler, M.J. Dunn, B. Fiorina, D. Geyer, A. Gomez, S. Hochgreb, M. Ihme, J. Janicka, A. Kempf, R.P. Lindstedt, A.R. Masri, W. Meier, H. Pitsch, S.B. Pope, E.S. Richardson, D. Roekaerts, A. Steinberg, L. Vervisch

INTRODUCTION

The series of workshops on Measurement and Computation of Turbulent Nonpremixed Flames (TNF) facilitates collaboration and information exchange among experimental and computational researchers in the field of turbulent combustion. The emphasis is on fundamental issues of turbulence-chemistry interaction in flames that are relatively simple in terms of both geometry and chemistry. The 1st TNF Workshop was held in Naples, Italy in July 1996. Its objectives were to select experimental data sets for testing combustion models and to establish guidelines for collaborative comparisons of measured and modeled results on those target flames. Subsequent workshops were held in Heppenheim, Germany (1997), Boulder, Colorado (1998), Darmstadt, Germany (1999), Delft, The Netherlands (2000), Sapporo, Japan (2002), Chicago, Illinois (2004), Heidelberg, Germany (2006), Montreal, Canada (2008), and Beijing, China (2010). Proceedings and summaries are available at <http://www.sandia.gov/TNF>.

The TNF Workshop series was initiated to address validation of RANS based models for turbulent nonpremixed flames, as well as partially premixed flames where combustion occurs mainly in a diffusion flame mode. Although the title has not changed, our scope has expanded since TNF9 (Montreal, 2008) to address three challenges:

- Development and validation of modeling approaches which are accurate over a broad range of combustion modes and regimes (nonpremixed, partially premixed, stratified, and premixed).
- Extension of quantitative validation work to include more complex fuels (beyond CH₄) and fuel mixtures that are of practical interest.
- Establishment of a more complete framework for verification and validation of combustion LES, including quality assessment of calculations, as well as development and utilization of approaches which extract knowledge and understanding from comparisons of detailed experimental measurements with detailed simulations.

One of the most useful functions of this workshop series has been to provide a framework for collaborative comparisons of measured and modeled results. Such comparisons are most informative when multiple modeling approaches are represented and when there has been early communication and cooperation regarding how the calculations should be carried out and what results should be compared. Experience has shown that comparisons on new target flames can generate significant new insights, but also many new questions. These questions motivate further research, both computational and experimental, and subsequent rounds of model comparisons. Our overall goal is to accelerate the development of advanced combustion models that are soundly based in fundamental science, rigorously tested against experiments, and capable of predicting flame behavior over a wide range of turbulent combustion modes and regimes.

TNF11 was attended by 84 researchers from 13 countries. The main sessions topics included:

- Turbulent stratified flames and model comparisons
- Differential diffusion effects in turbulent premixed flames
- Lifted flames in vitiated coflow

- Model comparisons on the Sydney Piloted Premixed Jet Burner (PPJB)
- Progress on DME flames and chemistry
- Oxy-fuel and MILD combustion
- Interpretation and utilization of temporally resolved data
- LES/DNS quality and best practice
- Turbulent opposed jet flames

This summary briefly outlines the presentations and key discussions points. Comments and conclusions given here are based on the perspectives of the authors and do not necessarily represent consensus opinions of the workshop participants. This summary does not attempt to address all topics discussed at the workshop or to define all the terms, acronyms, or references. Readers are encouraged to consult the complete TNF11 Proceedings and also the Proceedings of previous TNF Workshops, because each workshop builds upon what has been done before.

The complete Proceedings are available for download in pdf format from www.sandia.gov/TNF. The pdf file includes the list of participants, workshop agenda, summary abstracts of technical sessions, presentation slides, and two-page abstracts of the 34 contributed posters.

ACKNOWLEDGMENTS

The technical program for the TNF11 Workshop was co-chaired by Profs. Andreas Dreizler and Andreas Kempf with input from the Organizing Committee. Local arrangements were expertly coordinated by Ms Marion Mueller, Technical University of Darmstadt. Sponsorship funds from Andor, ANSYS, Continuum Lasers, Edgewave, General Electric, the GRK 1344 program, La Vision, the Leverhulme Trust, Numeca, Princeton Instruments, Quantel, Rolls-Royce, and Sirah Lasers are gratefully acknowledged. These contributions allowed reduction of the registration fees for university faculty, postdocs, and students. Support for the TNF web site has been provided by the U. S. Department of Energy, Office of Basic Energy Sciences, Division of Chemical Sciences, Geosciences, and Biosciences. Sandia National Laboratories is a multiprogram laboratory operated by Sandia Corporation, a Lockheed Martin Company, for the United States Department of Energy under contract DE-AC04-94-AL85000.

IMPORTANT NOTE ON USE OF THIS MATERIAL

Results in this and other TNF Workshop proceedings are contributed in the spirit of open scientific collaboration. Some results represent completed work, while others are from work in progress. Readers should keep this in mind when reviewing these materials.

It would be inappropriate to quote or reference specific results from these proceedings without first checking with the individual author(s) for permission and for the latest information on results and references.

HIGHLIGHTS OF PRESENTATIONS AND DISCUSSIONS

Turbulent Stratified Flames and Model Comparisons

Coordinators: Andreas Kempf and Benoit Fiorina

The objective of the session was to compare recent simulations of turbulent stratified flames against experimental data. Burner configurations from TU-Darmstadt and Cambridge University provided the target cases, both burning methane. Five groups were involved in the simulations: the Technische Universität Darmstadt (TUD), the Institute for Combustion Technology (ITV, Aachen), Lund University (LUND), the

EM2C laboratory at Ecole Centrale Paris (EM2C), and a team from Imperial College London and Duisburg-Essen University (IC-UDE).

All groups performed Large Eddy Simulations using Low Mach Number solvers. TUD applied a premixed flamelet tabulation with local flame thickening, ITV used a flamelet progress variable approach also based on premixed flamelet tabulation, LUND described the combustion chemistry through a 4-steps mechanism combined with Implicit LES, EM2C applied the model F-TACLES that is based on filtered premixed flamelet tabulation, and finally IC-UDE used a flame surface density approach. All modeling strategies were designed to predict a flame propagation speed equal to a laminar flame speed when the flame wrinkling is fully resolved on the LES grid. However different assumptions regarding the species transport description have been made. The TUD and ITV models assume that the flame front structure is similar to a 1-D premixed flamelet computed under unity Lewis assumption when subgrid scale flame wrinkling vanishes. At the opposite end, LUND and IC-UDE assumed that the flame front has the same structure as a 1-D premixed flamelet for which differential diffusion phenomena are considered. These assumptions regarding the multi-component transport properties affect the value of the effective laminar flame front propagation speed. EM2C proposed two model formulations with and without differential diffusion effects on the laminar flame speed.

The *Darmstadt stratified burner* consists of three 5-mm-staged concentric tubes placed in a 0.1 m/s coflow. Burnt gases exit from the central tube (pilot) to stabilize the flame. Different approaches have been taken to represent the computational domain: TUD computed the entire flow upstream within slot1, slot2 and the pilot tube; EM2C restricted the flow upstream computation to slot1 and slot2; LUND, IC-UDE and ITV used a more compact computational domain, starting simulations at the outlet of the inner nozzle, prescribing the measured velocity data. All groups performed simulations of the TSF-A reactive case. Also, ITV computed the TSF-Cr configuration, EM2C and IC-UDE the TSF-Ai (inert) case, and ICUDE the TSF-G (reactive) case.

Both adiabatic and isothermal assumptions have been considered to set up the pilot burner wall boundary conditions. To estimate the burner wall temperature, TUD developed an analytical analysis to model heat exchange between the pilot tube and stream 1, while EM2C performed a RANS 2D-axisymmetric computation of the fluid flow inside the burner coupled with conductive heat transfer within the burner wall. Both studies estimate a wall temperature for the pilot tube of around 700K. For the TSF-A case, an extensive comparison of simulation and experimental data was presented for the mean and RMS field of velocity, temperature, mixture fraction, and major species mass fractions. In general, good agreement has been observed between the numerical predictions and the measurements. All adiabatic computations predicted a flame anchoring at the burner lips, while the non-adiabatic simulations predicted a lift-off of the flame of half a pilot diameter. The comparison of the mean temperature field and the species formation/consumption against the experimental data provides evidence that accounting for heat losses improves the prediction of the flame position. However, the impact of heat losses on the combustion chemistry remains only one possible explanation of the flame lift-off. Other phenomena like an incomplete burning of the pilot gases could also explain this observation. Further measurements are needed to conclude on the effective stabilization mechanism.

It has been also observed that multi-component transport assumptions significantly affect the mean flame position. Accounting for differential diffusion phenomena in the direction normal to the flame front seems to improve the quality of the prediction. Another conclusion from numerical data analysis is that the effect of stratification on the flame front propagation remains weak for the TSF-A case. For future work on the Darmstadt burner, the focus should be shifted towards more stratified cases where the modeling of subgrid scale mixture fraction heterogeneities will be more challenging and influential.

The *Cambridge/Sandia burner* also consists of three concentric tubes in a laminar coflow, but the center tube is sealed with a ceramic cap, and the flame is stabilized by recirculation of combustion products downstream of this central bluff body. Computations were performed by EM2C and IC-UDE, both groups included the last part of the burner into the computational domain. Three non-swirling cases were considered: an isothermal reference case (SwBc), a homogeneous case with an equivalence ratio of 0.75 within both annular tubes (SwB1), and a stratified case with equivalence ratio of 1.0 in the inner and 0.5 in the outer tube (SwB5).

For the case SwBc, comparisons of mean and rms profiles for the axial and radial velocity component with PIV measurements were presented for various downstream locations. Both groups achieved good agreement with the measured flow field. For the reactive cases SwB1 and SwB5, comparisons of mean and rms profiles for the axial and radial velocity-component with PIV measurements and for temperature and equivalence ratio have been presented at various downstream locations. In general, good agreement between experiment and simulation was observed. However, significant deviations were observed within the recirculation zone: on the one hand, the predicted recirculation zone has a lower negative axial velocity magnitude and is shorter than the measured one, which is more visible with the modelling approach chosen by UDE-IC. One possible explanation could be that the real flame is lifted, in contrast to the anchored flame predicted by the adiabatic simulations. This theory is also supported by the temperature profiles for the stratified case SwB5, where the peak value is about 125 K lower than the one predicted by both simulations. As the maximum temperature is about 300 K higher compared to the homogeneous case SwB1, conduction and flame lift-off are likely to become more important. On the other hand, the measurement predicts a peak of the equivalence ratio profiles within the bluff body region, which is not visible in the simulation results. It could be assumed that this is caused by differential diffusion effects, as discussed in the next section, which are not taken into account with either model. More detailed investigation of the influence of mass and heat transfer near the bluff body could be an interesting topic for future studies. It was agreed that surface temperatures of the ceramic pilot tube of the TUD burner and the ceramic bluff body cap of the Cambridge burner would be measured using thermographic phosphor techniques at TU Darmstadt.

Differential Diffusion Effects in Turbulent Premixed Flames

Coordinators: Simone Hochgreb and Luc Vervisch

This session was devoted to understanding differential diffusion in turbulent premixed flames. Specifically, the focus was on bluff-body stabilised turbulent flames, and the role of the recirculation zone in enhancing the effect of differential diffusion.

Recent experiments involving premixed and stratified turbulent flames ($Re \sim 10^4$) stabilized on an annular burner with a central bluff body (the Cambridge/Sandia burner and a simpler single slot burner) showed that the carbon-hydrogen balance is not conserved across the flame in the region adjacent to the recirculation zone. Instantaneous and averaged measurements of equivalence ratio and the C/H atom ratio calculated from major species at a distance of 10 mm above the bluff body surface show a jump across the flame zone, unlike measurements made on laminar premixed flames or turbulent flames without a recirculation zone. The CO_2 mass fraction is higher than expected in the products, while the O_2 mass fraction is lower. This behavior has been attributed to the differential transport (diffusion and convection) among species. Near the flame stabilization point at the edge of the recirculation zone, there is strong shear due to the velocity difference between the reactant stream and products within the recirculation zone. In this region, the shear layer thickness is of the same order as the flame thickness. Diffusion acts across this layer to transport oxygen and fuel from the reactants toward products and CO_2 , H_2O , CO and H_2 from products back toward reactants. As in a planar flame with no shear (1D calculation), diffusion of CO_2 from products to reactants is slower than that of hydrogen containing species, hydrogen and water. In the bluff body case, however, the boundary conditions are affected by the presence of intense convection on the reactant side, and recirculating convection on the product side. The H-rich mixture on the reactant side is convected away (downstream), whilst the C-rich mixture on the product side is recirculated. In retrospect it appears that there was evidence of this same effect in published Raman/Rayleigh measurements on the TECFLAM premixed swirl burner.

Laminar and turbulent simulation results for a similar bluff body burner were presented by Vish Katta. These simulations included full transport and chemistry (GRI Mech 3.0). Results for state profiles across the flame (scalars vs. temperature) agree well with measurements, confirming that the effects of differential transport, including differential diffusion and shear near the bluff body, are responsible for the observed behavior.

This issue creates additional difficulties for modellers attempting to use such a database for validation, as differential diffusion is typically not accounted for in many LES models using mixture fraction and progress of reaction as scalar variables. Luc Vervisch considered the problem in the context of flamelet models, and

whether it is possible to find an approximate source term to take care of differential transport. The differential transport effect arises due to the difference in velocities across the reacting shear layer. The effect of differential diffusion can be estimated from the difference in residence time along the burner, and estimates from LES calculations without differential diffusion predict a difference of around 7% in mixture fraction. Further, it is possible to incorporate the differences in mixture fraction (defined either from the major species or minor species) by using a source term, defined as the remainder after the reaction and average diffusion term are subtracted from the calculations. LES results using this simple approach showed significant improvement in comparison with measurements from the Cambridge burner.

Key questions raised during discussion were how relevant differential diffusion may be as the level of turbulence is increased, as well as its role in energy transport.

Lifted Flames in Vitiating Coflow

Coordinators: Matthias Ihme and Ed Richardson

The focus of this presentation was threefold:

- Review and characterize relevant ignition and flame-stabilization scenarios in lifted and vitiating flames.
- Provide a comprehensive overview of recent research progress on the modeling of lifted flames, with specific focus on the modeling of jet-in-hot-coflow (JHC) burners from Adelaide and Delft and simulating the vitiating coflow burner (VCB) or “Cabra” burner. An overview of other related experimental configurations, new measurement-data, and consideration of additional operating conditions was given.
- Discuss the utilization of DNS-databases on lifted flames for analysis and model-development.

Three different flame-ignition mechanisms were identified and characterized:

- *Autoignition-mode:* The ignition and transition from unburned to burned states depends on the condition of the local scalar dissipation rate. This ignition mode requires that the local dissipation rate reduces below the so-called ignition-dissipation rate. If this condition is reached, onset of ignition occurs, in which radical-production and heat-release exceed the diffusion rate, promoting transition to a burning flame-structure. Conditions for the occurrence of the ignition location dependent on turbulent flow-field structure and duration over which the dissipation-rate remains below the ignition-dissipation rate.
- *Gradual/continuous transition:* This ignition mode pertains to the MILD combustion regime. In MILD combustion, the S-shape curve degenerates so that the notional ignition and quenching dissipation conditions merge into a single point. Under this condition, the S-shape curve has a single inflection point, promoting the transition between unburned and burning flame-states along the monotonically increasing S-shape curve.
- *Secondary ignition-mechanism:* This ignition mechanism is observed under conditions that promote transport of heat/radicals into the flame-region. Examples for this are strong flow recirculations, swirling flows, and cross-flow conditions. Under these conditions, the ignition onset is controlled by the flame-environment, and external heat/radical entrainment into the flame promotes ignition. Characterizing this ignition mode in terms of the S-shape curve shows up as direct crossing of unstable flamelet-branch, which is not feasible from fundamental 1D-flamelet arguments.

Vitiating coflow burner (VCB, “Cabra” burner): Since the last TNF-workshop, a number of groups have performed RANS and LES computations of the “Cabra” vitiating coflow burner, considering H₂- or CH₄-fuels. Recent RANS computations include DQMOM-computations by Lee, Park, and Kim of the H₂-VCB, and ADF-PCM computations by Collin & Michel. Several LES-computations on this burner have been reported, including conditional moment closure (Navarro-Martinez et al.), multiple mapping conditioning (Sundaram et al.), unsteady flamelet/progress variable model (Ihme & See), and flow-controlled chemistry tabulation (Enjalbert et al.). The presentation contains a discussion of all contributions, including a brief overview about the model-formulation, details regarding the numerical method and computational setup, and comparisons of model-results and experiments. Since all modelling efforts employed different discretization-schemes, grid-

resolutions, SGS-models, and temporal integration methods, only comparisons of individual modelling-results against experiments were discussions. An objective comparison of all models is not meaningful, and no quantitative conclusions about best model-practice or relative model-performance are given.

Adelaide jet-in-hot-coflow (AJHC) burner: The jet-in-hot-coflow (JHC) burner was developed at the University of Adelaide with the objective to investigate oxygen-diluted and three-stream combustion. Measurements in this burner include speciation, temperature, and mixture fraction for three operating conditions of decreasing oxygen-concentration (9%, 6%, and 3% O₂) in the coflow-stream. Recent studies by Medwell and Dally extended the measurements to other fuels and a wider range of operating conditions (including changing jet-exit Reynolds number, coflow temperature, and oxygen-concentration). The focus of recent measurements was on effects of operating conditions on the apparent lift-off height. For this, a combination of visualization, chemiluminescence, and long-exposure flame-photographs were used to characterize trends in lift-off heights as function of jet Reynolds number, coflow temperature and oxygen-level. It was concluded that the apparent “lift-off” is not a monotonic function of coflow-temperature, and also depends on the O₂-level and Reynolds-number.

In the AJHC-burner the oxygen-diluted coflow is provided through a secondary burner, resulting in inhomogeneous and transient scalar inflow conditions in the coflow stream. Effects of variations in scalar inflow conditions on the flame structure have been investigated by Ihme et al. (2011, 2012), and it was concluded that the effects of inflow inhomogeneities extend throughout the entire flame region. This was attributed to the low-Damköhler number combustion regime. These findings could also have implications for other vitiated burner configurations in which one or more oxidizer streams is generated from a secondary burner. Further measurements of temperature, velocity, and species (or a subset thereof) would be most useful to provide boundary conditions for model-inputs. Apart from mean data, it was discussed that measurements of second moment statistics (rms of temperature and species) and temporal correlations would be of direct relevance to modellers.

Delft jet-in-hot-coflow (DJHC) burner: The Delft-group has reported comprehensive measurements on a JHC-burner (Oldenhof, 2010, 2011, 2012) that is similar in design to the AJHC. Several operating conditions, fuel mixtures, and oxygen-dilution ratios (mostly at the upper limit of the MILD-regime) are considered, further extending the JHC-experimental database. Point-wise measurements for velocity and temperature have been reported. Of interest to modellers, these experiments also include PIV measurements, and enable comparisons with predictions of the velocity field. Oldenhof reported joint OH-PLIF-PIV measurements and analysed the velocity-statistics as a function of distance from the OH-layer. Comparisons with simulations have not been performed and can be subject of subsequent investigations.

Three groups provided contributions from recent modelling efforts. De et al. and Sarras et al. performed RANS computations using EDC and transported PDF-methods (JCPDF, JVPDF). These investigations considered the cases DJHC-I and DJHC-X, which correspond to oxygen mass fractions of 7.6% and 10.9% and Re_{jet} between 4100 and 8800. Analysis of model results and comparisons with experiments indicate that the ignition behaviour depends on consideration of molecular transport, PDF-method, and micro-mixing model. Similar to the findings in the context of the AJHC, it was observed that the prescription of inflow conditions is crucial for predicting the outer flame region; heat-losses to the burner wall and inhomogeneities in the secondary burner are not quantified and require further consideration in the model-formulation. Kulkarni & Polifke performed Fluent-LES computations of the DJHC-I and DJHC-X configurations using a stochastic fields approach. Predictions for velocity are in good agreement, but over predictions of temperature suggest higher predicted reactivities of the model compared to experiments. Similar observations have been made by other groups and require further investigations.

Insights and challenges from DNS: The preceding comparison of different modelling approaches for lifted flames in vitiated coflow is impaired by the high sensitivity of the model predictions to uncertain or unknown experimental boundary conditions, and to uncertain chemical kinetic models. Direct Numerical Simulation of turbulent lifted flames provides validation data with precisely known boundary conditions and physical models. The potential use of such DNS data for model development was raised as a topic for discussion at the workshop. A set of new DNS computations involving lifted flame stabilization has been contributed by the

group of J.H. Chen. These include a parametric study of the effect of co-flow temperature on lifted hydrogen jet flames (Yoo et al) and parametric investigation of jet in cross flow flame stabilisation with various fuel compositions and jet nozzle geometries (Grout et al.). It was noted that the parametric variation between these flames causes transition between auto-ignitive, propagative, and secondary stabilization processes, as defined above.

Models have previously been compared in terms of ensemble- (conditionally-) averaged profiles, with respect to predictions of the mean lift-off height. Given complete knowledge of the spatio-temporal evolution of all flow and chemical quantities from DNS, however, there is scope for more detailed and more quantitative comparison between the DNS and turbulent reacting flow model. The question of which flame features to consider when evaluating predictive model performance was discussed. The use of DNS data for a posteriori model validation for lifted flames in vitiated coflow was also discussed, taking the work of Knudsen et al. as a case study. Due to the relatively moderate Reynolds numbers which characterize current state-of-the-art DNS, conclusions about LES model performance must be drawn with care. The modeller should be careful to distinguish whether the model has been validated in the context of ‘high fidelity’ LES or ‘energy resolved’ LES, as discussed by Pope and Vervisch during presentations on LES quality at this meeting. The study by Knudsen et al. reveals certain advantages to working with DNS data as opposed to experimental data. The first advantage, as noted above, is exact knowledge of the boundary conditions and physical models. Second, the resulting three-dimensional turbulent solution is known completely. The third advantage, which was realized by Knudsen et al. when their initial attempts at modelling the flame were only partially successful, is that the DNS data provides very detailed information about why particular models do or do not work. By interrogating the DNS data, they were able to identify – and remedy – deficiencies in their modelling of scalar dissipation rate and molecular transport, achieving greatly improved agreement. It was noted during discussion that, while use of DNS data removes some layers of uncertainty from model comparison, implicitly filtered LES models (which are used predominantly) combine the effects of the modelling with the numerical method. This is a feature of most current LES methods which affects comparisons with both laboratory measurements and DNS, and which should be considered further.

Discussion points and future directions: Main discussion points and further research directions that came up during the workshop presentation were:

- Wall heat-losses in the secondary burner is of great importance in vitiated flames. Measurements of wall-temperature would provide valuable information for model comparisons.
- Information about spatial and/or temporal correlations could be used to further interrogate and scrutinize LES combustion models. High-speed laser-diagnostics could provide an accessible approach to evaluate temporal correlations, and spatial correlations could be evaluated from planar measurements.
- A major source of uncertainties is the specification of inflow-conditions. Measurements of exit profiles for temperature, species, and velocity could further assist model validation and reduce ambiguities in specifying boundary conditions. This issue becomes increasingly relevant for low-oxygen and low-Damköhler number combustion regimes and for configuration that supply reactants from secondary burners or mixing systems.
- Different metrics have been considered experimentally to quantify the lift-off height in vitiated flame. While most of them have been developed from experimental considerations, only few of them can be evaluated in simulations. Examples are chemiluminescence measurements or photographs with exposure times of the order of seconds cannot be considered in LES for the reason that these computations are often only conducted over a fraction of this period. Another reason is that excited species, such as OH*, CH*, CH₂* are not included in skeletal and some of the detailed mechanisms (such as GRI). Inclusion of such species is feasible, but will increase the computation time.
- Some valuable DNS-LES comparisons have been reported, and DNS researchers are encouraged to facilitate comparison with their data by providing full details of initial/boundary conditions and physical models, and, where possible, by providing access to the code used to implement the physical models and to generate the initial/boundary conditions. The data required for LES validation are, in the first instance, similar to those reported for laboratory flames, and DNS researchers are encouraged to provide profiles of single-point statistics of scalars and velocities as a minimum.

Piloted Premixed Jet Burner

Coordinators: Matthew Dunn, Assaad Masri, and Heinz Pitsch

The purpose of the session on the piloted premixed jet burner (PPJB) was to evaluate developments in large eddy simulation of the PPJB since TNF10. Four groups were involved in the simulations: Stanford/Aachen, Imperial College London/Sydney, University of Michigan, and Lund University. The PPJB was introduced as a modelling target flame at TNF10, with PDF and preliminary LES results reported. The LES results presented at TNF11 represent a significant step forward from the LES results presented at TNF10.

The Stanford/Aachen simulations utilised a steady premixed flamelet model, with a 4D tabulated chemistry table. The chemistry tabulation incorporated the rms mixture fraction, two mean mixture fraction variables, and reaction progress as parameterization coordinates so as to accommodate for mixing with the coflow and pilot. They reported essentially negligible difference in results between 4 and 9 million grid cell meshes. The University of Michigan results employed a steady nonpremixed flamelet based tabulation combustion model approach with two mixture fractions to account for the variation between pilot and coflow streams mixing with the jet.

The Lund simulations employed an ILES model, which allowed the incorporation of complex chemistry (19 transported species). As the ILES model is dependent on the mesh size and quality, model quality measures were developed, and it was shown for the PM1-150 flame good results were obtained up to and including $x/D=15$ with an unstructured hexahedral grid of 2 million cells. The Imperial College London/Sydney simulations employed a stochastic field LES model with eight stochastic fields. The stochastic field model utilized a complex chemistry approach (15 transported species) over a 4.8 million cell grid. Interestingly, the stochastic field approach results for the PM1-200 flame, whilst predicting a flame too short, produced the best results in terms of mean and rms profiles for this flame thus far. However, there is still greater improvement need before successful prediction can be claimed for this flame. Both of the LES methods that incorporated complex chemistry were able to predict some degree extinction and re-ignition for the PM1-150 flame. However the degree of extinction was typically much smaller than measured.

The four groups presented very promising results for the two low-velocity flames PM1-50 and PM1-100. However all groups predict an insufficient degree of extinction in the high velocity flames (PM1-150 and PM1-200) and thus predicted a flame length too short. All four groups presented good results in terms of the mean and rms scalar profiles close to the burner. The success of the tabulated LES flamelet models (Michigan and Stanford/Aachen) for the low velocity PM1-50 flame is somewhat to be expected due to the correlation of the flame structure observed from experiments to the fundamental flame structure assumptions of these models. Therefore, the success of the PM1-50 simulation results can be viewed as a validation for these models assumptions. However, the success of these tabulated chemistry models for the PM1-100 flame and the PM1-150 flame (in the near nozzle region up to and including $x/D=15$) that have a significant degree of turbulence chemistry interaction is somewhat unexpected due to the assumptions of the models. It was discussed and proposed that if the tabulated chemistry approaches were to have greater success for the PM1-150 and PM1-200 flames in the future, the composition space accessed during extinction must be incorporated in some manner, e.g., through an additional tabulation dimension.

In 2010 at TNF10 the RANS based PDF calculations were presented, showing good results for the low velocity flames and under prediction of the degree of extinction in the high velocity flames. In order to further improve the PDF models, experiments exploring the role of the pilot to jet heat release ratio and the micro mixing model were proposed to be necessary. Such modelling progress also needed additional experiments to be conducted. These experiments were also discussed at TNF11 and were considered to be of relevance to the development and validation of the LES results presented at TNF11.

As always for LES, the sensitivity to boundary conditions was emphasised by all participants. A strong consensus was that accurate profiles closer to the nozzle for temperature and velocity would be very beneficial, particularly near the pilot exit and the pilot-coflow interface. No model has yet been able to show a convincing predictive capability for the entire PM1-150 and PM1-200 flames, which feature significant

extinction and reignition. Attempting to solve this challenge will hopefully motivate future developments in combustion models and corresponding experiments, which will utilize the TNF workshop as a forum to drive such progression and collaboration.

Chemistry, Complex fuels, and New Combustion Modes

Coordinators: Peter Lindstedt and Dirk Roekaerts

This session was organized in two parts. The first part covered alternative fuels, with emphasis on recent work on dimethyl ether (DME). The second part was devoted to oxy-fuel combustion and fuel composition effects in MILD combustion.

Progress on alternative fuels: There has been a long-standing ambition for the TNF community to consider alternative fuels. At TNF10, a number of options were discussed, and it was decided to consider alternative fuels by including increasingly comprehensive data sets for DME and ethanol. This combination is particularly attractive as DME is a potential fuel for Diesel engines, while ethanol is already used extensively as a bio-derived fuel additive for gasoline. Furthermore, both fuels are comparatively simple, have the same molecular weight, and their different properties hence stem from the chemical structures. The review presented at TNF11 considered DME and covered a number of different aspects, including a new DME flame series, some of the chemistry background, recent modeling efforts, and the influence of differential diffusion in the context of transport approximations. To date, corresponding work on ethanol flames has not been performed. It is in this context important to note that the TNF community serves to identify and encourage collaborative research, but cannot provide direct funding streams.

Perhaps the key reason for the success of the TNF community has been the ability to evaluate the importance of turbulence-chemistry interactions in a coherent framework that is inclusive and permits a focus on the primary topic while reducing other complexities. In this context, the Sandia A-F flame series has served as a key component, and it is particularly important that the corresponding data sets are now in the process of being extended to alternative fuels. Experimental work on a new piloted DME flame series (A-G) currently features collaboration between Sandia National Laboratory and Ohio State University, with further contributions expected from TU Darmstadt and UT Austin. The applied diagnostics at Sandia include PIV, LIF, and Rayleigh scattering at low repetition rates as well as velocity and scalar imaging at high repetition rates. Raman spectroscopy and line measurements of temperature and species are being pursued in collaboration with the other institutions mentioned. As with the piloted CH₄/air flames, these DME flames show increasing probability of local extinction with increasing jet velocity (Re up to ~68,000). Preliminary experimental results are highlighted in the presentation. More extensive velocity and scalar measurements should be available before TNF12.

The chemistry of DME has been covered comparatively extensively by several groups with proposed mechanisms available. The latter include the work by Kaiser et al. (2000) and Zhao et al. (2008) as outlined by Fuest et al. (2012). There has also been a number of experimental low-pressure premixed flame studies, and a comparison of modeled species profile with measurements by Cool et al. (2007) was presented. There are indications that the key initial branching of DME leading to either methoxy (CH₃O) or formaldehyde (CH₂O) remains less well reproduced than desirable – particularly given the very different reactivities of methoxy and formaldehyde – and hence some updating of the chemical mechanisms may be required. The impact of differences in combustion chemistry is further highlighted by the LES-CMC computations performed at ITV Stuttgart by Kronenburg and co-workers, with very significant differences obtained in formaldehyde concentrations depending on the chemical mechanism used. The work thus further emphasizes the need to revisit key initial branching ratios. The need for accurate reduced mechanisms of DME remains a priority and should arguably form a focus point ahead of TNF12.

The impact of transport approximations (differential diffusion) upon the ability to predict DME flame structures was investigated in a collaboration between TU Bergakademie Freiberg, Engler-Bunte-Institute KIT, and TU Darmstadt. The work shows that differential diffusion effects are non-negligible and that problems in predicting the outer regions of the flames measured by Fuest et al. are present.

Oxy-fuel combustion and fuel composition effects in MILD combustion: The objective of this session was to review state of the art and identify research questions of particular relevance for the participants in the TNF-workshop.

In oxy-fuel combustion the oxidiser stream is oxygen or enriched air. Oxy-fuel combustion is used in partial oxidation (gasification) and in high temperature furnaces (e.g. glass furnaces), and it is part of a potentially efficient solution for carbon capture and sequestration (CCS). Oxy-fuel combustion is often used with CO₂ recycled into the oxidiser stream in order to lower NO_x emissions. In order to decide on recommended modeling approaches in applications of oxy-fuel combustion, it is of interest to investigate the role of turbulence-chemistry interaction and also the role of turbulence-radiation interaction in a range of configurations, from simple to semi-industrial.

In MILD or ‘flameless’ combustion, one or more of the fuel and oxidizer streams is diluted with products of combustion, which are at lower than adiabatic temperature. The combined effects of lowering of oxygen concentration and lower enthalpy have impact on the combustion process. Because high values of temperature are less frequent, NO_x formation by the thermal mechanism is lower. In flameless combustion, auto-ignition is observed to play an important role. To be able to exploit the benefits of MILD combustion in a wider range of applications, fundamental understanding is needed on how fuel composition influences the boundaries of operation in the MILD regime. The jet-in-hot-coflow (JHC) burner (with coflow of vitiated air) allows study of the MILD combustion phenomena in a turbulent jet flame configuration.

Results from several experimental and numerical studies on oxy-fuel and MILD combustion were highlighted, with emphasis on localized extinction, differential diffusion effects, radiation modeling, flame lift-off behavior, fuel effects with different hydrogen/hydrocarbon mixtures, and chemistry reduction. The reported experimental results provide interesting new opportunities for modeling studies. For example, the datasets on oxy-fuel jet flames can be used to study whether models capable to predict local extinction in turbulent jet flames burning in air are performing equally well in the case of oxy-fuel and whether they are able to capture the additional effects due to differential diffusion and influence of presence of CO₂ level in the oxidizer on CO-level in the flame. Datasets on jet flames of natural gas diluted with H₂ or CO₂ burning in vitiated coflow can be used to study whether models are able to predict the trends in lift-off height and the observed appearance and growth of ignition kernels. Datasets on MILD combustion in a lab-scale furnace can be used to study which level of modeling is needed to predict the boundaries of the regime with low emissions

Interpretation and Utilization of Temporally Resolved Data

Coordinators: Adam Steinberg, Wolfgang Meier, and Luc Vervisch

The two focus topics for this session were: 1) experimental considerations for creating ‘well-posed’ time-resolved experiments and 2) requirements for comparing time-resolved experiments and simulation.

The main experimental considerations highlighted were out-of-plane effects, limited detectable quantities, and data analysis. Experimental methods that accounted for out-of-plane effects were identified, which typically employ cross-plane or parallel plane imaging. The combined use of planar imaging with line-of-site integrated techniques also was discussed. Limitations imposed by detectable species arise due to the relatively low pulse energy of continuous duty-cycle high repetition-rate laser systems. Consequentially, OH PLIF, tracer PLIF, and 1D Rayleigh scattering are the most commonly reported high-repetition-rate spectroscopic techniques. Experiments must therefore be designed such that these measurements reveal the phenomena of interest. Moreover, effort should be made to visualize simulations in the same manner as experiments. The potential of custom-built pulse-burst laser systems, capable of achieving much higher pulse-energies for short-duration bursts (ca. 10-100 pulses), also was discussed. Several different analysis techniques for time-resolved data were then presented, and experiments that employ these techniques reviewed. Efforts should be made to standardize certain common techniques, such as proper orthogonal decomposition, and/or have a few common data sets on which different versions of the techniques can be tested.

The following issues were discussed during and after the workshop:

1. Attention must be given to the different meanings between ‘time-resolved’ in the context of experiments and simulations. What is the effect of the LES time step, pulse duration, and inter-measurement time on the interpretations?
2. For model development and validation, specific target phenomena should be sought in which time-resolved experiments can yield important new insight. What are the most important dynamic phenomena to model properly? An advantage of time-resolved image sequences is that the statistics can be conditioned and that it is possible to catch events which happen quite rarely.
3. Effort must be made to analyze time-resolved experiments and simulations using the same tools (filtering, POD, DMD, etc.). Standardized data sets should be used to test different versions of analysis algorithms. This will allow more quantitative comparisons of experiments and simulations.
4. It was proposed to distinguish between ignition dynamics and flame dynamics:
 - a. Ignition relates to a single instant in time and space, which must be isolated in both experiments and simulations; time series may be collected before and after ignition to better understand ignition conditions and implication on the subsequent flame development.
 - b. Flame dynamics studies rather go with time sequences (not always time resolved), with a necessary check of the statistical predictions to validate the simulation.
5. In simulations, the time analyses may be performed in either Lagrangian or Eulerian frameworks. Eulerian implies storing many fields and Lagrangian motivates the development of specific methods to track meaningful trajectories (not always matching the flow path-lines). Specialized budget equations may also be derived to isolate time evolution of a given quantity. It may be desirable to rewind time, which is not always that easy in practice.

LES/DNS Quality and Best Practice

Coordinators: Joe Oefelein, Luc Vervisch, and Steve Pope

LES and DNS have become topics of central interest in the TNF workshop due to 1) the potential benefits LES has over classical Reynolds-Averaged Navier-Stokes approaches, and 2) the potential DNS has for providing insights toward model development. There are still many open questions, however, related to implementation of these methods and the sensitivity of various inputs on the results and model accuracy. Efforts over the past several workshops have been focused on establishing robust performance metrics to assess the “quality” of a given simulation in a manner that minimizes potential sources of error. The goal for TNF11 was to continue to build off of these past efforts by first providing a broad summary of what has been learned to date followed by development of a new more formal set of criteria that provides improved quality metrics to assess model accuracy.

The need for improved quality metrics has been recognized now for many years. In TNF8, for example, attempts to model the bluff-body flames (e.g., HM1) produced many ambiguities. Two issues arose from initial comparisons: 1) uncertainty with respect to boundary conditions, and 2) uncertainty with respect to code and simulation parameters (i.e., numerics, grid-resolution, time-step, integration time, etc.). The combined uncertainties made it difficult to draw any conclusions regarding model accuracy. Codes with a variety of different numerical schemes and capabilities (e.g., with and without explicit artificial dissipation added for stability) were used. Geometric details of the burner (which are surprisingly complex) were not resolved in most cases. Limited computational resources imposed significant constraints on the levels spatial/temporal resolution applied, all of which is a typical dilemma. These types of uncertainties are even more severe for applications.

For TNF9, algebraic error indicators were applied to the HM1 flame to explore their utility in the context of the observations above. It was shown that these indicators could produce anomalous results. Dissipative schemes (or application in laminar flows) produced misleading performance trends. Use of bulk averages instead of instantaneous quantities was problematic. Measures of turbulent kinetic energy were shown to be divergent and/or anomalous (e.g. for dissipative schemes velocity fluctuations are damped and low values of

turbulent viscosity suggests good “resolution” as a consequence). Detailed analysis of results led to the conclusion that these types of indicators do not account for various sources of error correctly.

A second focal point in TNF9 and TNF10 was application of the error-landscape concept to LES (Geurts et al.). This method inherently accounts for the competing effects of numerical and modeling errors simultaneously. The primary advantage of this technique is that it identifies combinations of grid, filter, and model parameters that introduce incorrect flow and combustion physics. Thus, it allows one to simultaneously minimize the competing effects of modeling errors and numerical errors. The disadvantage, however, is that the error cannot be reduced to any arbitrary level and the method is expensive to implement (but still cheaper than refining the grid to eliminate non-optimal minimization of errors). Likewise, grid dependence studies were presented as part of TNF10 with emphasis placed on parametric uncertainties and recursive filter refinement.

Based on these findings, improved performance metrics, based on a new local resolution, criteria were proposed and presented. The new criteria are based on quantifying the sub-filter scales that a given turbulent combustion model is capable of representing as a function of critical parameters. The analysis and discussion led to the following progressive set of recommendations to guide ongoing research:

- Grid resolution and coupling between grid and filter spacing must be quantified
 - Simple global refinements are not sufficient
 - Pros/cons of implicit versus explicit filtering need to be better quantified
 - Local resolution criteria needs to be established as function of sub-filter scales
 - Local grid distributions need to be reported and checked in critical regions of flow
- Metrics for model applicability and implementation need to be reported
 - Grid spacing ... numerical parameter
 - Filter width ... model parameter
 - Competition between numerical and model errors
- More documentation of key simulation parameters is needed
 - Algorithmic characteristics of codes (spatial, temporal, stabilization method)
 - Local grid resolution, key length/time scales, related parameters
 - Boundary conditions and sub-model implementation
- Work toward UQ to determine sensitivity of uncertain parameters
 - Boundary conditions, model parameters, baseline model assumptions
 - Large space of uncertain parameters, general guidelines

The goal for TNF12 will be to apply these new criteria to key target flames to demonstrate the method and define a more precise set of requirements based on the recommendations above.

Turbulent Opposed Jet Flames

Coordinators: Dirk Geyer and Alesandro Gomez

The presentation started with an overview of the characteristics of existing turbulent opposed jet configurations, focusing on the last decade, and the experimental data available for these configurations. Currently, two main designs are available. The first is the turbulent opposed jet version from Darmstadt (DA), having a nozzle diameter of $D=30$ mm as well as nozzle separation of $H=30$ mm ($H/D=1$), which was especially designed to allow for laser beam access along the centerline, aiming for the measurement of scalar gradients over the reaction zone. This version was further developed by the group of Peter Lindstedt at Imperial College (IC) with an emphasis on the enhancement of the turbulent velocity fluctuations. The level of the turbulent fluctuations was enhanced by a factor of two by employing fractal grids instead of simple perforated plates. Moreover, the distribution of energy containing length scales was also substantially increased. The second design ($D=12.7$ mm, $H/D=1.5$), is from Sandro Gomez’s group at Yale. Here, the turbulence generation is based on a different scheme, forcing the flow through a high-blockage plate with a daisy-shaped orifice far upstream of the burner outlet. Using this scheme, turbulent Reynolds number up to approx 1200 could be realized. The discussion showed that the turbulent flow established near the stagnation plane exhibits different features, depending on the use of fractal grids (IC) or high blockage plates (Yale).

The most prominent difference is that large scale instabilities in the region of the reaction zone are much more pronounced in the Yale burner. Such instabilities necessitate the use of suitably formulated conditional statics.

Detailed information on the inflow conditions is crucial for all turbulent opposed jet configurations since the flow field depends strongly on the way the turbulence is generated. Such data are available for all opposed jet configurations (DA, IC, Yale). In particular, the DA group also ran high-speed PIV downstream of the turbulence generating plates. Different LES simulations performed for all configurations directly after the turbulence generating device by Andreas Kempf's group at IC were able to capture all prominent characteristics of the flow field very well. The compact domain of turbulent opposed jet geometries allows for a high resolution of the simulations inside the nozzle.

During recent years, the number of fuels and flame conditions was increased. While the earlier work focused methane as fuel, higher hydrocarbons like C_2H_4 or C_3H_8 , and liquid fuels like JP-10 have been investigated at IC. The flame conditions are ranging from non-premixed to very lean premixed, with the latter established in the fresh reactant versus burnt product configuration. Experiments with conditions of local extinction were briefly discussed under conditions of direct relevance to gas turbine operations.

A number of simulations (Monte-Carlo PDF, 2nd moment U-RANS, LES-Flamelet) have been performed in the past years on the three burner configurations and were compared to experimental data. Flow fields as well as scalar data obtained by experiments are available for all configurations, where in particular the type of scalar data varies from line concentration/temperature data up to 2D imaging at low and high speed. The compact computational domain in conjunction with aerodynamic stabilization of the flame provides potential advantages computationally, in particular for LES. Simulations with different methods (LEM, W. Calhoon or LES-PDF, S. Pope) are under way. The concluding discussion showed that there is an ongoing interest in the turbulent opposed jet flames in parts of the TNF community, especially since the recent increase of the turbulent Reynolds number allows for investigations more relevant to technical applications.

Priorities and Planning for TNF12

The TNF12 Workshop will be held in the San Francisco area prior to the 35th Combustion Symposium (San Francisco, August 3-8, 2014). It is likely that there will be some coordination on schedule and venue between the TNF Workshop and the International Sooting Flame (ISF) Workshop.

It is anticipated that more extensive model comparisons will be carried out for the Darmstadt and Cambridge stratified burners and for the Sydney Piloted Premixed Jet Burner. Interested modeler should contact Andreas Kempf or Matt Dunn, respectively. There is also ongoing interest in opposed jet flames and in lifted flames in hot coflow and crossflow. We anticipate significant new experimental progress on the series piloted DME jet flames, so model comparison should be possible. It is possible that other target flames will be added, and such announcements will be made as early as possible. Those interested in modeling these or other flames that are relevant to the TNF process are encouraged to contact the authors of work on those specific flames and appropriate members of the Organizing Committee.

We also expect to continue work toward developing a more complete framework for combustion LES validation. Progress and challenges in areas of LES quality assessment, parameter variation, uncertainty quantification, and the roles of DNS and highly resolved LES in model validation are likely to be on the agenda. Development of better methods for quantitative comparison of experiments and LES, particularly in the context of high speed imaging, will also be a priority for the next workshop.

In recognition of his hard work on preparations for TNF11, Benoit Fiorina has been invited to join the TNF Organizing Committee.

List of Participants

Surname	First name	E-Mail
Anker	Jan E.	jan.anker@numeca.be
Arndt	Christoph Michael	christoph.arndt@dlr.de
Arteaga Mendez	Luis D	l.d.arteagamendez@tudelft.nl
Avdic	Amer	avdic@ekt.tu-darmstadt.de
Barlow	Robert	barlow@sandia.gov
Blanquart	Guillaume	g.blanquart@caltech.edu
Böhm	Benjamin	bboehm@ekt.tu-darmstadt.de
Cavallo Marincola	Fabrizio	fc1809@imperial.ac.uk
Chen	J.-Y.	jychen@me.berkeley.edu
Chen	Jacqueline	jhchen@sandia.gov
Cleary	Matthew	m.cleary@sydney.edu.au
Coriton	Bruno	brcori@sandia.gov
Dally	Bassam	bassam.dally@adelaide.edu.au
Dederichs	Stefan	stefan.dederichs.ext@siemens.com
Dibble	Robert Woodrow	dokdibble@gmail.com
Dreizler	Andreas	dreizler@csi.tu-darmstadt.de
Dunn	Matthew John	matthew.dunn@sydney.edu.au
Fiolitakis	Andreas	andreas.fiolitakis@dlr.de
Fiorina	Benoit	benoit.fiorina@ecp.fr
Frank	Jonathan	jhfrank@sandia.gov
Frederick	Don	don.frederick@berkeley.edu
Fuest	Frederik	fuest.1@osu.edu
Gabet	Kathryn Nicole	gabet.1@osu.edu
Génin	Franklin Marie	franklin.genin@power.alstom.com
Geyer	Dirk	dirk.geyer@h-da.de
Gomez	Alessandro	alessandro.gomez@yale.edu
Gordon	Robert Lindsay	robert.gordon2@rolls-royce.com
Gruber	Andrea	andrea.gruber@sintef.no
Hasse	Christian	christian.hasse@iec.tu-freiberg.de
Hawkes	Evatt	evatt.hawkes@unsw.edu.au
Hiremath	Varun	vh63@cornell.edu
Hochgreb	Simone	simone.hochgreb@eng.cam.ac.uk
Hunger	Franziska	franziska.hunger@vtc.tu-freiberg.de
Ihme	Matthias	mihme@umich.edu
Janicka	Johannes	janicka@ekt.tu-darmstadt.de
Katta	Viswanath R	vrkatta@gmail.com
Kempf	Andreas	andreas.kempf@uni-due.de
Ketelheun	Anja	ketelheun@ekt.tu-darmstadt.de
Kim	Yongmo	ymkim@hanyang.ac.kr
Klimenko	Alexander Y	klimenko@mech.uq.edu.au
Krisman	Alexander	a.krisman@unsw.edu.au
Kronenburg	Andreas	kronenburg@itv.uni-stuttgart.de
Kuenne	Guido	kuenne@ekt.tu-darmstadt.de

List of Participants

Surname	First name	E-Mail
Lacaze	Guilhem	gnlacaz@sandia.gov
Lee	Jeongwon	wjddnjs@hanyang.ac.kr
Lindstedt	Peter	p.lindstedt@imperial.ac.uk
Maas	Ulrich	umaas@itt.uni-karlsruhe.de
Magnotti	Gaetano	gaetanomagnotti@gmail.com
Masri	Assaad	assaad.masri@sydney.edu.au
Medwell	Paul	paul.medwell@adelaide.edu.au
Meier	Wolfgang	wolfgang.meier@dlr.de
Mercier	Renaud Camille	renaud.mercier@ecp.fr
Messig	Danny	danny.messig@iec.tu-freiberg.de
Muradoglu	Metin	mmuradoglu@ku.edu.tr
Nambully	Suresh Kumar	nambulls@coria.fr
Navarro-Martinez	Salvador	s.navarro@imperial.ac.uk
North	Andrew John	anorth@berkeley.edu
Oefelein	Joseph	oefelei@sandia.gov
Park	Sang-woon	avenue-84@hanmail.net
Pfitzner	Michael	michael.pfitzner@unibw.de
Pitsch	Heinz	h.pitsch@itv.rwth-aachen.de
Pope	Stephen B	s.b.pope@cornell.edu
Pouransari	Zeinab	zeinab@mech.kth.se
Prasad	Vinayaka Nakul	vprasad@sydney.edu.au
Proch	Fabian	fabian.proch@uni-due.de
Raman	Venkat	v.raman@mail.utexas.edu
Ren	Zhuyin	Zhuyin.Ren@enr.uconn.edu
Renfro	Michael	renfro@enr.uconn.edu
Richardson	Edward	e.s.richardson@soton.ac.uk
Roekaerts	Dirk	d.j.e.m.roekaerts@tudelft.nl
Sarras	Gerasimos	g.sarras@tudelft.nl
Schneider	Silvan	schneider@csi.tu-darmstadt.de
Settersten	Tom	Tbsette@sandia.gov
Stahler	Thabo	stahler@csi.tu-darmstadt.de
Stein	Oliver T	o.stein@itv.uni-stuttgart.de
Steinberg	Adam	steinberg@utias.utoronto.ca
Sundaram	Brruntha	brruntha.sundaram@uqconnect.edu.au
Sutton	Jeffrey	sutton.235@osu.edu
Tong	Chenning	ctong@clemson.edu
Trisjono	Philipp	p.trisjono@itv.rwth-aachen.de
Vervisch	Luc	vervisch@coria.fr
Wandel	Andrew P.	andrew.wandel@usq.edu.au
Williams	Forman A.	faw@ucsd.edu

Conference Agenda

Thursday, 26th July 2012

4:00 pm to 5:00 pm | **Registration and Poster Setup**
(Room Kopernikus)

5:00 pm to 9:00 pm | **Reception**
(includes refreshments and dinner)
(Restaurant Herrengarten)

7:00 pm to 9:00 pm | **Poster Session**
(Room Kopernikus)

Friday, 27th July 2012

8:30 am to 9:00 am | **Introduction and Announcements**
(Andreas Dreizler)

9:00 am to 10:30 am | **Turbulent Stratified Flames and Model Comparison**
(Coordinators: B. Fiorina, A. Kempf)

10:30 am to 11:00 am | **Coffee Break (Poster Session)**

11:00 am to 12:30 pm | **Differential Diffusion Effects in Turbulent Flames**
(Coordinators: S. Hochgreb, L. Vervisch)

1:00 pm to 2:00 pm | **Lunch (included)**

2:00 pm to 3:30 pm | **Lifted Flames in Vitiated Coflow**
(Coordinators: M. Ihme, E. Richardson)

3:30 pm to 4:00 pm | **Coffee Break (Poster Session)**

4:30 pm to 6:00 pm | **Piloted Premixed Jet Burner**
(Coordinators: A. Masri, M. Dunn, H. Pitsch)

7:00 pm to 8:00 pm | **Dinner (included)**

8:00 pm to ... | **Poster Session**
(Room Kopernikus)

Saturday, 28th July 2012

8:30 am to 9:30 am	Chemistry, Complex Fuels, and New Combustion Modes (Coordinators: D. Roekaerts, P. Lindstedt)
9:30 am to 10:30 am	Interpretation and utilization of Time Resolved data (Coordinators: W. Meier, A. Steinberg)
10:30 am to 11:00 am	<i>Coffee Break (Poster Session)</i>
11:00 am to 12:30 pm	LES/DNS: Quality and Best Practice (Coordinators: J. Oefelein, S. Pope)
12:30 pm to 1:30 pm	<i>Lunch (included)</i>
1:30 pm to 2:30 pm	Turbulent Opposed Jet Flames (Coordinators: D. Geyer, S. Gomez)
2:30 pm to 3:00 pm	Open Discussion, Action Items and Planning for TNF12 (Discussion Leader: J. Janicka)
3:00 pm to 3:30 pm	<i>Coffee Break (Remove Posters)</i>
6:00 pm to 8:00 pm	<i>Beer and Dinner (included, but registration required)</i> Keynote Address: Braustüb'l, Goebelstr. 7, darmstadt, close to main station, 2 km from Welcome Hotel

Turbulent stratified flames and model comparisons

Andreas Kempf and Benoît Fiorina

The objective of the session was to compare recent simulations of turbulent stratified flames against experimental data. Two configurations, investigated at TU-Darmstadt and at Cambridge, respectively, have been selected as target flames. Five groups were involved in the simulations: the Technische Universität Darmstadt (TUD), the Institute for Combustion Technology (ITV, Aachen), Lund University (LUND), the EM2C laboratory (EM2C, Ecole Centrale Paris) and a team from Imperial College London and Duisburg-Essen University (IC-UDE).

All groups performed Large Eddy Simulations using Low Mach Number solvers. TUD applied a premixed flamelet tabulation with local flame thickening (structured FASTEST code), ITV used a flamelet progress variable approach also based on premixed flamelet tabulation (structured CIAO code), LUND described the combustion chemistry through a 4-steps mechanism combined with Implicit LES (i.e. no explicit combustion or subgrid model was used with the unstructured OPENFOAM code), EM2C applied the model F-TACLES that is based on filtered premixed flamelet tabulation (unstructured YALES2 code) and finally IC-UDE used a flame surface density approach (structured PsiPhi code).

All modeling strategies were designed to predict a flame propagation speed equal to a laminar flame speed when the flame wrinkling is fully resolved on the LES grid. However different assumptions regarding the species transport description have been made. The TUD and ITV models assume that the flame front structure is similar to a 1-D premixed flamelet computed under unity Lewis assumption when subgrid scale flame wrinkling vanishes. At the opposite end, LUND and IC-UDE assumed that the flame front has the same structure as a 1-D premixed flamelet for which differential diffusion phenomena are considered. These assumptions regarding the multi-component transport properties affect the value of the effective laminar flame front propagation speed. EM2C proposed two model formulations with and without differential diffusion effects on the laminar flame speed. Note that all the present modeling strategies assume that differential diffusion is restricted to the direction normal to the flame front. Complex transport across iso-mixture fractions is, for instance, not considered.

The question of heat transfer has also been considered within the numerical simulations. In addition to adiabatic computations, several groups have performed non-adiabatic simulation, in particular for the Darmstadt flame, where the impact of heat losses on the chemistry has been modeled.

Darmstadt stratified flame

The burner consists of three 5mm-staged concentric tubes (from the center: pilot, slot1 and slot2) placed in a 0.1m/s air co-flow. Burnt gases exit from the central tube (pilot) to stabilize the flame. Different approaches have been taken to represent the computational domain: TUD computed the entire flow upstream within slot1, slot2 and the pilot tube. EM2C restricted the flow upstream computation to slot1 and slot2. LUND, IC-UDE and ITV used a more compact computational domain, starting simulations at the outlet of the inner nozzle, prescribing the measured velocity data. All groups performed simulations of the TSF-A reactive case. Also, ITV computed the TSF-Cr configuration, EM2C and IC-UDE the TSF-Ai (inert) case and IC-UDE the TSF-G (reactive) case.

Both adiabatic and isothermal assumptions have been considered to set up the pilot burner wall boundary conditions. To estimate the burner wall temperature, TUD developed an analytical analysis to model heat exchange between the pilot tube and stream 1 while EM2C

performed a RANS 2D- axisymmetric computation of the fluid flow inside the burner coupled with conductive heat transfer within the burner wall. Both studies estimate a wall temperature for the pilot tube of around 700K. For the TSF-A case, an extensive comparison of simulation and experimental data has been presented for the mean and RMS field of velocity, temperature, mixture fraction, and major species mass fractions. In general, a good agreement has been observed between the numerical predictions and the measurements. All adiabatic computations predicted a flame anchoring at the burner lips, while the non-adiabatic simulations predicted a lift-off of the flame of half a pilot diameter. The comparison of the mean temperature field and the species formation/consumption against the experimental data provides evidence that accounting for heat losses improves the prediction of the flame position. However, the impact of heat losses on the combustion chemistry remains only one possible explanation of the flame lift-off. Other phenomena like an incomplete burning of the pilot gases could also explain this observation. Further measurements are needed to conclude on the effective stabilization mechanism.

It has been also observed that multi-component transport assumptions significantly affect the mean flame position. Accounting for differential diffusion phenomena in the direction normal to the flame front seems to improve the quality of the prediction. Another conclusion from numerical data analysis is that the effect of stratification on the flame front propagation remains weak for the TSF-A case. For future work, focus should be shifted towards more stratified cases where the modeling of subgrid scale mixture fraction heterogeneities will be more challenging and influential.

Cambridge flame

The burner consists of three concentric tubes with outer diameters of 12.7 mm, 25.4 mm and 38.1 mm. The inner tube is sealed with a ceramic cap, the outer tubes have a thickness of 0.9 mm respectively 1.65 mm (named from center: bluff body, inner tube, outer tube). The mean velocity is adjusted to 8.31 m/s in the inner and 18.7 m/s in the outer tube, the burner is surrounded by an air co-flow of 0.4 m/s.

Computations were performed by EM2C and IC-UDE, both groups included the last part of the burner into the computational domain. Three cases are considered, an isothermal reference case (SwBc), a homogeneous case with an equivalence ratio of 0.75 within both tubes (SwB1) and a stratified case with equivalence ratio of 1.0 in the inner and 0.5 in the outer tube (SwB5).

For the case SwBc, comparisons of mean and rms profiles for the axial and radial velocity-component with PIV measurements have been presented for various downstream locations. A good agreement has been observed between the experimental and the simulated data, both groups were able to give a good prediction for the resulting flow field, including the recirculation zone behind the bluff body.

For the reactive cases SwB1 and SwB5, comparisons of mean and rms profiles for the axial and radial velocity-component with PIV measurements and for temperature and equivalence ratio with CO-LIF measurements have been presented at various downstream locations. In general, a good agreement between experiment and simulation has been observed. However, significant deviations were observed within the recirculation zone: on the one hand, the predicted recirculation zone has a lower negative axial velocity magnitude and is shorter than the measured one, which is more visible with the modelling approach chosen by UDE-IC. One possible explanation could be that the real flame is lifted, in contrast to the anchored flame predicted by the adiabatic simulations. This theory is also supported by the temperature profiles for the stratified case SwB5, where the peak value is about 125 K lower than the one predicted by both simulations. As the maximum temperature is about 300 K higher compared to the homogeneous case SwB1, conduction and flame lift-off are likely to become more

important. On the other hand, the measurement predicts a peak of the equivalence ratio profiles within the bluff body region, which is not visible in the simulation results. It could be assumed that this is caused by differential diffusion effects, which are not taken into account with either model.

More detailed investigation of the influence of mass and heat transfer near the bluff body could be an interesting topic for future studies.

Turbulent stratified flames and model comparisons

Andreas Kempf
Duisburg Essen University

Benoît Fiorina
Ecole Centrale Paris
EM2C - CNRS

1

Content

- Introduction (*Kempf*)
- Darmstadt Burner (*Fiorina*)
 - Heat losses
 - Modelling Approaches
 - Results
- Cambridge Burner (*Kempf*)
 - Modelling Issues
 - Results
- Summary
- Outlook: Challenges and Questions for TNF12

2



TECHNISCHE
UNIVERSITÄT
DARMSTADT

Guido Kuenne, Anja Ketelheun, Amer Avdic,
Amsini Sadiki, Johannes Janicka, Florian
Seffrin, Frederik Fuest, Dirk Geyer, Andreas
Dreizler, Thabo Stahler



Philipp Trisjono, Konstantin Kleinheinz and
Heinz Pitsch



Christophe Duwig



Simone Hochgreb, Mark Sweeney, Matt
Dunn and Rob Barlow



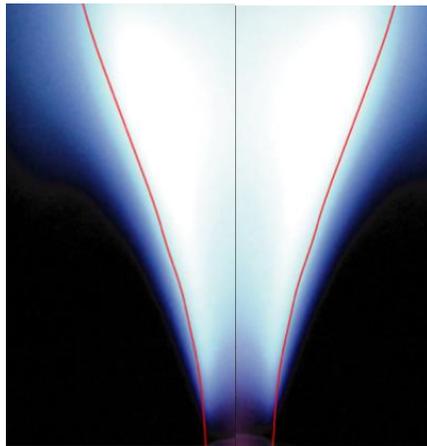
Fabrizio Cavallo, Fabian Proch and Andreas
Kempf



Renaud Mercier and Benoît Fiorina

3

Target flames



Turbulente Stratified Flame
TSF

Darmstadt, TNF10, TNF11



Swirled stratified flame
SWB

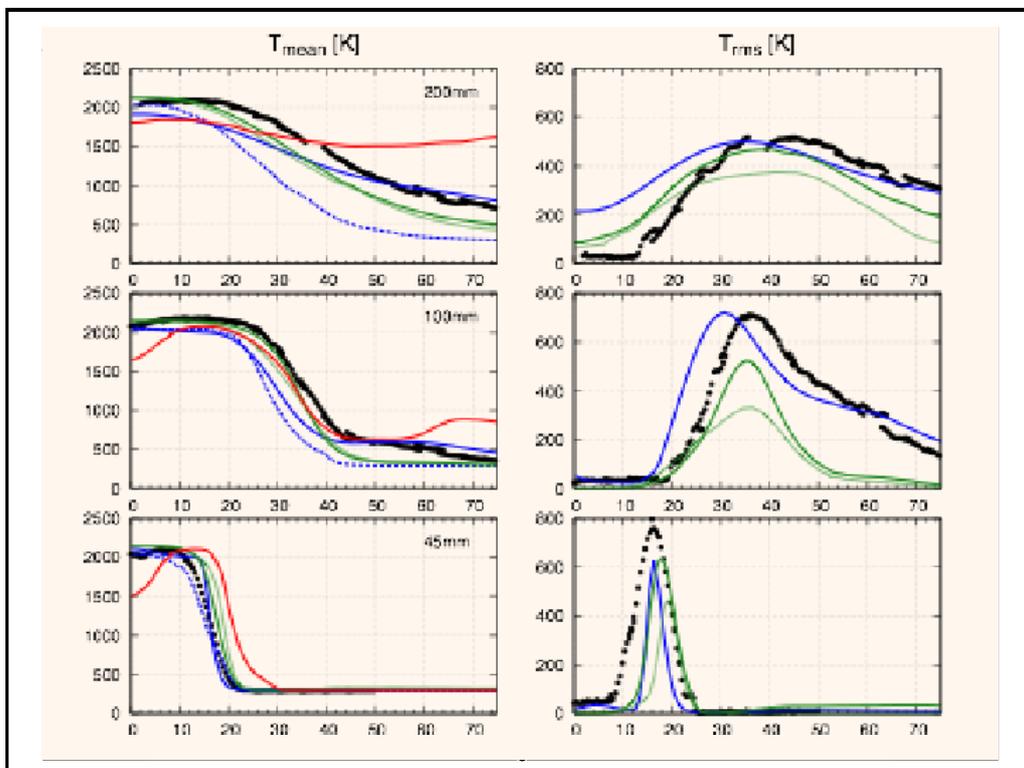
Cambridge - Sandia, TNF 11

4

Context

- Darmstadt Stratified Flame new target for TNF10
- TNF shows progress
- TNF is about developments
- Reminder: Temperature predictions from TNF10

5



Turbulent Stratified Flame TSF (TUD)

1. Experiments

- i) Brief description of the TUD flame configuration
- ii) Modeling issues

1. Simulations

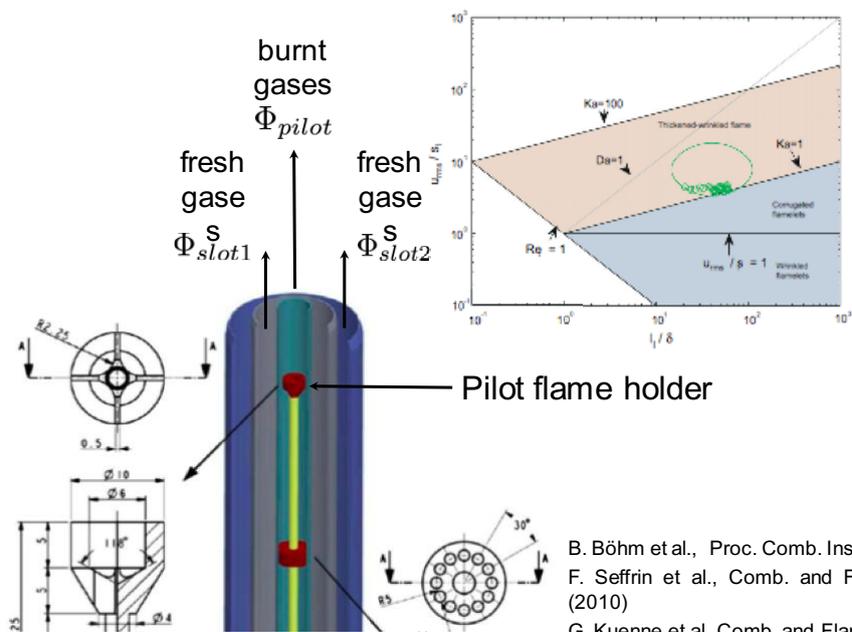
- i) Modeling approaches
- ii) Code descriptions
- iii) Computational domains

1. Result analysis



7

Turbulent Stratified Flame (TUD)



Darmstadt Stratified Burner

Configuration	Φ_{flue}	\dot{V}_{flue} (m/s)	Φ_{inlet}	\dot{V}_{inlet} (m/s)	Re_{inlet}	Φ_{out2}	\dot{V}_{out2} (m/s)	Re_{out2}	P_{total} (kW)	l (mm)
TSF_A_r	0.9	1	0.9	10		0.6	10		72	120
TSF_A_i1	0.9	1	0	10	13,800	0	10	13,300		
TSF_A_i2	0	10	0	10		0	10			
TSF_B_r	0.9	1.5	0.9	15		0.6	15		109	150
TSF_B_i1	0.9	1.5	0	15	20,700	0	15	20,000		
TSF_B_i2	0	15	0	15		0	15			
TSF_C_r	0.9	1	0.9	10	13,800	0.6	5	6700	53	110
TSF_C_i1	0.9	1	0	10		0	5			
TSF_D_r	0.9	1	0.9	10	13,800	0.6	20	26,600	111	130
TSF_D_i1	0.9	1	0	10		0	20			
TSF_E_r	0.9	1	0.9	10	13,800	0.9	5	6700	64	110
TSF_F_r	0.9	1	0.9	10	13,800	0.75	10	13,300	83	120
TSF_G_r	0.9	1	0.9	10	13,800	0.9	10	13,300	94	130
TSF_H_r	0.9	0.6	0.6 (C ₂ H ₄)	10	14,000	0.9 (C ₂ H ₄)	5	6800	53	110
TSF_L_r	0.9	0.6	0.6 (C ₂ H ₄)	10	14,000	0.6 (C ₂ H ₄)	10	13,500	63	150
TSF_J_r	0.9	0.6	0.6	10		0.9	5		52	(320)
TSF_J_i1	0.9	0.6	0	10	13,700	0	5	6600		
TSF_J_i2	0	6	0	10		0	5			
TSF_K_r	0.9	0.6	0.6	10	13,700	0.6	10	13,300	61	(250)

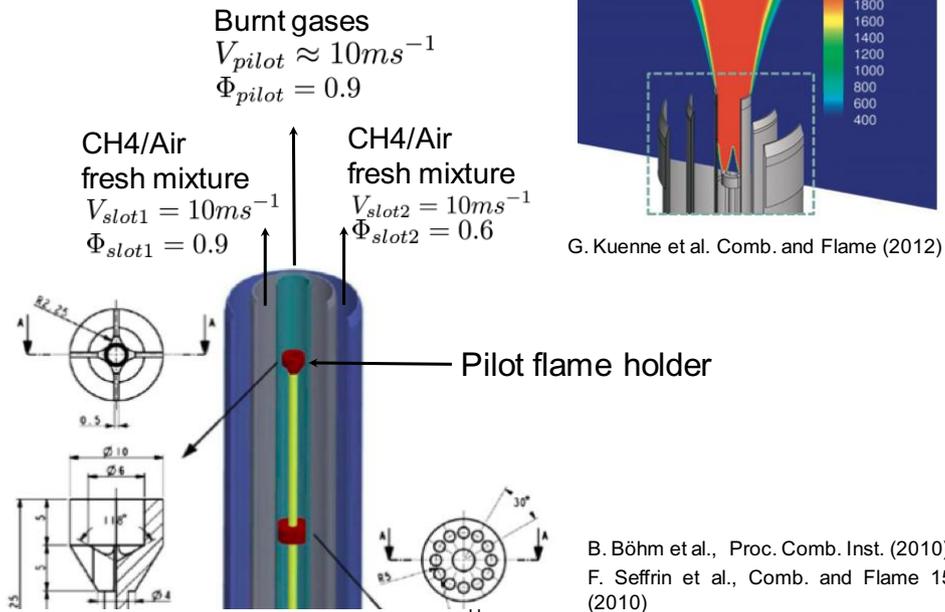
9

Contributions

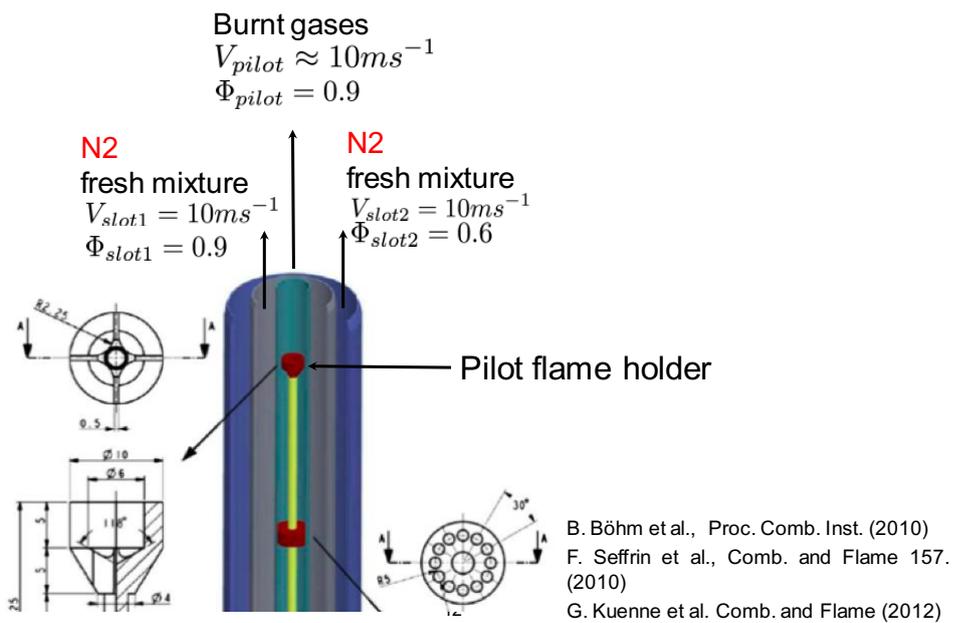
Code	TSF Ai	TSF Ar	TSF Cr	TSF Gr
ITV		X	X	
EM2C	A1	X		
LUND		X		
TUD		X		
IC-UDE	A2	X		X

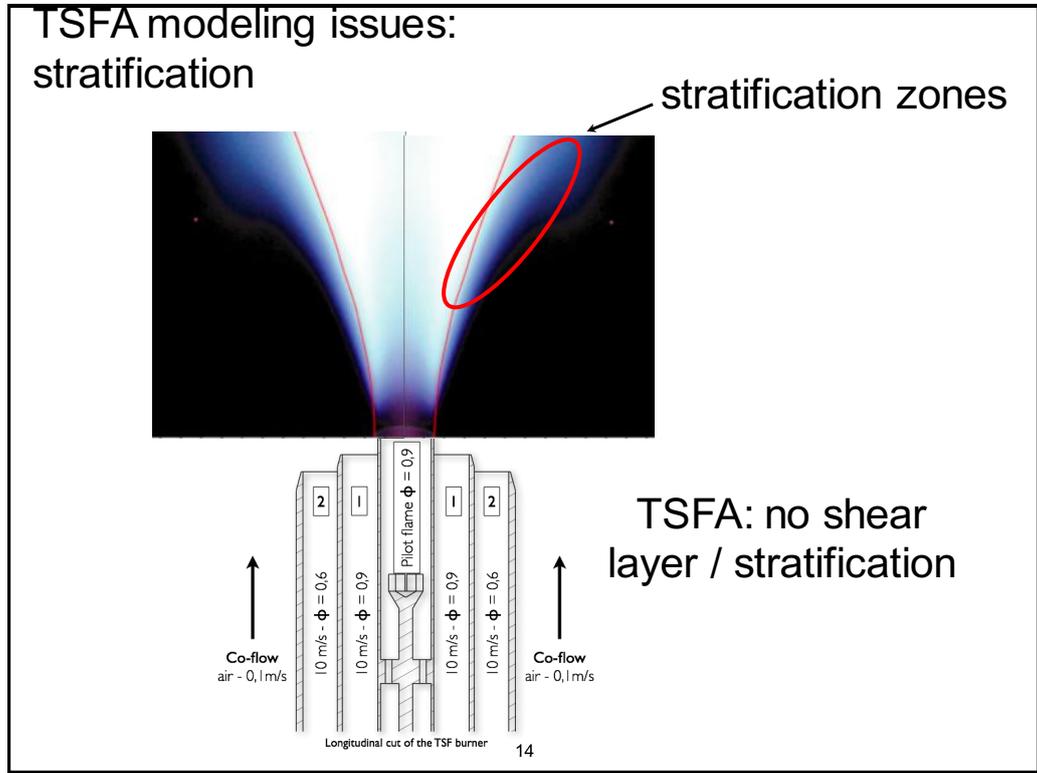
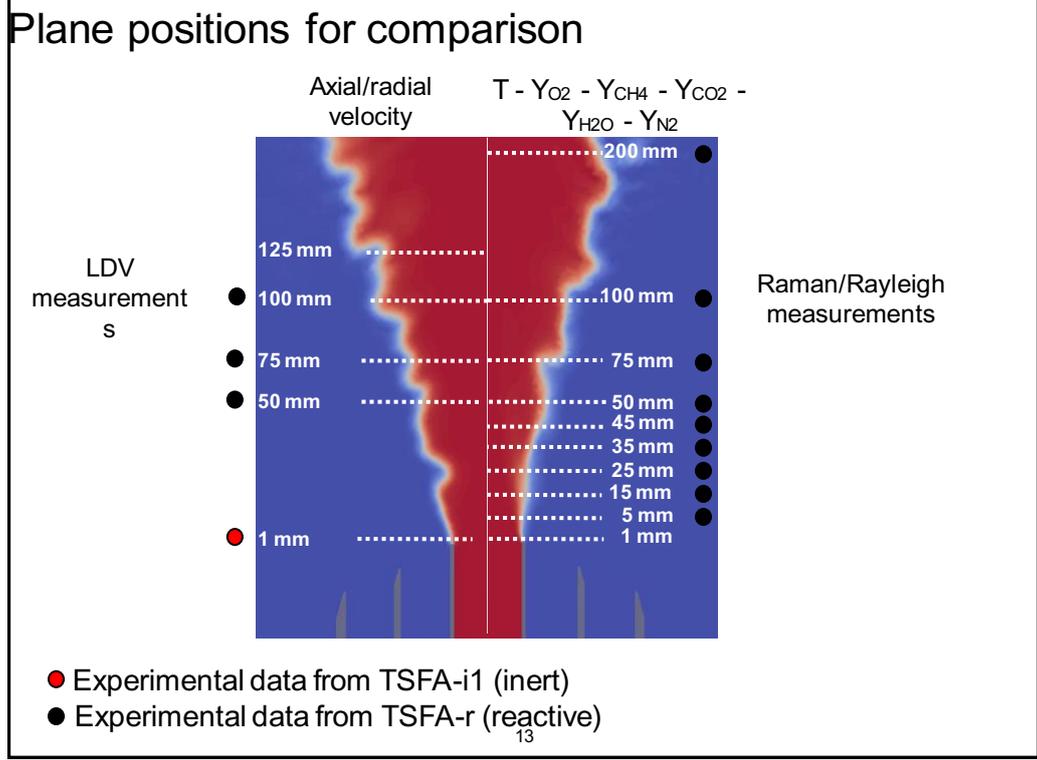
10

TSF - Ar / Reactive

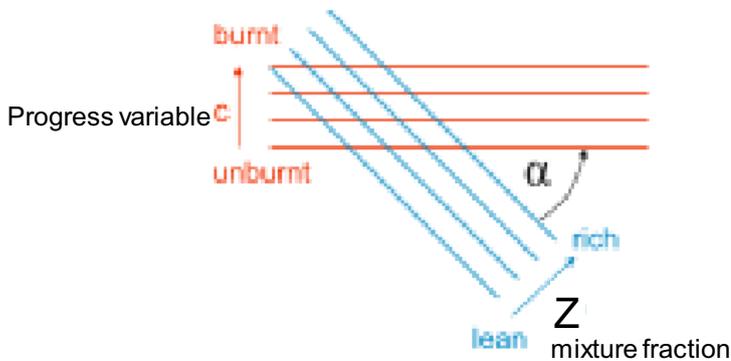


TSF - Ai / Inert





Modeling issues - stratified combustion

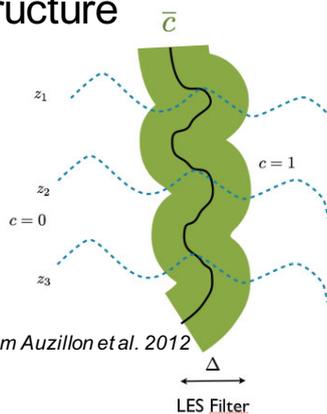


From Kuenne et al. 2012

Burning rate influenced by the orientation of iso-c versus iso-z

15

Orientation of iso-c versus iso-z will affect the flame structure



From Auzillon et al. 2012

Reaction rate is influenced

$$\rho \chi_{cz} = \rho D \nabla c \cdot \nabla z$$

Domingo et al. 2002

Modeling issues:

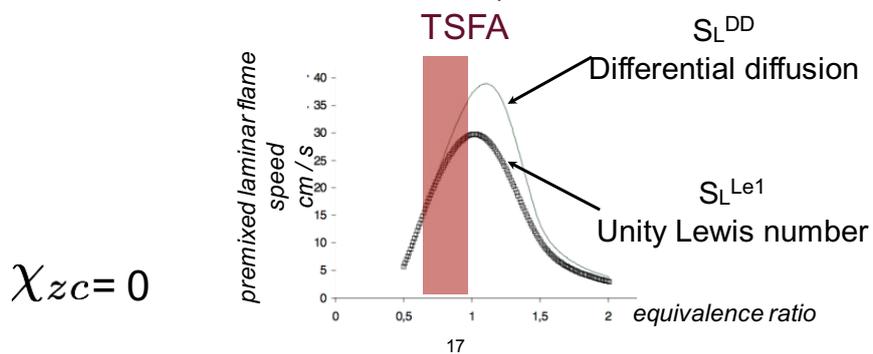
- Capture the effect of χ_{zc} on the chemistry
- Model for $\overline{\chi_{zc}}$

16

Modeling issues - differential diffusion

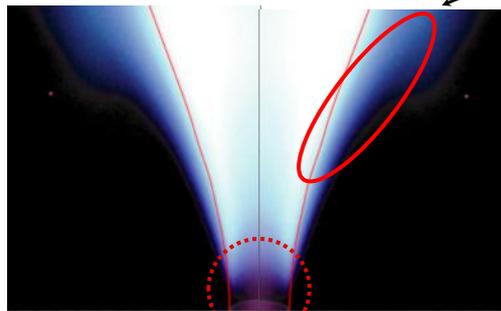
In stratified flame, differential diffusion occurs both across iso-z (mixture fraction) and iso-c (progress variable)

Only the impact of differential diffusion across iso-c on the flame propagation is discussed here (diff-diff across iso-z is discussed in next session)

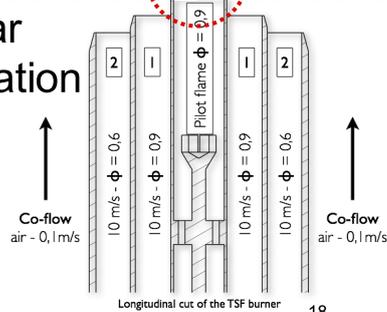


TSFA: no shear layer / stratification

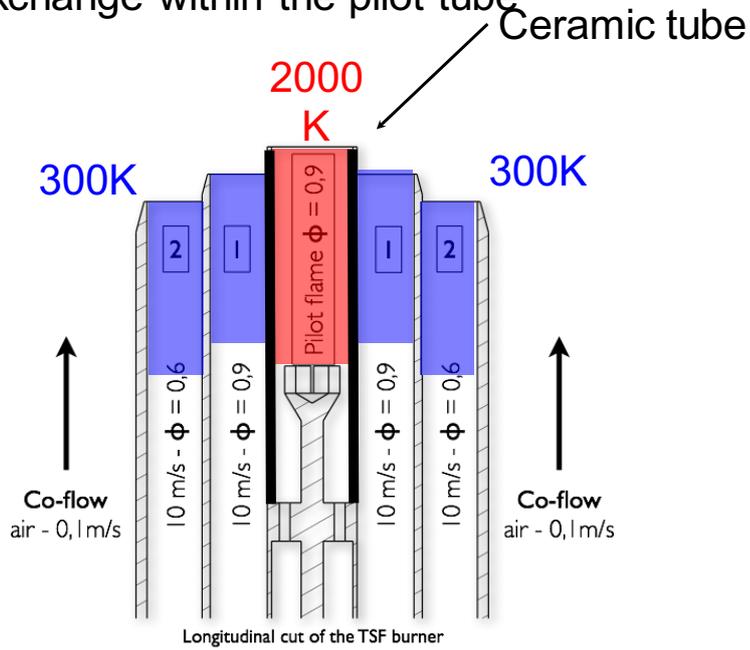
stratification zones



no shear
no stratification

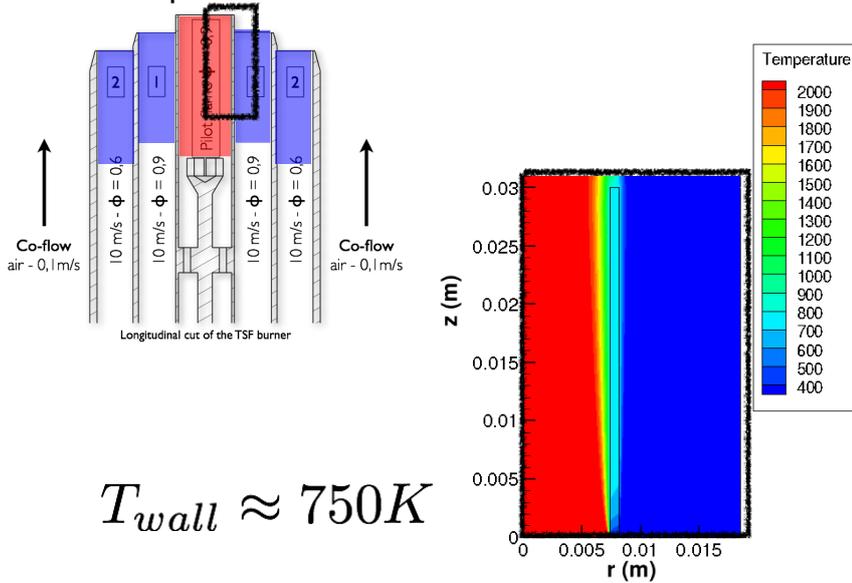


One possible explanation is the heat exchange within the pilot tube



Heat exchange within the pilot tube

Coupled fluid-solid RANS Simulation

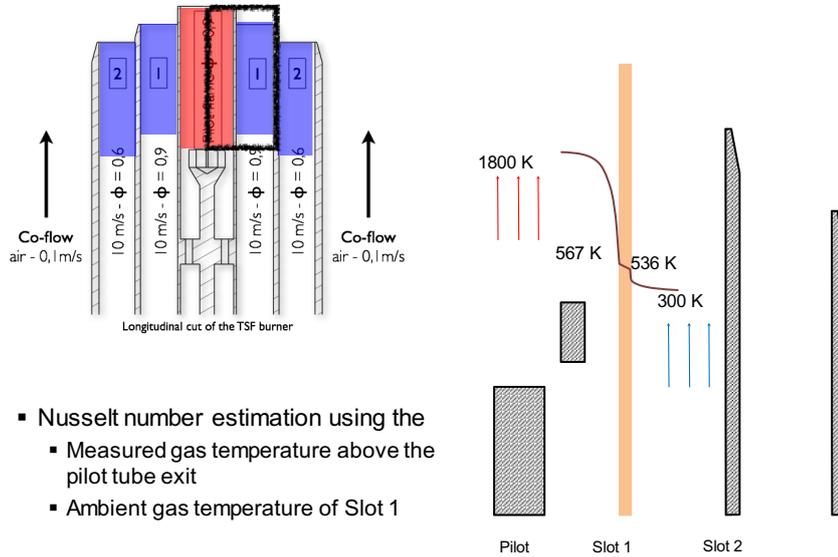


20

Mercier et al. 2012 - FM2C

Heat exchange within the pilot tube

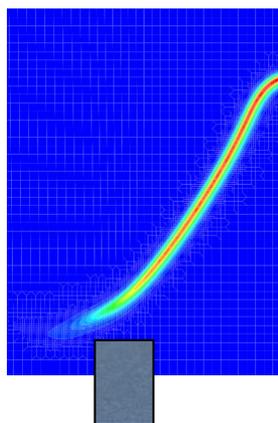
Analytical analysis from empirical laws



- Nusselt number estimation using the
 - Measured gas temperature above the pilot tube exit
 - Ambient gas temperature of Slot 1

21 *Kuene et al, 2012 - TUD*

Modeling issues: capture the effect of heat losses on the combustion chemistry



Detailed chemistry computation of a laminar premixed flame stabilized above an isothermal burner (Fiorina et al. CTM. 2003)

22

Turbulent Stratified Flame (TUD)

1. Experiments

- i) Brief description of the TUD flame configuration
- ii) Modeling issues

1. Simulations

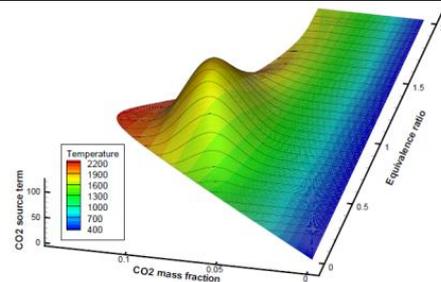
- i) Modeling approaches
- ii) Code descriptions
- iii) Computational domains

1. Result analysis

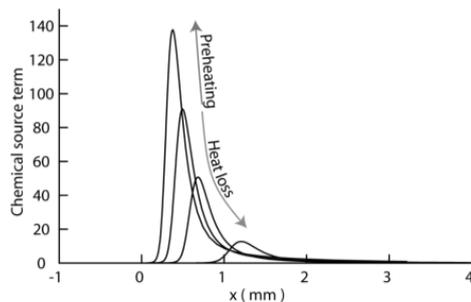
23

TUD: Artificial thickening and FGM

- Artificial thickening
 - Grid adaptive based on local cell size
 - Dynamic based on a flame sensor
 -
- FGM tabulated chemistry
 - Build by freely propagating premixed flames
 - 3-Dimensional
 - Progress Variable
 - Mixture fraction
 - Enthalpy

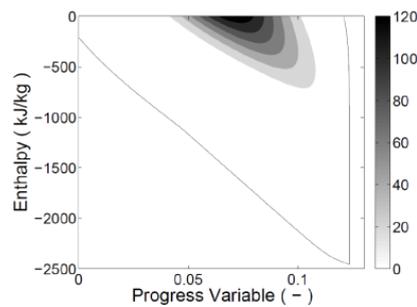


Representation of the chemistry table within the progress variable and mixture fraction space (i.e. for one enthalpy level)



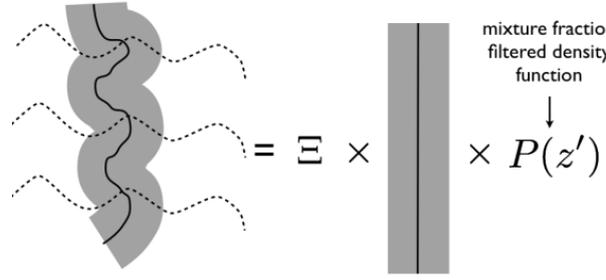
Flamelets computed for different enthalpy levels

24



Representation of the chemistry table within the progress variable and enthalpy space (i.e. for one mixture fraction)

EM2C: Filtered Tabulated Chemistry for LES (F-TACLES)



mixture fraction
filtered density
function
↓
 $P(z')$

Presumed Beta
FDF

$$\tilde{\rho\dot{\omega}_{Y_c}} = \Xi \times \int_0^1 \langle \rho\dot{\omega}_{Y_c} | z = z' \rangle P(z') dz'$$

with $\langle \rho\dot{\omega}_{Y_c} | z = z' \rangle = \int_{-\infty}^{+\infty} \rho^* \dot{\omega}_{Y_c}^*(x'_n, z') G_{\Delta}(x_n - x'_n) dx'_n$

1-D premixed flamelets Gaussian filter

25

F-TACLES: non adiabatic formulation

See R. Mercier poster

Mixture fraction

$$\partial_t(\bar{\rho}\tilde{z}) + \nabla \cdot (\bar{\rho}\tilde{\mathbf{u}}\tilde{z}) = \nabla \cdot \left[\left(\frac{\mu}{Sc} + \frac{\mu_t}{Sc_t} \right) \nabla \tilde{z} \right]$$

Progress variable

$$\begin{aligned} \frac{\partial \bar{\rho}\tilde{Y}_c}{\partial t} + \nabla \cdot (\bar{\rho}\tilde{\mathbf{u}}\tilde{Y}_c) = & \nabla \cdot \left(\Xi \gamma(\tilde{z}, \tilde{z}''^2, \Delta\tilde{h}) \alpha_{Y_c}^{ad}[\tilde{Y}_c, \tilde{z}, \tilde{z}''^2, \Delta] \rho_0 D_0 \nabla \tilde{Y}_c \right) \\ & - \Xi \gamma(\tilde{z}, \tilde{z}''^2, \Delta\tilde{h}) \Omega_{Y_c}^{ad}[\tilde{Y}_c, \tilde{z}, \tilde{z}''^2, \Delta] \\ & + \Xi \gamma(\tilde{z}, \tilde{z}''^2, \Delta\tilde{h}) \bar{\rho}\tilde{\omega}_{Y_c}^{ad}[\tilde{Y}_c, \tilde{z}, \tilde{z}''^2, \Delta], \end{aligned}$$

$$\gamma(\tilde{z}, \tilde{z}''^2, \Delta\tilde{h}) = \frac{\tilde{S}_l(\tilde{z}, \tilde{z}''^2, \Delta\tilde{h})}{\tilde{S}_l(\tilde{z}, \tilde{z}''^2, \Delta h = 0)}$$

Charlette et al. wrinkling model

Lookup table based on adiabatic 1-D filtered
flamelets²⁶

ITV: Flamelet Progress Variable

Governing Equations:

$$\frac{\partial}{\partial t} (\bar{\rho} \tilde{Z}) + \frac{\partial}{\partial x_\beta} (\bar{\rho} \tilde{u}_\beta \tilde{Z}) = \frac{\partial}{\partial x_\beta} \left(\bar{\rho} \tilde{D} \frac{\partial \tilde{Z}}{\partial x_\beta} \right) + \frac{\partial}{\partial x_\beta} (\bar{\Xi}_{\beta,Z,ssf})$$

$$\frac{\partial}{\partial t} (\bar{\rho} \tilde{C}) + \frac{\partial}{\partial x_\beta} (\bar{\rho} \tilde{u}_\beta \tilde{C}) = \frac{\partial}{\partial x_\beta} \left(\bar{\rho} \tilde{D} \frac{\partial \tilde{C}}{\partial x_\beta} \right) + \frac{\partial}{\partial x_\beta} (\bar{\Xi}_{\beta,C,ssf}) + \bar{m}_C$$

No use of a G-equation to capture the flame position

All scalars, fluid properties, source term follow:

$$\tilde{\phi}_k(\tilde{Z}, \tilde{Z}^{\prime 2}, \tilde{C}) = \int_C \int_Z \phi(Z, C) \beta(Z; \tilde{Z}, \tilde{Z}^{\prime 2}) \delta(C - \tilde{C}) dC dZ$$

Assumptions:

- Unity Lewis number
- Z convoluted with beta-pdf, C convoluted with delta-pdf
- Dynamic Smagorinsky-type model for $\bar{\Xi}_{\beta,C,ssf}$ and $\bar{\Xi}_{\beta,Z,ssf}$

27

ITV: Accounting for heat losses

Idea:

- \bar{m}_C approximated through generic Arrhenius source term

$$\bar{m}_C = A \cdot (C_{\max} - \tilde{C}) \cdot \exp\left(-\frac{E_a}{R\tilde{T}}\right)$$

- Taylor series expansion and linear regression leads to

$$\frac{E_a}{R} = -\tilde{T} \cdot \left(\frac{\bar{m}_C}{A \cdot (C_{\max} - \tilde{C})} \right)$$

- Corrected source term yields

$$\bar{m}_C(\tilde{T}_{flm} + \Delta T) = \bar{m}_C(\tilde{T}_{flm}) \cdot \exp\left(-\frac{E_a}{R\tilde{T}_{flm}} \left(\frac{\tilde{T}_{flm}}{\tilde{T}_{flm} + \Delta T} - 1 \right)\right)$$

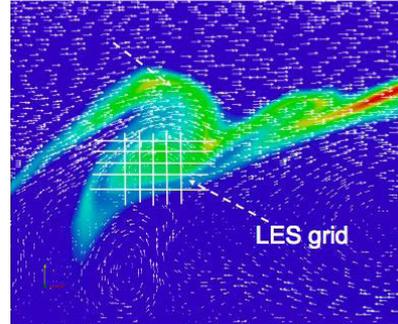
29

LUND: Implicit LES Model

Implicit LES model

$$\overline{\dot{w}_j(Y_i, T)} = \dot{w}_j(\tilde{Y}_i, \tilde{T})$$

Rather suitable for high
Ka number (here $Ka \approx 1$)



resolve the reaction
layer with the LES grid

Chemistry described by the four steps mechanism of
Lindstedt & Jones (Combustion and Flame 1988)

30

IC-UDE

- Mixture fraction

$$\partial_t(\bar{\rho}\tilde{z}) + \nabla \cdot (\bar{\rho}\tilde{\mathbf{u}}\tilde{z}) = \nabla \cdot \left[\left(\frac{\mu}{Sc} + \frac{\mu_t}{Sc_t} \right) \nabla \tilde{z} \right]$$

- Progress variable (Fureby, Duwig)

$$\partial_t(\bar{\rho}\tilde{c}) + \nabla \cdot (\bar{\rho}\tilde{\mathbf{u}}\tilde{c}) \approx \nabla \cdot (\bar{\rho}D\nabla\tilde{c}) + \bar{\omega}_c + \frac{2}{\tilde{z}}\bar{\rho}D\nabla\tilde{c} \cdot \nabla\tilde{z}$$

- Generalised Flame Surface Density Approach (Boger, Veynante, Trouvé)

$$\nabla \cdot (\bar{\rho}D\nabla\tilde{c}) + \bar{\omega}_c = (\bar{\rho}S_d)_s \Sigma_{gen} \quad \Sigma_{gen} = \Xi |\nabla\tilde{c}|$$

- FSD model for wrinkling factor (Fureby)

$$\Xi = \left[1 + \Gamma \left(\frac{u'_{\Delta}}{S_u} \right) \right]^{(D_f - 2)}$$

31

Combustion modeling approaches

	Turbulent combustion model	chemistry	Adiab	Non adiab	Lewis number	SL
TUD	Thickened flame TFLES	Tabulated from premixed flamelets	X	X	=1	S_L^{LE1}
EM2C	Filtered flame F-TACLES	Tabulated from premixed flamelets	X	X	=1	S_L^{LE1}
					$\neq 1$ across iso-c = 1 across iso-z	S_L^{DD}
ITV	Flamelet progress variable FPV	Tabulated from premixed flamelets	X	X	=1	S_L^{LE1}
LUND	no model ILES	4 steps mechanism		X	=1	S_L^{DD}
IC UDE	Flame Surface Density	flame speed interpolated	X			S_L^{DD}

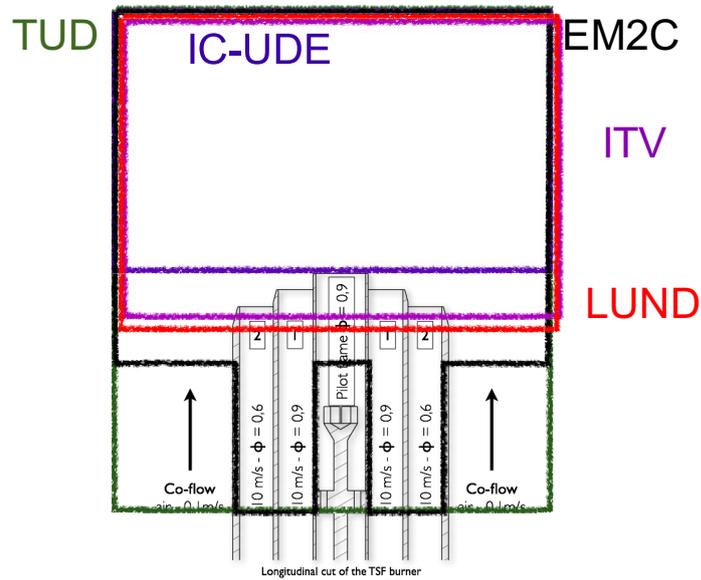
33

Computational set up

	Code	Mesh Scheme order	LES closure	$\frac{\Delta x}{\delta_l}$	Grid
TUD	AST ST Low Mach	struct 2 nd	Dyn. Smag.	0.3-1.5	6.5M nodes
EM2C	AL S2 Low Mach	unstruct 4 th	Dyn. Smag.	1	5 M nodes (32M tetra)
ITV	A Low Mach	struct 2 nd	Dyn. Smag	0.3-1	3M nodes
LUND	en oam Low Mach	unstruct 2 nd	Smag.	0.4-0.5	3M nodes (3M hexa)
IC UDE	si hi $\rightarrow \sqrt{\quad}$ Low Mach	struct 2 nd	Smag.	0.5	28M nodes

34

Computational domains



Non-adiabatic boundary conditions

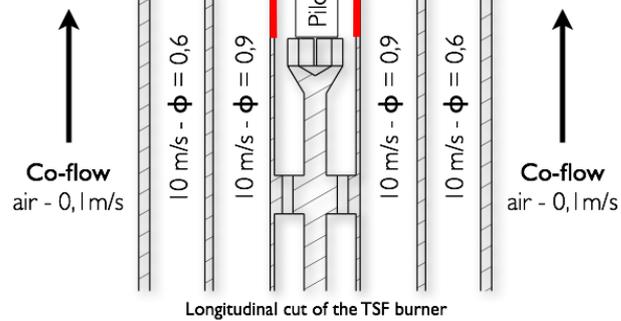
TUD: $T_{wall} = 560K$

LUND: $T_{wall} = \&$ T_{inlet} fitted to match the $x=15mm$ temperature measurement

EM2C: $T_{wall} = 800K$ & T_{inlet} fitted to match the $x=15mm$ temperature measurement

ITV: T_{inlet} fitted to match the $x=5mm$ temperature measurement

IC-UDE: T_{inlet} fitted to match the $x=15mm$ temperature measurement



Turbulent Stratified Flame (TUD)

1. Experiments
 - i) Brief description of the TUD flame configuration
 - ii) Modeling issues
2. Simulations
 - i) Modeling approaches
 - ii) Code descriptions
 - iii) Computational domains

3. Result analysis

37

Result analysis

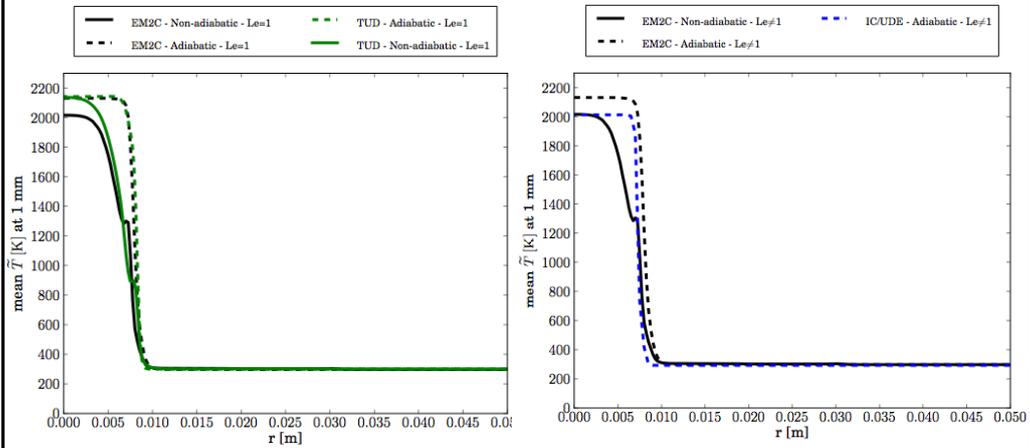
Case A

- Temperature
- *Impact of heat losses*
- *Impact of Lewis number assumption*
- Velocity
- Species and mixture fraction
- *Discussion on stratification*

Cases C & G

38

T MEAN



adiab & non-adiab

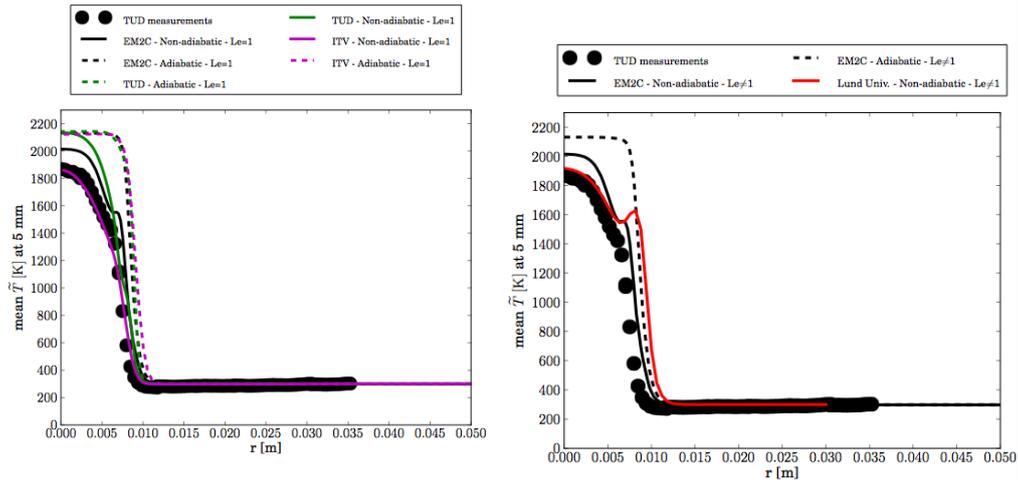
Unity Lewis number assumption

adiab & non-adiab

Differential diffusion effects on flame speed

39

T MEAN



adiab & non-adiab

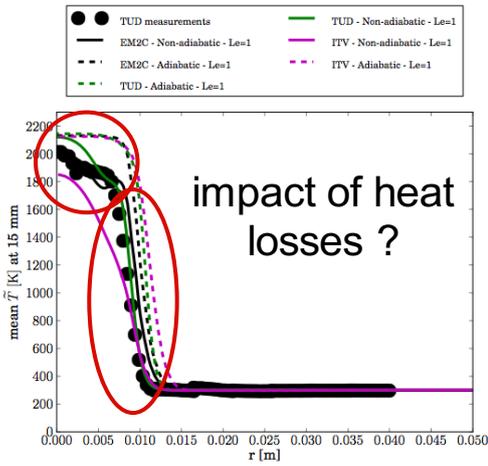
Unity Lewis number assumption

adiab & non-adiab

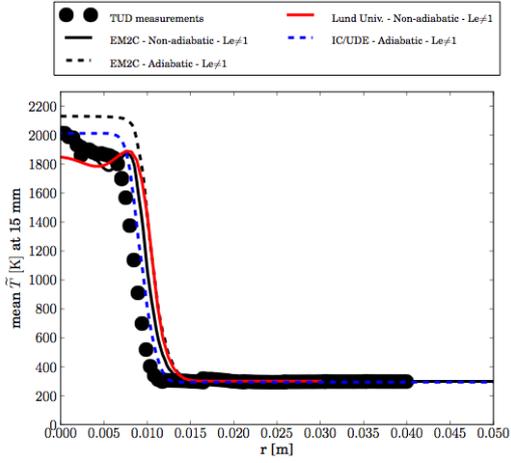
Differential diffusion effects on flame speed

40

T MEAN



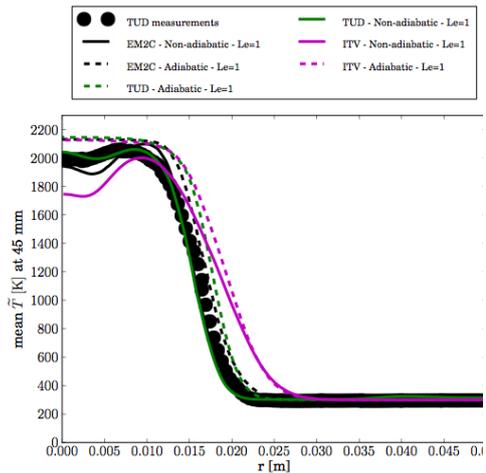
adiab & non-adiab
Unity Lewis number assumption



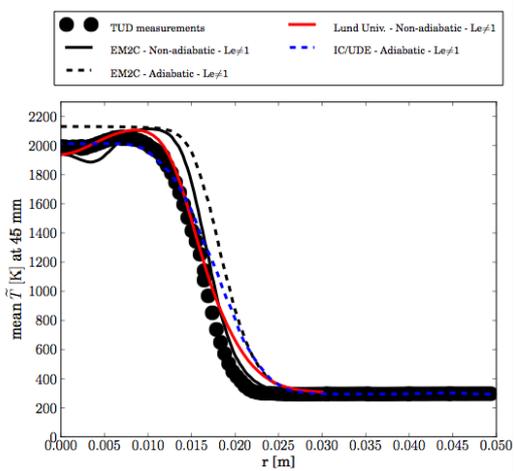
adiab & non-adiab
Differential diffusion effects on flame speed

41

T MEAN



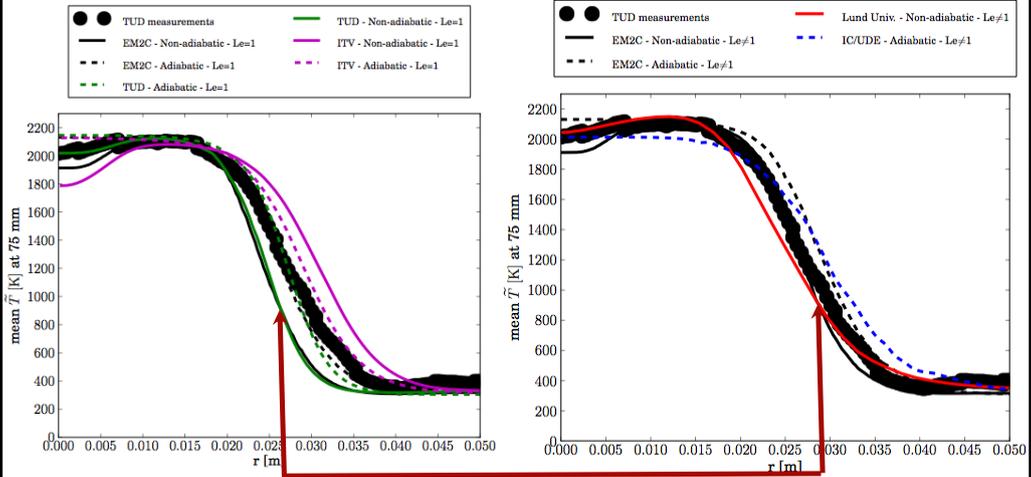
adiab & non-adiab
Unity Lewis number assumption



adiab & non-adiab
Differential diffusion effects on flame speed

44

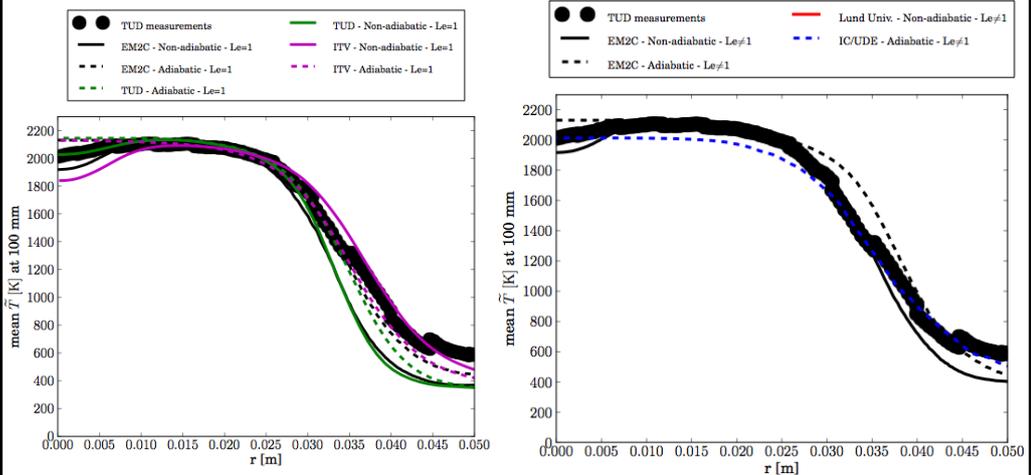
T MEAN



Impact of diff-diff

adiab & non-adiab
Unity Lewis number assumption
adiab & non-adiab
Differential diffusion effects on flame speed

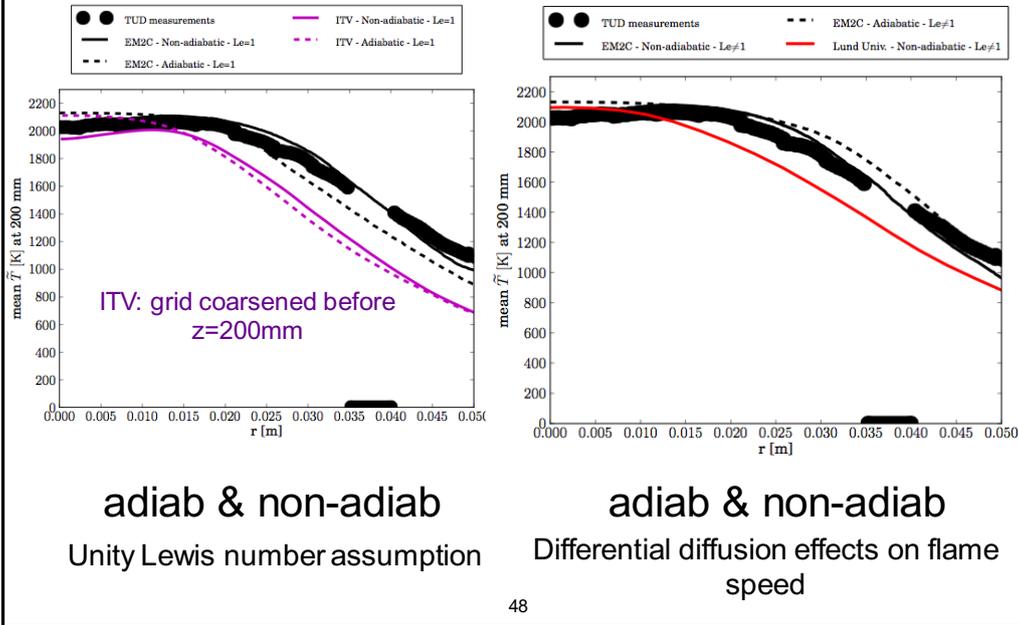
T MEAN



adiab & non-adiab

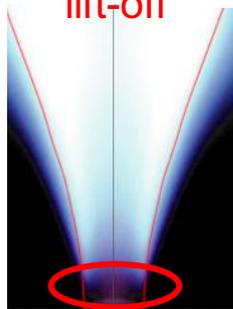
Unity Lewis number assumption
Differential diffusion effects on flame speed

T MEAN

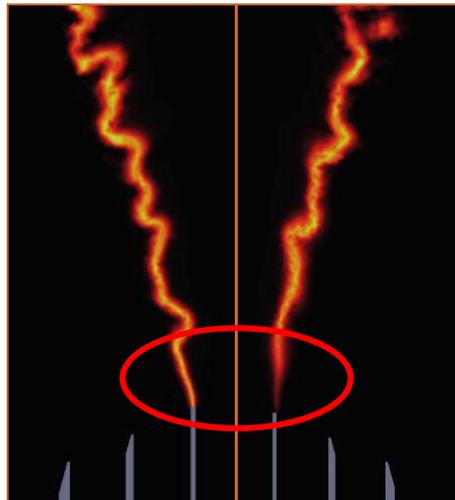


Effect of heat losses on mean temperature profile

Simulations with heat losses predict a flame lift-off



Adiabatic Non-adiabatic



Same conclusions for the others models

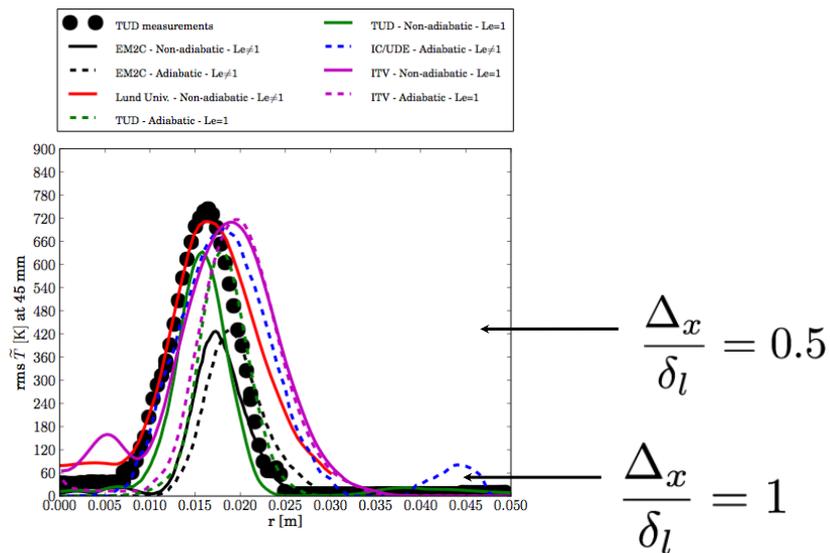
EM2C, 2012

Mean temperature profile analysis

- Heat losses would explain a flame lift-off of half a diameter. Other physical explanation ???
- Accounting or not for differential diffusion effects across iso-progress variable affects the flame speed of the filtered flame front. The effect is noticeable on the simulations. Differential diffusion effects across iso-z has not been considered.
- Accounting for heat losses improves the prediction. Conclusion is not so clear when accounting for diff-diff effects on the flame speed.

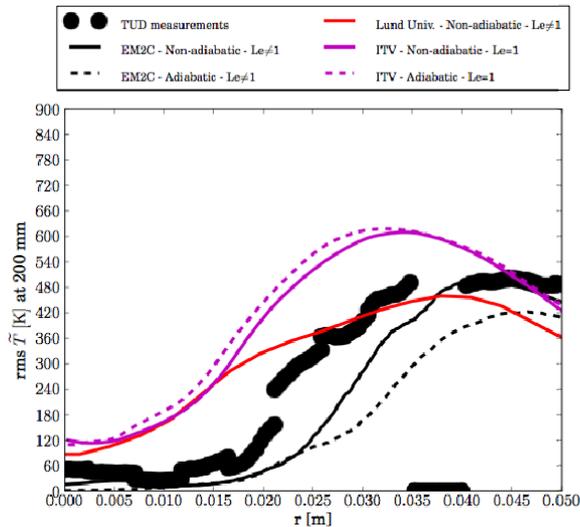
50

T RMS



51

T RMS



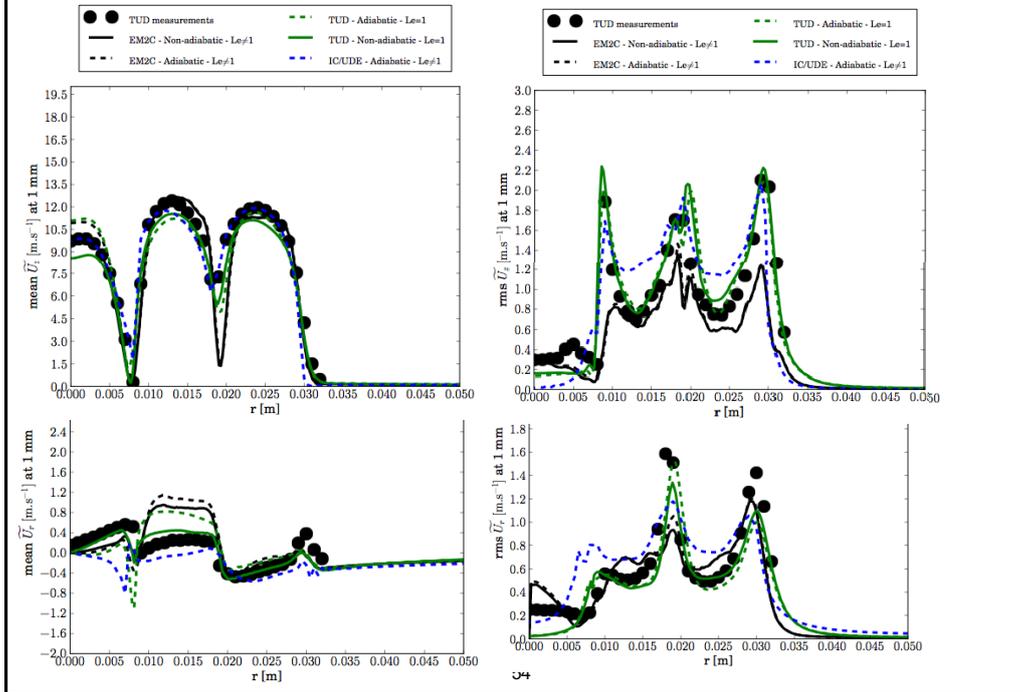
52

Analysis of RMS temperature profile

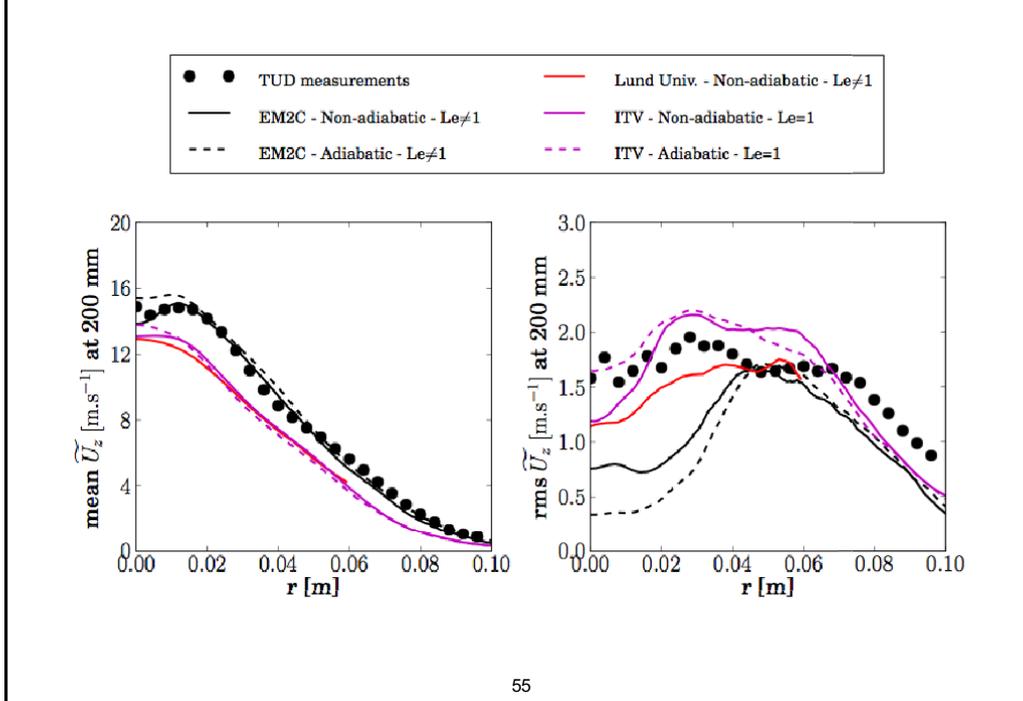
- Heat losses
- No impact on RMS level
- Same shift of temperature than for mean profiles (due to the flame lift-off)
- The amplitude of RMS is, as expected, directly correlated to the size of the resolved scales

53

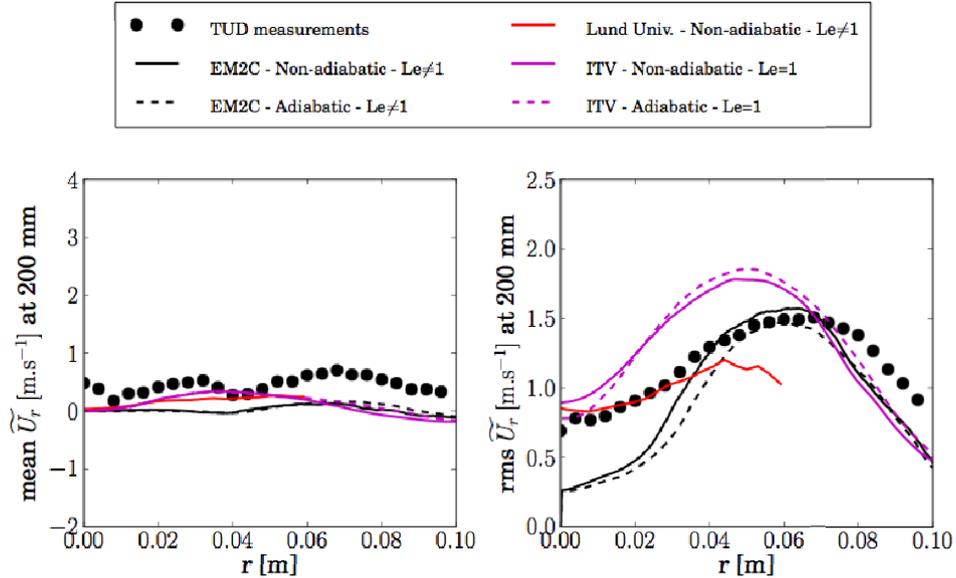
Velocity at the injection plane



Uz mean & RMS



Ur mean & RMS



56

Analysis of velocity profiles

- Impact of heat losses visible on axial velocity profiles
- High level of axial velocity RMS downstream. Not captured by all approaches

57

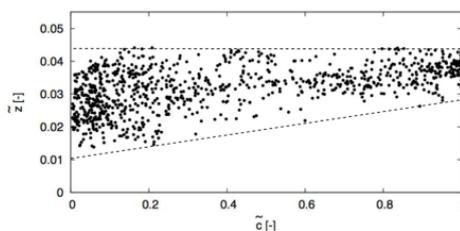
Analysis of major species profiles

- not shown but consistent with temperature results: because of heat losses, the flame is lifted and the profiles are shifted.

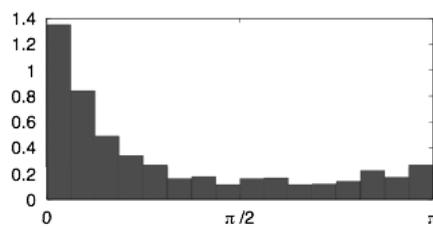
58

Stratification in flame A

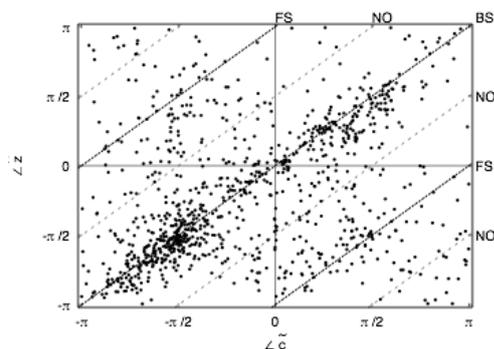
Darmstadt Stratified Burner, A-r (stratified, no shear)



1) Mixture fraction vs. progress variable



2) Angle between gradients of z , c

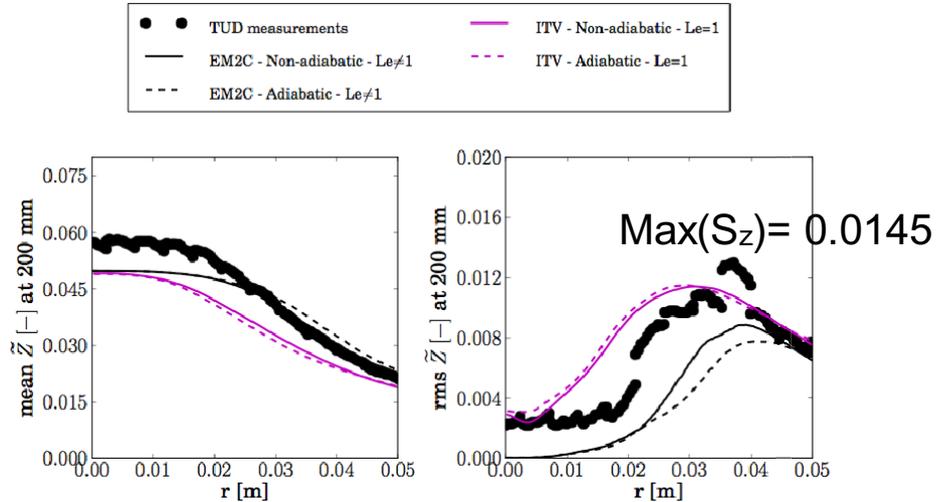


3) Angles of gradients relative to centreline

ICE-UDE

59

Z mean & RMS



60

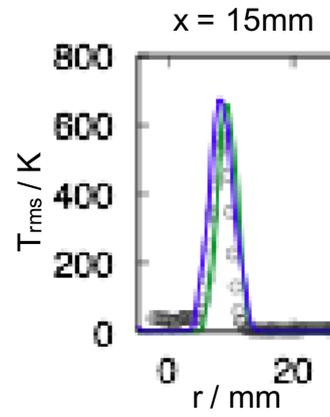
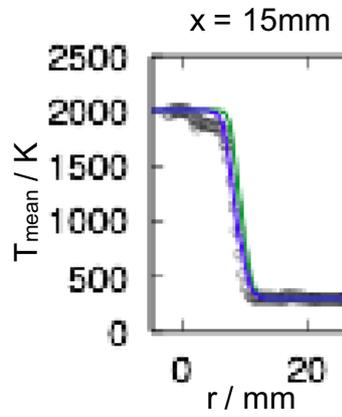
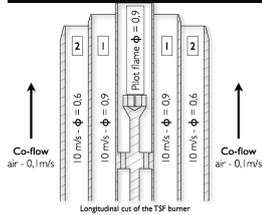
Analysis of stratification

- Weak fluctuations of mixture fraction:
 $\text{Max}(S_z) = 0.0145$ at the resolved scale
- iso-c and iso-z are mainly aligned at the resolved scale

61

Flame lift-off?

Testcase: lift-off enforced (5mm+10mm, IC-UDE)



62

Case C

$$V_{pilot} \approx 10 \text{ m s}^{-1}$$

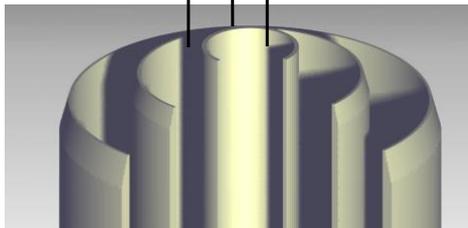
$$\Phi_{pilot} = 0.9$$

$$V_{slot1} = 10 \text{ m s}^{-1}$$

$$\Phi_{slot1} = 0.9$$

$$V_{slot2} = 5 \text{ m s}^{-1}$$

$$\Phi_{slot2} = 0.6$$



Case G

$$V_{pilot} \approx 10 \text{ m s}^{-1}$$

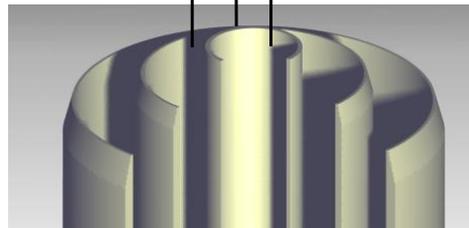
$$\Phi_{pilot} = 0.9$$

$$V_{slot1} = 10 \text{ m s}^{-1}$$

$$\Phi_{slot1} = 0.9$$

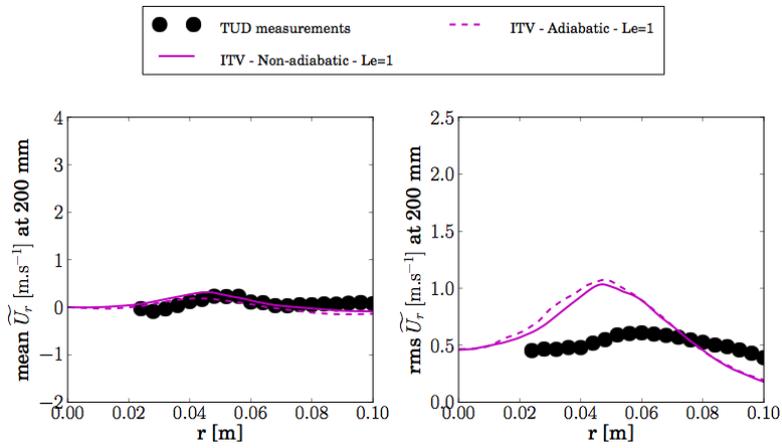
$$V_{slot2} = 10 \text{ m s}^{-1}$$

$$\Phi_{slot2} = 0.9$$



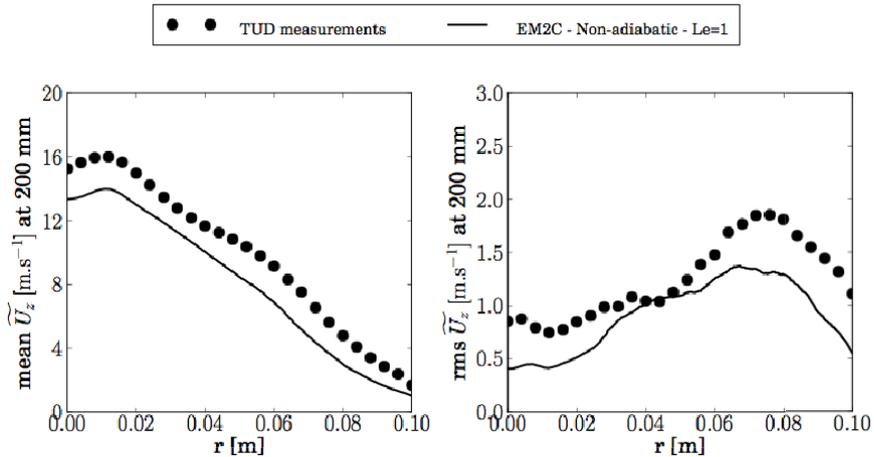
53

Velocity comparison for Case C



64

Velocity comparison for Case G



65

Conclusions

Flame A is divided in three zones, from bottom to top:

- The base of the flame is lifted: «transitional» or «lifted»
- Then the flame is well established and mainly burn at $\Phi=0.9$.
- A more diluted flame front region due to the coflow air entrainment

Modeling the effect of subgrid scale mixture fraction on the chemistry does not seem critical to capture the flame position. This may not be true for higher shear or different equivalence ratios...

66

Cambridge Stratified Flames



EM2C: Renaud Mercier, Benoît Fiorina

UDE/IC: Fabian Proch, Fabrizio Cavallo-Marincola, Andreas Kempf

*Cambridge/Sandia: Mark Sweeney, Simone Hochgreb, Matt Dunn,
Rob Barlow*



Introduction

- First time TNF test-case
- Differences to Darmstadt TSF
 - Smaller
 - Stabilisation by recirculation, not pilot
 - Heat losses?
 - Flame lift off?
 - Mixing?
 - Stability of recirculation zone?
 - No chamfer for tubes (min. structure size 0.9mm)
 - Stoichiometric reference case ($\Phi = 1.0$ instead of 0.9)
 - Stronger stratification (ratios of 2, 3 instead of 1.5)
 - Shear
 - Recirculations zone - with differential diffusion

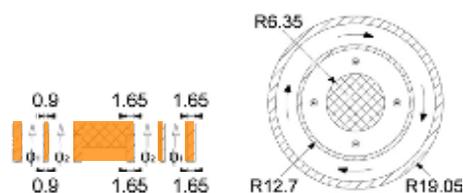
68

Configuration



Photograph and snapshot from LES (Proch)

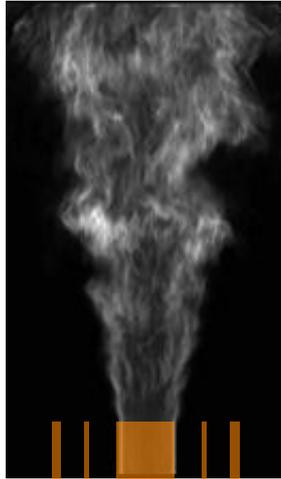
Cases	Cold	SW1	SW5	SW9
Φ_i / Φ_o		1	2	3
Φ_i		0.75	1.0	1.125
Φ_o		0.75	0.5	0,375
U_i / ms^{-1}		8.31		
U_o / ms^{-1}		18.7		
U_{co} / ms^{-1}		0.4		
Swirl		0		
Fuel		CH ₄ / air		
EM2C	✓	✓	✓	
UDE	✓	✓	✓	✓



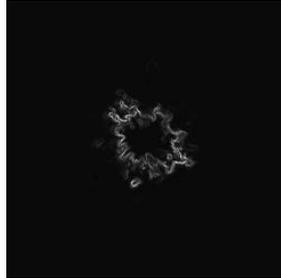
69

Overview

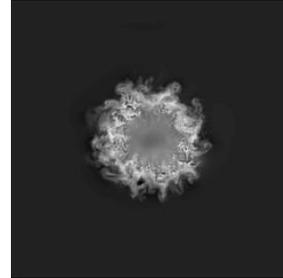
LES by F. Proch



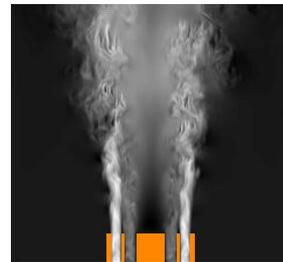
Volume rendered source term



Source term



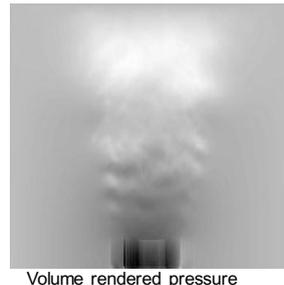
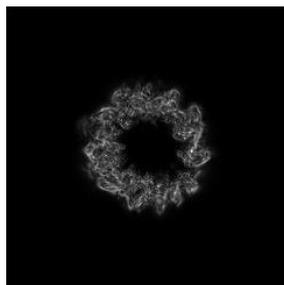
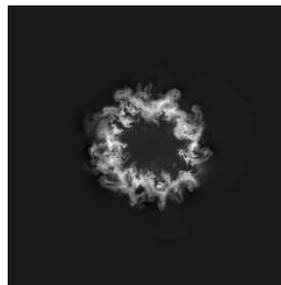
Axial velocity



70

Overview

LES by F. Proch



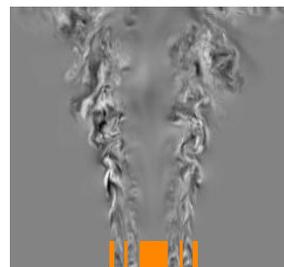
Volume rendered pressure



Axial momentum



Turbulent viscosity

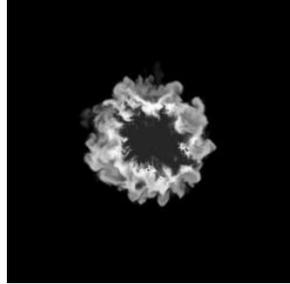
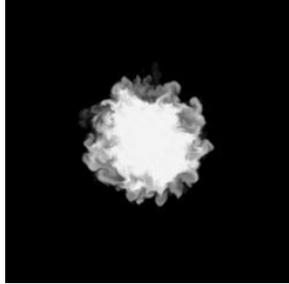
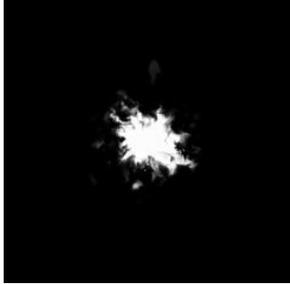


Out of plane velocity

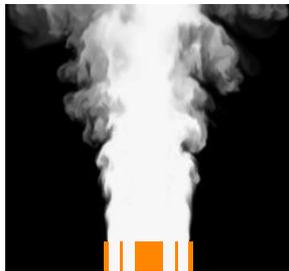
71

Overview

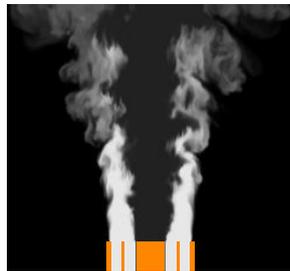
LES by F. Proch



Progress variable



Equivalence Ratio

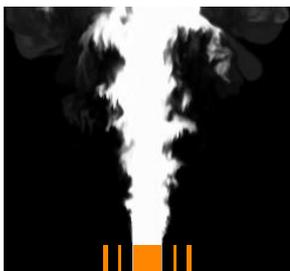
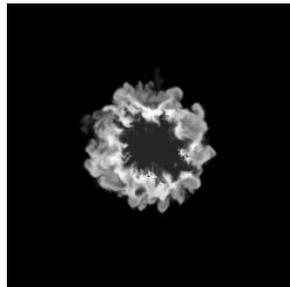
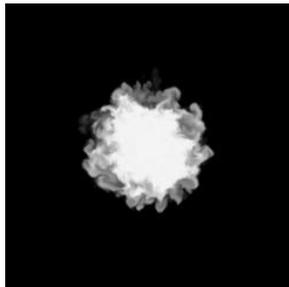
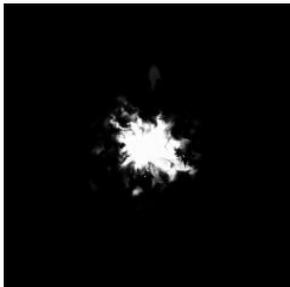


Mixture density

72

Overview

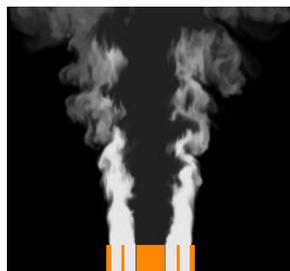
LES by F. Proch



Progress variable



Equivalence Ratio



Mixture density

73

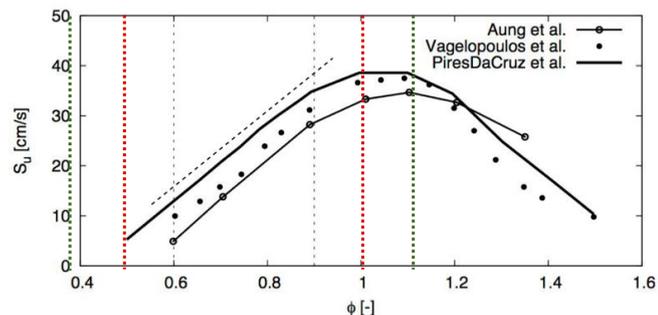
Contributions

Contributor	EM2C, École Central, Paris R. Mercier , Fiorina	Universität Duisburg-Essen Proch , Cavallo Marincola, Kempf
Cases	NR, Sw1, Sw5	NR, Sw1, Sw5
Turbulence model	Dynamic Germano	Smagorinsky $C_s = 0.173$
Combustion model	F-TACLES	Fureby FSD Fureby-Duwig approach Algebraic wrinkling factor
Code	YALES2	PsiPhi
Schemes	O(4)	CDS2 (Momentum) TVD (Scalars) O(3) RK in time
Domain and grid	unstructured NR, SwB1: 2.6M/13M SwB5: 5.3M/30M	13.5M cubic cells, (0.5mm) ³ immersed boundaries
Cost (Core heures)	5,000h SGI Altix 15,000h SGI Altix	10,000h Infiniband Cluster

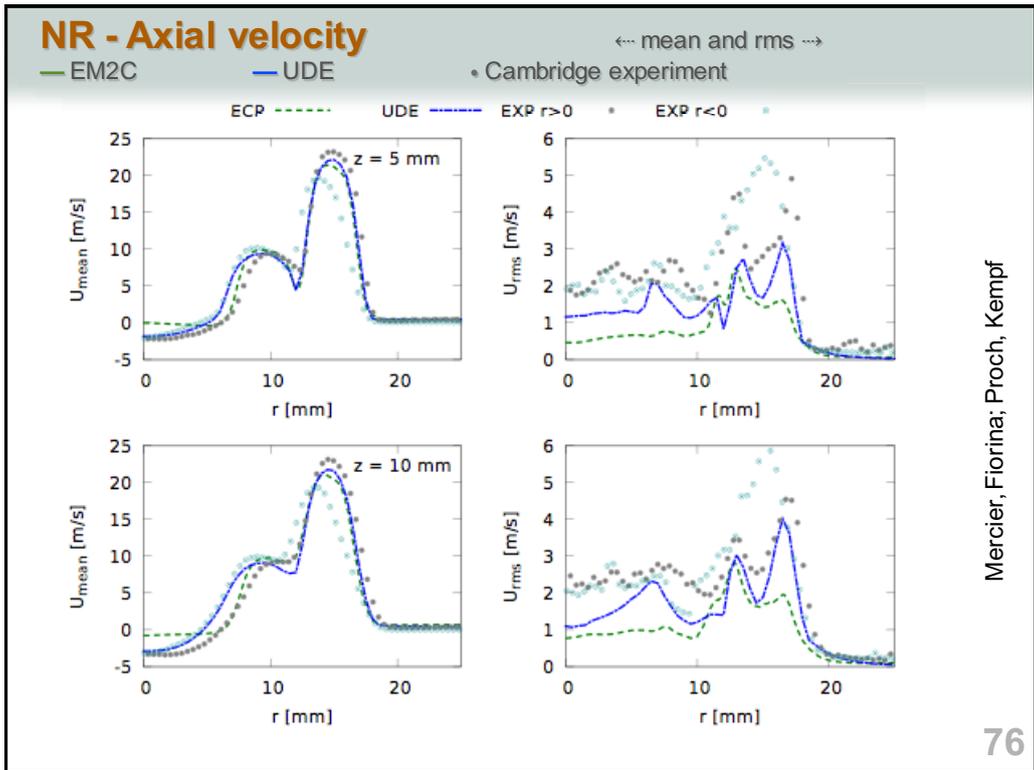
74

Modelling

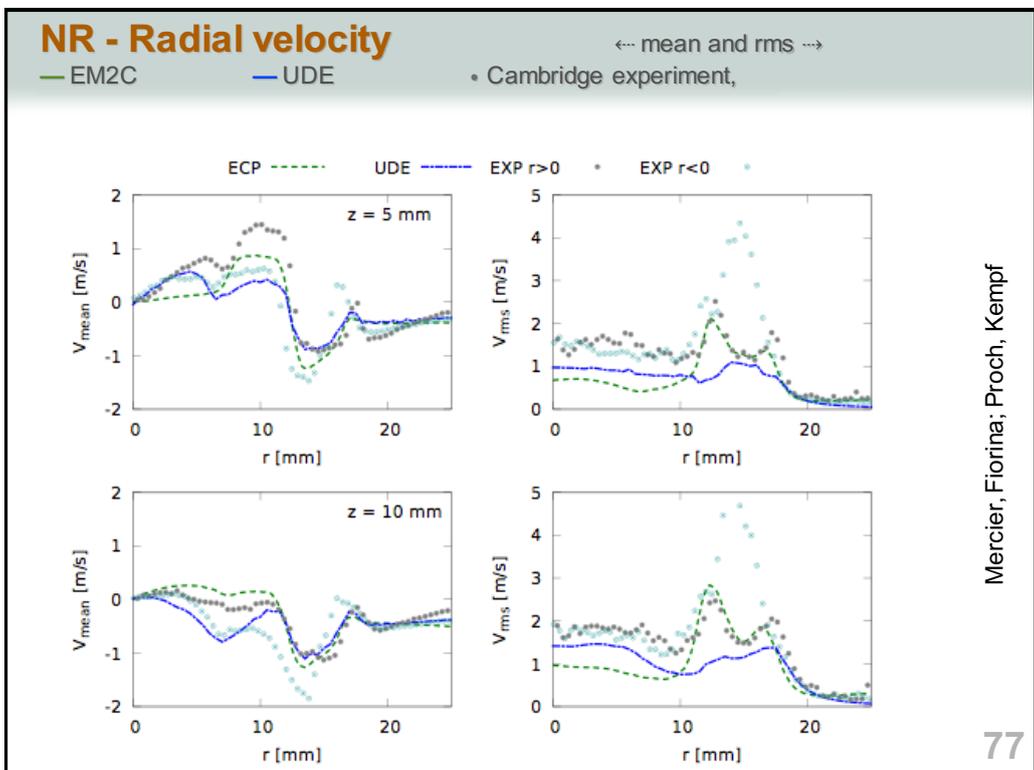
- As for TSF
- For UDE, note that:
- Immersed boundaries
- Flame speed closure
- Implicit modelling of effect of mixture fraction SG-distribution
- Good results for TSF flames ($0.6 < \phi < 0.9$). And here?



75



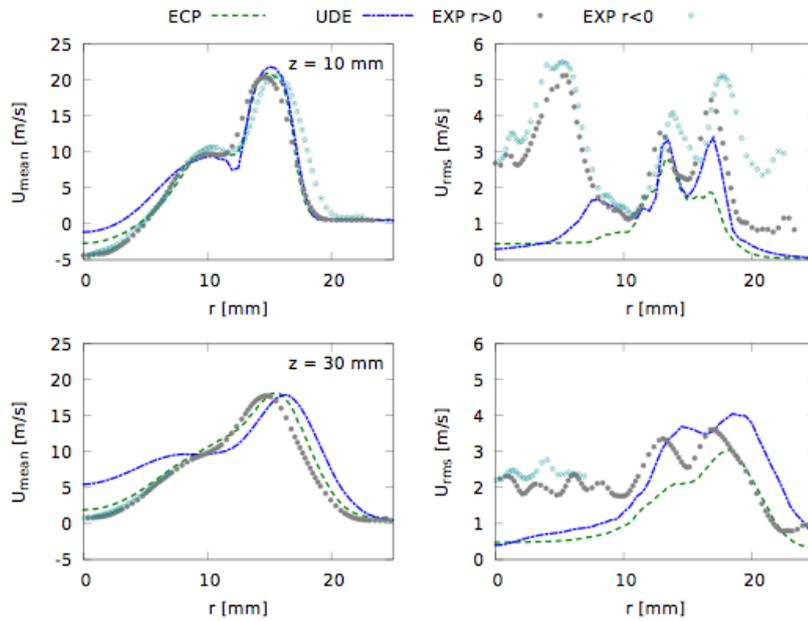
Mercier, Fiorina, Proch, Kempf



Mercier, Fiorina, Proch, Kempf

Sw1 - Axial velocity

← mean and rms →
 — EM2C — IC/UDE • ● Cambridge experiment, $r > 0$, $r < 0$

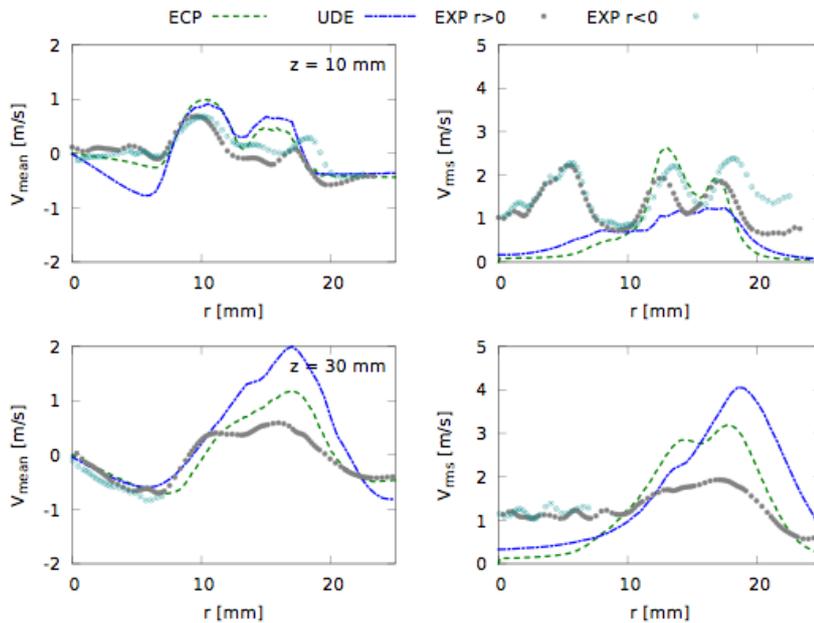


Mercier, Fiorina; Proch, Kempf

78

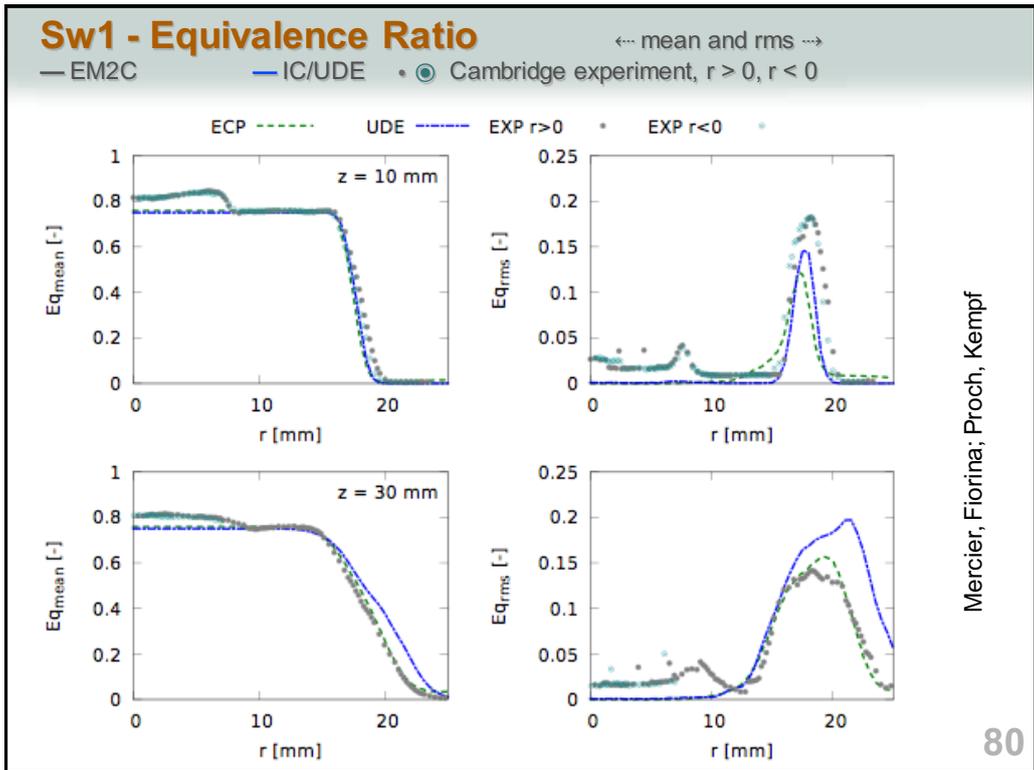
Sw1 - Radial velocity

← mean and rms →
 — EM2C — IC/UDE • ● Cambridge experiment, $r > 0$, $r < 0$

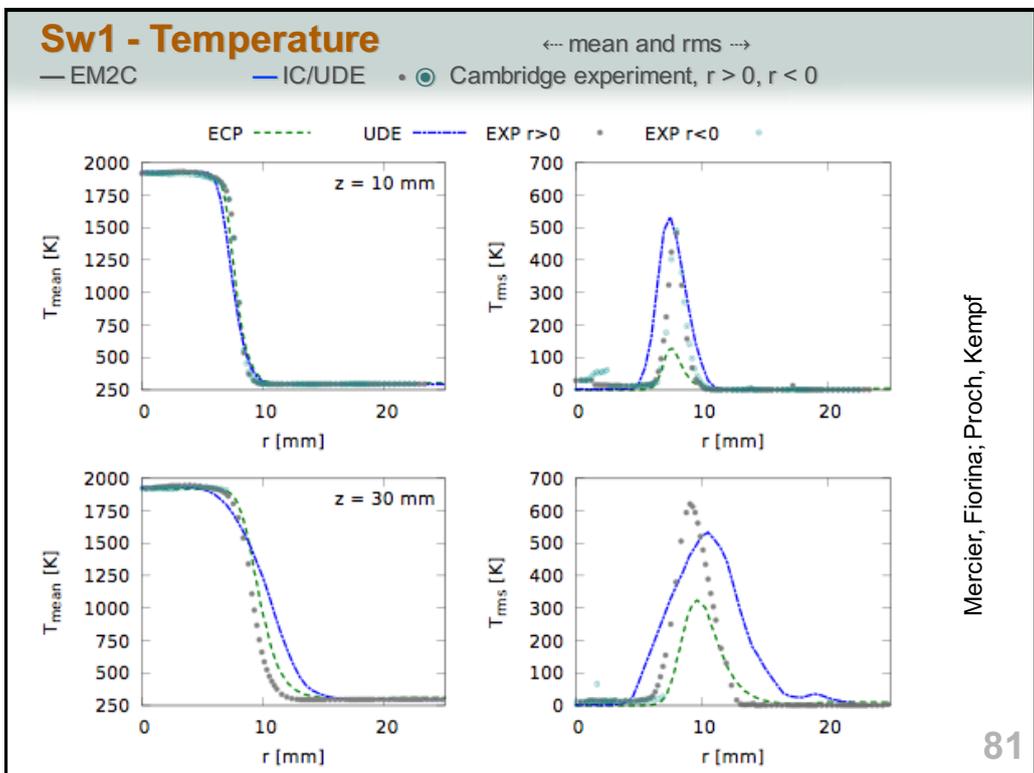


Mercier, Fiorina; Proch, Kempf

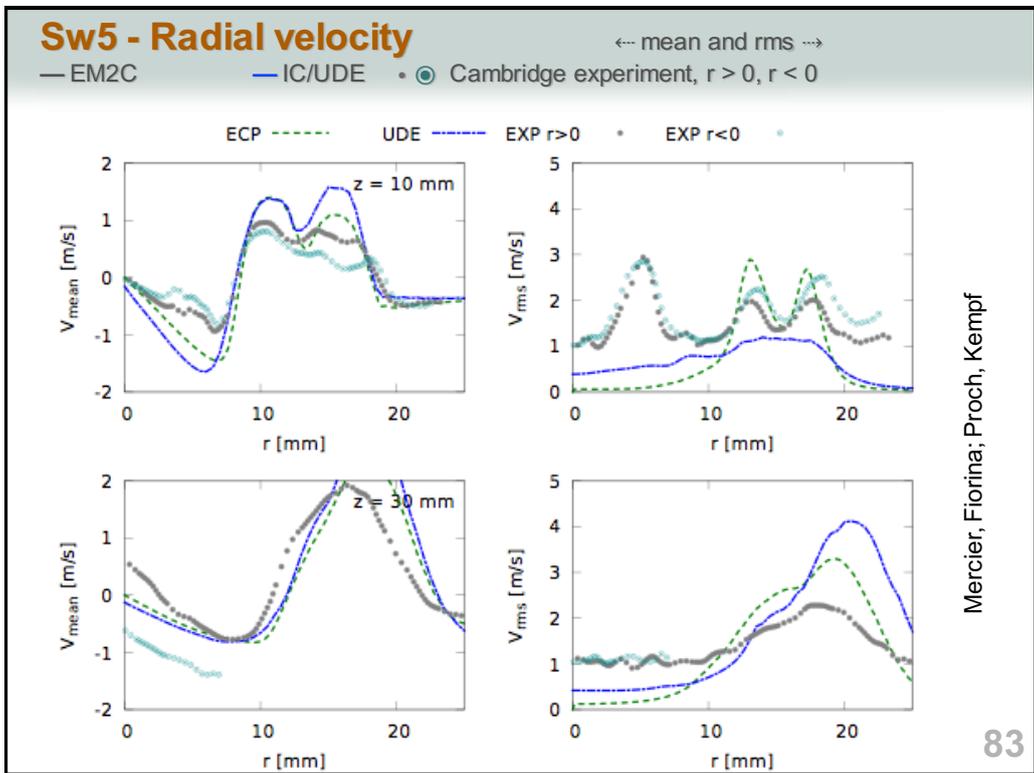
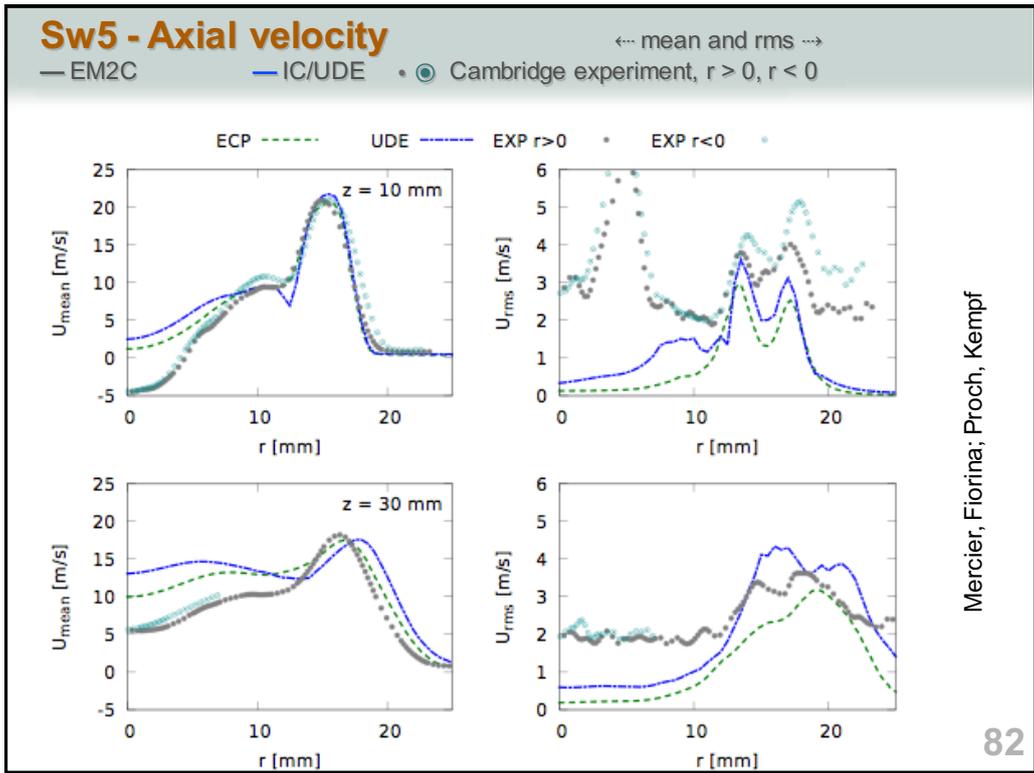
79



Mercier, Fiorina; Proch, Kempf



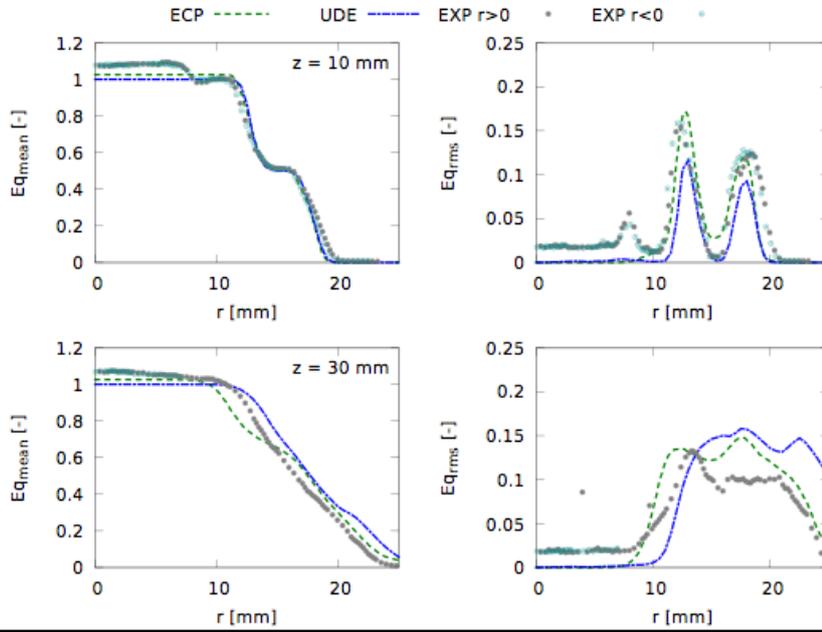
Mercier, Fiorina; Proch, Kempf



Sw5 - Equivalence Ratio

— EM2C — IC/UDE • ● Cambridge experiment, $r > 0$, $r < 0$

← mean and rms →



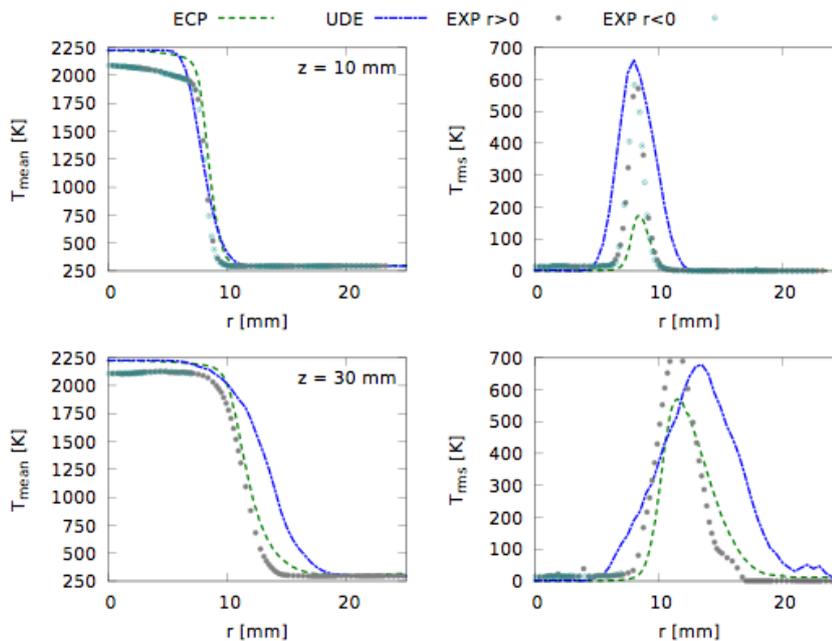
Mercier, Fiorina; Proch, Kempf

84

Sw5 - Temperature

— EM2C — IC/UDE • ● Cambridge experiment, $r > 0$, $r < 0$

← mean and rms →

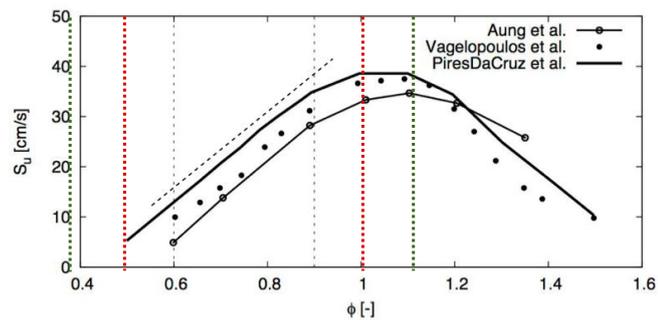


Mercier, Fiorina; Proch, Kempf

85

Observations I

- F-TACLES seems to work well
- Flame spreading rate overpredicted
- FSD with „implicit“ modelling approach works less well than with TSF
 - Add an explicit SG model
 - Algebraic model cannot resolve the production of wrinkling
 - FSD models can produce excessive wrinkling on fine grids

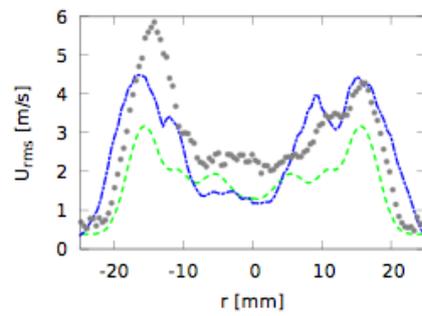
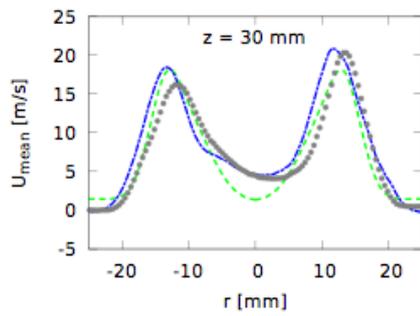
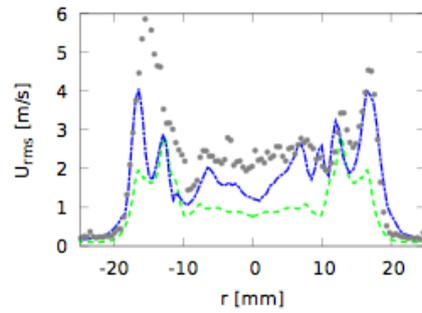
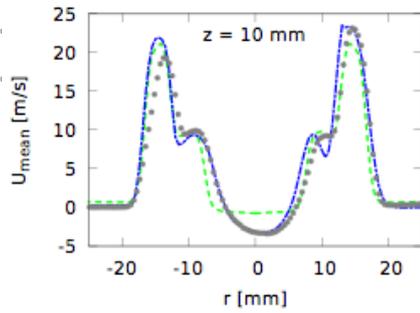


86

Observations II

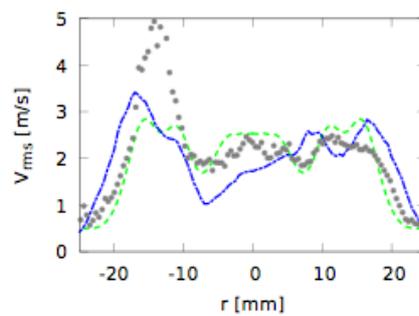
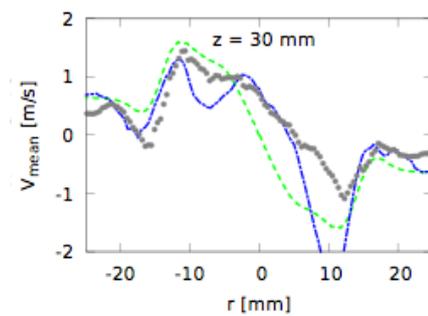
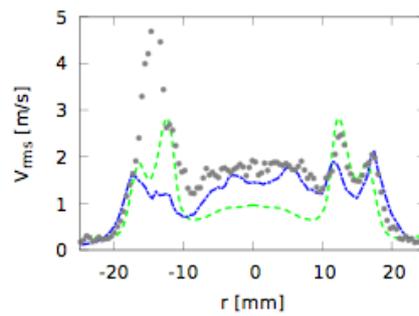
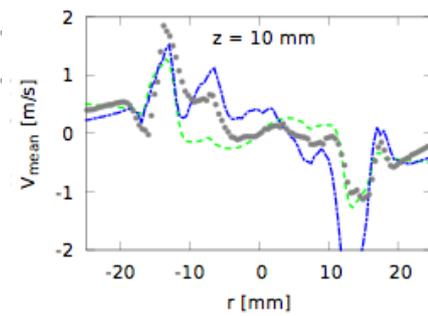
- Is the flow prone to asymmetry?
- Evidence:
 - High fluctuations on centreline
 - Very long recirculation zone
 - Strong effect of small asymmetry in BCs
 - Asymmetric experimental profiles

Observations II

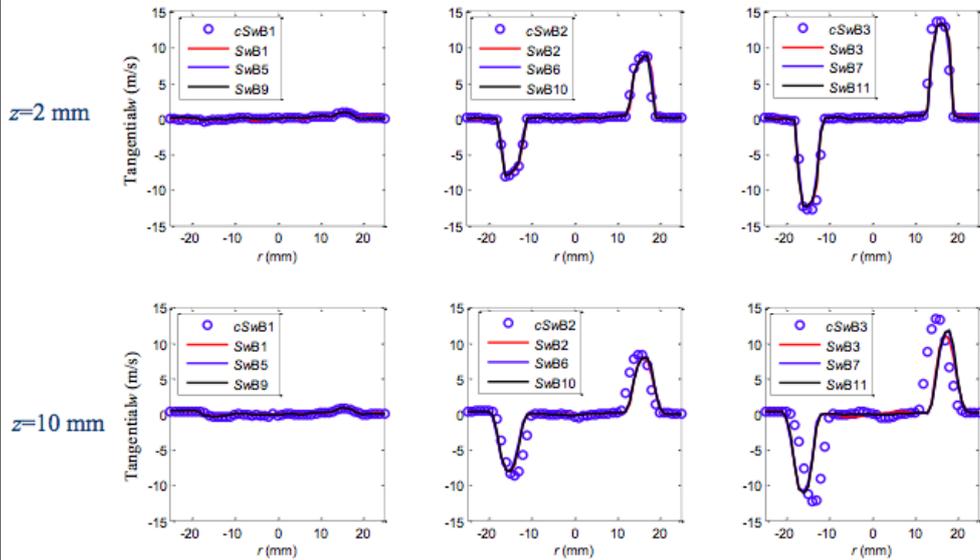


Observations II

New data, more symmetric



Observations II



90

Summary

Cambridge Flame

- First time TNF test-case
- Sensible predictions from EM2C, UDE
- Recirculation zone is not predicted correctly

91

Challenges and opportunities for TNF12

Cambridge Flame

- Fluidmechanics in recirculation zone? Symmetry?
- Impact of flame lift off from bluff body? (Similar to Sydney flame?)
- Potential for very fine LES ($\Delta < 250\mu\text{m}$)
- This TNF: testcase established
- Next TNF: focus on (strong) stratification

- Differential diffusion? \Leftrightarrow next session

92

Summary - Stratified Flames I

- **Darmstadt Flames** - TNF10, TNF11
 - Very good progress since 2012
 - Minor problems
 - Lift-off? Heat loss?
 - Stratification
 - Well predicted in macroscopic quantities
 - How to better analyse stratification?
 - How to better „stress the models“?
- Future
 - Shear, details (turbulence - chemistry)

Summary - Stratified Flames II

- **Cambridge Flames - TNF 11**
 - First time at TNF
 - Reasonable/good predictions already
 - Difficulty with recirculation zone
- Future
 - Swirl? Shear?
 - Higher stratification
 - Differential diffusion → Luc, Simone

Acknowledgements

- All contributors from
 - Aachen, Cambridge, Darmstadt, Duisburg-Essen, Imperial, Lund, Paris, Sandia
- Plots, analysis and helpful discussions
 - Renaud Mercier, Fabian Proch**
- Thank you for your attention and inspiring questions!

TNF11 – Differential Diffusion Effects in Turbulent Flames

Luc Vervisch (INSA-CORIA) and Simone Hochgreb (University of Cambridge)

Summary

The session was devoted to understanding differential diffusion in turbulent premixed flames. Specifically, the focus was on bluff-body stabilised turbulent flames, and the role of the recirculation zone in enhancing the effect of differential diffusion. Key questions raised were how relevant differential diffusion may be as the level of turbulence is increased, as well as its role in energy transport.

Background

Recent experiments by Barlow et al. [1] and Sweeney et al. [2-3], involving premixed and stratified turbulent flames ($Re \sim 10^4$) stabilized on an annular burner with a central bluff body, showed that the carbon–hydrogen balance across the flame is not conserved for regions near the flame stabilization point. Instantaneous and averaged measurements of equivalence ratio and the C/H atom ratio calculated from major species in these flames show a jump across the flame zone (Fig. 1), unlike measurements made on laminar premixed flames or turbulent flames without a recirculation zone. The CO_2 mass fraction is higher than expected in the products, while the O_2 mass fraction is lower. The discrepancy decreases as mixing and reaction evolve downstream. This behaviour has been attributed to the differential transport (diffusion and convection) among species [1] and has been confirmed by laminar [3] and turbulent simulations, shown later on in this summary.

Near the flame stabilization point at the edge of the recirculation zone, there is strong shear. The shear is manifested by the difference in convection velocities between the reactant stream and the recirculation zone velocities, which are near zero. In this region, the velocity boundary layer thickness is of the order of the same order as the flame thickness. Across this layer, diffusion acts to transport oxygen and fuel from the reactants toward products, and CO_2 , H_2O , CO and H_2 from products back toward reactants. The experiments show that most of the difference in mass fractions appears for CO_2 and O_2 . The following rationale has been offered: diffusion of CO_2 from products to reactants is slower than that of hydrogen-containing species, hydrogen and water. In a free flame or a strained flamelet model, differential diffusion is always present. In the current situation, however, the boundary conditions are affected by the presence of intense convection on the reactant side, and recirculating convection on the product side. The H-rich mixture on the reactant side is convected away (downstream), whilst the C-rich mixture on the product side is recirculated.

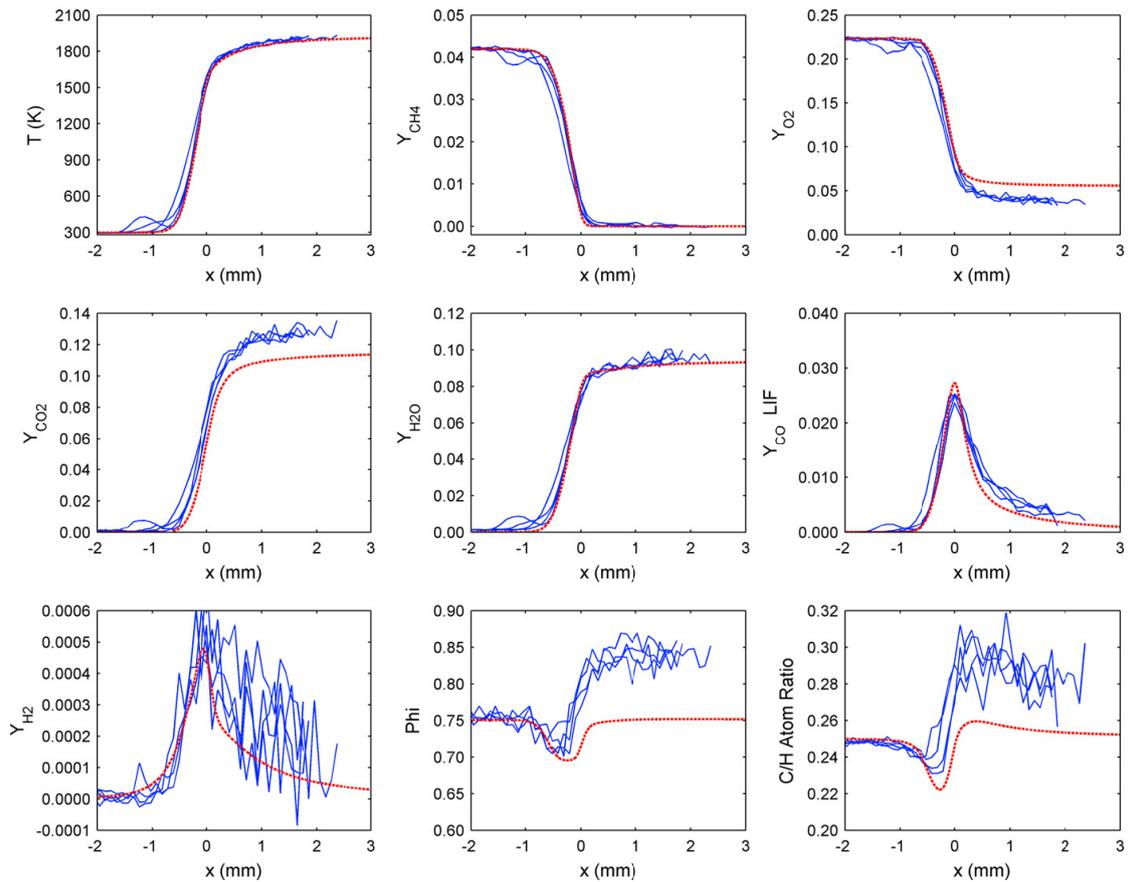


Figure 1. Scalar profiles for a premixed turbulent flame with a bluff body, at low axial distances ($z = 10$ mm), for $\phi = 0.75$, Case SwB1 [1].

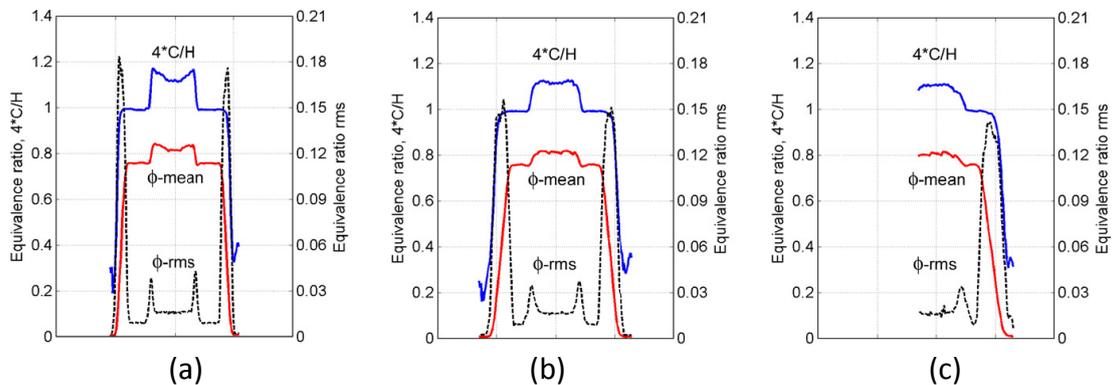


Figure 2. Equivalence ratio and C/H profiles and rms fluctuations, for $\phi = 0.75$, Case SwB1 for increasing distances from the bluff body [1].

Simulations

Simulation results of the bluff-body burner were presented by Vish Katta (Figure 3). These simulations include full transport and chemistry (GRI Mech 3.0), as described in [4], and the turbulent calculations simply added a κ - ϵ model to the laminar base case.

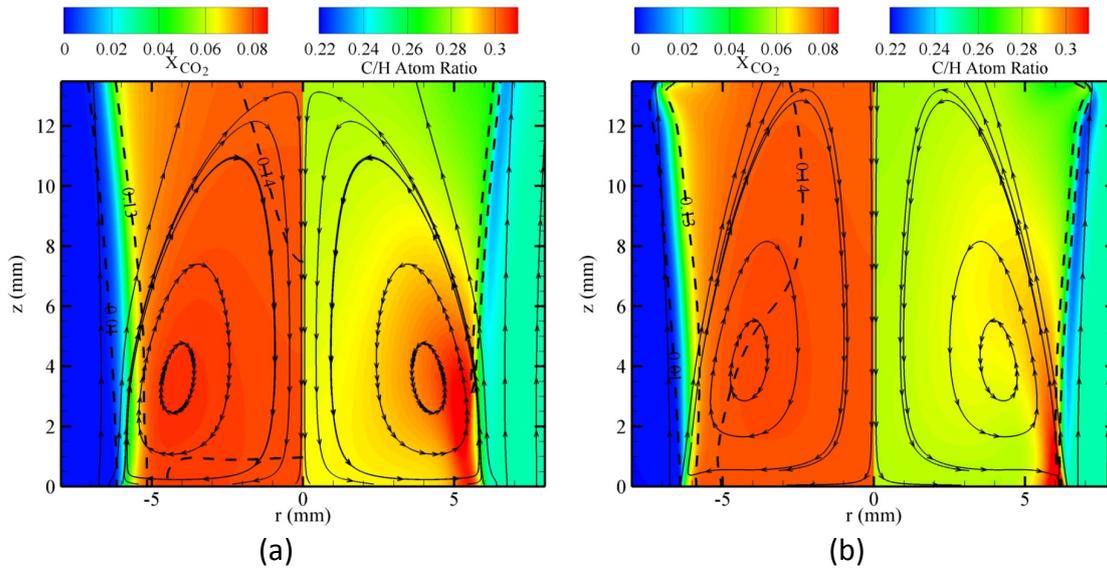


Figure 3. Calculated CO_2 and C/H atom ratio for laminar (a) and turbulent (b) calculations near the recirculation zone. Premixed flame, $\phi = 0.75$, velocity in the first annulus = 8.31 m/s.

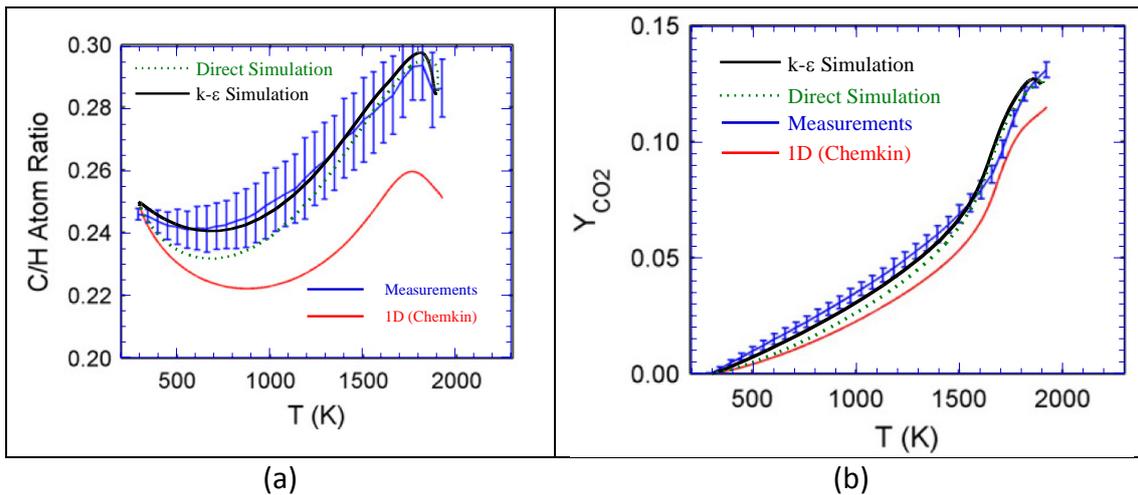


Figure 4. State space plots of C/H atom ratio (a) and CO_2 mass fraction, including experimental measurements (at 10 mm height), and calculations (at 6.5 mm height) Premixed flame, $\phi = 0.75$, velocity in the first annulus = 8.31 m/s.

The state profiles in Figure 4 agree remarkably well with the experiments. Turning off the differential diffusion mechanism eliminates the gradients in C/H. This shows that the effects of differential transport, including differential diffusion and shear near the bluff body, are responsible for the observed behaviour.

How can this behaviour so far not have been observed? In part, this appears to be a result of the very small number of high accuracy species measurements in turbulent premixed flames. Indeed, a revisiting of prior data from the TECFLAM premixed swirl burner, which has a central bluff body and recirculation zone, displays a discrepancy between the measured and modelled spatial equivalence ratio distribution at low axial distances from the burner [5], which may well be due to the same phenomenon.

The issue creates additional difficulties for modellers attempting to use such a database for validation, as differential diffusion is typically not accounted for in many LES models using mixture fraction and progress of reaction as scalar variables. Luc Vervisch considered the problem in the context of flamelet models, and whether it is possible to find an approximate source term to take care of differential transport, as described in the following section.

Modelling

The differential transport effect arises due to the difference in velocities across the reacting shear layer. The effect of differential diffusion can be estimated from the difference in residence time along the burner, and estimates from LES calculations without differential diffusion predict a difference of around 7% in mixture fraction. Further, it is possible to incorporate the differences in mixture fraction (defined either from the major species or minor species) by using a source term, defined as the remainder after the reaction and average diffusion term are subtracted from the calculations. The simple approach appears to be successful, as shown in Figure 5.

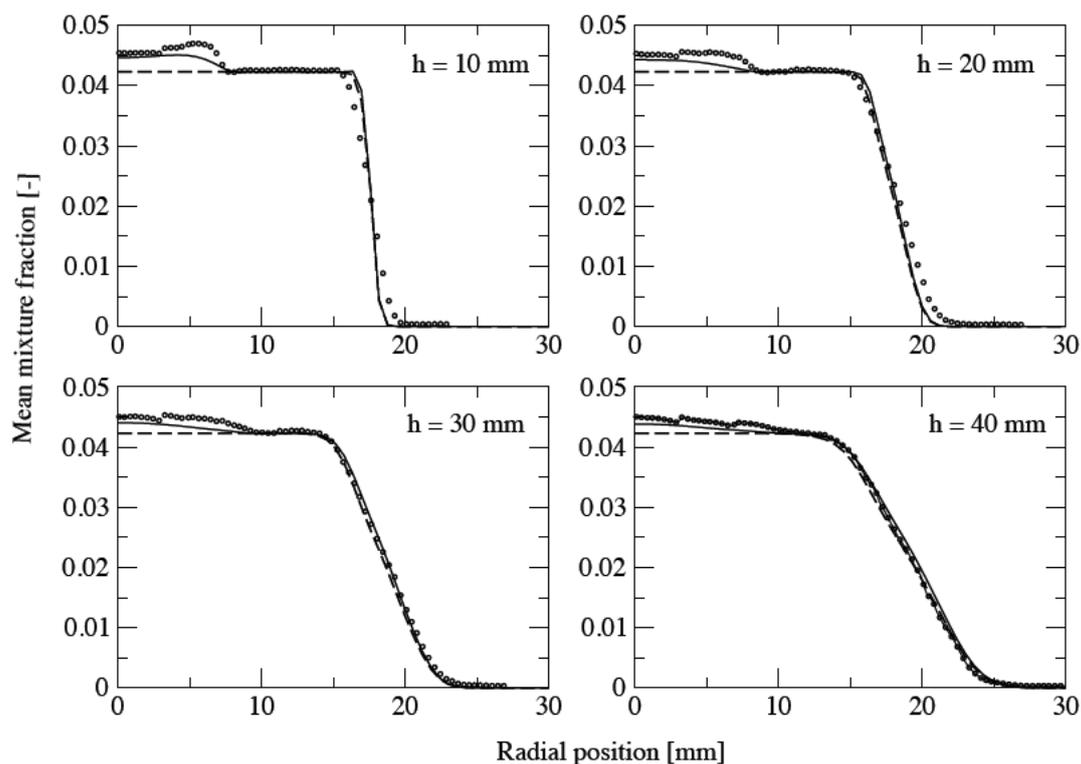


Figure 5. LES calculations of premixed flame in Figs 1-2, using the flamelet differential diffusion source approach within an FDF-PDF model [6].

Discussion

There was consensus that the differential diffusion effect is real, and needs to be considered in comparisons of models and experiments. Simplified models that may

take differential diffusion into account may need to be further developed. Further considerations were given in the discussion to the following issues:

- (a) Is a recirculation zone required for these strong differential diffusion effects to appear or are they simply a consequence of high shear?
- (b) If CO₂ and H₂O are transported differentially, what is the consequence for the energy balance? Does this affect temperature? Should energy equation be correspondingly altered to take into account differential diffusion? A post-meeting contribution has shown that there is a more pronounced decrease in maximum temperature with increasing annular velocity, which would support the assumption [7].

There are now a few more groups modelling the effects in this flame series, and it will be interesting to see how these questions and answers will evolve into TNF12.

References

1. Barlow, R. S., Dunn, M. J., Sweeney, M. S. and Hochgreb, S. *Combustion and Flame* 159 (2012) 2563–2575, <http://dx.doi.org/10.1016/j.combustflame.2011.11.013>.
2. Sweeney, M. S., Hochgreb, S., Dunn, M. J. and Barlow, R. S., *Combustion and Flame* 159 (2012) 2896–2911 doi: 10.1016/j.combustflame.2012.06.001.
3. Sweeney, M. S., Hochgreb, S., Dunn, M. J. and Barlow, R. S., *Combustion and Flame* 159 (2012) 2912–2929, doi:/10.1016/j.combustflame.2012.05.01.
4. Katta, V., Roquemore, W. M., *Proc. Comb. Inst.*, in press, <http://dx.doi.org/10.1016/j.proci.2012.06.033>.
5. Kuenne, G., Ketelheun, A. and Janicka, J. *Combustion and Flame* 158 (2011) 1750–1767., <http://dx.doi.org/10.1016/j.combustflame.2011.01.005>.
6. Nambully S., Domingo P., Moureau V., Vervisch L. (2012) Modeling differential diffusion in large-eddy simulation of nonpremixed flames. 7th International Symposium on Turbulence, Heat and Mass Transfer, THMT, Palermo, Sicily, Italy 24-27 Sept.
7. Dunn, M. J., Barlow, R. S., *Proc. Comb. Inst.*, in press, <http://dx.doi.org/10.1016/j.proci.2012.06.070>.

Differential Diffusion Effects in Turbulent Flames

Simone Hochgreb, Luc Vervisch

TNF 2012

Darmstadt, 26-28 May 2012

Outline

- Part I :Experimental (S. Hochgreb, U. Cambridge)
- Part II: Comparison of experiments and simulations: (Vish Katta, ISS)
- Part III: Modelling differential diffusion in premixed flames (Luc Vervisch, CORIA)

Outline

- Part I :Experimental (S. Hochgreb, U. Cambridge)
 - Background
 - Experimental work Sandia/Cambridge
 - Methodology
 - Single shot and favre averages
 - Relationship with velocity fields
- Part II: Comparison of experiments and simulations: (Vish Katta, ISS)
- Part III: Modelling differential diffusion in premixed flames (Luc Vervisch, CORIA)



Differential Transport Effects in Turbulent Flames

Mark Sweeney
Ruigang Zhou
Simone Hochgreb: University of Cambridge

Rob Barlow: Sandia National Labs

Matt Dunn: University of Sidney



Differential diffusion in turbulent premixed flames

Scalar
diffusivity

T

Y_i

$$Le = \alpha_T / \mathcal{D}$$

$$Le_i = \alpha_T / \mathcal{D}_i$$

$$\beta_i = \mathcal{D} / \mathcal{D}_i$$

TD instability/dilatation
counter-gradient
diffusion

Differential transport of
species within flame

Abdel-Gayed et al, 1985
Troune & Poinso, JFM 1994
Chakraborty et al (Phys. Fluids 2009,
FTC 2011)
Swaminathan et al (CNF2001)
Aspden et al (JFM2011)

Pope and Anand (PCI1984)
Richardson et al (CNF2010, 2012)
De Swart et al (FTC 2012)
Barlow & Dunn (CNF2011)
Sweeney et al (CNF 2012a, 2012b)

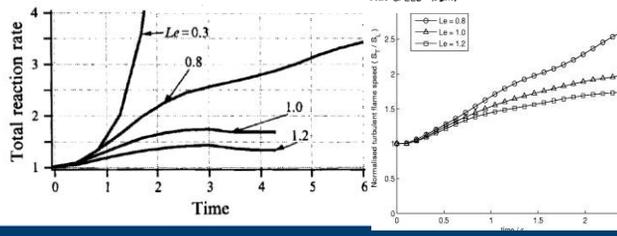
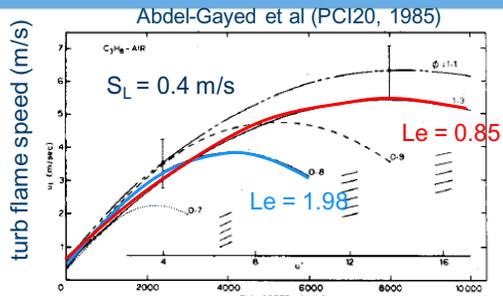


Differential diffusion in turbulent premixed flames

$$Le = \alpha_T / \mathcal{D}$$

TD instability \rightarrow **more area**
Secondary effects of strain,
temperature, curvature

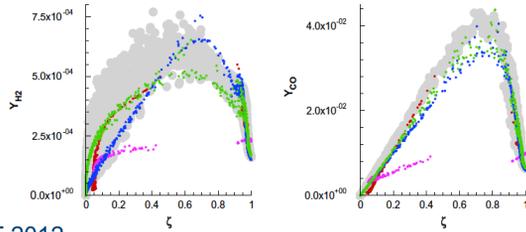
Abdel-Gayed et al (PCI20, 1985)
Haworth & Poinso (JFM 1992)
Troune & Poinso (JFM 1994)
Chakraborty et al (PoF 2005,
2009,
FTC 2011)
Swaminathan et al (CNF2001)
Aspden et al (JFM2011)
Troune & Poinso (JFM 1994)
Chakraborty et al
(PoF 2005)



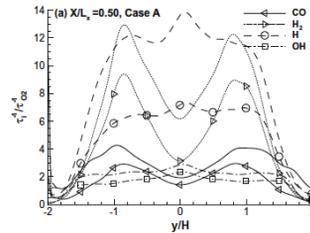
Preferential diffusion of species in turbulent premixed flames

$$Le_i = \alpha_T / \mathcal{D}_i \quad \beta_i = \mathcal{D} / \mathcal{D}_i$$

Differential diffusion for species within flame



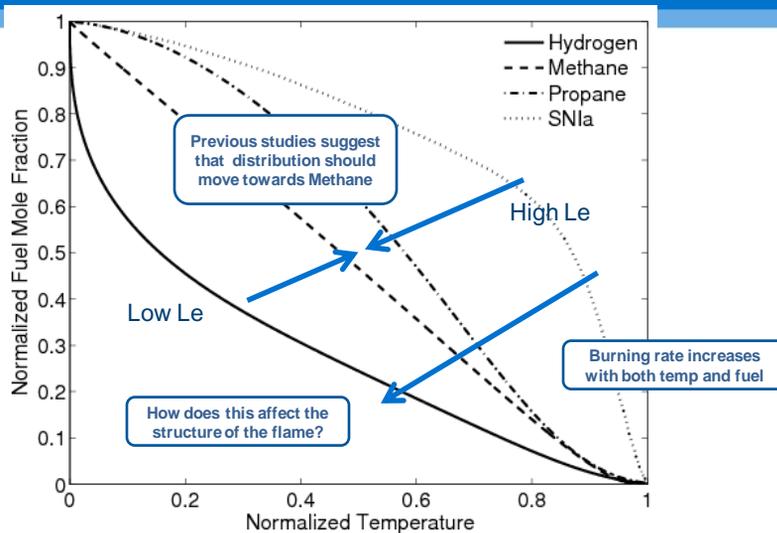
Richardson & Chen, CNF 2012



Richardson et al, CNF 2010



Lewis Number Effects – Aspden et al

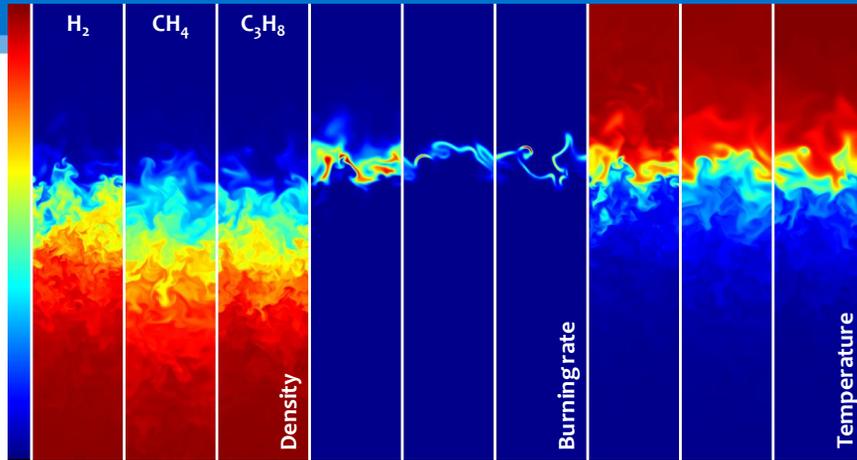


How does this affect the structure of the flame?



ccse.lbl.gov

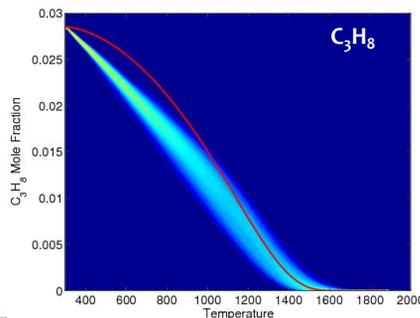
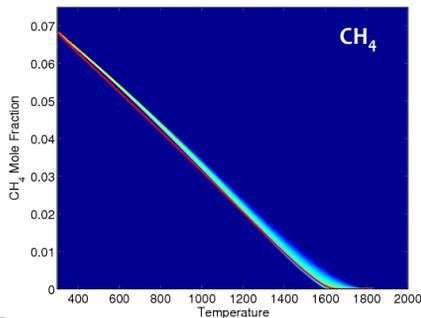
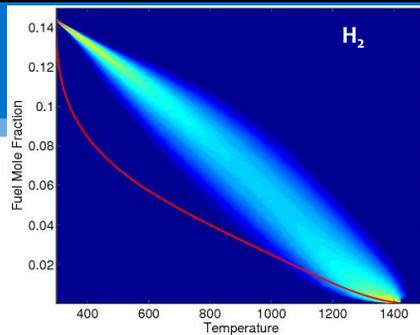
2D Slices: $Ka_F=410$ and Damköhler number $Da_F=0.0015$



- Similar broad distribution in density and temperature fields
- Only real difference can be seen in the burning rate
 - H_2 is broader than CH_4 and C_3H_8 , relatively more intense

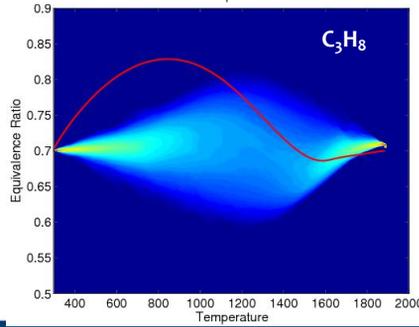
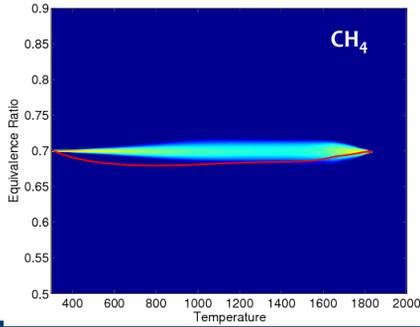
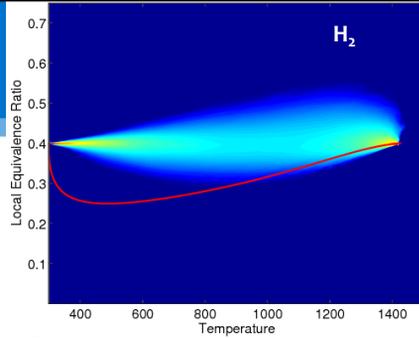
Temp-Fuel JPDF

- Again all profiles similar
- Narrow distribution
- Close to linear
- Characteristic of distributed flame



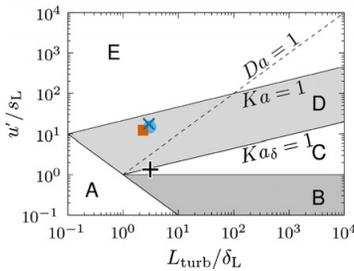
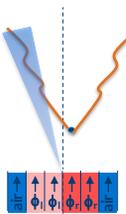
Temp-Phi JPDF

- Laminar flame as solid red line
- Similar response in all cases
- Moves towards constant
- Characteristic of distributed flame

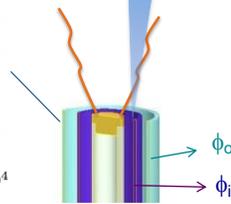


Experimental: Stratified flame studies/swirling flame with bluff body

Slot burner



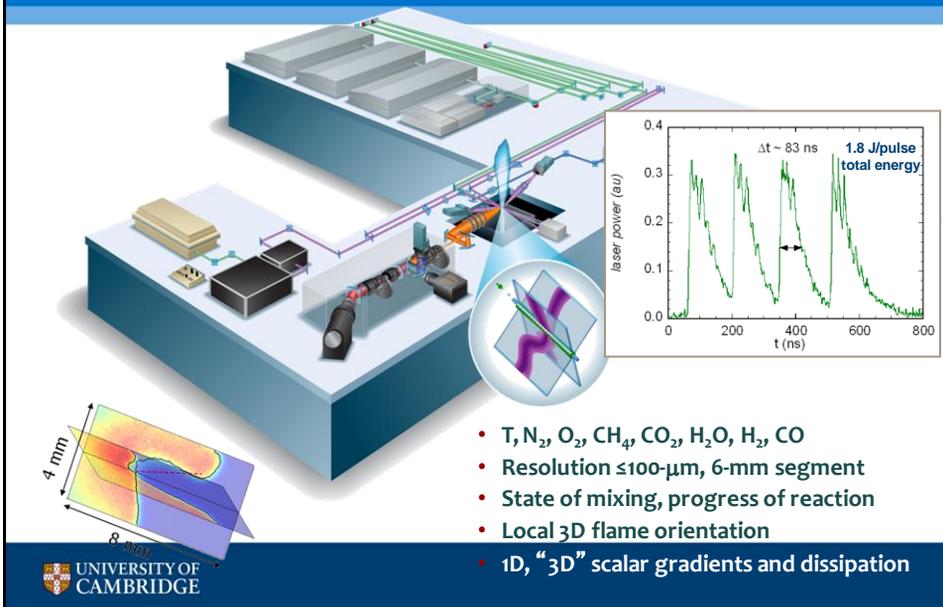
Swirl burner



U_1 (m/s)	3.0	U_2 (m/s)	3.0
u'/U (-)	0.1	u'/S_L (-)	1.3
Re_{h1}	2316	Re_{h2}	2316
L_t (mm)	1.9	Re_t	38
Da	0.8	Ka	10

U_1 (m/s)	8.3	U_2 (m/s)	18.7
u'/U (-)	0.2-0.4	u'/S_L (-)	4-8
Re_{h1}	5800	Re_{h2}	10800
L_t (mm)	1.9	Re_t	100-500
Da	1-4	Ka	10-60

Raman/Rayleigh/CO PLIF diagnostics in stratified flames



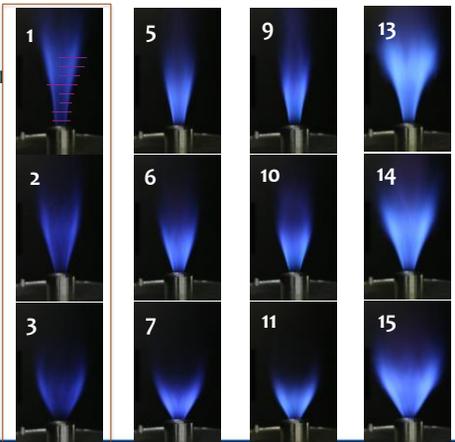
Sandia-Cambridge Stratified Swirl Burner

$U_i = 8.3 \text{ m/s}$ $U_o = 18.7 \text{ m/s}$ $U_{cf} = 0.4 \text{ m/s}$
 $Re_i = 5,960$ $Re_o = 11,500$

Vary stratification ratio and swirl

- Radial profiles
 - $z = 10, 20, 30, \dots \text{ mm}$
 - 300 shots at each location, 1500 in flame brush
 - $103 \mu\text{m}$ data spacing
- Long records
 - crossing of flame & mixing layer
 - 30,000 shots
 - $20 \mu\text{m}$ data spacing
 - Wavelet denoising
 - $60 \mu\text{m}$ effective resolution

SR = 1	SR = 2	SR = 3	SR = 1
$\phi_i = 0.75$	$\phi_i = 1.0$	$\phi_i = 1.125$	$\phi_i = 1.0$
$\phi_o = 0.75$	$\phi_o = 0.5$	$\phi_o = 0.375$	$\phi_o = 1.0$

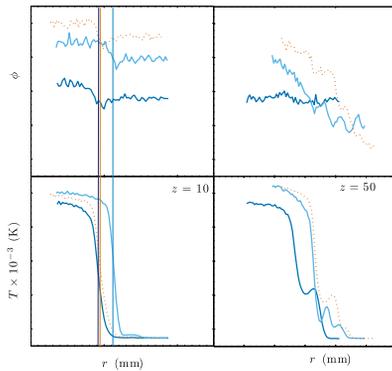


UNIVERSITY OF CAMBRIDGE

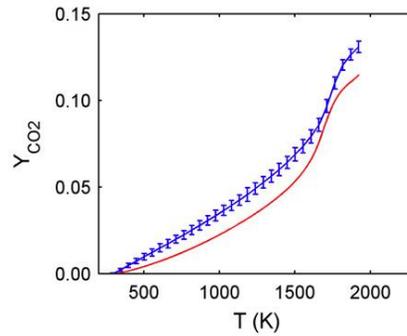
Sweeney et al, CNF 2012a, b, c

Swirl burner measurements SwB1 (pmx, $\phi = 0.75$), $z = 10$ mm

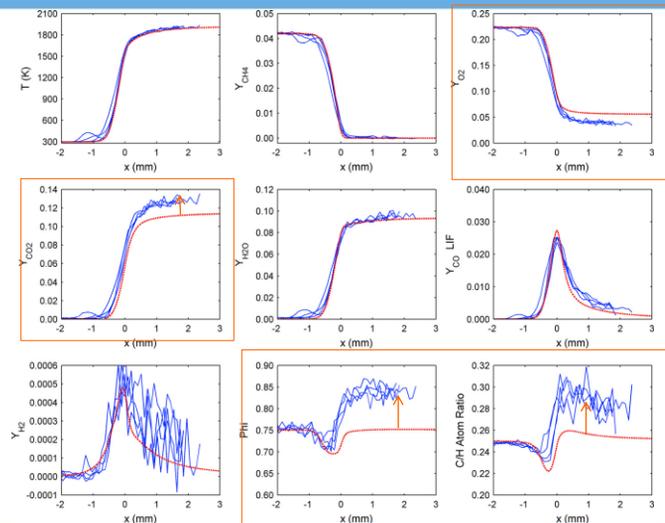
Single-shot



Average

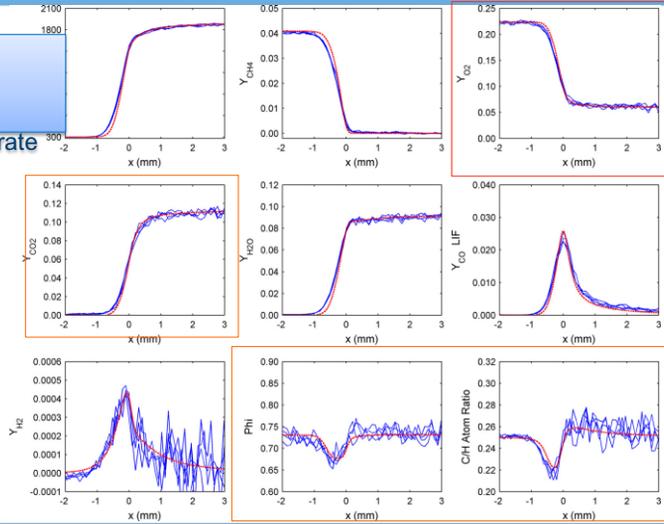


Species concentrations conservation across SwB1 (pmx, $\phi = 0.75$), $z = 10$ mm



Laminar flame results $\phi = 0.73$

Very good agreement:
experimental
technique accurate

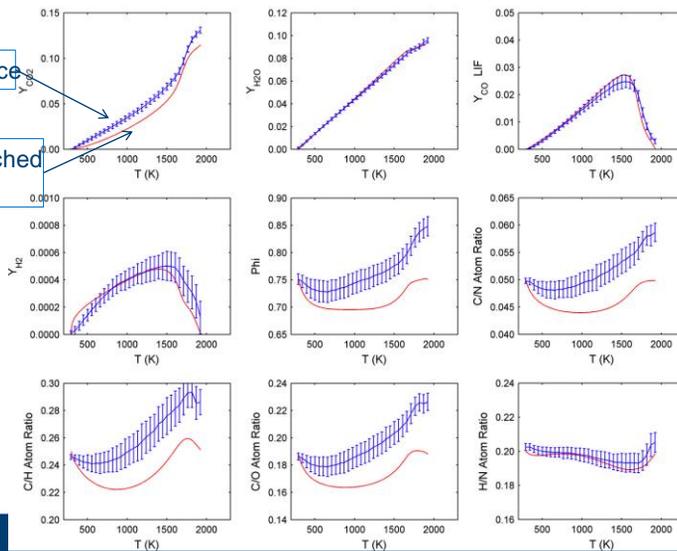


Equivalence ratio conservation across SwB1 ($\rho m x, \phi = 0.75, z = 10 \text{ mm}$)

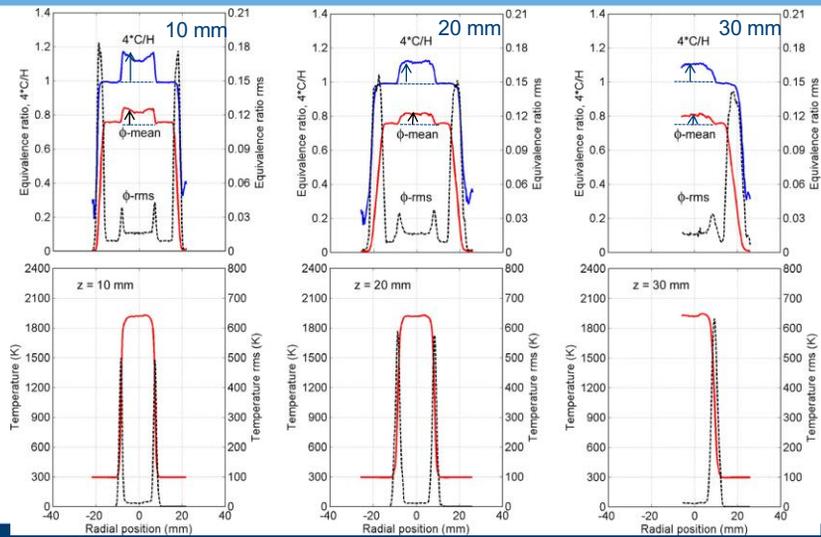
average+variance

laminar unstretched
calculations

$$\phi = \frac{\beta_C + \beta_H/4}{\frac{1}{2}\beta_O}$$

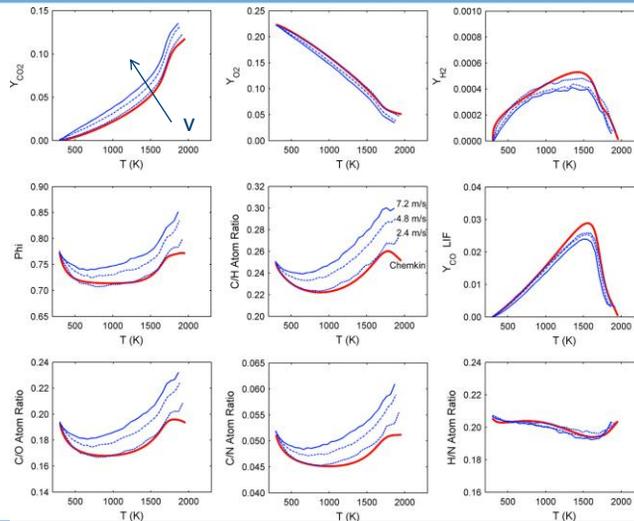


Equivalence ratio conservation across SwB1 ($\rho m x, \phi = 0.75$), for different heights



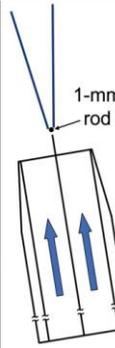
UNIVERSITY OF CAMBRIDGE

Simplified bluff-body burner (BarlowDunn)

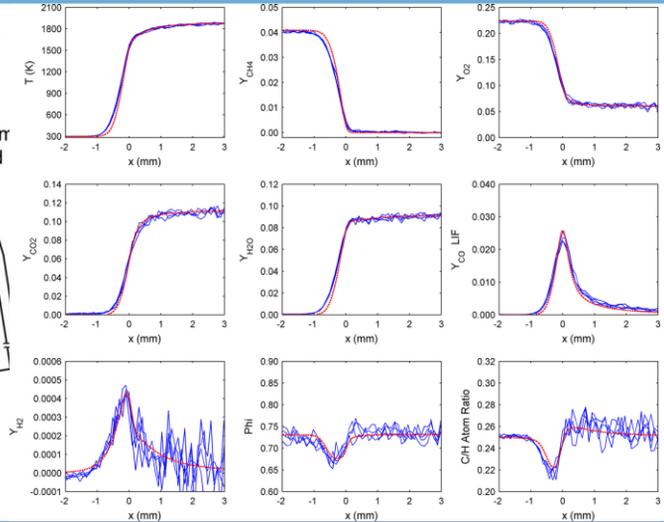


UNIVERSITY OF CAMBRIDGE

Simplified turbulent splitter plate burner

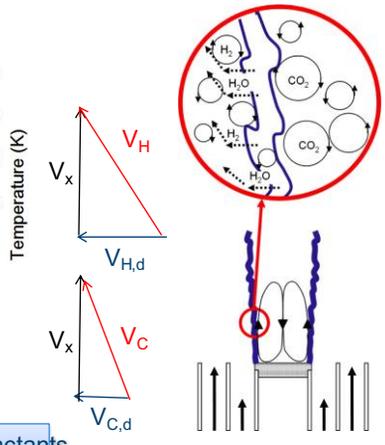
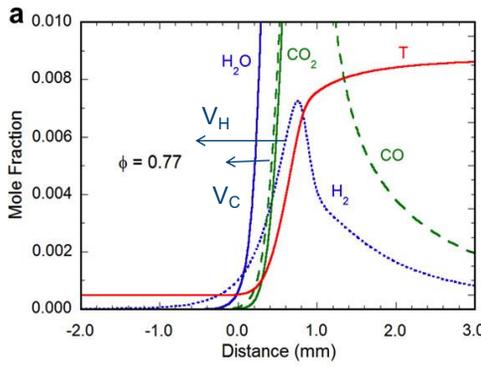


agreement similar to laminar flame



UNIVERSITY OF CAMBRIDGE

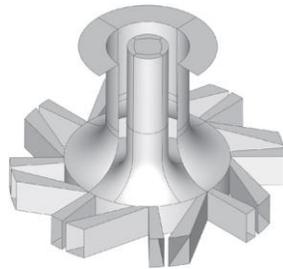
What is happening? Mechanism for differential transport in stabilized burners



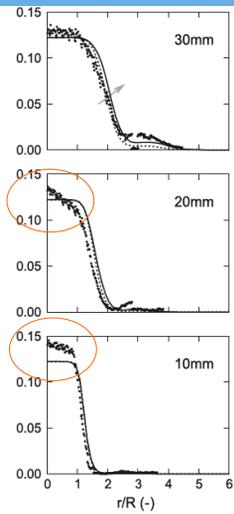
More H than C diffuses towards the reactants
Reactants swept downstream by axial flow

UNIVERSITY OF CAMBRIDGE

Evidence of differential mass diffusion in other systems ?



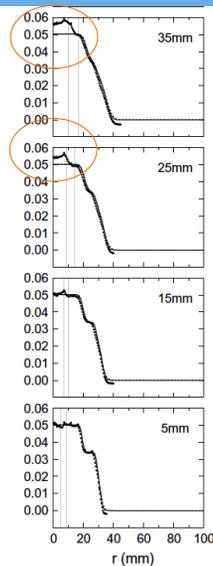
Premixed burner
Kuenne et al, CNF 158 (2011) 1750–1767



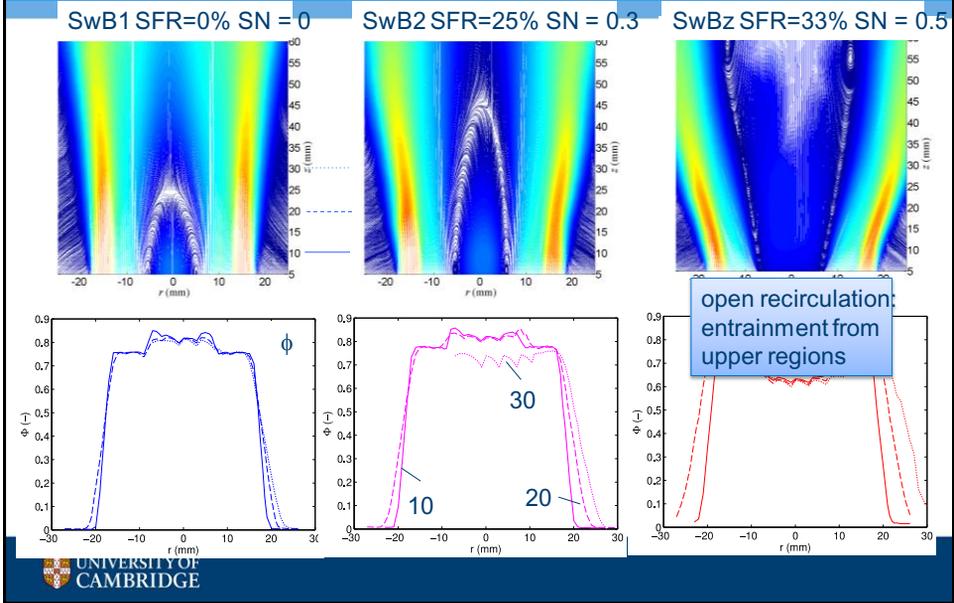
And absence (?) in piloted systems



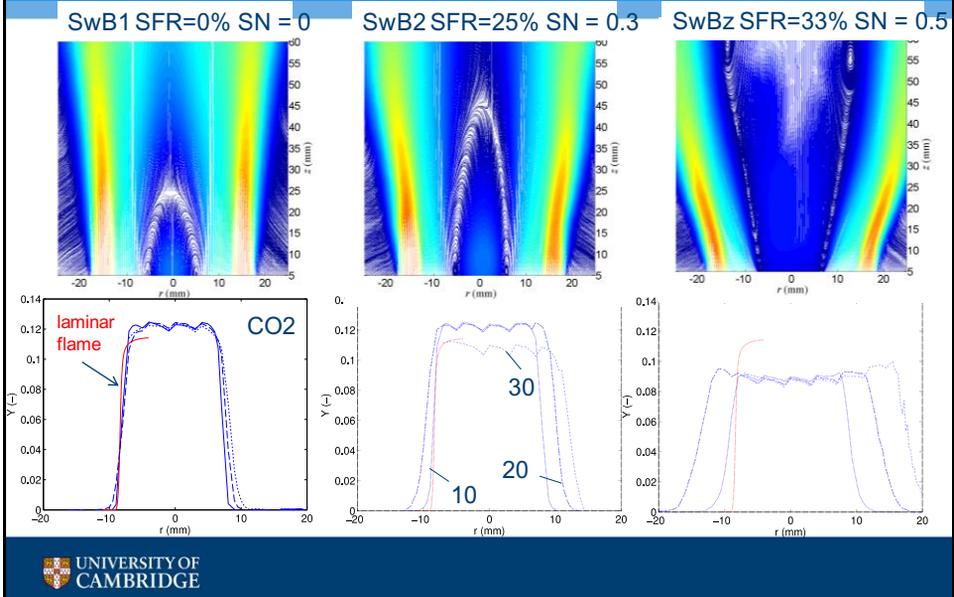
TUD stratified piloted burner
Kuenne et al, CNF 2012



PIV : recirculation zone behavior, premixed, $\phi = 0.75$



PIV : recirculation zone behavior, premixed, $\phi = 0.75$



Summary

- Differential **diffusion** of C-containing species vs H-containing species leads to C/H and ϕ dip across flame
- Differential **convection** across the reaction zone due to presence of shear near flame stabilization point leads to jump in CO₂ and C/H in bluff-body flames
- Effect may be present in other flames with similar ratios of differential diffusion and convection

Lifted flames in vitiated coflow

Presented by Matthias Ihme and Edward Richardson

Contributions from:

S. Navarro-Martinez, A. Kroneburg, B. Jones, G. Sarras, M. Stöllinger, D. Roekaerts, P. Medwell, B. Dally, E. Oldenhof, M. Tummers, E. van Veen, R. Kulkarni, Y. C. See, W. L. Chan, F. Collonval, M. Zellhuber, W. Polifke, O. Colin, J.-B. Michel, J. Lee, S. Park, Y. Kim, Y. Chen, B. Sundaram, M. Cleary, A. Klimenko, J. H. Chen, H. Kolla, C. Duwig, L. Fuchs

The focus of the session on “lifted flames in vitiated coflows” was threefold:

1. Review and characterize relevant ignition and flame-stabilization scenarios in lifted and vitiated flames.
2. Provide comprehensive overview about recent research progress on the modeling of lifted flames, with specific focus on the modeling of (i) jet-in-hot-coflow (JHC) burner from Adelaide and Delft and (ii) simulating the vitiated coflow burner (VCB) by Cabra et al. An overview over related experimental configurations, new measurement-data, and consideration of additional operating conditions is given.
3. Discussion on the utilization of DNS-database for analysis and model-development of lifted-flame.

1 Overview of flame-ignition and stabilization mechanisms

Three different flame-ignition mechanisms were identified and characterized in terms of the S-shape curve of the flamelet-model. This characterization is based on analysing the intersection of the Lagrangian flamelet-trajectory with the steady-flamelet S-shaped curve. The ignition modes are schematically illustrated in the presentation that accompanies this document.

- 1) *Autoignition-mode*: The ignition and transition from unburned to burned states depends on the condition of the local scalar dissipation rate. This ignition mode requires that the local dissipation rate reduces below the so-called ignition-dissipation rate. If this condition is reached, onset of ignition occurs, in which radical-production and heat-release exceed the diffusion rate, promoting transition to a burning flame-structure. Conditions for the occurrence of the ignition location dependent on turbulent flow-field structure and duration over which the dissipation-rate remains below the ignition-dissipation rate.
- 2) *Gradual/continuous transition*: This ignition mode pertains to the MILD combustion regime. In MILD combustion, the S-shape curve degenerates so that the notional ignition and quenching dissipation conditions merge to a single point. Under this condition, the S-shape curve has a single inflection point, promoting the transition between unburned and burning flame-state along the monotonically increasing S-shape curve.
- 3) *Secondary ignition-mechanism*: This ignition mechanism is observed under conditions that promote transport of heat/radicals into the flame-region. Examples for this are strong flow-recirculations, swirling flows, and cross-flow conditions. Under these conditions, the ignition onset is controlled by the flame-environment, and external heat/radical entrainment into the flame promotes ignition. Characterizing this ignition mode in terms of the S-shape curve shows up as direct crossing of unstable flamelet-branch, which is not feasible from fundamental 1D flamelet-arguments. The accompanying presentation gives an example for this ignition mode in the context of a jet-in-cross-flow configuration.

2 Model comparisons of lifted and vitiated flames

A focus of this session was on discussing recent modelling results for lifted and vitiated flames, present comparisons with experiments, discuss new experimental contributions and experimental facilities that are operational since the last TNF-workshop, and highlight further research-directions. We hereby focused on the VCB flame-series (by Cabra and Gordon) and the jet-in-hot-coflow (JHC) burners, available at Adelaide and Delft. In that order, the current modelling status is summarized in the following subsections.

2.1 Vitiated coflow burner (VCB, “Cabra” burner)

The lifted-flame in vitiated co-flow has been a TNF target flame, and past TNF-workshops discussed model-comparisons for this flame-series. Comprehensive measurements for speciation, temperature, and velocity, and lift-off heights are document in the work by Cabra et al. and publications by Rob Gordon, who considered a wider range of operating conditions. The database can be considered to be fairly complete, and no new measurements since the last TNF-workshop have been reported.

Since the last TNF-workshop, a number of groups performed RANS and LES computations of the burner, considering H₂ or CH₄-fuel. Recent RANS computations include DQMOM-computations by Lee, Park, and Kim on the H₂-VCB, and ADF-PCM computations by Collin & Michel.

Several LES-computations on this burner have been reported, including conditional moment closure (Navarro-Martinez et al. (2011)), multiple mapping conditioning (Sundaram et al.), unsteady flamelet/progress variable model (Ihme & See (2010)), and flow-controlled chemistry tabulation (Enjalbert et al. (2012)). The accompanying presentation contains a discussion of all contributions submitted to this session, including a brief overview about the model-formulation, details regarding the numerical method and computational setup, and comparisons of model-results and experiments.

Since all modelling efforts employed different discretization-schemes, grid-resolutions, SGS-models, and temporal integration methods, only comparisons of individual modelling-results against experiments were discussions. An objective comparison of all models is not meaningful, and no quantitative conclusions about best model-practice or relative model-performance are given.

2.2 Jet-in-hot-coflow (JHC) burner (Adelaide/Delft JHC-burner)

2.2.1 Adelaide jet-in-hot-coflow (AJHC) burner

The jet-in-hot-coflow (JHC) burner was developed by Dally and coworkers at the University of Adelaide with the objective to investigate oxygen-diluted and three-stream combustion. Measurements in this burner include speciation, temperature, and mixture fraction for three operating conditions of decreasing oxygen-concentration in the coflow-stream (ranging from 9% down to 3% oxygen). Recent studies by Medwell & Dally (2012) extended the measurements to other fuels and a wider range of operating conditions (including changing jet-exit Reynolds number, coflow-temperature, and oxygen-concentration). The focus of recent measurements was on investigating effects of operating conditions on the apparent lift-off height. For this, a combination of visualization, chemiluminescence, and long-exposure flame-photographs were used to characterize trends in lift-off heights as function of jet Reynolds number, coflow temperature and oxygen-level. It was concluded that the apparent “lift-off” is not a monotonic function of coflow-temperature, and also depends on the O₂-level and Reynolds-number. Although only lift-off height as a global quantity was reported in these investigations, this data provides further information for model-assessments beyond the baseline configurations (HM1 (9% O₂), HM2 (6% O₂), and HM3 (3% O₂)).

In the AJHC-burner the oxygen-diluted coflow is provided through a secondary burner, resulting in inhomogeneous and transient scalar inflow-conditions in the coflow stream. Effects of variations in scalar inflow-conditions on the flame-structure have been investigated by Ihme et al. (2011, 2012), and it was concluded that the effects of inflow-inhomogeneities extend throughout the entire flame-region. This was attributed to the low-Damkoehler number combustion regime. These findings could also have implications for other vitiated burner configurations in which one or more oxidizer streams

is generated from a secondary burner. Further measurements of temperature, velocity and species (or a subset thereof) would be most useful to provide boundary conditions for model-inputs. Apart from mean-data, it was discussed that measurements of second moment statistics (rms of temperature and species) and temporal correlations would be of direct relevance to modellers.

2.2.2 Delft jet-in-hot-coflow (DJHC) burner

Recently, the Delft-group initiated a comprehensive measurement campaign on a JHC-burner that is similar in design to the AJHC (Oldenhof, 2010, 2011, 2012). Several operating conditions, fuel-mixtures, and oxygen-dilution ratios (mostly at the upper limit of the MILD-regime) are considered, further extending the JHC-experimental database. Point-wise measurements for velocity and temperature have been reported, but data for speciation are currently not available.

Of interest to modellers, these experiments also include PIV measurements, and enable comparisons with predictions of the velocity field. Oldenhof reported joint OH-PLIF-PIV measurements and analysed the velocity-statistics as function of distance to the OH-layer. Comparisons with simulations have not been performed and can be subject of subsequent investigations.

Three groups provided contributions from recent modelling efforts. De et al. (2011) and Sarras et al. (2012) performed RANS computations using EDC and transported PDF-methods (JCPDF, JVPDF). These investigation considered the cases DJHC-I and DJHC-X, which correspond to oxygen massfractions of 7.6% and 10.9% and Re_{jet} between 4100 and 8800. Analysis of model results and comparisons with experiments indicate that the ignition behaviour depends on consideration of molecular transport, PDF-method, and micro-mixing model. Similar to the findings in the context of the AJHC, it was observed that the prescription of inflow conditions is crucial for predicting the outer-flame region; heat-losses to the burner wall and inhomogeneities in the secondary burner are not quantified and require further consideration in the model-formulation.

Kulkarni & Polifke (2012) performed Fluent-LES computations of the DJHC-I and DJHC-X configurations using a stochastic fields approach. Predictions for velocity are in good agreement, but overpredictions of temperature suggest higher predicted reactivities of the model compared to experiments. Similar observations have been made by other groups and require further investigations.

3 Insight and challenges from DNS

The preceding comparison of different modelling approaches for lifted flames in vitiated coflow is impaired by the high sensitivity of the model predictions to uncertain or unknown experimental boundary conditions, and to uncertain chemical kinetic models. Direct Numerical Simulation of turbulent lifted flames provides validation data with precisely known boundary conditions and physical models. The potential use of such DNS data for model development was raised as a topic for discussion at the workshop.

A set of new DNS computations involving lifted flame stabilization has been contributed by the group of J.H. Chen (Sandia National Laboratories) and co-workers. These include a parametric study of the effect of co-flow temperature on lifted hydrogen jet flames (Yoo et al 2011, 2012) and parametric investigation of jet in cross flow flame stabilisation with various fuel compositions and jet nozzle geometries (Grout et al. 2012). It was noted that the parametric variation between these flames causes transition between auto-ignitive, propagative, and *secondary* stabilization processes, as defined above.

DNS quantities for model validation: Models have previously been compared in terms of ensemble (conditionally-) averaged profiles, with respect to predictions of the mean lift-off height. Given complete knowledge of the spatio-temporal evolution of all flow and chemical quantities from DNS, however, there is scope for more detailed and more quantitative comparison between the DNS and turbulent reacting flow model. The question of which flame features to consider when evaluating predictive model performance was discussed.

Take the example of the jet lift-off height in a vitiated coflow, which provides a measure of the cumulative influence of turbulence-chemistry interaction up to the point of ignition, and which has been used widely as a measure of predictive model performance. It can be difficult to uniquely define a lift-off height from experimental measurement, especially under conditions of MILD-combustion, hence the quantitative compositional information available from DNS is valuable for comparison with model predictions. Furthermore, DNS provides fully three-dimensional information on the dynamics of the lift-off location (among other processes). For applications in which the ability to predict flame dynamics is a requirement, DNS provides the opportunity to evaluate statistically the ability of different models to describe relevant dynamical processes. It was emphasized during discussion at the meeting, however, that model performance should be judged only based on the overall prediction of quantities that are of practical significance: In general we should not demand that models describe all underlying dynamical processes, provided that the major quantities of interest are captured.

DNS data for a posteriori validation: The use of DNS data for *a posteriori* model validation for lifted flames in vitiated coflow was also discussed, taking the work of Knudsen et al. (2012) as a case study. Due to the relatively moderate Reynolds numbers which characterize current state-of-the-art DNS, conclusions about LES model performance must be drawn with care. The modeller should be careful to distinguish whether the model has been validated in the context of ‘high fidelity’ LES or ‘energy resolved’ LES, as discussed by Pope and Vervisch during presentations on LES quality at this meeting.

The study by Knudsen et al. (2012) reveals certain advantages to working with DNS data as opposed to experimental data. The first advantage, as noted above, is exact knowledge of the boundary conditions and physical models. Second, the resulting three-dimensional turbulent solution is known completely. The third advantage, which was realized by Knudsen *et al.* when their initial attempts at modelling the flame were only partially successful, is that the DNS data provides very detailed information about *why* particular models do or do not work. By interrogating the DNS data, they were able to identify – and remedy – deficiencies in their modelling of scalar dissipation rate and molecular transport, achieving greatly improved agreement.

It was noted during discussion that, while use of DNS data removes some layers of uncertainty from model comparison, implicitly filtered LES models (which are used predominantly) combine the effects of the modelling with the numerical method. This is a feature of most current LES methods which affects comparisons with both laboratory measurements and DNS, and which should be considered further.

4 Discussions and future directions

Main discussion points and further research directions that came up during the workshop presentation were:

- 1) *Experimental characterization of heat-transfer:* Wall heat-losses in the secondary burner become of importance in vitiated flames. Direct measurements of wall-temperature provide valuable information for model comparisons. These data can be used to estimate wall heat-fluxes, support the analysis by conducting conjugate heat-transfer simulations, or adjust boundary-conditions. This issue is not only of relevance to the VCB and JHC-flame-series, but was also subject of discussion in the context of the stratified flame-experiments and the piloted premixed jet burner.
- 2) *Consideration of two-point correlations for model comparisons:* Information about spatial and/or temporal correlations could be used to further interrogate and scrutinize LES-combustion models. High-speed laser-diagnostics could provide an accessible approach to evaluate temporal correlations, and spatial correlations could be evaluated from planar measurements.
- 3) *Inflow conditions:* A major source of uncertainties is the specification of inflow-conditions. Measurements of spatial burner-exit profiles for temperature, species, and velocity could

further assist model-validation and reduce ambiguities in specifying boundary conditions. This issue becomes increasingly relevant for low-oxygen and low-Damköhler number combustion regimes, and for configuration that supply reactants from secondary burners or mixing systems.

- 4) *Characterization of lift-off height*: Different metrics have been considered experimentally to quantify the lift-off height in vitiated flame. While most of them have been developed from experimental considerations, only few of them can be evaluated in simulations. Examples are chemiluminescence measurements or photographs with exposure times of the order of seconds cannot be considered in LES for the reason that these computations are often only conducted over a fraction of this period. Another reason is that excited species, such as OH*, CH*, CH₂* are not included in skeletal and some of the detailed mechanisms (such as GRI). Inclusion of such species is feasible, but will increase the computation time.
- 5) *Use of DNS data for LES validation*: Some valuable DNS-LES comparisons have been reported, and DNS researchers are encouraged to facilitate comparison with their data by providing full details of initial/boundary conditions and physical models, and, where possible, by providing access to the code used to implement the physical models and to generate the initial/boundary conditions. The data required for LES validation are, in the first instance, similar to those reported for laboratory flames, and DNS researchers are encouraged to provide profiles of single-point statistics of scalars and velocities as a minimum.

References

- Michel, J.-B., Colin, O. Angelberger, C., and Veynante, D., "Using the tabulated diffusion flamelet model ADF-PCM to simulate a lifted methane-air jet flame." *Combust. Flame*, 156(7) 1318-1331, 2009.
- Grout, R.W., Gruber, A., Yoo, C.S. and Chen, J.H., "Direct Numerical Simulation of Flame Stabilization Downstream of a Transverse Fuel Jet in Cross-Flow." *Proceedings of the Combustion Institute* 33(1)1629-1637, 2011.
- Grout, R.W., Gruber, A., Kolla, H., Brember, P.-T., Bennett, J.C., Gyalassy, A. and Chen, J.H., "A direct numerical simulation study of turbulence and flame structure in transverse jets analysed in jet-trajectory based coordinates" *Journal of Fluid Mechanics* 706, 351-383, 2012.
- Ihme, M. and See, Y. C., "LES flamelet modelling of a three-stream MILD combustor: Analysis of flame sensitivity to scalar inflow conditions." *Proc. Combust. Inst.* 33, 1309-1317, 2011
- Ihme, M., Zhang, J., He, G., and Dally, B., "Large-eddy simulation of a jet-in-hot-coflow burner operating in the oxygen-diluted combustion regime." *Flow Turbulence Combust.*, 89(3) 449-464, 2012.
- Ihme, M. and See, Y. C., "Prediction of autoignition in a lifted methane/air flame using an unsteady flamelet/progress variable model." *Combust. Flame*, 157(10), 1850-1862, 2010.
- Knudsen, E., Richardson, E.S., Doran, E.M., Pitsch, H. and Chen, J.H., "Modeling scalar dissipation and scalar variance in large eddy simulation: Algebraic and transport equation closures", *Physics of Fluids*, 24, 055103, 2012.
- Medwell, P. R. and Dally, B. B., "Experimental observation of lifted flames in a heated and diluted coflow." *Energy & Fuels*, 26, 5519-5527 (2012).
- Oldenhof, E., Tummers, M. J., van Veen, E. H., and Roekaerts, D. J. E. M., "Ignition kernel formation and lift-off behaviour of jet-in-hot-coflow flames." *Combust. Flame*, 157(6), 1167-1178, 2010.

- Oldenhof, E., Tummers, M. J., van Veen, E. H., and Roekaerts, D. J. E. M., "Role of entrainment in the stabilisation of jet-in-hot-coflow flames." *Combust. Flame*, 158(8), 1553-1563, 2011.
- Oldenhof, E., Tummers, M. J., van Veen, E. H., and Roekaerts, D. J. E. M., "Transient response of the Delft jet-in-hot coflow flames." *Combust. Flame*, 159(2), 697-706, 2012.
- De, A., Oldenhof, E., Sathiah, P., and Roekaerts, D., "Numerical simulation of Delft-jet-in-hot-coflow (DJHC) flames using eddy dissipation concept model for turbulence-chemistry interaction." *Flow Turbulence Combust.* 87(4) 537-567, 2011.
- Enjalbert, N., Domingo, P., and Vervisch, L., "Mixing time-history effects in large eddy simulation of non-premixed turbulent flames: Flow-controlled chemistry tabulation." *Combust. Flame*, 159(1), 336-352, 2012.
- Sarras, G., Stollinger, M. K., and Roekaerts, D. J. E. M., "Transported PDF simulations of the Delft-jet-in-hot-coflow burner based on 3D FGM tabulation chemistry." *Turbulence Heat and Mass Transfer*, 7, 2012.
- Kulkarni, R. M. and Polifke, W., "LES of Delft-jet-in-hot-coflow (DJHC) with tabulated chemistry and stochastic fields combustion model." *Fuel Processing Technology*, 2012.
- Narvarro-Martinez, S. Kronenburg, A., "Flame stabilization mechanisms in lifted flames." *Flow Turbulence Combust.* 87(2-3), 377-406, 2011.
- Yoo, C.S. and Chen, J.H., "A Comparative Study of Turbulent Lifted Hydrogen Jet Flames in Mildly-Heated Coflows", in preparation, 2012.



Computational Modeling and Experimental Investigation of Combustion-dynamic Processes in Turbulent Reacting Flows

Session Coordinators:
Ed Richardson and Matthias Ihme

Contributions:

S. Navarro-Martinez, A. Kroneburg, B. Jones, G. Sarras, M. Stöllinger, D. Roekaerts, P. Medwell, B. Dally, E. Oldenhof, M. Tummers, E. van Veen, R. Kulkarni, F. Collonval, M. Zellhuber, W. Polifke, O. Colin, J.-B. Michel, J. Lee, S. Park, Y. Kim, Y. Chen, B. Sundaram, M. Cleary, A. Klimenko, J. H. Chen, H. Kolla, C. Duwig, L. Fuchs

Overview



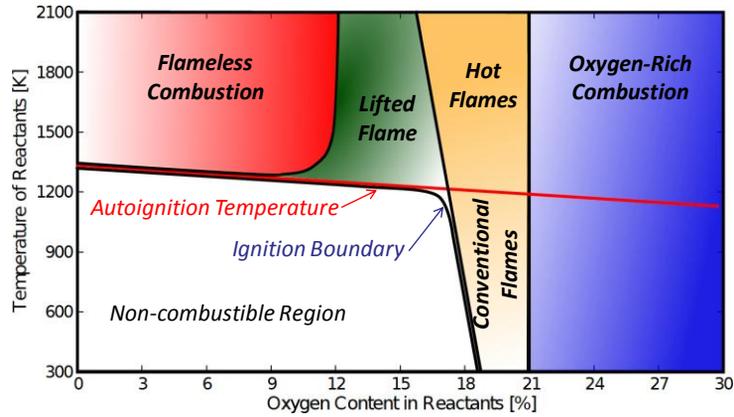
- Review of combustion-physics of lifted flames
 - Ignition-scenarios
 - Comparison of lifted flames in vitiated coflows
 - Model comparison
 - MILD combustion
 - Overview of experimental configurations, available measurements
 - Model comparison
 - Utilization of DNS-data for model-development
 - Discussion
-

2

Lifted-flames in Vitiated Coflows



- Regime-diagram¹
 - Heated and diluted oxidant conditions (methane/air)



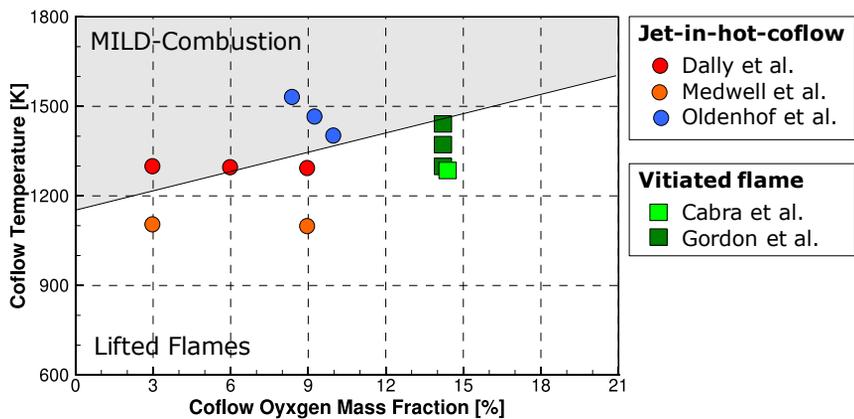
¹ Rao & Levy, 8th Int. Symp. On High Temp. Air Combustion and Gasification Poland, 2010.

3

Lifted-flames in Vitiated Coflows



- Regime-diagram



4

Lifted-flames in Vitiated Coflows

Flame Ignition/Stabilization Mechanisms



- Oxygen-concentration and temperature in coflow control ignition and flame-stabilization
- Ignition/Stabilization scenarios
 - 1) Autoignition → vitiated lifted flames
 - 2) Gradual/Continuous transition → MILD combustion
 - 3) Secondary ignition → recirculating flows (JICF)

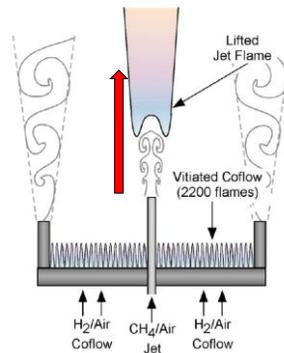
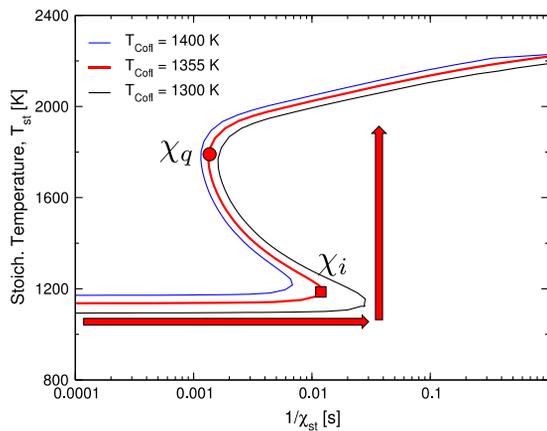
5

Lifted-flames in Vitiated Coflows

Flame Ignition/Stabilization Mechanisms



1) Autoignition → vitiated lifted flames¹



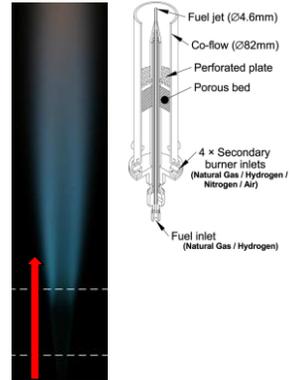
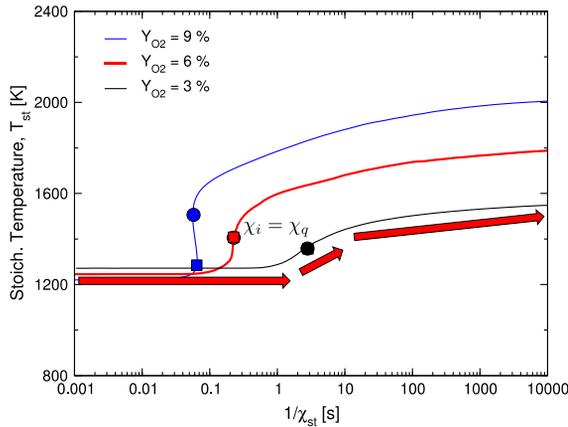
¹ Cabra, Chen, Dibble, Karpets, Barlow, Combust. Flame, 143 (2005)

6

Lifted-flames in Vitiated Coflows Flame Ignition/Stabilization Mechanisms



2) Gradual/Continuous Transition → MILD combustion¹



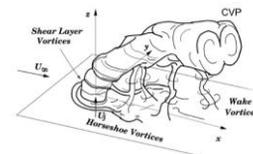
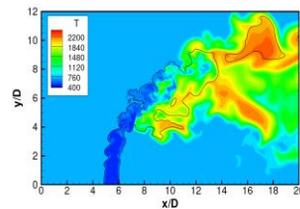
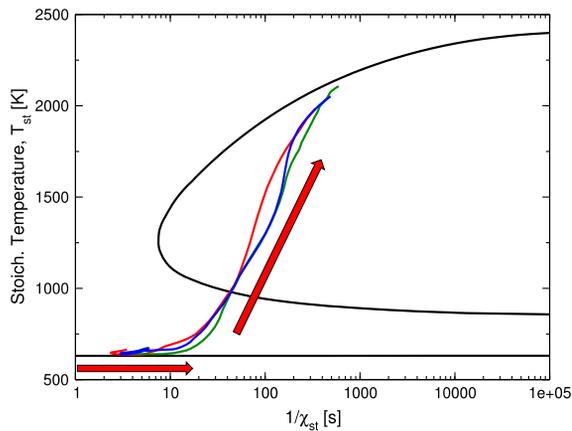
¹ Dally, Karpetis, Barlow, Proc. Combust. Inst. 29 (2002)

7

Lifted-flames in Vitiated Coflows Flame Ignition/Stabilization Mechanisms



3) Secondary ignition → Recirculating flows (JICF¹), transport, propagation (edge-flame)



¹ Grout, Gruber, Yoo, and Chen, Proc. Combust. Inst., 33 (2011)

8

Overview



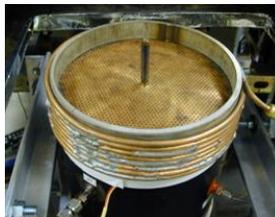
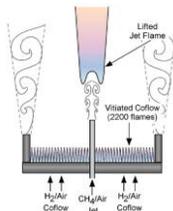
- Review of combustion-physics of lifted flames
 - Ignition-scenarios
- Comparison of lifted flames in vitiated coflows
 - Model comparison
- MILD combustion
 - Overview of experimental configurations, available measurements
 - Model comparison
- Utilization of DNS-data for model-development
- Discussion

9

Model Application



- Experimental configuration
 - Lifted flame in vitiated co-flow
 - Fuel
 - H₂/N₂: 1:3; Z_{st} = 0.47; T_{co}=1045 K
 - CH₄/air: 1:2; Z_{st} = 0.177, T_{co}=1350 K
 - Jet exit Reynolds number: ~23,000 (V_j~100 m/s)
 - Measurements: Raman/Rayleigh/LIF: Z, T, O₂, N₂, H₂, H₂O, OH & NO



Cabra, Proc. Comb. Inst. 29 2002
Cabra, Chen, Dibble, Karpetsis, Barlow, CF, 143, 2005

Modeling of Cabra VCB: H₂-flame



Authors/Groups	Turb.-model	Comb. Model	Reaction Chemistry
RANS			
Cabra, Myhrvold, Chen, Dibble, Karpetsis, Barlow, PCI 29, (2002)	k-eps, LRR, RSM	EDC, PDF	GRI 2.11
Masri, Cao, Pope, Goldin, CTM, 8 (2004)	k-eps	PDF	GRI 2.11
Cao, Pope, Masri, CnF, 142, 2005	k-eps	JCPDF	Mueller, Li
Gkagkas, Lindstedt, CTM, 13 (2009)	K-eps	JCPDF	Detailed
Myhrvold, Ertesvag, Gran, Cabra, Chen, CST, 178 (2006)	k-eps (mod), RSM	EDC	GRI 2.11
Gordon, Masri, Pope, Goldin, CTM, 11 (2007)	k-eps	PDF, ISAST	Mueller
Lee, Park, Kim (2012)	Mod k-eps	DQMOM	Mueller
LES			
Duwig & Fuchs, CST, 180 (2008)	FSFM	PSR	GRI 1.2, Li
Navarro-Martinez, Kroneburg, Jones(2011)	Dyn. SGS, Sct	CMC	Yetter
Sundaram, Cleary, Klimenko (2012)	Dyn SGS	MMC-FDF	Mueller, Li

11

Modeling of Cabra VCB: CH₄-flame



Authors/Groups	Turb.-model	Comb. Model	Reaction Chemistry
RANS			
Gordon, Masri, Pope, Goldin, CnF, 151, (2007)	k-eps	PDF	Detailed
Gkagkas, Lindstedt, PCI, 31 (2007)	k-eps	JCPDF	Detailed, based on Lindstedt & Meyer, Rizos
Michel, Colin, Angelberger, Veynante, CnF, 156 (2009)	k-eps	Flamelet ADF-PCM	GRI 3.0
Colin, Michel (2012)	k-eps	ADF-PCM CMC	GRI 3.0
LES			
Domingo, Vervisch, Veynante, CnF,, 152, (2008)	Dyn. SGS	FPI-AI	GRI 3.0
Navarro-Martinez, Kronenburg, PCI, 32 (2009)		CMC	Detailed mech (44 spec)
Ihme & See, CnF, 157 (2010)	Dyn. SGS	UFPV	GRI 2.11
Navarro-Martinez, Rigopoulos, FCT, 87 (2011)	Dyn. SGS, Sct	CMC	RCCE
Enjalbert, Domingo, Vervisch, CnF, 159 (2012)	Dyn. SGS	FCCT (PaSR, tab. chem)	GRI 3.0

12



DQMOM-based PDF Transport Modeling for VCB: H2/N2-flame

J. Lee, S. Park, and Y Kim
 Department of Mechanical Engineering
 Hanyang University, Seoul Korea

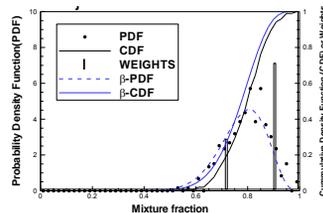
13

DQMOM for VCB: H2-flame

Lee, Park, Kim



- Objective
 - Apply DQMOM-based transported PDF model to auto-ignition, flame liftoff, local extinction and re-ignition processes



- Formulation
 - Closed joint composition PDF-transport equation

$$\frac{\partial f_\phi}{\partial t} + \langle U_i \rangle \frac{\partial f_\phi}{\partial x_i} - \frac{\partial}{\partial x_i} \left(\Gamma_i \frac{\partial f_\phi}{\partial x_i} \right) = - \frac{\partial}{\partial \Psi_i} \left[\left(C_\phi \frac{\varepsilon}{k} (\langle \phi_i \rangle - \Psi_i) + S_i(\Psi) \right) f_\phi \right]$$

- PDF-formulation

$$f_r(Y; x, t) = \prod_{n=1}^{N_r} p_n(x, t) \prod_{\alpha=1}^{N_\alpha} d(Y_\alpha - \langle f_\alpha \rangle_n(x, t))$$

14

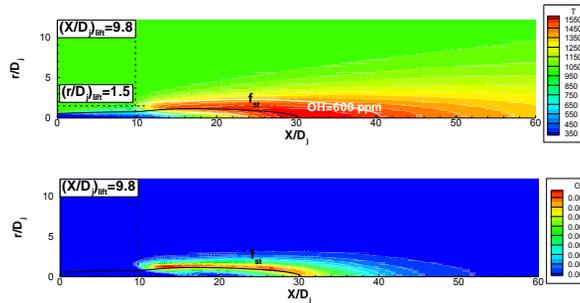
DQMOM for VCB: H2-flame

Lee, Park, Kim



- Computational setup

- Modified k-epsilon model
- Consideration of buoyancy and radiative heat loss
- Detailed chemistry with NOx: Mueller (9 species, 21 rxn)
- 2 DQMOM-environments
- Mixing model: $C_\phi = 2$



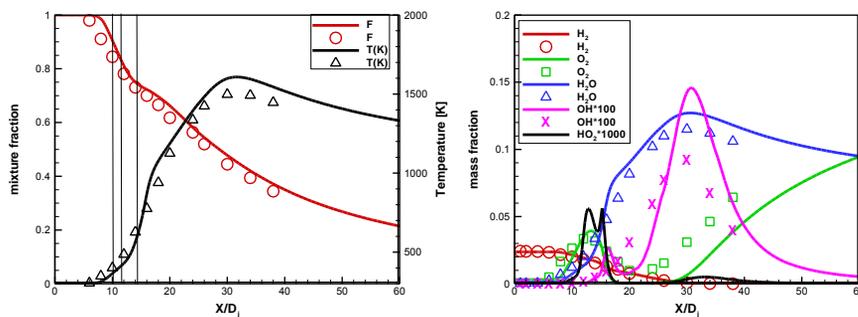
15

DQMOM for VCB: H2-flame

Lee, Park, Kim



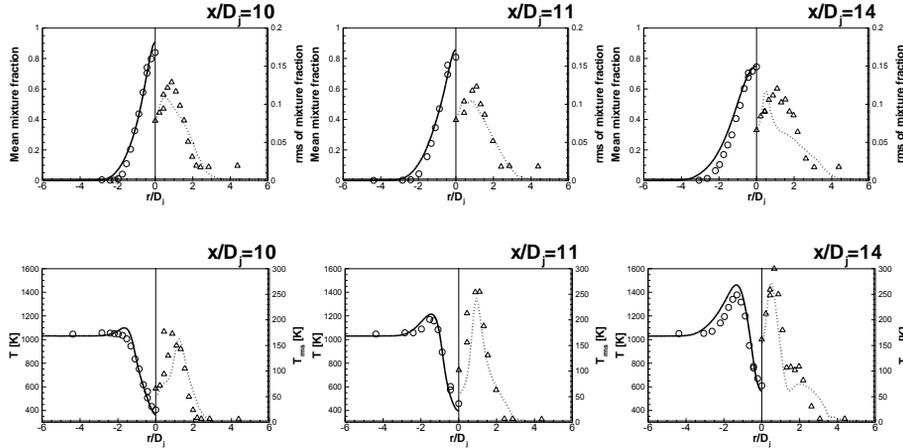
- Results: axial profiles



16



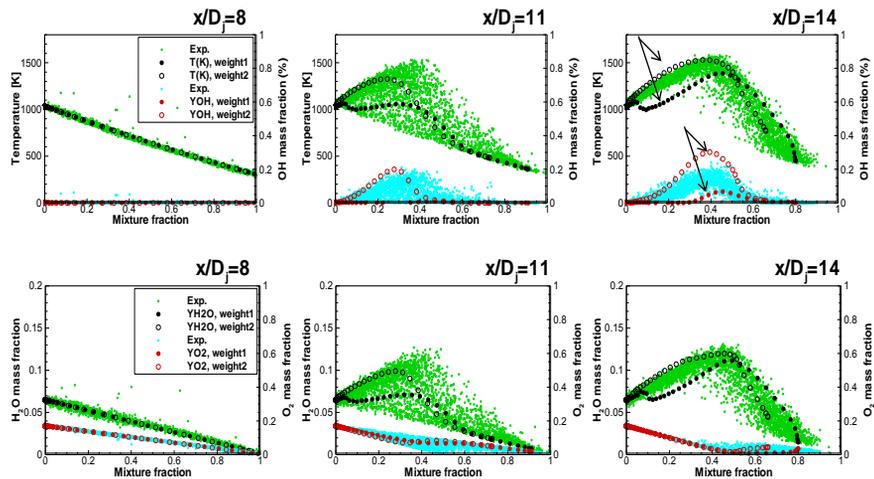
• Results: Radial profiles



17



• Results: Conditional Data



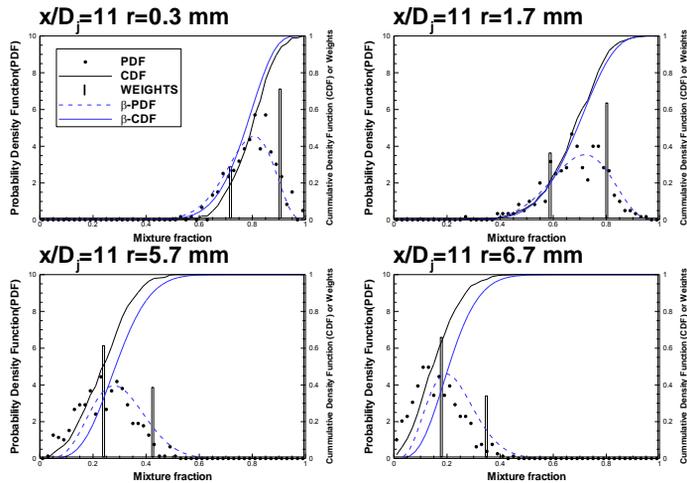
18

DQMOM for VCB: H2-flame

Lee, Park, Kim



- Results: PDFs



19

DQMOM for VCB: H2-flame

Lee, Park, Kim



- Summary and Conclusions

- Application of DQMOM-based transported PDF method to VCB
- Predicted mean and rms in good agreement; underestimation of lift-off height
- Results are dependent on DQMOM-environments
- DQMOM captures evolution of PDF in physical and compositional space

- Future work

- Micro-mixing models

20



Tabulated CMC-Approach for Methane/Air Cabra-flame: CH₄-flame

Olivier Colin, Jean-Baptiste Michel
IFP

21

Tabulated CMC for VCB: CH₄-flame Colins, Michel



- Approach
 - Second-order CMC
 - Reaction rate pre-tabulated from homogeneous auto-ignition reactor computation (ADF-PCM concept)
 - Conditional reaction rates closed using presumed PDF for normalized progress variable
- CMC-equations solved on same mesh as conservation equations
- Computational setup
 - Standard k-epsilon model with C2 correction
 - HR table generated with GRI3.0 with 100 points in C and eta
 - Reference mixture fraction resolution: $N_{\eta} = 50$
 - Reference case: $U_{jet} = 100$ m/s, $U_{co} = 5.4$ m/s, $T_{co} = 1350$ K

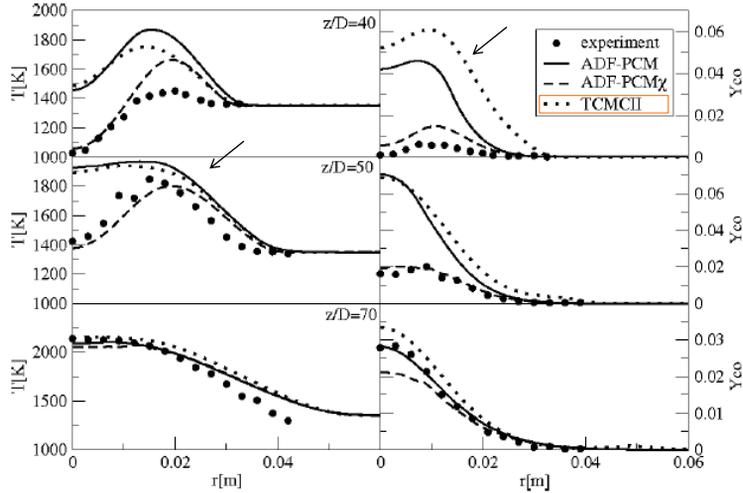
22

Tabulated CMC for VCB: CH₄-flame

Colins, Michel



• Results: Temperature



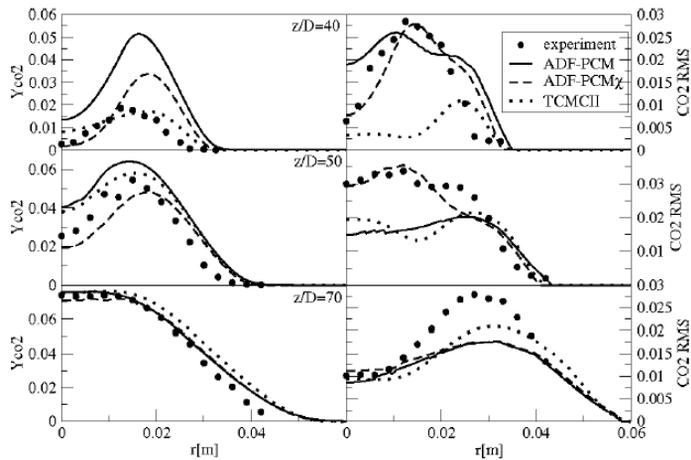
23

Tabulated CMC for VCB: CH₄-flame

Colins, Michel



• Results: CO₂



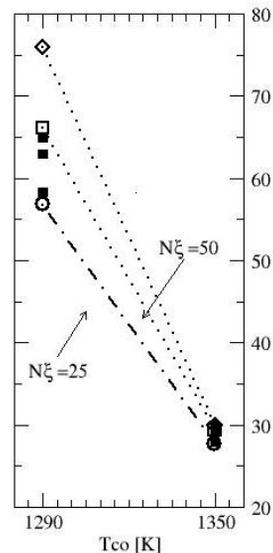
24

Tabulated CMC for VCB: CH4-flame

Colins, Michel



- Lift-off height-sensitivity to T_{coflow}
 - Good relative variation of lift-off with T_{coflow}
 - large sensitivity to N_{ξ} for $T_{co}=1290$ K



25

Tabulated CMC for VCB: CH4-flame

Colins, Michel



- Summary and conclusions
 - Formulation of CMC model based on progress variable and tabulation
 - Allows resolution of CMC equations on CFD mesh
 - Acceptable increase of CPU time compared to flamelet model (ratio TCMCII/ADF-PCM = 9 approximately for $N_{\xi}=50$)
- Model results
 - Acceptable temperature and species profiles, but no improvement compared to ADF-PCMchi
 - Better variations of lift-off height compared to ADF-PCMchi
 - Strong differences in conditional profiles for flamelet and CMC models → strong differences in stabilization mechanism

26



Multiple Mapping Conditioning Approach for H₂-Vitiated Coflow Burner

B. Sundaram, M.J. Cleary, A.Y. Klimenko

University of Queensland
University of Sydney

27

MMC for VCB: H₂-Flame

Sundaram, M.J. Cleary, A.Y. Klimenko



- Background on mathematical model
 - Hybrid Eulerian/Lagrangian approach
 - Eulerian LES simulates filtered velocities, pressure and the reference variable (mixture fraction f)
 - LES-Solver; *Flowsi*, Dynamic Smagorinski model
 - MMC-FDF of reactive scalars is modelled with a sparse distribution of stochastic particles that are transported by the underlying LES flow field
 - MMC is based on mapping to a set of reference variables.
 - Eulerian mixture fraction is chosen as the reference variable
 - Mixing is enforced between particles which are closest in the extended space (physical location and mixture fraction)
 - **Extent of mixing is controlled by a localisation parameter f_m .** As this parameter decreases, mixing becomes more local in mixture fraction space
 - Particle field is coupled back to LES through density and an equivalent enthalpy method

28

MMC for VCB: H₂-Flame

Sundaram, M.J. Cleary, A.Y. Klimenko



• Computational setup

- Eulerian Grid:
 - Staggered, cylindrical
 - Physical size: 298.5 mm (65d) axial x 228.5 mm (50d) radial
 - Number of Cells: 1026 axial x 55 radial x 32 azimuthal
 - 6 cells used to resolve nozzle
- Lagrangian particles
 - 23000 or 1L/8E (one Lagrangian particle per eight Eulerian cells)
- Simulations are run for:
 - Reaction mechanisms - Mueller (9 species, 21 reactions), Li (13 species, 25 reactions)
 - $T_c = 1020, 1030, 1045, 1060$ and 1080 K
 - $f_m = 0.01, 0.02, 0.03, 0.04, 0.045$ and 0.05
- Reactions restricted to particles of $0.00 < Z < 0.95$
- Lift-off is measured at first location where $Y_{OH} = 2 \times 10^{-4}$

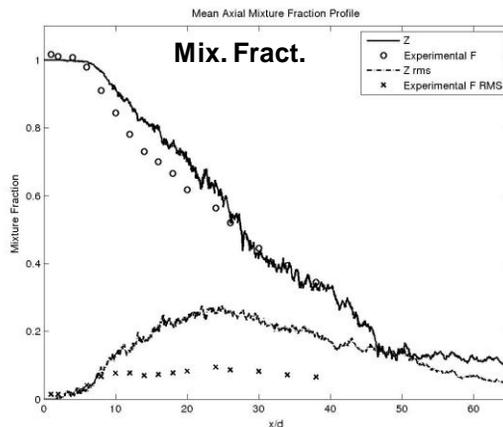
29

MMC for VCB: H₂-Flame

Sundaram, M.J. Cleary, A.Y. Klimenko



- Axial Profiles: $f_m=0.04$, $T_c=1045$ K, Mueller-mech.



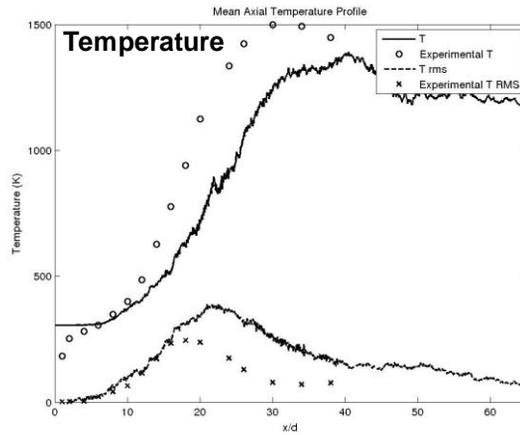
30

MMC for VCB: H2-Flame

Sundaram, M.J. Cleary, A.Y. Klimenko



- Axial Profiles: $f_m=0.04$, $T_c=1045$ K, Mueller-mech.



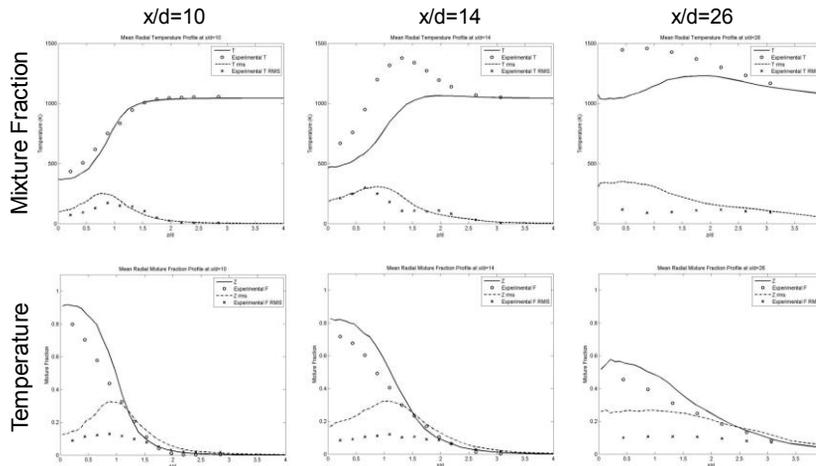
31

MMC for VCB: H2-Flame

Sundaram, M.J. Cleary, A.Y. Klimenko



- Radial Profiles: $f_m=0.04$, $T_c=1045$ K, Mueller-mech.



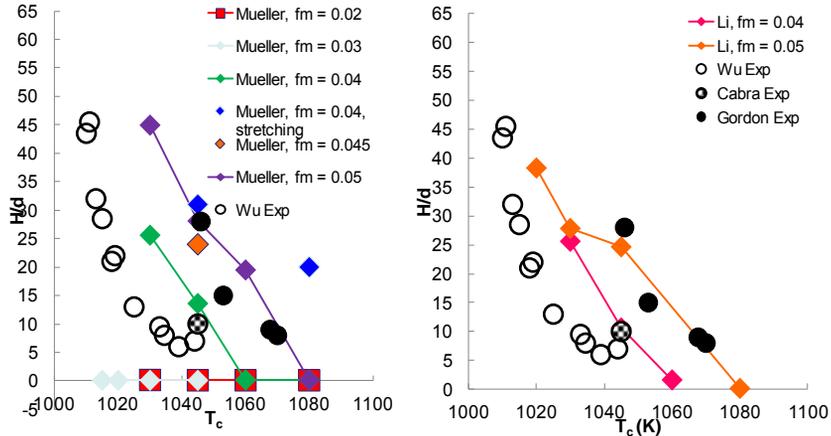
32

MMC for VCB: H2-Flame

Sundaram, M.J. Cleary, A.Y. Klimenko



- Lift-off height sensitivity to co-flow temp, rxn-mech and mixing localization



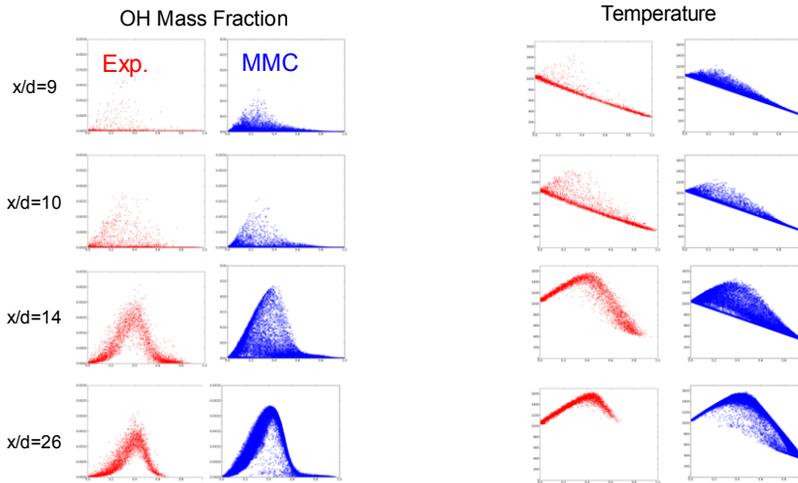
33

MMC for VCB: H2-Flame

Sundaram, M.J. Cleary, A.Y. Klimenko



- Scatter plots: $f_m=0.04$, $T_c=1045$ K, Mueller-mech.



34



LES-CMC of Cabra CVB: H₂, CH₄-Flame

Salvador Navarro-Martinez
Andreas Kronenburg
Bill Jones

35

MMC for VCB

Navarro-Martinez, Kronenburg, Jones



- Computational setup

Flame	Grid (<i>cylindrical</i>)	Combustion Models	Smagorinsky	Studies
Hydrogen	256 x 110 x 64	CMC, PDF	Dynamic, Sc _{sgs} =0.7	T sensitivity
Methane	320 x 80 x 48 512 x 120 x 64	CMC, PDF	Dynamic Sc _{sgs} =0.7	1D vs. 2D CMC Chemistry Kinetics

- Discretization scheme

- Low Mach number formulation staggered code (BOFFIN)
- Crank-Nicholson temporal integration
- Central Difference for momentum, TVD for scalars
- Stochastic field for PDF equation N=16 fields

- Chemical kinetics

- H₂-Mech: Yetter *et al.* 9 species and 19 steps
- CH₄-Mech: Lindstedt *et al.*, RCCE reduction to N_c=10, 19; ARM from GRI 3.0

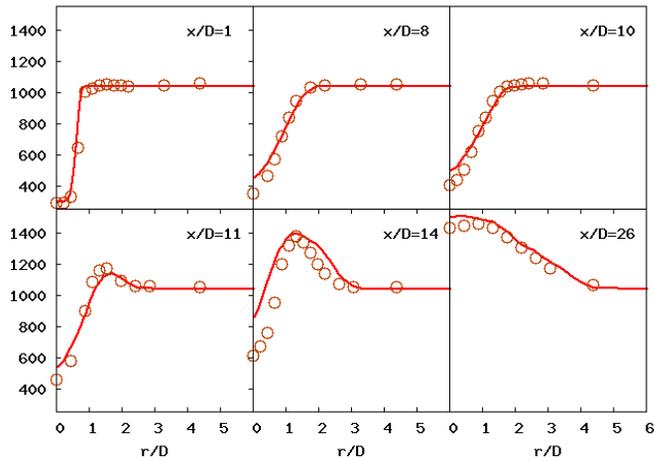
36

MMC for VCB – H₂-flame

Navarro-Martinez, Kronenburg, Jones



- Radial Temperature profiles (LES-1D-CMC)



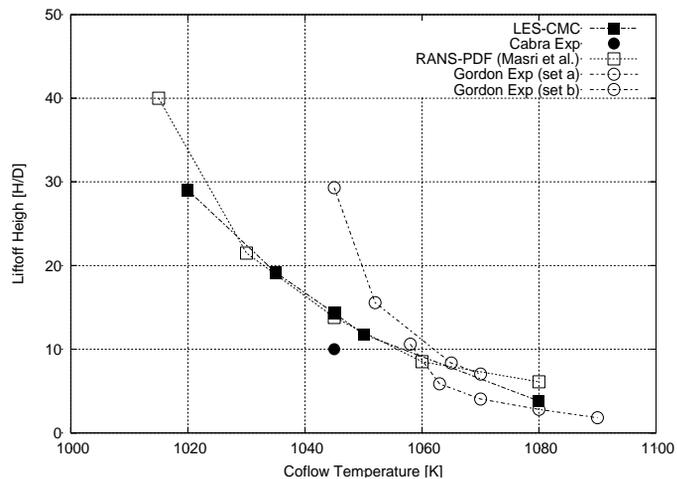
37

MMC for VCB – H₂-flame

Navarro-Martinez, Kronenburg, Jones



- Lift-off height (LES-1D-CMC)



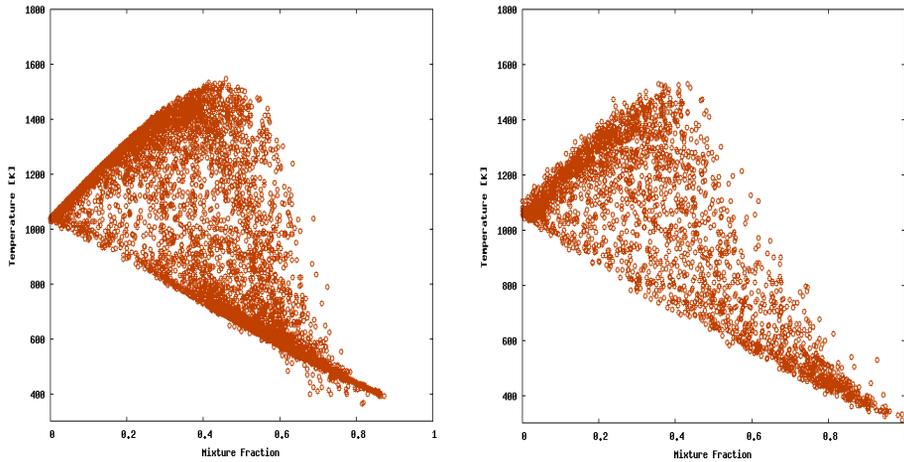
38

MMC for VCB – H₂-flame

Navarro-Martinez, Kronenburg, Jones



- Temperature scatter plots (LES-1D-CMC)



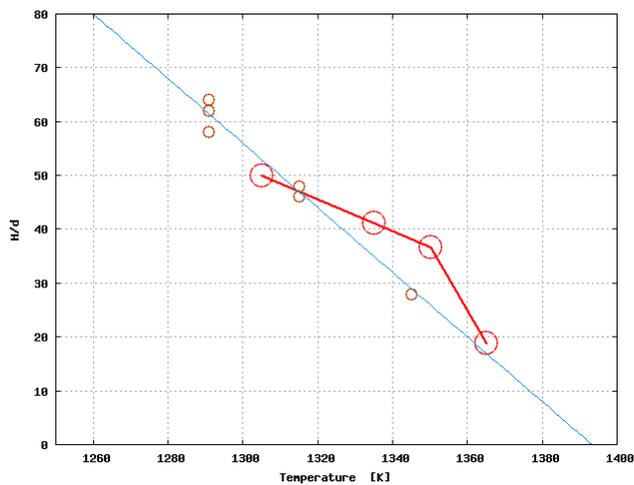
39

MMC for VCB – CH₄-flame

Navarro-Martinez, Kronenburg, Jones



- Lift-off height (LES-CMC)



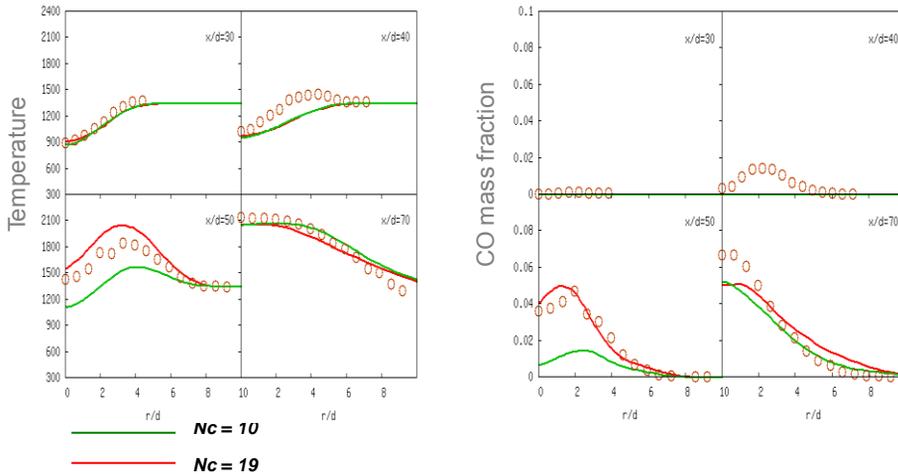
40

MMC for VCB – CH₄-flame

Navarro-Martinez, Kronenburg, Jones



- Chemistry effects (LES-CMC)



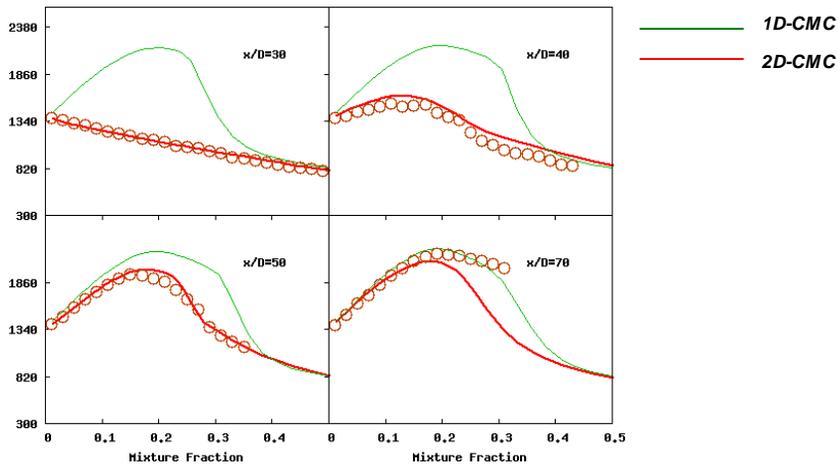
41

MMC for VCB – CH₄-flame

Navarro-Martinez, Kronenburg, Jones



- Conditional Temperature (LES-CMC)



42

MMC for VCB – **CH₄-flame**

Navarro-Martinez, Kronenburg, Jones



- Summary and Conclusions
 - Application of CMC to Cabra-flame
 - 1D-CMC adequate for H₂ but 2D-CMC required for methane configuration
- Question
 - Why is higher model-fidelity needed for CH₄-flame?

43

Overview



- Review of combustion-physics of lifted flames
 - Ignition-scenarios
- Comparison of lifted flames in vitiated coflows
 - Model comparison
- MILD combustion
 - Overview of experimental configurations, available measurements
 - Model comparison
- Utilization of DNS for model-development
- Discussion

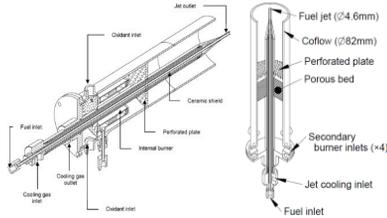
44

JHC-Burner



Adelaide JHC

• Burner design^{1,2}:

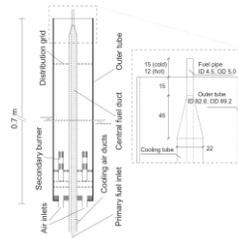


• (nominal) operating conditions:

- Coflow-O₂ composition: 3, 6, 9%
- Coflow-temperature: 1100, 1200, 1300, 1400 K
- Jet Reynolds number: 5000 - 25000
- Fuel: CH₄/H₂, C₂H₄/ {N₂, H₂, air}

Delft JHC

• Burner design^{3,4}:



• (nominal) operating conditions:

- Coflow-O₂ composition: 7.6, 8.8, 10.9%
- Coflow-temperature: 1395, 1460, 1540 K
- Jet Reynolds number: 2500 - 8800
- Fuel: CH₄/N₂, CH₄/C₂H₆/N₂

1 Dally et al., Proc. Combust. Inst, 29 (2002), 2 Medwell, Combust. Flame, 148 (2007); 152 (2008)
 3 Oldenhof et al. Combust. Flame, 158 (2011); 4 Oldenhof et al. Combust. Flame, 158 (2011)

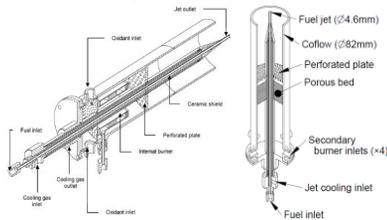
45

JHC-Burner



Adelaide JHC

• Burner design^{1,2}:



• (nominal) operating conditions:

- Coflow-O₂ composition: 3, 6, 9%
- Coflow-temperature: 1100, 1200, 1300, 1400 K
- Jet Reynolds number: 5000 - 25000
- Fuel: CH₄/H₂, C₂H₄/ {N₂, H₂, air}

1 Dally et al., Proc. Combust. Inst, 29 (2002), 2 Medwell, Combust. Flame, 148 (2007); 152 (2008)
 3 Oldenhof et al. Combust. Flame, 158 (2011); 4 Oldenhof et al. Combust. Flame, 158 (2011)

46

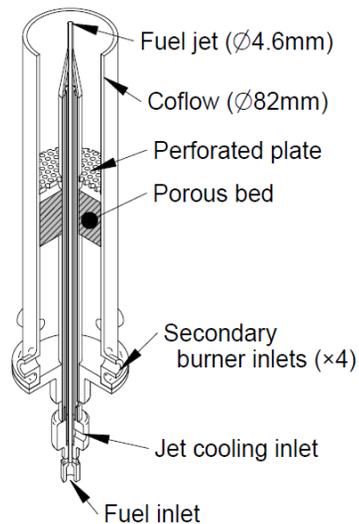
- Adelaide JHC-Burner - Lifted Flames in Heated and Diluted Coflows

Paul Medwell and Bassam Dally

Adelaide JHC Lift-off height characterization



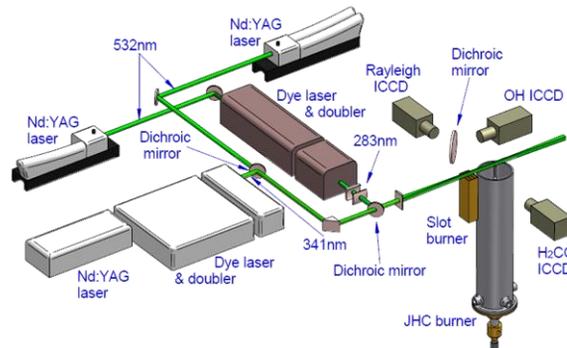
- Emulate MILD combustion with Jet in Hot Coflow (JHC) burner
- Coflow stream of products from secondary burner creates hot and diluted O₂ oxidant for jet flame
 - Full control of conditions
- Hot and diluted O₂ conditions create a fundamentally different type of flame (MILD combustion)
- Full optical access
- Investigation of different fuels
- Subsequently duplicated by Delft



Adelaide JHC Lift-off height characterization



- Conducted extended measurements to include simultaneous imaging of temperature, OH and formaldehyde
- Investigated role of turbulence on flame structure, effect of fuel composition on stability, discovered transitional behaviour of "lifted" flames in the heated and low O₂ coflow

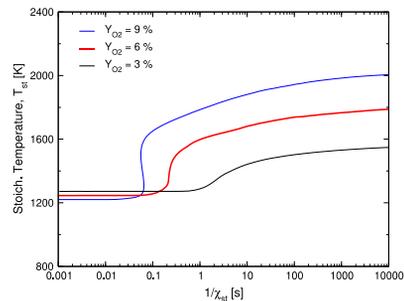


49

Adelaide JHC Lift-off height characterization



- Apparent lift-off transition¹
 - At 3% O₂, the reaction zone can become sufficiently weak to allow O₂ penetration across the flame front
 - Weak reaction zone promotes diffusion of O₂ through flame front to the fuel rich side
 - This 'partial premixing' makes flames under MILD conditions less susceptible to lift-off
 - Different mechanism than adding air to the fuel stream, since the penetrated O₂ is hot
 - Partial premixing with cold air cools the flame
 - Adding air is not as effective at improving flame stability as the small amount of hot O₂ through diffusion
 - At 9% O₂, the reaction intensity is higher, such that O₂ is fully consumed across flame front

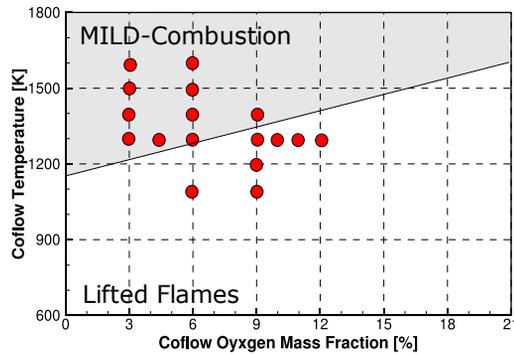


¹ Medwell, Kalt and Dally, Combust. Sci. Tech. 181 (2009) 937-953

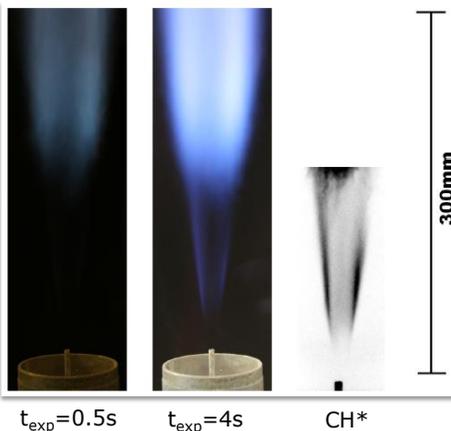
50



- To investigate lift-off processes, performed systematic and comprehensive measurement campaign, considering effects of:
 - O₂-concentration in coflow, H₂/NG ratio
 - Jet-exit Reynolds number, coflow-speed
 - Coflow-temperature



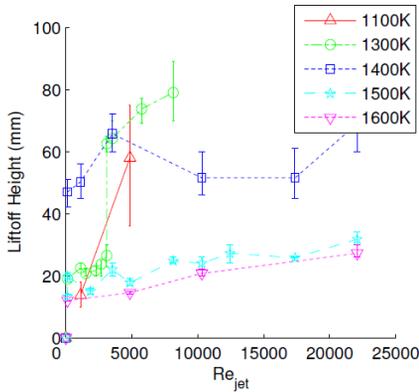
- Using a combination of visualization, flame photographs and CH* chemiluminescence, use the JHC burner to cover a wide range of conditions and plot the lift-off height



- Flames have low luminosity → uncertainties in visual observation
 - Error-bars are range of perceivable lift-off heights (not measure of actual error)
 - Definition of "lift-off height" becomes ambiguous (no steep gradients)



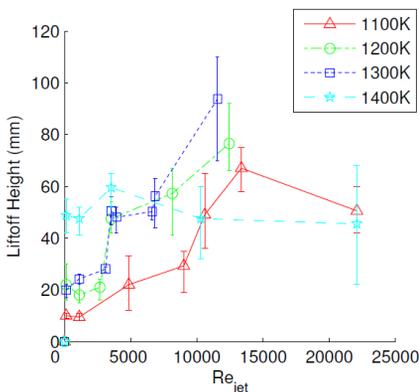
- 3% O₂ in coflow
 - starting with coflow temperature at 1300K and increase: the liftoff height increases then decrease



- Once certain temperature limit is exceeded, the flame behaves like a conventional flame
- Temperature limit is intimately coupled with O₂-level: not just function of temperature



- 9% O₂ in coflow
 - Similar observation: lift-off height increases, then decreases, with increasing coflow temperature)



- Once certain temperature limit is exceeded, flames behave like conventional lifted flames
- For fixed jet momentum, increasing the coflow temperature:
 - reduces density
 - increases viscosity
 - reduces mixing
- Temperature limit is intimately coupled with the O₂ level

Adelaide JHC

Lift-off height characterization



- JHC/MILD flames are not lifted in the same sense as conventional flames
 - Exhibit a *transition* at a point resembling the lift-off height
 - 'Lift-off' not a monotonic function of coflow temperature
 - **Note to modellers:** molecular diffusion plays an important role, even at turbulent conditions

55



Modeling of Adelaide JHC-Burner

Modeling of Adelaide JHC-Burner



- Modeling efforts

Authors/Groups	Turb.-model	Comb. Model	Reaction Chemistry	Configurations
RANS				
Aminian et al., FTC, 88 (2012); Appl. Therm. Engg. 31 (2011)	K-eps (Stand. Modified, realiz., RNG)	EDC	KEE-58, DRM-{19,22}	HM{1,2,3}
Wang et al., CST, 184 (2012)	Mod. K-eps; Radiation	EDC	Global reaction mech: {2,3,4}-step	HM{1,2,3}
Mardani et al., CTM, 15 (2011); CTM, 14 (2010)	Mod. k-eps	EDC	DRM-22, GRI2.11	HM{1,2,3}
Frassoldati et al., Appl. Therm. Engg., 30 (2009)	k-eps (Stand., Mod.), RSM, Radiation	EDC	Detailed chemistry	HM{1,2,3}
Christo & Dally CnF, 142 (2005)	k-eps (Stand, RNG, realiz.)	EDC, steady flamelet	Skeletal, detailed mech.	HM{1,2,3}
Kim et al., PCI, 30, 2004	Mod. K-eps	CMC	GRI2.11	HM{1,2,3}
LES				
Ihme et al., PCI 33 (2011); FTC (2012)	Dyn. SGS	3-stream FPV	GRI-2.11	HM{1,2,3}

57



- Adelaide JHC-Burner - Three-Stream flamelet/progress variable model

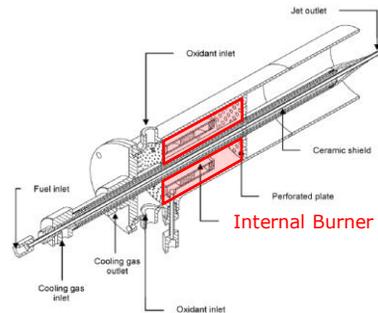
Y.C. See, J. Zhang, M. Ihme, B. Dally

Adelaide JHC

See, Zhang, Ihme, Dally



- Three-stream Jet-in-Hot-Coflow (JHC) burner¹
- Consideration of three operating conditions with successively diluted oxygen-concentration in vitiated coflow



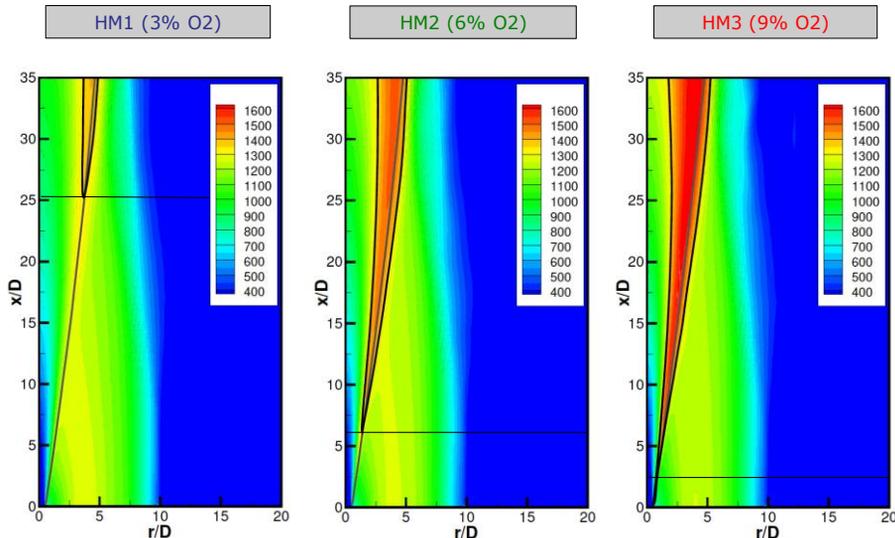
Configuration	Damköhler #	Coflow-Composition O ₂ /N ₂ /H ₂ O/CO ₂ [%]
HM3	0.47	9/79/6.5/5.5
HM2	0.17	6/82/6.5/5.5
HM1	0.03	3/85/6.5/5.5

¹ Dally, Karpetsis, & Barlow, Proc. Combust. Inst., 29, 1147 (2002)

59

Adelaide JHC

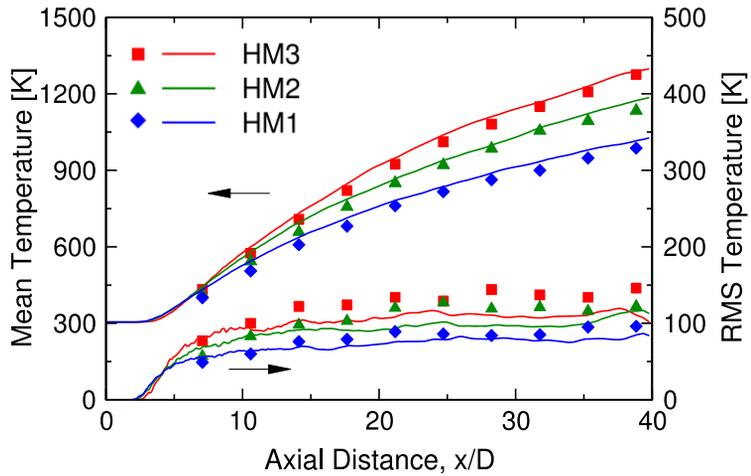
See, Zhang, Ihme, Dally



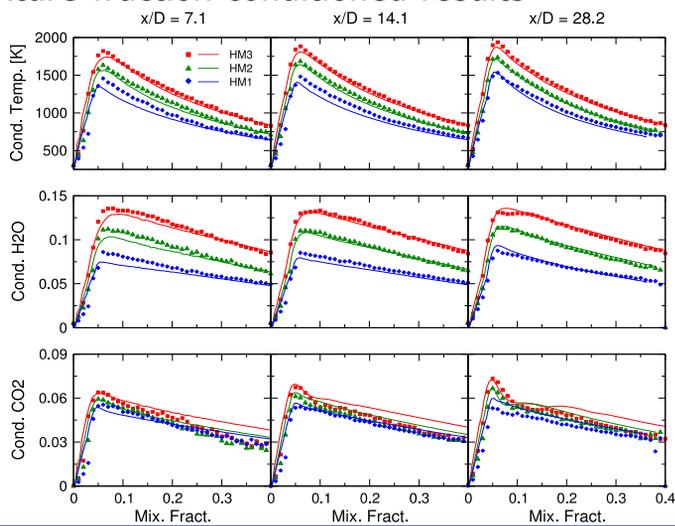
60



- Centerline temperature profiles

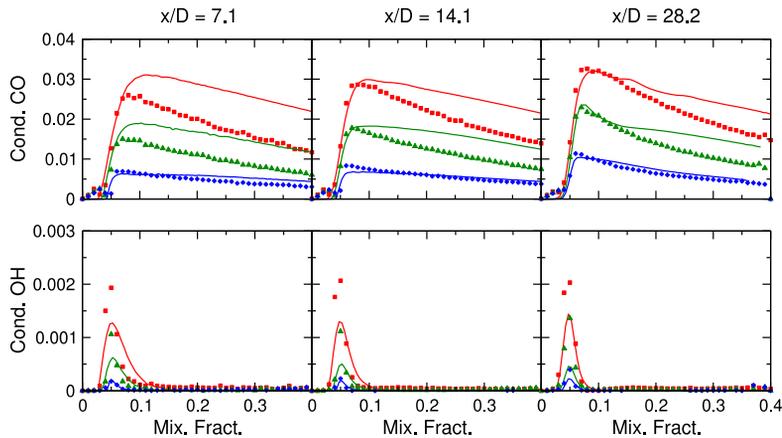


- Mixture-fraction conditioned results





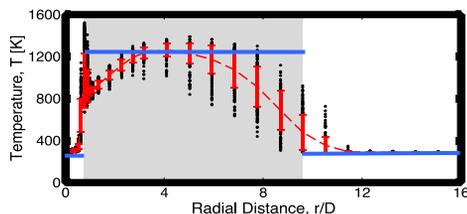
- Mixture-fraction conditioned results



63



- Application of three-stream FPV-combustion model to highly diluted JHC-burner: $Da = [0.47 \dots 0.03]$
- Model accurately captures dilution effects on flame structure and major species
 - Identification of transition region between unburned and burned mixture
- Discrepancies for CO, OH predictions on fuel-rich side are attributed to
 - Sensitivity of CO-CO₂ conversion to scalar inflow composition

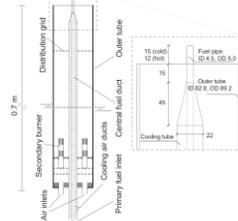


64



Delft JHC

- Burner design^{3,4}:



- (nominal) operating conditions:
 - Coflow-O₂ composition: 7.6, 8.8, 10.9%
 - Coflow-temperature: 1395, 1460, 1540K
 - Jet Reynolds number: 2500 - 8800
 - Fuel: CH₄/N₂, CH₄/C₂H₆/N₂

1 Dally et al., Proc. Combust. Inst, 29 (2002), 2 Medwell, Combust. Flame, 148 (2007); 152 (2008)
3 Oldenhof et al. Combust. Flame, 158 (2011); 4 Oldenhof et al. Combust. Flame, 158 (2011)



- Delft JHC-Burner - Conditional Velocity Statistics: PLIF-PIV Measurements in DJHC

E. Oldenhof, M.J. Tummerts,
E.H. van Veen, D.J.E.M. Roekaerts
TU Delft



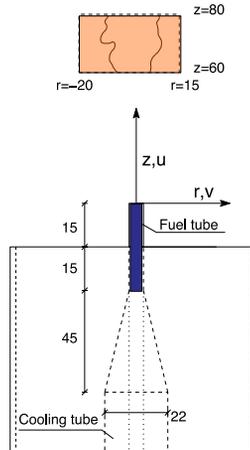
• Objective

- Determine flow field characteristics conditional on distance to reaction zone (OH) for the case of a fuel jet issuing into slower-moving low-turbulent surroundings of combustion products of lean combustion

• Conditions

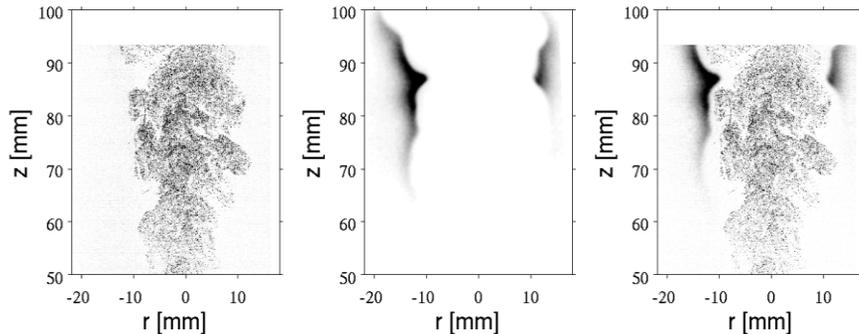
Case name	Fuel	Nozzle D [mm]	Vol. flow [nl/min]	Re _{jet} [-]	Z _{st} [-]	U _{jet,70} [m/s]	r _{jet,70} [mm]
DNG 0.5 (=DJHC-1)	Dutch Natural Gas (DNG)	4.5	30	8800	0.019	28.2	11.1
Premix 0.5	Air+DNG (3:1)	4.5	32	9000	0.168	35.6	10.2
DNG 2.0	DNG	2.0	11	5900	0.019	27.9	11.1

Measurement Region



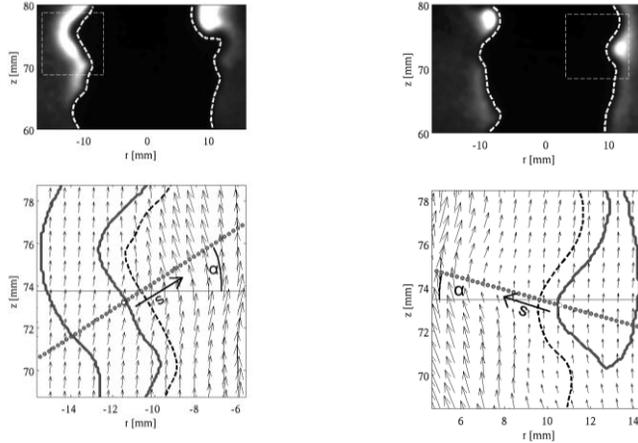
• Joint OH-PLIF PIV measurements

- Both coflow and jet seeded for PIV
- $f_{PIV} = 100$ Hz, $f_{PLIF} = 10$ Hz
- OH-PLIF laser pulse temporally centered between two PIV pulses

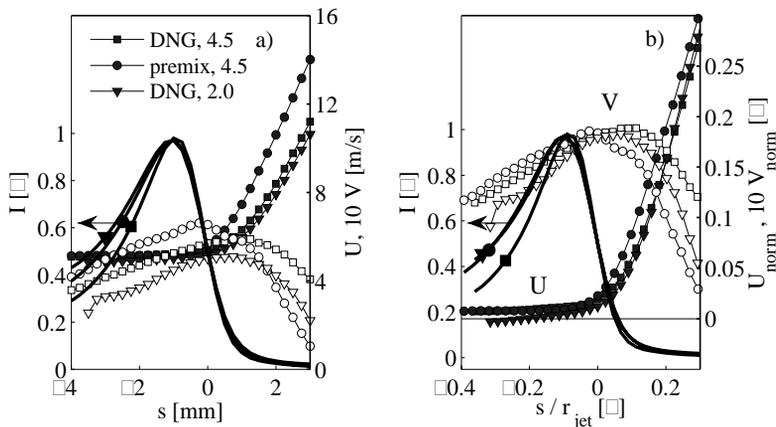




- Flame-structure analysis via local coordinate transformation
 - origin at jet side boundary of OH zone, directed orthog. to OH layer

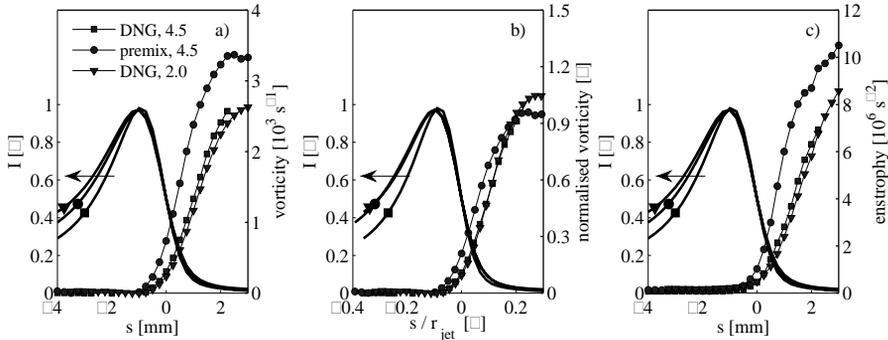


- Flame-structure analysis via local coordinate transformation
 - Mean axial and radial velocity vs local coordinate





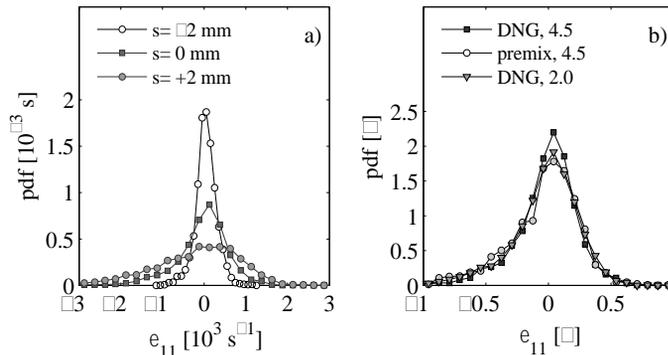
- Flame-structure analysis via local coordinate transformation
 - Mean OH and vorticity
 - Weakly strained flame zones but no vorticity



71



- Flame-structure analysis via local coordinate transformation
 - At $s=0$ mean strain neither compressive nor extensive
 - At $s=2$ mm the strains are on average compressive, and the pdf is considerably wider



72



• Summary and Conclusions

- Velocity statistics conditional on distance to OH-zone were determined
- Statistics within flame zone differ strongly from those closer to jet
- Vorticity is low at flame zones but they are weakly strained

- Sharp division of flow field in turbulent jet region and quasi-laminar coflow region

- Fluid dynamic properties of coflow stream determine turbulence-chemistry interaction

Modeling of Delft JHC-Burner



• Modeling efforts

Authors/Groups	Turb.-model	Comb. Model	Reaction Chemistry	Configurations
RANS				
De et al., <i>FTC</i> , 87 (2011)	K-eps (Stand. Realiz., RNG)	EDC	DRM-19	DJHC-I_S DJHC-X_S
Sarras, Stoellinger, Roekaerts, <i>Turb. Heat Mass Transfer</i> , 7 (2012)	K-eps	JCPDF, JVCPDF, 3D-FGM EDC	GRI 3.0 Skeletal Mech (Smooke)	DJHC_I (Re=4100)
LES				
Kulkarni, Collonval, Zellhuber, Polifke, (2012); Kulkarni & Polifke, <i>Fuel Process. Tech.</i> , (2012)	LES	Stochastic field method	GRI 3.0	DJHC_I DJHC_V



RANS of DJHC Transported PDF Method Using 3D FGM

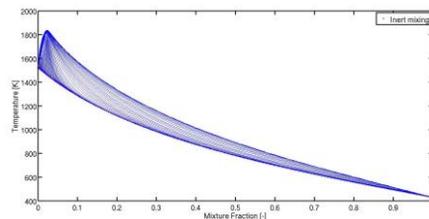
Gerasimos Sarras, Michael Stoellinger,
Dirk Roekaerts

Department Process & Energy
Department of Multi-Scale Physics,
Delft University of Technology

Modeling of Delft JHC-Burner Sarras, Stoellinger, Roekaerts



- Model formulation
 - Flame-structure evaluation from unsteady laminar diffusion flamelets
 - Detailed chemistry
 - Definition of reaction progress variable and thermo-chemistry



$$Y = \frac{Y_{H_2}}{M_{H_2}} + \frac{Y_{H_2O}}{M_{H_2O}} + \frac{Y_{CO_2}}{M_{CO_2}}, c = \frac{Y - Y_{\min}(Z_1)}{Y_{\max}(Z_1) - Y_{\min}(Z_1)} \quad \phi(x, t) \rightarrow \phi(Z_1, Y; Z_2)$$

- Lagrangian particle Eulerian mesh
 - Joint composition PDF approach (JCPDF)
 - Joint velocity composition PDF approach (JVCPDF)
- Cases considered:
 - DJHC-I: $Re = \{4100, 8800\}$, $T_{co} = 1540$, $X_{O_2, co} = 7.6\%$

Modeling of Delft JHC-Burner

Sarras, Stoellinger, Roekaerts



JCPDF

- Particle position:

$$dX_i^* = \frac{\tilde{u}_i}{\langle r \rangle} dt + \sqrt{\frac{2G_T}{\langle r \rangle}} dW$$

- Turbulent velocity fluctuations:

$$\langle u_i'' | \tilde{y} \rangle = -G_T \frac{F}{r}$$

- Algebraic scalar flux model:

$$\langle r \rangle \overline{u_j'' f_a} = -G_T \frac{\tilde{f}}{x_j}$$

JVCPDF

- Particle position and velocity:

$$dX_i^* = (\tilde{U}_i + u_i^*) dt$$

$$du_i^* = -u_j^* \frac{\tilde{u}_i}{x_j} dt + \frac{1}{\langle r \rangle} \frac{\overline{u_i'' u_j''}}{x_j} dt + a_i^* dt$$

- Differential scalar flux

$$\frac{1}{\langle r \rangle} \overline{u_j'' f_a} = \dots + \langle r a_i f_a \rangle + \langle r a_i q_a \rangle$$

$$a_i^* dt = G_{ij} u_j^* dt + \sqrt{C_0 \epsilon} dW_i$$

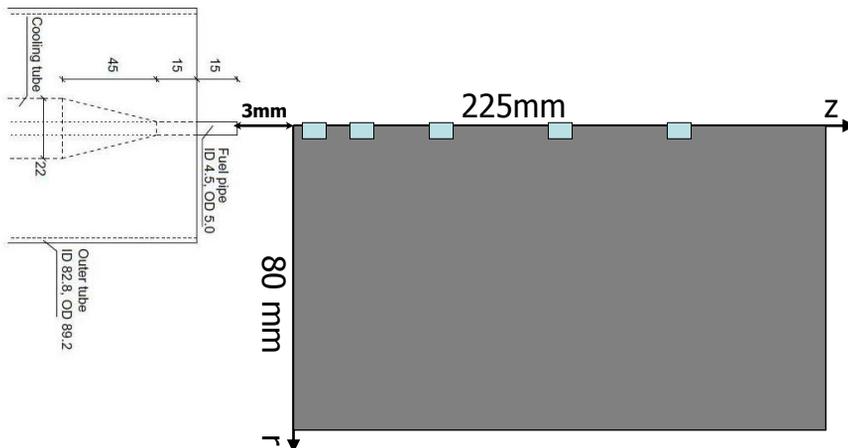
77

Modeling of Delft JHC-Burner

Sarras, Stoellinger, Roekaerts



- Computational Setup: 2D axisymmetric domain (150x110 grid-points)



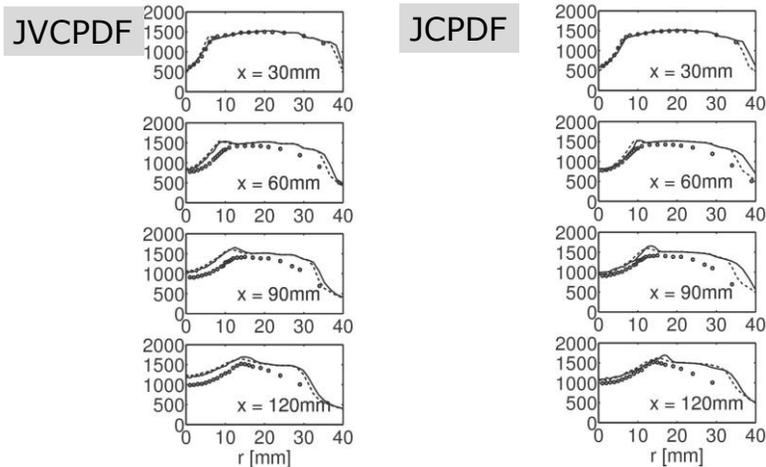
78

Modeling of Delft JHC-Burner

Sarras, Stoellinger, Roekaerts



- PDF approaches with IEM (dashed line) and EMST (solid line) mixing models



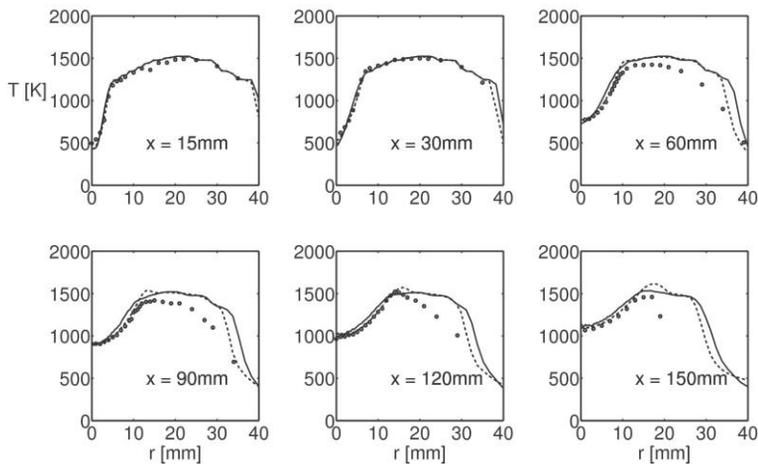
79

Modeling of Delft JHC-Burner

Sarras, Stoellinger, Roekaerts



- JVCPDF (solid, $C_\phi=1$) and JCPDF (dashed, $C_\phi=1$) with Modified Curl



80

Modeling of Delft JHC-Burner

Sarras, Stoellinger, Roekaerts



- Summary and Conclusions

- PDF simulations of DJHC are performed using RANS/Monte Carlo particle method
- JCPDF results are closer to experiments comparing to JCVPDF
- outer region not well predicted due to wrong inflow boundary conditions used
- ignition behavior depending on
 - inclusion of mean molecular diffusion
 - PDF method (scalar or velocity-scalar)
 - Micro-mixing model
- Modified Curl performs better than IEM and EMST for both PDF approaches

- Ongoing/future work

- Consideration of enthalpy
- LES using OpenFOAM

81



LES of DJHC Stochastic field method and tabulated chemistry

R. Kulkarni, F. Collonval, M. Zellhuber,
W. Polifke
TU Munich

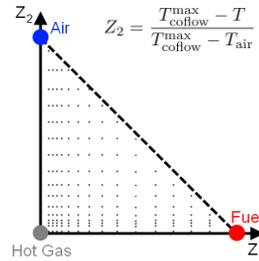
Modeling of Delft JHC-Burner

Kulkarni, Collonval, Zellhuber, and Polifke



- Model formulation
 - Reaction chemistry tabulation from homogeneous reactor simulations
 - Chem. Mech: GRI 3.0
 - Composite progress variable:

$$Y_C = \text{CH}_2\text{O} + \text{CO} + \text{CO}_2$$
- Assumptions:
 - Correlation btw. Temp. and Y_{O_2} in coflow
 - Neglect strain-rate effects
 - No differential diffusion
- Transported pdf using Eulerian stochastic fields
- Mixing model: IEM + drift term
- Closure for species source terms and heat release



$$\tilde{\omega}_\alpha = \bar{\rho} \frac{1}{N} \sum_{n=1}^N \dot{\omega}_\alpha(Z_1^n, Z_2^n, Y_C^n)$$

R. Kulkarni, W. Polifke, Fuel Processing Technology, in press, 2012

83

Modeling of Delft JHC-Burner

Kulkarni, Collonval, Zellhuber, and Polifke



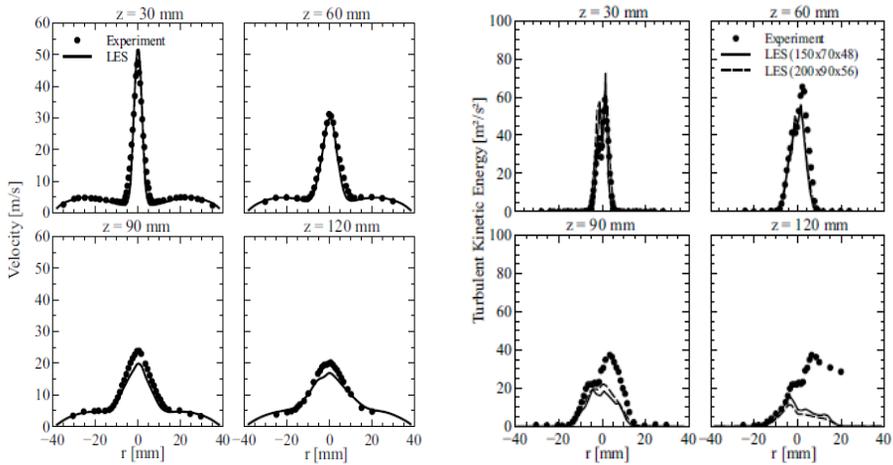
- Numerical method
 - LES performed with FLUENT 13
 - Segregated pressure-based
 - Dynamic Smagorinsky model
 - Turbulent Schmidt number: 0.9
 - Discretization: 2nd order in time & space
 - Time step: 2 μs (CFL < 0.7)
- Computational mesh
 - O-grid mesh \sim 650 000 cells
 - 150 x 70 x 48 (x, r, ϕ)
 - Clustered towards axis
 - Δx_{grid} [0.1mm, 1.5mm]
 - Turbulent inlet: Vortex method
- Cases considered:
 - DJHC-I: $\text{Re} = \{4100, 8800\}$, $T_{\text{co}} = 1540$, $X_{\text{O}_2, \text{co}} = 7.6\%$
 - DJHC-V: $\text{Re} = 4600$, $T_{\text{co}} = 1460$, $X_{\text{O}_2, \text{co}} = 8.8\%$

R. Kulkarni, W. Polifke, Fuel Processing Technology, in press, 2012

84



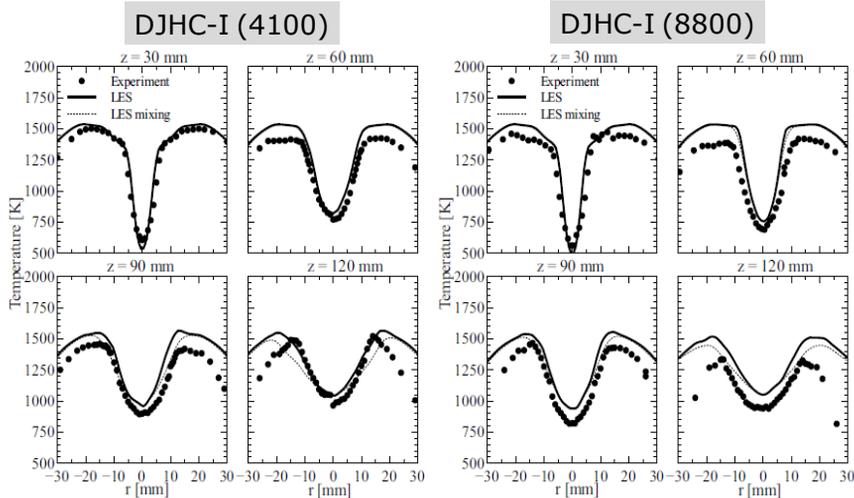
• Model Results: DJHC-I (8800)



85



• Model Results:



86

Overview



- Review of combustion-physics of lifted flames
 - Ignition-scenarios
- Comparison of lifted flames in vitiated coflows
 - Model comparison
- MILD combustion
 - Overview of experimental configurations, available measurements
 - Model comparison
- Utilization of DNS for model-development
- Discussion

87

Overview



- Review of combustion-physics of lifted flames
 - Ignition-scenarios
- Comparison of lifted flames in vitiated coflows
 - Model comparison
- MILD combustion
 - Overview of experimental configurations, available measurements
 - Model comparison
- Utilization of DNS for model-development
- Discussion

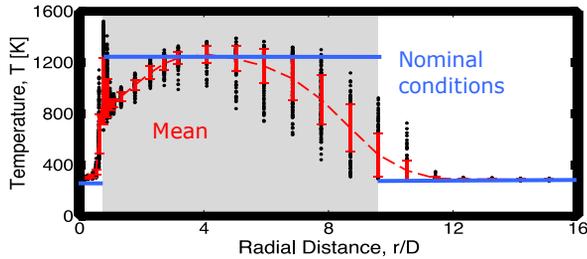
88

Discussion



- MILD-combustion

- Sensitivity of flow-field, heat-release, and species to scalar/velocity inflow boundary conditions



Example:
Scatter data at
burner-exit of
HM3-AJHC

- Quantitative understanding of lift-off mechanisms (Bassam)
 - Importance of coflow O₂ and temperature?
 - Effects of flow/velocity field on lift-off?
 - Interplay of operating parameters: T, O₂, ...
 - Effects of other species, flow-field?

89

Discussion



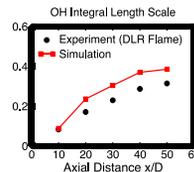
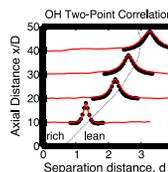
- Lifted flames

- Definition of lift-off height
 - link btw. measurements and simulation
 - relevant diagnostics
- Inclusion of CH*/OH* in simulation



- Utilization/need for additional measurements

- Scalar inflow boundary conditions
- High-speed diagnostics
- Spectral information
- Two-point correlations
(Ex.: DLR-A 2-pt OH-correlation)



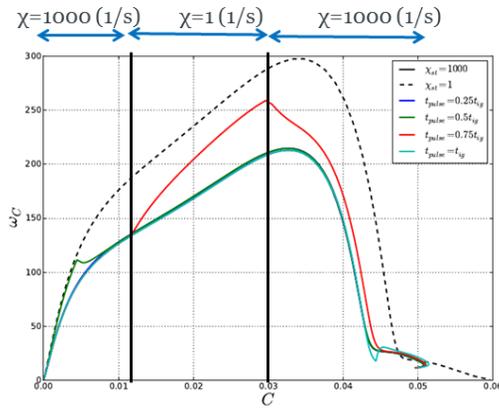
90

Discussion



- Combustion modeling
 - High-resolution LES
 - Resolving instead of modeling?
 - Convergence in combustion-model formulations?
 - DNS-data
 - Infra-structure for DNS-data-access
 - Direct access, local-processing, server, pre-processing

Implications for modelling



Unsteady igniting flamelets with a time-varying dissipation rate: $20\mu\text{s}$ step pulse

- Error due to tabulation using constant dissipation rates is greatest around thermal runaway.

- Delayed response suggests a Lagrangian averaging/relaxation model* for an 'equivalent'** dissipation rate $\hat{\chi}$:

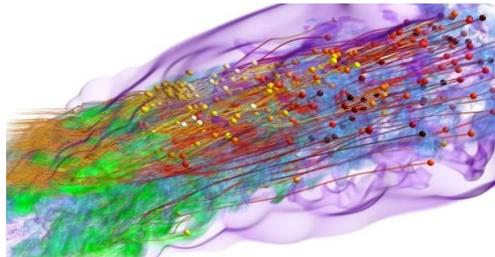
$$\frac{D\hat{\chi}}{Dt} = \frac{1}{\tau_{\chi}} (\chi - \hat{\chi}).$$

- The DNS database provides deep insight into the chemical and diffusive contributions to the relaxation time τ_{χ} .

* Adapting the Lagrangian averaged modelling approach by Meneveau *et al.* (1996)

** Related concept of equivalent *strain* concept by Cuenot *et al.* (2000)

Modelling of Lifted Flames in Vitiated Coflow: Insight and Challenges from DNS

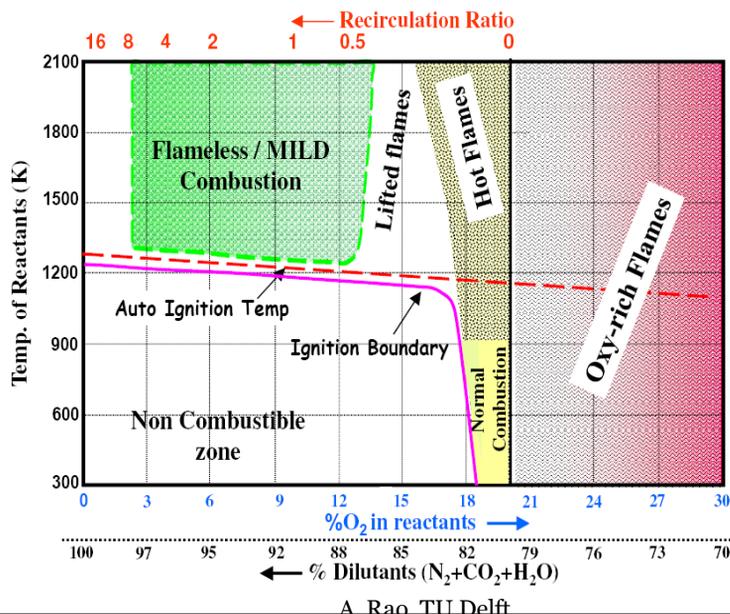


Lagrangian particles tracking the turbulent flow in an autoigniting jet of ethylene fuel. DNS by Yoo et al.

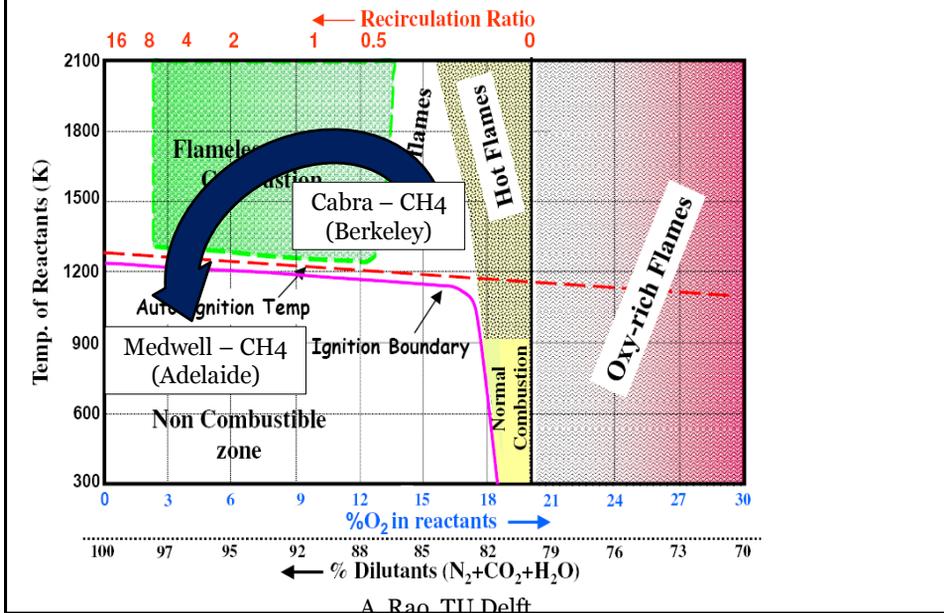
Contributions from:

Jackie Chen, Hemanth Kolla (Sandia National Laboratories, Ca),
Ray Grout (NREL), Andrea Gruber (SINTEF), Chunsang Yoo (UNIST, Korea),
Ed Knudsen (CTR, Stanford/ Bosch), Heinz Pitsch (RWTH Aachen)

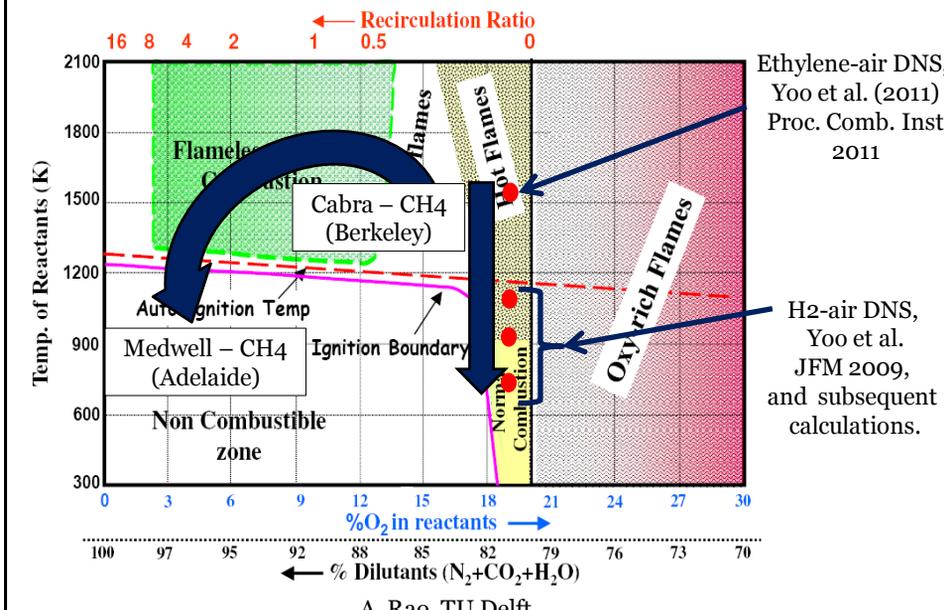
Role of preheat and dilution



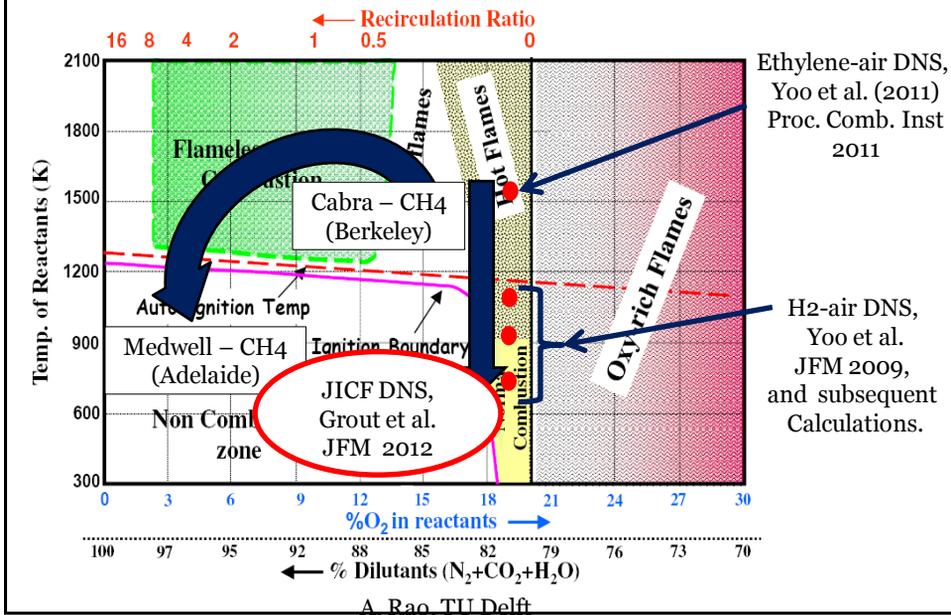
Role of preheat and dilution: Autoignition → Distributed Ignition



Role of preheat and dilution: Autoignition → Propagation



Role of preheat and dilution: Jet-in-Cross-Flow (multi-mode)



Modelling of Lifted Flames in Vitiated Coflow: Insight and Challenges from DNS

DNS analysis of lifted flame stabilization

- 1) Stabilization dynamics,
- 2) Transition from deflagration to ignition fronts,
- 3) Chemical characterization of igniting flow,
- 4) Stabilization of Jets-in-Cross-Flow.

Q. What quantities could/should be compared between model & DNS/experiment?

Q. Which stabilization physics do you want in TNF data sets?

DNS for *a posteriori* validation

- 1) Advantages and limitations,
- 2) Case study: Flamelet modelling of a lifted jet flame.

Sandia DNS of jet flame stabilization in hot air with detailed/reduced chemistry

Lifted Hydrogen jet flames in hot coflow: 750K, 950K, 1100K coflow

- Conditions spanning the ignition temperature.
- Jet Reynolds number $\sim 11,000$

C.S. Yoo et al. JFM 2009

Lifted Ethylene jet flames in hot coflow: 1550K coflow.

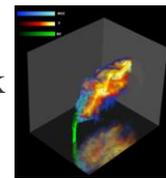
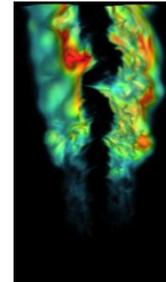
- Strongly autoignitive conditions.

C.S. Yoo et al. PCI 2011

Jet in cross flow: Hydrogen and CO/hydrogen flames: 750K

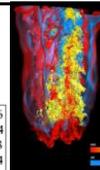
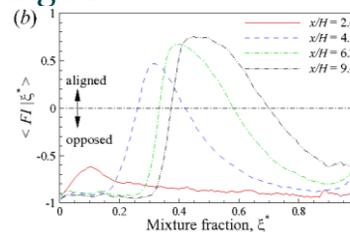
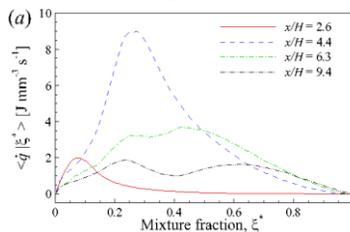
- Stabilized by mixing in the jet wake.

R.W. Grout et al. JFM 2012



7

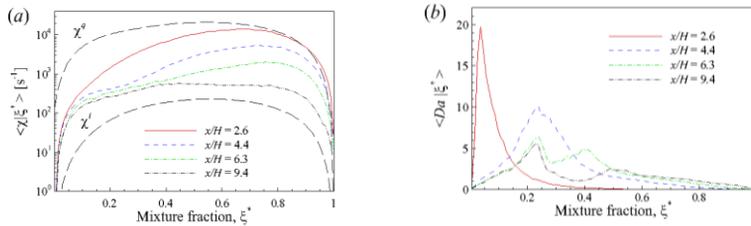
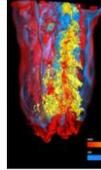
Hydrogen lifted flame in 1100K coflow: Mixedness & Burning Mode



- Mean HRR condtl on ξ , $\langle \dot{q} | \xi^* \rangle$
 - HRR starts to increase in lean mixtures ahead of the flamebase
 - Shift in the peak $\langle \dot{q} | \xi^* \rangle$ from lean to rich
 - Two peaks in $\langle \dot{q} | \xi^* \rangle$ form further downstream
 - One centered neat the stoichiometric
 - The other in fuel-rich condition
- Mean FI condtl on ξ , $\langle FI | \xi^* \rangle$
 - $FI = \nabla Y_F \cdot \nabla Y_O / |\nabla Y_F| |\nabla Y_O|$
 - Near the flamebase, $\langle FI | \xi^* \rangle$ exhibits negative values
 - HRR occurs in nonpremixed mode
 - Downstream, $\langle FI | \xi^* \rangle$ shows positive for stoichiometric and fuel-rich mixtures
 - The reactants are well mixed and HRR occurs in both nonpremixed and premixed mode

8

Hydrogen lifted flame in 1100K coflow: Conditional Statistics

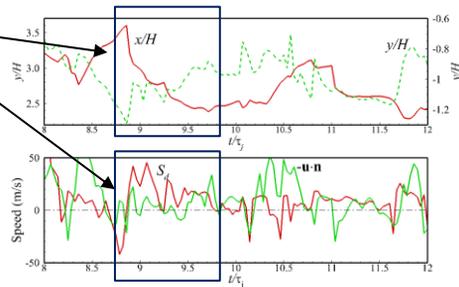


- Mean χ condntl on ξ , $\langle \chi | \xi^* \rangle$
 - The mean value is substantially lower than corresponding 1-D extinction χ and greater than 1-D ignition χ
 - The variance of χ is substantially larger than the conditional mean value
 - Local ignition \rightarrow local instantaneous χ decreases below 1-D ignition χ
 - Local extinction \rightarrow local instantaneous χ increases above 1-D extinction χ
- Mean Da condntl on ξ , $\langle Da | \xi^* \rangle$
 - $Da = \frac{\dot{\omega}_k}{|-\nabla \cdot (\rho Y_k \mathbf{V}_k)|}$
 - At the flame base, $\langle Da | \xi^* \rangle \gg O(1)$
 - Auto-ignition is the main source of stabilization of the lifted flame
 - Further downstream, $\langle Da | \xi^* \rangle$ approaches unity near stoichiometric and fuel-rich mixtures
 - Transition from auto-ignition to normal flames

9

1) Dynamics of the Stabilization Point

- Early period
 - In low velocity, high displacement speed, and small mixture fraction
 - Far away from the core jet
 - **The flame base moves upstream and inward slowly**
- Later period
 - The flame base approaches the core jet region with large mixture fraction
 - The flame base encounters high axial velocity and high scalar dissipation rate
 - The flame base moves downstream and outward fast

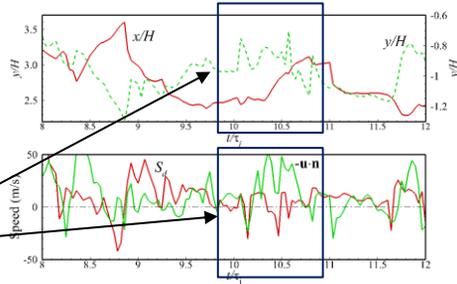


Temporal evolution of the axial stabilization point with axial velocity, S_d (top) and mixture fraction, heat release rate, and scalar dissipation rate (bottom)

10

1) Dynamics of the Stabilization Point

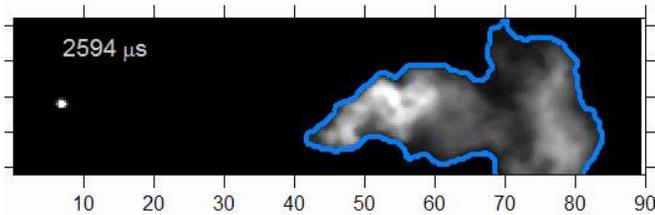
- **Early period**
 - In low velocity, high displacement speed, and small mixture fraction
 - Far away from the core jet
 - The flame base moves upstream and inward slowly
- **Later period**
 - The flame base approaches the core jet region with large mixture fraction
 - The flame base encounters high axial velocity and high scalar dissipation rate
 - **The flame base moves downstream and outward fast**



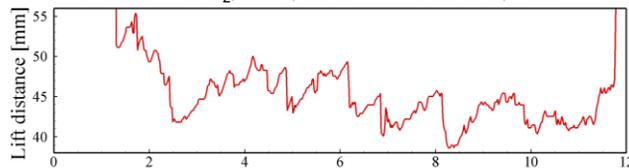
Temporal evolution of the axial stabilization point with axial velocity, S_d (top) and mixture fraction, heat release rate, and scalar dissipation rate (bottom)

1) Dynamics of the Stabilization Point: Diesel lifted jet flame

- Lifted diesel jet in a constant volume vessel under high pressure (Lyle Pickett et al. Proc. Combust. Inst. 31 (2009))
- Ignition plays key role to stabilize the flame base

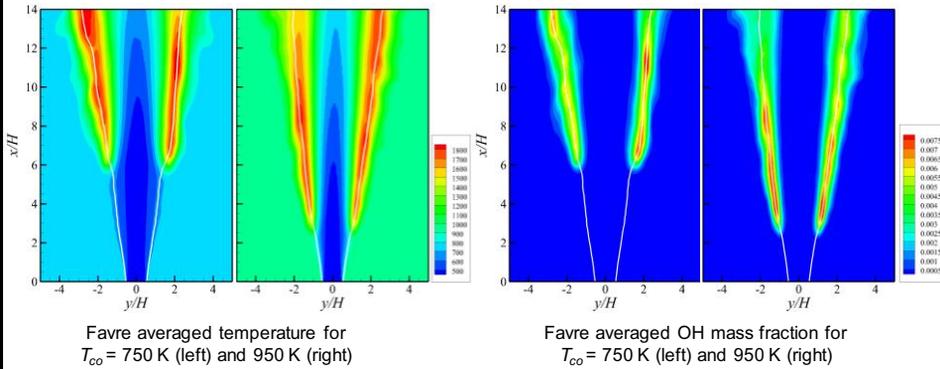


Chemiluminescence from diesel lift-off stabilization for #2 diesel, ambient 21% O_2 , 850K, 35 bar L. Pickett et al, 2009.



Q. Is this "Saw-tooth" shaped movement a useful measure of model validity?

2) Transition from deflagration to ignition physics: Lifted H₂ Jet Flames in Mildly-Heated Coflow

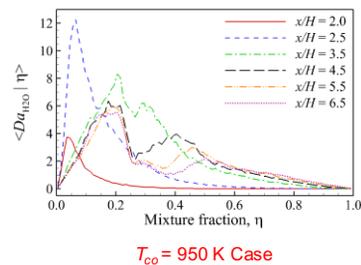
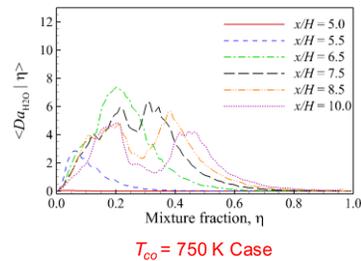


- To compare the stabilization mechanisms of lifted flames
 - $T_{co} = 750$ K (< auto-ignition temperature)
 - $T_{co} = 950$ K (> auto-ignition temperature)

13

2) Transition from deflagration to ignition physics: Damköhler Number

- Conditional mean Da , $\langle Da | \eta \rangle$
 - $Da_k = \frac{\dot{\omega}_k}{|\nabla \cdot (\rho Y_k \mathbf{V}_k)|}$
- 750 K case
 - At the flame base, $\langle Da | \eta \rangle \sim O(1)$
 - Reaction counter-balances diffusion
- 950 K case
 - At the flame base, $\langle Da | \eta \rangle \gg O(1)$
 - Auto-ignition is the main source of stabilization of the lifted flame

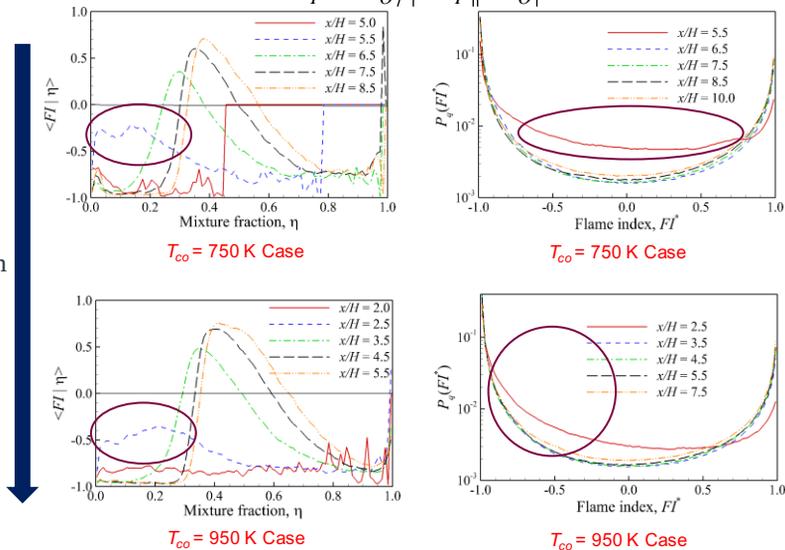


14

2) Transition from deflagration to ignition physics:

$$\text{Flame Index } FI = \nabla Y_F \cdot \nabla Y_O / \|\nabla Y_F\| \|\nabla Y_O\|$$

Transition
between
deflagration
and ignition
fronts



750 K: Shows increased contribution from 'premixed' ($FI > 0$) mode.

15

3) Chemical characterization of igniting flow: Chemical Explosive Mode Analysis (CEMA)

T. Lu, C.S. Yoo, J. H. Chen, C. K. Law, J. Fluid Mech. 2010

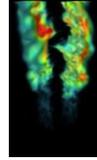
- Governing equations for a chemically reacting flow

$$\frac{d\mathbf{y}}{dt} = \mathbf{g}(\mathbf{y}) = \boldsymbol{\omega}(\mathbf{y}) + \mathbf{s}(\mathbf{y})$$

\mathbf{y} : the vector of variables (e.g. species concentration and temperature)
 $\boldsymbol{\omega}$: chemical source term
 \mathbf{s} : other source terms (e.g. diffusion)

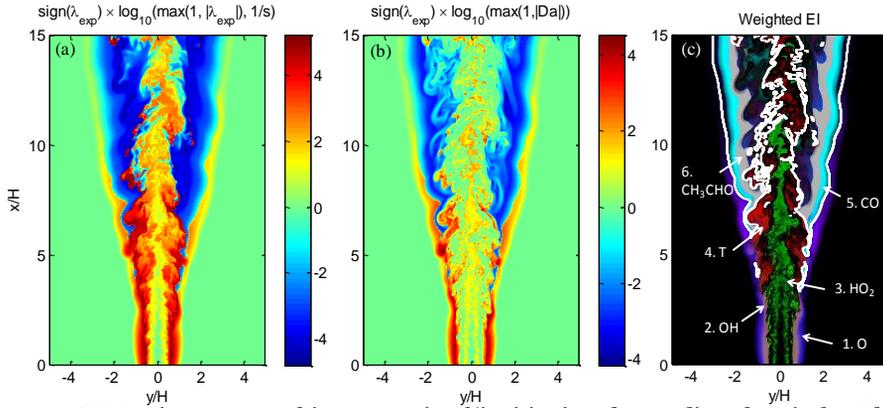
- The chemical Jacobian $\mathbf{J}_\omega = \frac{d\boldsymbol{\omega}}{d\mathbf{y}}$
- Chemical mode $f = \mathbf{b} \cdot \mathbf{g}$ \mathbf{b} : a left eigenvector of \mathbf{J}_ω
- Positive eigenvalue, λ_{exp} , of \mathbf{J}_ω indicates chemical explosive mode

3) Chemical characterization of igniting flow: CEM, Da, Weighted explosion index



- Ethylene-air lifted flame in 1550K coflow

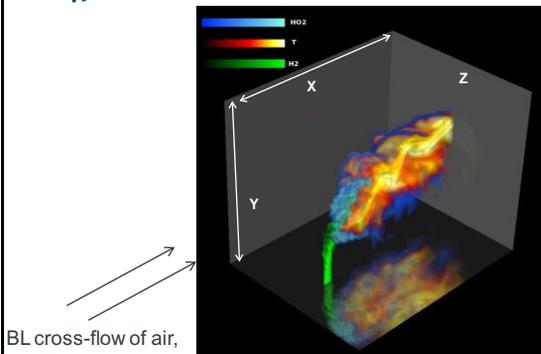
Z. Luo, C. S. Yoo, E. S. Richardson, J. H. Chen, C. K. Law, T. Lu *Combust. Flame* 2012



- CEMA gives an unambiguous metric of 'ignition', and preceding chemical modes (Explosion indices)

- Q.** Do our models predict the same chemical characteristics?

4) Stabilization of Jets in Cross-flow



BL cross-flow of air,
 $T_{cf} = 750$ K,
 $u_{cf} = 55$ m/s

N_2 diluted (30%) H_2 rich fuel
 jet,
 $T_j = 420$ K, $R_m = 3.4$
 effective dia = 1 mm

	X	Y	Z
size (mm)	25	20	20
N_{pts}	1408	1080	1100
Δ (μ m)	17.8	18.2	10.2-24.3
BCs	inflow/ outflow	isothermal wall/ outflow	periodic

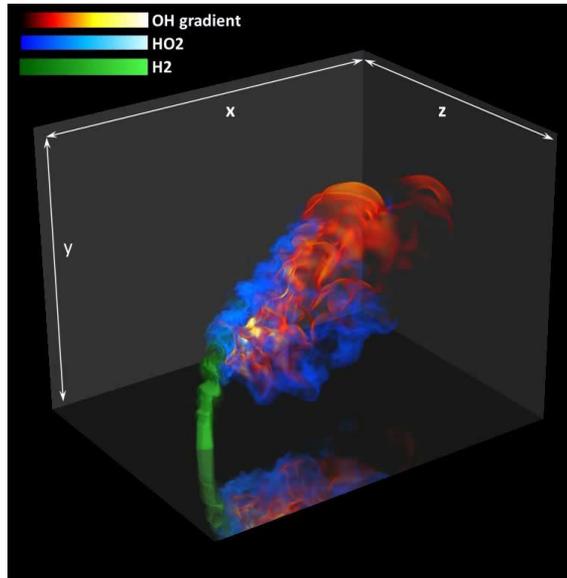
Parametric variation:

Nozzle: round, elliptical, square

Injection angle: $90^\circ, 75^\circ$

Fuel composition ($H_2:CO$): 1:0 (pure H_2); 16:1; 1:1

4) Stabilization of Jets in Cross-flow



Volume rendering of OH, HO₂, H₂ (DNS by Grout et al., Visualisation by H. Yu, Sandia)

4) Stabilization of Jets in Cross-flow: DNS analysis

Instantaneous flame characteristics:

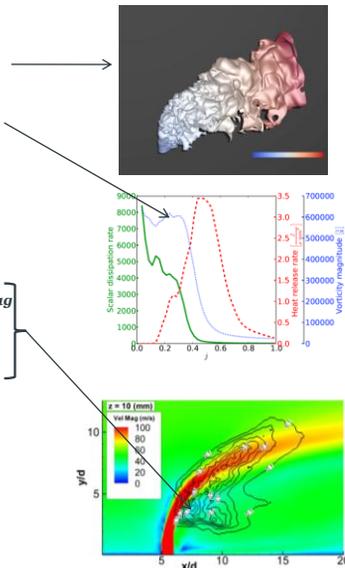
- novel *jet path parametrization* to describe instantaneous jet trajectory meaningfully.
- region in vicinity of flame root characterized by intense turbulence.
- (grad ξ) and (grad \mathbf{c}) not aligned: possibly distributed combustion

Mean flame characteristics:

- flame anchors, on average, in regions of low V_{mag} and ξ_{st} .
- flame anchoring conclusively observed only on jet leeward side (windward branch not evident).
- extensive counter-gradient diffusion of ξ due to pressure/anisotropy (symposium poster).

Flame blow-off:

- two-phased transient blow-off identified when angle transitioned from 90° to 75°



DNS analysis of lifted flame stabilization: Possible modelling targets

- Flame base dynamics – reveals contributions from interaction of chemistry with flow,
- Transition from propagative to ignitive stabilization,
- Prediction of chemical characteristics (CEMA) of igniting flow.

DNS for *a posteriori* validation

Advantages

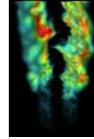
- Known ‘physics’: chemistry, boundary conditions,
 - 3D, multi-scalar validation data:
- Can determine where and why a model fails.

Limitations

- Moderate Reynolds number; moderate chemical complexity; simple geometry,
- Computational expense

Q. What is the best format for DNS & Modellers to interact?

Case study: Flamelet modelling of DNS Of Lifted C_2H_4 Flame

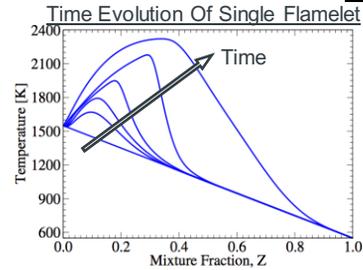


- Unsteady flamelet model

$$\frac{\partial \phi_i}{\partial \tau} - \frac{\chi Z}{2} \frac{\partial^2 \phi_i}{\partial Z^2} = \dot{\omega}_i$$

- Parameterize flamelets using

- Mixture fraction, Z
- Progress variable, C
- Reference dissipation rate, $\chi_{z,ref}$



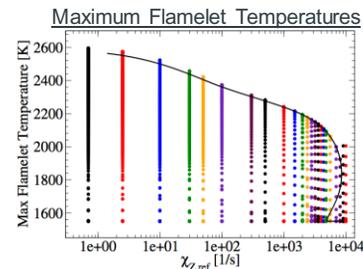
- Presume PDFs

- Beta-PDF for Z , Delta-PDFs otherwise

$$\tilde{\phi} = \tilde{\phi}(\tilde{Z}, \tilde{Z}''^2, \tilde{\chi}_{z,ref}, \tilde{C})$$

- Map chemistry into an LES

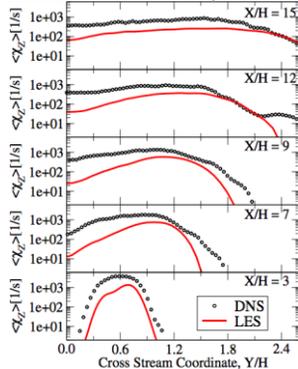
- Filter to Kolmogorov ratio: $\Delta/\eta = 8$



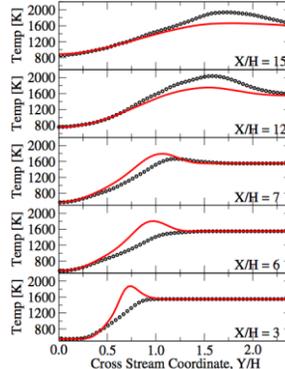
E. Knudsen, E. S. Richardson, Shashank, E. M. Doran, H. Pitsch, and J. H. Chen, Phys. Fluids 2012.

LES Results: Algebraic Models, Unity Lewis numbers

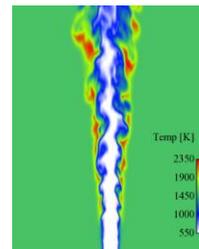
Mixture Fraction Dissipation Rate



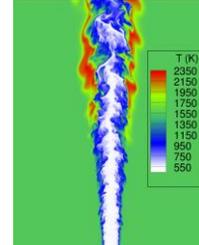
Temperature



LES Temperature Field



DNS Temperature Field

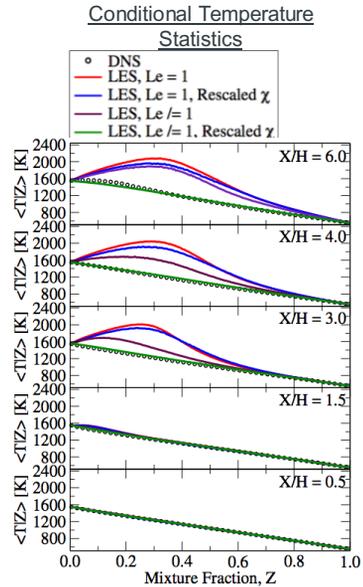


- Algebraic dissipation rate model: $\tilde{\chi}_z = 2(D_z + D_t)|\nabla \tilde{Z}|^2$
- Algebraic scalar variance model: $\tilde{Z}''^2 = C_{Zvar} \Delta^2 |\nabla \tilde{Z}|^2$
- LES significantly under-predicts flame lift-off

24

Combustion Model Sensitivities

- Compare 4 LES runs:
 - Unity Lewis #'s, original $\tilde{\chi}_z$ model
 - Unity Lewis #'s, $\tilde{\chi}_z$ rescaled to match DNS
 - Non-unity Lewis #'s, original $\tilde{\chi}_z$ model
 - Non-unity Lewis #'s, $\tilde{\chi}_z$ rescaled to match DNS
- Two equally critical modeling challenges
 - Identifying Lewis # importance
 - Improve transport ($\tilde{\chi}_z$) model



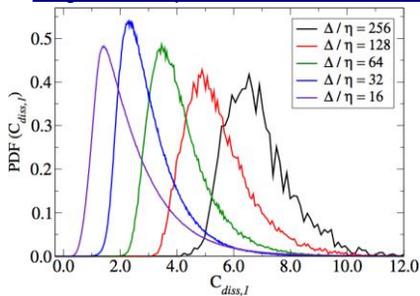
A 'Borrowed' Dynamic LES Model for dissipation rate

- Accept that dynamic models are not applicable to small scale quantities
- Idea: borrow dynamic information from another quantity - the subfilter scalar variance

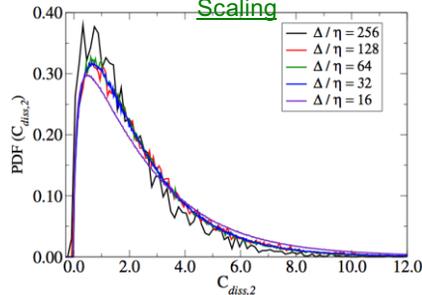
$$C_{diss} = C_{diss,2} \cdot \left(\frac{C_{Zvar}}{C_{Zvar}^0} \right) \quad \text{where } C_{Zvar} \text{ comes from } \widetilde{Z''^2} = C_{Zvar} \Delta^2 |\nabla \widetilde{Z}|^2$$

- Transport equation for mixture fraction variance

Original Dissipation Coefficient PDFs



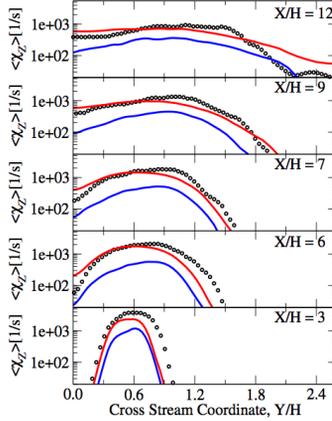
Coefficient PDFs After Dynamic Scaling



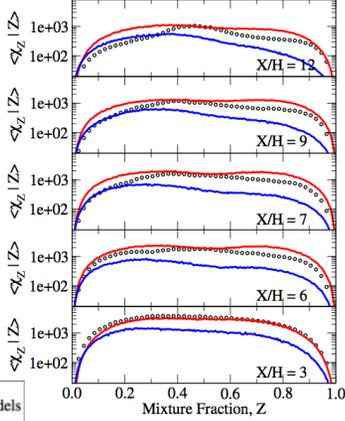
26

LES Results: Dissipation Rate

Unconditional Scalar Dissipation Rate



Conditional Scalar Dissipation Rate

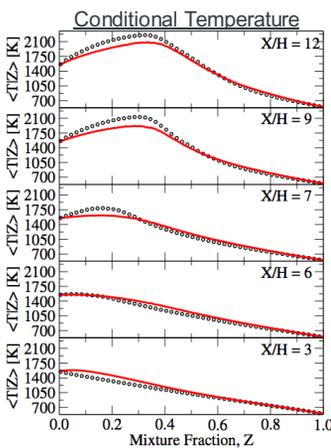


○ DNS
 — LES, Transport Eq. Models
 — LES, Algebraic Models

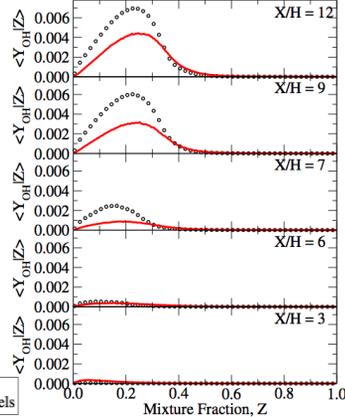
- Compare transported and algebraic models for scalar dissipation
- Transport equation model most accurately predicts DNS

27

LES Results, Non-Unity Lewis numbers



Conditional OH

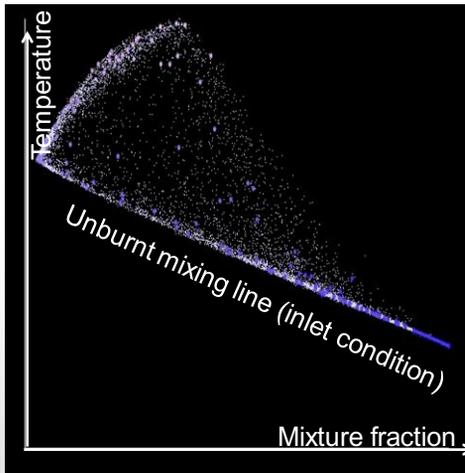
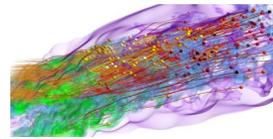


○ DNS
 — LES, Transport Eq. Models

- Improved fidelity of dissipation and variance models improves lift-off height prediction
- Conditional data shows temperatures still too low: [sensitive to entrainment](#)

28

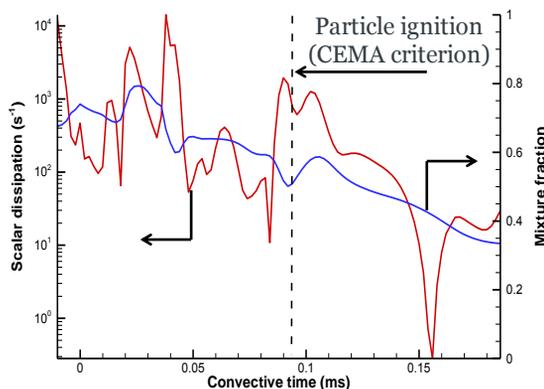
'History' effects in the lifted jet, missing in the flamelet modelling



Lagrangian evolution of fluid 'particles' in the jet flame

- High scalar dissipation retards or prevents ignition – response to dissipation fluctuations.
- In the jet configuration, fluid mixes with material of different 'age'.

Lagrangian analysis of dissipation rate fluctuations



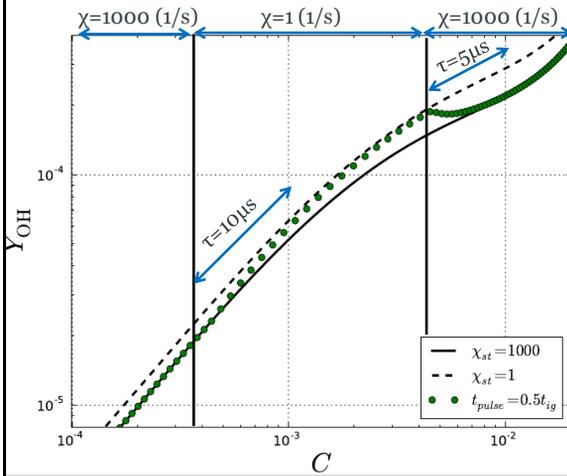
Dissipation history of one Lagrangian particle inside the turbulent shear layer.

The particle burns after 0.1ms in the domain, at a mixture fraction where $\tau_{ign} > 1\text{ms}$, due to mixing with slow-moving 'older' fluid that has already burned.

- Dissipation rate is highly intermittent with order-of-magnitude fluctuations over $5\mu\text{s}$ - $100\mu\text{s}$.
- Stochastic modelling for the dissipation rate is well developed (e.g. contributions by S. B. Pope, R.O. Fox), **but the transient effect on autoignition chemistry is not captured in tabulated flamelets.**

Response times of igniting flamelets

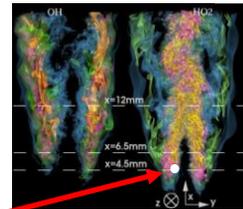
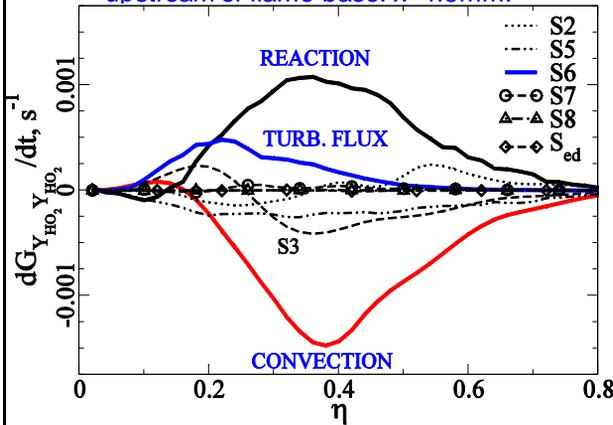
Unsteady igniting flamelets with a time-varying dissipation rate: 20μs step pulse



- The chemical state transitions between two constant-dissipation manifolds.
- The response time, $\sim 10\mu\text{s}$ or $\sim 0.1\tau_{\text{ign}}$, corresponds to dissipation fluctuation timescales.
- LES-flamelet tables only contain constant dissipation information.

Mixing of fluid with different 'age'

Budget for conditional variance of HO₂, upstream of flame base: x=4.5mm.



Conditional turbulent flux mixes fluid with different convective 'age', generating conditional fluctuations.

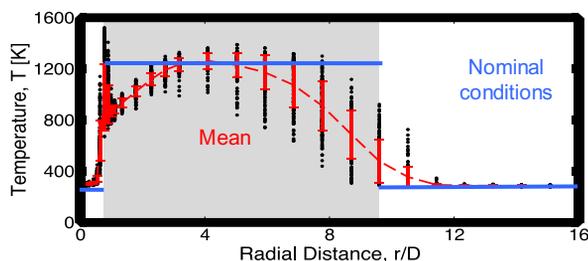
- Dissipation rate fluctuations, S7, have a limited rôle in this lifted jet configuration.
- Chemistry and turbulent convection dominate – the mixture's *history* is important. E.Richardson, C.S. Yoo, and J.H. Chen. Proc. Combust. Inst. 32 (2009)

Summary: *a posteriori* flamelet modelling of lifted C₂H₄ flame DNS

- Demonstrated that differential diffusion must be included,
- Identified deficiency in the dissipation and variance sub-models, improved models developed.
- The final unsteady flamelet model achieves an accurate prediction of lift-off height, but conditional statistics show some deviation.
- DNS analysis suggests need to extend model to include effects of 'history':
 - Response to dissipation fluctuations
 - Mixing of fluid with different 'age'
- Comparison with DNS removes uncertainty over physical models and boundary conditions → direct evaluation of turbulent-combustion model performance.

Discussion

- MILD-combustion
 - Sensitivity of flow-field, heat-release, and species to scalar/velocity inflow boundary conditions



Example:
Scatter data at
burner-exit of
HM₃-AJHC

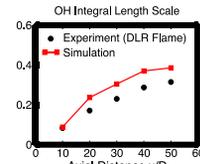
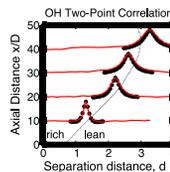
- Quantitative understanding of lift-off mechanisms (Bassam)
 - Importance of coflow O₂ and temperature?
 - Effects of flow/velocity field on lift-off?
 - Interplay of operating parameters: T, O₂, ...
 - Effects of other species, flow-field?

Discussion

- Lifted flames
 - Definition of lift-off height
 - link btw. measurements and simulation
 - relevant diagnostics
 - Inclusion of CH^*/OH^* in simulation



- Utilization/need for additional measurements
 - Scalar inflow boundary conditions
 - High-speed diagnostics
 - Spectral information
 - Two-point correlations
(Ex.: DLR-A 2-pt OH-correlation)



Discussion

- Combustion modeling
 - High-resolution LES
 - Resolving instead of modeling?
 - Convergence in combustion-model formulations?
 - DNS-data
 - Infra-structure for DNS-data-access
 - Direct access, local-processing, server, pre-processing

LES computations of the Piloted Premixed Jet Burner

Session co-ordinators: Matthew J. Dunn, Assaad R. Masri, Heinz Pitsch.

The purpose of the session on the piloted premixed jet burner (PPJB) at TNF11 was to evaluate developments in large eddy simulation of the PPJB since TNF10. Four groups were involved in the simulations: Stanford/Aachen, Imperial College London/Sydney, University of Michigan, and Lund University. The PPJB had been presented as a modelling target flame at TNF10, with PDF and preliminary LES results reported. The LES results presented at TNF11 represent a significant step forward from the LES results presented at TNF10.

The Stanford/Aachen simulations utilised a steady premixed flamelet model, with a 4D tabulated chemistry table. The chemistry tabulation incorporated the rms mixture fraction, two mean mixture fraction variables, and reaction progress as parameterization coordinates so as to accommodate for mixing with the coflow and pilot. They reported essentially negligible difference in results between 4 and 9 million grid cell meshes. The University of Michigan results employed a steady flamelet based tabulation combustion model approach with two mixture fractions to account for the variation between pilot and coflow streams mixing with the jet.

The Lund simulations employed an ILES model, which allowed the incorporation of complex chemistry (19 transported species). As the ILES model is dependant on the mesh size and quality, model quality measures were developed, and it was shown for the PM1-150 flame good results were obtained up to and including $x/D=15$ with an unstructured hexahedral grid of 2 million cells. The Imperial College London/Sydney simulations employed a stochastic field LES model with eight stochastic fields. The stochastic field model utilized a complex chemistry approach (15 transported species) over a 4.8 million cell grid. Interestingly, the stochastic field approach results for the PM1-200 flame, whilst predicting a flame too short, produced the best results in terms of mean and rms profiles for this flame thus far. However, there is still greater improvement need before successful prediction can be claimed for this flame. Both of the LES methods that incorporated complex chemistry were able to predict some degree extinction and re-ignition for the PM1-150 flame. However the degree of extinction was typically much smaller than measured.

The four groups presented very promising results for the two low-velocity flames PM1-50 and PM1-100. However all groups predict an insufficient degree of extinction in the high velocity flames (PM1-150 and PM1-200) and thus predicted a flame length too short. Close to the burner all four groups presented good results in terms of the mean and rms scalar profiles. The success of the tabulated LES flamelet models (Michigan and Stanford/Aachen) for the low velocity PM1-50 flame is somewhat to be expected due to the correlation of the flame structure observed from experiments to the fundamental flame structure assumptions of these models. Therefore the success of the PM1-50 simulation results can be viewed as a validation for these models assumptions. However, the success of these tabulated chemistry models for the PM1-100 flame and the PM1-150 flame (in the near nozzle region up to and including $x/D=15$) that have a significant degree of turbulence chemistry interaction is somewhat unexpected due to the assumptions of the models. It was discussed and proposed that if the tabulated chemistry approaches were to have greater success for

the PM1-150 and PM1-200 flames in the future, the composition space accessed during extinction must be incorporated in some manner, e.g., through an additional tabulation dimension.

In 2010 at TNF10 the RANS based PDF calculations were presented, showing good results for the low velocity flames and under prediction of the degree of extinction in the high velocity flames. In order to further improve the PDF models, experiments exploring the role of the pilot to jet heat release ratio and the micro mixing model were proposed to be necessary. Such modelling progress also needed additional experiments to be conducted. These experiments were also discussed at TNF11 and were considered to be of relevance to the development and validation of the LES results presented at TNF11.

As always for LES, the sensitivity to boundary conditions was emphasised by all participants. A strong consensus was that accurate profiles closer to the nozzle for temperature and velocity would be very beneficial, particularly near the pilot exit and the pilot-coflow interface. Perhaps the greatest surprise from the results presented at the TNF11 workshop was that the four LES results, despite being a significant progression from the two LES results reported at TNF10, did not convincingly show a superior predictive capability to the RANS transported PDF calculations presented by Cornell at TNF10. Also, no model has yet been able to show a convincing predictive capability for the entire PM1-150 and PM1-200 flames, which feature significant extinction and re-ignition. Attempting to solve this challenge will hopefully motivate future developments in combustion models and corresponding experiments, which will utilize the TNF workshop as a forum to drive such progression and collaboration.

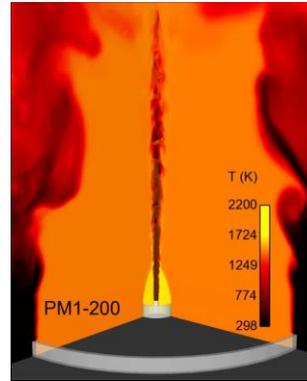
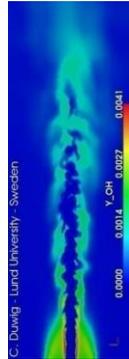
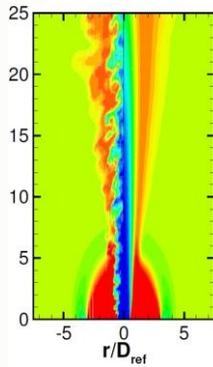
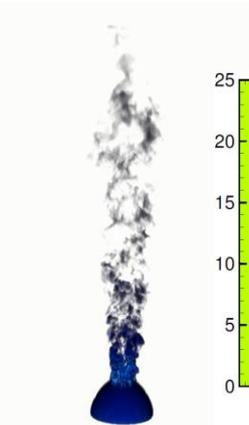
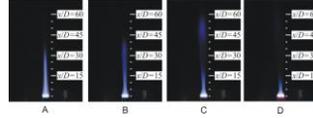
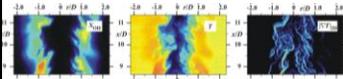
LES computations of the Piloted Premixed Jet Burner (PPJB)

Session co-ordinators

Matthew J. Dunn

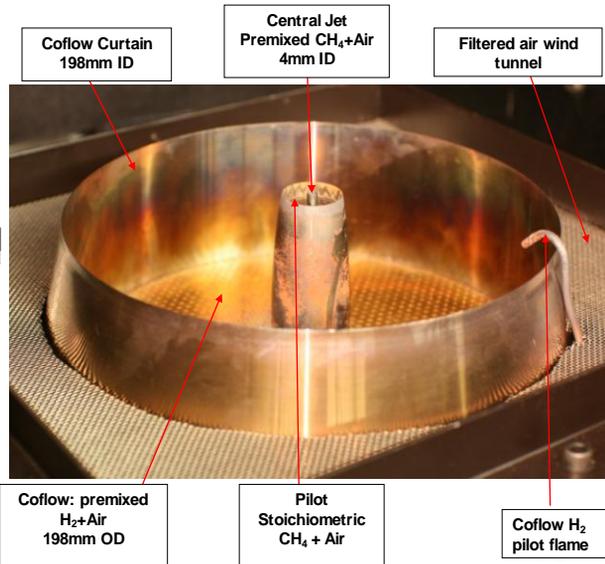
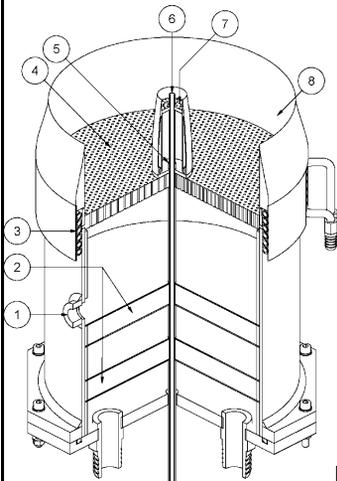
Assaad Masri

Heinz Pitsch



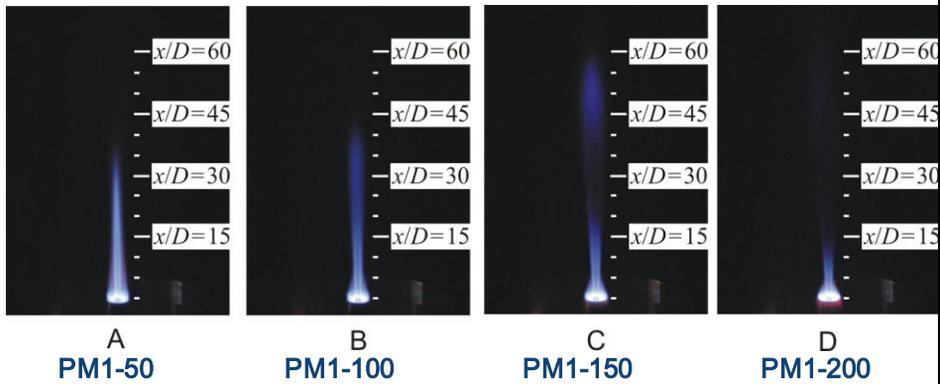
TNF 11 Workshop, Darmstadt 2012

PPJB Overview



TNF 11 Workshop, Darmstadt 2012

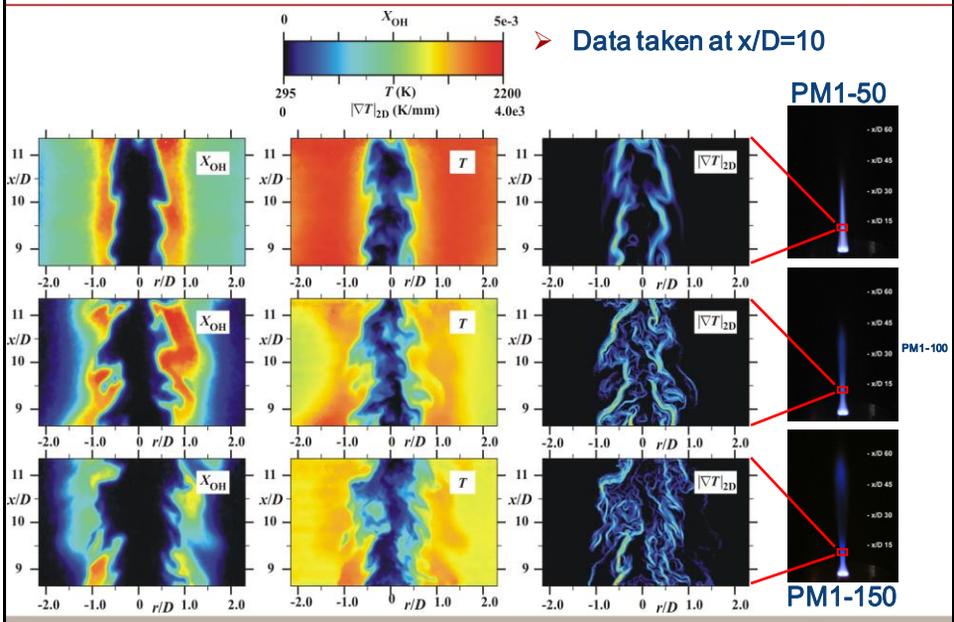
PPJB PM1 Flame Selection



- Transition for central jet velocities 50, 100, 150 and 200m/s:
 - ($Re \sim 12500, 25000, 37500$ and 50000), $T_{Coflow} = 1500K$, $\phi_{Jet} = 0.5$

TNF 11 Workshop, Darmstadt 2012

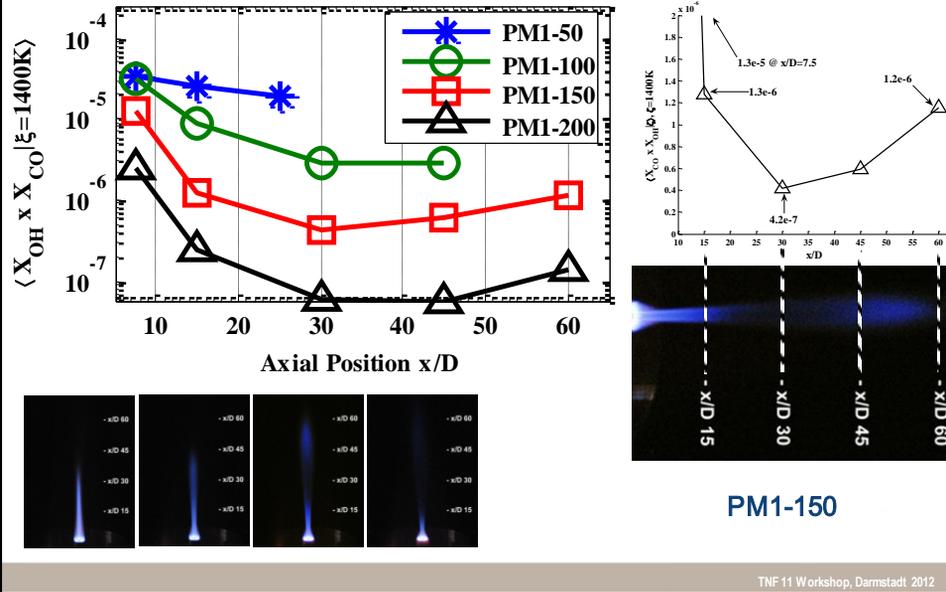
High Resolution Temperature-OH images



TNF 11 Workshop, Darmstadt 2012

Application of $\langle [CO][OH] \rangle_T$ to PM1 Flame Series

➤ Results for all flames $\langle [CO][OH] \rangle_{\xi=1400K}$



4 LES Contributions



V.N. Prasad^{#,**,*}, K.H. Luo and W.P. Jones

[#]Imperial College London
^{**}The University of Southampton
^{***}The University of Sydney



Varun Mittal
 Heinz Pitsch
 Stanford University

Contributors that
 will present own
 work



Yuntao Chen and Matthias Ihme
 Department of Aerospace Engineering
 University of Michigan



Christophe Duwig^{*,**}
^{*}Dept. of Energy Sciences, Lund University, Sweden
^{**}Haldor Topsøe A/S, DK-2800 Lyngby

TNF 11 Workshop, Darmstadt 2012

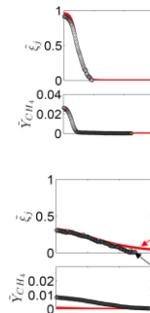
TNF10 Summary (2xLES, 2xPDF)

- **LES calculations (Lund/Stanford):**
 - All presented results first pass/preliminary
- **Conclusions**
 - **Stanford**
 - Need to implement tabulation for mixing
 - Need to model pilot chamfer
 - For the highest velocity cases, reaction progress over predicted
 - **Lund**
 - Good results for PM1-50 case
 - Questions raised over resolution requirements
 - Subsequent publication addressed the resolution requirements
 - Poor spatial resolution results in over predicted reaction rate (flame too short)

TNF 11 Workshop, Darmstadt, 2012

TNF10 Summary

- **RANS PDF calculations:**
 - Can predict the mixing fields well
 - Good results for the PM1-50 case
 - For the highest velocity cases, reaction progress over predicted
- **Questions raised:**
 - Suitability of chemical mechanisms
 - Subsequent publication showed no difference for San Diego mechanism
 - Mixing model deficient?
 - Implied scalar dissipation too low



PM1-150

TNF 11 Workshop, Darmstadt, 2012

TNF10 -> TNF11

- **Plan of attack: LES focusing on the following measures:**
 - **#1 Mixing fields (mixture fraction)**
 - **#2 Reaction progress fields (Temperature/CH₄ acceptable alternative)**
 - **#3 Reaction rate (CO, OH and <[CO][OH][T]>)**

TNF 11 Workshop, Darmstadt 2012

Lund LES Calculations



LUND
UNIVERSITY

Lund LES Calculations

Christophe Duwig^{*,**}

** Dept. of Energy Sciences, Lund University, Sweden*

*** Haldor Topsøe A/S, DK-2800 Lyngby*

*Primary contact Dr Christophe Duwig (Christophe.Duwig@energy.lth.se)

TNF 11 Workshop, Darmstadt 2012

Large Eddy Simulation using OpenFOAM

Customized solver based on the OpenFOAM library

reactingLMFoam

Filtered continuity and Navier-Stokes

low-Mach number assumption

pressure coupling is PISO

Smagorinski SGS closure

ideal gas assumption

Filtered specie- and enthalpy-equations:

$$\frac{\partial(\bar{\rho}\tilde{Y}_i)}{\partial t} + \nabla \cdot (\bar{\rho} \cdot \tilde{u} \tilde{Y}_i) = \nabla \cdot \left(\bar{\rho} \cdot \left(D_i + \frac{v_\Delta}{Sc_\Delta} \right) \nabla \tilde{Y}_i \right) + \omega_r(\tilde{Y}_j)$$

$$\frac{\partial(\bar{\rho}\tilde{h})}{\partial t} + \nabla \cdot (\bar{\rho} \cdot \tilde{u} \tilde{h}) = \nabla \cdot \left(\bar{\rho} \cdot \left(D_h + \frac{v_\Delta}{Pr_\Delta} \right) \nabla \tilde{h} \right)$$

ILES or

“no model”:

We resolve the reaction layer in the LES grid!!

HALDOR TOPSOE 

TNF 11 Workshop, Darmstadt, 2012

Large Eddy Simulation using OpenFOAM

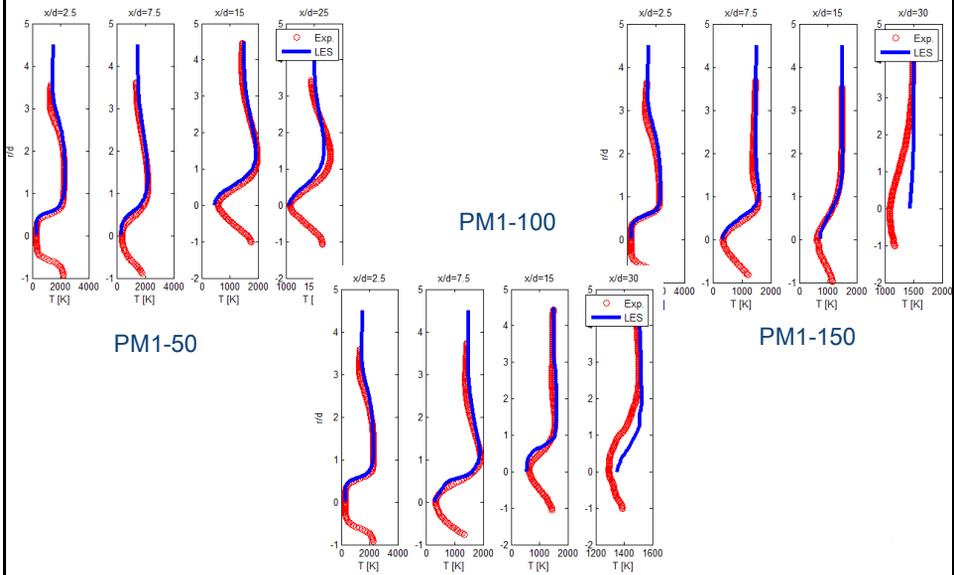
customized solver reactingLMFoam

• Numerical methods

- spatial discretization: second order
- temporal discretization: second order upwind
- solver CG with AMG-preconditioning for pressure
- Gauss-Seidel smoother
- ‘turbulent’ inflow conditions: vortex dipoles technique (Kornev&Hassel, PoF, 2007)

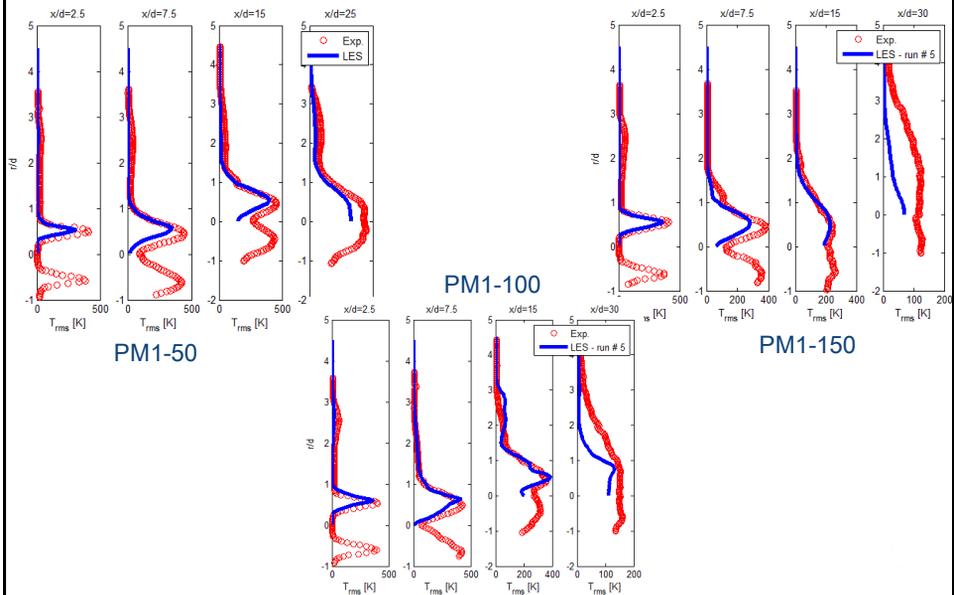
TNF 11 Workshop, Darmstadt, 2012

Lund LES: Mean Temperature

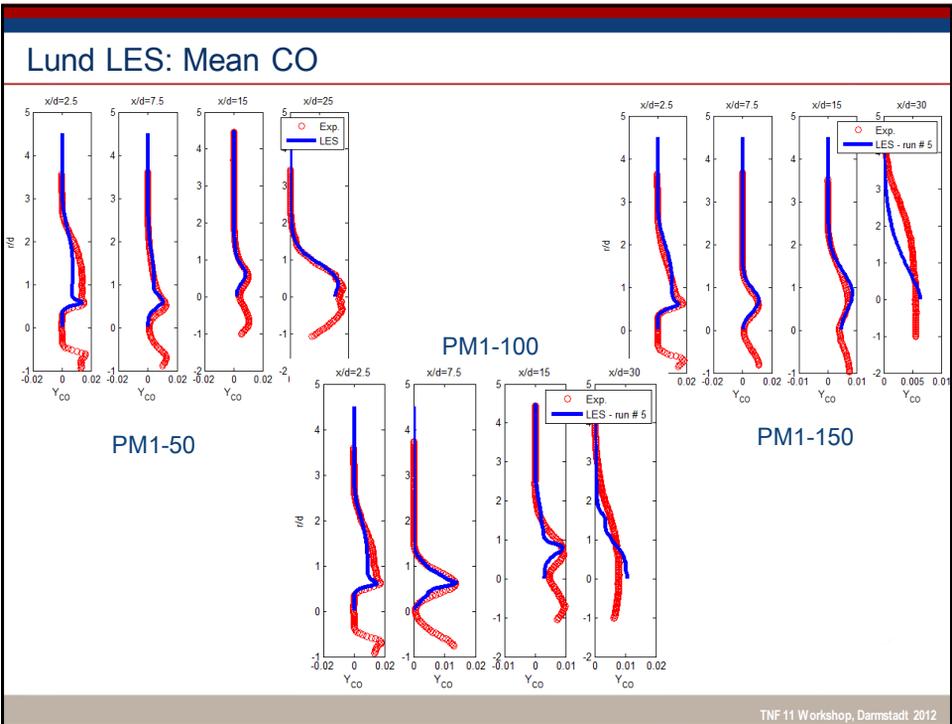
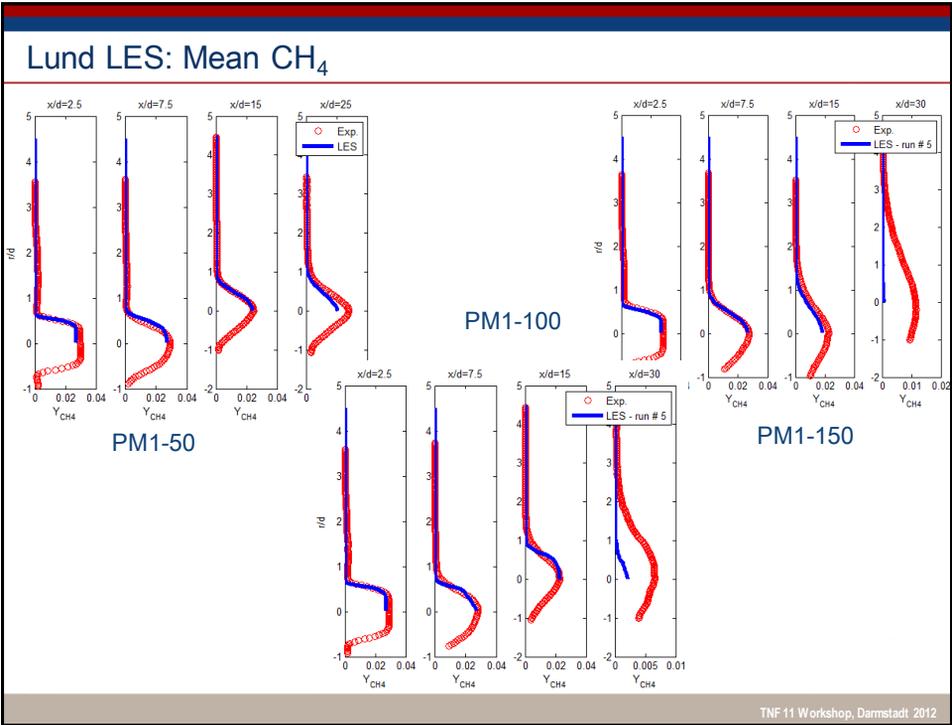


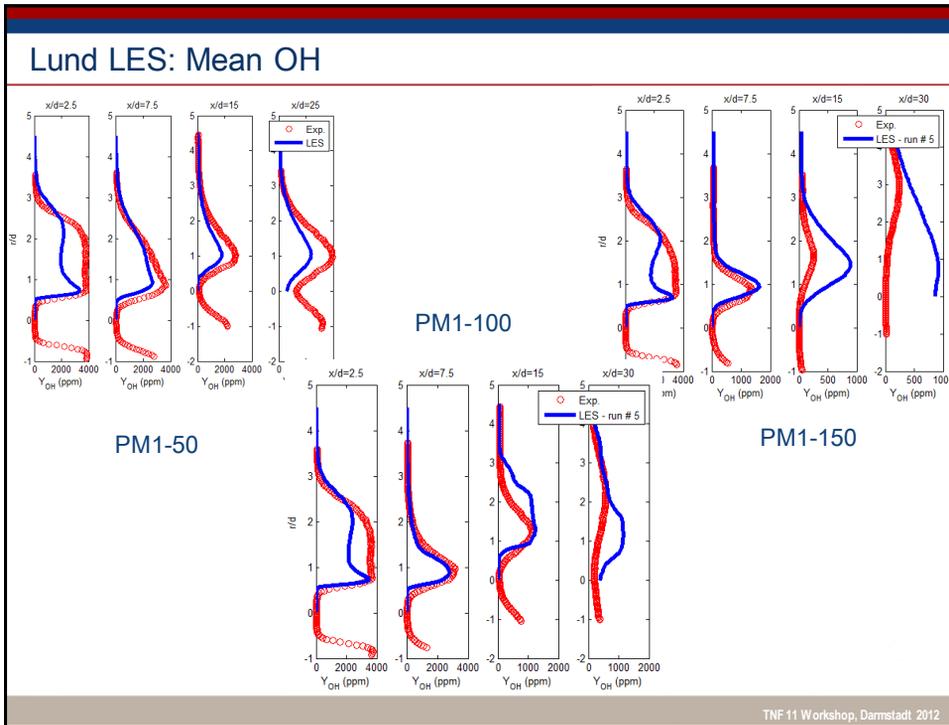
TNF 11 Workshop, Darmstadt 2012

Lund LES: RMS temperature



TNF 11 Workshop, Darmstadt 2012





Imperial College
London

UNIVERSITY OF
Southampton

LES-SF simulation of the PM1-x series

V.N. Prasad, K.H. Luo and W.P. Jones

Transported pdf approach

- joint scalar *sgs-pdf* contains all statistical moments (mean, variance etc.)

$$\tilde{P}_{sgs}(\boldsymbol{\psi}; \mathbf{x}, t) = \frac{1}{\bar{\rho}} \int_{\Omega} \rho G_{\Delta} \times \prod_{\alpha=1}^{N_s} \delta[\psi_{\alpha} - \phi_{\alpha}(\mathbf{x}', t)] d\mathbf{x}'$$

- sgs-pdf* can be obtained from modeled transport equation:

$$\begin{aligned} \bar{\rho} \frac{\partial \tilde{P}_{sgs}(\boldsymbol{\psi})}{\partial t} + \bar{\rho} \tilde{u}_j \frac{\partial \tilde{P}_{sgs}(\boldsymbol{\psi})}{\partial x_j} + \sum_{\alpha=1}^{N_s} \frac{\partial}{\partial \psi_{\alpha}} \left[\bar{\rho} \omega_{\alpha}(\boldsymbol{\psi}) \tilde{P}_{sgs}(\boldsymbol{\psi}) \right] = & \text{closed!!} \\ - \frac{\partial}{\partial x_j} \left[\left(\frac{\mu}{\sigma} + \frac{\mu_{sgs}}{\sigma_{sgs}} \right) \frac{\partial \tilde{P}_{sgs}(\boldsymbol{\psi})}{\partial x_j} \right] - \frac{\bar{\rho}}{2\tau_{sgs}} \sum_{\alpha=1}^{N_s} \frac{\partial}{\partial \psi_{\alpha}} \left[(\psi_{\alpha} - \tilde{\phi}_{\alpha}(\mathbf{x}, t)) \tilde{P}_{sgs}(\boldsymbol{\psi}) \right] & \text{LSME} \end{aligned}$$

- chemical source terms closed, but additional model term introduced (micro-mixing)

21

Stochastic field method

- pdf* reconstructed by an ensemble of Eulerian stochastic fields

$$\tilde{P}_{sgs}(\boldsymbol{\psi}; \mathbf{x}, t) = \frac{1}{N} \sum_{m=1}^N \frac{1}{\bar{\rho}} \int_{\Omega} \rho G(\mathbf{x} - \mathbf{x}', \Delta(\mathbf{x})) \times \prod_{\alpha=1}^{N_s} \delta[\psi_{\alpha} - \zeta_{\alpha}^m(\mathbf{x}, t)] d\mathbf{x}'$$

- transport equation by Valiño (1998):

$$\begin{aligned} \bar{\rho} d\zeta_{\alpha}^m = & - \bar{\rho} \tilde{u}_i \frac{\partial \zeta_{\alpha}^m}{\partial x_i} dt + \frac{\partial}{\partial x_i} \left[\Gamma_i' \frac{\partial \zeta_{\alpha}^m}{\partial x_i} \right] dt + \bar{\rho} \sqrt{\frac{2\Gamma_i'}{\bar{\rho}}} \frac{\partial \zeta_{\alpha}^m}{\partial x_i} dW_i^m \\ & - \frac{\bar{\rho}}{2\tau_{sgs}} (\zeta_{\alpha}^m - \tilde{\phi}_{\alpha}) dt + \bar{\rho} \omega_{\alpha}^m(\zeta^m) dt \end{aligned} \quad \begin{array}{l} \text{Wiener process} \\ dW = \mathcal{N}(0, 1) \Delta t^{1/2} \end{array}$$

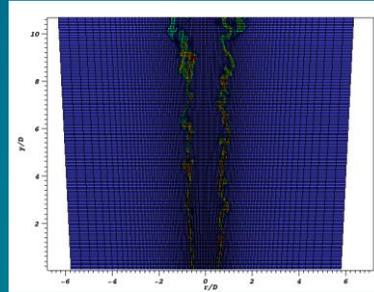
- statistical moments straightforward to compute:

$$\tilde{\phi}_{\alpha} = \frac{1}{N} \sum_{n=1}^N \zeta_{\alpha}^n$$

22

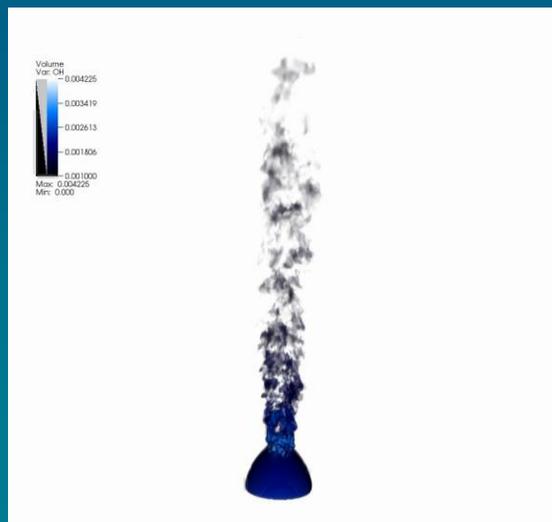
Modelling and numerics

- LES code BOFFIN developed by Bill Jones at Imperial College
- inflow generator by Klein *et al.*
- GRI 3.0 reduced mechanism by Sung *et. al* (15 steps, 19 species)
- 4.8 M cells (30 cells in jet)
- 8 stochastic fields, CD=2.0



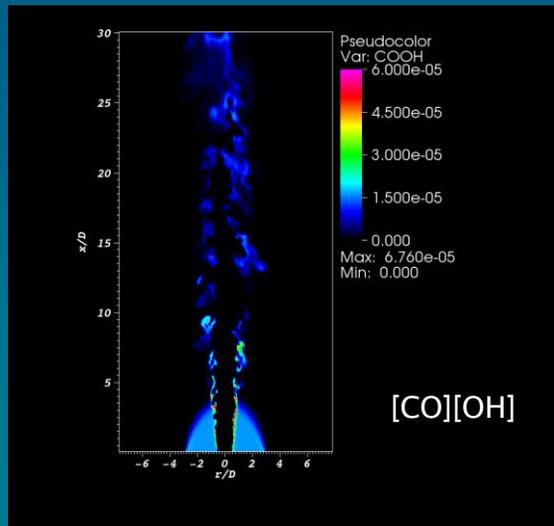
23

3d animation of OH (PM1-200)



24

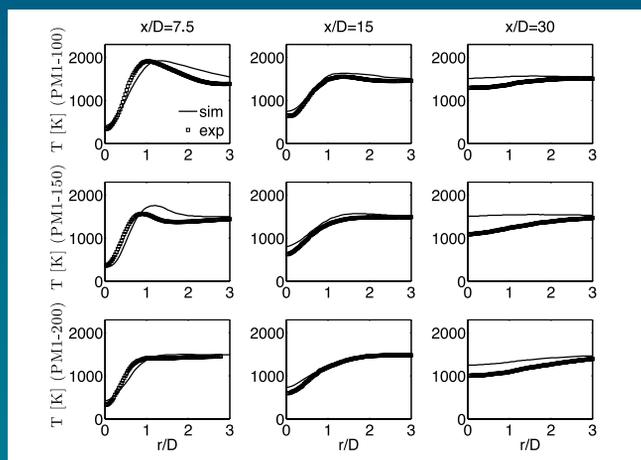
Snapshot (PM1-150)



25

Mean radial temperature profiles

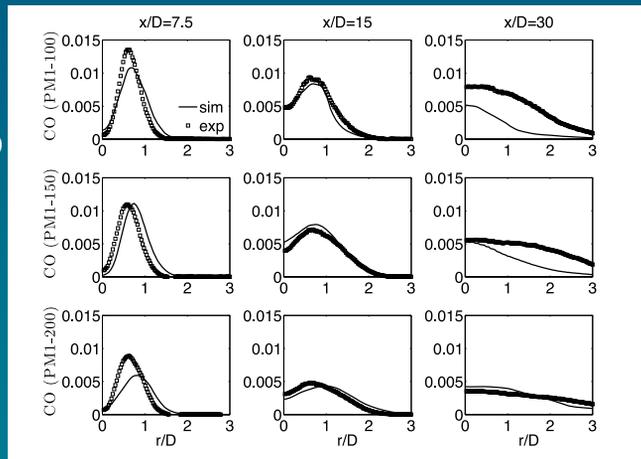
- Spreading captured well
- Flame too short!



26

Mean CO radial profiles

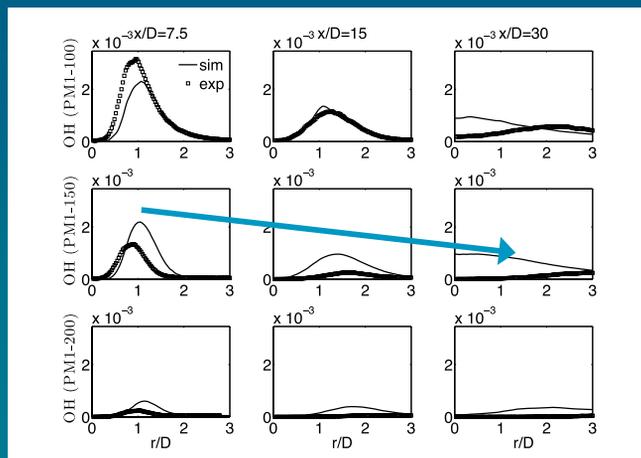
- CO profiles overall in good agreement up to $x/D=15$



27

Mean OH radial profiles

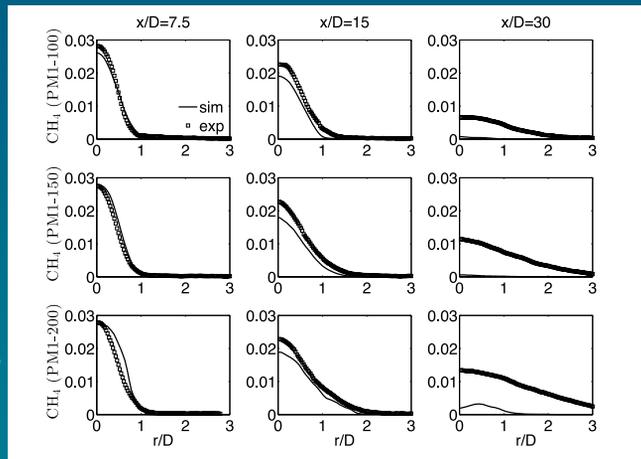
- OH decay reproduced
- OH depression much less pronounced than in experiment



28

Mean CH4 profiles

- Fuel consumption good up to $x/D=15$
- Excessive fuel consumption from $x/D=15$ to 30



29

Conclusions and Outlook

- Basic features reproduced
 - Simulation results consistent for all three flames
 - Dip in reaction rates from $x/D=7.5$ to $x/D=15$
 - Flames too short for all three cases
- How can we further reduce reaction rates?
 - “global” problem (grid...)?
 - Sub-grid problem (number of fields, micro-mixing)

30



Flame Characterization of a Piloted Premixed Jet Burner

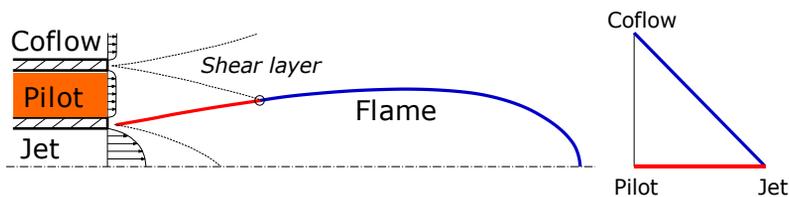
Yuntao Chen and Matthias Ihme

*Department of Aerospace Engineering
University of Michigan*

Flamelet Formulation for 3-Stream Combustion



- Extension to multi-stream systems

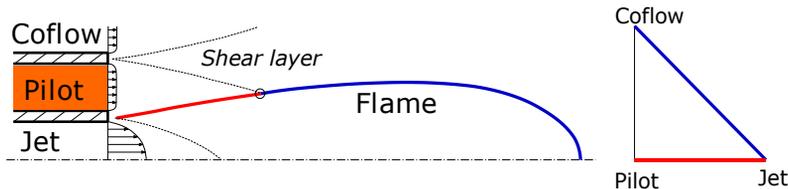


- Flame is established between fuel and oxidizer streams having different compositions
- Flamelet formulation remains valid; requires **consideration of local composition** in fuel and oxidizer streams

Flamelet Formulation for 3-Stream Combustion



- Extension to multi-stream systems



- Modeling approach:
 - Introduce additional scalar to account for variations in oxidizer streams

$$\psi(Z=0) = \psi^{\text{Oxi}}(W)$$

- Oxidizer split W

$W = 0$: In Pilot Stream

$W = 1$: In Coflow Stream

33

Presumed PDF-closure



- The chemistry-turbulence interaction is modeled through a presumed PDF approach
- Two-dimensional Dirichlet distribution is used
 - Mixture fraction Z and oxidizer split W live in a unit triangle
 - PDF is given as

$$P(Z, W) = \frac{\Gamma(a+b+c)}{\Gamma(a)\Gamma(b)\Gamma(c)} Z^{a-1} W^{b-1} (1-Z-W)^{c-1}$$

- a , b , and c are parameters determined from the mean and variances of Z and W
- Progress variable C is assumed to follow a delta distribution

34

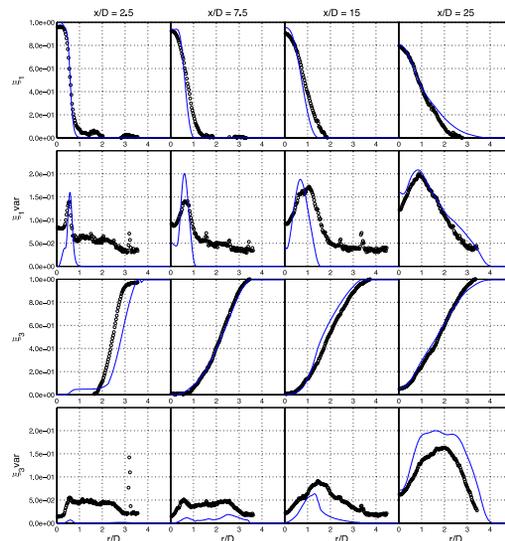
Computational Setup



- 3D cylindrical simulation domain
 - Computational domain: $60 D_{\text{ref}}$ (axial), $20 D_{\text{ref}}$ (radial), 2π (azimuthal)
 - Mesh size: 256 (axial), 280 (radial), 64 (azimuthal)
 - Total grid points: **4.6 million**
- Velocity profile
 - Central jet: turbulent pipe flow ($Re = 12500 \sim 37500$)
 - Pilot and coflow: tanh profile
- Chemical compositions calculated by CHEMKIN
 - Detailed chemistry for Methane-Air reaction
 - GRI-MECH 3.0: 50 species and 250 reactions
- Precomputed chemistry using steady-state flamelet solution

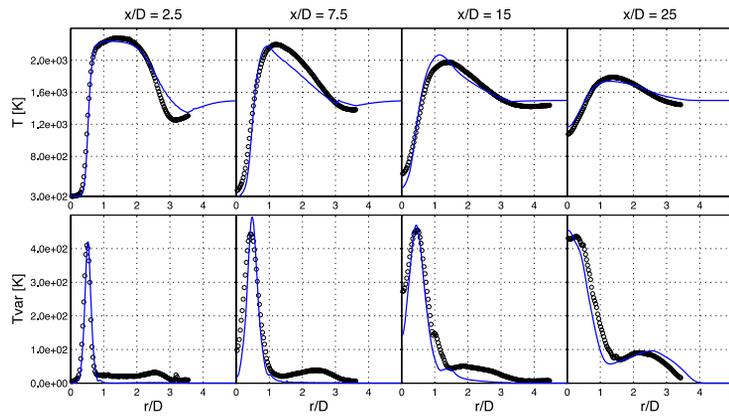
35

Results (PM1-50) Mixture Fraction (ξ_1, ξ_3)



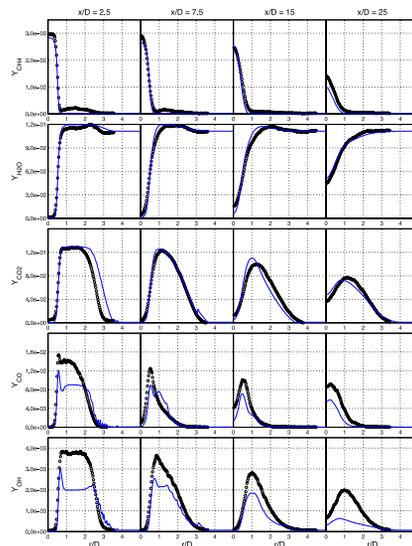
36

Results (PM1-50) Temperature



37

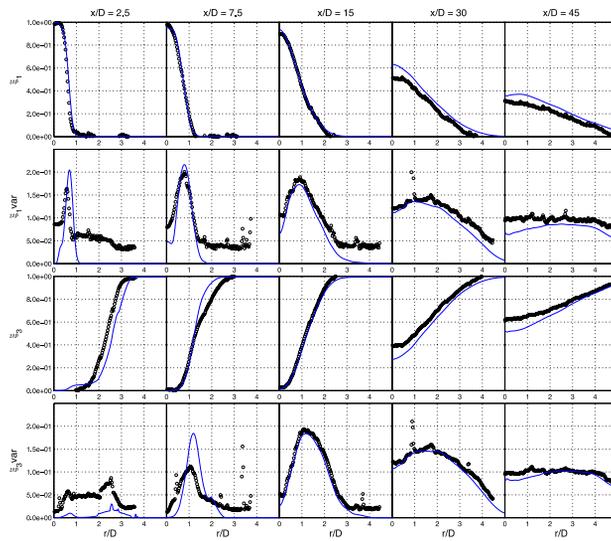
Results (PM1-50) Species



38

Results (PM1-100)

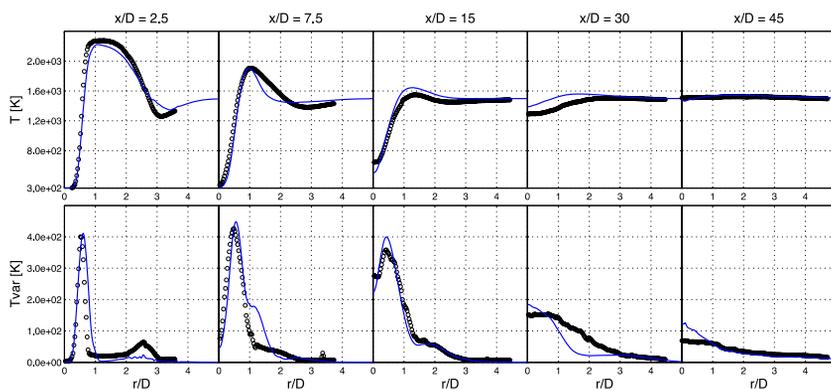
Mixture fractions (ξ_1, ξ_3)



39

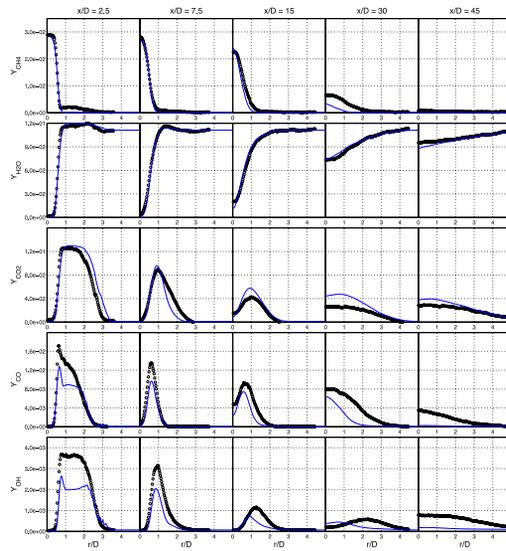
Results (PM1-100)

Temperature



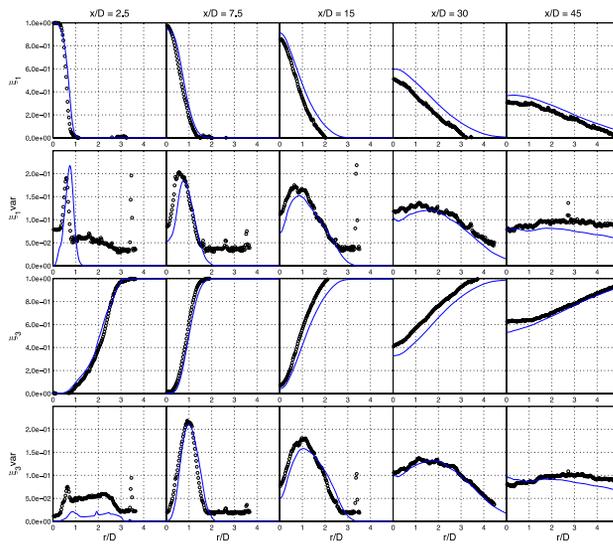
40

Results (PM1-100) Species



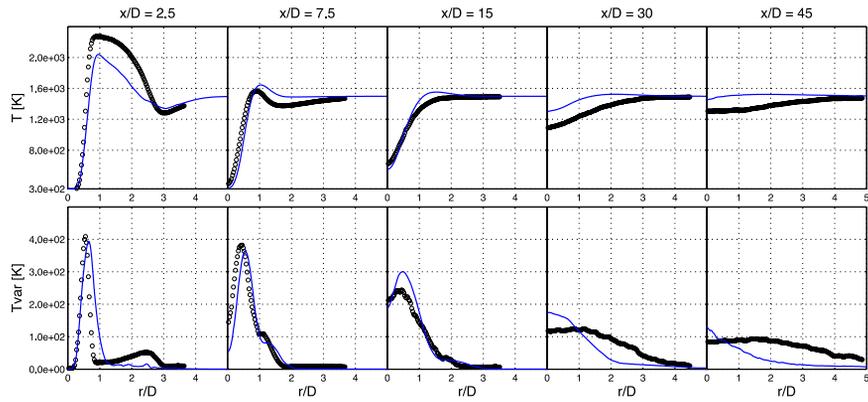
41

Results (PM1-150) Mixture fractions (ξ_1, ξ_3)



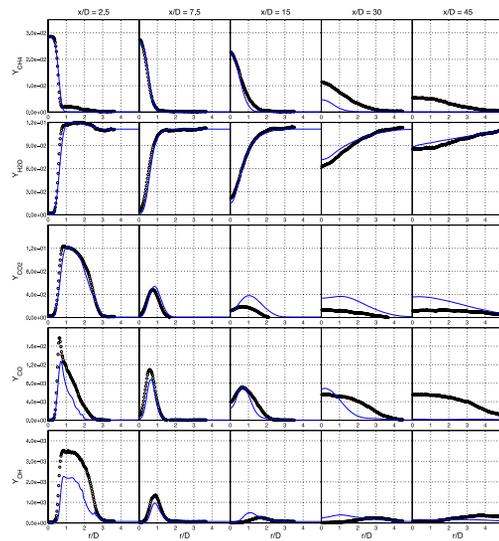
42

Results (PM1-150) Temperature



43

Results (PM1-150) Species



44



Simulation of Piloted Premixed Flames with Strong Finite Rate Chemistry

Varun Mittal
Heinz Pitsch

Stanford University

TNF Session, 2012

Jul 25th, 2012

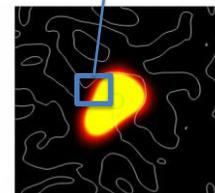
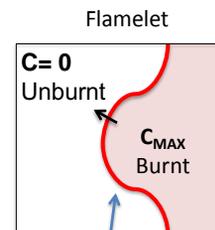
Steady Premixed Flamelet Model



- Combustion aligned with gradients in reaction progress, C
 - C : Sum of product mass fractions
 - $C = 0$: Unburnt, $C \sim 0.3$: Burnt
- Combustion happens on small length scales
- Combustion timescales are fast compared to the flow timescale
- Model combustion as *steady* 1D 'flamelets' along the arrows

$$\cancel{\frac{\partial (\rho Y_i)}{\partial t}} + \frac{\partial (\rho v_j Y_i)}{\partial x_j} = \frac{\partial}{\partial x_j} \left(\rho D \frac{\partial Y_i}{\partial x_j} \right) + \rho \dot{w}_i$$

- Solution precomputed along 1D with exact chemistry
- Transform to C direction : $x_j \rightarrow C$
- Include mixture fraction Z for different fuel/air ratios



Temperature Profile

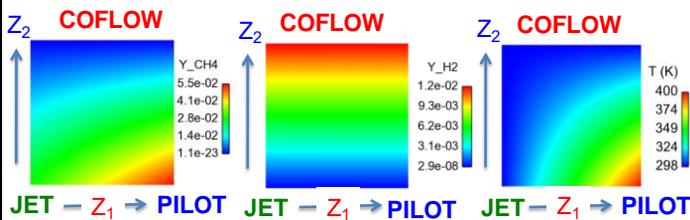
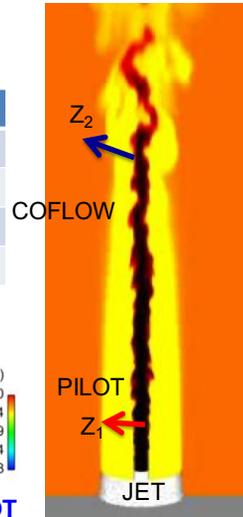
Jul 25th, 2012

Model Extension for Jet Flame



- Traditional mixture fraction cannot be used due to multiple streams/multiple fuel
- Two different mixture fractions used here

	Stream				Z1		Z2	
	Fuel	State	phi	Tu (K)	0.0	1.0	0.0	1.0
JET	CH ₄	Unburnt	0.5	298	1.0	0.0	1-Z1	0.0
PILOT	CH ₄	Burnt	1.0	400	0.0	1.0	Z1	0.0
COFLOW	H ₂	Burnt	0.43	298	0.0	0.0	0.0	1.0

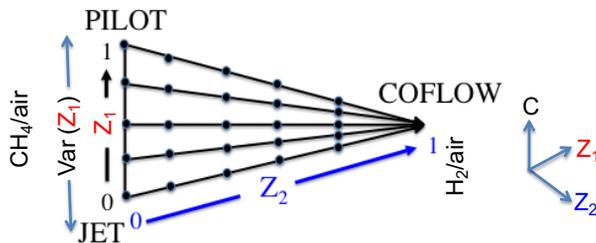
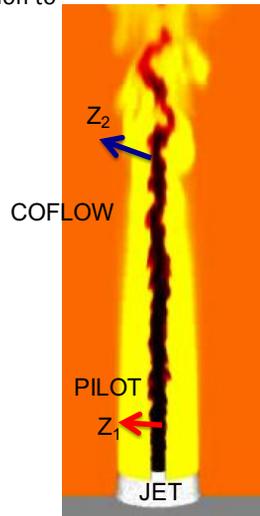


Jul 25th, 2012

Model Setup



- Unstretched premixed flamelets solved at each circle location to obtain chemical solutions
 - Boundary conditions obtained by linear mixing at each location
- 4D tabulation based on Z_1 , Z_2 , $\text{Var}(Z_1)$ and C
 - Table resolution : 50x30x30x50
 - Variance of Z_2 ignored

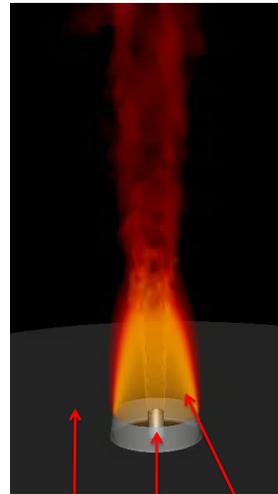


Jul 25th, 2012

Simulation Parameters



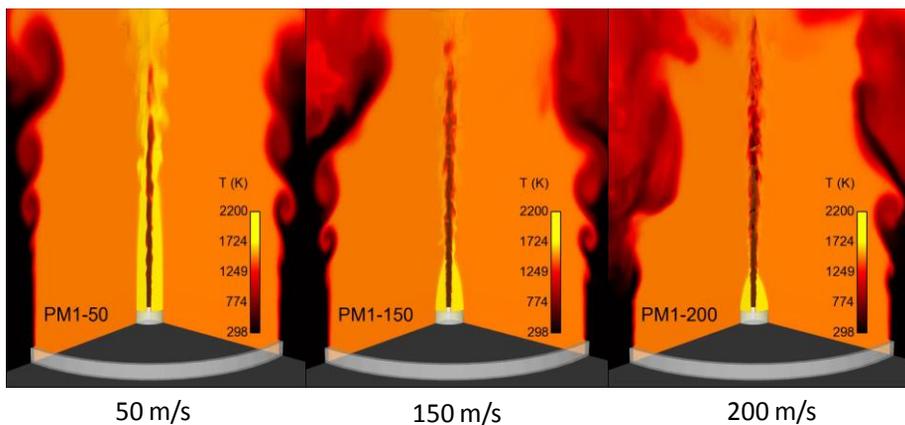
- GRI-3.0 chemical mechanism
- Different grid points in simulation
 - 4 million
 - 9 million
- 3D Domain
 - Periodic in third direction
- Run on 192 processors
- Cold flow velocity comparisons done
- Variable density non-reactive velocity comparisons done
- Similar results with both meshes



COFLOW JET PILOT

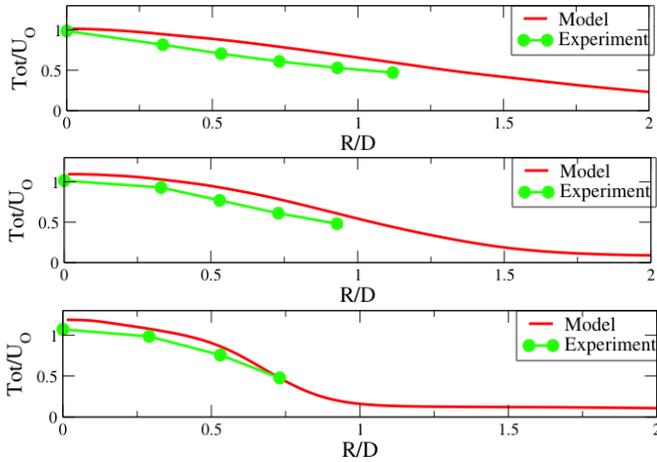
Jul 25th, 2012

Simulation Results



Jul 25th, 2012

Velocity : PM1-50



Jul 25th, 2012

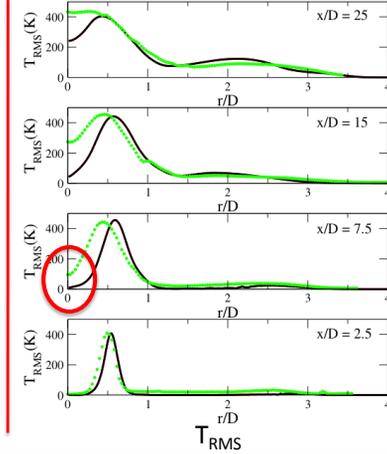
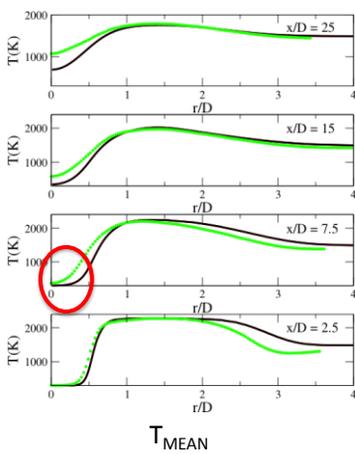


Temperature : PM1-50

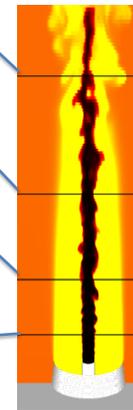


- Lower burning along centerline
- Smaller T fluctuations along centerline

— Model
• Experiment



Jul 25th, 2012

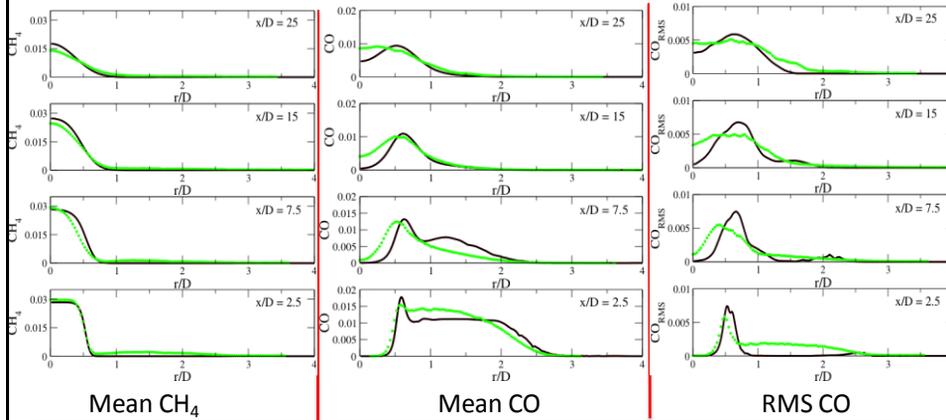


Species : PM1-50



- Consistent with temperature comparison
- Effect of buoyancy, level set, Lewis numbers analyzed
- No significant change due to any of them

— Model
• Experiment



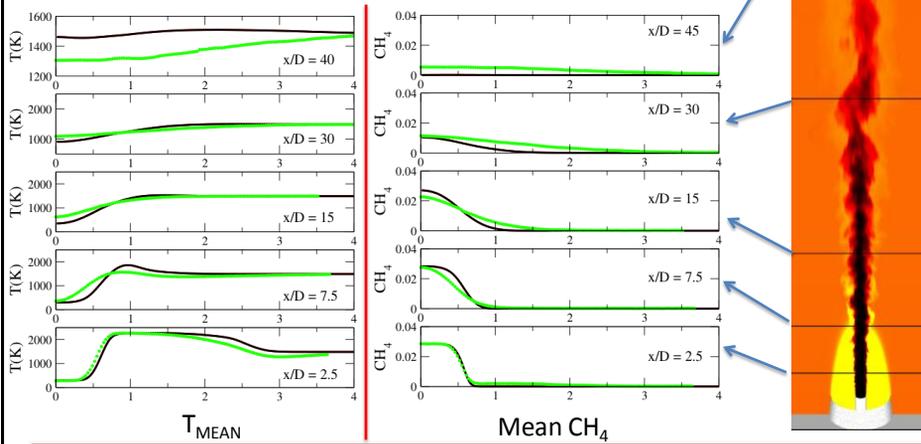
Jul 25th, 2012

Comparison : PM1-150



- Similar issues along centerline
- Extinction around $x/D = 45$ in experiment

— Model
• Experiment



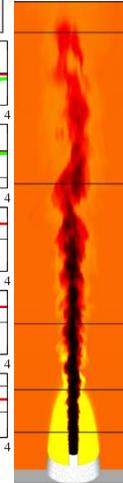
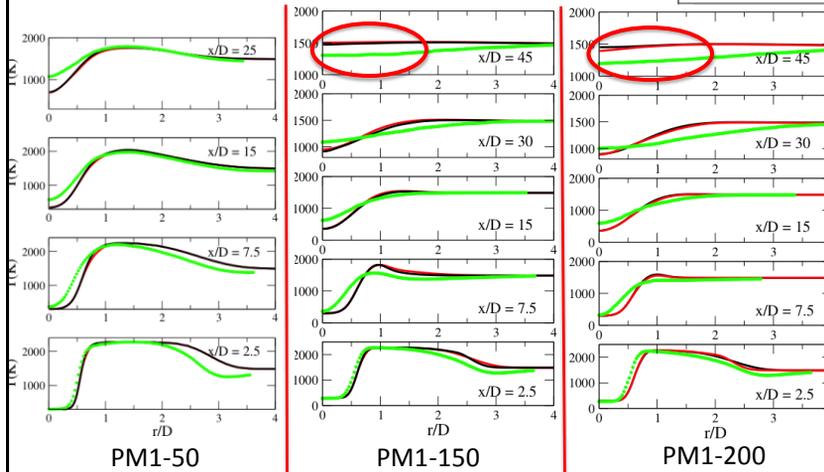
Jul 25th, 2012

Mean Temperature



- Good agreement close to the nozzle
- Extinction not captured accurately

— No LVL
— LVL
• Exp



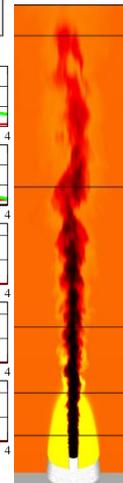
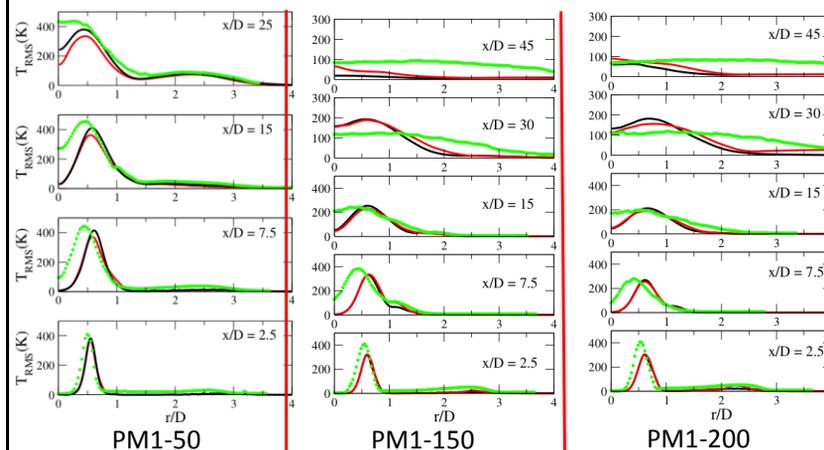
Jul 25th, 2012

Temperature RMS



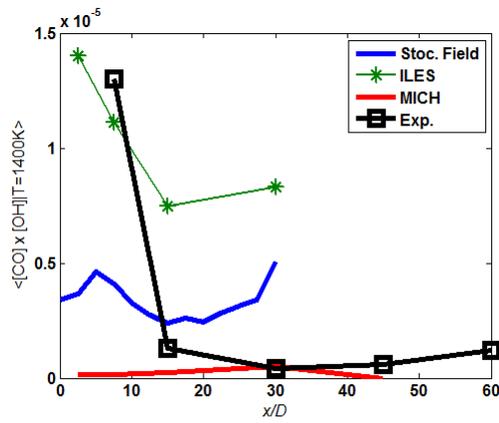
- Centerline temperature RMS is under predicted
- Velocity fluctuations agree well
- Various effects investigated (Lewis number, buoyancy)

— No LVL
— LVL
• Exp



Jul 25th, 2012

PM1-150 LES: Reaction rate for 3/4 simulations



- No model correctly predicts the rate of extinction as function of axial distance, hence flame length is predicted to be too short

TNF 11 Workshop, Darmstadt, 2012

LES Discussion

- Similarities between modeling approaches and results
- Have we now established the “limits” of flamelet/tabulation LES?
- Close to the burner exit all get good results
- Why is extinction still under-predicted and higher velocity flames predicted to be too short?
- Has LES shown greater predictive capability compared to RANS PDF?

TNF 11 Workshop, Darmstadt, 2012

TNF11

Session on Chemistry, Complex Fuels and New Combustion Modes

Coordinated by Peter Lindstedt and Dirk Roekaerts

Part 1. Chemistry and Complex Fuels

Presented by R.P. Lindstedt

The first part of the session considered alternative fuels. There has been a long-standing ambition for the TNF community to consider alternative fuels and consideration has been given to a number of options. At TNF10, the latter were reviewed and it was decided to consider alternative fuels by gradually including increasingly comprehensive data sets for DME and ethanol. This combination is particularly attractive as DME is a potential fuel for Diesel engines, while ethanol is already used extensively as a bio-derived fuel additive for gasoline. Furthermore, both fuels are comparatively simple, have the same molecular weight and their different properties hence stem from the chemical structures.

The review presented at TNF11 considered DME and covered a number of different aspects such as a new DME flame series, analogous to the Sandia A-F flame series that has formed one of the cornerstones of the TNF community, some of the chemistry background, modeling efforts and the influence of differential diffusion in the context of transport approximations.

To date, corresponding work on ethanol flames has not been performed. It is in this context important to note that as usual the TNF community serves to identify and encourage collaborative research, but cannot provide direct funding streams.

A DME Flame Series

Perhaps the key reason for the success of the TNF community has been the ability to evaluate the importance of turbulence-chemistry interactions in a coherent framework that is inclusive and permits a focus on the primary topic while reducing other complexities. In this context, the Sandia A-F flame series has served as a key component and it is particularly important that the corresponding data sets are now in the process of being extended to alternative fuels. The experimental work on the new DME A-G flame series currently features a collaboration between Sandia National Laboratory (Barlow, Coriton, Frank, Magnotti), Ohio State University (Fuest, Sutton) with further contributions expected from TU Darmstadt and UT Austin.

The applied diagnostics at Sandia includes velocity, LIF and Rayleigh scattering at low repetition rates as well as flame imaging at high repetition rates with Raman spectroscopy and line measurements of temperature and species pursued in collaboration with the other institutions mentioned. Some of the work has been published by Fuest et al. [1].

The overview presentation outlined the experimental setup with examples of preliminary data from DME Flame D with a $Re \sim 27,000$.

- **Slides 6-8.**

Mean and rms of species mole fractions at $x/d = 1$ and $x/d = 40$ are shown along with an analysis of a preliminary scatter plot of temperature at $x/d = 10$. The latter highlights an area of particular experimental uncertainty at mixture fractions in the range 0.5 – 0.9 due to potential interference and non-detectable hydrocarbons. A significant deviation from a laminar flamelet computation is also noted in this region and may be linked to either the experimental uncertainties or difficulties associated with aspects of the chemistry such as thermal decomposition reactions.

- **Slides 11-14.**
Differences between the behavior of DME and CH₄ for partially premixed flames at the same stoichiometric mixture fraction have been clearly outlined and substantial changes in the extinction strain rates observed.
- **Slides 15-16.**
The significant role of formaldehyde in the chemistry of DME has been highlighted along with the diagnostic challenges.

The Chemistry of DME

The chemistry of DME has been covered comparatively extensively by several groups with proposed mechanisms available. The latter include the work by Kaiser et al. (2000) and Zhao et al. (2008) as outlined by Fuest et al. [1].

- **Slides 19-22.**
There has also been a number of experimental low-pressure premixed flame studies with the work by Cool et al. (2007) (T.A. Cool, K. Wang, N. Hansen, P.R. Westmoreland, F.L. Dryer, Z. Zhao, A. Kazakov, T. Kasper and K. Kohse-Höinghaus, (2007) Proc. Combust. Inst. 31:285-293) selected to serve as an illustration of current capabilities (computations by S.W. Park, PhD Thesis, Imperial College, 2012). The work illustrates the key initial branching of DME leading to either methoxy (CH₃O) or formaldehyde (CH₂O). Both pathways lead to the methyl radical and intermediate species remain computed with good accuracy. However, there are indications that the initial branching remains less well reproduced than desirable – particularly given the very different reactivities of methoxy and formaldehyde – and hence some updating of the chemical mechanisms may be required.
- **Slides 23-26.**
The impact of differences in combustion chemistry is further highlighted by the LES-CMC computations performed at ITV Stuttgart by Kronenburg and co-workers with very significant differences obtained in formaldehyde concentrations depending on the chemical mechanism used. The work thus further emphasizes the need to revisit key initial branching ratios.
- The need for accurate reduced mechanisms of DME remains a priority and should arguably form a focus point ahead of TNF12.

The Impact of Transport Approximations

The impact of transport approximations (differential diffusion) upon the ability predict DME flame structures was investigated in a collaboration between TU Bergakademie Freiberg, Engler-Bunte-Institute KIT and TU Darmstadt.

- **Slides 27-31.**
The work shows that differential diffusion effects are non-negligible and that problems in predicting the outer regions of the flames measured by Fuest et al. [1] are present.

Conclusions

Significant steps are being taken towards the inclusion of DME as an alternative reference fuel in the TNF community. It is hence expected that a substantial body of work will be available for review at TNF12.

Alternative Fuels: DME - Summary

TNF 11, Darmstadt, Germany, July 26 – 28, 2012

Peter Lindstedt and Dirk Roekaerts

Objective

Objective

- Assess where we stand in terms of our ability to predict DME flames.

1D species and temperature measurements in new DME flame series A-G

Frederik Fuest, Jeffrey A. Sutton
The Ohio State University

Robert S. Barlow, Gaetano Magnotti
Sandia National Laboratory



Department of Mechanical and
Aerospace Engineering



Outline

- Experimental setup
- Preliminary data, DME flame D, $Re \sim 27000$
- Heights: $x/d = 1, 5, 10, 20, 40$
- Spatial mean and rms profiles of species, temperature and mixture fraction
- Example scatter plot of temperature at $x/d = 10$



Department of Mechanical and
Aerospace Engineering

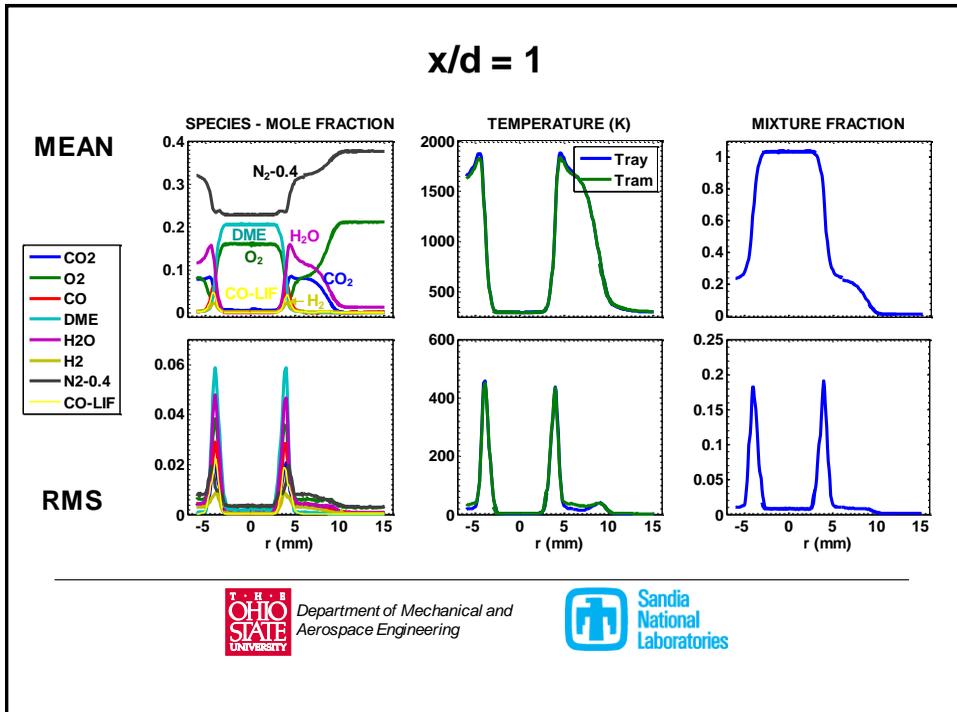


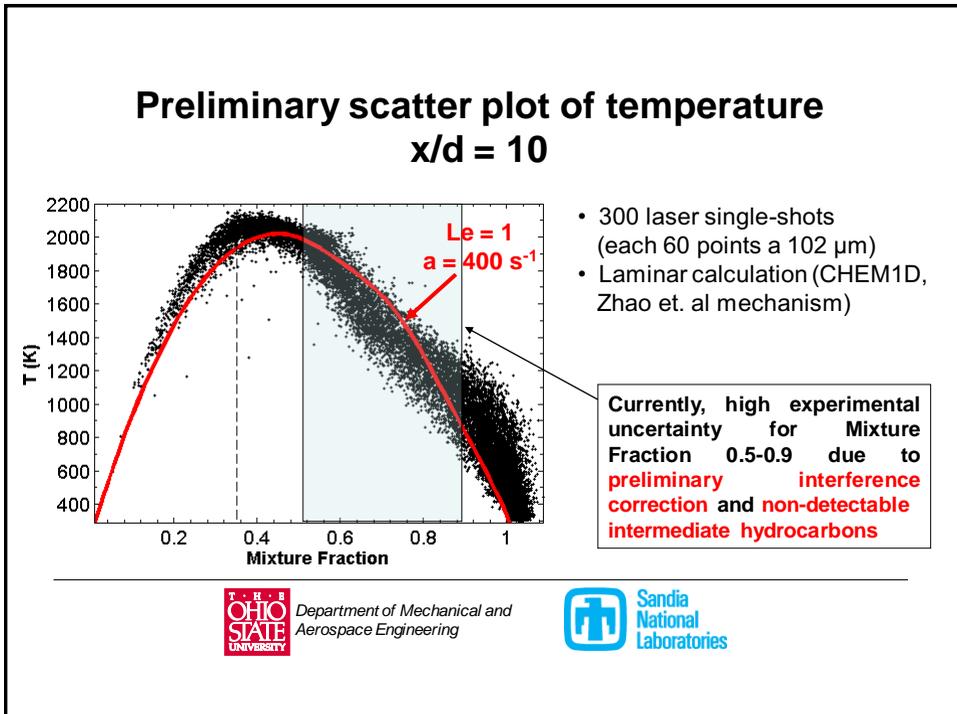
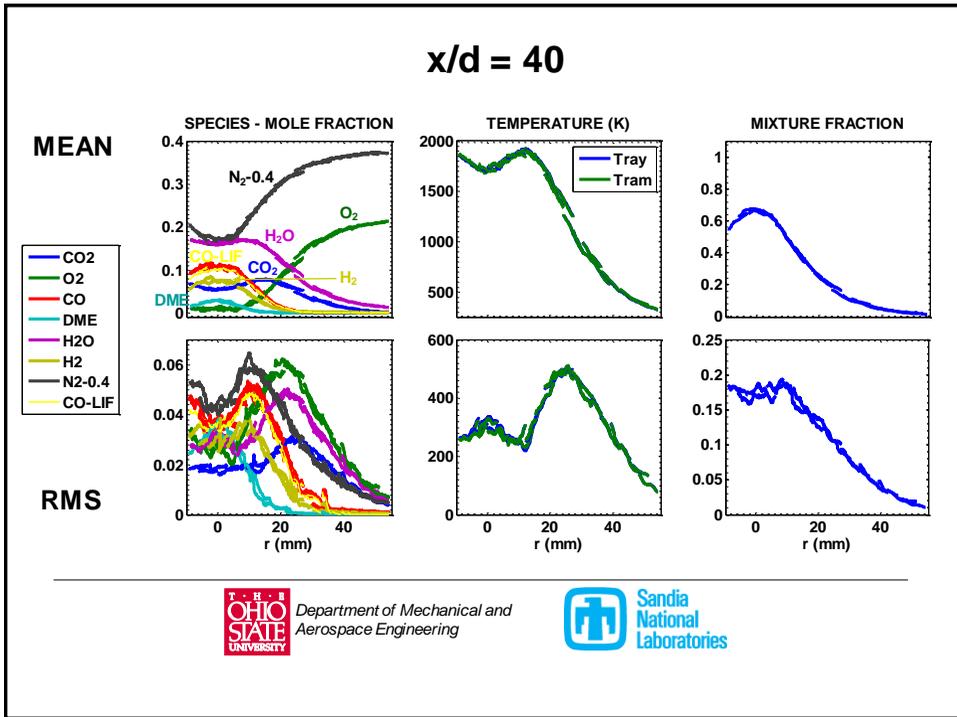
Experimental setup Sandia National Laboratory

- Raman scattering for major species concentrations
- Rayleigh scattering for temperature measurement
- Laser Induced Fluorescence of CO (CO-LIF)
- 1D probe volume length: 6 mm
- Laser beam diameter: $\sim 200 \mu\text{m}$ ($1/e^2$)
- Spatial resolution: $102 \mu\text{m}$
- Sandia piloted jet burner $d = 7.2 \text{ mm}$



Department of Mechanical and
Aerospace Engineering





Future work

- Improvement of interference correction
- Addressing limitations due to non-detectable intermediate hydrocarbons (according to Fuest et. al CNF 159:2533–2562, 2012)
- Further checks of flow rates, fuel/air ratios, pilot compositions
- DME flames E-G
- Development of new data processing techniques for accessing intermediate hydrocarbons

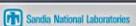


Department of Mechanical and
Aerospace Engineering



New Target Flame Series: Turbulent Partially Premixed Piloted Dimethyl Ether/Air Jet Flames

Jonathan Frank, Bruno Coriton
*Combustion Research Facility
Sandia National Laboratories
Livermore, CA*





Turbulent Partially Premixed Piloted DME/air Jet Flames



- Target flames for studying turbulence-chemistry interactions in combustion of an oxygenated fuel
- Series of jet flames with varying probabilities of localized extinction
- Analogous to Sandia piloted CH₄/air jet flames, using the same piloted Sydney burner






Comparison of DME-air and CH₄-air flame series

Fuel mixture: 20% DME, 80% air

Flame	Re_d
D	~27,200
E	~40,700
F	~54,300
G	~68,000

$\xi_{st} = 0.353$

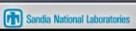
pilot: 2% power of main flame
 $\phi = 0.60$

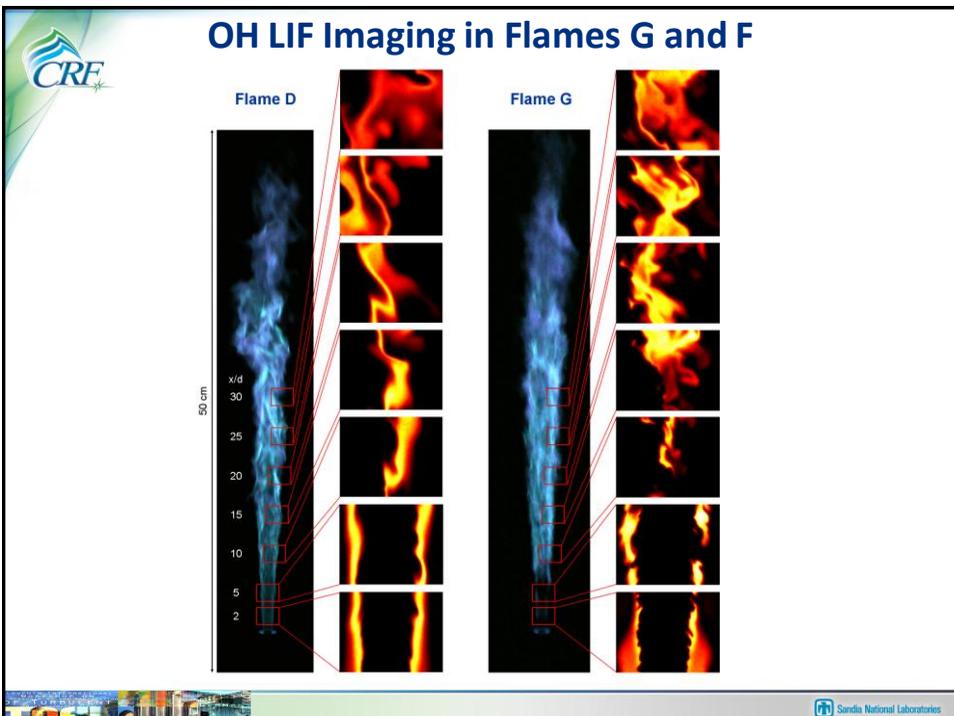
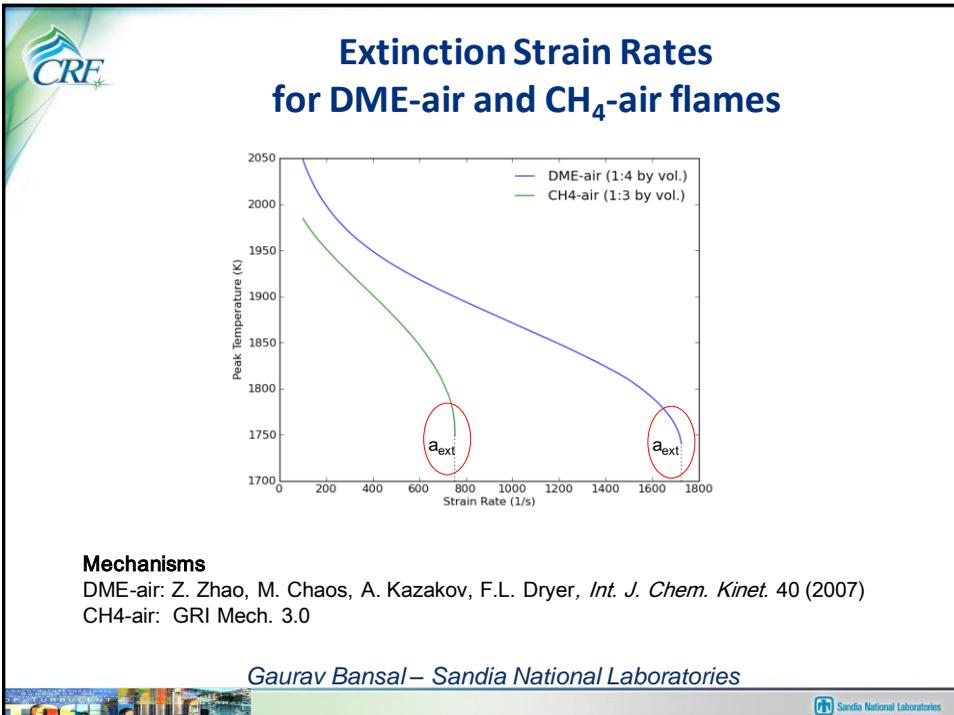
Fuel mixture: 25% CH₄, 75% air

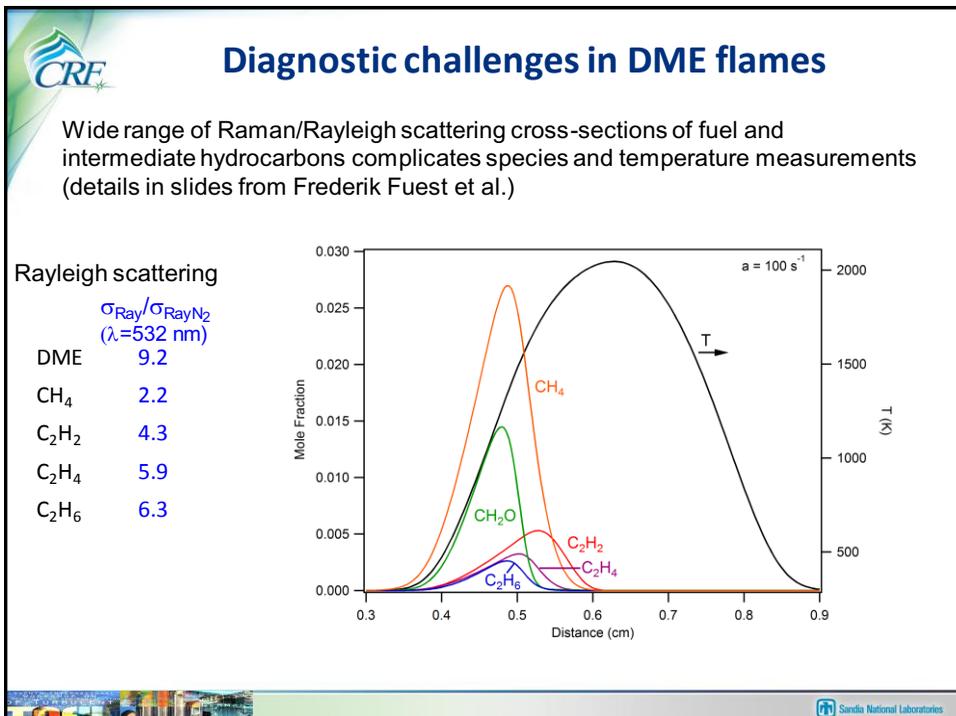
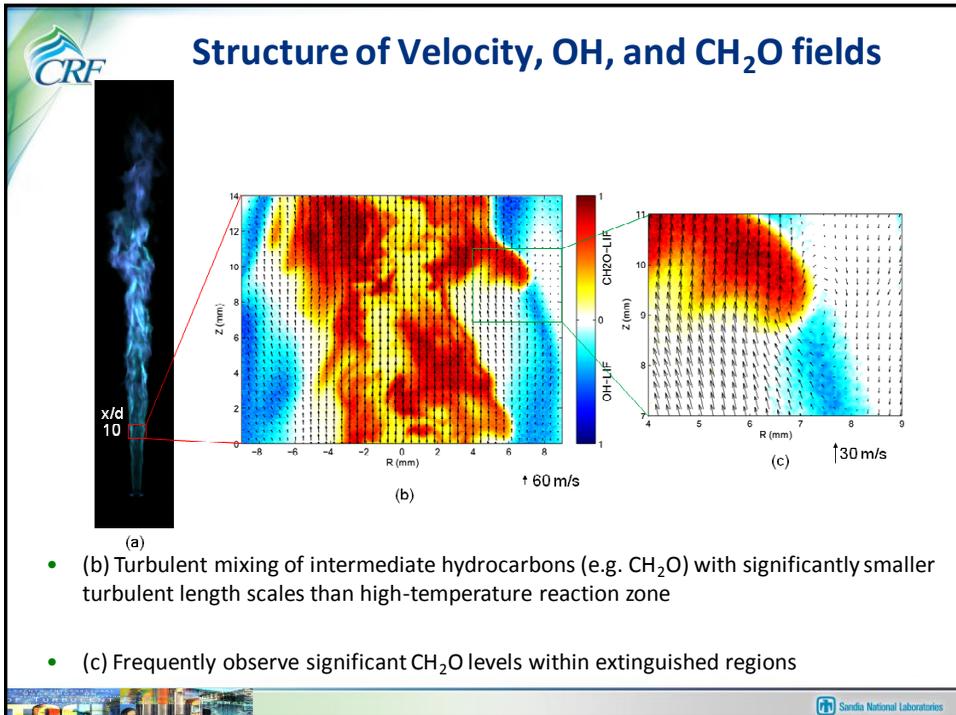
Flame	Re_d
C	~13,400
D	~22,400
E	~33,600
F	~44,800

$\xi_{st} = 0.353$

pilot: 6% power of main flame
 $\phi = 0.77$

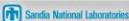






Current Efforts on DME/Air Jet Flames

- Imaging measurements (Sandia)
 - Low rep-rate velocity, LIF, Rayleigh scattering
 - High rep-rate imaging of flame dynamics
- Raman spectroscopy and line measurements of temperature/species (Sandia, TU Darmstadt, Hochschule Darmstadt, OSU, UT Austin)
- Simulations using LES/CMC (Stuttgart University)
- Others?

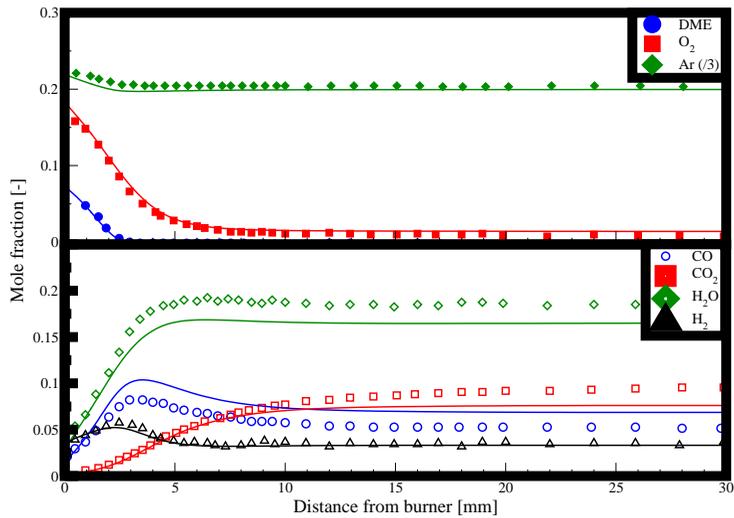


Imperial College
London

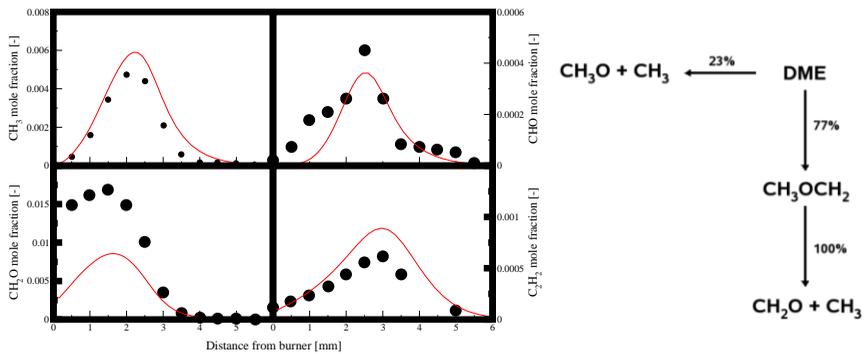
Chemistry Work

- Previous mechanisms for DME have good points and tend to work quite well.
- Some issues arise in terms of species predictions and with respect to major branching ratios.
- Some examples given.

**Low Pressure Flat Flame – Fuel Rich ($\Phi = 1.2$) DME Mixture
(Data from Cool et al. 2007)**

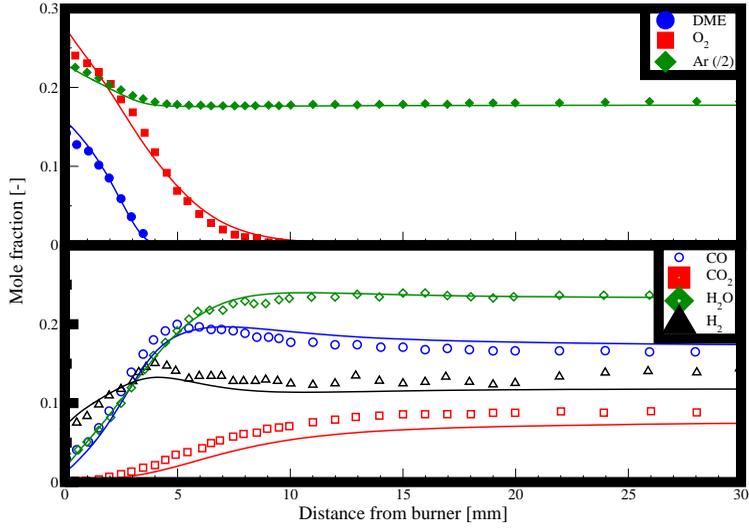


**Low Pressure Flat Flame – Fuel Rich ($\Phi = 1.2$) DME Mixture
(Data from Cool et al. 2007)**

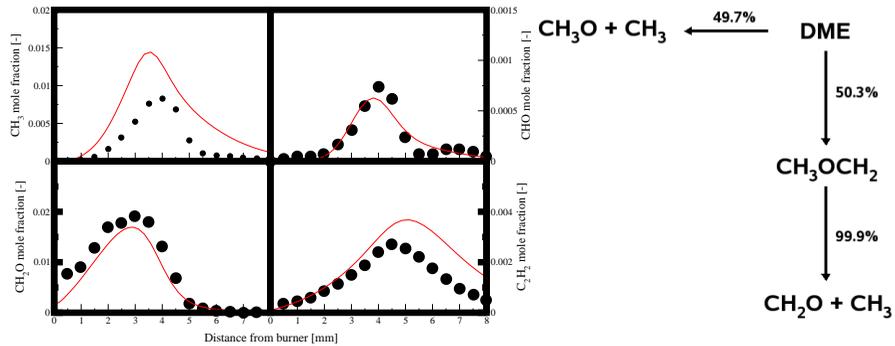


Minor species well reproduced. The formaldehyde concentration a bit low which may point to some uncertainties in branching and the methoxy chemistry. However, overall good agreement.

**Low Pressure Flat Flame – Fuel Rich ($\Phi = 1.68$) DME Mixture
(Data from Cool et al. 2007)**



**Low Pressure Flat Flame – Fuel Rich ($\Phi = 1.68$) DME Mixture
(Data from Cool et al. 2007)**



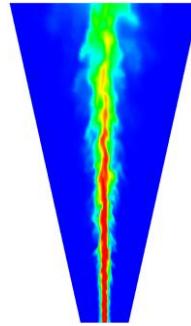
Minor species well reproduced. The formaldehyde concentration is satisfactory which along with the increased branching to methoxy may suggest a remaining issue with the initial DME branching.

LES-CMC of a turbulent piloted DME/air jet flame

Masoomeh Zendeheel
Satoshi Ukai
Oliver Stein
Andreas Kronenburg

Institut für Technische Verbrennung
Universität Stuttgart

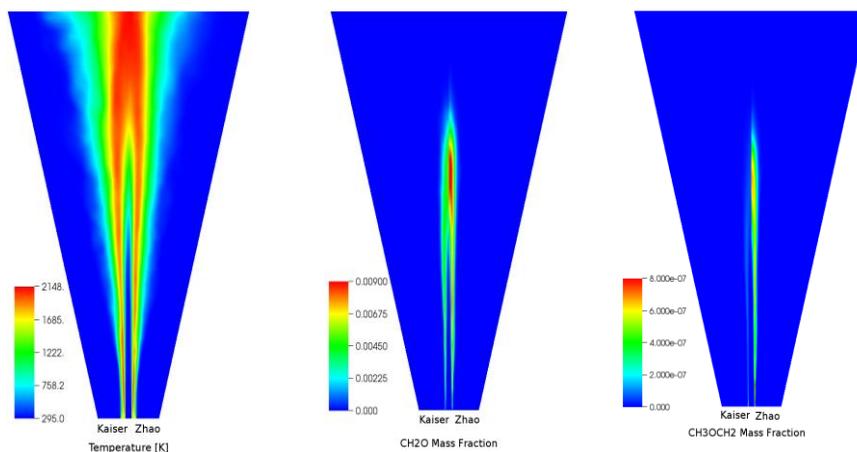
11th International Workshop on
Measurement and Computation of
Turbulent Flames



Configuration

- Turbulent piloted DME/air flame, stabilised on the Sandia piloted jet burner, velocities comparable with Flame D.
- Similar flames previously studied by Fuest et. al., current experimental campaign by J. Frank (PIV/LIF) at Sandia.
- $D_{\text{jet}} = 7.2 \text{ mm}$, $D_{\text{pilot}} = 18.2 \text{ mm}$
- $W_{\text{jet}} = 49.1 \text{ m/s}$, $W_{\text{pilot}} = 5.8 \text{ m/s}$, $W_{\text{coflow}} = 0.9 \text{ m/s}$
- Fuel jet: DME/air flow rates are 24/96 LPM, respectively.
- LES resolution: 70x70x240 cells
- The DME reaction chemistry is based on two available mechanisms:
 - Kaiser/Fischer et al., 78 species and 351 reactions
 - Zhao et al., 55 species and 290 reactions

Comparison of Favre-averaged mean contours from the two mechanisms



- F. Fuest, R.S. Barlow, J.-Y. Chen, A. Dreizler, *Combust. Flame*, DOI:10.1016/j.combustflame.2011.11.001
- E.W. Kaiser, T.J. Wallington, M.D. Hurley, J. Platz, H.J. Curran, W.J. Pitz, C.K. Westbrook, *J. Phys. Chem. A*, 104(35), 8194 (2000).
- S.L. Fischer, F.L. Dryer, H.J. Curran, *Int. J. Chem. Kinet.*, 32(12), 713 (2000).
- Z. Zhao, M. Chaos, A. Kazakov, F.L. Dryer, *Int. J. Chem. Kinet.*, 40, 1 (2008).

TECHNISCHE UNIVERSITÄT BERGAKADEMIE FREIBERG

Die Ressourcenuniversität. Seit 1765.




Modeling of partially premixed dimethyl ether flames using detailed chemistry and transport approaches

D. Messig^a, J. Keller^b, F. Fuest^c, A. Dreizler^c, C. Hasse^a

11th TNF Workshop, Darmstadt July, 26th-28th 2012

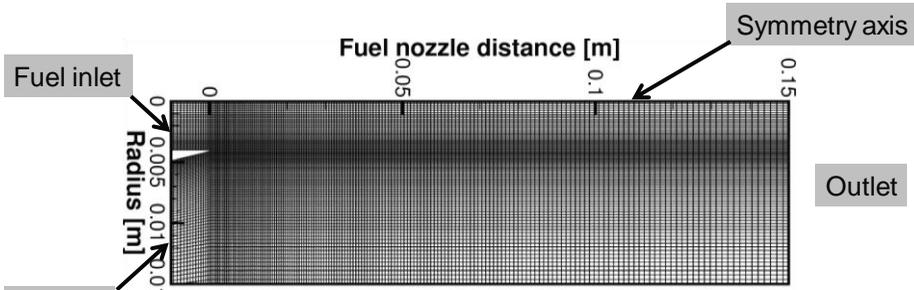
^a Chair of Numerical Thermo-Fluid Dynamics, TU Bergakademie Freiberg
^b Engler-Bunte-Institut, KIT
^c CSI – Center of Smart Interfaces, TU Darmstadt

TU Bergakademie Freiberg | Professur für Numerische Thermofluidynamik
 Institut für Energieverfahrenstechnik und Chemieingenieurwesen
 Reiche Zeche | 09596 Freiberg | Tel. +49(0)3731/39 4850 | Fax +49(0)3731/39 4555
 www.ntfd.tu-freiberg.de

Case description

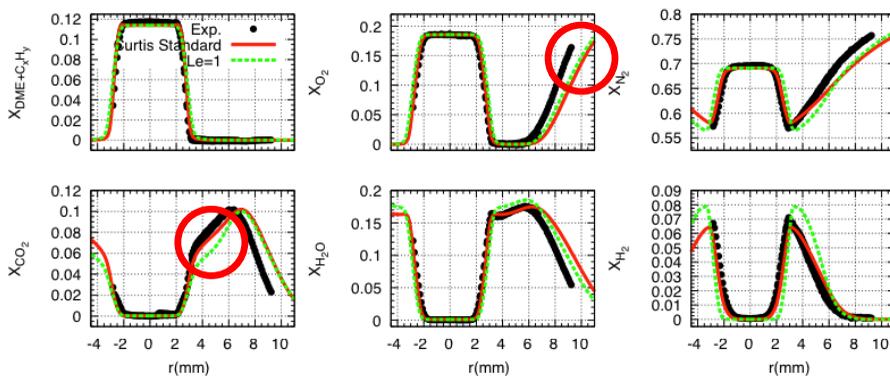
Boundary conditions (Fuest et al. 2012)

	T in K	u in m/s	Species in wt%
Air inlet	290	0.3	$Y_{Ar} = 1.3, Y_{H_2O} = 0.4, Y_{N_2} = 75.2,$ $Y_{O_2} = 23.1$
Fuel inlet		2.7	$Y_{Ar} = 1.1, Y_{DME} = 17.0, Y_{N_2} = 62.7,$ $Y_{O_2} = 19.2$



Mesh of L1-flame

- 2D axisymmetric
- Geometry data (Fuest et al. 2012)
 - domain extrusion inside the nozzle
 - 28870 non-uniform volume cells
- Fully developed velocity profile at inlets
- detailed chemistry with Zhao mechanism (Zhao et al. 2008)
 - 55 species
 - 290 reactions
 - Different diffusion models



Numerical radial results at $x = 0.02$ m for the Curtis Standard vs. $Le = 1$ model in comparison with experimental data from [5]



Results

Comparison of diffusion models



Conclusions:

- Differential diffusion effects are non-negligible
- Good agreement is obtained for the inner flame region
- In outer flame region ($r \geq 6$ mm) larger differences can be observed

31

Imperial College
London

Conclusions

- ❑ DME work is gaining strength. Very likely that we will have a substantial body of work at our next meeting.
- ❑ Some issues (as usual at this stage) but very encouraging.

Part 2.

Oxy-fuel Combustion and Fuel Composition Effects in MILD Combustion.

Presented by D. Roekaerts and B. Dally

The second part of the session was devoted to oxy-fuel combustion and to fuel composition effects in MILD combustion. The objective was to review state of the art and identify research questions of particular relevance for the participants in the TNF-workshop. In the following we first recall the motivation to put these subjects on the agenda of TNF, then list the contributions contained in the slides and finally give some conclusions.

Oxy-fuel Combustion

In oxy-fuel combustion the oxidiser stream is oxygen or enriched air. Oxy-fuel combustion

- is used in partial oxidation (gasification) for economic reason (lower investment).
- is used in high temperature furnaces (e.g. glass furnaces): to reach lower NO_x formation.
- is part of a potentially efficient solution for Carbon Capture and Sequestration (CCS).

Even in the case of combustion with oxygen and fuel not containing nitrogen, NO_x formation can be a problem in applications since small amounts of N₂ due to air leaks (in a furnace) can give high NO_x emission by the thermal mechanism. To lower NO_x formation, oxyfuel combustion often is used with CO₂ recycle into the oxidizer stream.

In order to decide on the recommended modeling approach in applications of oxyfuel combustion it is of interest to investigate the role of turbulence-chemistry interaction and also the role of turbulence-radiation interaction in a range of configurations, from simple to semi-industrial.

Fuel Composition Effects in MILD Combustion

In MILD or 'flameless' combustion, one or more of the fuel and oxidizer streams is diluted with products of combustion, which are at lower than adiabatic temperature. The combined effects of lowering of oxygen concentration and lower enthalpy have impact on the combustion process. Because high values of temperature are less frequent, NO_x formation by the thermal mechanism is lower. In flameless combustion, auto-ignition is observed to play an important role.

To be able to exploit the benefits of MILD combustion in a wider range of applications, fundamental understanding is needed on how fuel composition influences the boundaries of operation in the MILD regime. The jet-in-hot-coflow (JHC) burner (with coflow of vitiated air) allows study of the MILD combustion phenomena in a turbulent jet flame configuration.

Contributions by TNF11 Participants

- **Slides 5-11.**
Structure of the near field of turbulent oxy-fuel jet flames using Raman/Rayleigh laser diagnostics. (Sevault, Barlow, Dunn, Ditaranto). The aim of this work is to look at turbulent oxy-fuel flame structure, especially local extinction, in the near field of a series of oxy-fuel flames of CH₄/H₂ and to create data library for use in validation studies of turbulent combustion models. In the case of combustion with an oxygen-CO₂ mixture of about 30% O₂, the combustion is as stable as combustion with air (21% O₂). This is the result of the combined effect of difference in heat transfer properties (diffusive and radiative) and heat capacity. However the precise percentage depends on the mixing process. The results of Raman/Rayleigh measurements for a CO₂ diluted case with 32% O₂, shows the trends in local

extinction with Reynolds number and fuel composition. Effects of differential diffusion and impact of CO₂ dilution on CO levels are addressed. This work in the mean time has been published [2].

- **Slides 12-14.**
Experimental and numerical investigation of a partial oxidation oxy-fuel flame (Hunger, Stelzner, Voss, Trimis, Hasse). This study concerns a confined laminar flame operated at globally rich conditions, representing a gasifier. The configuration is 'inverse' in the sense that the oxidiser is in the central jet and the fuel in the coflow. The comparison of modeling and experiment draws conclusions on the role of differential diffusion, radiation modeling using an optically thin assumption and the applicability of flamelet analysis.
- **Slides 15-19.**
MILD combustion in JHC with different fuels (Medwell and Dally). A study was made of JHC flames with as fuel mixtures of 50% hydrogen and 50% of the following three: methane, ethylene and propane. The results presented in the slides have also been published [3].
- **Slides 20-21.**
Experiments on ignition and flame stabilization for Dutch NG diluted with H₂ or CO₂ burning in cold air and diluted coflow (Arteaga-Mendez, Tummers, Roekaerts). The lift-off behaviour of JHC flames was studied as function of fuel composition. The previously reported Delft JHC database for the case of natural gas (Oldenhof et al) is being extended to natural gas mixed with either H₂ or CO₂, both up to level of 25%.
- **Slides 24-41.** (Presented at the workshop by Bassam Dally)
MILD oxy-combustion of gaseous fuels (Dally, Li and Mi). Results are reported of studies of oxy-fuel combustion in a lab-scale (20 kW) MILD combustion furnace. The burner is a parallel jet burner, with exhaust nozzles situated in between the injection nozzles, making it possible to reach the levels of dilution by exhaust gases, required for reaching MILD combustion. The study uses three different fuels (natural gas, LPG and ethylene). Effect of dilution of O₂ by CO₂ up to 60% is also considered. It evaluates the effects of equivalence ratio, fuel-nozzle diameter and CO₂ level on performance parameters, in-furnace temperature and global emissions. The transition between conventional and MILD combustion occurs at different equivalence ratio, depending on the level of dilution of the fuel with CO₂. The conclusion is that oxy-fuel MILD combustion can be achieved using different gaseous fuels, even with pure oxygen as oxidant. However, in the case of dilution of oxygen with CO₂, MILD combustion can only be achieved when the equivalence ratio is greater than a critical value. The fuel-jet momentum appears to be the most critical parameter for establishment of the MILD oxy-combustion. It is suggested that the flame speed of a particular fuel could also be a vital parameter determining the occurrence of MILD combustion.

Contributions by Others

In addition to the contributions listed above some other contributions were invited providing links with cases showing extra complexity due to additional physical processes (soot formation) or due to the application (furnaces). Although these slides were not presented at the workshop they are provided here as reference and to provide leads to more widespread application of the models developed by the TNF community.

- **Slides 45-49.**
Soot formation and radiation in oxygen enriched combustion (Haworth, Mehta). Reports on the effects of oxygen enrichment on soot formation and the relative success of different turbulent combustion models.

- **Slides 50-52.**
Experiments on combustion of coke oven gas (COG) and blast furnace gas (BFG) in a lab-scale MILD combustion furnace (Gambale, Lupant). A relatively detailed dataset of in furnace probe measurements is available for the case of combustion of NG and provides a database for model validation studies.
- **Slides 53-56.**
Modeling of oxy-fuel combustion in a semi-industrial furnace (Galletti, Giovannini, Coraggio, Tognotti). Reports on CFD predictions of oxy-fuel combustion in a 3 MW furnace. Identifies some of modeling issues (chemistry reduction, spectral radiation effects).

Conclusions

The reported experimental results provide interesting new opportunities for modeling studies with some examples outlined below.

- The datasets on oxyfuel jet flames [2] can be used to study whether models capable to predict local extinction in turbulent jet flames burning in air are performing equally well in the case of oxyfuel and whether they are able to capture the additional effects due to differential diffusion and influence of presence of CO₂ level in the oxidizer on CO-level in the flame.
- Datasets on jet flames of natural gas diluted with H₂ or CO₂, burning in vitiated coflow can be used to study whether models are able to predict the trends in lift-off height and the observed appearance and growth of ignition kernels.
- Datasets on MILD combustion in a lab-scale furnace can be used to study which level of modeling is needed to predict the boundaries of the regime with low emissions.

References

- [1] Fuest, F., Barlow, R.S., Chen, J.-Y., Dreizler, A. (2012) Raman/Rayleigh scattering and CO-LIF measurements in laminar and turbulent jet flames of dimethyl ether, *Combust. Flame* 159 (8) 2533-2562.
- [2] Sevault, A., Dunn, M., Barlow, R.S., Ditaranto, M. (2012) On the structure of the near field of oxy-fuel jet flames using Raman/Rayleigh laser diagnostics, *Combust. Flame* 159 (11) 3342-3352.
- [3] Medwell, P.R., Dally, B.B. (2012) Effect of fuel composition on jet flames in a heated and diluted oxidant stream, *Combust. Flame* 159 (10) 3138–3145.

TNF 11, Darmstadt, Germany, July 26 – 28, 2012
Chemistry, complex fuels, and new combustion modes

- Oxy-fuel combustion

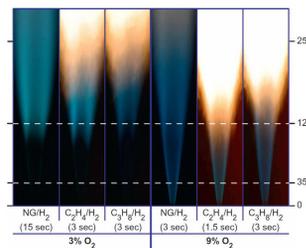
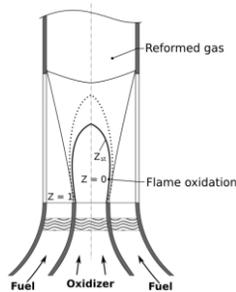
- Fuel composition effects in MILD combustion

Coordinators: Peter Lindstedt and Dirk Roekaerts



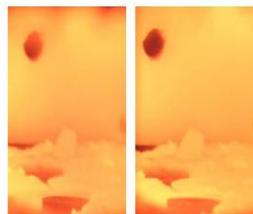
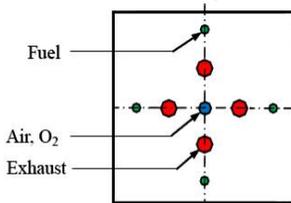
TNF workshop

We would like to know more about



Characteristics of JHC flames of various fuels

Fundamentals of oxyfuel flames



How to achieve MILD (oxyfuel) combustion in furnaces

Oxy-fuel combustion

Motivation

- Used in **partial oxidation** (gasification) for economic reason (lower investment)
- Used in **high temperature furnaces** (e.g. Glass furnaces): lower NO_x formation
However: small amounts of N₂ due to air leaks can give high NO_x emission by the thermal mechanism
- Flame temperature can be lowered via CO₂ recycle into the oxidizer stream
- Potentially efficient solution for **Carbon Capture and Sequestration**

Contributions to this presentation by TNF11 participants

- Local extinction in the near field of a series of oxy-fuel flames (Sevault, Barlow, et al)
- Confined laminar flame representing gasifier (Hasse et al)
- Oxy-fuel combustion in a lab-scale MILD combustion furnace (Dally et al)

Contributions by others

- Soot formation and radiation in oxygen enriched combustion (Mehta, Haworth)
- Modeling of oxy-fuel combustion in a 3MW furnace (Galletti et al)

Ref: Oxygen-enhanced combustion, C.E. Baukal Jr (Editor), CRC Press 1998

Fuel composition effects in MILD combustion

Motivation:

- Benefits of MILD combustion to be obtained in a wider range of applications
- Need fundamental understanding on how fuel composition influences **the boundaries of operation in the MILD regime**

Contributions to this presentation by TNF11 participants:

- Experiments and modeling of the JHC burner, Adelaide (Medwell and Dally)
- Experiments in the Delft JHC burner (Arteaga et al)

Contribution by others

- Experiments on combustion of coke oven gas (COG) and blast furnace gas (BFG) in a lab-scale MILD combustion furnace (Gambale and Lupant)

**STRUCTURE OF THE NEAR FIELD OF
 TURBULENT OXY-FUEL JET FLAMES
 USING RAMAN/RAYLEIGH LASER DIAGNOSTICS**

Alexis Sevault, Robert S. Barlow,
 Matthew Dunn and Mario Ditaranto



I. Background and motivations

a. Oxy-fuel combustion

BIGCO2 project considers it as a great potential among the CCS technologies

CO₂ capture achieved through simple water removal from flue gas

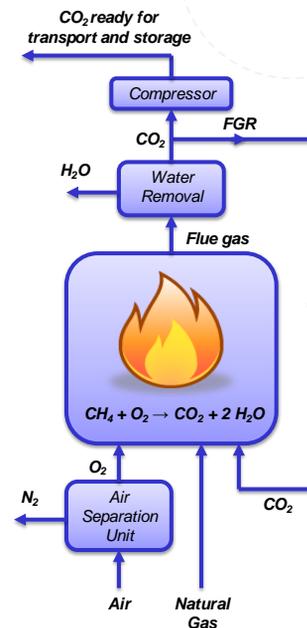
High flame temperature reduced by using flue gas recirculation

Great potential for retro-fitting current gas-fired plants

Main limit: O₂ supply is energy-consuming

Literature:

- Well documented for system and processes
- Not well documented about fundamentals on CO₂-diluted oxy-fuel flames



I. Background and motivations

7

b. Research topic

Aims of the research:

- Look at turbulent oxy-fuel flame structure
- Create data library eventually used for validation of turbulent combustion codes

Specific objective:

- Investigate turbulent non-premixed CO₂-diluted oxy-fuel jet flame from a coflow burner

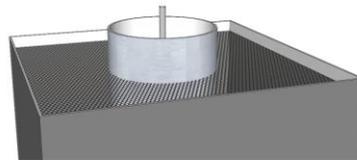
Flame properties:

- 32 % O₂ in oxidizer
- Overall equivalence ratio: 1.25

Flame	%H ₂ in fuel	Re _{Fuel}	Jet speed (m/s)	Coflow speed (m/s)
A-1	55	15,000	98.2	0.778
A-2	45	15,000	84.4	0.755
A-3	37	15,000	75.8	0.739
B-1	55	12,000	78.6	0.622
B-2	55	15,000	98.2	0.778
B-3	55	18,000	117.8	0.933

Coflow burner

- Fuel nozzle:
 - Fuel: CH₄/H₂
 - 5mm ID
 - Wall thickness 0.5 mm
 - Squared-off end
- Coflow tube:
 - Oxidizer: O₂/CO₂
 - 96.5 mm ID
 - Air coflowing at 0.5 m/s



www.ntnu.edu

Investigation of Turbulent Oxy-Fuel Jet Flames Using Raman/Rayleigh Laser Diagnostics – A. Sevault

Why 32 % O₂ in oxidiser ?

8

- Difference in heat transfer due to difference in properties between CO₂ and N₂
- Different heat capacity
- Different radiative properties
CO₂ radiates more than N₂,
leading to lower temperature and higher occurrence of local extinction
This can have an impact on flame stabilization

It has been found that combustion with air (21 % O₂)
is as stable as combustion with oxygen/CO₂ mixture with about 30% O₂

However, the precise percentage depends on the mixing process,
e.g. Kutne et al (PCI, 2011), using a burner with partial premixing and swirl, find that
oxyfuel combustion with 20% oxygen in the oxidiser gives a stable flame

. Sevault et al. C&F, 2012



www.ntnu.edu

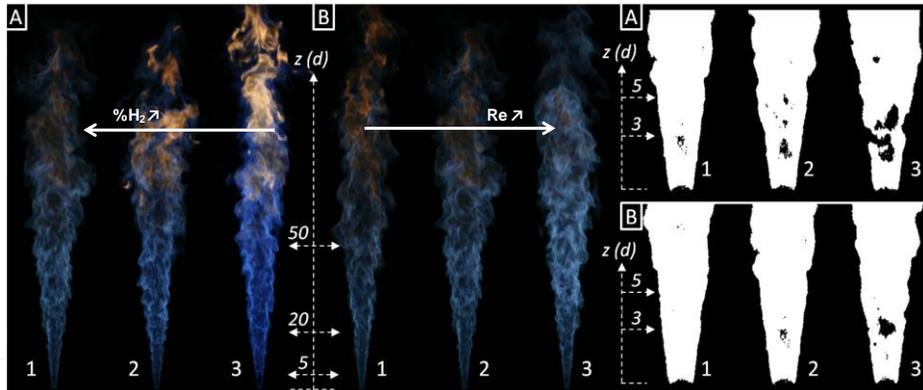
III. Results analysis

9

a. Localized extinction (1/3)

Localized extinction:

- Occurs when turbulent mixing rates between fuel and oxidizer become competitive with critical rates of chemical reactions
- Takes place in the near-field
- Probability of localized extinction increases with decreasing H₂ content in fuel and increasing jet Reynolds number.



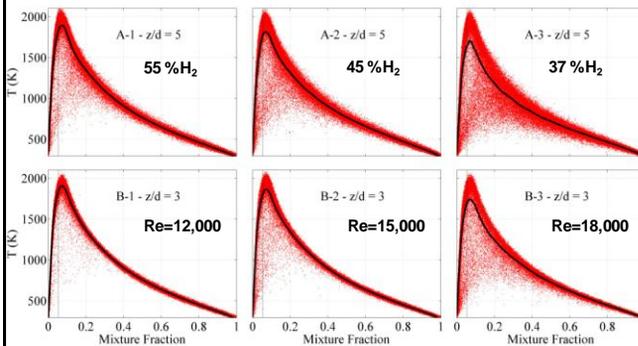
www.ntnu.edu

Investigation of Turbulent Oxy-Fuel Jet Flames Using Raman/Rayleigh Laser Diagnostics – A. Sevault

III. Results analysis

10

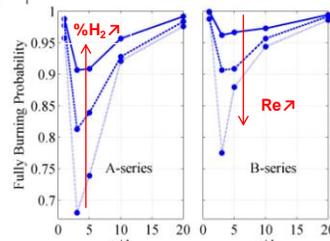
a. Localized extinction (2/3)



Leads to local temperatures drops due to increasing heat removal rates from convection and diffusion along with decreasing chemical reaction rates.

Fully burning probability:

- Enables to quantify the degree of extinction
- Based on pdf of temperatures above T_b in the mixture fraction region $F_{B-St} \pm \sigma$
- Here, with $T_b = 1700$ K and $\sigma = 0.02$



www.ntnu.edu

Investigation of Turbulent Oxy-Fuel Jet Flames Using Raman/Rayleigh Laser Diagnostics – A. Sevault

IV. Conclusions

11

Parametric study of CO₂-diluted oxy-fuel jet flames varying:

- CH₄/H₂ volume fraction from 37 % H₂ to 55 % H₂
- jet Reynolds number from 12,000 to 18,000

Observations could be made about :

- Evolution of degree of localized extinction along the flame
- Higher level of differential diffusion in the near-field
- Enhanced CO concentrations due to high CO₂-dilution levels

Scalar measurements of the temperature and mass fractions of main species displayed reasonable accuracy and are available upon request

Next step:

-Supplementary Raman measurements were performed at NTNU Trondheim in laminar premixed H₂/O₂/CO₂ and CH₄/O₂/CO₂ flat flames and transitional non-premixed H₂-O₂/CO₂ jet flames, with varying oxygen content in the oxidizer.. This parameter showed a strong influence on local CO concentration, spontaneous flame luminosity and flame stability. Measurements also available upon request.



www.ntnu.edu

Investigation of Turbulent Oxy-Fuel Jet Flames Using Raman/Rayleigh Laser Diagnostics – A. Sevault

TECHNISCHE UNIVERSITÄT BERGAKADEMIE FREIBERG

Die Ressourcenuniversität. Seit 1765.



11th TNF Workshop, Darmstadt
July, 26th-28th 2012

Experimental and Numerical Investigation of a Partial Oxidation Oxy-Fuel Flame *

F. Hunger, B. Stelzner, S. Voss, D. Trimis, C. Hasse

*B. Stelzner, , F. Hunger , S. Voss , J. Keller , C. Hasse , D. Trimis: Experimental and Numerical Study of Rich Inverse Diffusion Flame Structure, accepted for Proceedings of the Combustion Institute, 2012

TU Bergakademie Freiberg | Akademiestraße 6 | 09599 Freiberg
Fax: +49 3731 394555 | www.tu-freiberg.de

Geometry

- Inverse, confined, co-flow diffusion flame

Conditions

- Fuel: CH₄/CO₂ (1:1 molar), 300 K
- Oxidizer: O₂, 300 K
- Global equivalence ratio $\phi = 2.5$

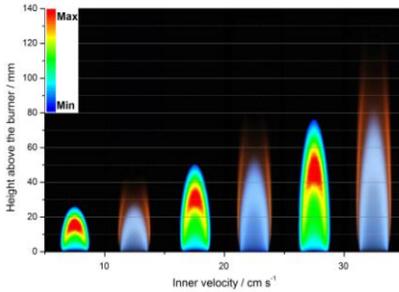


Fig. 3 Scheme of an IDF and the geometry of the FG-flame

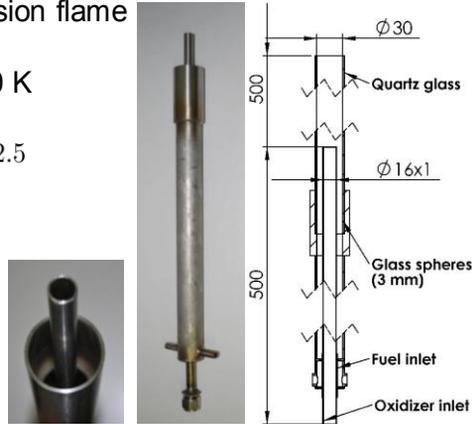
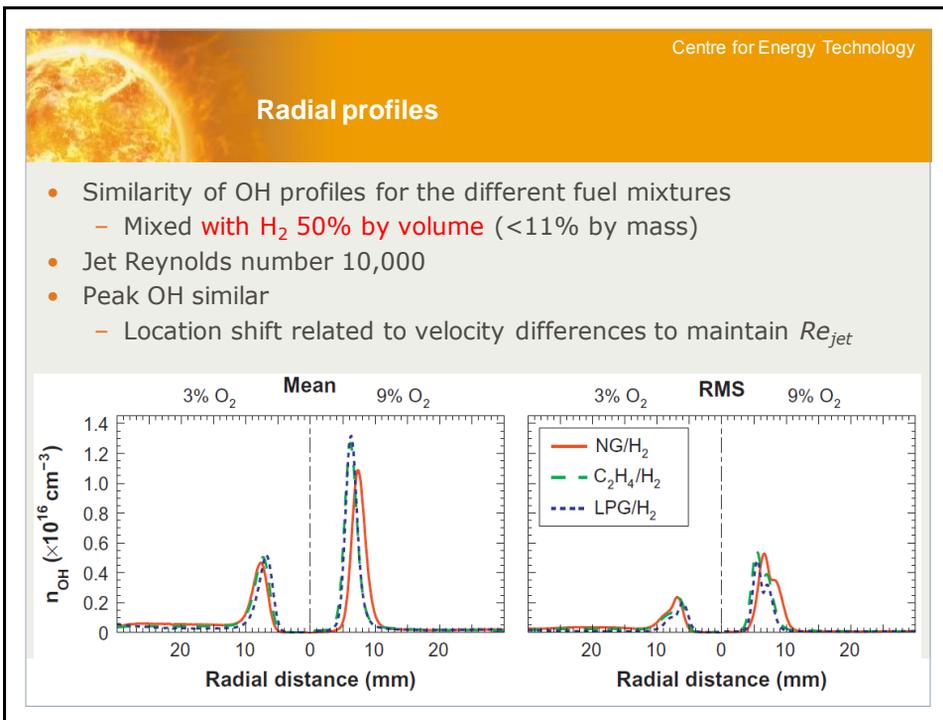
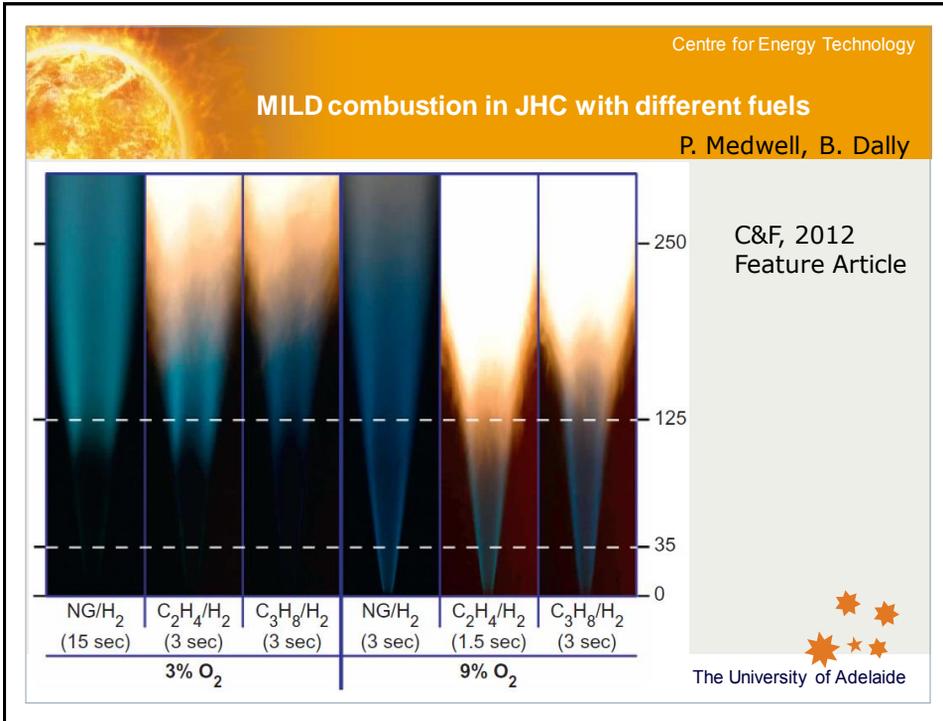


Fig. 4 Photograph of the burner setup and the engineering drawing.

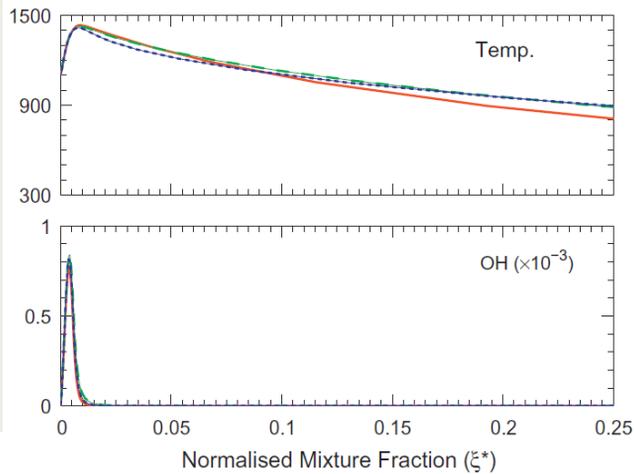
Summary of results

- Reference flame for model development and testing for gas-phase reaction in partial oxidation flames developed
 - Inverse and confined diffusion flame
 - Oxy-fuel process
- Numerical results
 - Diffusion modeling
 - Differential diffusion important
 - Thermal diffusion must be included
 - Radiation modeling
 - Optically thin assumption does not give a reasonable agreement downstream in the reforming zone
 - Flamelet analysis
 - Steady flamelet model not applicable in the post-flame zone
 - Lagrangian flamelet matches species development



Supporting the measurements...

- Laminar flame calculations also suggest that the kinetics are similar **under these MILD conditions...**

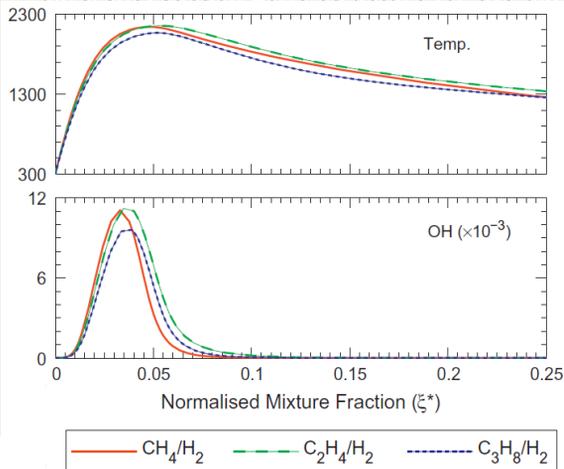


- 3% O₂
- 1100K

The University of Adelaide

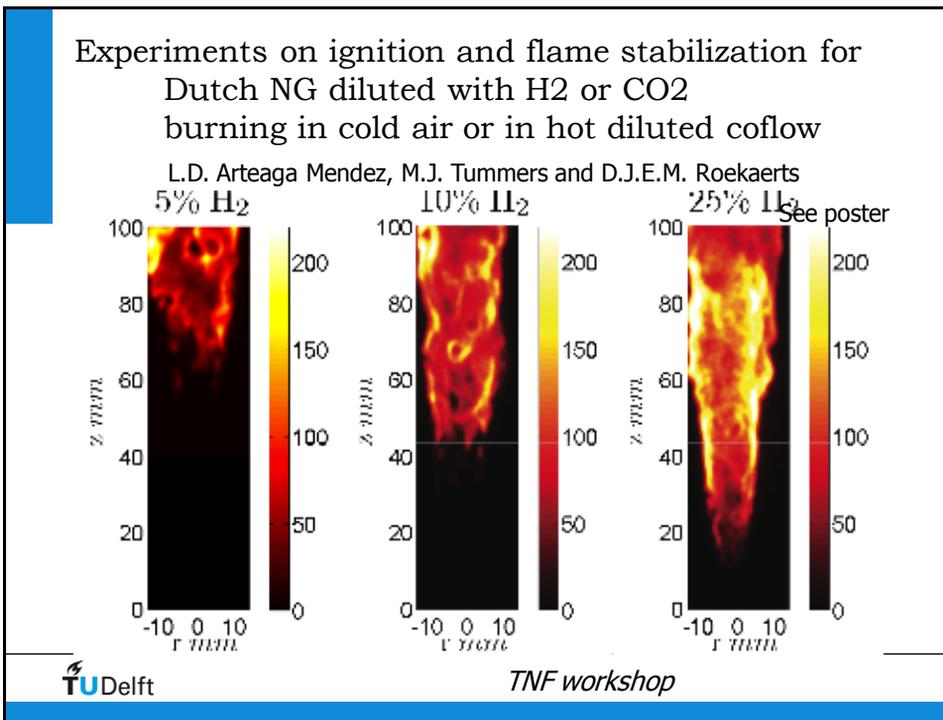
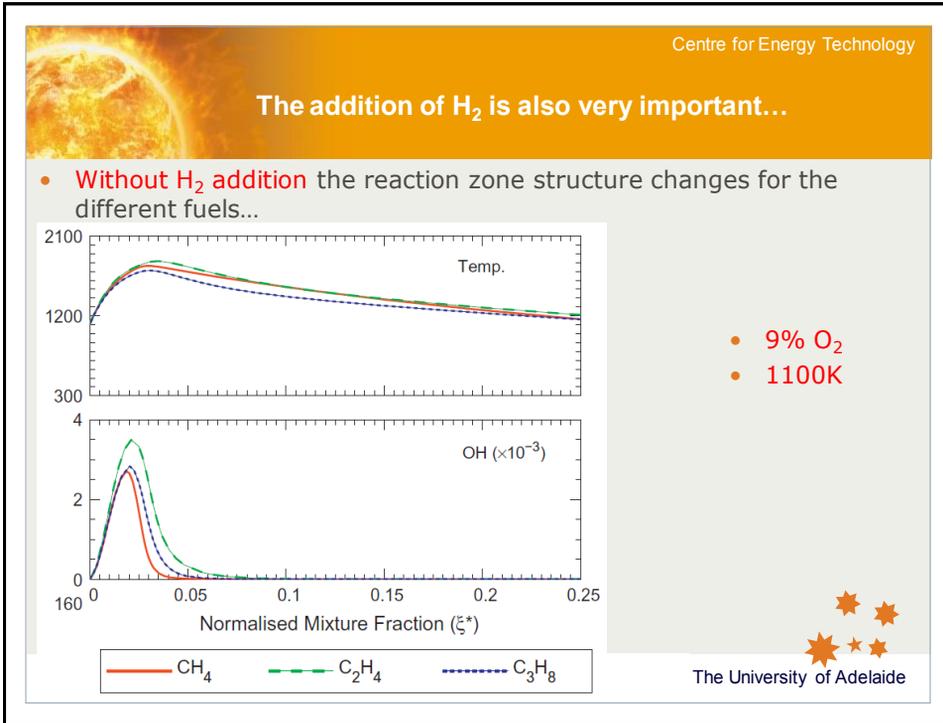
In contrast...

- The same fuel mixture, but **not under MILD** gives clearly different reaction zone structure for the different fuels...

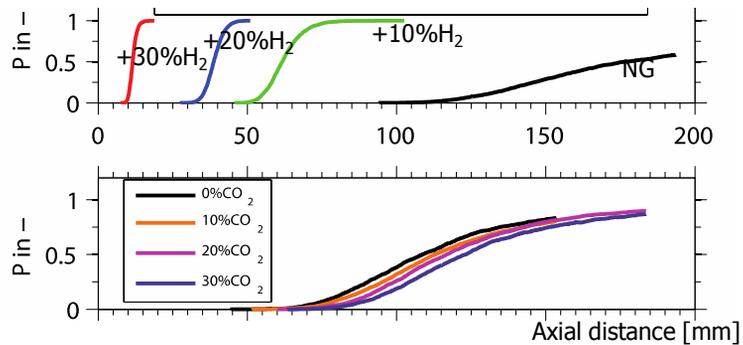


- 21% O₂
- 300K

The University of Adelaide



Probability of flame luminescence



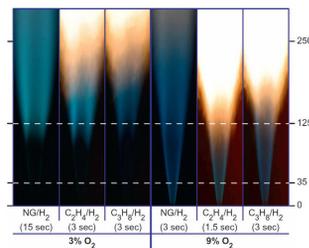
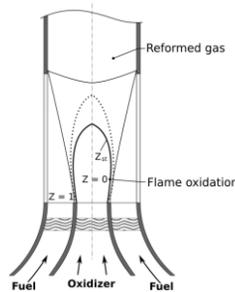
Overall conclusion: for case of hot vitiated coflow, % hydrogen added to NG has strong effects, but addition of carbon dioxide leads to comparably small effects.

Current work:
detailed study of the flame stabilization region using combined PIV – luminescence (ignition kernel appearance and evolution in relation to flow field properties)



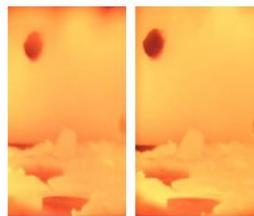
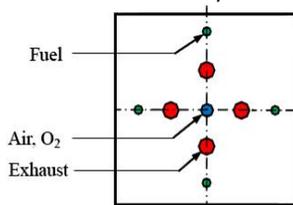
TNF workshop

We learned a lot, but can we predict it ?



Characteristics of JHC flames of various fuels

Fundamentals of oxyfuel flames



How to achieve MILD (oxyfuel) combustion in furnaces

On the agenda for modelers:

- Modeling of turbulent oxy-fuel jet flames using models appropriate for describing local extinction:
 - predict trends in burning probability
- Modeling of lifted flames of natural gas diluted with H₂ or CO₂
 - predict ignition kernel appearance and growth...
- Modeling of combustion furnaces
 - predict boundaries of the regime with low emissions



MILD Oxy-Combustion of Gaseous Fuels

Bassam Dally

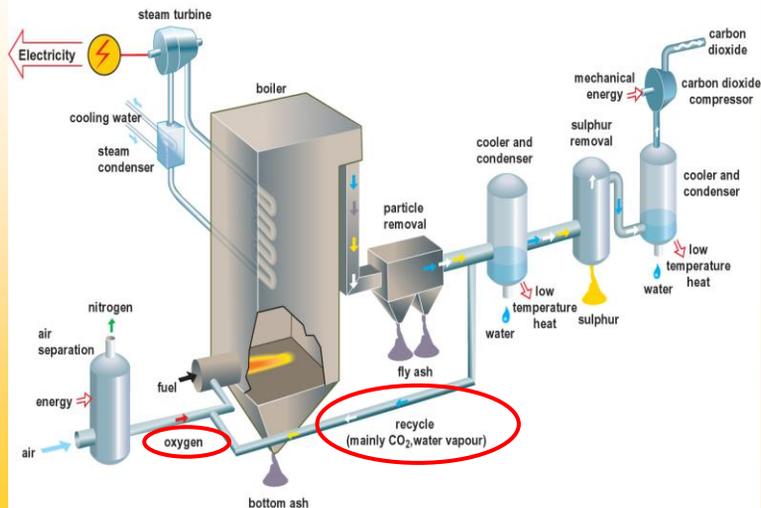
Center of Energy Technology & School of Mechanical
Engineering, The University of Adelaide

P. Li and J. Mi

College of Engineering, Peking University

Oxy-fuel Combustion

O₂/CO₂ recycle (oxyfuel) combustion capture



July, 2012

Copyright © 2012 The University of Adelaide, Australia. All rights reserved.

25

This Work

Characteristics of MILD combustion using:

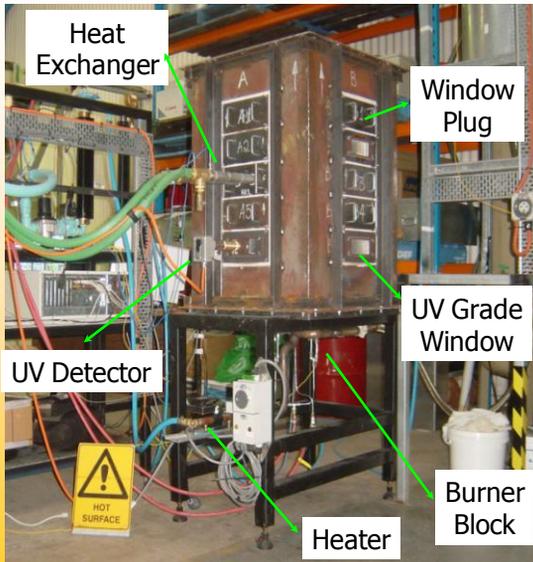
- Natural Gas (90% CH₄)
- Liquefied Petroleum Gas (92% C₃H₈)
- Ethylene (99.9% C₂H₄)
- Temperature distribution
- Effect of equivalence ratio (Φ)
- Effect of the fuel-nozzle diameter (D_f)
- Effect of the CO₂ level
- NO_x emission

July, 2012

Copyright © 2012 The University of Adelaide, Australia. All rights reserved.

26

Experimental Furnace (MCF)



Technical Specs

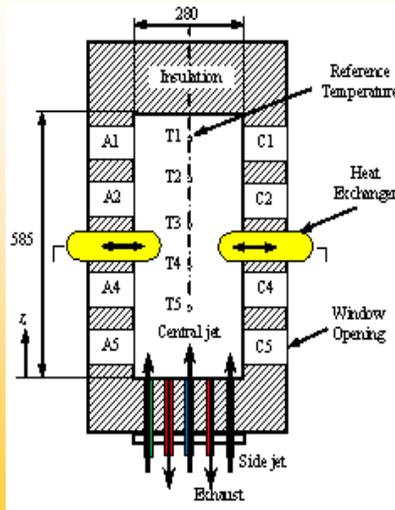
<u>Dimensions:</u>	280 × 280 × 585
	mm ³
<u>Fuel type:</u>	NG, LPG , Ethylene
<u>Max. capacity:</u>	20kW
<u>Turn down ratio:</u>	1:3
<u>Max. furnace temp.:</u>	1400° C
<u>Max. exhaust temp.:</u>	800° C
<u>Max. heat extraction:</u>	40%

July, 2012

Copyright © 2012 The University of Adelaide, Australia. All rights reserved.

27

What can be Measured?



Performance parameters

- Thermal Input
- Heat load
- Heat exchanger location

In-furnace temperature

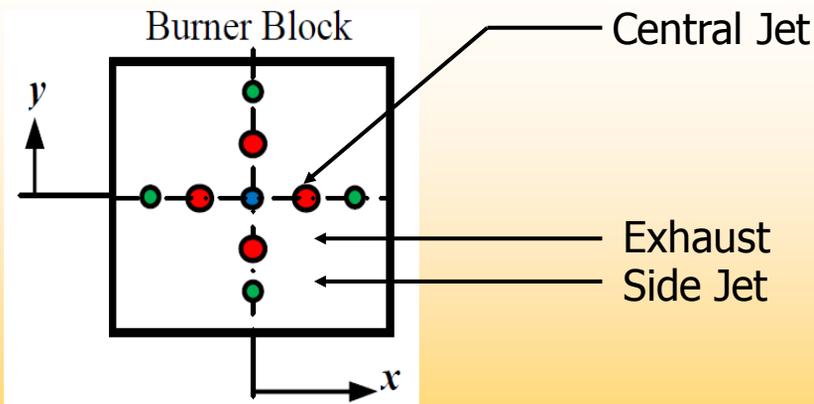
- Global emissions (O₂, CO, CO₂, H₂, NO_x, UHC)

July, 2012

Copyright © 2012 The University of Adelaide, Australia. All rights reserved.

28

Parallel Jet Burner



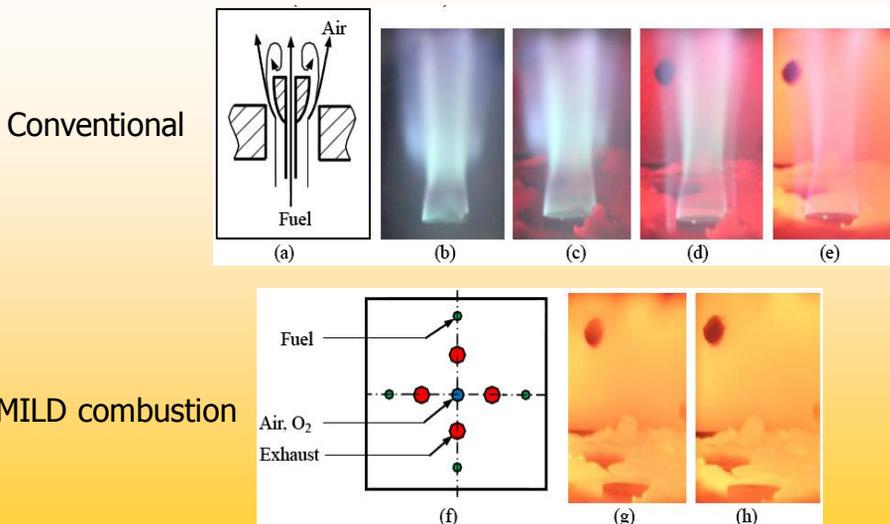
- For NG as a fuel, the air or O_2 / CO_2 were introduced into the furnace from the central nozzle.
- For LPG or Ethylene as fuel, the air or the O_2 were injected from the central jet while the fuel diluted with CO_2 issued from the side jets.

July, 2012

Copyright © 2012 The University of Adelaide, Australia. All rights reserved.

29

CONVENTIONAL versus MILD combustion



July, 2012

Copyright © 2012 The University of Adelaide, Australia. All rights reserved.

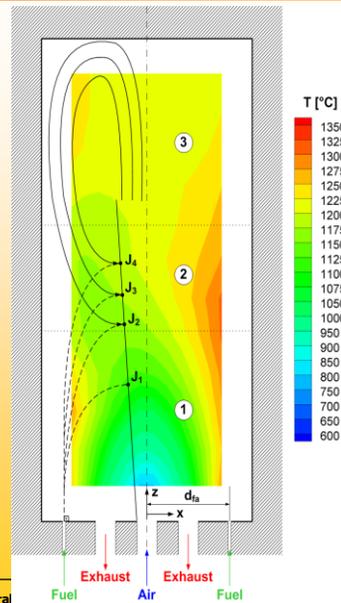
30

How to Establish MILD Combustion?

Recirculation Zone

Main Reaction Zone

Fuel Preconditioning



July, 2012

Copyright © 2012 The University of Adelaide, Australia

Effect of equivalence ratio (ϕ) - NG

$Y_{CO_2} = 0\%$

$Y_{CO_2} = 30\%$

$Y_{CO_2} = 60\%$

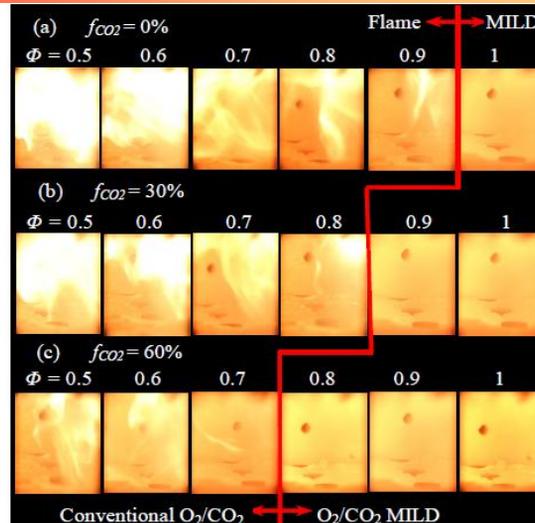


Figure 3. Images showing the effect of equivalence ratio on the in-furnace appearance of O_2/CO_2 combustion, at different initial mass fractions of CO_2 in the oxidant stream. NG was used as fuel while the O_2 / CO_2 mixture was injected through the central nozzle.

July, 2012

Copyright

Temperature distribution – NG ($\phi=0.82$)

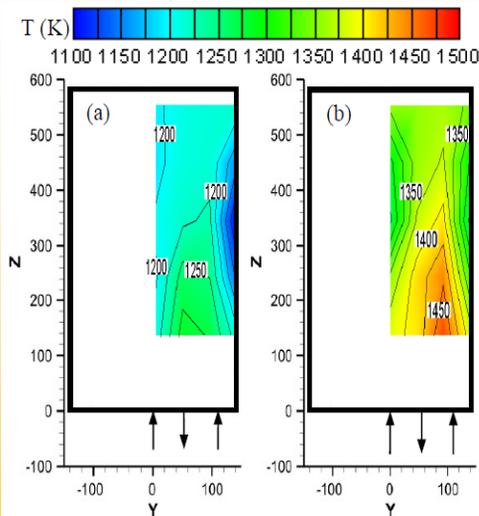


Figure 2. Measured temperature distribution of NG at $\phi = 0.82$, plane $x = 0$. (a) MILD combustion in air; (b) Oxy-fuel MILD combustion.

Similar Observations:

- thermal field is quite uniform;
- the high temperatures are located in the lower part of the furnace;

Difference:

- the average temperature of the oxy-fuel MILD combustion case is higher than the MILD combustion in air case;
- $\dot{M}(\text{CO}_2/\text{O}_2) = 6.557 \text{ kg/h}$
- $\dot{M}(\text{Air}) = 18.870 \text{ kg/h}$

July, 2012

Copyright © 2012 The University of Adelaide, Australia. All rights reserved.

33

Effect of the CO_2 level – NG ($\phi=0.90$)

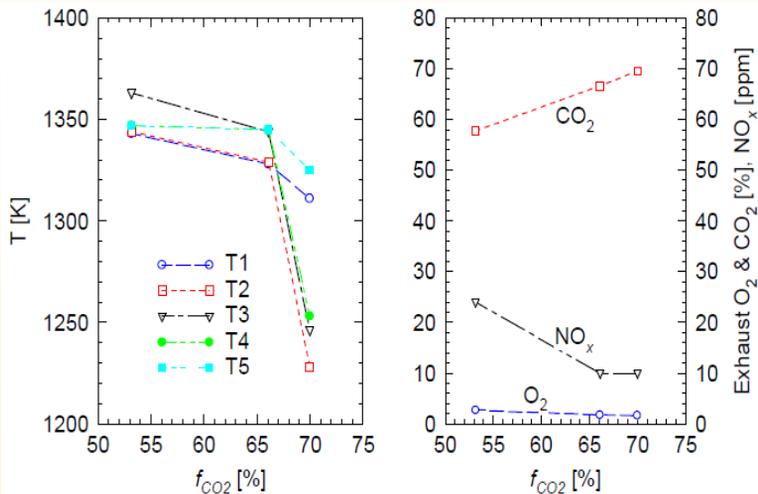


Figure 5. Effect of initial CO_2 mass fraction on the in-furnace temperatures and emissions of NG MILD oxy-combustion at $\phi = 0.90$.

July, 2012

Copyright © 2012 The University of Adelaide, Australia. All rights reserved.

34

Effect of the fuel-nozzle diameter (D_f)

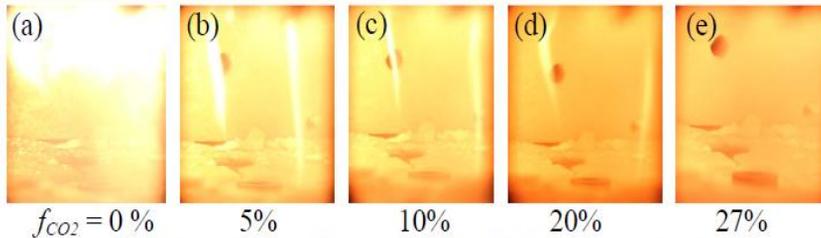


Figure 4. Effect of CO_2 dilution on the MILD oxy-combustion using LPG as fuel ($D_f = 2 \text{ mm}$), $\Phi = 0.92$.

- Two nozzle diameters, i.e. $D_f = 4 \text{ mm}$ and 2 mm , were used in the experiment for the four side fuel jets;
- When $D_f = 4 \text{ mm}$, the oxy-fuel MILD combustion could not be established for any of the fuels.

July, 2012

Copyright © 2012 The University of Adelaide, Australia. All rights reserved.

35

Effect of the CO_2 level – LPG ($\phi = 1.0$)

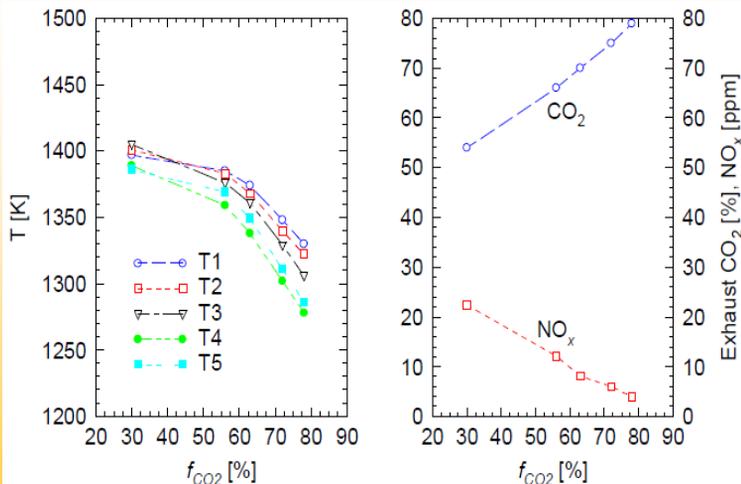


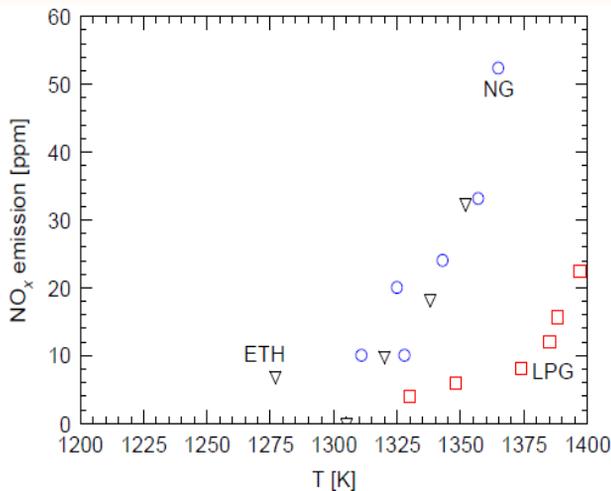
Figure 6. Effects of initial CO_2 mass fraction on the in-furnace temperature and emissions of LPG MILD oxy-combustion at $\Phi = 1$.

July, 2012

Copyright © 2012 The University of Adelaide, Australia. All rights reserved.

36

NO_x emissions – NG and LPG



The origin of the nitrogen in this case is in the fuel stream. N₂ content of NG, LPG and Eth by volume is respectively, 1.28%, 0.73% and <0.1%.

Figure 7. Relationship between the furnace temperature and NO_x emission of MILD oxy-combustion for NG, ETH and LPG as fuels.

July, 2012

Copyright © 2012 The University of Adelaide, Australia. All rights reserved.

37

Effect of different fuels

- when $D_f = 2$ mm and NG was used as fuel, the MILD combustion was achieved without any dilution.
- However, when LPG or ETH was used with $D_f = 2$ mm, if the fuel was not premixed with CO₂, the MILD combustion could not be achieved, even the central jet of oxygen was premixed with large amount of CO₂.

Table 1. Properties of the fuels under investigation

Fuel	Density (kg/m ³)	LHV (kJ/Nm ³)	Momentum rate at $D_f = 2$ mm (kg·m/s ²)
NG	0.7719	35906	0.006703855
LPG	2.0102	93244	0.003329352
ETH	1.2605	59482	0.004855839

July, 2012

Copyright © 2012 The University of Adelaide, Australia. All rights reserved.

38

Concluding Remarks

- The oxy-fuel MILD combustion can be achieved using different gaseous fuels, even with pure oxygen as oxidant;
- The amount of CO₂ dilution level, the MILD combustion can be achieved only when the equivalence ratio is greater than a critical value.
- The fuel-jet momentum appears to be the most critical parameter for establishment of the MILD oxy-combustion.

Concluding Remarks

- The flame speed of a particular fuel is perhaps also a vital parameter that determines the occurrence of MILD combustion.
- MILD regime is easier with NG than with ETH.

What can TNF Contribute?

Effect of CO₂ Concentration

- Impact of injection position of CO₂ relative to the reaction zone (oxidant stream versus fuel stream);
- Impact on radiation characteristics of flame;
- Impact on CO oxidation and emission.

Effect of Pure O₂ Injection

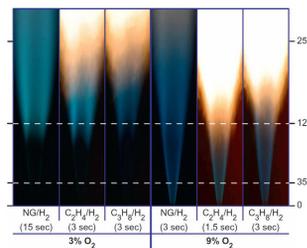
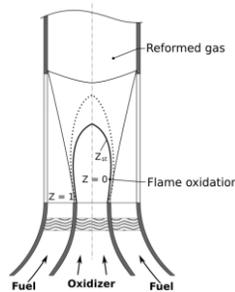
- Effect of molecular diffusion at elevated temperatures on O₂ penetration of reaction zone;
- Measuring flame speed under relevant conditions.

July 2012

Copyright © 2012 The University of Adelaide, Australia. All rights reserved.

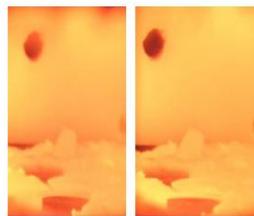
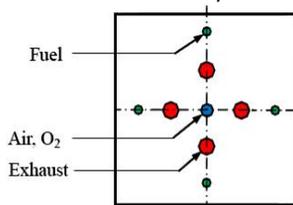
41

We learned a lot, but can we predict it ?



Characteristics of JHC flames of various fuels

Fundamentals of oxyfuel flames



How to achieve MILD (oxyfuel) combustion in furnaces

Applicability of models:
(from Pope et al. TNF9)

Models applicable to all modes of combustion based on full composition

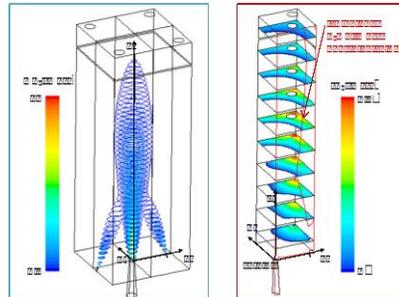
- DNS
- PDF and LES/FDF
- RANS with neglect of fluctuations
- Thickened flame front
- Eddy break-up models
- Eddy dissipation concept (EDC)
- LEM, ODT, other

Models applicable to adiabatic two-supply flames (A2)

- Z, c (or Z, Y_F , or ...)
- Z, G

Models applicable to non-adiabatic two-supply flames (N2)

- Z, c, h
- Z, G, h



Simulation of Mons furnace (Lupant)

Other contributions

Soot formation and radiation in oxygen-enriched turbulent jet flames

Daniel C. Haworth
Ranjan S. Mehta
July 2012

PENNSSTATE



Department of Mechanical & Nuclear Engineering
The Pennsylvania State University

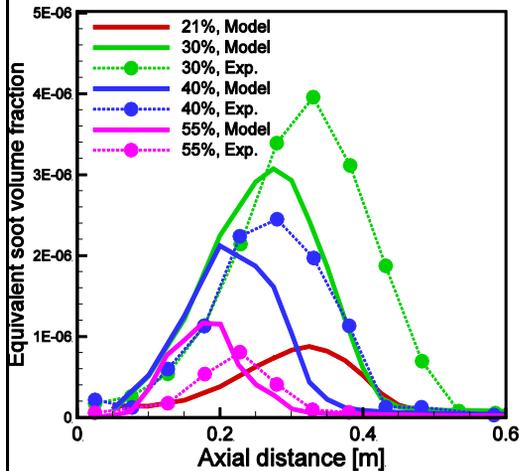
Oxygen-Enriched Sooting Turbulent Jet Flames

Flame	Fuel	Oxidizer	Jet Reynolds Number
III	90% CH ₄ -10% C ₂ H ₄	Air	6700
IV	90% CH ₄ -10% C ₂ H ₄	30% O ₂	6700
VI	90% CH ₄ -10% C ₂ H ₄	40% O ₂	6700
VI	90% CH ₄ -10% C ₂ H ₄	55% O ₂	6700

Naming based on R.S. Mehta, D.C. Haworth & M.F. Modest (2010) *Combust. Flame* 157:982.

- Detailed characterization of turbulent jet flames with Oxygen Enrichment undertaken by Turns and co-workers at the Pennsylvania State University.** [L.Wang, N.E. Endrud, S.R. Turns, M.D. D'Agostini and A.G. Slavejkov, *A study of the influence of oxygen index on soot, radiation, and emission characteristics of turbulent jet flames*, *Combust. Sci. Tech.* 178(8) (2002), pp. 45–72.]
- Number of experiments to understand effect of key parameters on soot, radiation and emission characteristics of jet flames
- Line-of-sight laser extinction measurements – correlated to an “equivalent soot volume fraction”
- Radiative flux measurements along the wall to find total radiant fractions (with oxygen enrichment)
- Experiments are conducted with modeling requirements in mind (Boundary conditions well characterized etc).

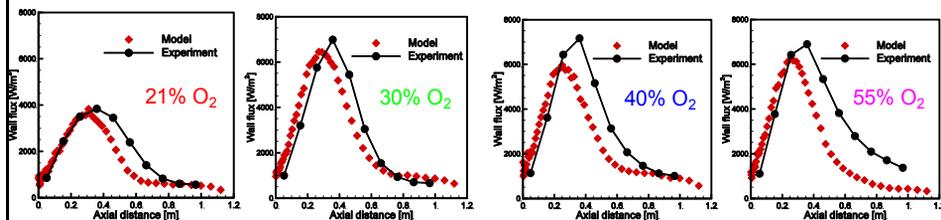
Modeling Study of the Oxygen-Enriched Flames



R.S. Mehta, D.C. Haworth & M.F. Modest (2010)
Combust. Flame 157:982.

1. Sooting tendency first increases with oxygen enrichment and then decreases
2. Competing effects due to increased oxygen
 - Increased H radicals due to Oxygen aid in soot surface growth by the HACA mechanism (Hydrogen-Abstraction acetylene addition mechanism)
 - Increased O₂ oxidises both soot precursors and soot itself
3. Increase in soot surface growth outpaces the oxidation rates initially
4. Later on, soot and precursor oxidation becomes dominant than the HACA rates with higher oxygen

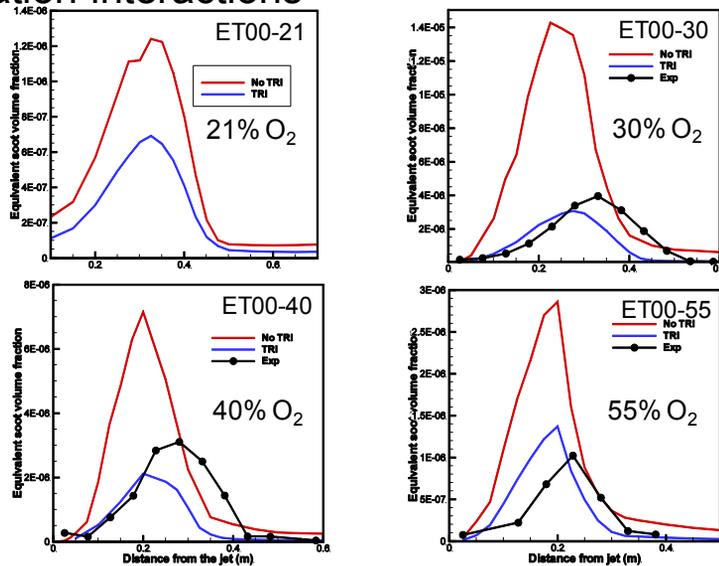
Modeling Study Continued...



R.S. Mehta, D.C. Haworth & M.F. Modest (2010)
Combust. Flame 157:982.

1. Composition PDF Method for turbulent combustion coupled with a Photon Monte Carlo method accounting for turbulence-radiation interactions
2. Accounting for TRI is shown to be extremely important in sooting flames
3. All flames simulated with a single set of model parameters: (No parameter tuning to get better match etc.)
4. Parameters include: k-epsilon constants, PDF method – mixing model constants)
 - Approaches are being developed to realize the benefits of PDF methods using more conventional numerical methods and/or reduced computational resources
 - *In situ* adaptive tabulation (ISAT)
 - Eulerian field PDF methods

Computed soot levels decrease by as much as a factor of four with consideration of turbulence-radiation interactions

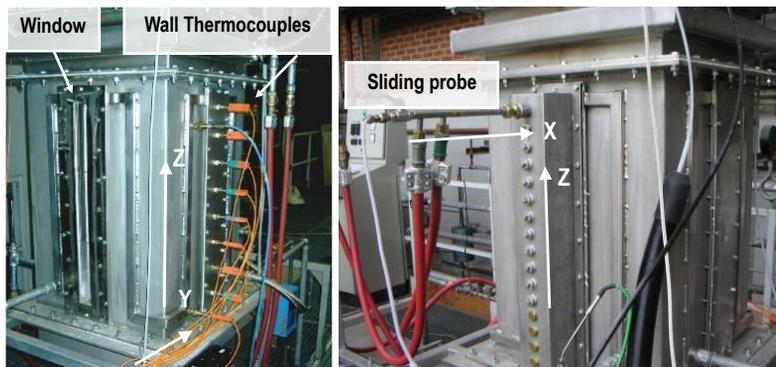


Flameless combustion of COG/BFG

A. Gambale and D. Lupant

Generation of a stable flame can be difficult because of the variable calorific value and ignition characteristics of their components.

Flameless oxidation for stable combustion and low emissions.

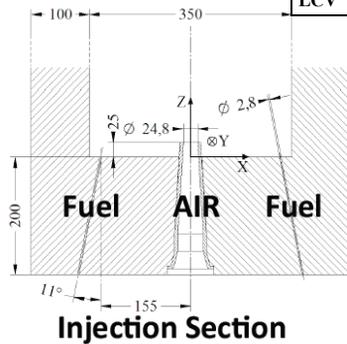


33kW MILD combustion furnace

Flameless combustion of COG/BFG

Natural gas (ref), **Coke Oven gas (COG)** and blend with **Blast Furnace Gas (BFG)**

Gas	NG	BFG100% <i>Not tested yet</i>	COG100%	COG50%- BFG50%
H₂	0	0,03	<u>0,62</u>	0,325
CO	0	0,205	0,06	0,1325
CH₄	0,92	0	0,285	0,1425
N₂	0,02	0,54	0,02	0,28
CO₂	0,01	0,225	0,015	0,12
C₂H₆	0,05	0	0	0
LCV [kJ/m³N]	37 183	<u>4059</u>	19 646	11 852



Measured emissions

	NO [ppm]	CO [ppm]
NG	7 ± 1	12 ± 20
COG	10 ± 1	21 ± 20
BGF – COG	6 ± 1	13 ± 20

Low NO (≈ 10 ppm) and CO (≈ 20 ppm) emissions
Negligible differences between COG and NG

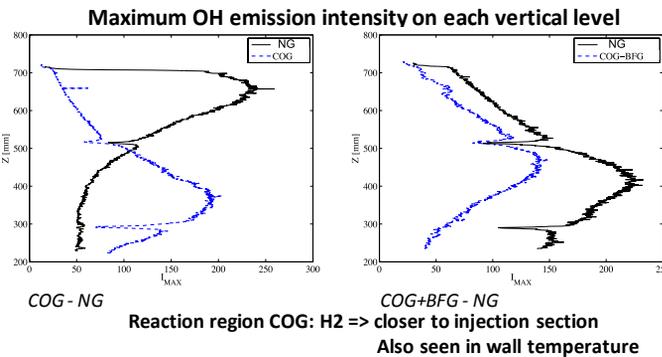
Université de Mons

11th International Workshop on Measurement and Computation of Turbulent Flames

Chemiluminescence

Reacting zone closer to the injectors for COG than for NG: effect of the high hydrogen content of COG (62%).

Substituting Natural Gas with Coke Oven Gas or a mixture of Coke Oven gas and Blast Furnace Gas in a flameless combustion chamber is feasible with high efficiency and low, emissions.



What is in it for TNF ?

- Extensive dataset of in furnace probe measurements for NG case (PhD Thesis D. Lupant, delphine.lupant@umons.ac.be)
- Results of first series of model validation studies, with EBU and with EDC show significant discrepancies with measurements. Asks for further computational studies with more detailed models.

Université de Mons

Supported by the Walloon Government, the IEA and ArcelorMittal



Università
di Pisa



International
Flame Research
Foundation

MODELLING OF OXY-FUEL COMBUSTION IN A SEMI-INDUSTRIAL FURNACE

C. Galletti¹, L. Giovannini², G. Coraggio², L. Tognotti^{1,2}

¹Dept. of Chemical Engineering, University of Pisa, Italy ²IFRF - Livorno, Italy

IFRF NG and coal oxy-combustion tests in FoSper (3 MW furnace) have been used to validate a modeling approach for oxy-fuel combustion of NG and coal.

Here only NG results are presented.

- Validation of sub-models (e.g. oxidation schemes, combustion and radiation models) for CO₂-enriched atmosphere
- Validation of sub-models at large scale where different effects may arise (e.g. radiation)
- Procedures for a systematic validation

FoSper furnace : 2m x 2 m x 6.25 m, 8 cooling loops

TEA-C burner: Low NO_x burner,

Oxidiser fed by the secondary and tertiary ducts (swirled), NG fed by 8 gas lances

- **Experimental data:**

Coraggio, G., Laiola, M., Tognotti, L., 2009, Combustion of NG and pulverized coal in a mixture of oxygen and RFG, IFRF report 110/y/01, Livorno, Italy.

Reference: paper presented at the 17th IFRF int. member conference, Paris, 2012



Università
di Pisa



International
Flame Research
Foundation

Physical models

FLUENT by Ansys 13

Turbulence Model	Combustion Model	Kinetic Scheme	Radiation Model	Spectral Model	BCs@ walls
SST k- ω	EDM	WDair [1]	P1	WSGG [4]	T, e
SST k- ω	EDC	WDair [1]	P1	WSGG [4]	T, e
SST k- ω	EDC	WDoxy [2]	P1	WSGG [4]	T, e
SST k- ω	EDC	Jlair[3]	P1	WSGG [4]	Heat Flux
SST k- ω	EDC	Jloxy [2]	P1	WSGG [4]	T, e
SST k- ω	EDM	WDair [1]	P1	WSGGoxy [5]	T, e
SST k- ω	EDC	WD air[1]	P1	WSGGoxy [5]	T, e

[1] Westbrook, C.K., Dryer, F.K., 1981, Combust Sci Technol, 27:31-43.

[2] Andersen, J., Rasmussen, C.L., Giselsson, T., Glarborg, P., 2009, Energy Fuels, 23:1279-1389.

[3] Jones WP, Lindstedt RP., 1989, Combust Flame, 73:233-249.

[4] Smith, F., Shen, Z.F., Friedman, J.N., 1982, J. Heat Transfer, 104:602-608.

[5] Johansson, R., Andersson, K., Leckner, B., Thunman, H., 2010, Int J Heat Mass Trans, 53:220-230.

MODELING ISSUES: choice of submodels

- constraints → global reaction mechanism and simple spectral/radiation models to make the simulations affordable (with 4 millions cells)

CPU time (24 cores)

Runs with EDM ~7 days

Runs with EDC (ISAT with tolerance 10⁻⁵) ~15 days

ASSUMPTION: Air leakage distribution

- air leakage evaluated from species balances minimizing errors on CO₂ and O₂

17th IFRF International Member Conference – Paris, 11th-13th June 2012

54

Introduction
Experimental
Modeling approach
Numerical model
Oxy-NG results
Oxy-COAL results
Conclusions



Università di Pisa



International Flame Research Foundation

Introduction

Experimental

Modeling approach

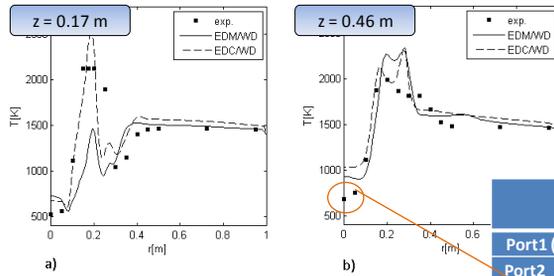
Numerical model

Oxy-NG results

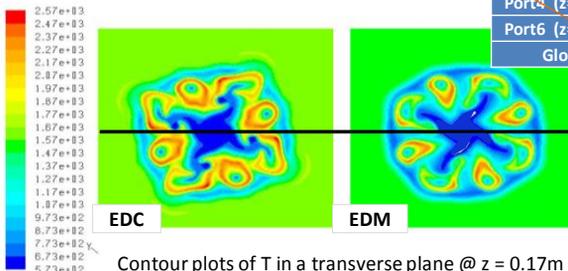
Oxy-COAL results

Conclusions

Results: effect of combustion model



Only EDC model predicts the high temperature peak at $z = 0.17$ m



Contour plots of T in a transverse plane @ $z = 0.17$ m

	EDM Wdair	EDC Wdair
Port1 ($z=0.17$ m)	23.2	14.3
Port2 ($z=0.46$ m)	12.7	12.3
Port4 ($z=1.02$ m)	6.2	7.3
Port6 ($z=1.64$ m)	2.8	3.0
Global	12.8	10.2

Low temperature data near the axis is non captured by CFD predictions (even using different kinetic schemes) → we need a different explanation!

17th IFRF International Member Conference – Paris, 11th-13th June 2012

55



Università di Pisa



International Flame Research Foundation

Introduction

Experimental

Modeling approach

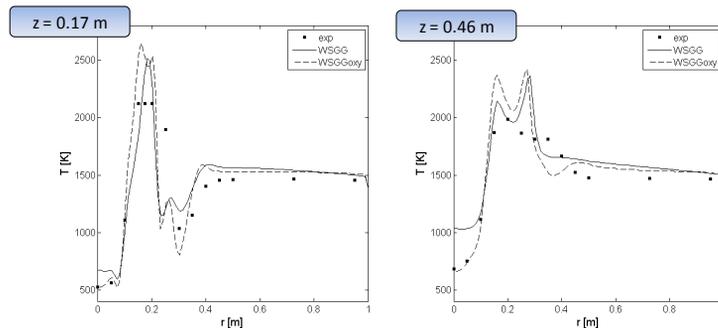
Numerical model

Oxy-NG results

Oxy-COAL results

Conclusions

Results : effect of spectral model



- Large impact of spectral model
- Need to revise WSGG schemes for FoSper oxy-fuel conditions (RFG + air leakage)!

	EDC WD WSGG	EDC WD WSGGoxy
Port1 ($z=0.17$ m)	14.3	13
Port2 ($z=0.46$ m)	12.3	8.5
Port4 ($z=1.02$ m)	7.3	5.6
Port6 ($z=1.64$ m)	3.0	4.8
Global	10.2	8.7

17th IFRF International Member Conference – Paris, 11th-13th June 2012

56

Radiation : Nongray-Gas effects

- Comparison of models for the case of a 12mx12mx4m enclosure at 1500 K with wall having emissivity 0.725 at temperature 750 K
Chungen Yin, Energy&Fuels, 2012
- Comparison between
 - Gray WSSGM for air-fuel combustion
 - Gray WSGGM for oxy-fuel combustion derived using
 - statistical narrow band model (SNBM)
 - exponential wide band model ((EWBM)
 - Nongray model : box-model based on EWBM
 - Nongray model : spectral line based WSGG (SLW)
- Case of wet flue gas recycle and dry flue gas recycle
- Results :
 - SNBM and EWBM in close correspondence
 - Use of oxy-fuel WSGGM can significantly improve predictive capability
 - Air-fuel WSGGM gives appreciable underprediction of radiative heat flux at wallErrors are more pronounced for high CO₂ concentration environment

Interpretation and Utilization of Time-Resolved Data

Session Co-ordinators: Adam Steinberg (University of Toronto), Wolfgang Meier (German Aerospace Center), Luc Vervisch (INSA de Rouen)

This session had two primary focuses: (1) experimental considerations for creating ‘well-posed’ time-resolved experiments and (2) requirements for comparing time-resolved experiments and simulations.

The main experimental considerations highlighted were out-of-plane effects, limited detectable quantities, and data analysis. Experimental methods that accounted for out-of-plane effects were identified, which typically employ cross-plane or parallel plane imaging. The combined use of planar imaging with line-of-site integrated techniques also was discussed. Limitations imposed by detectable species arise due to the relatively low pulse energy of continuous duty-cycle high-repetition-rate laser systems. Consequentially, OH PLIF, tracer PLIF, and 1D Rayleigh scattering are the most commonly reported high-repetition-rate spectroscopic techniques. Experiments must therefore be designed such that these measurements reveal the phenomena of interest. Moreover, effort should be made to visualize simulations in the same manner as experiments. The potential of custom-built pulse-burst laser systems, capable of achieving much high pulse-energies for short-duration bursts (ca. 10-100 pulses), also was discussed. Several different analysis techniques for time-resolved data were then presented, and experiments that employ these techniques reviewed. Efforts should be made to standardize certain common techniques, such as proper orthogonal decomposition, and/or have a few common data sets on which different versions of the techniques can be tested.

The following issues were discussed during and after the workshop:

1. Attention must be given to the different meanings between ‘time-resolved’ in the context of experiments and simulations. What is the effect of the LES time step, pulse duration, and inter-measurement time on the interpretations?
2. For model development and validation, specific target phenomena should be sought in which time-resolved experiments can yield important new insight. What are the most important dynamic phenomena to model properly? An advantage of time-resolved image sequences is that the statistics can be conditioned and that it is possible to catch events which happen quite rarely.
3. Effort must be made to analyze time-resolved experiments and simulations using the same tools (filtering, POD, DMD, etc.). Standardized data sets should be used to test different versions of analysis algorithms. This will allow more quantitative comparisons of experiments and simulations.
4. It was proposed to distinguish between ignition dynamics and flame dynamics:
 - a. Ignition relates to a single instant in time and space, which must be isolated in both experiments and simulations; time series may be collected before and after ignition to better understand ignition conditions and implication on the subsequent flame development.
 - b. Flame dynamics studies rather go with time sequences (not always time resolved), with a necessary check of the statistical predictions to validate the simulation.
5. In simulations, the time analyses may be performed in either Lagrangian or Eulerian frameworks. Eulerian implies storing many fields and Lagrangian motivates the development of specific methods to track meaningful trajectories (not always matching the flow path-lines). Specialized budget equations may also be derived to isolate time evolution of a given quantity. It may be desirable to rewind time, which is not always that easy in practice.



Interpretation and Utilization of Time Resolved Data

11th International Workshop on Measurement and Computation of Turbulent Flames
Darmstadt, Germany

Part 1 – Experimental Perspective: Adam Steinberg¹ and Wolfgang Meier²

Part 2 – LES/DNS Perspective: Luc Vervisch³

¹Institute for Aerospace Studies, University of Toronto

²Institute for Combustion Technology, German Aerospace Center

³CORIA, l'INSA de Rouen



Contributors

- Christoph Arndt – DLR Stuttgart
- Isaac Boxx – DLR Stuttgart
- Campbell Carter – Air Force Research Laboratory
- James Dawson – Cambridge University
- Andreas Dreizler – TU Darmstadt
- Jim Driscoll – University of Michigan
- Sébastien Ducruix – École Centrale Paris
- Jonathon Frank – Sandia National Laboratory
- Frédéric Grisch – CORIA
- Peter Hamlington – UC Boulder
- Assaad Masri – University of Sydney
- William O'Loughlin – Sydney University
- Elaine Oran – Naval Research Laboratory
- Jeffrey Sutton – Ohio State University
- Mark Tummers – TU Delft



Overview

- How do we create a well-posed high-speed experiment?
 - Objectives of high-speed imaging
 - Considerations for (quantitatively) analyzing dynamic phenomena
 - Current utilization of high-speed data
 - Moving forward/best practices
- Caveat: We will only cover flames that are relevant to TNF, not in-engine processes
- Caveat: Only imaging techniques will be considered
 - Chemiluminescence of OH* or CH*
 - Particle Image Velocimetry (PIV) for flow velocities
 - Planar laser induced fluorescence (PLIF) of OH, NO, CH₂O, tracers
 - Rayleigh scattering for gas density, (temperature)



Objectives of Obtaining Temporally Resolved Data

- Main objective of temporally resolving data are to
 1. Observe cause-and-effect relationships
 - Gain new physical understanding of combustion processes
 2. Quantify cause-and-effect relationships in a meaningful way
 - Describe basic processes
 - Assess and develop detailed models
 - Explain large scale dynamics
- Must quantify both the dynamics of individual events and the statistics of the dynamics**
- Some areas where high-speed data is useful
 - (Local) flame extinction
 - Turbulence-flame interactions
 - (Auto) ignition
 - Flame stabilization, flash-back, blow-off
 - Flame/flow dynamics, periodic instabilities



Designing Well-Posed High-Speed Experiments

- For high-speed experiments, special consideration is required of
 - Dimensionality
 - What can be measured
 - How the measured quantities, in the available number of dimensions, can be employed usefully to solve problems



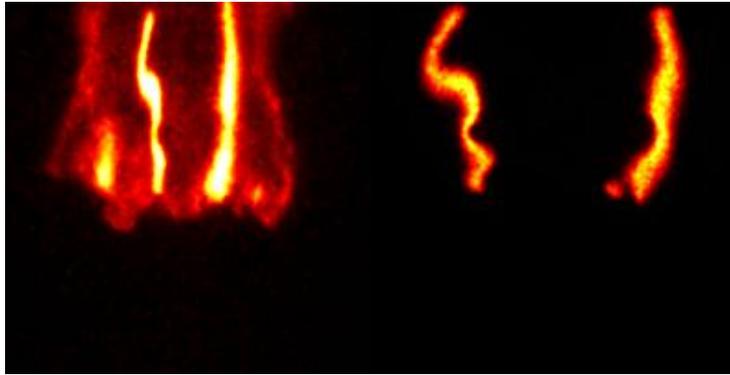
Dimensionality

- Because the way we use high-speed data is different than non-temporally resolved data, 3D effects are very important
 - Out-of-plane flow and flame motion
 - Out-of-plane flame orientation, velocity gradients
- Without proper consideration of out-of-plane effects, what you see is NOT necessarily what is happening
- Generally requires either
 - 4D data
 - Some measure of out-of-plane effects
 - A statistical approach where out-of-plane effects are unimportant
 - Line-of-sight integrated techniques

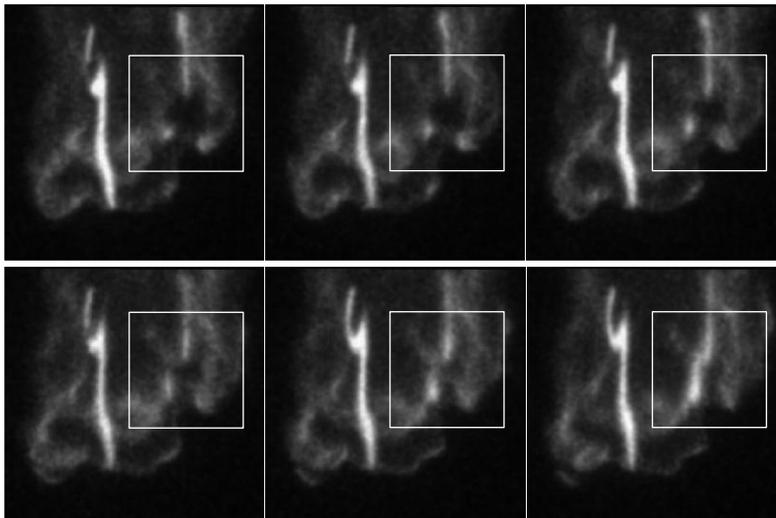


Dimensionality

- Lifted jet flame
 - 10 kHz OH PLIF and OH* chemiluminescence
 - OH* chemiluminescence viewing angle is 30° relative to the PLIF



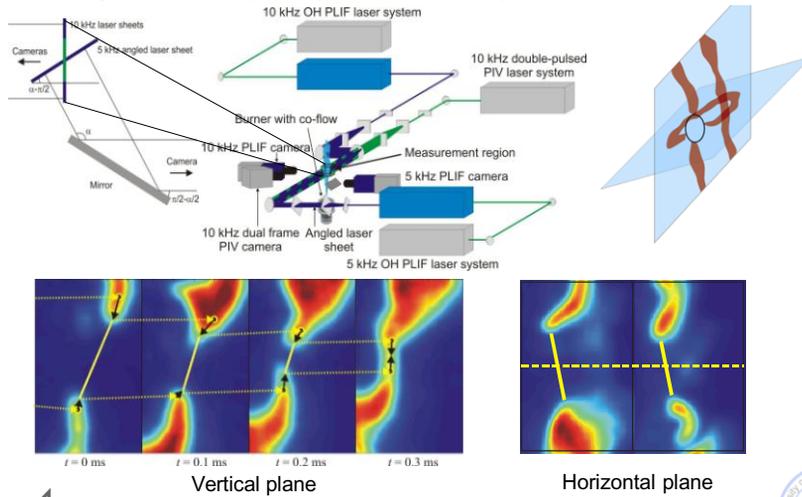
Dimensionality



Dimensionality

➤ Simultaneous cross-plane OH PLIF and PIV

To get a 10% uncertainty in the quantities of interest, only 4% of the data could be used

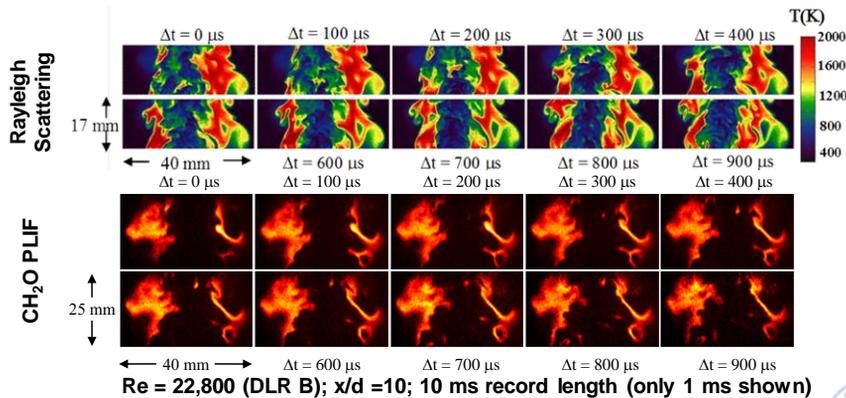
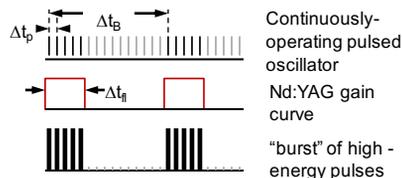


Limited Detectable Quantities

- Accurately quantifying scalars using high-speed systems is difficult
 - Laser limitations
 - High-speed imaging hardware limitations
- Most published work is based on OH PLIF
 - Continuous duty cycle DPSS lasers and dye lasers (Edgewave/Credo Monopoly)
 - $O(0.1 \text{ mJ/pulse})$ – Two orders of magnitude less than 10 Hz systems
- Many measurements require considerably more laser power
 - CH_2O
 - CH
 - Temperature
- New continuous duty cycle lasers are approaching the power levels needed for CH_2O PLIF
 - 6-12 mJ/pulse @ 355 nm, 5 kHz
- Continuous duty cycle systems vs. pulse burst

Limited Detectable Quantities

- Pulse-burst systems can be used to detect lower signal quantities over short-durations (Sutton et al. – Ohio State)



Doing Something Useful (Data Analysis)

- Must design experiments in which the acquired data can be used
 - To study dynamic cause-and-effect processes in a well-posed manner
 - With sufficient certainty to improve current understanding/models
- Consideration must be given to
 - The specific dynamic nature of the process
 - Tracking individual, frequently occurring events?
 - Identifying instants of one particular event?
 - Determining large scale dynamics?
 - The number of dimensions needed for the analysis
 - What species can be measured and what they represent with respect to the problem
- Details of how high-speed data is analyzed will likely remain problem specific
- There are common analysis 'themes' that are well suited for high-speed data



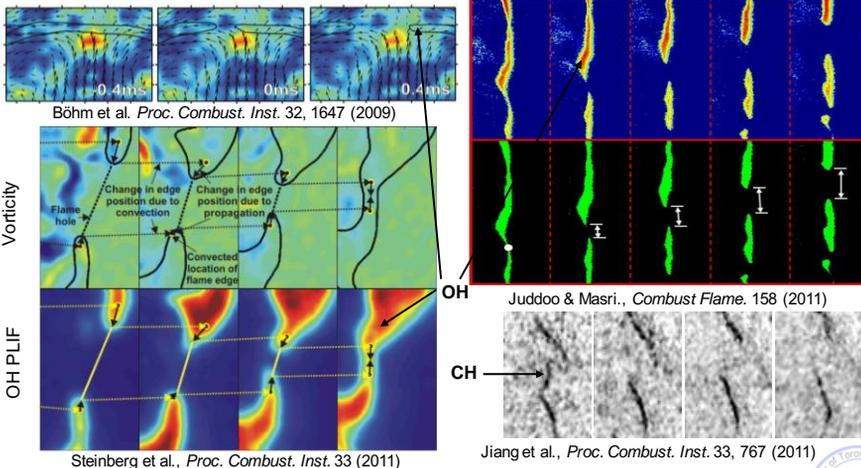
Doing Something Useful (Data Analysis)

- Event analysis (from which event statistics can be derived)
 - Lagrangian analysis
 - Eulerian analysis
 - Spatio-temporal correlation analysis
 - Event lead-up/timing
- Modal analysis
 - Proper orthogonal decomposition
 - Dynamic mode decomposition
- Spectrum and cross-spectrum analysis
- We will look at
 1. (Local) flame extinction
 2. Turbulent flame dynamics
 3. (Auto) ignition
 4. Flame stabilization, including flash-back and blow-off
 5. Other large-scale flame dynamics (thermo-acoustics)



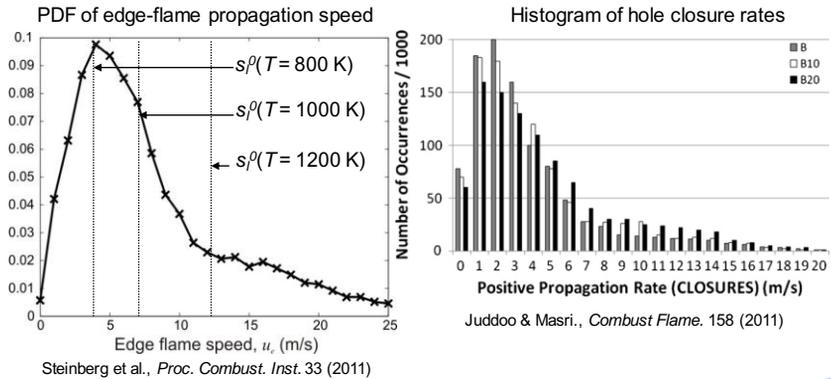
Local Flame Extinction

- Local flame extinction is a short-duration process that can be readily studied using high-speed diagnostics



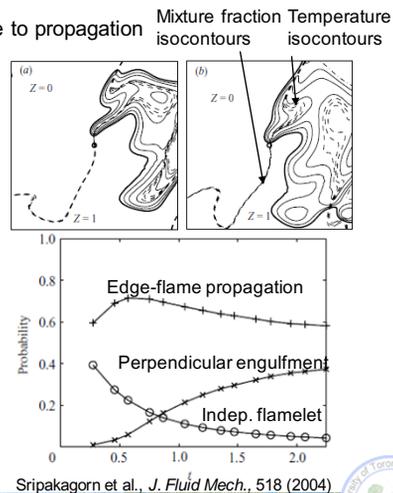
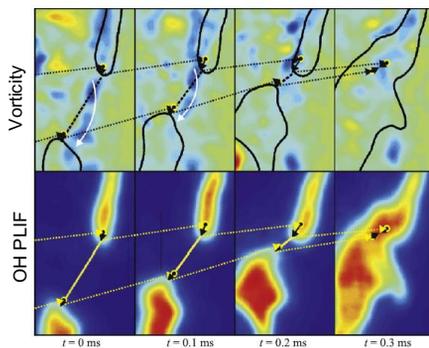
Local Flame Extinction

- Measured edge-flame propagation speeds are similar to measured hole-closure rates
 - The majority of flame-hole closure is due to propagation
 - Convective reignition is relatively minor



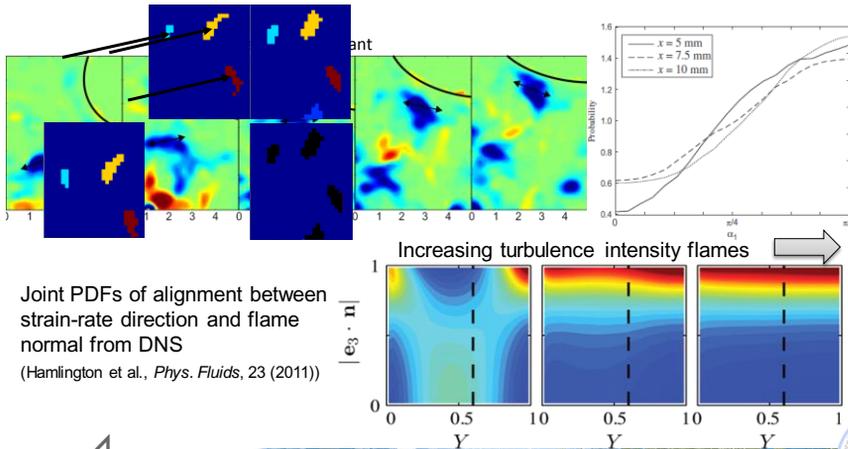
Local Flame Extinction

- Measured edge-flame propagation speeds are similar to measured hole-closure rates
 - The majority of flame-hole closure is due to propagation
 - Convective reignition is relatively minor



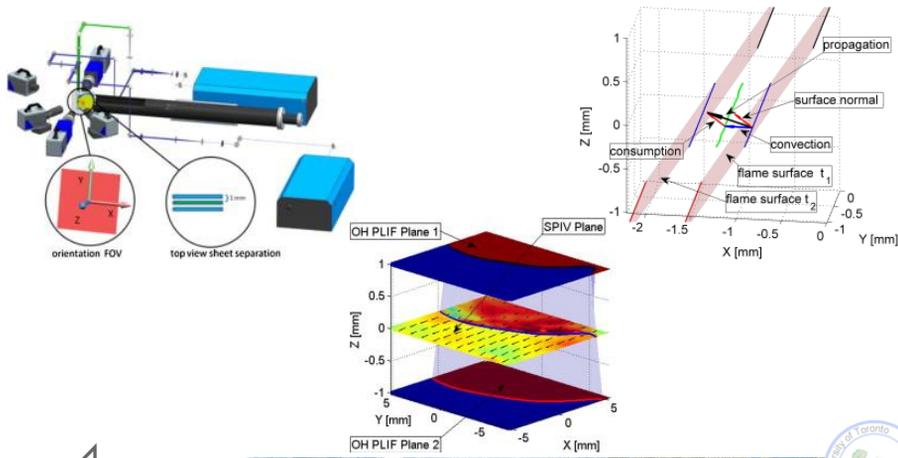
Turbulence-Flame Interactions

- Turbulence-flame interactions treated by following fluid elements as they interact with the flame (Steinberg et al., *Combust. Flame*, 159 (2012))



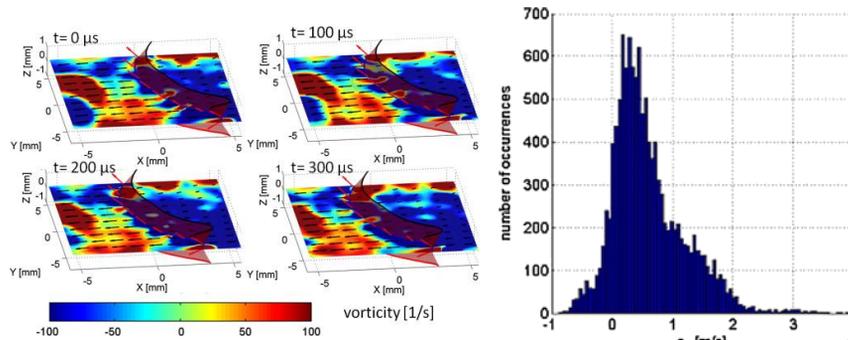
Turbulence-Flame Interactions

- Flame surface tracking to determine propagation speeds during turbulence-flame interactions (Trunk et al., *Proc. Combust. Inst.*, 34 (2012))



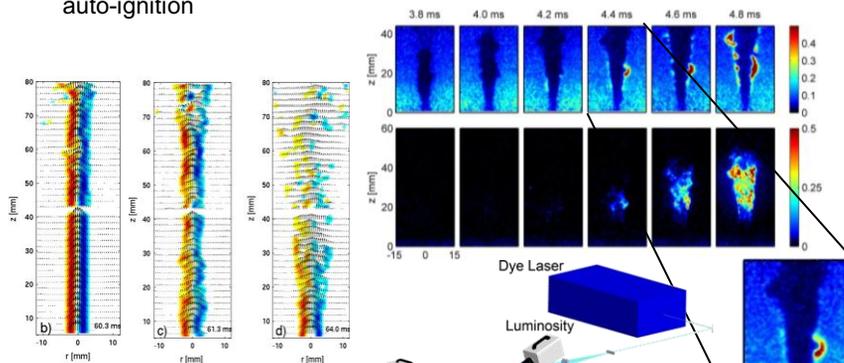
Turbulence-Flame Interactions

- Flame surface tracking to determine propagation speeds during turbulence-flame interactions (Trunk et al., *Proc. Combust. Inst.*, 34 (2012))
 - Consumption speed statistics computed
 - Conditioned statistics and rate-controlling turbulence-flame interactions can be determined from this form of analysis



Auto-ignition

- High-speed diagnostics can be used to capture the lead-up and onset of auto-ignition



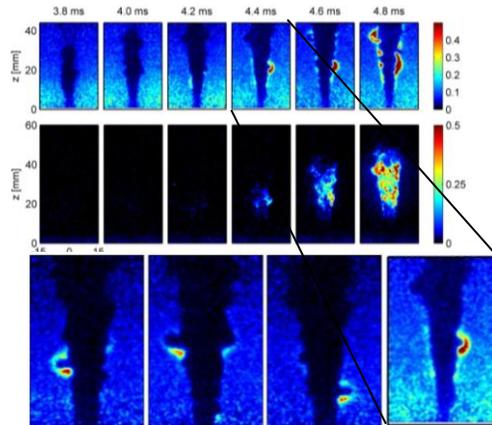
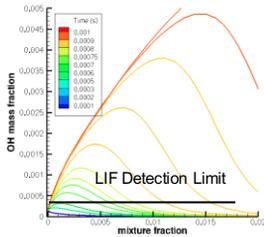
Laminar-to-turbulent transition prior to auto-ignition
Oldenhof et al., *Combust. Flame*, 159 (2012)

Kernel and jet topology at auto-ignition
Arndt et al., *Proc. Combust. Inst.*, 34 (2012)



Auto-ignition

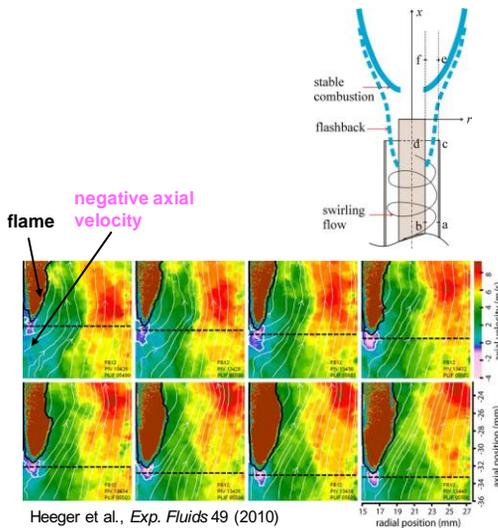
- High-speed diagnostics can be used to capture the lead-up and onset of auto-ignition
- How to define auto-ignition
- Sensitivity analysis of the PLIF system: ignition kernel detectable when $[OH]_{\text{kernel}} = 2x [OH]_{\text{coflow}}$



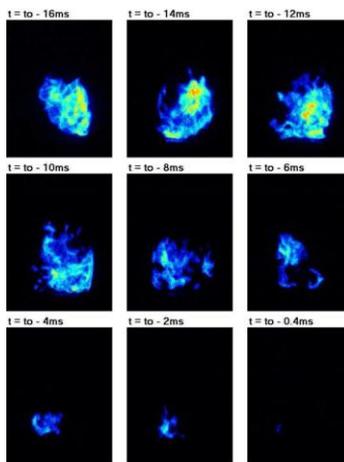
Kernel and jet topology at auto-ignition
Arndt et al., *Proc. Combust. Inst.*, 34 (2012)



Flame stabilization, flash-back, and blow-off



Heeger et al., *Exp. Fluids* 49 (2010)

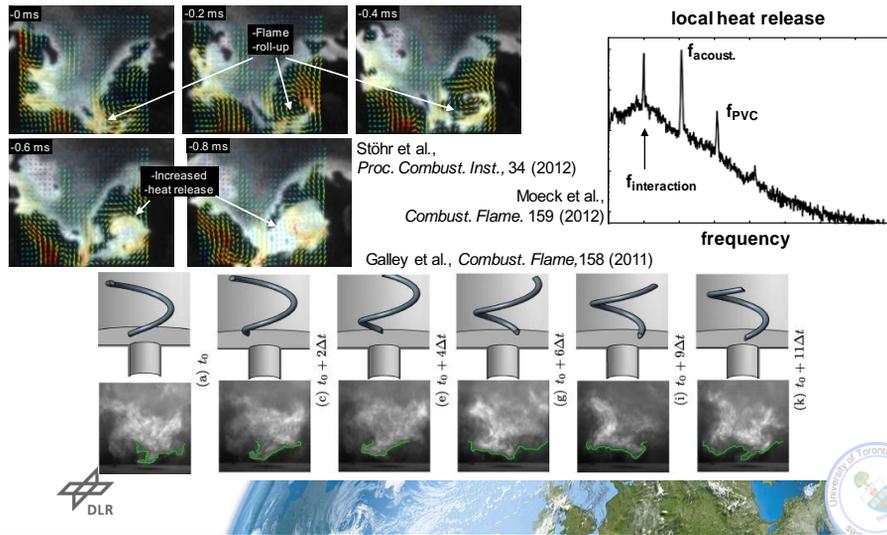


Dawson et al., *Proc. Combust. Inst.*, 33 (2011)



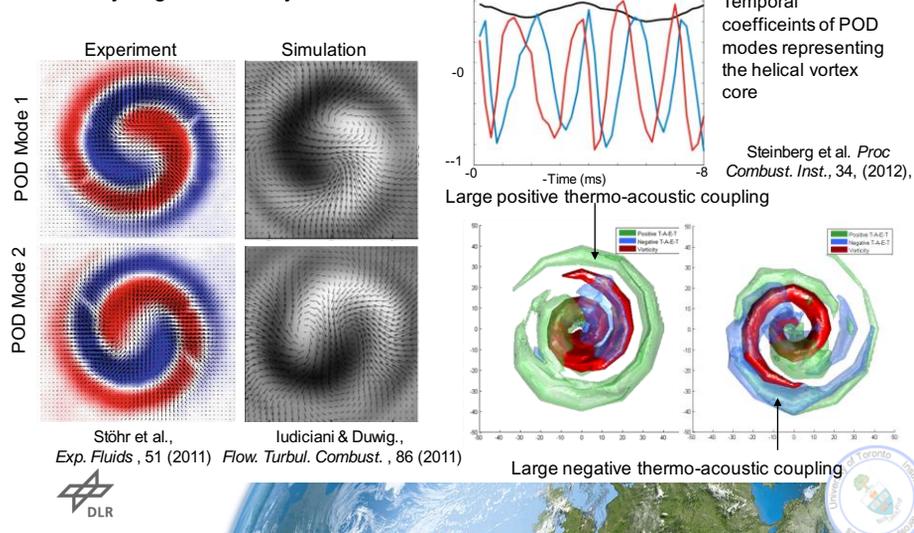
Energetic Dynamics in Swirl Flames

- Energetic flow and flame dynamics are being studied using event analysis, modal analysis, and spectral analysis



Energetic Dynamics in Swirl Flames

- Proper orthogonal decomposition has emerged as a powerful tool for analysing coherent dynamics



Conclusion/Best Practices

- Considerations for designing well-posed high-speed experiments are different than traditional experiments
 - Particular emphasis should be placed on accounting for 3D effects
 - Much more important for interpretation of time-resolved data than for statistical analysis of individual measurements
- Data analysis will remain problem specific, but there are several common techniques
 - Effort should be made over the coming years to standardize particularly useful analysis techniques
 - POD, DMD, correlation analysis
 - Allow for consistent data analysis and comparison between different experiments, as well as experiments and simulations



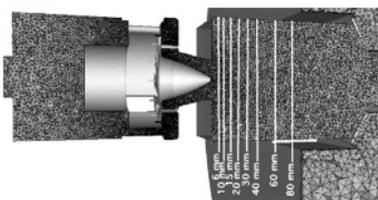
Time resolved data - A perspective from DNS & LES

- Steady (GT) vs Unsteady (IE) Combustion Systems

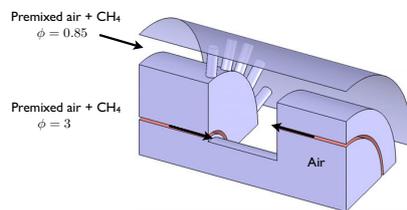
- Flame Dynamics vs Ignition Dynamics

✓ Ignition: A single instant in time and space, which must be isolated in both experiment and simulation

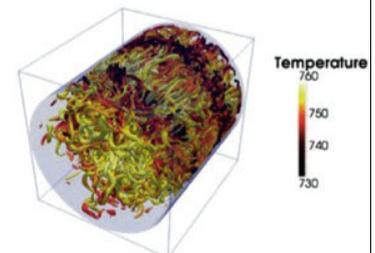
✓ Flame dynamics: Time sequences (not always time resolved), eventually featuring same statistics in experiments and simulations



B. Franzelli et al. Combust. Flame 159(2): 621-637, 2012



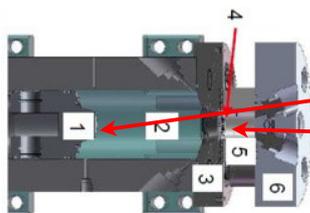
Luc Vervisch,



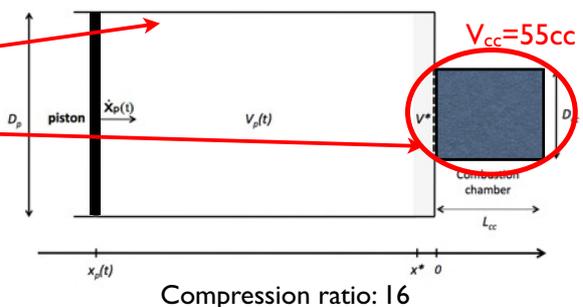
Lodier et al. Combust. Flame in press

Guillaume Lodier, Cindy Merlin, Pascale Domingo, Vincent Moureau
INSA de Rouen & CNRS CORIA

The extreme case: A rapid compression with ignition

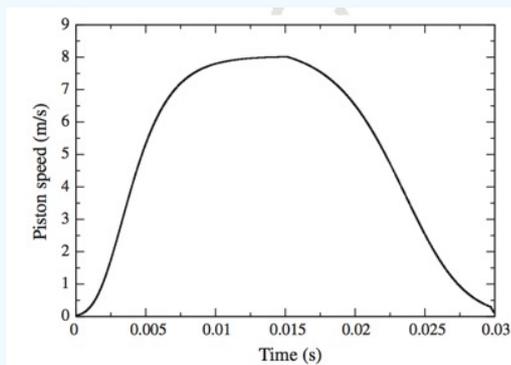


Guibert et al. (FTaC 84(1): 79-95, 2010)



- Velocity: 2D PIV

- PLIF: Localisation of ignition kernel and flame development



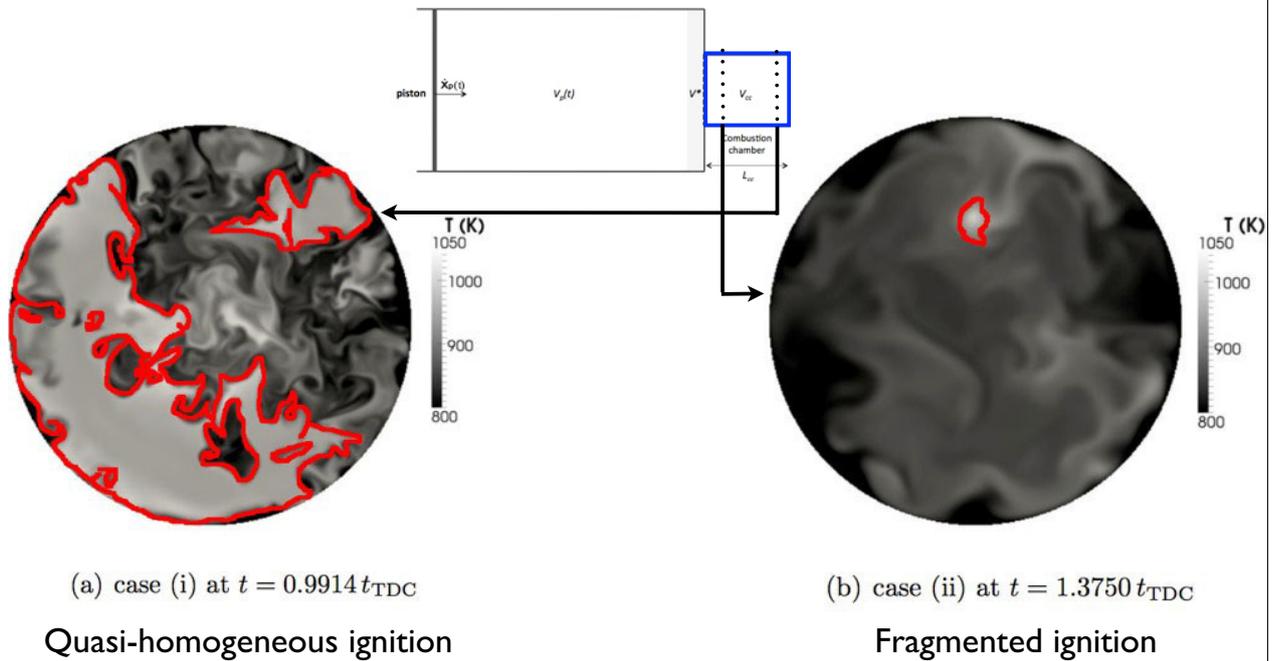
- DNS needs the exact piston speed to be relevant

$$U(r, \theta, t) = U_o(t)F^+(r) + u(r, \theta, t)$$

$$U_o(t) = \frac{R_v}{1 + R_v} \left(\frac{D_p}{D_{cc}} \right)^2 \dot{x}_p(t)$$

Time resolved ignition: Specific post-processing tools

- DNS resolution of 20 μm

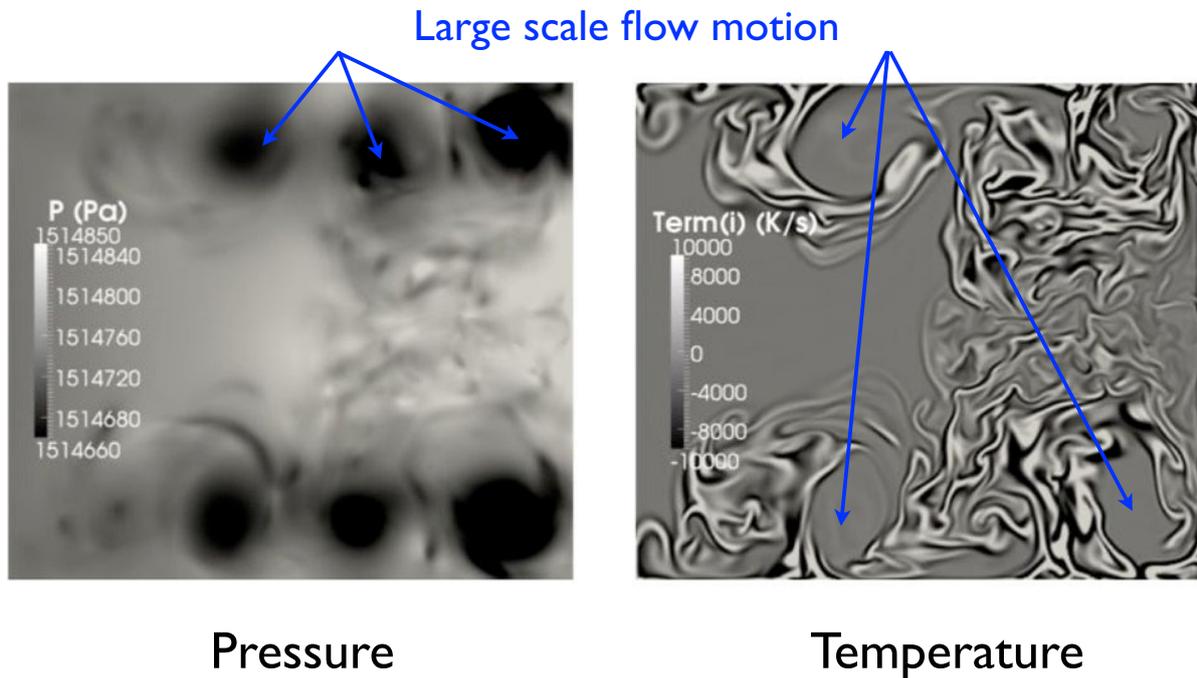


Time resolved ignition: Specific post-processing tools

- Localisation of the ignition kernel
- Time resolved analysis of the subsequent flame development
 - ✓ Eulerian: Store many 3D fields
 - ✓ Lagrangian: Follow flow path-lines (See E. Richardson et al. CTR SPI2)
- Introduce specific flow budgets which can be tracked in time
 - ✓ For instance a specific form of energy budget:

$$\text{---} = \frac{1}{\rho} \left(\underbrace{\nabla \cdot (\lambda \nabla)}_{(i)} + \underbrace{\dot{\omega}_T}_{(ii)} + \frac{1}{\gamma - 1} \underbrace{\dot{v}}_{(iii)} \right) - (\gamma - 1) \nabla \cdot \mathbf{u}$$

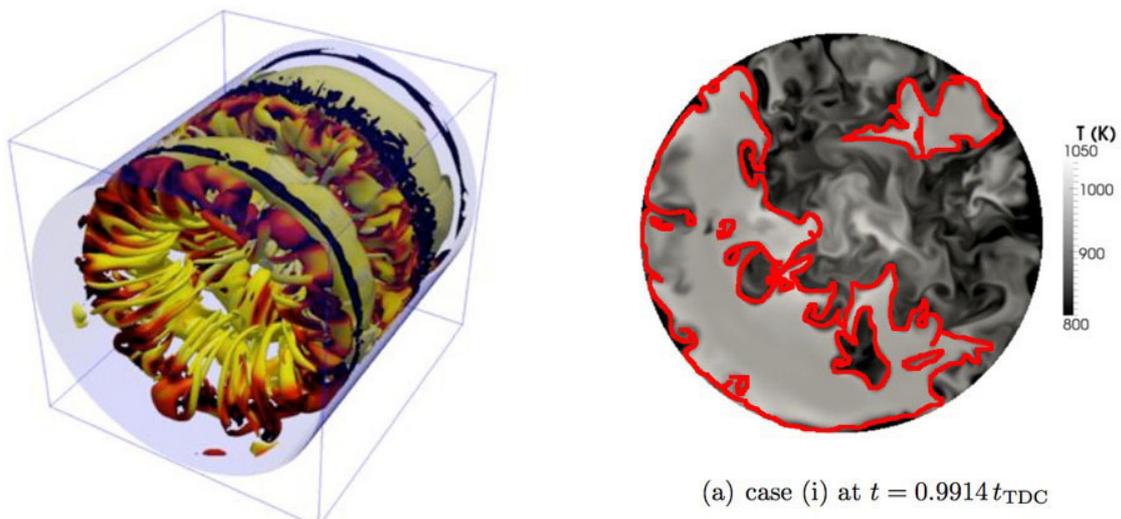
Time resolved ignition: Flow rollers are thermally insulated



5

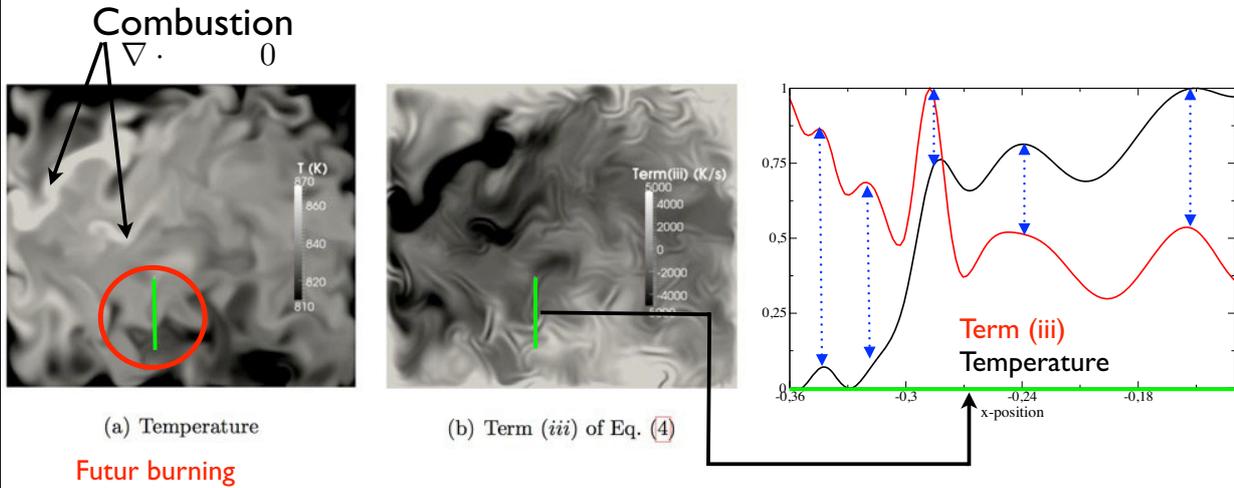
Time resolved ignition: Quasi-homogeneous ignition

- DNS & Experiment reveal that short ignition delays lead to quasi-homogeneous ignition because of 'thermally isolated' coherent structures



Time resolved ignition: Fragmented ignition

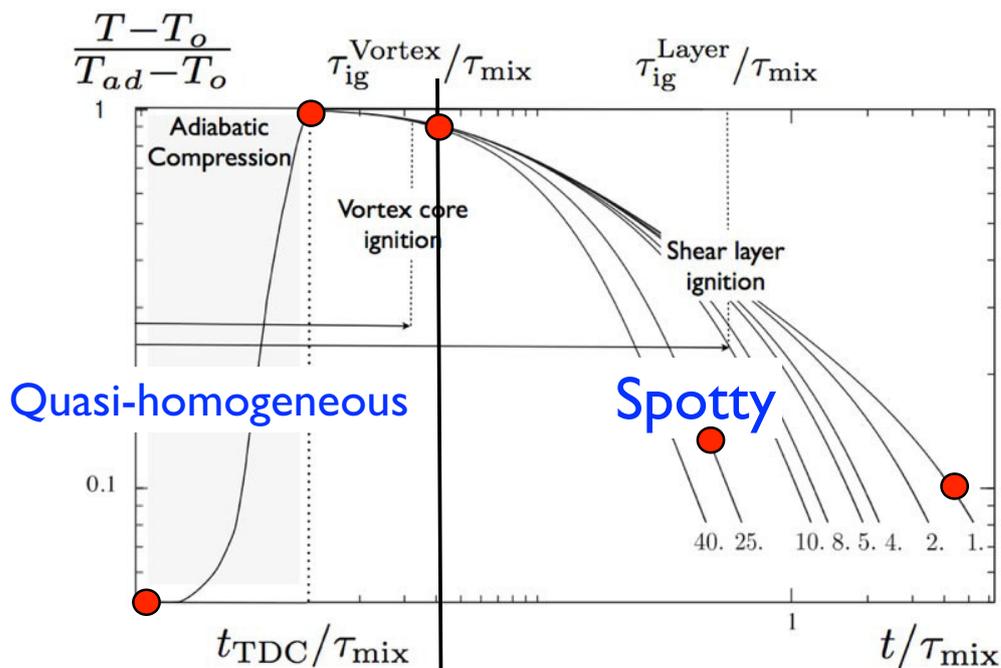
- Need to rewind time (not always that easy...)



$$\frac{\dot{Q}}{\rho v} = \frac{1}{\rho v} \left(\underbrace{\nabla \cdot (\lambda \nabla T)}_{(i)} + \underbrace{\dot{\omega}_T}_{(ii)} + \frac{1}{\gamma - 1} \underbrace{\nabla \cdot \mathbf{u}}_{(iii)} \right) - (\gamma - 1) \nabla \cdot \mathbf{u}$$

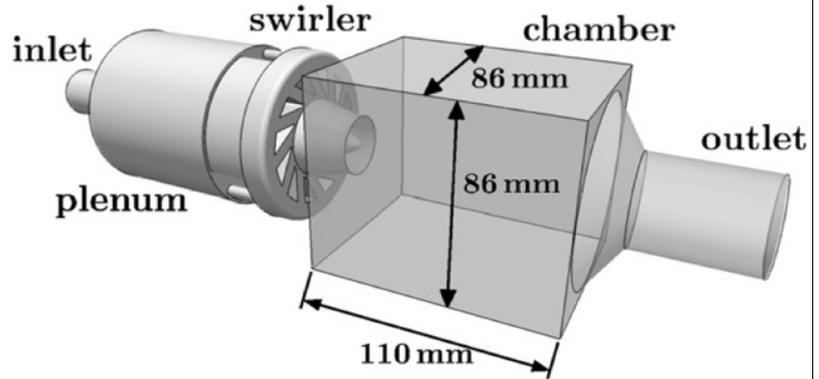
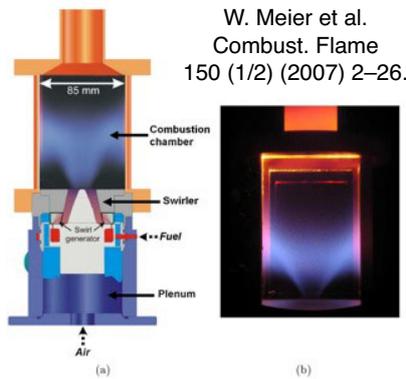
7

Summarize time-resolved analysis in a 'global picture'



Lodier et al. Combust. Flame in press

Flame Dynamics in burners which are steady in mean



Re	u'	Re_T	Re_λ	l_T	τ_t	η_K
40000	3.5 m/s	1480	149	7 mm	2 ms	29 μ m

S_L	δ_L	Da	Ka
29 cm/s	0.424 mm	7.51	7.23

Time resolved measurements compared against LES?

- Experiments and LES are unlikely to be resolved at the same scale
 - ✓ Perform LES for various resolutions
 - ✓ Post-process experiments and LES using same tools:

- ◆ Filtering
- ◆ POD
- ◆ DMD

Varying LES resolution (Moureau et al. 2011)

Cells in Million	1.7	14	110	329
Δ [mm]	1.2	0.6	0.3	0.2
$\ell_T \Delta$	5.8	11.7	23.3	35.0
$\Delta \eta$	41.4	20.7	10.3	6.9
$\delta_L \Delta$	0.35	0.71	1.41	2.12
c	0.8	0.7	0.25	0.15

- **Localized Dynamic Smagorinsky Closure**

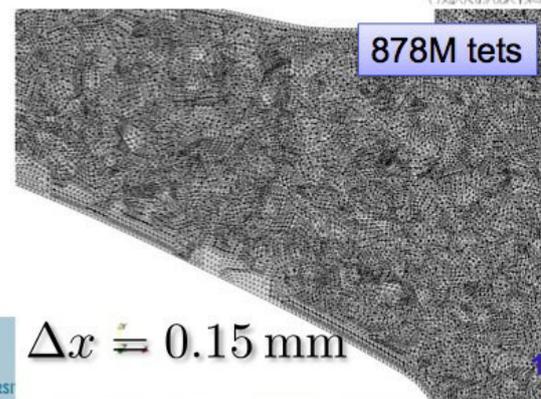
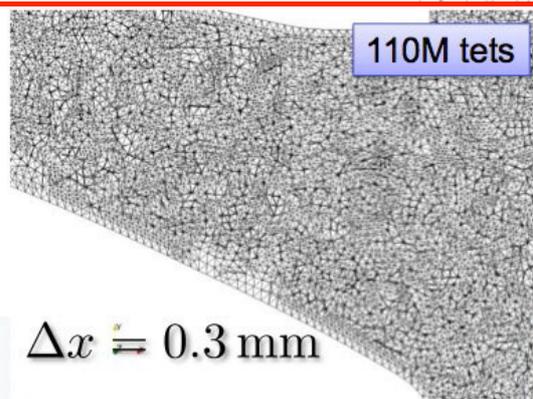
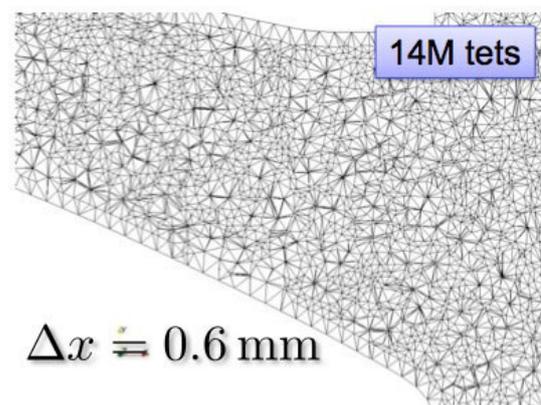
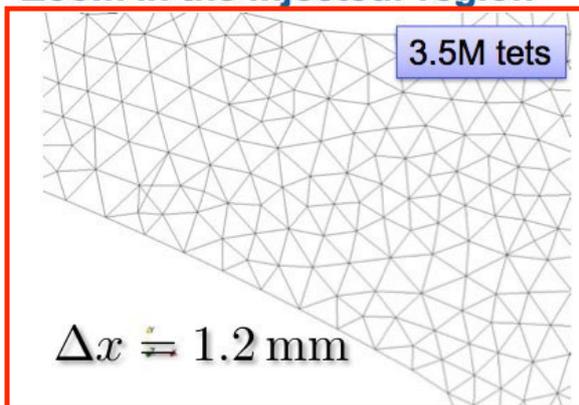
Germano et al. *Phys. Fluids* 3 (7): 1760–1765, 1991

- **Premixed flamelet modeling with Beta-Presumed PDF**

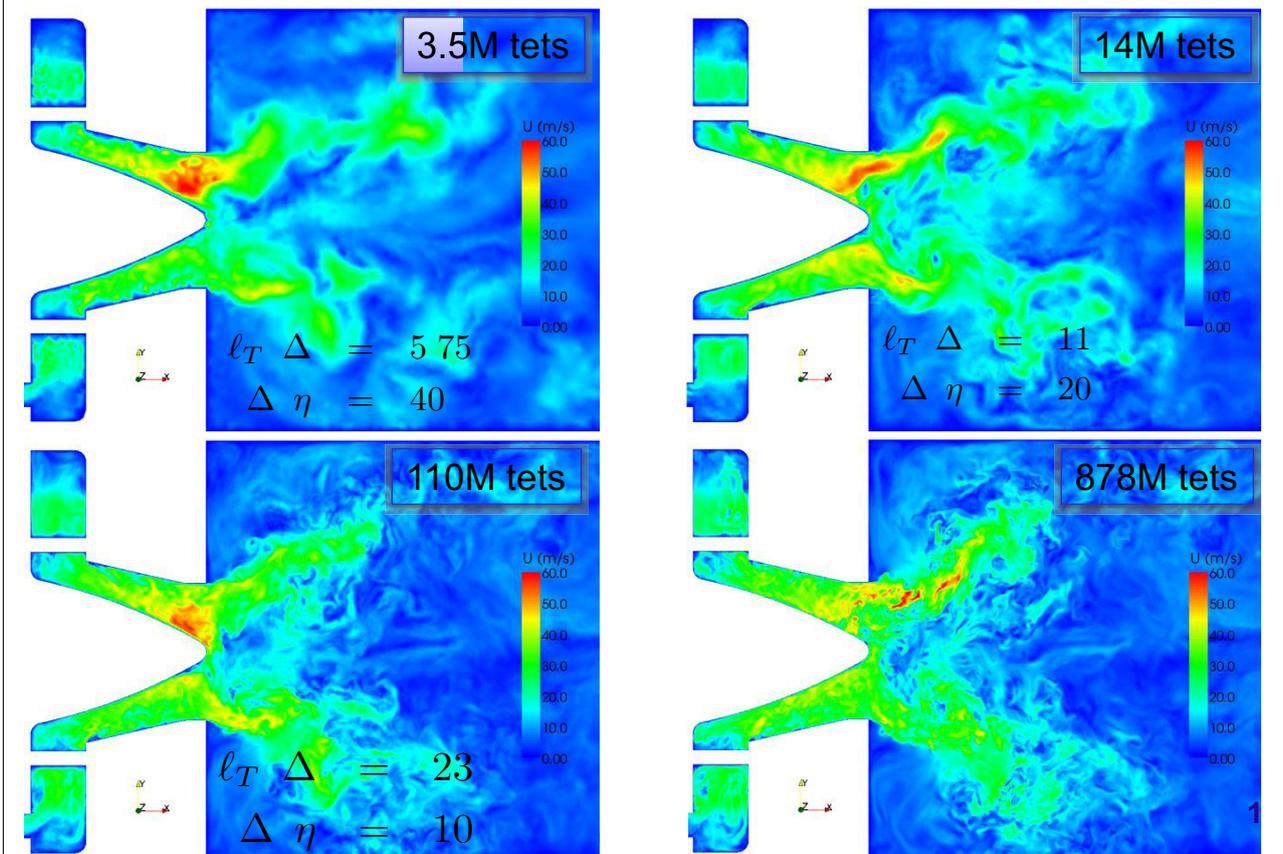
J. Galpin et al. *Combust. Flame* 155(1–2): 247–266, 2008

The mesh

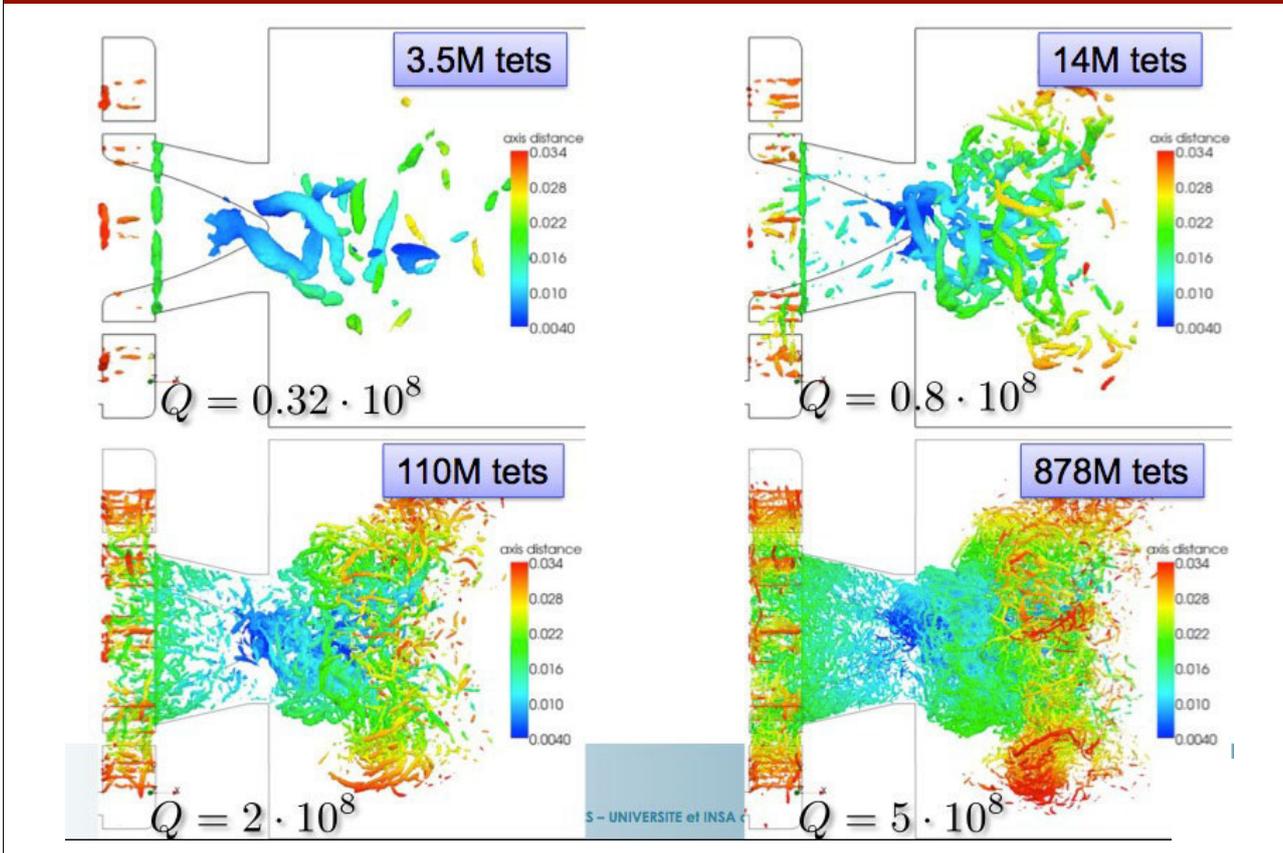
► Zoom in the injecteur region



Varying LES resolution (Moureau et al. 2011)

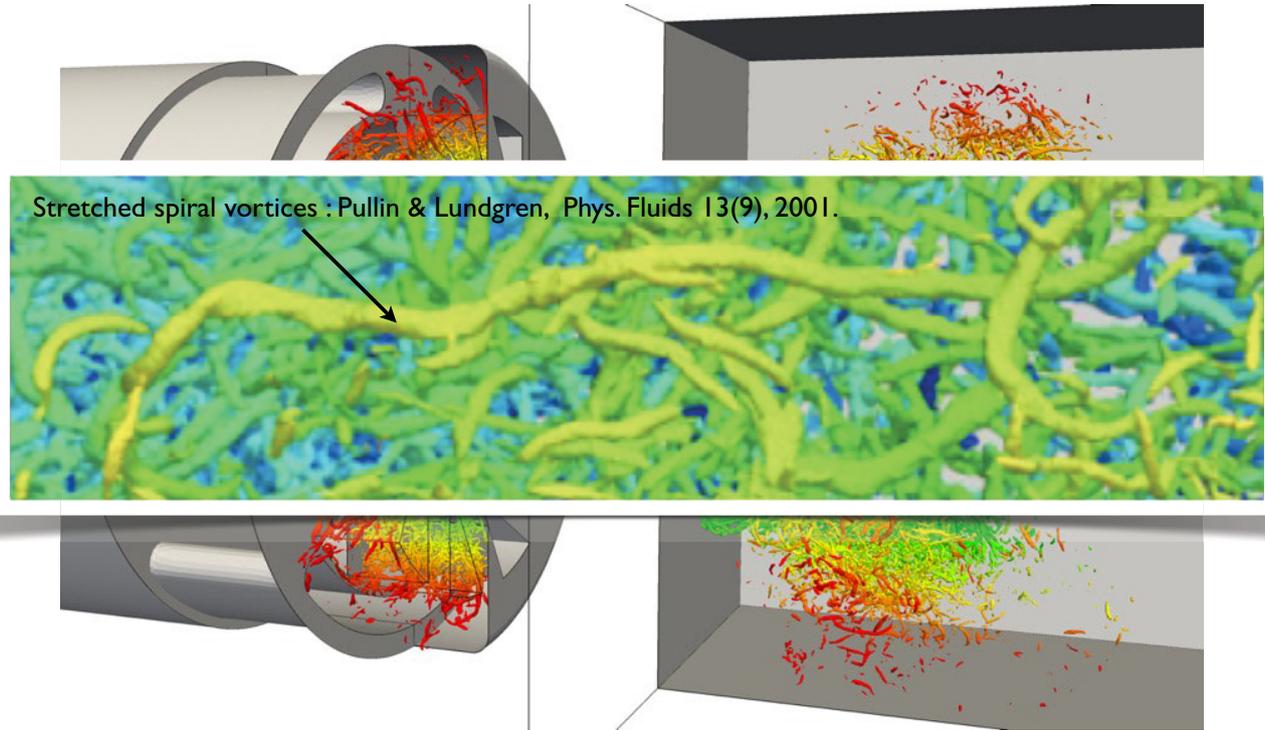


Varying LES resolution (Moureau et al. 2011)

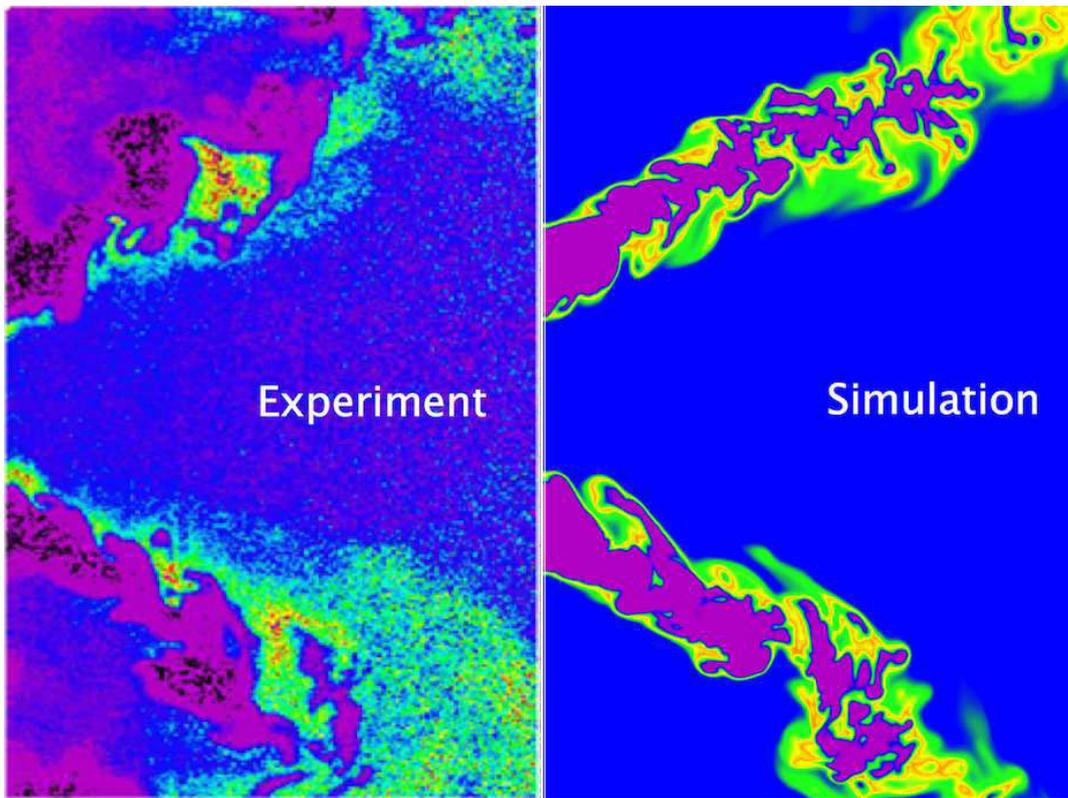


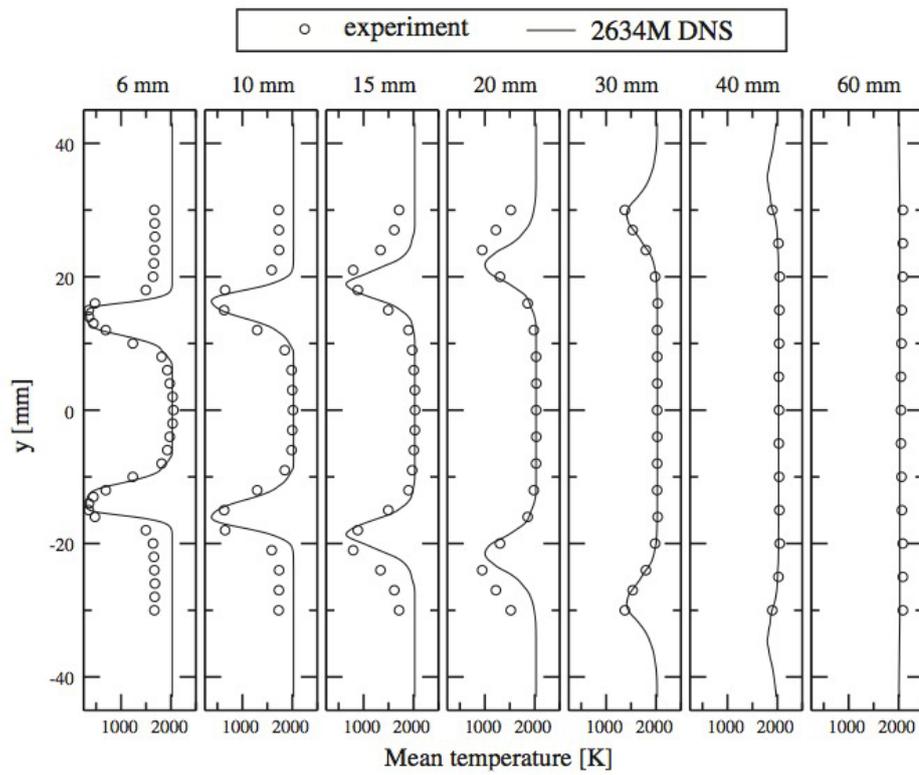
PLIF against Quasi-DNS

2.6B cells (YALES2 up to I45B this summer)

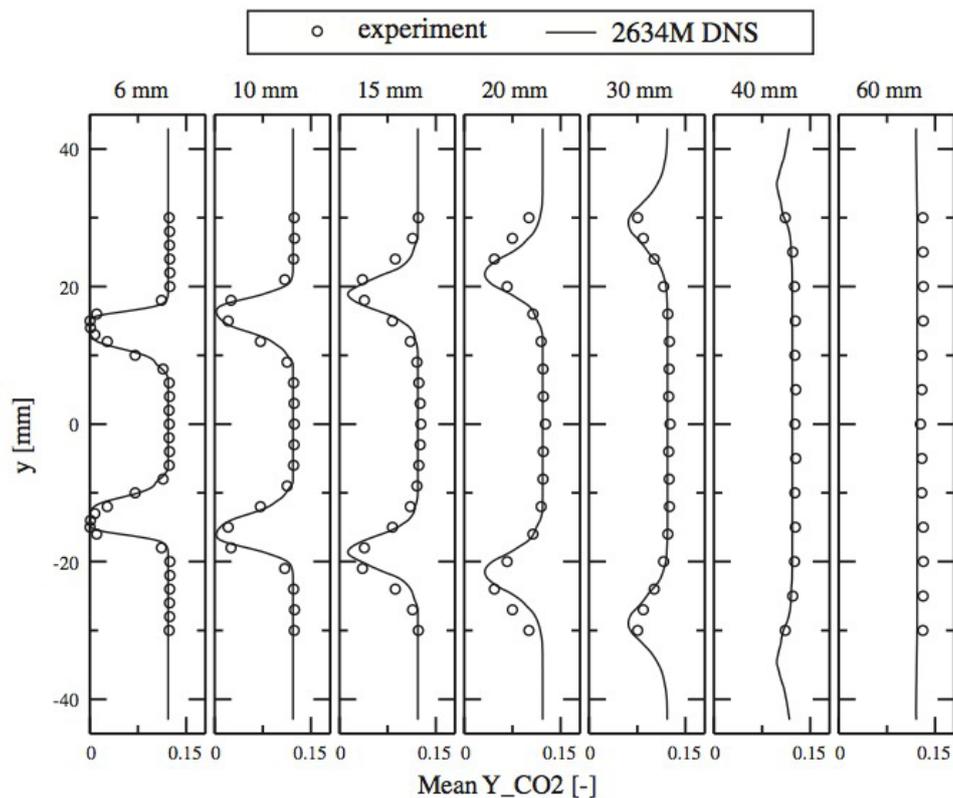


PLIF against Quasi-DNS





V. Moureau et al. *Combust. Flame* 158(7): 1340-1357, 2011



V. Moureau et al. *Combust. Flame* 158(7): 1340-1357, 2011

Flame dynamics in Trapped Vortex Combustor

Burguburu et al. ASME GT2010
Merlin et al. Submitted

TECC-AE

Main Lean-premixed

$$\phi = 0.85$$

$$\dot{m}_{Air} = 20 \text{ g/s}$$

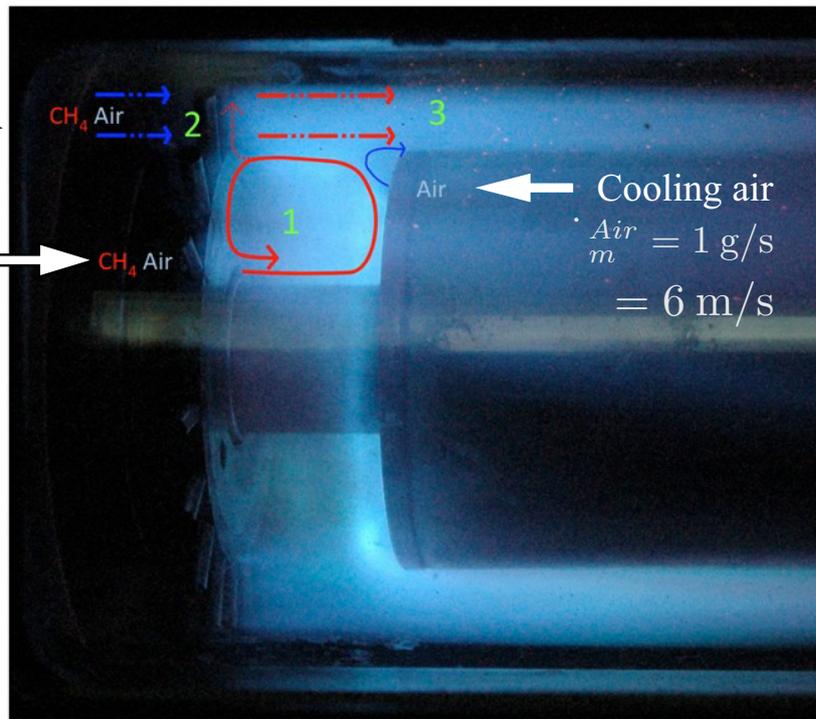
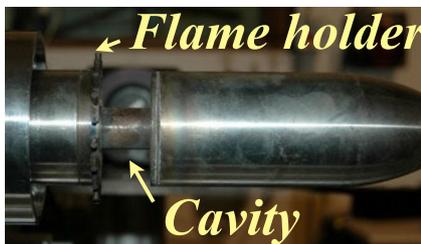
$$= 8 \text{ m/s}$$

Rich-premixed pilot

$$\phi = 3.0$$

$$\dot{m}_{Air} = 0.7 \text{ g/s}$$

$$= 8 \text{ m/s}$$



Fully compressible immersed boundaries

SiTCom

P. Domingo et al. (2008) *Combust. Flame* 152(3): 415-432.

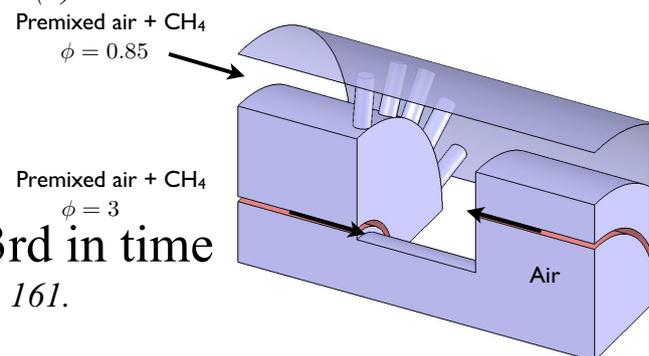
- Finite Volume Scheme
 - Fully compressible
 - 4th order in space and 3rd in time
- Ducros et al. (2000), *J. Comput. Phys.* 161.

- 3D-NSCBC boundary conditions

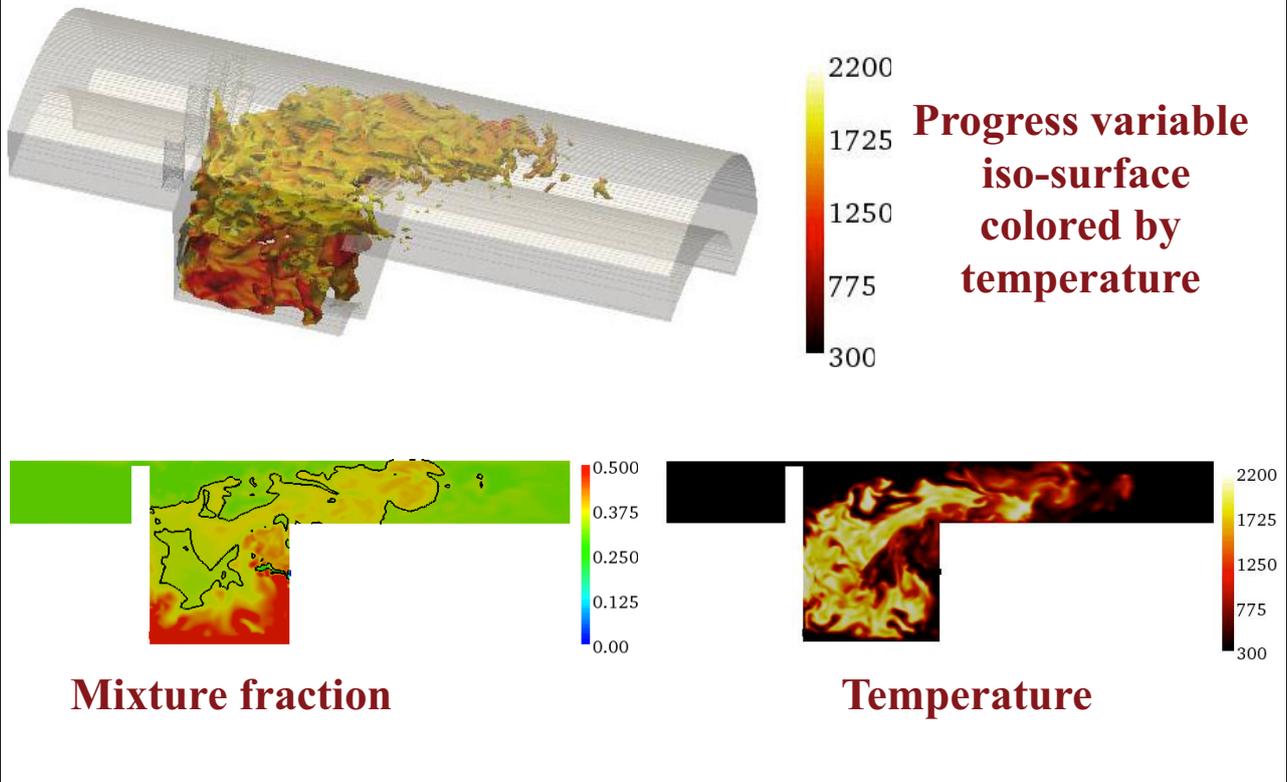
Lodato et al. (2008), *J. Comput. Phys.* 22.

- Immersed Boundary Method for cartesian mesh with acoustic BC

Merlin et al., *FTaC*, Submitted



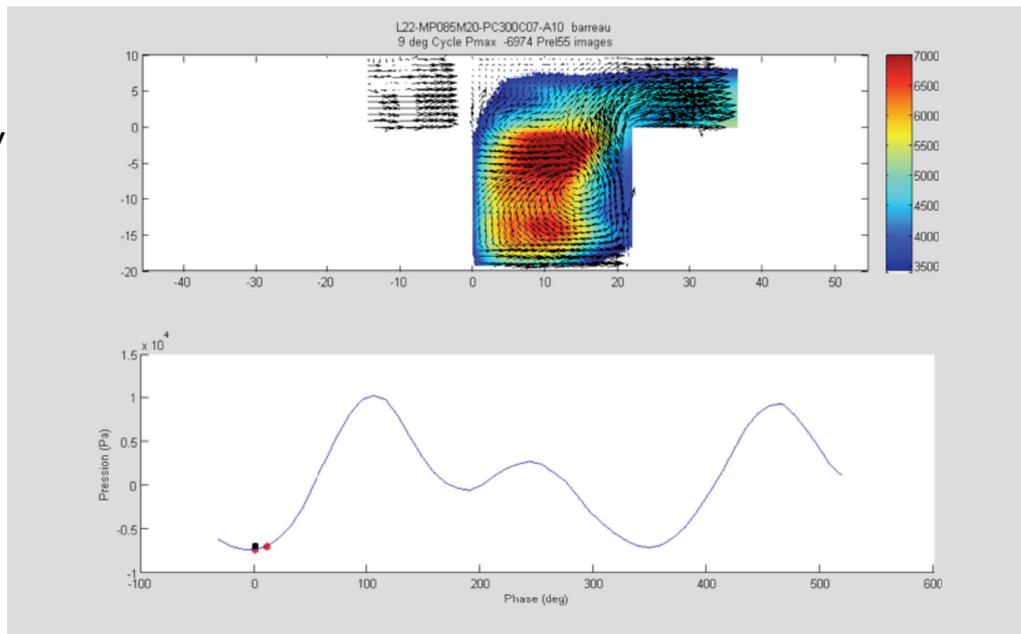
Flame dynamics



Flame dynamics in Trapped Vortex Combustor

Not resolved in time, but time sequences can be compared

Instantaneous PIV
flow field-Mean
CH* emissions

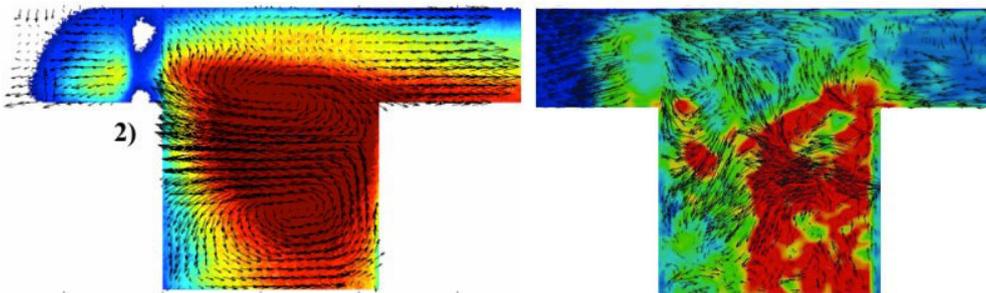
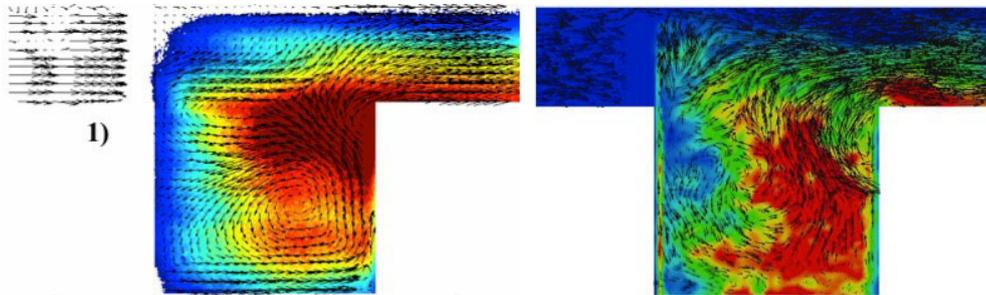


Burguburu et al. ASME GT2010
Merlin et al. Submitted

Flame dynamics in Trapped Vortex Combustor

Experiment

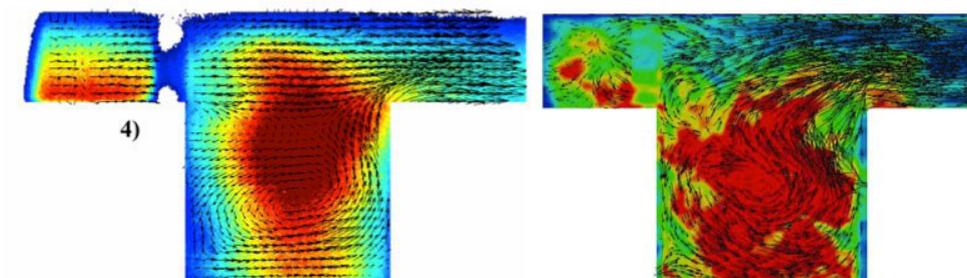
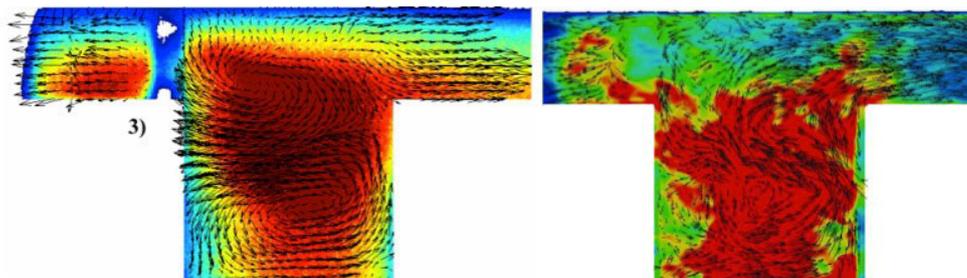
LES



Flame dynamics in Trapped Vortex Combustor

Experiment

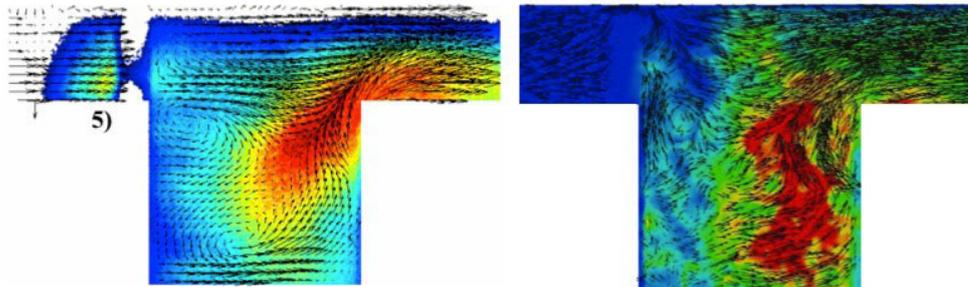
LES



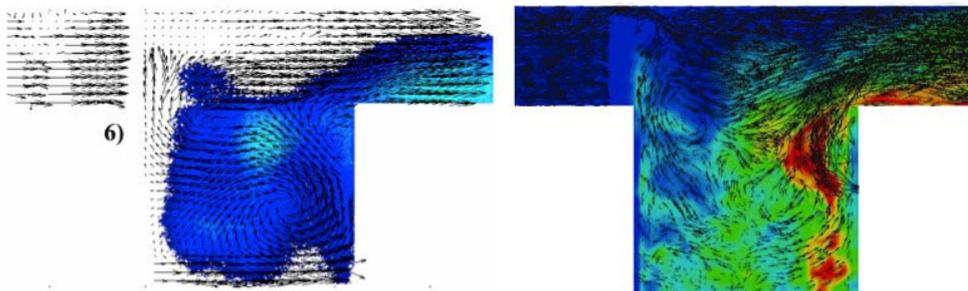
Flame dynamics in Trapped Vortex Combustor

Experiment

LES

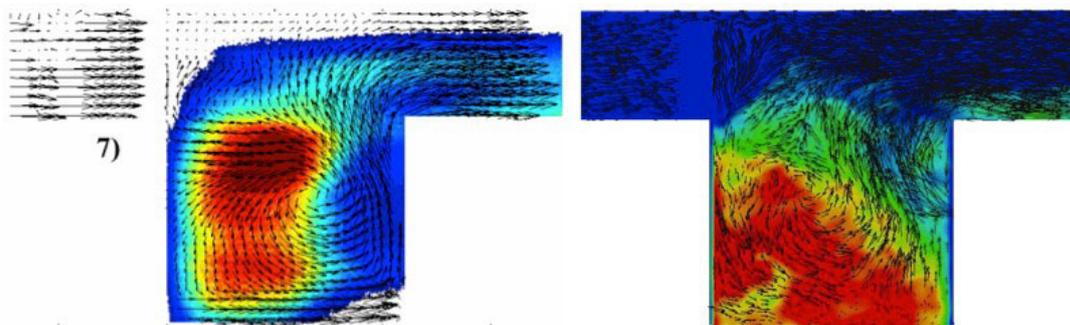


(c) $\theta = 229^\circ$



(a) $\theta = 289^\circ$

Flame dynamics in Trapped Vortex Combustor



(b) $\theta = 349^\circ$

- Flame dynamics can be compared
- More is learned on turbulent flames
- Reproduce first flame dynamics or statistics?

LES/DNS Quality and Best Practices

Joe Oefelein, Luc Vervisch, Steve Pope

LES and DNS have become topics of central interest in the TNF workshop due to 1) the potential benefits LES has over classical Reynolds-Averaged Navier-Stokes approaches, and 2) the potential DNS has for providing insights toward model development. There are still many open questions, however, related to implementation of these methods and the sensitivity of various inputs on the results and model accuracy. Efforts over the past several workshops have been focused on establishing robust performance metrics to assess the “quality” of a given simulation in a manner that minimizes potential sources of error. The goal for TNF11 was to continue to build off of these past efforts by first providing a broad summary of what has been learned to date followed by development of a new more formal set of criteria that provides improved quality metrics to assess model accuracy.

The need for improved quality metrics has been recognized now for many years. In TNF8, for example, attempts to model the bluff-body flames (e.g., HM1) produced many ambiguities. Two issues arose from initial comparisons: 1) uncertainty with respect to boundary conditions, and 2) uncertainty with respect to code and simulation parameters (i.e., numerics, grid-resolution, time-step, integration time, etc.). The combined uncertainties made it difficult to draw any conclusions regarding model accuracy. Codes with a variety of different numerical schemes and capabilities (e.g., with and without explicit artificial dissipation added for stability) were used. Geometric details of the burner (which are surprisingly complex) were not resolved in most cases. Limited computational resources imposed significant constraints on the levels spatial/temporal resolution applied, all of which is a typical dilemma. These types of uncertainties are even more severe for applications.

In TNF9, algebraic error indicators were applied to the HM1 flame to explore their utility in the context of the observations above. It was shown that these indicators could produce anomalous results. Dissipative schemes (or application in laminar flows) produced misleading performance trends. Use of bulk averages instead of instantaneous quantities was problematic. Measures of turbulent kinetic energy were shown to be divergent and/or anomalous (e.g. for dissipative schemes velocity fluctuations are damped and low values of turbulent viscosity suggests good “resolution” as a consequence). Detailed analysis of results led to the conclusion that these types of indicators do not account for various sources of error correctly.

A second focal point in TNF9 and TNF10 was application of the error-landscape concept to LES (Geurts et al.). This method inherently accounts for the competing effects of numerical and modeling errors simultaneously. The primary advantage of this technique is that it identifies combinations of grid, filter, and model parameters that introduce incorrect flow and combustion physics. Thus, it allows one to simultaneously minimize the competing effects of modeling errors and numerical errors. The disadvantage, however, is that the error cannot be reduced to any arbitrary level and the method is expensive to implement (but still cheaper than refining the grid to eliminate non-optimal minimization of errors). Likewise, grid dependence studies were presented as part of TNF10 with emphasis placed on parametric uncertainties and recursive filter refinement.

Based on these findings, improved performance metrics based on a new local resolution criteria was proposed and presented. The new criteria is based on quantifying the sub-filter

scales that a given turbulent combustion model is capable of representing as a function of critical parameters. The analysis and discussion led to the following progressive set of recommendations to guide ongoing research:

- Grid resolution and coupling between grid and filter spacing must be quantified
 - Simple global refinements are not sufficient
 - Pros/cons of implicit versus explicit filtering need to be better quantified
 - Local resolution criteria needs to be established as function of sub-filter scales
 - Local grid distributions need to be reported and checked in critical regions of flow
- Metrics for model applicability and implementation need to be reported
 - Grid spacing ... numerical parameter
 - Filter width ... model parameter
 - Competition between numerical and model errors
- More documentation of key simulation parameters
 - Algorithmic characteristics of codes (spatial, temporal, stabilization method)
 - Local grid resolution, key length/time scales, related parameters
 - Boundary conditions and sub-model implementation
- Work toward UQ to determine sensitivity of uncertain parameters
 - Boundary conditions, model parameters, baseline model assumptions
 - Large space of uncertain parameters, general guidelines

The goal for TNF12 will be to apply these new criteria to key target flames to demonstrate the method and define a more precise set of requirements based on the recommendations above.

LES/DNS Quality and Best Practices

Joe Oefelein, Luc Vervisch, Steve Pope

Eleventh International Workshop on Measurement and
Computation of Turbulent (Non)Premixed Flames

Darmstadt Germany, July 26-28 2012

Outline

1. Summary of past TNF discussions in this area
 2. Toward development of improved “formal” resolution criteria for LES
 3. Analysis of (need for??) explicit filtering in the context of reacting flows and resolving scalar gradients
 4. Discussion with a goal of adopting at least some improved performance metrics and criteria
- Items 1, 2 – Oefelein; Items 2, 3 – Vervisch; Item 4 – Pope
 - ... Toward TNF12

TNF8: Attempts to model bluff-body flames produced many ambiguities

- **Two issues arose from initial comparisons**
 - **Uncertainty with respect to boundary conditions**
 - **Uncertainty with respect to code parameters (numerics, grid-resolution, time-step, integration time, etc.)**
- **Combined uncertainties make it difficult to draw any conclusions regarding model accuracy**
 - **Codes with a variety of different numerics and capabilities**
 - **Geometric details of burner (which are surprisingly complex) are not resolved in most cases**
 - **Limited computational resources impose significant constraints on spatial/temporal resolution applied**
- **A typical dilemma ...**

Even more difficult for applications ... tougher conditions, less data

- **GT aircraft engines**
 - **Spray inevitably leads to partial premixing**
 - **Multiple streams**
 - **Augmentors – stratified; multiple streams**
 - **Combustion instabilities**
- **GT for power generation**
 - **Almost premixed**
 - **Small mixture inhomogeneities influence performance**
 - **Combustion instabilities**
- **IC engines**
 - **Diesel – high-pressure DI, stratified**
 - **Gasoline – low-pressure DI**
 - **HCCI – Small mixture inhomogeneities influence performance**

TNF9: Algebraic error indicators applied to HM1 flame (Kempf et al.)

Contributions

- ANSYS-CFX/Fluent, G. Goldin

ANSYS

TNF9: Algebraic error indicators applied to HM1 flame (Kempf et al.)

Cases

NRBB

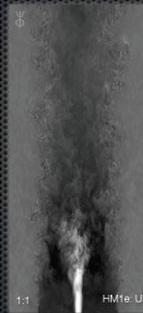
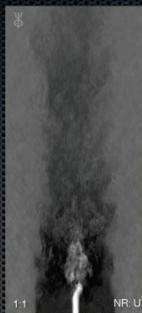
air, 20 m/s, 61 m/s
velocity measurements

HM1e

fuel, 35 m/s, 108 m/s
velocity measurements

HM1

fuel, 40 m/s, 118 m/s
scalar measurements



Imperial College
London

TNF9: Algebraic error indicators applied to HM1 flame (Kempf et al.)

- Viscosity ratio

$$VR = \frac{\mu_t}{\mu_{lam}}$$

- Energy ratio ('Pope criterion' with Lilly model)

$$ER \approx \frac{E_{res}}{E_{res} + \langle E_{sgs} \rangle}; \quad \langle E_{sgs} \rangle = \left(\frac{\langle \nu_t \rangle}{c\Delta} \right)^2; \quad c = 0.094$$

- LES-IQ (Celik, based on viscosity)

$$LESIQ_v = \frac{1}{1 + 0.05 \left(\frac{\nu + \nu_t}{\nu} \right)^{0.53}}$$

- LES-IQ (Celik, based on grids)

$$LESIQ_\nu(x) = \left(1 + \left(1 - \frac{K^c}{K^l} \right) \left/ \left(\left(\frac{\Delta}{\Delta'} \right)^p - 1 \right) \right. \right)^{-1}$$

- Systematic Grid and Model Variation (Klein)

$$ER = \frac{E_{res}}{E_{DNS}} \approx \frac{E_{res}}{E_{res} + E_{sgs}} \quad E_{sgs}^{Klein} = \frac{E_3 - E_1}{1 - \alpha} + \frac{(E_2 - E_1) - (E_3 - E_1) \frac{1 - \beta^m}{1 - \alpha}}{1 - \beta^n}$$

Imperial College
London

TNF9: Algebraic error indicators applied to HM1 flame (Kempf et al.)

- Can produce anomalous results
 - Dissipative schemes or application in laminar flows produce misleading performance trends
 - Use of bulk averages instead of instantaneous quantities can be problematic (but converse is true also ...)
- $LESIQ_v$ is well defined instantaneously, but
 - Measure of energy can be divergent (>80% criteria can be biased by this)
- For dissipative schemes
 - Velocity fluctuations damped
 - Low values of turbulent (Smagorinsky) viscosity
 - Suggests good “resolution” as a consequence (perfect quality for MILES approach)

These indicators do not account for various sources of error correctly

Discretization and modeling introduce errors:

$$\begin{aligned}\partial_j(\overline{u_i u_j}) &= [\delta_j(\overline{u_i u_j}) + \mathcal{D}_i] + \partial_j \tau_{ij} \\ &= [\delta_j(\overline{u_i u_j}) + \mathcal{D}_i] + \{\partial_j m_{ij} + \mathcal{R}_i\} \\ &= \delta_j(\overline{u_i u_j}) + \delta_j m_{ij} + (\mathcal{D}_i + \mathcal{R}_i + \mathcal{D}_i^{(m)})\end{aligned}$$

Distinguish:

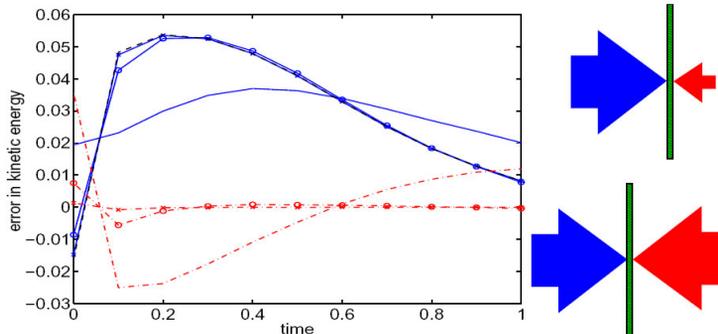
- \mathcal{D}_i : discretization error from using method δ_j
- $\mathcal{R}_i = \partial_j(\tau_{ij} - m_{ij})$: total 'model-residue'
- $\mathcal{D}_i^{(m)}$: error when treating model m_{ij} , e.g., filtering

Q1: Justified to ignore \mathcal{D}_i ? Grid-(in)-dependent LES?

Q2: Interacting errors? Error-decomposition? Dominance?

TNF9: Error-landscape concept applied to LES (Geurts et al.)

Competing effects of numerical and modeling errors must be considered simultaneously (paradoxical error cancellation)



Decaying turbulence: discretization, modeling and total-error

- better model may result in worse predictions
- better numerics may result in worse predictions

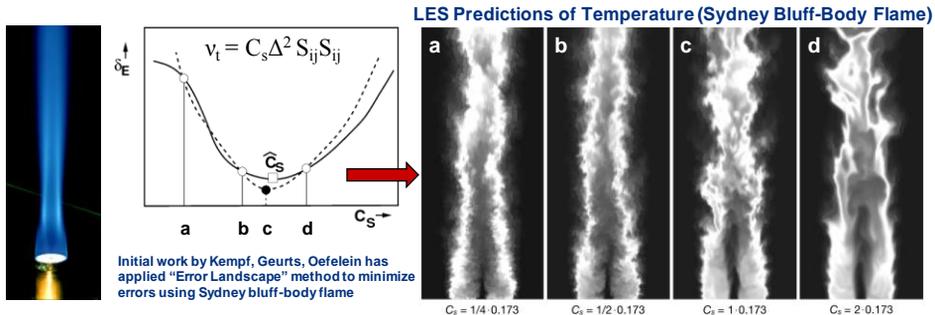
TNF9: Error-landscape concept applied to LES (Geurts et al.)

- Error defined for A quantities at M locations using expression of the form:

$$E^2 = \sum_{\alpha=1}^A \sum_{i=1}^M W_{\alpha,i} \left(\xi_{\alpha,i}^{(LES)} - \xi_{\alpha,i}^{(exp)} \right)^2$$

- Provides total simulation error in terms of differences that occur in mean, RMS flow properties
 - Makes use of available experimental data
 - Measurements of velocity, temperature, mixture fraction
 - Data collected different positions and sampling times

TNF9: Error-landscape concept applied to LES (Geurts et al.)



- Recent calculations have demonstrated how to minimize errors associated with the baseline Smagorinsky model
 - Small values of C_s allow structures on order of cell spacing to form where numerical errors dominate
 - Large values suppress structures due to artificial diffusion
 - Convergence via Successive Inverse Polynomial Interpolation

A. M. Kempf, B. J. Geurts and J. C. Oefelein (2011). Error analysis of large eddy simulation of the turbulent non-premixed Sydney bluff-body flame. *Combustion and Flame*, 158:2408-2419.

TNF9: Error-landscape concept applied to LES (Geurts et al.)

- **Advantage:**
 - Identifies combinations of grid, filter, and model parameters that introduce incorrect flow and combustion physics
 - Simultaneously minimizes competing effects of modeling errors and numerical errors
- **Disadvantage:**
 - Error cannot be reduced to any arbitrary level
 - Method is expensive to implement (but cheaper than refining the grid to eliminate non-optimal minimization of errors)

TNF10: Pitsch et al.

- Overview of best practices for LES
- Grid dependence studies in complex geometries (e.g., Hahn, Olbricht, Sadiki, Janicka)
- Parametric uncertainty (Error Landscape)
- Recursive filter refinement ...

TNF10: Recursive filter refinement (V. Raman)

- **Scalar variance should tend to zero as filter width tends to zero**

Normalized scalar variance is used as refinement measure

$$= \frac{Z^2 \leftarrow \text{Instantaneous variance}}{\tilde{Z}(1 - \tilde{Z}) \leftarrow \text{Maximum variance}}$$

Grid should be designed to reduce normalized variance

- **Based on 20% limit for normalized variance**

Filter widths/ grid size at current (n) and future level (n+1)

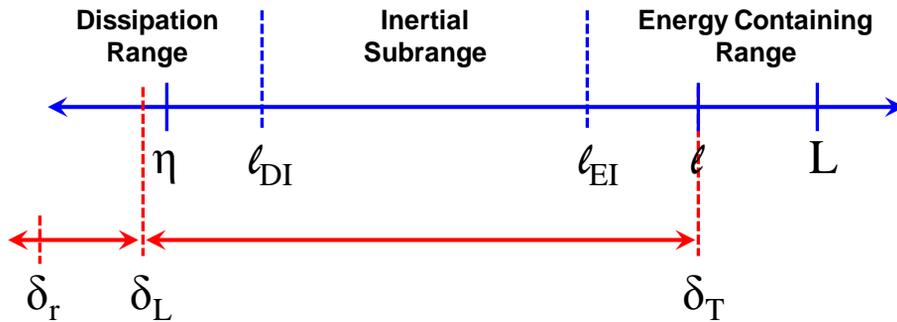
$$\frac{n+1}{n} = 0.2 \frac{\tilde{Z}(1 - \tilde{Z})}{Z^2}^{2/3}$$

Provides a quantitative estimate of necessary local refinement

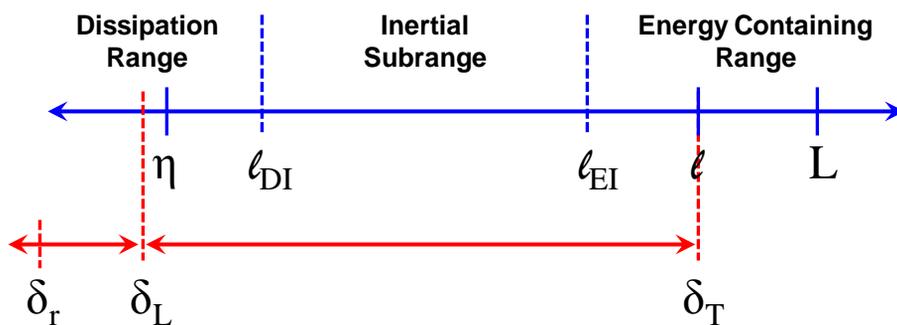
Recommendations (these are progressive)

- **Focus on grid resolution and coupling between grid and filter spacing (implicit versus explicit filtering)**
 - Simple global refinements are not sufficient
 - Local resolution criteria needs to be established
 - Local grid distributions need to be reported and checked
- **Develop better metrics for model applicability, implementation**
 - Grid spacing ... numerical parameter
 - Filter width ... model parameter
 - Competition between numerical and model errors
- **Provide more documentation of key simulation parameters**
 - Algorithmic characteristics of codes (spatial, temporal, stabilization method)
 - Local grid resolution, key length/time scales, related parameters
 - Boundary conditions and sub-model implementation
- **Incorporate UQ to determine sensitivity of uncertain parameters**
 - Boundary conditions, model parameters, baseline model assumptions
 - Large space of uncertain parameters, no general guidelines

Development of local resolution criteria



Development of local resolution criteria

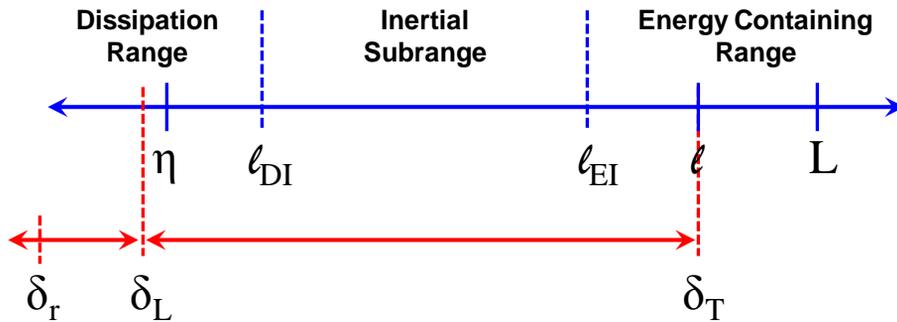


δ_T = thickness, time averaged scalars

δ_L = thickness, flame structure

δ_r = thickness, inner reaction zone

Development of local resolution criteria

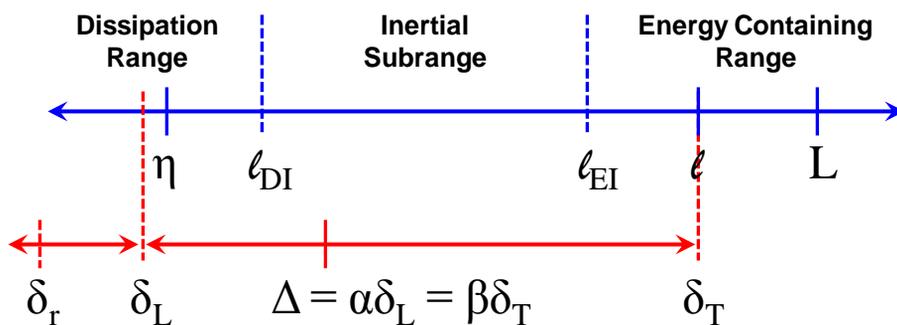


$$h_{\text{DNS}} = \delta_L / N$$

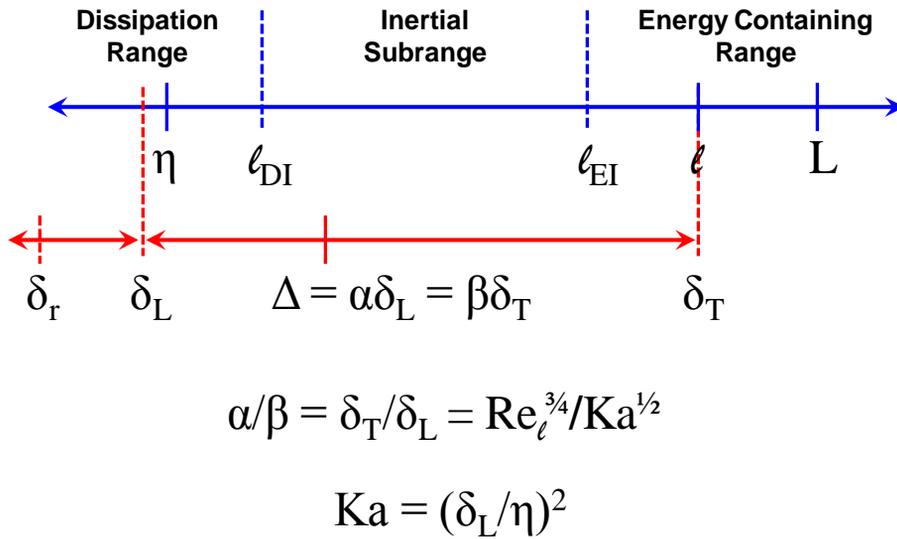
$$h_{\text{RANS}} = \delta_T / N$$

$$h_{\text{LES}} = \Delta / N = \alpha h_{\text{DNS}} = \beta h_{\text{RANS}}$$

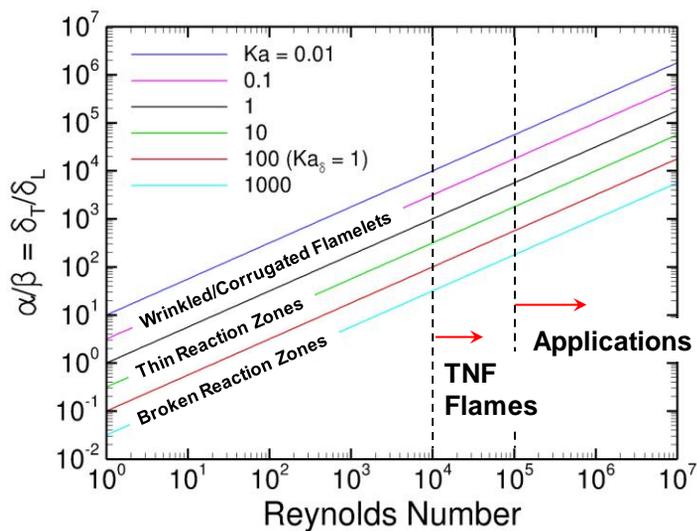
Development of local resolution criteria



Development of local resolution criteria



Can a robust criteria be developed and used as a quantitative metric ...



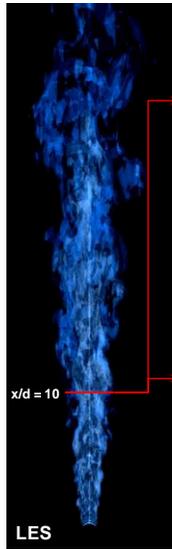
Example: Resolution criteria for DLR-A established and scaled to high-Re case



Experiment

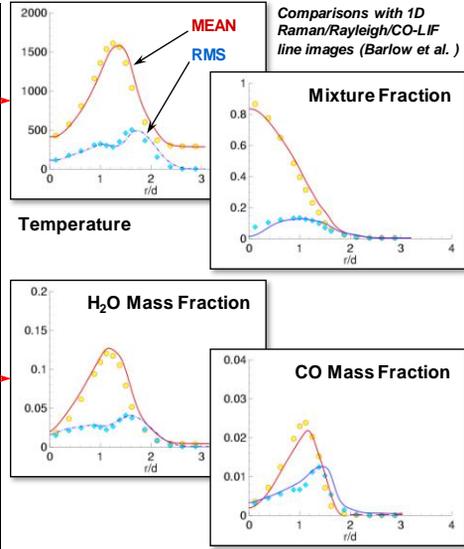
DLR-A Flame: $Re_d = 15,200$
 Fuel: 22.1% CH₄, 33.2% H₂, 44.7% N₂
 Coflow: 99.2% Air, 0.8% H₂O

Detailed Chemistry and Transport: 12-Step Mechanism (J.-Y. Chen, UC Berkeley)

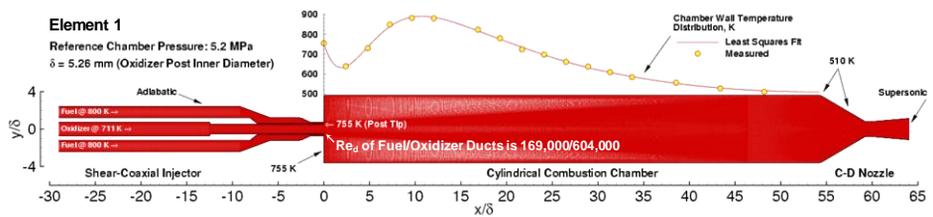


$x/d = 10$

LES

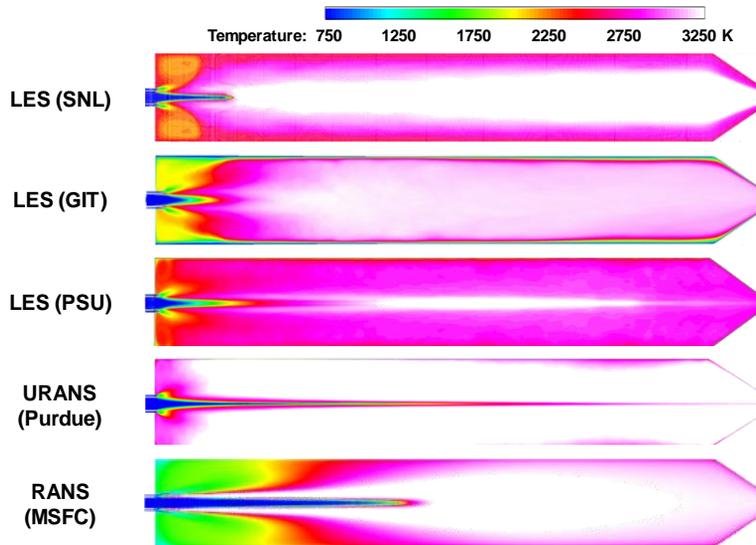


NASA/PSU high-pressure uni-element rocket

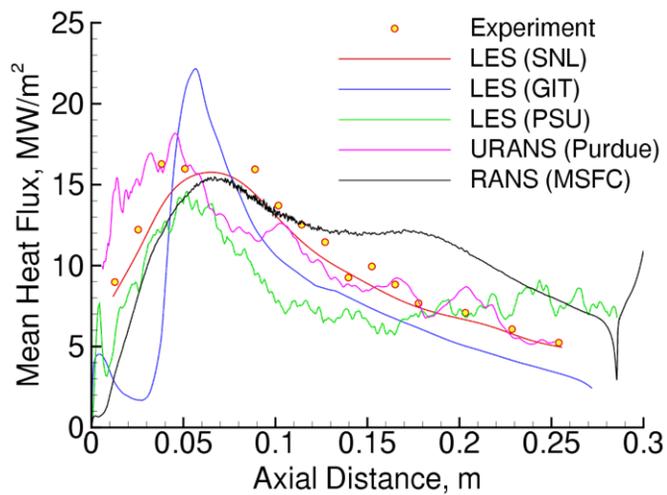


	Element 1		Element 2	
	GOX	H2	LOX	H2
Pressure, MPa	5.2		8.0	
Temperature, K	711	800	120	295
Density, kg/m ³	26.8	3.33	1118	6.18
Bulk Velocity, m/s	155	771	14.9	353
Mach Number	0.302	0.524	0.0255	0.26
Reynolds Number	604,000	169,000	547,000	455,000

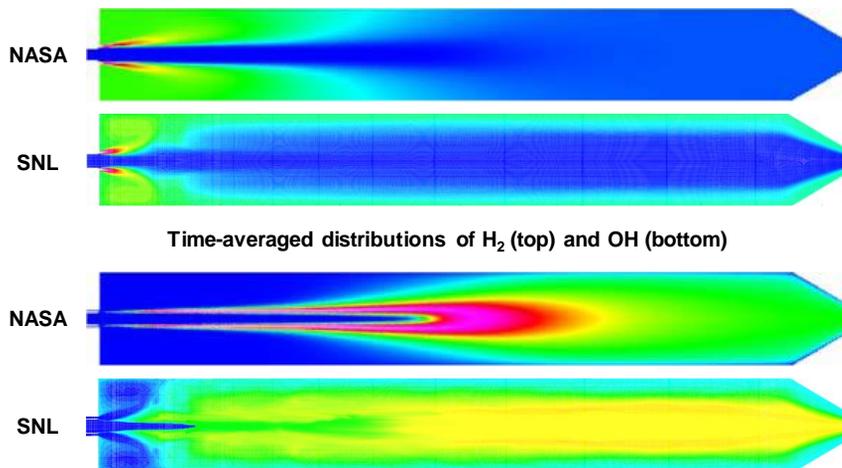
Same domain, BC's, and chemistry ... different codes, resolution, and models



Heat flux at chamber wall ... why?



Need to determine trade-off's between cost, accuracy, fidelity, models ...



Vervisch et al. (C&F 157, 2010) ... criteria based on minimizing residuals

Discretization and modeling introduce errors:

$$\begin{aligned}
 \partial_j(\overline{u_i u_j}) &= \left[\delta_j(\overline{u_i u_j}) + \mathcal{D}_i \right] + \partial_j \tau_{ij} \\
 &= \left[\delta_j(\overline{u_i u_j}) + \mathcal{D}_i \right] + \left\{ \partial_j m_{ij} + \mathcal{R}_i \right\} \\
 &= \delta_j(\overline{u_i u_j}) + \delta_j m_{ij} + \left(\mathcal{D}_i + \mathcal{R}_i + \mathcal{D}_i^{(m)} \right)
 \end{aligned}$$

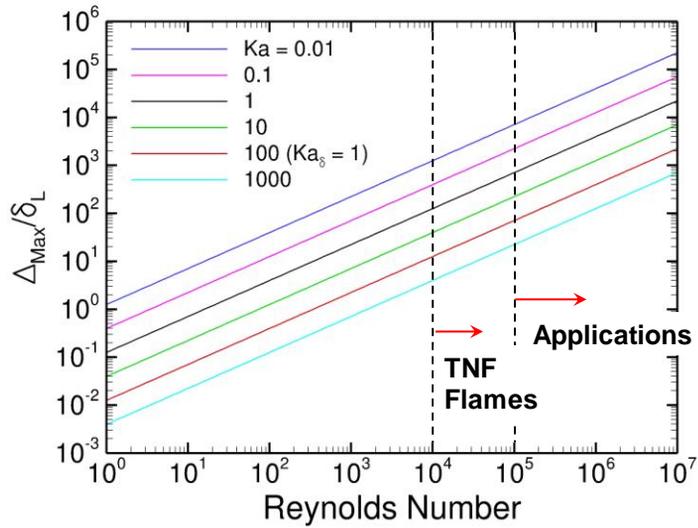
Distinguish:

- \mathcal{D}_i : discretization error from using method δ_j
- $\mathcal{R}_i = \partial_j(\tau_{ij} - m_{ij})$: total 'model-residue'
- $\mathcal{D}_i^{(m)}$: error when treating model m_{ij} , e.g., filtering

Q1: Justified to ignore \mathcal{D}_i ? Grid-(in)-dependent LES ?

Q2: Interacting errors? Error-decomposition? Dominance?

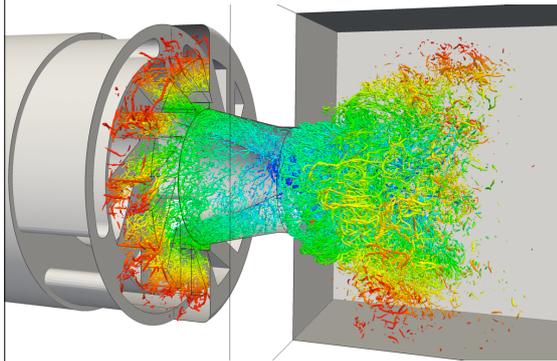
Vervisch et al. (C&F 157, 2010) ... criteria based on minimizing residuals



Luc Vervisch

Filtering and SGS modeling: Some unanswered questions

- LES is supposed to provide space filtered quantities
 - ✓ Is filtering under control?
 - ✓ Does the real filter size matter?



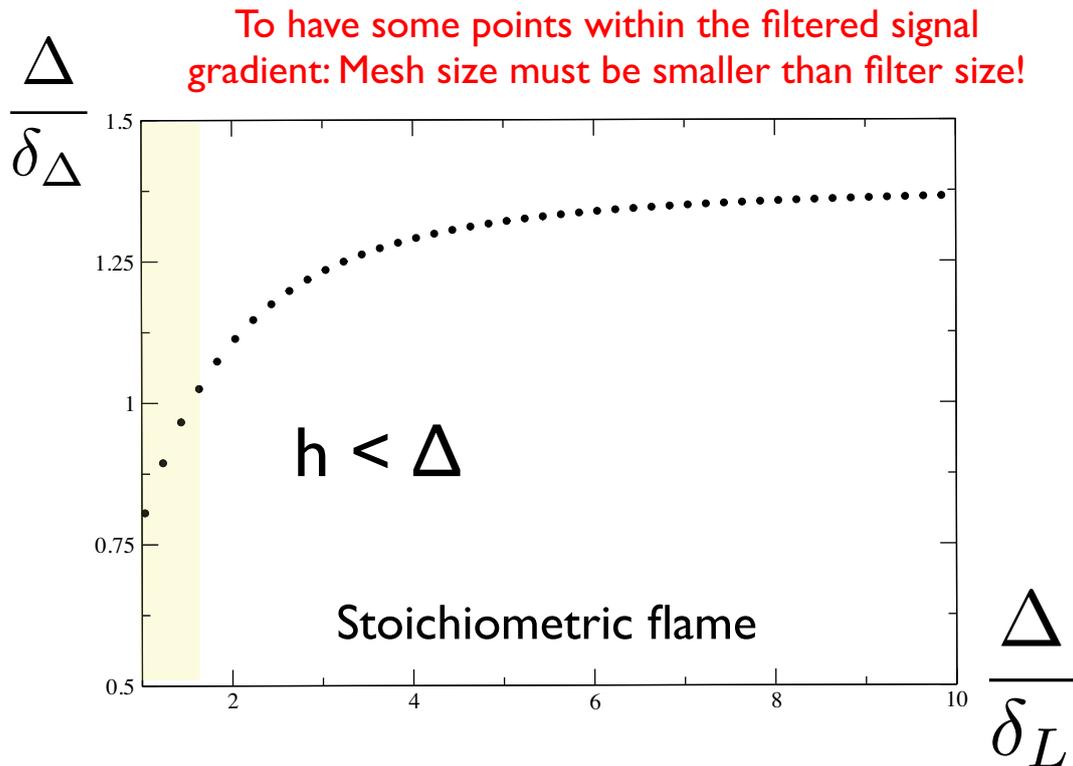
- From VLES to Quasi-DNS
 - ✓ Scaling of SGS scalar energy
 - ✓ Impact of SGS molecular diffusion

Luc Vervisch, Suresh Nambully,
Pascale Domingo, Vincent Moureau
INSA de Rouen & CNRS CORIA

The length scales

- The mesh size: h
- The filter size: Δ
- The characteristic signal thickness: $\delta_L = (\Delta\varphi) / \max(|\nabla\varphi|)$
- The characteristic filtered signal thickness: $\delta_\Delta = (\Delta\tilde{\varphi}) / \max(|\nabla\tilde{\varphi}|)$
- We expect: $\delta_L < h \leq \Delta$
- Also: $\Delta/\delta_\Delta < 1$

Filter (Gaussian) a CH₄/Air laminar premixed flame



Number of points within filtered signals

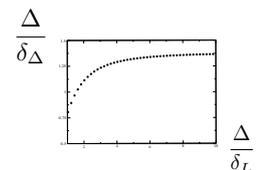
- Number of grid points necessary to resolve the signal: N

- LES Mesh size is h

- The filtered signal thickness depends on the filter size Δ

$$\delta_{\Delta} = \delta_{\Delta}(\Delta) = N \times h$$

Depends on signal
filtering



- The explicit filter size is in fact fully determined by the flame physics

How large can the flame filter size be?

Turbulent SGS Eddy viscosity

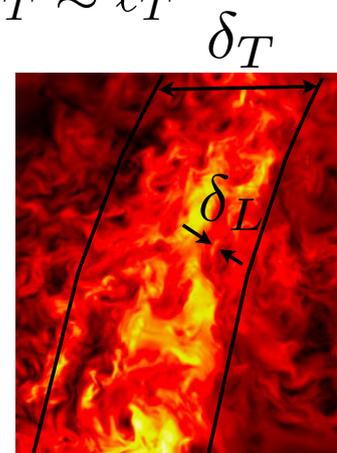
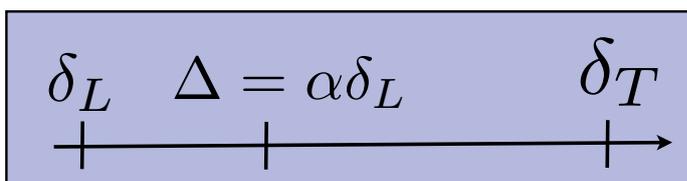
$$\left(\frac{\nu_T}{\nu}\right)^{LES} \propto Re_\Delta = \frac{\Delta k_{SGS}^{1/2}}{\nu} = \frac{\Delta}{\ell_T} \frac{\ell_T k_{SGS}^{1/2}}{\nu} \approx \beta \frac{\ell_T k_{SGS}^{1/2}}{\nu}$$

$$\lim_{\beta \rightarrow 1} \left(\frac{\nu_T}{\nu}\right)^{LES} \approx \left(\frac{\nu_T}{\nu}\right)^{RANS}$$

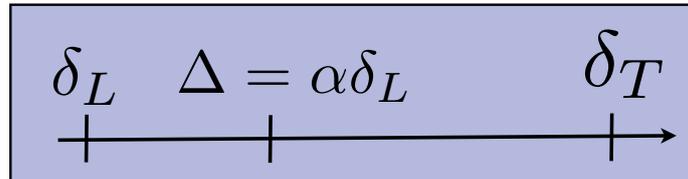
$$\beta = \frac{\Delta}{\ell_T} < 1$$

Three length scales

- Laminar flame thickness: δ_L
- Mean turbulent flame brush thickness: $\delta_T \approx \ell_T$
- LES filter length: Δ



Three length scales



$$\Delta = \alpha\delta_L = \beta\delta_T$$

Flame thickness
Mean flame brush

$$\alpha > 1 \text{ and } \beta < 1$$

Resolution is linked to SGS energy

SGS unresolved energy

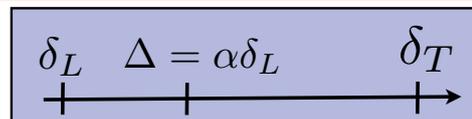
Total energy

$$k_{SGS} = \gamma K$$

Resolution factor < 0.2
80% of energy is resolved

Δ in inertial range

$$\frac{k_{SGS}^{3/2}}{\Delta} \approx \frac{K^{3/2}}{\delta_T} \quad \beta = \frac{\Delta}{\ell_T} = \gamma^{3/2}$$



Resolution is linked to SGS energy

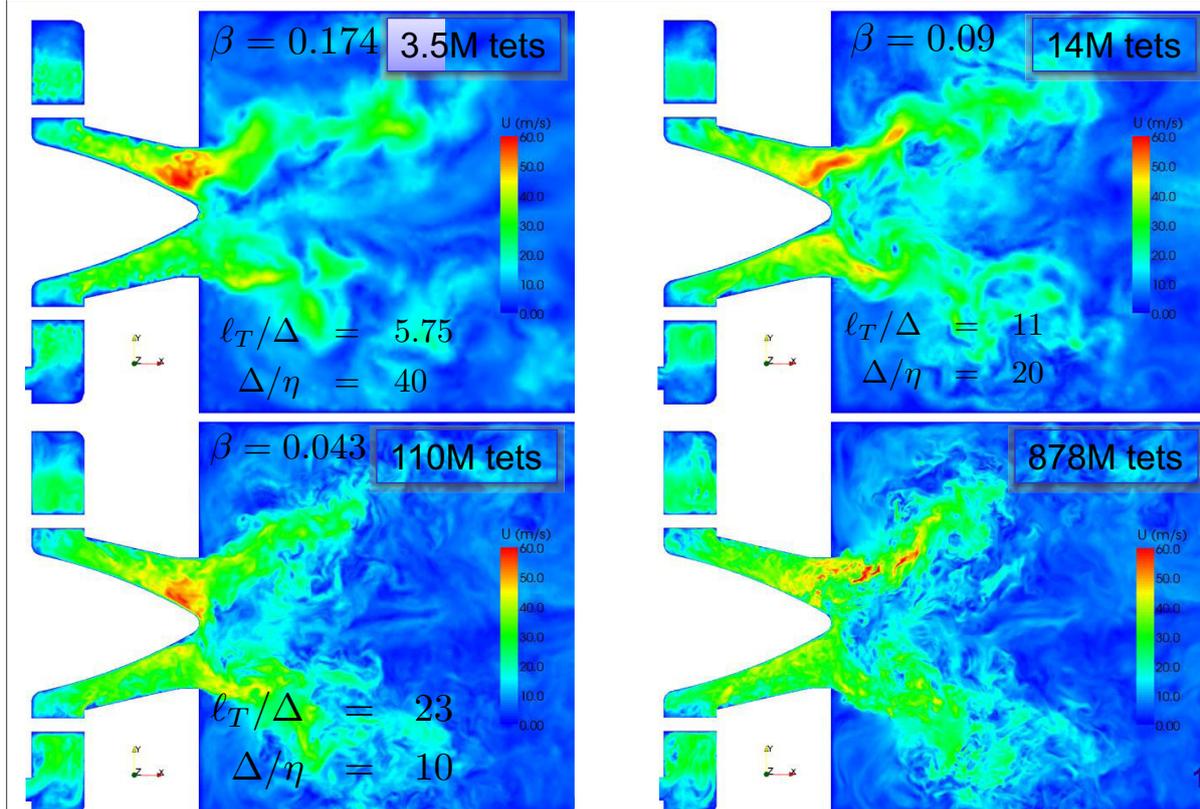
From Equilibrium: $\beta < \beta_R = \gamma_R^{3/2} = 0.09$

$$\Delta / \ell_T < 0.1$$

This is only a first approximation...

Seen flow topology (V. Moureau et al. 2011)

YALES2



Impact on SGS scalar energy

$$\varphi_v^* = \overline{\varphi^2} - \overline{\varphi}^2$$

- Used to calibrate SGS scalar activities in many turbulent combustion models;
- For reconstructing total fluctuations (Resolved + SGS) to compare with experiments;
- A standard tool also in RANS...

Impact on SGS scalar energy

$$\varphi(\underline{x}, t) = \overline{\varphi}(\underline{x}, t) + r_\varphi(\underline{x}, t)$$

SGS energy

$$\overline{r_\varphi^2} - \left(\overline{\varphi^2} - \overline{\varphi}^2 \right) = \overline{\varphi}^2 + \overline{\varphi}^2 - 2\overline{\varphi\overline{\varphi}}$$

SGS variance

A.W. Cook and J.J. Riley,
Phys. Fluids 8(6), 1994



The SGS energy is
the SGS variance if:

$$\begin{aligned} \overline{\varphi}^2 &= \overline{\varphi}^2 \\ \overline{\varphi\overline{\varphi}} &= \overline{\varphi}^2 \end{aligned}$$

Impact on SGS scalar energy

RANS or measurements: Total Energy of fluctuating field

$$\langle \varphi^2 \rangle$$

LES - **Known**: Energy of the resolved fluctuating field

$$\langle \overline{\varphi}^2 \rangle$$

+

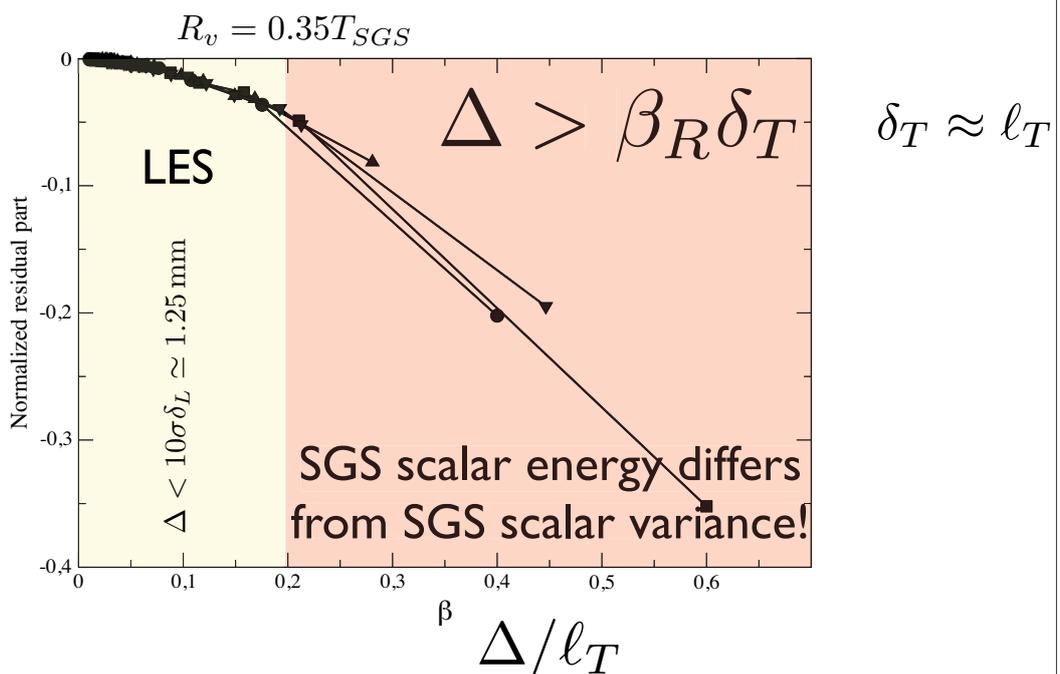
Energy of the SGS fluctuating field

$$\langle \overline{\varphi^2} \rangle - \langle \overline{\varphi}^2 \rangle$$

Not true when the mesh is too coarse

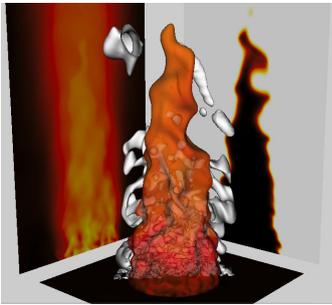
Impact on SGS scalar energy

SGS scalar energy decomposition error:



Impact on DNS

DNS should have a range of scales sufficient to perform a priori LES studies



$$Re_{\ell_t} > \left(\frac{\alpha_R \delta_L}{\beta_R \eta_k} \right)^{4/3}$$

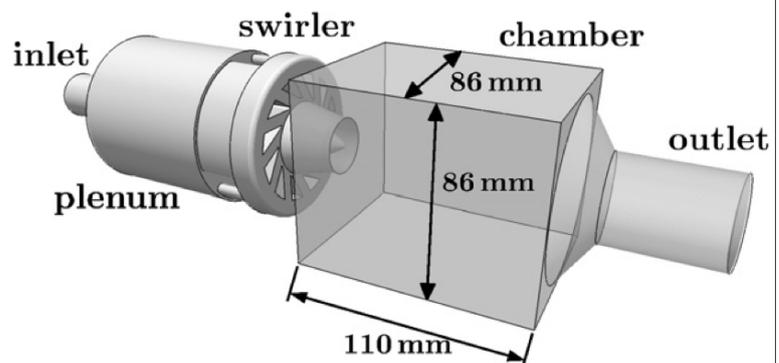
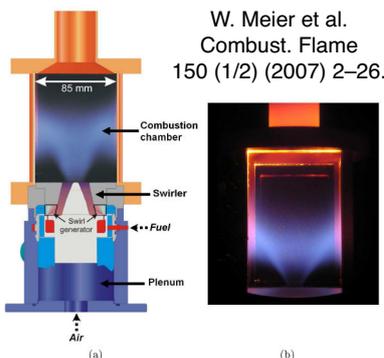
$$Re_{D_R} = \frac{U_b D}{u' \ell_t} \left(\frac{\alpha}{\beta_R} \right)^{4/3} Ka^{2/3}$$

$u'^2 = 0.1U_b^2$, $\ell_t = 0.5D$, $\alpha = 10$, $\beta_R = 0.2$ and $Ka = 50$: $Re_{D_R} = 15790$

$$Re_D > 15000$$

Combustion and Flame 157 (2010) 778–789

SGS Energy & Molecular Diffusion

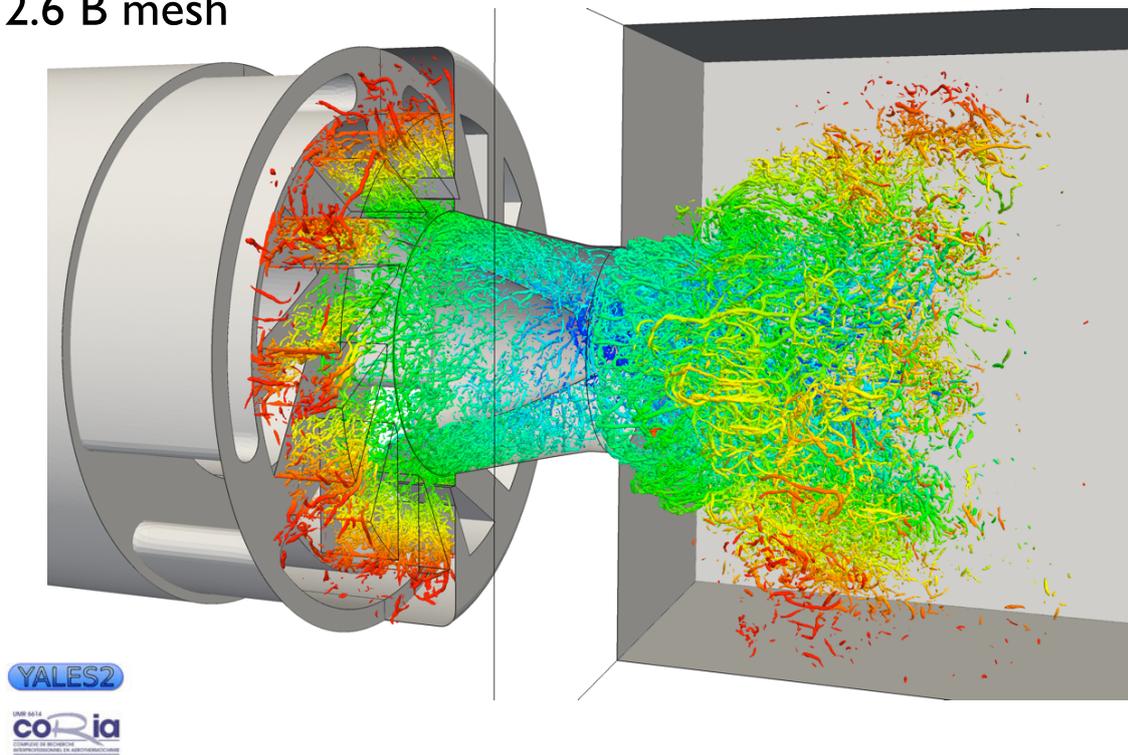


Re	u'	Re_T	Re_λ	ℓ_T	τ_t	η_K
40000	3.5 m/s	1480	149	7 mm	2 ms	29 μ m

S_L	δ_L	Da	Ka
29 cm/s	0.424 mm	7.51	7.23

DNS of the shear layers (not at wall $y^+ = 10$)

2.6 B mesh



Filtering DNS for Analysis

Δ/h_{DNS}	4	8	16	32
Δ/δ_L	0.9432	1.88	3.77	7.54
Δ/ℓ_T	0.0572	0.1144	0.2288	0.4576
Δ/Δ'	1.35	1.45	1.8	2.4

Scalar variance scaling in Δ or Δ^2 ?

BML pdf:

$$\bar{P}(c^*; \underline{x}, t) = \alpha(\underline{x}, t)\delta(c^*) + \beta(\underline{x}, t)\delta(1 - c^*) + \frac{\bar{\Sigma}(\underline{x}, t)}{\mathcal{G}(c^*)}H(c^*)H(1 - c^*)$$

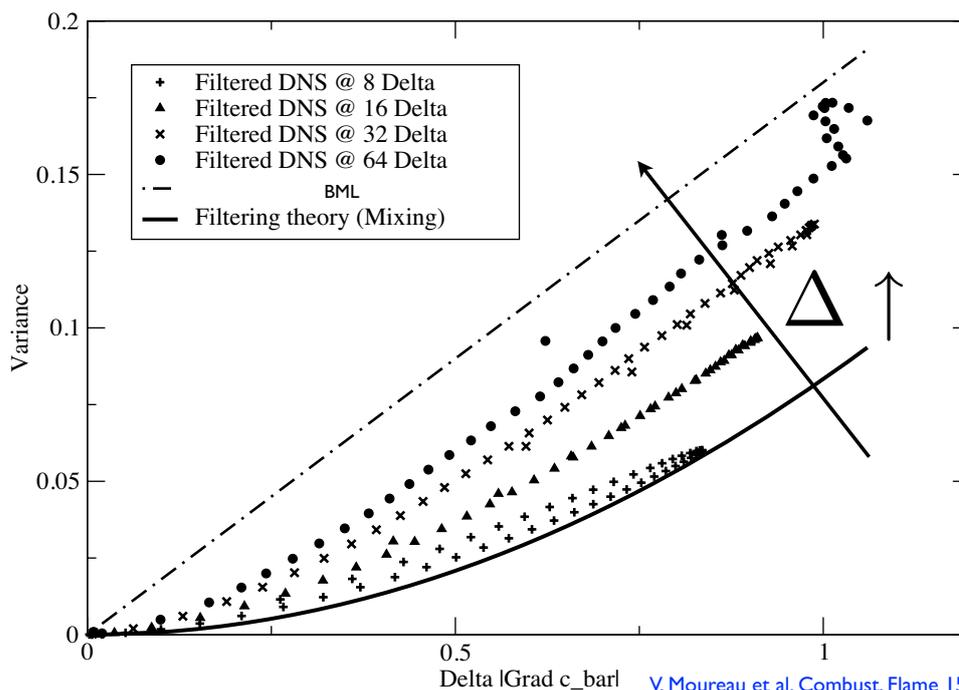
$$\bar{\Sigma} = \frac{\bar{c}(1 - \bar{c}) - (\bar{c}^2 - \bar{c}^2)}{\delta_c} \quad \delta_c = \int_{\epsilon}^{1-\epsilon} \frac{c^*(1 - c^*)}{\mathcal{G}(c^*)} dc^*$$

$$c_v = \bar{c}^2 - \bar{c}^2 = \left(C_c^{\text{or}} - \frac{\delta_c \bar{\Sigma}}{\Delta} \right) \Delta |\nabla \bar{c}|$$

Equilibrium hypothesis:

$$c_v = C(\Delta |\nabla c|)^2$$

Scaling depends on filter size, therefore on resolution



V. Moureau et al. *Combust. Flame* 158(7): 1340-1357, 2011

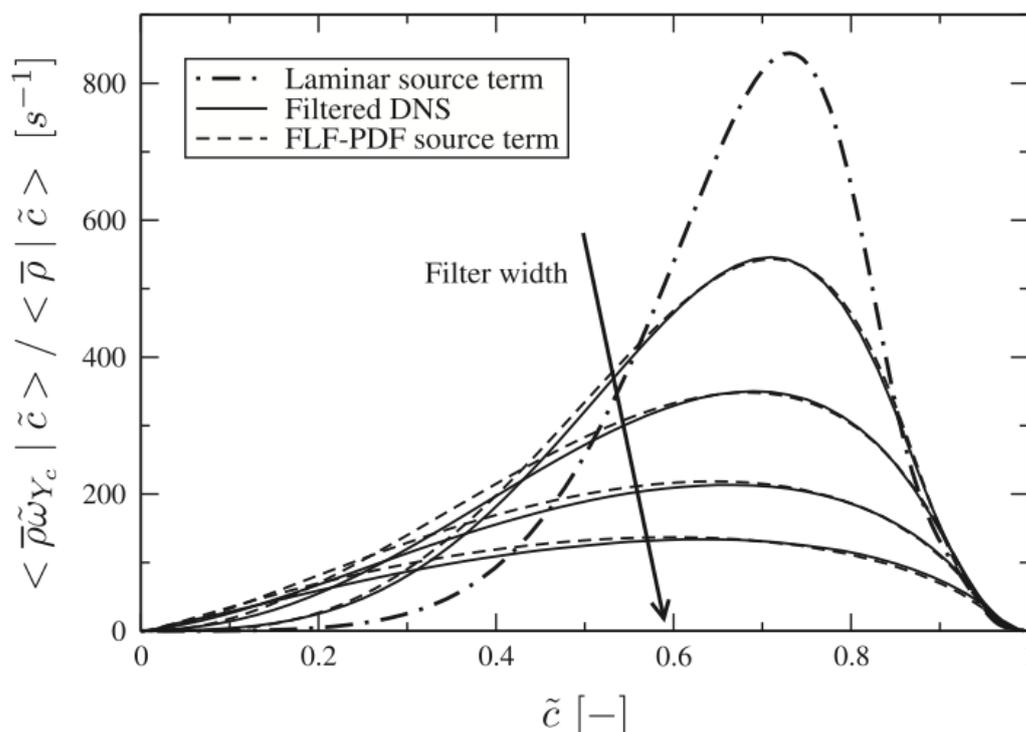
- The filter for the flame can hardly be the mesh
- The flame filter-size should not be uniform

$$\Delta' = \Delta'(\tilde{c}, c_v)$$

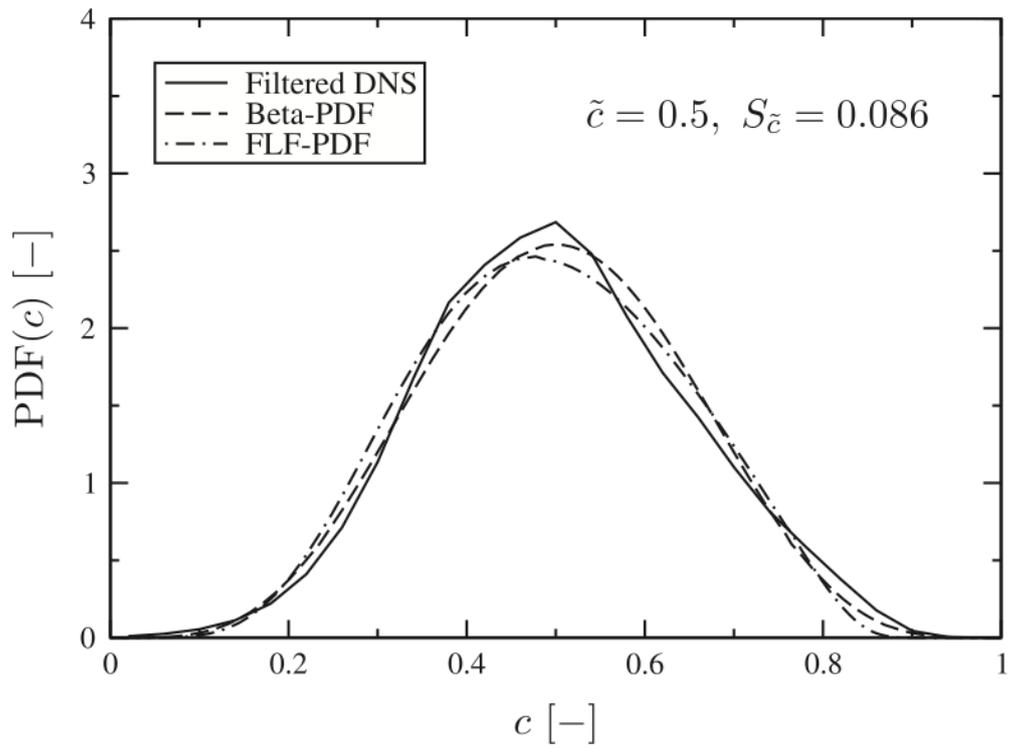
$$\tilde{P}(c^*; \tilde{c}, \Delta') = \frac{\rho(c^*) G_{\Delta'}(\tilde{x}^{\Delta'}(\tilde{c}^{\Delta'}) - x(c^*))}{\bar{\rho}^{\Delta'} |\nabla c|_F}$$

- Select the filter size that reproduces the (LES) SGS variance when filtering laminar flamelets
- Use this non-uniform filter for computing the burning rate

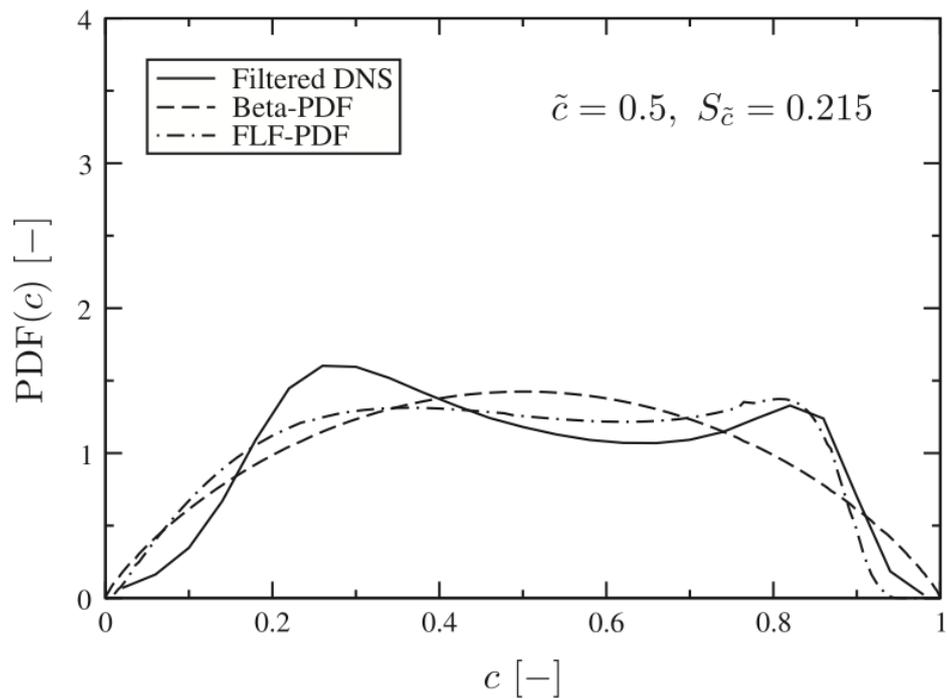
FLF - PDF



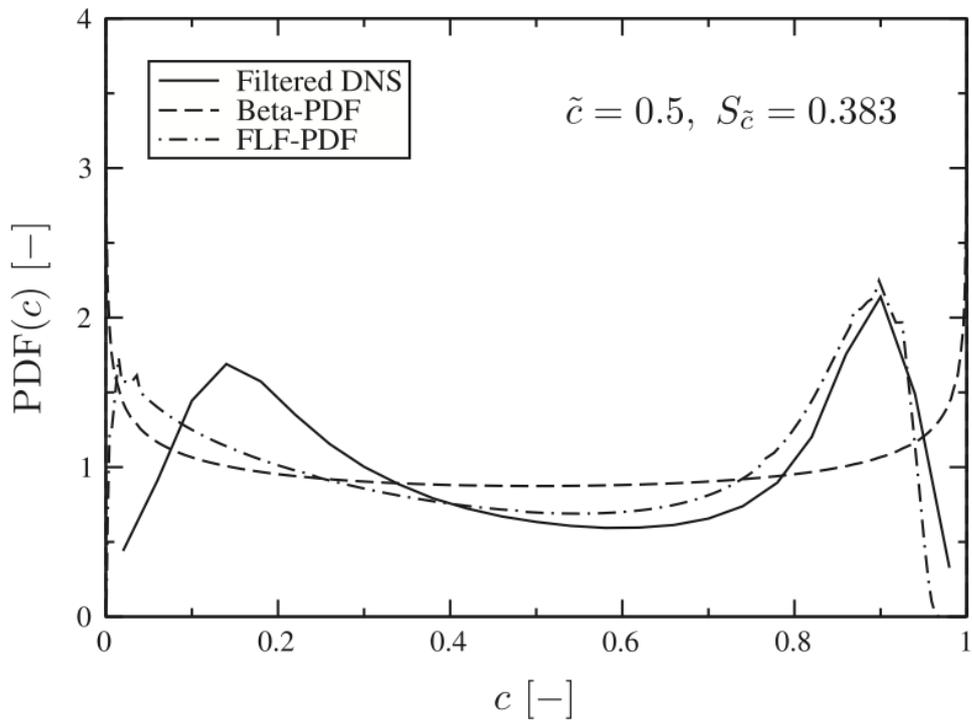
FLF - PDF



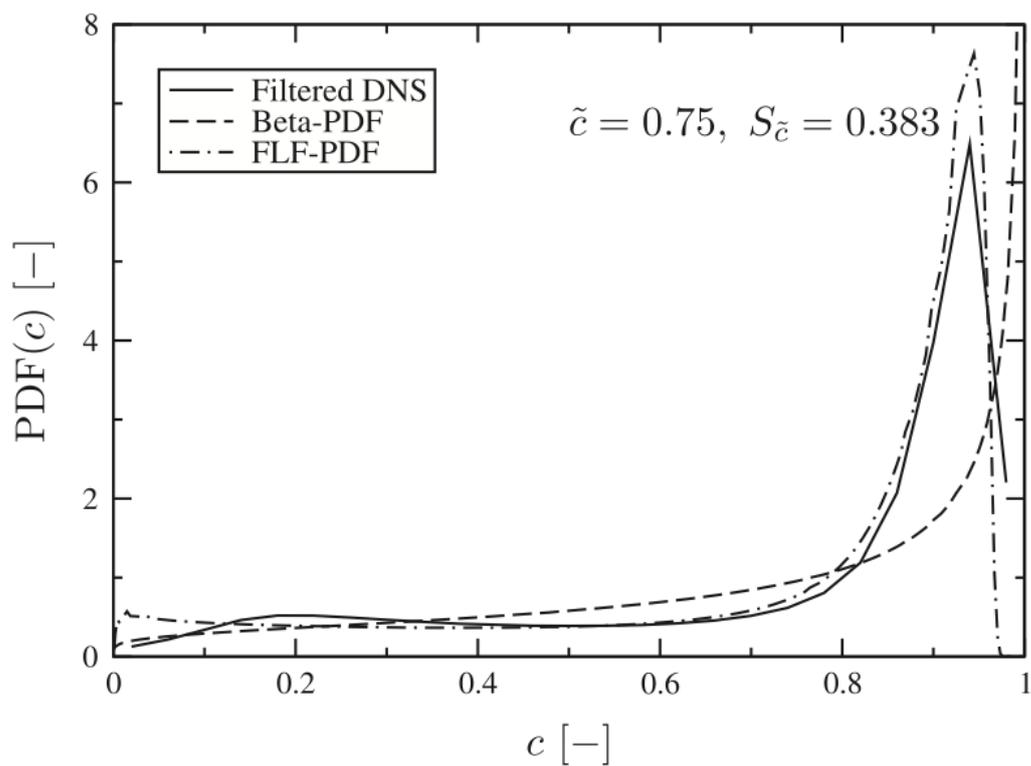
FLF - PDF



FLF - PDF



FLF - PDF



Modeling SGS molecular diffusion in LES?

- The diffusive budget is usually expressed neglecting its unresolved SGS fluctuations (infinite Re hypothesis):

$$\nabla \cdot \left(\overline{(\mu/S_c) \nabla \phi} \right) \approx \nabla \cdot \left((\mu(\tilde{T})/S_c) \nabla \tilde{\phi} \right)$$

- Strictly speaking there are two competing divergences of SGS flux:

$$\nabla \cdot (\tau_{\phi_D}) = \nabla \cdot \left(\overline{(\mu/S_c) \nabla \phi} - (\mu(\tilde{T})/S_c) \nabla \tilde{\phi} \right)$$

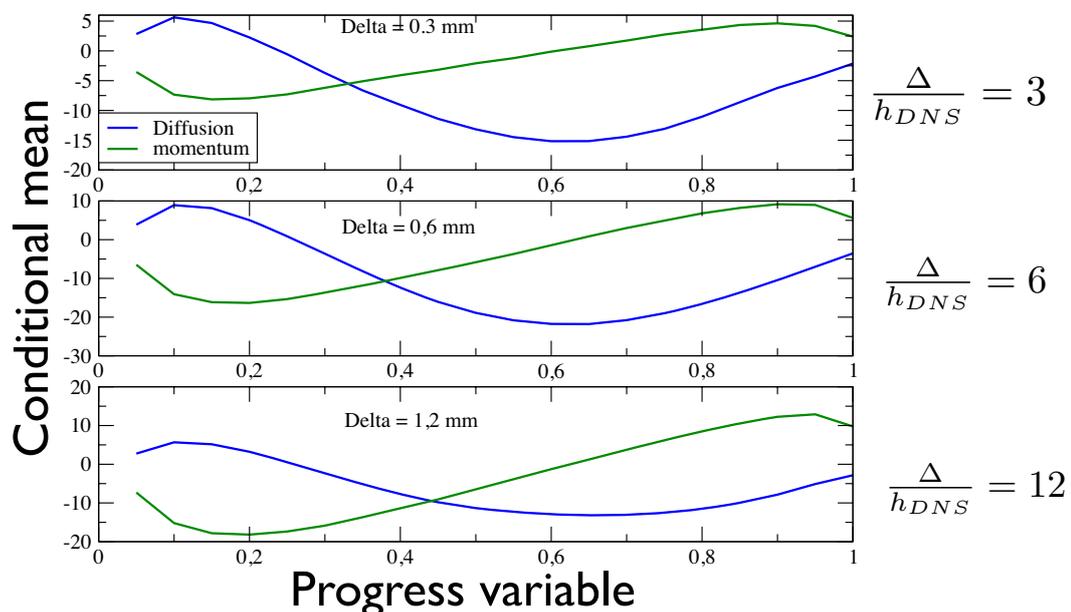
$$\nabla \cdot (\tau_{\phi}) = \nabla \cdot \left(\overline{\rho \mathbf{u} \phi} - \bar{\rho} \tilde{\mathbf{u}} \tilde{\phi} \right)$$

The two are of the same order of magnitude in most LES

$$\nabla \cdot (\tau_{\phi_D}) = \nabla \cdot \left(\overline{(\mu/S_c) \nabla \phi} - (\mu(\tilde{T})/S_c) \nabla \tilde{\phi} \right)$$

$$\nabla \cdot (\tau_{\phi}) = \nabla \cdot \left(\overline{\rho \mathbf{u} \phi} - \bar{\rho} \tilde{\mathbf{u}} \tilde{\phi} \right)$$

$h = 0.1 \text{ mm}$



- SGS modeling will still be needed for many years
- It takes about $t_0 + 7$ years for almost everyone in industry to benefit from the computing power available in academic labs at t_0
- LES is already a design tool for aeronautical engines (see CERFACS-SAFRAN work)

Discussion ...

- **Grid resolution and coupling between grid and filter spacing (implicit versus explicit filtering)**
 - Simple global refinements are not sufficient
 - Local resolution criteria needs to be established
 - Local grid distributions need to be reported and checked
- **Better metrics for model applicability, implementation**
 - Grid spacing ... numerical parameter
 - Filter width ... model parameter
 - Competition between numerical and model errors
- **More documentation of key simulation parameters**
 - Algorithmic characteristics of codes (spatial, temporal, stabilization method)
 - Local grid resolution, key length/time scales, related parameters
 - Boundary conditions and sub-model implementation
- **Toward UQ to determine sensitivity of uncertain parameters**
 - Boundary conditions, model parameters, baseline model assumptions
 - Large space of uncertain parameters, no general guidelines

Turbulent Opposed Jet Flames

The presentation started with an overview of the characteristics of existing turbulent opposed jet configurations, focusing on the last decade, and the experimental data available for these configurations. Currently, two main designs are available. The first design is the turbulent opposed jet version from Darmstadt (DA), having a nozzle diameter of $D=30$ mm as well as nozzle separation of $H=30$ mm ($H/D=1$), which was especially designed to allow for laser beam access along the centerline, aiming for the measurement of scalar gradients over the reaction zone. This version was further developed by the group of Peter Lindstedt at Imperial College (IC) with an emphasis on the enhancement of the turbulent velocity fluctuations. In the presentation it was shown that Lindstedt's group enhanced the level of the turbulent fluctuations by a factor of two by employing fractal grids instead of simple perforated plates. Moreover, the distribution of energy containing length scales was also substantially increased by this measure. The second design ($D=12.7$ mm, $H/D=1.5$), is the one from Sandro Gomez's group at Yale. Here, the turbulence generation is based on a different scheme, by forcing the flow through a high-blockage plate with a daisy-shaped orifice far upstream of the burner outlet. As a result, significantly larger turbulent Reynolds number, with values of up to approx 1200 could be realized. The discussion showed that the turbulent flow established near the stagnation plane exhibits different features, depending on the use of fractal grids (IC) or high-blockage plates (Yale). The most prominent difference are large scale instabilities in the region of the reaction zone, which are much more pronounced in case of the Yale burner. Such instabilities necessitate the use of suitably formulated conditional statistics.

Detailed information on the inflow conditions are crucial for all turbulent opposed jet configurations since the flow field depends strongly on the way the turbulence is generated. Such data are available for all opposed jet configurations (DA, IC, Yale). In particular, the DA group also ran high-speed PIV downstream the turbulence generating plates. Different LES simulations performed for all configurations directly after the turbulence generating device by Andreas Kempf's group at IC were able to capture all prominent characteristics of the flow field very well. The compact domain of turbulent opposed jet geometries allows for a high resolution of the simulations inside the nozzle.

During recent years, the number of fuels as well as the flame conditions were varied. While the earlier work focused methane as fuel, higher hydrocarbons like C_2H_4 or C_3H_8 , and liquid fuels like JP-10 have been added (IC). The flames conditions are ranging from non-premixed to very lean premixed, with the latter established in the fresh reactant versus burnt product configuration. Experiments with conditions of local extinction were briefly discussed under conditions of direct relevance to gas turbine operations.

A number of simulations (Monte-Carlo PDF, 2nd moment U-RANS, LES-Flamelet) were performed in the past years on the three configurations (DA, IC, Yale) and were compared to experimental data. Flow fields as well as scalar data obtained by experiments are available for all configurations, where in particular the type of scalar data varies from line concentration/temperature data up to 2D imaging at low and high speed. The compact computational domain in conjunction with the aerodynamical stabilization of the flame provides potential advantages computationally, in particular for LES. Simulations with different methods (LEM, William Calhoon or LES-PDF, Steve Pope) are under way. The concluding discussion showed that there is an ongoing interest in the turbulent opposed jet flames in parts of the TNF community, especially since the recent increase of the turbulent Reynolds number allows for investigations close to technical applications.

Opposed Jet Flames ,TNF II Darmstadt

Session coordinators: Dirk Geyer, Sandro Gomez

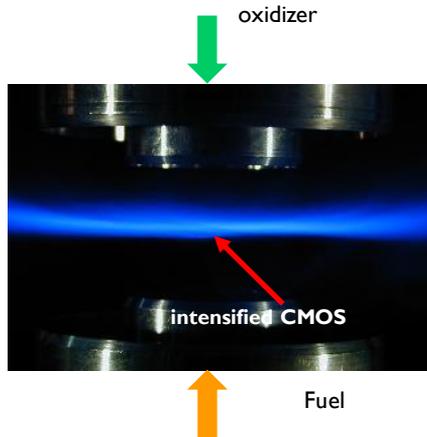


Outline

- ▶ Opposed Jet configurations
 - Characteristics
 - Recent developments
- ▶ Inflow conditions
 - experiments and simulations
- ▶ Flames
 - Darmstadt
 - Imperial college
 - Yale
- ▶ Summary

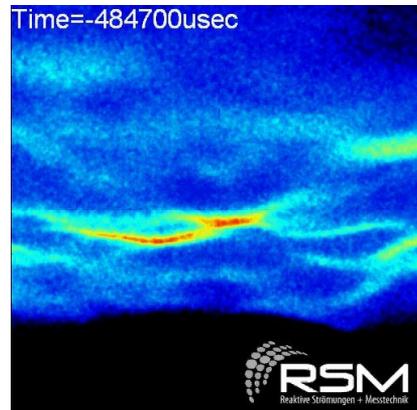


Turbulent opposed-jet - *chemiluminescence*



Photography
(90° viewing angle)

Spatial location and propagation of
extinction 'holes'



High speed imaging,
intensified CMOS 10 kHz
(45° viewing angle)

▶ 3

Pros and cons of opposed-jet flames

- ▶ Pros
 - Simple, very compact flow field
 - Aerodynamic stabilization of flame
 - Spatially confined reaction zone
 - factor of ~50 in the cylindrical volume of the chemiluminescent regions
 - Computational cost dramatically reduced
 - Better statistics at the same computational cost
 - Good optical access for non-intrusive laser diagnostics

Images:
opposed jet-flame and jet-flame, same scaling,
~identical Re (10000) and Re_c (1000)

A. Gomez, Yale.

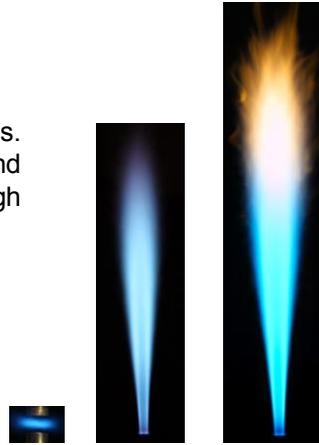


▶ 4

Advantage from a Soot Perspective (C_2H_4 Flames)

X_f	0.10	0.15	0.20
Re	9,480	10,400	10,000
Re_t	1050	995	995

In counterflow, mean residence time < 1 ms.
Thus, one can avoid soot complications and study turbulence of even fuels with high soot propensity.



▶ 5

Pros and cons of opposed-jet flames

▶ Pros

- Simple, very compact flow field
- Aerodynamic stabilization of flame
- Spatially confined reaction zone
 - factor of ~50 in the cylindrical volume of the chemiluminescent regions
 - Computational cost dramatically reduced
 - Better statistics at the same computational cost
- Good optical access for non-intrusive laser diagnostics
- Short residence time in reaction zone \Rightarrow PAH formation reduced

▶ Cons

- Re number limited - **in the past**
- Turbulence might be not fully developed



▶ 6

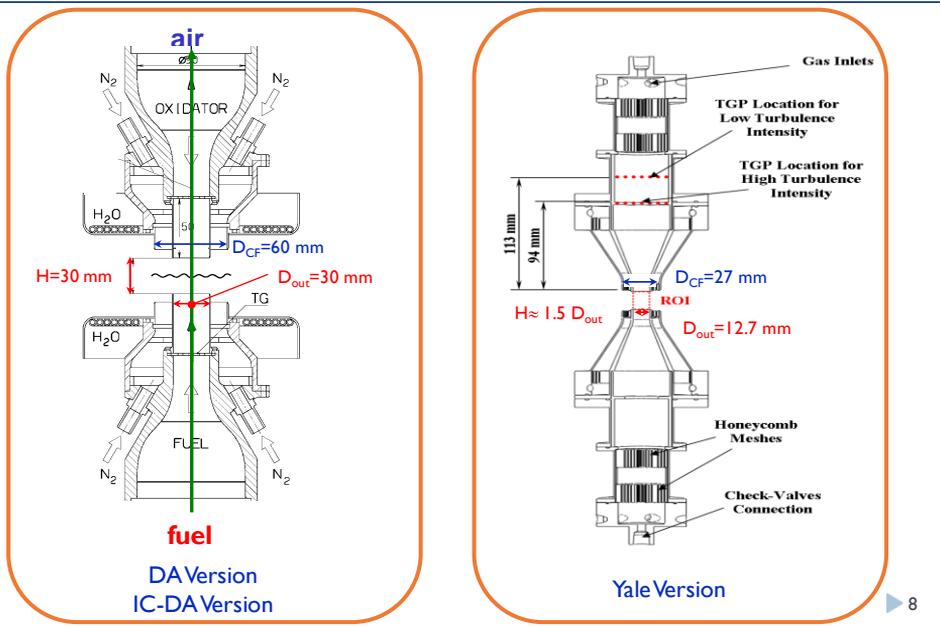
Overview of experiments (other configurations)

Experiments in the 90s

- ▶ Kostiuk et al. (1989, 1993, 1999)
- ▶ Mounaim-Rouselle, Gökalp (1994)
- ▶ Tsuji, H., Yoshida, A., and Endo (1994)
- ▶ Kitajima et al. (1996, 2004)
- ▶ Imperial college
 - Mastorakos, Taylor, Whitelaw, (1992-1995)
 - Sardi, Taylor, Whitelaw, (1998)
 - Luff, Lindstedt (2003-2007)

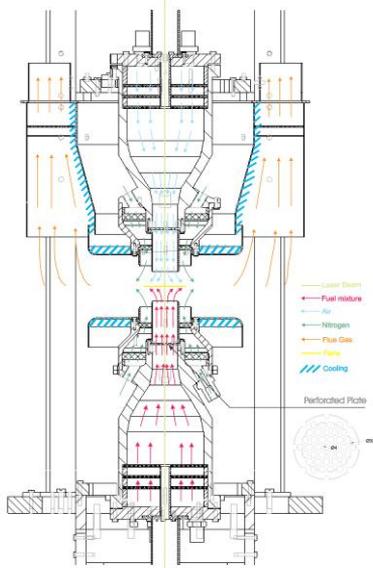
▶ 7

'current' turbulent opposed-jet designs – dimensions



▶ 8

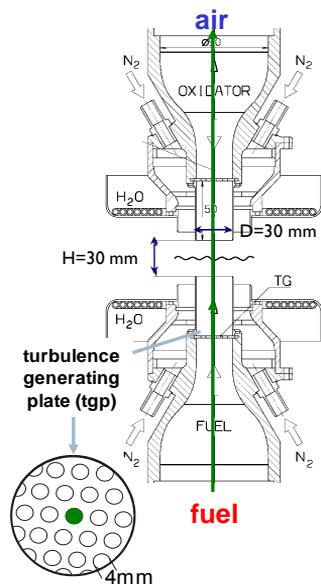
'current' turbulent opposed-jet designs – DA Version



- ▶ Two identical opposed nozzles, $D=H=30\text{mm}$
- ▶ Accurate alignment of nozzles
- ▶ N_2 coflow prevents ambient air mixing
- ▶ Designed to allow for laser beam access along centerline
 - ⇒ Measurements of scalars (temperature, concentrations) and their gradients along centerline

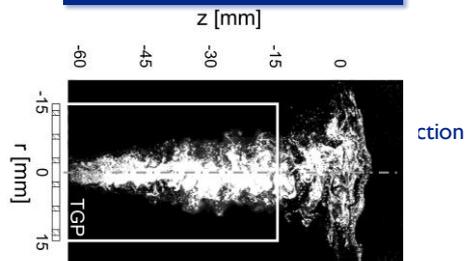
▶ 9

'current' turbulent opposed-jet designs – DA Version



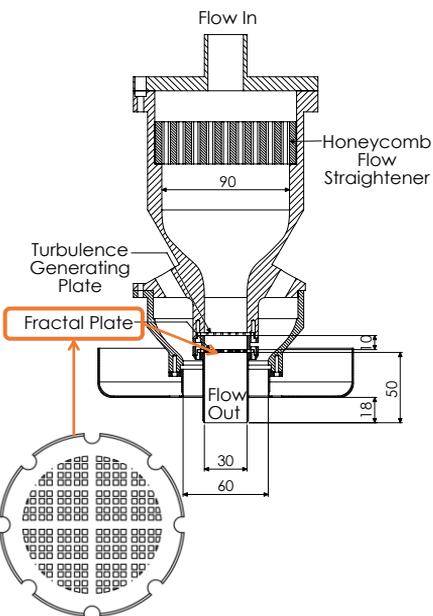
- ▶ Turbulence generation
 - Turbulence generating plate
 - 4.0 mm holes, 45% blockage, hexagonally arranged
 - Access for laser beam along burner axis → no beam steering

Snapshot of axial velocity, central jet seeded, PIV
Böhm, Stein, Kempf, Dreizler (2010)



▶ 10

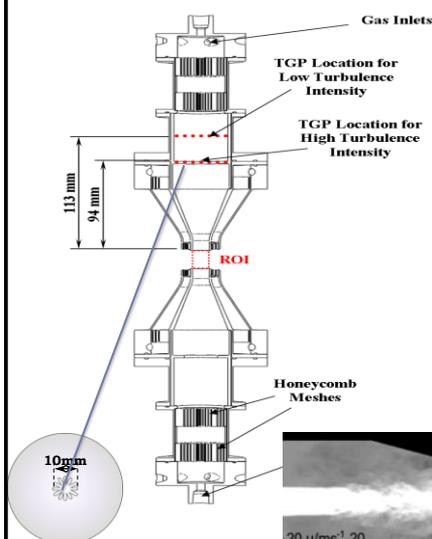
'current' turbulent opposed-jet designs – IC-DA Version



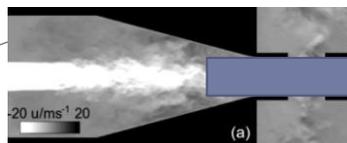
- ▶ Turbulence generation
 - DA:TGP, 4.0 mm holes
⇒ IC now: fractal grids
⇒ leads to multiscale turbulence.
 - fractal enhanced turbulence, stable bulk flow. Geipel et al. (2010).
- ▶ Turbulence intensity:
 - 12 or 20 % at nozzle exit, depending of fractal grid configuration.
 - Grid design provides a balance between Re_t and Da numbers.
- ▶ Operating conditions
 - Isothermal
 - Non-Premixed
 - Premixed
 - Different fuels

▶ 11

'current' turbulent opposed-jet designs – Yale Version



- ▶ Turbulence generation
 - Different approach to generate turbulence
 - High blockage Turbulence Generation Plate (TGP)
- ▶ Turbulence intensity:
 - ~20% - 30% at nozzle exit
- ▶ Operating conditions
 - Cold and non-premixed
 - Premixed against discharges of a jet of hot combustion products



Snapshot of axial velocity, highly resolved LES

Geipel, M.W., Coriton, B., Geipel, A., Kempf, A.M (2011)

▶ 12

Characterization of inflow conditions

- ▶ Turbulence generating devices \Rightarrow careful characterization of inflow conditions (inside nozzle or @ nozzle exit)
- ▶ In isothermal flow
 - DA
 - PIV and high-speed PIV inside glass nozzle
 - Highly resolved LES
 - Böhm, Stein, Kempf, Dreizler (2010) & Stein, Böhm, Kempf, Dreizler (2011)
 - IC
 - PIV inside glass nozzle. Geipel, Goh, Lindstedt (2010)
 - Highly resolved LES. Wysocki (2012)
 - Yale
 - HWA @ nozzle exit. Coppola & Gomez 2009
 - Highly resolved LES & HWA inside nozzle. Pettit, Coriton, Gomez, Kempf (2011)

▶ 13

Conditions at nozzle exit, isothermal flow

- ▶ Inflow conditions at nozzle exit, some numbers at nozzle exit

	Config.	D [mm]	max. Re_B	$u'/\langle u \rangle$	L_t [mm]	Re_t	Flame type
1	DA	30	7200	0.10	~4.7	~ 90	Partially premixed $\Phi=2.0, CH_4$
2	IC-DA	30	33,600	0.12 (0.20)	~4.2	550 (920)	back to burnt $\Phi=1.0, CH_4$
3	Yale	12.7	10,000	0.20 0.30	3-4	~1200	non-premixed wide range prem

$$Re_B = \frac{u_B}{\nu \cdot D}$$

$$Re_t = \frac{u'}{\nu \cdot L_t}$$

▶ 14

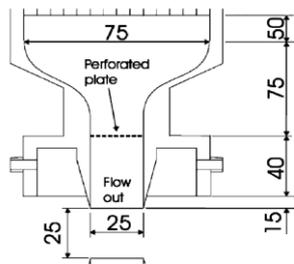
Turbulent Opposed Jet Experiments & Simulations - Focus on Inflow Conditions -

Oliver Stein^{1,*}, ITV, Stuttgart University
Andreas Kempf^{*}, IVG, Duisburg-Essen University
Benjamin Böhm², Andreas Dreizler, EKT/CSI, Darmstadt University
Stefan Wysocki, Mike Pettit, Imperial College London

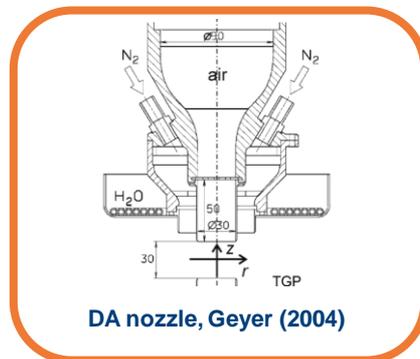
¹LES contact: o.stein@itv.uni-stuttgart.de, ²Experimental contact: bboehm@ekt.tu-darmstadt.de
^{*}Previous address: Department of Mechanical Engineering, Imperial College London

Experimental Set-Up: TOJ-TGP

- Two identical opposed nozzles vertically aligned
- Turbulent conditions established by turbulence generating plates (TGP) upstream of the nozzle exit
- Excellent optical access and a wealth of experimental validation data available
- Operation modes: non-reacting, non-premixed, premixed (this presentation: non-reacting/premixed)
- Previous LES analyses: Kempf et al. (2000), Kempf (2003)

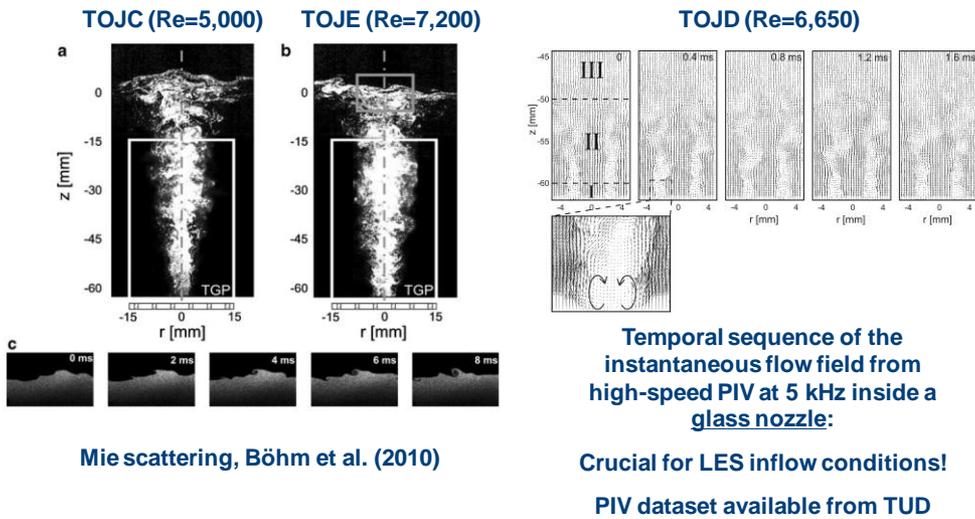


(Old) IC nozzle, Luff et al. (2003)



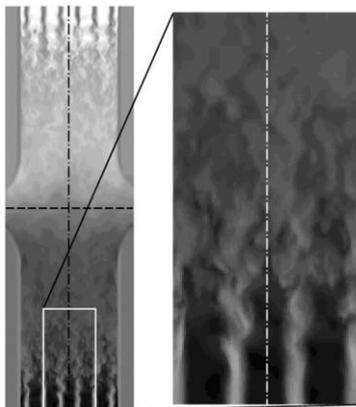
DA nozzle, Geyer (2004)

Experiments: High-Speed PIV of the in-nozzle flow

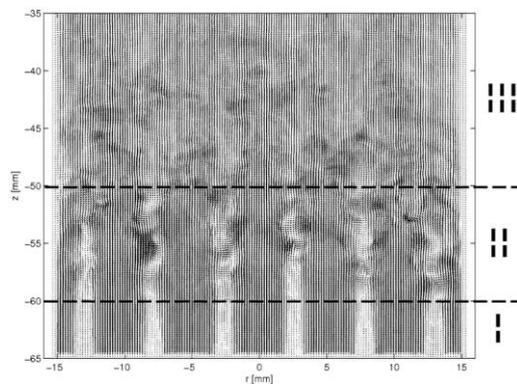


Mie scattering, Böhm et al. (2010)

Highly-resolved LES (quasi-DNS between the nozzles)



Axial velocity from LES
Stein et al. (2011)



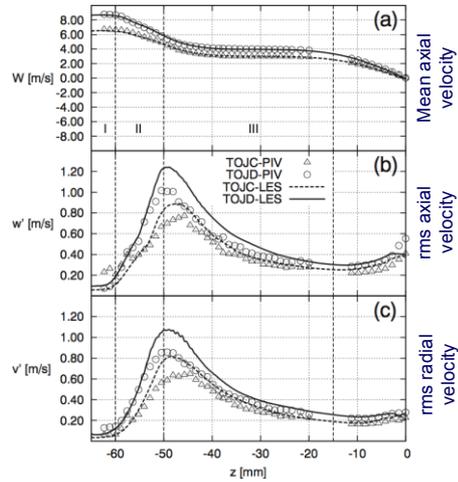
LES vectors: 3 distinct flow regions

- I: initial jet development
- II: strong jet interaction
- III: turbulence decay/homogenisation

LES parameter sensitivity and axial statistics

Parameter	Sensitivity	Typical value (TOJD)
Dimensions	Low-med.	$130 \times 44 \times 44 \text{ mm}^3$
Grid resolution	Med.-high	$706 \times 242 \times 242 \approx 40 \text{ M cells}$ $\Delta x = 0.18 \text{ mm}$
Statistical sampling	Med.-high	$t_R \approx 0.5 \text{ s}$; 2,250 samples
CFL number	Low-med.	$C_{FL} = 0.7 / \text{const. } \Delta t$
Pressure residual	Low	0.01
Smagorinsky constant	Med.	$C_s = 0.0$ (sgs model off)
TGP hole radius	High	1.8 mm
TGP mask filtering	High	10 iterations
Inflow turbulence level	High	$u'_i u'_i = 5 \times 10^{-3} \text{ m}^2/\text{s}^2$
Inflow length scale	Med.	1.15 mm
Inflow field length	Med.-high	$50D$

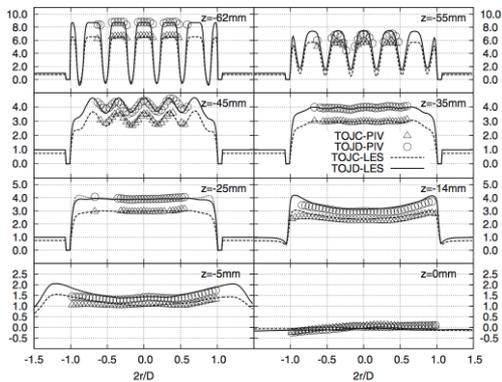
LES parameter sensitivity analysis (excerpt)



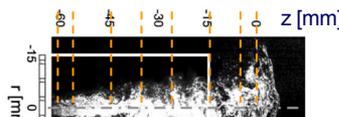
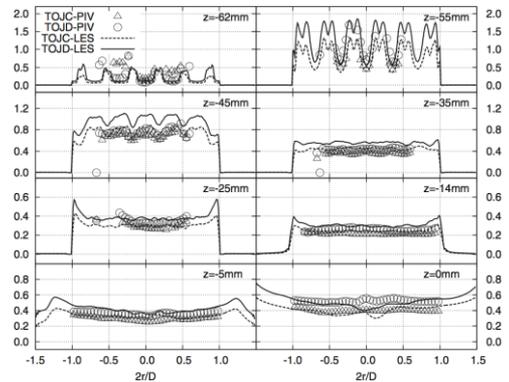
In-nozzle axial statistics
Stein et al. (2011)

LES (quasi-DNS) & PIV of the in-nozzle flow field

Radial profiles of the mean axial velocity

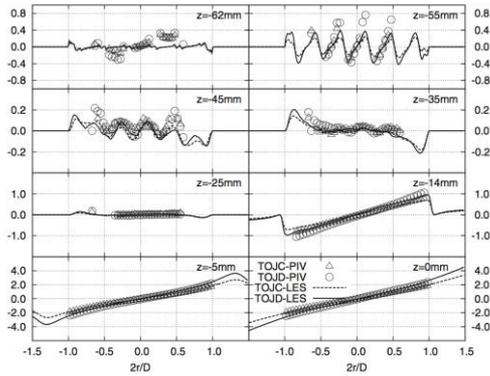


Radial profiles of the axial velocity fluctuation

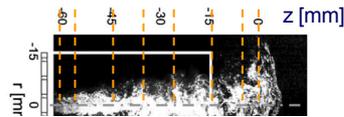
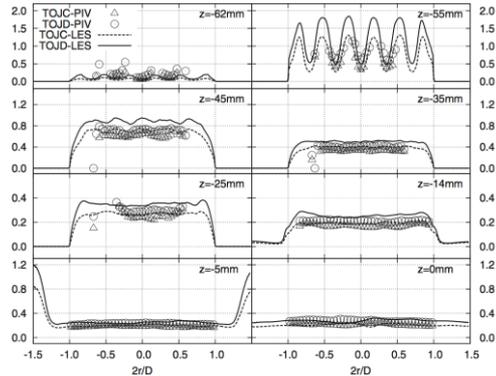


LES of the in-nozzle flow field (quasi-DNS)

Radial profiles of the mean radial velocity

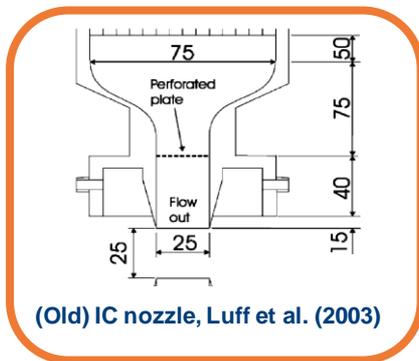


Radial profiles of the radial velocity fluctuation

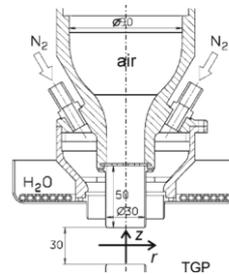


Experimental Set-Up: TOJ-TGP

- Two identical opposed nozzles vertically aligned
- Turbulent conditions established by turbulence generating plates (TGP) upstream of the nozzle exit
- Excellent optical access and a wealth of experimental validation data available
- Operation modes: non-reacting, non-premixed, premixed (this presentation: non-reacting/premixed)
- Previous LES analyses: Kempf et al. (2000), Kempf (2003)



(Old) IC nozzle, Luff et al. (2003)



DA nozzle, Geyer (2004)

Premixed Flames: (Algebraic) Flame Surface Density Modelling

Progress variable c , definition:

$$c = \frac{T - T_u}{T_b - T_u}$$

T_u = unburnt gas temperature
 T_b = burnt gas temperature

Unfiltered c transport equation:

$$r \frac{\partial c}{\partial t} + r u_k \frac{\partial c}{\partial x_k} = \frac{\partial}{\partial x_k} \left(\frac{\rho}{\rho_0} \epsilon D \frac{\partial c}{\partial x_k} \right) + W$$

Favre-filtered c transport equation:

$$\bar{r} \frac{\partial \tilde{c}}{\partial t} + \bar{r} \tilde{u}_j \frac{\partial \tilde{c}}{\partial x_j} + \frac{\partial}{\partial x_j} \left(\frac{\rho}{\rho_0} \tilde{c} \tilde{u}_j \right) - \tilde{u}_j \tilde{c} \frac{\partial \tilde{c}}{\partial x_j} = \frac{\partial}{\partial x_j} \left(\frac{\rho}{\rho_0} \tilde{\epsilon} D \frac{\partial \tilde{c}}{\partial x_j} \right) + \bar{W}$$

FSD reaction rate closure (algebraic):

$$\frac{\partial}{\partial x_j} \left(\frac{\rho}{\rho_0} \tilde{\epsilon} D \frac{\partial \tilde{c}}{\partial x_j} \right) + \bar{W} = (r S_d)_s S_{gen}$$

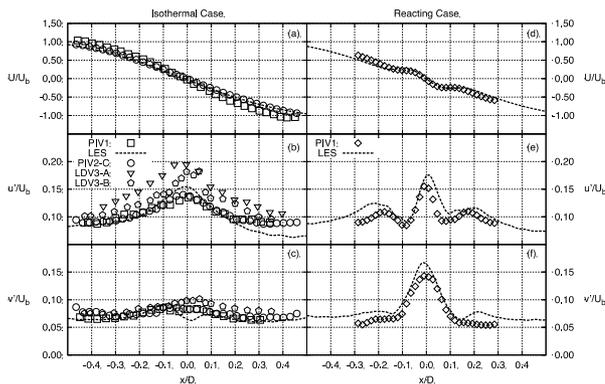
Here: $\Sigma_{gen} = 4 \beta / \Delta \cdot \bar{c} (1 - \bar{c})$ where $\Xi = \frac{S_T}{S_L}$ = wrinkling factor (Boger et al., PCI27, 917-925, 1998)

Experimental data for further LES validation

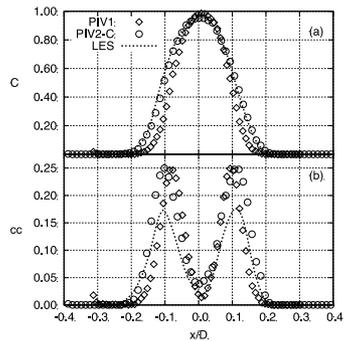
Key	Chemical State	Experimental Technique	TOJ Region	Reference
PIV1(-ISO)	isothermal	PIV	between nozzles	Lindstedt et al. (2005)
PIV1(-PRM)	CH ₄ /air, $\phi = 0.8$	PIV	between nozzles	Lindstedt et al. (2007)
PIV2-C	isothermal	PIV	between nozzles	Geipel (2008, 2009)
PIV2-C	CH ₄ /air, $\phi = 0.8$	PIV	between nozzles	Geipel (2008, 2009)
LDV3-A	isothermal	LDV	between nozzles	Mastorakos (1993), fig. 3.2.7
LDV3-B	isothermal	LDV	between nozzles	Mastorakos (1993), fig. 3.2.9

Result between the nozzles – isothermal / premixed FSD-LES

Velocity Profiles along Centreline



C-Profiles along Centreline



Fractal Generated Turbulence

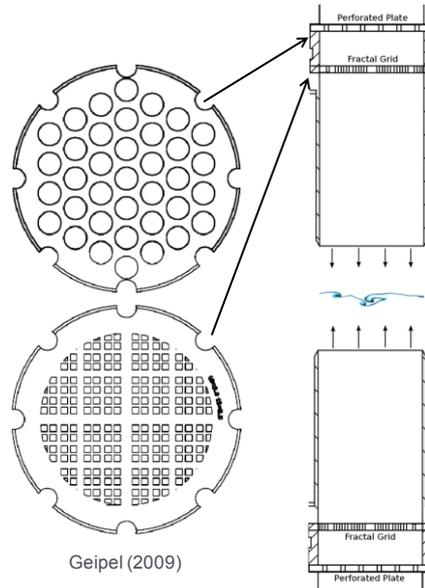
Aim to produce

- Fully-developed, isotropic turbulence
- High turbulent Reynolds number

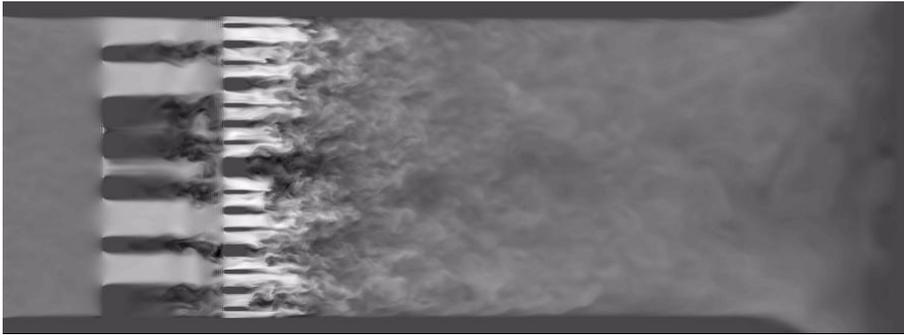
Fractal grid for higher Re_t at same bulk strain

- Inspired by Vassilicos et al., 2007
- Designed and tested by Geipel, 2009
- Re_t increased from ~ 50 to ~ 90
- Bulk strain remains constant
- Turbulent strain is increased

U_b	4 m/s
D	30 mm
H	30 mm
Grid blockage	65 %
Re_{grid}	~ 750
U_{grid}	~ 10 m/s



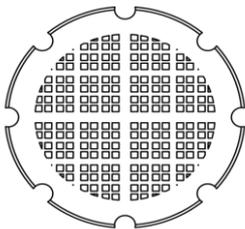
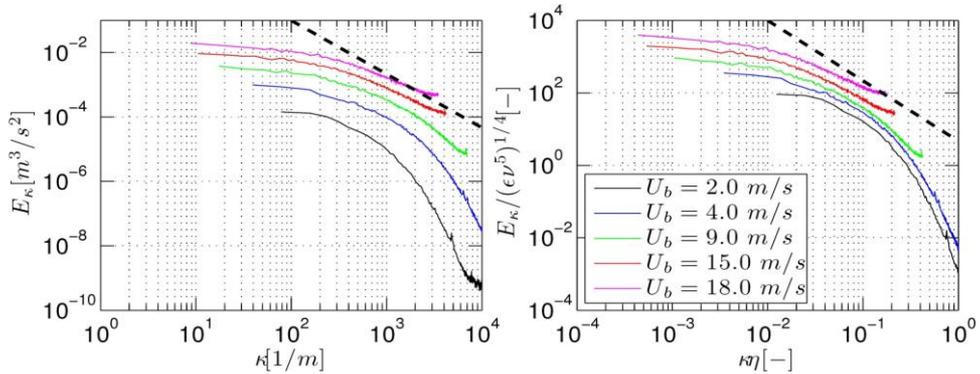
Flow Visualisation



Instantaneous axial velocities, $900 \times 320 \times 320 = 92.2\text{M}$ cells

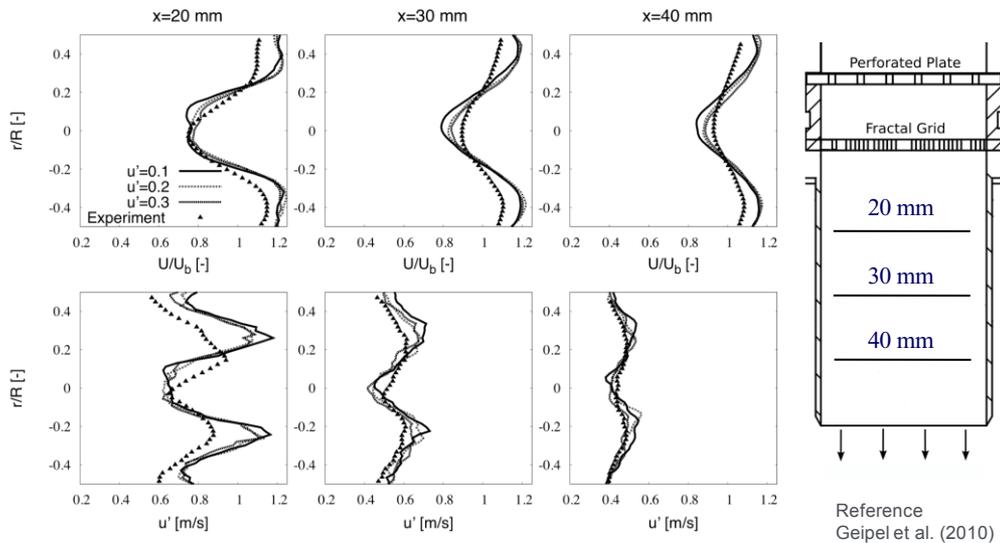
K.H.H. Goh, P. Geipel, R.P. Lindstedt

Imperial College
London



Energy spectra at nozzle exit in
isothermal flow,
obtained with hot-wire anemometry

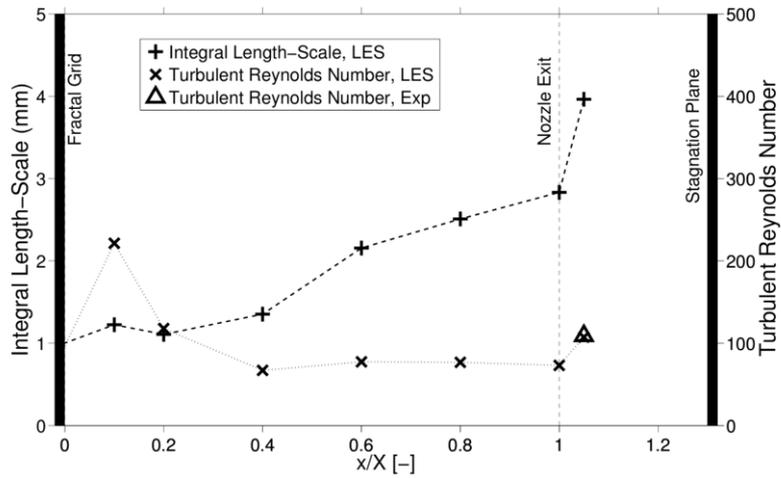
Result radial profiles – isothermal, inlet turbulence



References

- B. Böhm, *Experiments for the validation of large eddy simulations: Turbulence-Flame interactions in extinguishing turbulent opposed jet flames*, PhD thesis (2008), DA.
- B. Böhm, O. Stein, A. Kempf, A. Dreizler, *Flow, Turb. Combust.* 85 (2010) 73-93.
- P. Geipel, *Research on Turbulent Reacting Flows*, Technical Report (2008), IC.
- P. Geipel, *Experimental Research on Turbulent Reacting Flows using Gaseous and Liquid Fuels*, PhD thesis (2009), IC.
- P. Geipel, K.H. Henry Goh, P. Lindstedt, *Flow Turbulence Combust.* 85 (2010) 397-419
- D. Geyer, *1D Raman/Rayleigh experiments in a turbulent opposed-jet*, PhD thesis (2004), DA.
- D. Geyer, A. Kempf, A. Dreizler, J. Janicka, *Combust. Flame* 143 (2005) 524-548.
- A. Kempf, *Large Eddy Simulation of Non-Premixed Turbulent Flames*, PhD thesis (2003), DA.
- A. Kempf, H. Forkel, A. Sadiki, J. Janicka, *Proc. Combust. Inst.* 28 (2000) 35-40.
- R. Lindstedt, D. Luff, J. Whitelaw, *Flow, Turb. Combust.* 74 (2005) 169-194.
- R. Lindstedt, D. Luff, J. Whitelaw, *Proc. Combust. Inst.* 31 (2007) 1459-1466.
- D. Luff, E. Korusoy, R. Lindstedt, J. Whitelaw, *Exp. Fluids* 35 (2003) 618-626.
- E. Mastorakos, *Turbulent combustion in opposed jet flows*, PhD thesis (1993), IC.
- O. Stein, *Large Eddy Simulation of Combustion in Swirling and Opposed Jet Flows*, PhD thesis (2009), IC.
- O. Stein, B. Böhm, A. Dreizler, A. Kempf, *Flow, Turb. Combust.* 87 (2011) 425-447.
- J.C. Vassilicos, J.C.R. Hunt, *Math. Phys. Sci.* 435 (1991) 505-534

Time Series Analysis – Integral Length-Scale, Re_t



Experiments and simulations on reacting cases of DA opposed-jet

Benjamin Böhm, Dirk Geyer, Andreas Kempf, C. Heeger,
Andreas Nauert, Johannes Janicka, Andreas Dreizler



Overview of experiments and computations

- ▶ Velocity field
 - LDV, isothermal and reacting conditions
 - PIV & OH-LIF(10 Hz)
 - PIV & OH-LIF(high speed)
 - In-nozzle PIV (10 Hz & high speed)
- ▶ Scalar quantities
 - 2D OH-LIF imaging
 - PIV & OH-LIF(10 Hz) (see velocity field)
 - PIV & OH-LIF(high speed) (see velocity field)
 - High-speed quantitative OH concentration, on centerline (with Purdue)
 - Temperatures, concentrations and their gradients along centerline
- ▶ Simulations
 - MC-PDF of TOJ2D (J.Y. Chen)
 - LES of isothermal flow field (FLOWSI)
 - LES of reacting cases (FLOWSI)
 - LES of turbulence production in nozzle (PsiPhi) (Stein & Kempf, IC)

Publications:

Stein et al. (2011) FTC, Böhm et al. (2010), Proc. Combust. Inst.; Böhm et al. (2008), Proc. Combust. Inst.; Böhm et al. (2006), Proc. Combust. Inst.; Venkatesan et al. (2006), Flow Turb. and Combust.; Geyer et al. (2005) Combust. and Flame; Geyer et al. (2005), Proc. Combust. Inst.; Geyer et al. (2005), Proc. Combust. Inst.; Omar et al. (2004), Prog. in Comp. Fluid Dynamics.

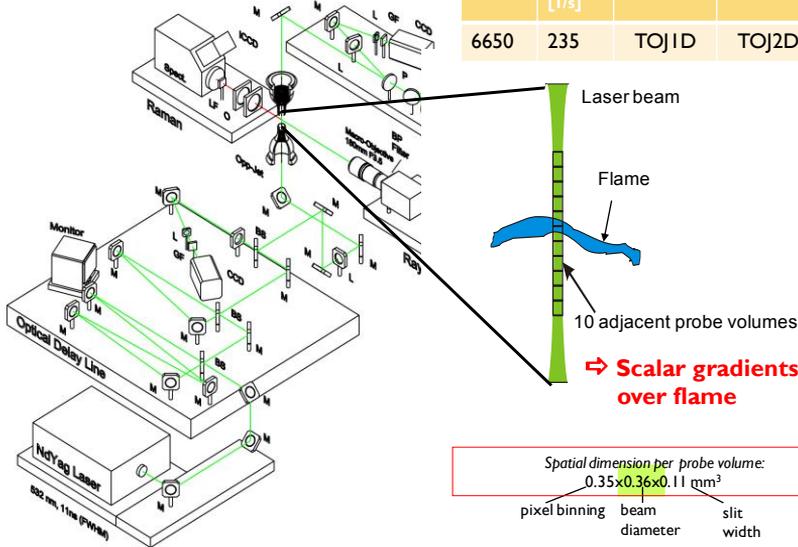


Temperature and concentration fields

Geyer, Kempf, Dreizler, Janicka (2005)

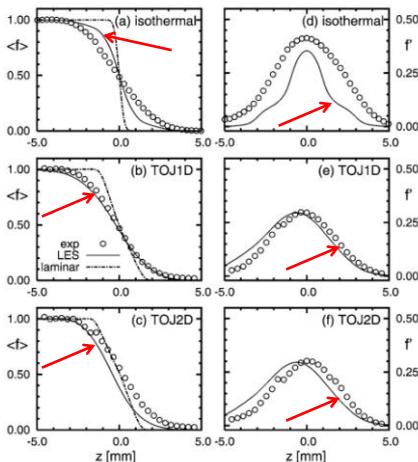
Flow configuration – CH₄ flames

Re _{Air}	a _m / [1/s]	Φ=3.18	Φ=2.0	Isoth. Φ=3.18
6650	235	TOJ1D	TOJ2D	TOJ1Dn



▶ 3

Selected results – mixture fraction along centerline



Mean profiles of mixture fraction

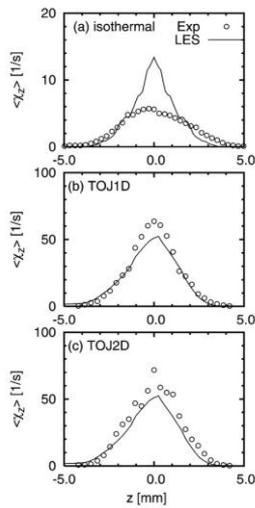
Fluctuations of mixture fraction

LES by A. Kempf

▶ 4

- Isothermal and reacting flow show similar mean profile shapes
- Mean profile of isothermal flow distinctly widened by intermittence
- In flames: turbulent mixing is damped by higher viscosity
 - ⇒ Mean profiles less widened
 - ⇒ Mixture fraction fluctuations in flames smaller than the very high ones in isothermal flow
- ⇒ change in fuel composition between TOJ1D and TOJ2D has only a minor impact on the profiles

Selected results – scalar dissipation rate along centerline



Scalar dissipation rate profiles along centerline isothermal flow (a) and partially premixed flames TOJ1D (b) and TOJ2D (c)

- Statistics of instantaneous 1D-scalar dissipation rate along centerline

$$\chi_z = 2D_f (\nabla_z f)^2$$

- Maximum at mean stagnation plane
- Again almost no influence of fuel composition
 \Rightarrow flow field effects dominate
- χ_z approximately 10 times higher in reacting flow than in isothermal
- Scalar gradients smaller in flame, but diffusivity increases in reacting flow
- LES resembles experiments very well

Combined PIV/OH-PLIV experiments (B. Böhm et al.)

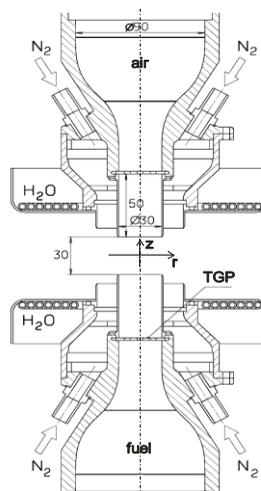


Extinguishing flames

- TOJ can be operated close to extinction by increasing flow momentum
- global extinction starts in the region of the stagnation point

	stable flame	
	TOJ2D	TOJ2C
Re	6650	5000
ϕ	2.0	2.0
Bulk velocity [ms^{-1}]	3.4	2.55
Bulk strain rate [s^{-1}]	231	175

extinguishing flame



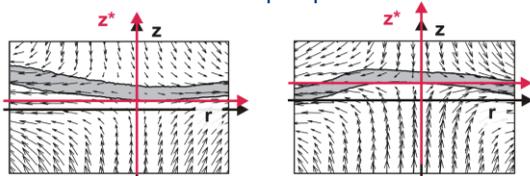
Benjamin Böhm | 1



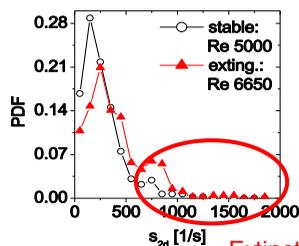
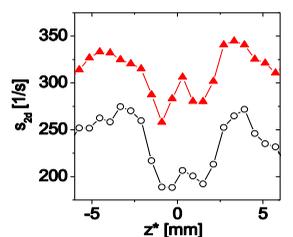
Temporally uncorrelated data



- Conditioning on instantaneous stagnation point
- PIV/OH-PLIF @ 1Hz:
- Flow field from flame perspective $\rightarrow z^*$



- Extinguishing flame:
 - \rightarrow higher value of mean strain (2D)
 - \rightarrow broader pdf of strain
 - \rightarrow wing towards high strain

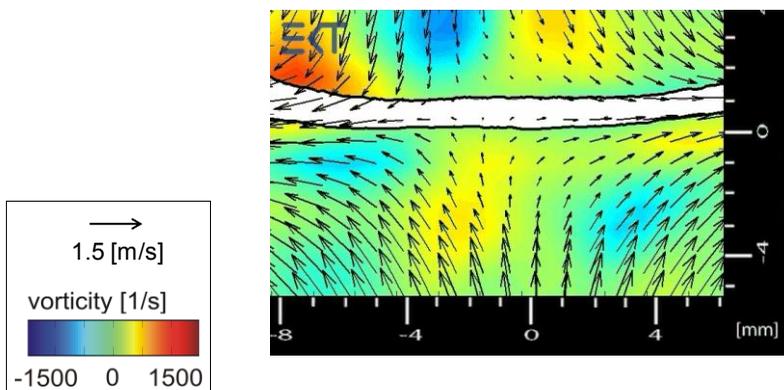


Benjamin Böhm | 2



Individual Extinction Event

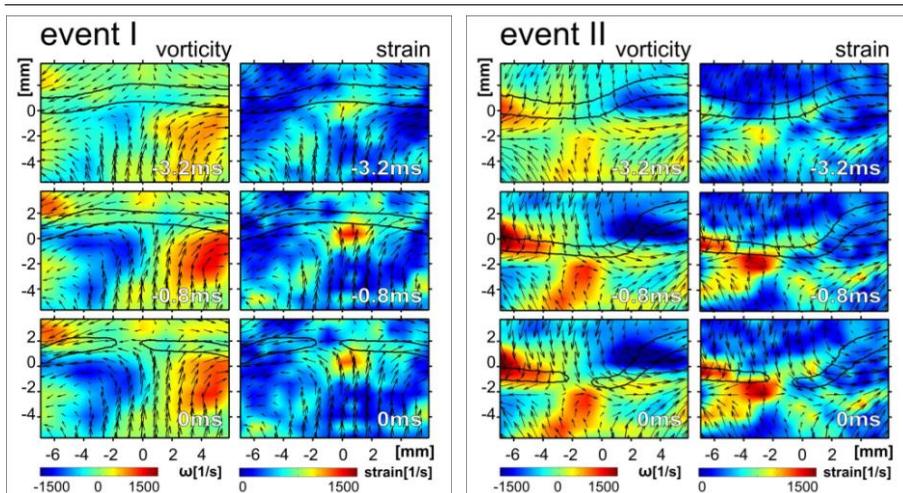
- instantaneous flow field, flame front recorded by OH-PLIF and vorticity map processed from the band-pass filtered flow field



Benjamin Böhm | 3



Individual Extinction Events



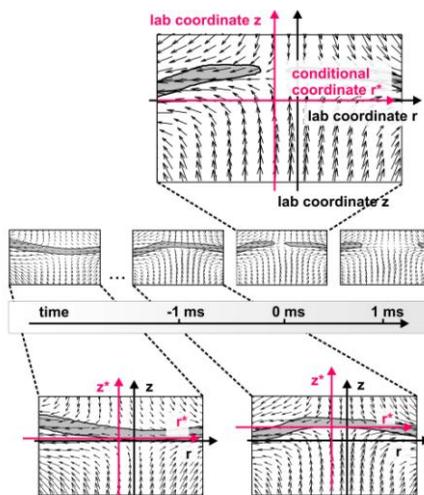
→ multiple vortices act coherently generating regions of high strain close to the flame at the onset of extinction



Multidimensional Conditioning

- how to build up meaningful statistics?

→ conditioning in time and space z^* , r^* , and t^*

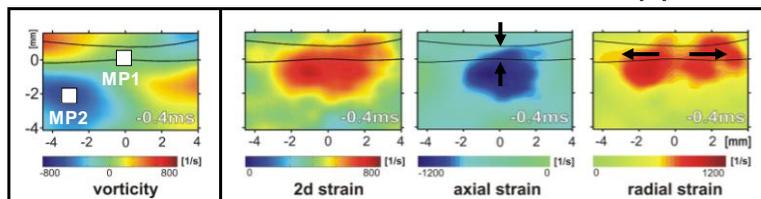
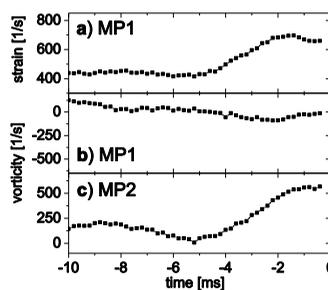


Benjamin Böhm | 5



Conditional Average

- maximum of axial strain surrounded by maxima of radial strain
- imposed strain requires time to cause extinction
- time history is important
- diffusion requires time to reduce scalar gradients



Benjamin Böhm | 6



Conditional Statistics, Length Scales and Energy Distribution in Fractal Generated Turbulence in Opposed Jets

11th International Workshop on Measurement and Computation of Turbulent Flames **TNF** **10**

26. – 28. July 2012, Darmstadt

P Geipel^{a,b}, KHH Goh^a and RP Lindstedt^a

^aMechanical Engineering, Imperial College, London.

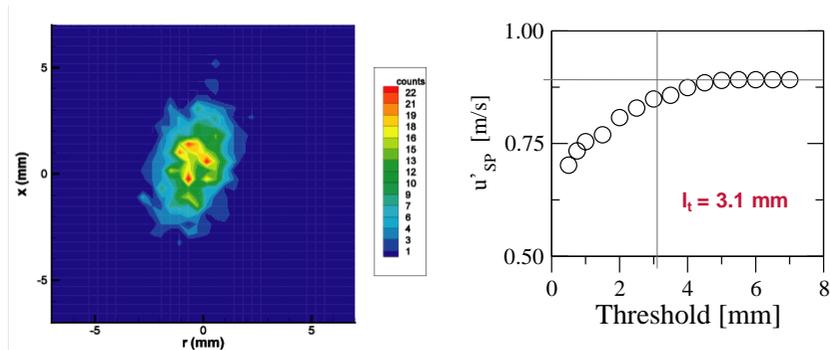
^bSiemens Industrial Gas Turbines, Finspong, Sweden.

Opposed Jets – Current Data Set

- ❑ Fractal grid generated turbulence is multiscale in nature and appears fundamentally different from that produced by conventional turbulence generators.
- ❑ The data sets should provide a particularly interesting test for LES and, for cases with low Da numbers, time resolved transported PDF based methods.
- ❑ The data includes combustion regime transitions.
- ❑ All measurements free of bulk flow instabilities – statistics available – see overleaf.

Statistical Analysis of the Stagnation Point Location

- The examples shown are the PDFs of the instantaneous stagnation point locations. Two planar filtering algorithms developed for data analysis.
- The movement of the stagnation point is often not only a result of turbulent motion but also due to a low frequency bulk movement of the flow.



K.H.H. Goh, P. Geipel, R.P. Lindstedt, Conditional statistics in turbulent premixed opposed jet flames, TNF10 Workshop, Beijing, July 2010.

Opposed Jets – Current Data Set

- Data sets cover premixed and flameless combustion modes. The stoichiometric range is focussed on fuel lean combustion
- The flow inside a nozzle measured to provide comprehensive boundary conditions.
- Velocity statistics implies normal and radial velocities as well as length scale information. The Re_t varied between 110 and 320. The upper limit determined by turbulent strain induced extinction.
- Scalar statistics implies the reaction progress variable and variance. The Da numbers varied from around 0.3 to 6.
- Conditional statistics implies conditional velocities and scalar fluxes.
- Flow structures implies spectra and/or conditional spectra and/or proper orthogonal decomposition (POD) data and/or conditional POD data and/or flame surface related properties.

Opposed Jets – Current Data Set

	Type	Fuel	Velocity Statistics	Scalar Statistics	Conditional Statistics	Flow Structures
1	Isothermal	--	Yes	--	--	Yes
2	Premixed	CH ₄	Yes	Yes	Yes	Yes
3	Premixed with increased Re _t .	CH ₄ C ₂ H ₄ C ₃ H ₈	Yes	Yes	Yes	Yes
4	Flameless	JP-10	Yes	Yes	Yes	Yes

- Data set 1 is available, set 2 is under review, set 3 to be submitted in September and set 4 will be available after the Symposium.
- Data sets 1, 2 and 4 share very similar boundary conditions (in the case of one nozzle for set 4) and work on the isothermal flow should translate directly.
- High-speed PIV and OF-PLIF (Frank Beyrau) data will be available.



Highly Turbulent Counterflow Flames: a Laboratory-scale Benchmark for Turbulent Combustion Studies



Alessandro Gomez¹, Bruno Coriton^{1,2} and Jonathan H. Frank²

¹Yale Center for Combustion Studies
Department of Mechanical Engineering and Materials Science
Yale University, New Haven, CT 06520-8284
<http://www.eng.yale.edu/gomez-lab/>

²Combustion Research Facility, Sandia National Laboratories

TNF11, July 2012

Turbulent Counterflow Flames

Previous Experimental Work

Kostiuk et al., 1989-1993 (Cambridge)
Mastorakos et al., 1992-1995 (Imperial College)
Dreizler, Kempf et al 2000-2005 (Darmstadt)

Problems/Challenges

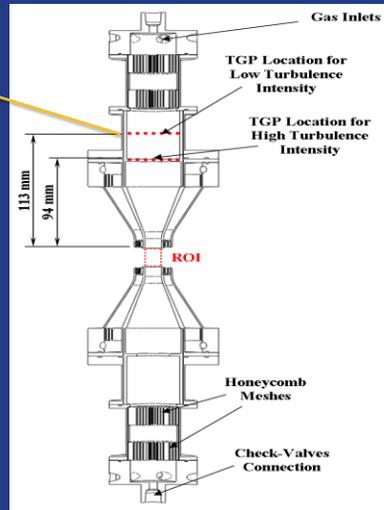
- Main limitation was the small, $O(50-100) Re_t$ (integral scale based)
- Young turbulence $\leftarrow \rightarrow$ eddy turnover time $\tau_e \gg \tau_r$
- Intrinsic instabilities cause large scales oscillations of the stagnation surface

TNF11, July 2012

Burner Design for High Turbulence

Main Ingredients

- High blockage Turbulence Generation Plate (TGP)
- Feed Stream composition to allow for robust flames at very high strain rates
- Burner dimensions:
 - $D_{out} = 12.7 \text{ mm}$
 - $D_{cf} = 27 \text{ mm}$
- Nozzle separation of $\sim 1\text{-}2 D_{out}$
- Characteristic inlet conditions
 - $Re_d \sim 10000$
 - Strain rates $\sim O(1000) \text{ s}^{-1}$



3

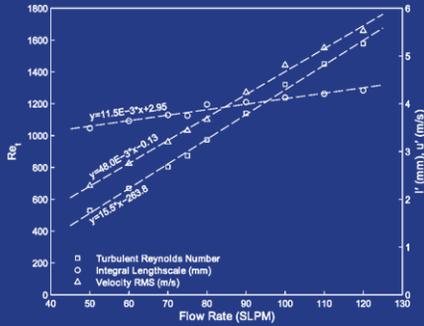
TNF11, July 2012

Nonreactive (Cold) Flows

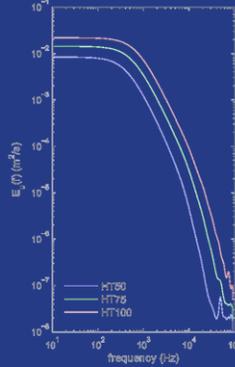
TNF11, July 2012

Flow Field Characterization

Integral Length scale and turbulent Reynolds number



Power Spectrum

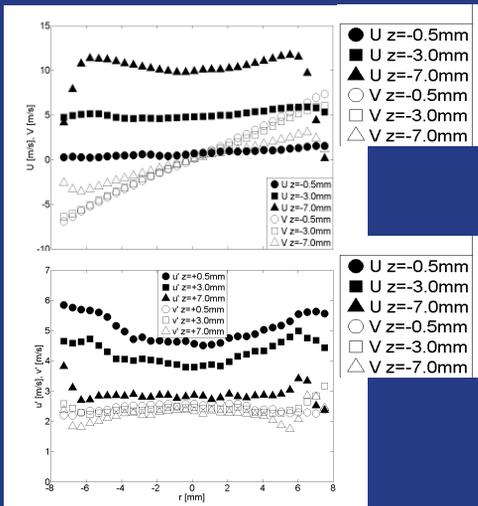


- Velocity Measurements by PIV and HW
- Turbulent Reynolds number range: 100 – 1000.
- Integral length scale: ≈ 3-4 mm
- Estimated Taylor scale at 0.8 mm
- Without TGP, the flow is laminar

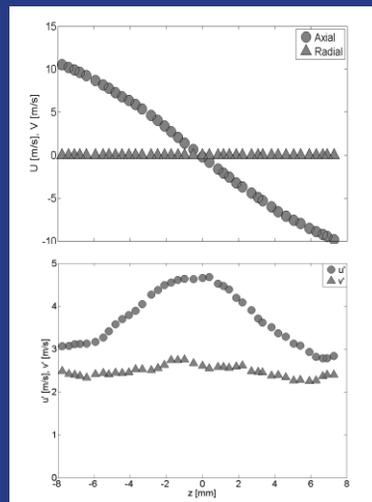
TNF11, July 2012

Mean and RMS Velocity

Radial



Axial



6

TNF11, July 2012

Instabilities and Coherent Structures

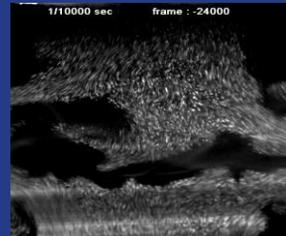
TNF11, July 2012

Large Scale Instabilities

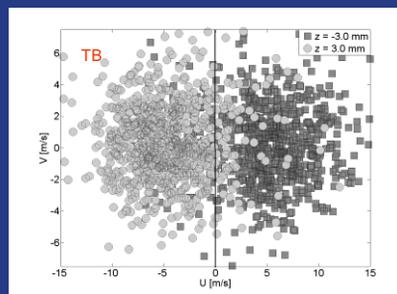
Cold



Hot

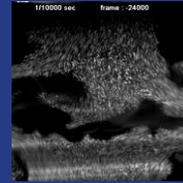


Turbulence generators trigger large scale oscillations of the stagnation surface at frequencies < 200 Hz.



TNF11, July 2012

Some Characteristic Times



- Characteristic period of instability: $t_i > 5 \text{ ms}$
- Mean Residence time: $t_r \sim 1/S_b \sim 1.0 \text{ ms}$
- Eddy turnover time: $t' \sim L'/k^{0.5} \sim 0.8 \text{ ms}$

Since $t_i \gg t_r > t'$

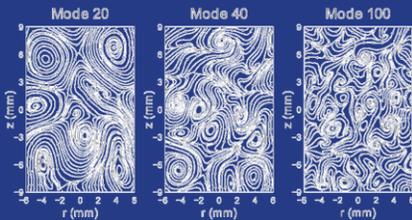
- ➔ Instabilities are not part of the turbulence
- ➔ Young turbulence concern does not apply

Still, should we care about them?

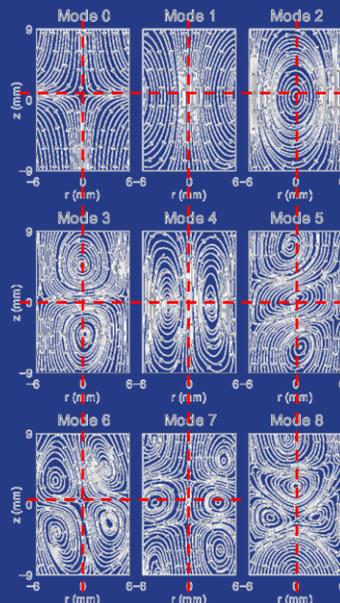
TNF11, July 2012

Coherent and Incoherent Structures

- Coherent structures symmetry is consistent with the burner geometry
- Incoherent structures are disorganized

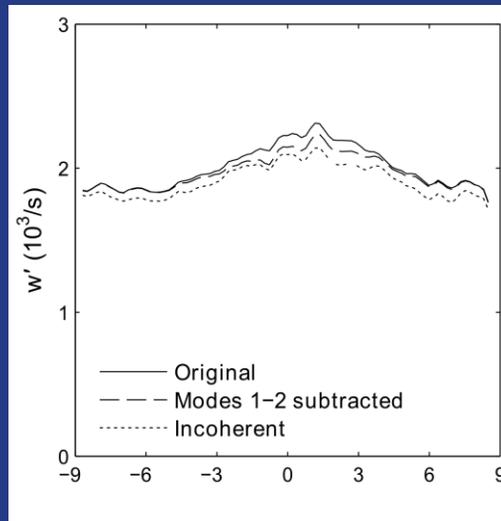


- Vortical structures become finer at higher modal order



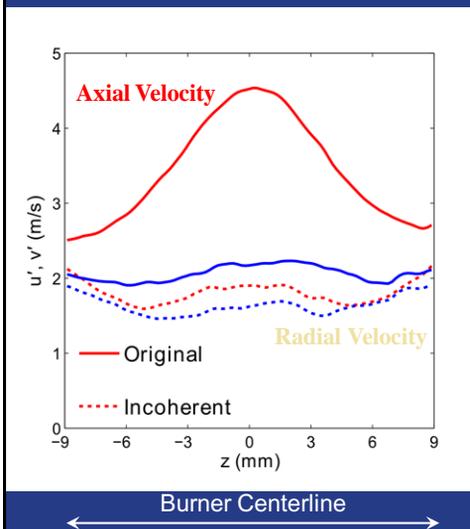
TNF11, July 2012

Vorticity fluctuations



TNF11, July 2012

Velocity Fluctuations



- Velocity fluctuations increase near the plane of symmetry of the burner.
- Effect is due to the instabilities of the gas mixing layer.
- Incoherent (turbulent) flow field is nearly isotropic.
- But instabilities need to be screened to eliminate artifacts in measurements, using for example POD

TNF11, July 2012

Turbulent Counterflow Flames: Challenges

- ~~Main limitation was the small, $O(50-100)$ Re_t (integral scale based)~~
- ~~Young turbulence $\leftarrow \rightarrow$ eddy turnover time $\tau_e \gg \tau_f$~~
- Intrinsic instabilities cause large scales oscillations of the stagnation surface, whose artifacts can be screened by POD.
- Instabilities might be suppressed by active/passive control (?)

TNF11, July 2012

Conclusion

- Highly turbulent Re_t (~ 1000) can be achieved in the counterflow configuration with a well behaved flow pattern
- Low-frequency instabilities are not part of turbulence, but may cause artifacts that need to be screened through suitable data processing

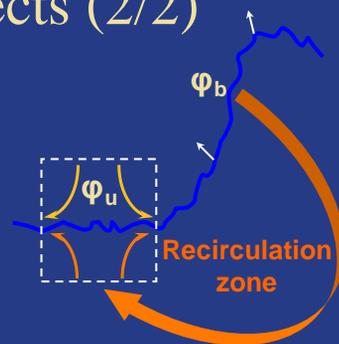
TNF11, July 2012

Premixed Flames: An Opportunity to Introduce Real Flame Effects in a Bench-top Set-up

TNF11, July 2012

Real Flame Effects (2/2)

- *Real* turbulent flames are exposed to external perturbations such as heat loss/gain, dilution by hot products, a large bulk strain rate, mixture stratification...
- Experimental investigation of the non-flamelet regime is a challenge because of blowoff.
- Pilot flames, swirls or bluff bodies have been designed to improve the flame stability at elevated Karlovitz numbers, but may present difficulties computationally in the prescription of the B.C.



Highly Swirled Flame



Piloted Jet Flame



Bluff-Body Flame

(Source: International Workshop on Premixed Flames)

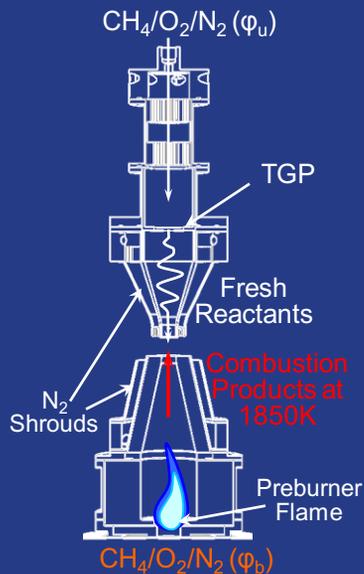
TNF11, July 2012

Objectives

- Investigate the structure of highly turbulent premixed flames
- Characterize flames in the non-Flamelet Regime in a laboratory-scale burner
- Characterize factors causing a departure from the Flamelet Regime, mimicking real flames

TNF11, July 2012

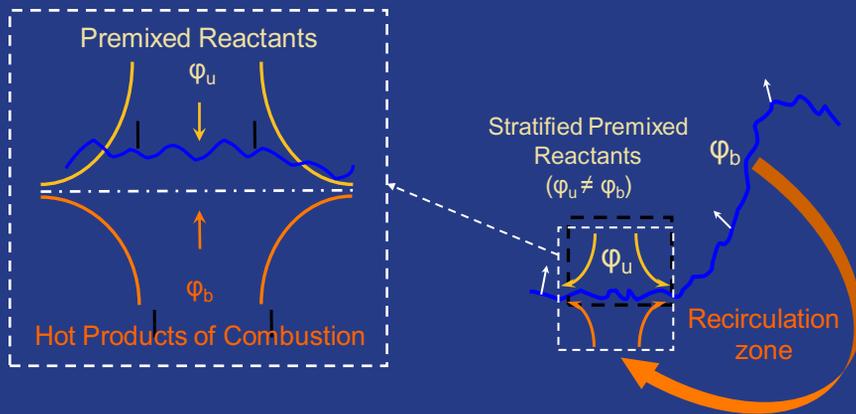
Burner Modification



- Upper nozzle is the same as in the nonpremixed flame configuration;
- Lower nozzle (castable zirconium ceramics in a stainless steel shell) discharges a jet of hot products of combustion in thermochemical equilibrium;
- No TGP is used in the lower nozzle;

TNF11, July 2012

Effects to Be Studied Systematically: Strain, Heat Loss and Stratification



TNF11, July 2012

Upper nozzle

- $Re_t = 470 - 1050$
- $T_u = 294K$
- $\phi_u = 0.3 - 1.2$
- $X(N_2/Air) = 70\%$

Lower nozzle

- Not turbulent
- $T_b = 1500K - 2000K$
- $\phi_b = 0.7, 1.0$ or 1.2
- $X(N_2/Air) = 63 - 74\%$

Pulsed Nd:YAG Laser

OPO SHG

230 nm

286 nm

Pulsed Nd:YAG Laser

Dye Laser

SHG

Beam Profile CO LIF

CO cell

OH LIF Camera

CO LIF Camera

Imaging of Reaction Rates

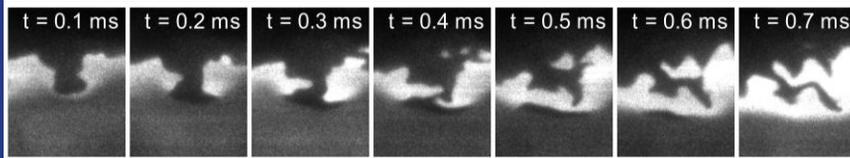
- CO-LIF and OH-LIF measurements yield reaction rate for:
 $CO + OH \rightarrow CO_2 + H$
- CH_2O -LIF and OH-LIF measurements yield reaction rate for:
 $CH_2O + OH \rightarrow H_2O + HCO$

TNF11, July 2012

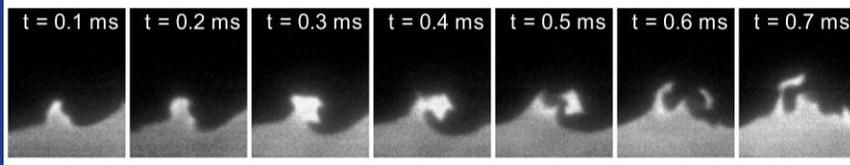
Extinction / Ignition Events

- Flame interaction with combustion products results in series of extinction and ignition events
- 10kHz OH-LIF image sequences

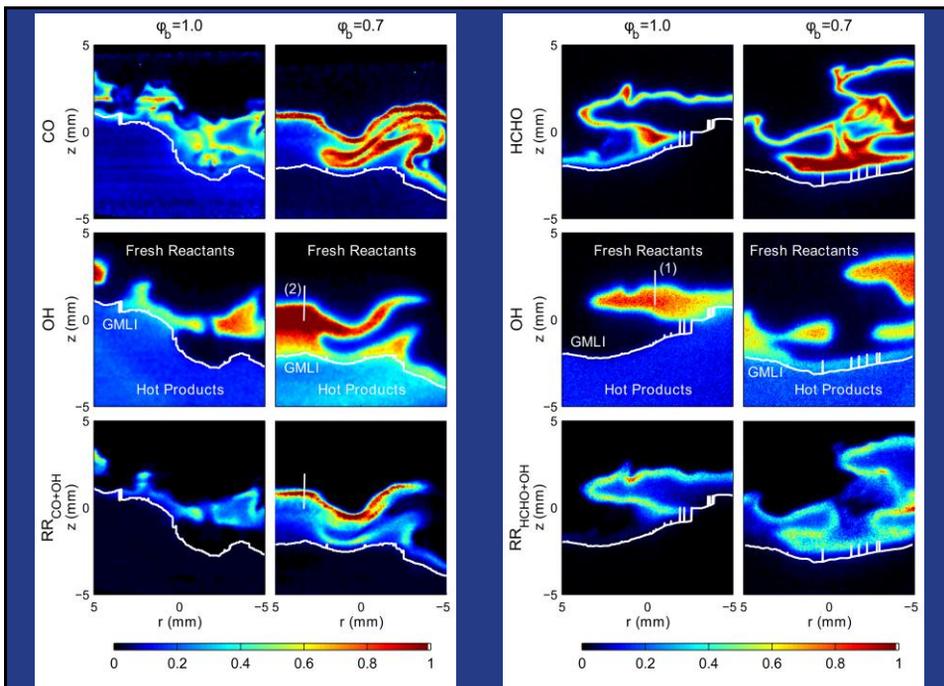
$\phi_u = 1.0$ – Formation and disappearance of a local extinction



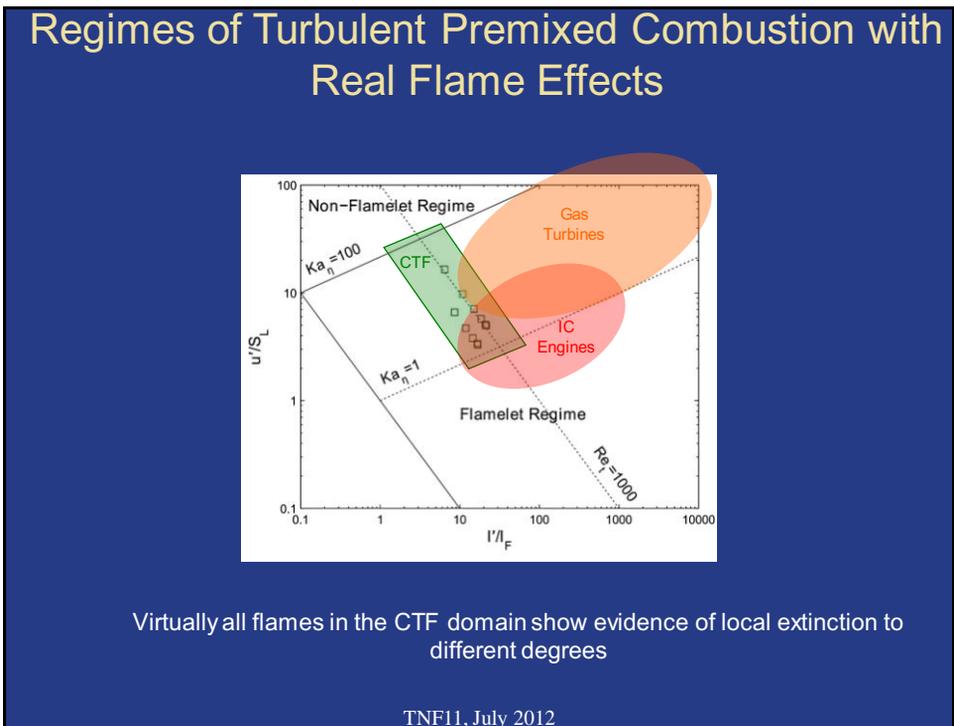
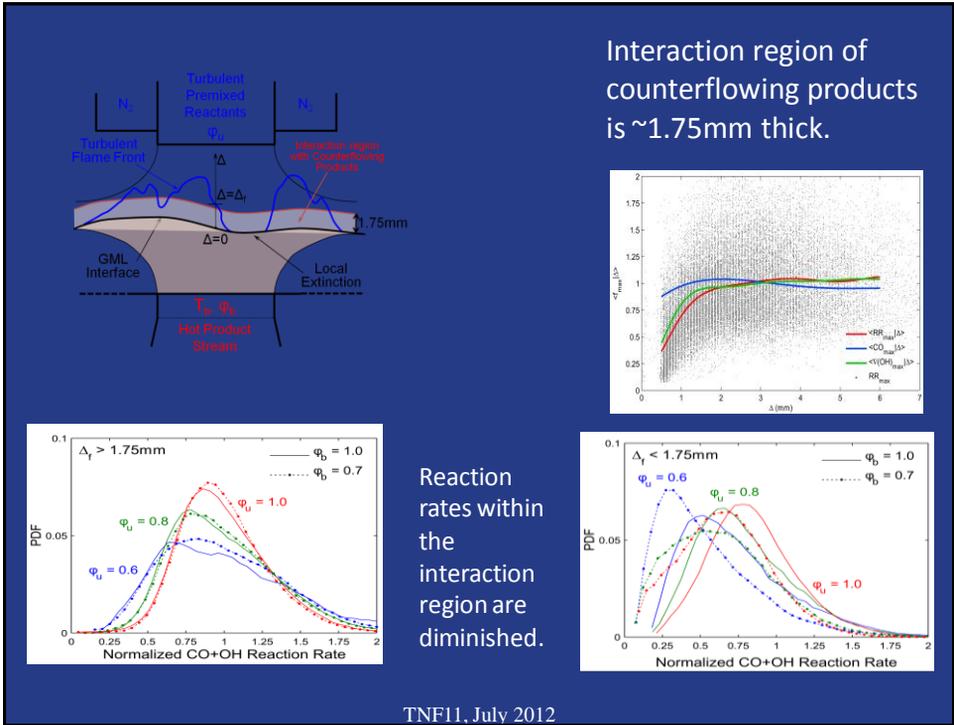
$\phi_u = 0.3$ – Local ignition spots



TNF11, July 2012



TNF11, July 2012



Conclusions (Premixed)

- The counterflow burner achieves a range of turbulent Reynolds numbers and Karlovitz numbers overlapping those of practical systems
- It has the potential to redefine the boundaries of the Flamelet Regime to account for real flame effects (strain, volumetric heat loss/gain, gas composition stratification, slow CO oxidation, etc.)
- Comparison of flames with the same coordinates in the Borghi diagram show very distinct behavior and seemingly paradoxical trends. Trends are confirmed by laminar flame calculations

TNF11, July 2012

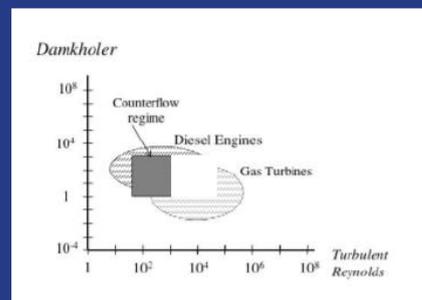
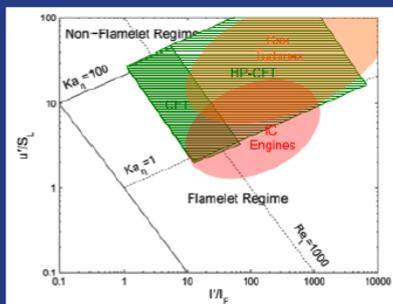
Concluding Remarks

- Highly turbulent counteflow flames ($Re_t=O(1000)$) can be stabilized in bench-top experiments in regimes of relevance to practical systems, including conditions of local extinction and non-flamelet behavior
- Flame compactness and short residence time are advantageous, especially for computational modeling
- Flames are aerodynamically stabilized, eliminating the need for bluff bodies and pilot flames with attending complications
- Soot is suppressed

TNF11, July 2012

High Pressure Extension

- Collaboration between Yale, Sandia and KAUST (Bill Roberts)
- Facility under construction at KAUST to operate up to 40 atm with pre-heating
 - Greater overlap with regimes of practical relevance



TNF11, July 2012

Summary Opp-Jet session

- ▶ Recent developments on configurations
 - Re_t number has been substantially increased
 - Re number has been raised, depending of flame configuration
- ▶ Experimental data sets
 - Substantial amount of experimental data available
 - Diversity on fuels one major activity
- ▶ Simulations, current activities

• Lindstedt et al.:	IC	Monte-Carlo PDF, 2nd moment U-RANS
• Kempf, Stein, et al.	DA, IC, Yale	LES
• Calhoun et al.	DA ?	LEM
• Pope	Yale	LES
- ▶ TNF perspective
 - Configurations of interest as a target flame ?
 - Activities planned ?

Notes

TNF11

July 2012



Open Discussion, Action Items and Planning for TNF12

J. Janicka



Institute for Energy and Powerplant
Technology



General Remarks



- **Impression**
 - Considerable progress
 - Young scientists!
- **Identification of target flames**
 - **Focus**
 - **Fundamental aspects** of turbulence chemistry interaction
 - **good** experiments
 - comparisons of **different** models
 - Phenomena **not understood?**
 - **Bottom up: driven by scientific interest and funding**
 - **Self adjusting systems**
 - **Simple! 2+3**
- **Increasing importance**
 - **Diff-Diff**
 - **Enthalpy as an additions variable**
 - **Use of DNS data for model development**



Perspective TNF12



- **Focal point: multiple calculation for target flames**

- **Stratified burner**
 - **Impressive progress → continue**

 - **Darmstadt burner**
 - Different models
 - Future: strained flames, different fuels

 - **Cambridge burner**
 - More models helpful
 - Recirculation zone prediction

 - **For both**
 - limits for premixed flame models (higher stratification)
 - Diff-diff effects



Perspective TNF12



- **Diff-diff effects**
 - **Picture for diffusion flames „clear“?**
 - **Open for stratified and premixed flame**
 - **Of tremendous technical importance (H2 addition)**

 - **Continue**
 - Evaluation of importance
 - Model formulation?



Perspektive TNF12



▪ Lifted flames, vitiated coflows, mild combustion

- VCB flames
 - Understood?
 - Like Flame D, TECFLAME?
- Potential for future target flames (mild combustion)
 - Interesting questions
 - Challenging
 - More model comparison needed
- Diff-diff
- Role of DNS



Perspektive TNF12



▪ Piloted premixed burner

- Cases with lower velocities ok
- PM1 200 not understood
 - Good news
 - Rethink
 - Additional iteration between model and experiment



Perspektive TNF12



▪ Piloted premixed burner

- Cases with lower velocities ok
- PM1 200 not understood
 - Good news
 - Rethink
 - Additional iteration between model and experiment



Perspektive TNF12



▪ Chemistry, complex fuels and new combustion modes

- DME
 - Test cases available
 - Understood?
- Oxyfuel (including mild combustion)
 - Ditto
- Strong funding perspective
- High potential for future activities
- High H₂ addition?



Perspektive TNF12



▪ Turbulent opposed jet flames

- Very good data base
 - Extinction, ignition, reignition, strain, stratification,..
 - Extension to higher Re number
 - Different fuels
 - Boundary conditions?
- Very suitable for model development and validation
- Future target flames?



Perspektive TNF12



▪ Interpretation and utilization of time resolved data

- Understanding of phenomena
- Particular suitable for statistically not stationary effects
 - (ignition, extinction, flashback,..)
 - POD, DMD
- Open
 - What can we learn for model development?
 - Future subject for TNF's



Perspective TNF12



- **LES/DNS: Quality and Best Practice**
 - **Uncertainties**
 - **Error analysis methods**
 - **Recommendations**
 - **Needed: Methods for high Re systems in complex geometry**

- **In progress → continue**



Acknowledgements



- **Local committee (Monika, Simone, Andreas²)**
- **Everybody preparing a lecture or a poster**
- **All discussion contributors**
- **Everybody for joining TNF11**

- **TNF12 in California**

→ Rob



Authors and Titles of Poster Abstracts (ordered by first author)

C. Arndt, R. Schießl, J. Gounder, W. Meier

Influence of Temperature and Velocity on Auto-Ignition and Flame Stabilisation of Pulsed Methane Jets in a Hot Coflow.

L.D. Arteaga Mendez, M.J. Tummers, D.J.E.M. Roekaerts

Effect of Fuel and Oxidizer Composition on Jet-in-Coflow Flames.

B. Coriton, J. H. Frank

Dependence of Localized Extinction and Thermal Dissipative Structures on Nozzle Diameter in Turbulent Non-Premixed Jet Flames.

B. Coriton, M. Gamba, S.-K. Im, G. Mungal, J. H. Frank

Simultaneous OH/CH₂O LIF Imaging and PIV Measurements in Turbulent Partially Premixed Dimethyl Ether/Air Jet Flames.

A. Fiolitakis, P. R. Ess, P. Gerlinger, M. Aigner

Transported PDF Calculations of a Turbulent, Non-Premixed, Hydrogen-Air Flame ("H3-flame").

D. Frederick, A. North, R. Dibble, J.Y. Chen, A. Gruber

The Effects of Diffusion Models, Turbulence, and Pressure on Autoignition Delay Time for a H₂/N₂ Jet Flame in a Vitiated Co-flow using a 1-D Laminar Mixing Model and the Linear Eddy Model.

F. Fuest, R. S. Barlow, J. A. Sutton, A. Dreizler

Signal-to-Noise and Signal-to-Background Ratios in Laminar and Turbulent Flames of Ethylene and Ethane in 1D Raman/Rayleigh Scattering and COLIF Measurements.

K. N. Gabet, F. Fuest, J. A. Sutton

Quantification and Accuracy of a CMOS-Based Raman Scattering Imaging System for High-Speed Measurements in Flames.

Y. Ge, B. Sundaram, M. J. Cleary, A. Y. Klimenko

Localisation and Convergence Testing in Sparse-Lagrangian MMC Simulations.

P. Geipel, K. H. H. Goh, F. Hampp, R. P. Lindstedt, **Conditional Statistics, Length Scales and Energy Distribution in Fractal Generated Turbulence.**

A. Gruber, H. Kolla, D. Valiev, J.H. Chen

DNS of Boundary Layer Flashback in Turbulent Channel Flow.

V. Hiremath, S. Pope

Combined Reduction-Tabulation based Strategies for Computationally-Efficient Implementation of Combustion Chemistry.

S. Hochgreb, M. S. Sweeney, R. Zhou, M. J. Dunn, R. S. Barlow

Scalar and Velocity Results in a Turbulent Stratified CH₄/Air Swirl Burner.

V. R. Katta, W. M. Roquemore

Preferential Diffusion in Bluff-Body Stabilized Turbulent Premixed Flames.

H. Kolla, A. Gruber, R. Grout, J.H.Chen

Fundamental Insight into Flame Stabilization in Transverse Jets in Cross-Flow using Direct Numerical Simulations (DNS).

K. Kopp-Vaughan, S. Tuttle, T. Jensen, B. Cetegen, M. Renfro

Bluff-Body Flame Blowoff Dynamics under Stratified Fueling and Thermoacoustic Coupling.

A. Krisman, E. R. Hawkes, J. C. K. Tang, J. E. C. Chan, S. Kook, J. H. Chen

Evaluating Mixing Models for Transported Probability Density Function Simulations of Nonpremixed Turbulent Flames.

Authors and Titles of Poster Abstracts (continued)

- G. Kuenne, A. Ketelheun, A. Avdic, A. Sadiki, J. Janicka
Investigation of Heat Loss effects within the Darmstadt Stratified Burner by means of Large Eddy Simulation and a Joint ATF-FGM Approach.
- G. Lacaze, J. C. Oefelein
Investigations of DME Jet Flames with Emphasis on Stabilization, Transport and Turbulence-Chemistry Interactions.
- J. Lee , S. Park , Y. Kim
DQMOM-based PDF Transport Modeling for Turbulent Lifted Flame with Vitiated Co-flow.
- G. Magnotti, A. Cutler
Dual Pump CARS Measurements in a Supersonic Combusting Free-Jet.
- P. Medwell, B. Dally
Experimental Observation of Lifted Flames in a Heated and Diluted Coflow.
- R. Mercier, P. Auzillon, V. Moureau, N. Darabiha, O. Gicquel, D. Veynante, B. Fiorina
Modeling Flame Stabilization by Heat Losses using Filtered Tabulated Chemistry for Large Eddy Simulation.
- D. Messig, J. Keller, C. Hasse
Modeling of Laminar Partially Premixed Dimethyl Ether Flames.
- S. Nambully, P. Domingo, V. Moureau, L. Vervisch
Modeling Differential Diffusion in Large Eddy Simulation of a Bluff Body Stabilized Premixed Weakly Turbulent Flame.
- North, A., Frederick, D., Dibble, R. W., Chen, J. Y., Gruber, A.
The Effect of Pressure, Environment Temperature, Jet Velocity and Nitrogen Dilution on the Liftoff Characteristics of a Hydrogen Jet Flame in a Vitiated Co-flow.
- Z. Pouransari, L. Vervisch, A. V. Johansson
Non-premixed Turbulent Flames Close to Wall.
- F. Proch, F. Cavallo Marincola, A.M. Kempf
LES of the Cambridge Stratified Flame Series.
- Z. Ren, T. Lu, G. Goldin
Dynamic Adaptive Chemistry for Turbulent Flame Simulations.
- G. Sarras, M. K. Stöllinger, D. J. E. M. Roekaerts
Simulation of the Delft-jet-in-hot-coflow burner using transported PDF methods and FGM tabulated chemistry.
- T. Stahler, S. Schneider, G. Kuenne, D. Geyer, A. Dreizler
Advances in Raman Spectroscopy for Model Validation on Turbulent Flames.
- Y. Yang, S. Pope, J. Chen
Empirical Low-Dimensional Manifolds in Composition Space.
- M. Zendejdel, S. Ukai, O.T. Stein, A. Kronenburg
LES-CMC Predictions of Turbulent Piloted DME Jet Flames.
- R. Zhou, M. S. Sweeney, S. Hochgreb, R. S. Barlow
Flow Field Studies of Cambridge Stratified Swirl Burner.

Influence of Temperature and Velocity on Auto-Ignition and Flame Stabilisation of Pulsed Methane Jets in a Hot Coflow

Christoph M. Arndt¹, Robert Schießl², James D. Gounder¹, Wolfgang Meier¹

¹*Deutsches Zentrum für Luft- und Raumfahrt (DLR), Institut für Verbrennungstechnik
Pfaffenwaldring 38-40, 70569 Stuttgart, Germany*

²*Karlsruher Institut für Technologie (KIT), Institut für Technische Thermodynamik
Kaiserstraße 12, 76131 Karlsruhe, Germany*

Christoph.Arndt@DLR.de

Auto-ignition of fuel in an environment of hot oxygen-rich combustion products (vitiating air) plays an important role in practical combustion devices like piston and gas turbine (GT) engines. In GT combustion, auto-ignition can lead to an undesired flame in the premixing region or mixing duct of reheat combustion systems where fuel is injected into hot, oxygen-containing exhaust gas. Auto-ignition events have previously been investigated under various conditions in shock tubes, rapid compression machines, flow reactors, and laminar and turbulent flames.

In this study, high-speed laser diagnostics and imaging techniques at repetition rates of up to 20 kHz were used to investigate the pulsed injection of a methane jet into the hot, oxygen-rich combustion products of a lean premixed hydrogen / air flat flame. High-speed OH* chemiluminescence was used to determine the time and location of the auto-ignition and to study the initial flame kernel development. Planar laser-induced fluorescence of the OH radical was used to characterize the auto-ignition process and flame kernel development with greater spatial resolution. After the ignition process, the jet burned as a stable lifted flame. The underlying stabilization mechanism was studied by imaging the flame dynamics at the flame base for approximately 0.7 s after the initial auto-ignition.

Preceding studies on the same burner [1] have shown that the auto-ignition kernels tend to form in bulges of the inflowing jet, where strain and scalar dissipation are expected to be low. In order to assess the influence of strain during the auto-ignition process, detailed model simulations and experiments were performed for a variety of coflow temperatures in the range between 1566 K and 1810 K [2]. It was found that strain is a key factor in the auto-ignition process in this configuration. The downstream location of auto-ignition and the auto-ignition delay time were found to be very sensitive to small changes of the co-flow temperature and composition.

In the present study, the influence of strain is studied in more detail experimentally. Measurements with varying jet and coflow velocity were performed and the auto-ignition height and time as well as the lift-off height of the steady state jet flame under these conditions were evaluated. In Figure 1 the averaged OH* chemiluminescence signal for the steady state jet flame for different coflow velocities is shown. The images are based on an average of 500 statistically independent chemiluminescence frames. The coflow temperature T_{coflow} for these cases was held constant at 1650 K and the jet velocity v_{jet} was held constant at 100 ms^{-1} . It can be seen that the lift-off height of the jet flame decreases with increasing coflow velocity, probably due to the smaller gradient in axial velocities between the inflowing jet and the coflow.

As was shown in previous studies in similar burner configurations, the jet flame was stabilized by auto-ignition. In this study, it was frequently observed for coflow temperatures below 1700 K (depending on the coflow velocity) that auto-ignition kernels formed upstream

of the flame base and propagated to the flame root. An example image sequence of such an event is shown in Fig. 2. The operating conditions for this case were $v_{coflow} = 4 \text{ ms}^{-1}$, $v_{jet} = 100 \text{ ms}^{-1}$ and $T_{coflow} = 1650 \text{ K}$. Here, an ignition kernel forms in the second frame of the image sequence and propagates downstream. The kernel slowly grows in size and intensity and finally merges with the flame base approximately 0.6 ms after its first occurrence. Such events can be observed regularly in an image sequence. However, for some of the higher coflow velocities (at the jet velocity shown here) no such events could be observed.

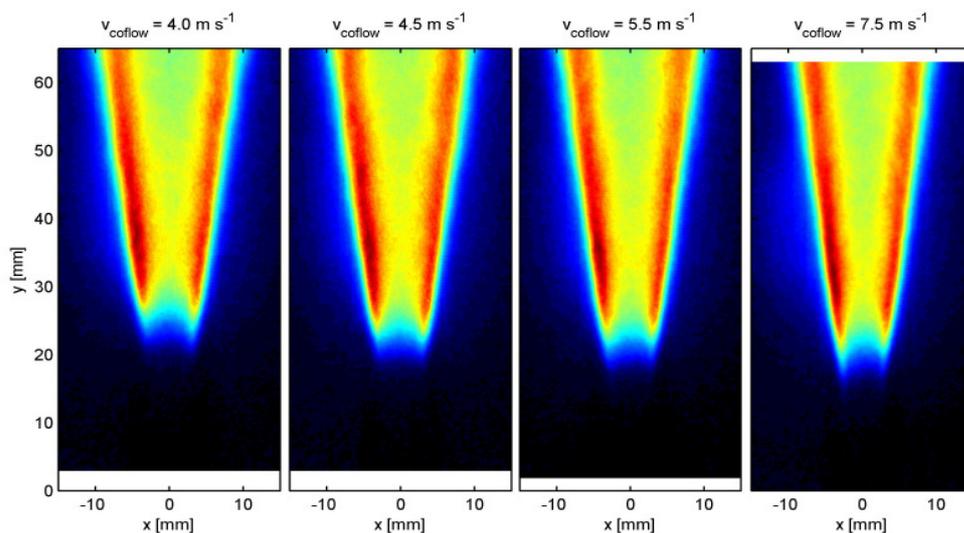


Figure 1: Influence of the Coflow Velocity on the lift-off height.

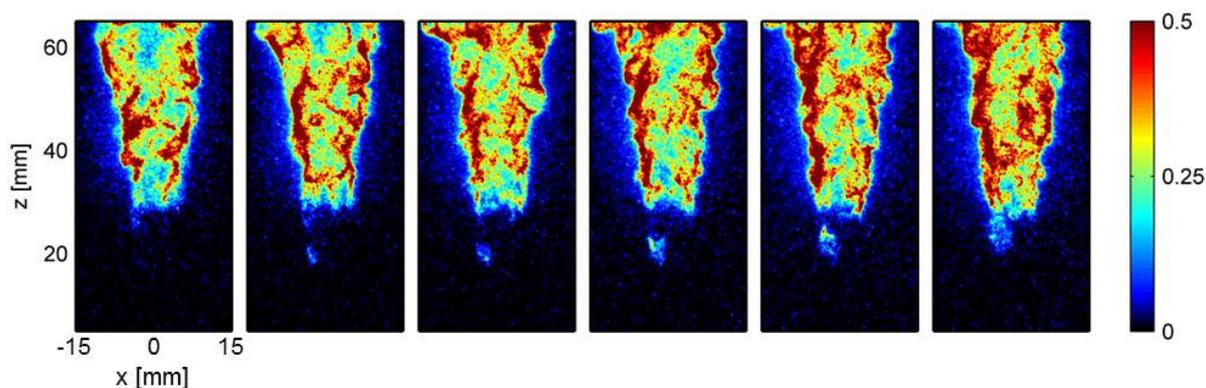


Figure 2: Image Sequence of an auto-ignition kernel forming below the flamebase. Time between frames is 0.15 ms.

References

- [1] C.M. Arndt et al., Appl. Phys. B (2012), DOI : 10.1007/s00340-012-4945-5
- [2] C.M. Arndt et al., Proc. Combust. Inst. (2012), DOI : 10.1016/j.proci.2012.05.082

Effect of fuel and oxidizer composition on jet-in-coflow flames

L.D. Arteaga Mendez, M.J. Tummers and D.J.E.M. Roekaerts

Department of Multi-Scale Physics, Delft University of Technology, The Netherlands

L.D.ArteagaMendez@tudelft.nl

In flameless oxidation reactants and combustion products mix prior to combustion leading to strongly reduced pollutant emissions as compared to traditional combustion processes. Important benefits may result from the application of flameless oxidation to non-conventional fuels such as coke oven gas, refinery gas and biogas. The effect of hydrogen and carbon dioxide on the stabilization mechanism of Dutch natural gas (DNG) jet flames oxidized in cold and hot coflows is currently being studied using high speed recordings of the flame luminescence and time resolved particle image velocimetry. The hot coflow has relatively low oxygen content mimicking the characteristic oxidizer conditions in flameless oxidation.

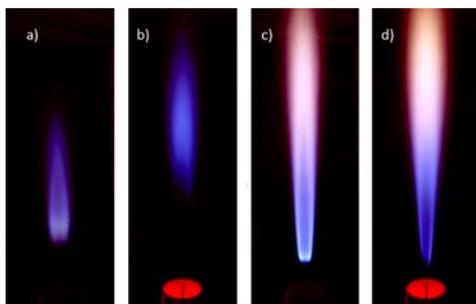


Fig. 1 Visual appearance of four studied flames: a) 10/90 CO₂/DNG in cold coflow, b) 10/90 CO₂/DNG in hot coflow, c) 10/90 H₂/DNG } in cold coflow and d) 10/20 H₂/DNG in hot coflow. For the hot coflow the O₂ concentration is 9.92% (mass basis) and the temperature is 1460 K. The window height is approximately 70 cm.

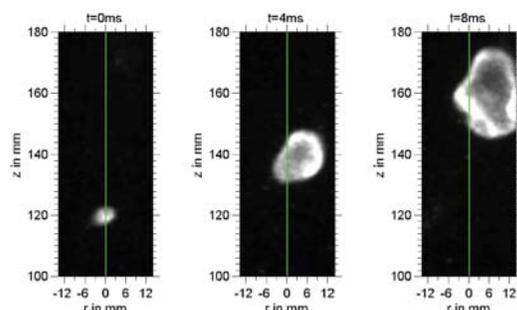


Fig. 2 Sequence of flame luminescence images showing the evolution of an autoignition kernel for a DNG flame in hot coflow. The time between images is 4 ms.

Figure 1 presents the visual appearance of four exemplary flames that were considered in this study. Addition of hydrogen to DNG results in flames that stabilize closer to the fuel pipe nozzle while increasing the visible flame length. Addition of carbon dioxide to DNG has the opposite effect.

Flames oxidized in cold air have a sharp but irregular boundary between the reactants and the flame zone. The position of the sharp boundary is fluctuating in time. The fuel composition affects the mean liftoff height and the RMS value of the fluctuations in liftoff height. These fluctuations increase when the liftoff height increases due to the presence of larger turbulent structures at greater distances from the fuel pipe nozzle.

Flames oxidized in hot coflow with low oxygen concentration exhibit a different stabilization mechanism. In this type of flames stabilization is achieved by autoignition kernels that grow while being convected downstream. The sequence of images of the flame luminescence in Fig. 2 shows the evolution of an autoignition kernel with time intervals of 4 ms for a DNG flame in hot coflow. Figure 3 shows the probability of flame luminescence as a function of height above the fuel pipe nozzle. The liftoff height was defined as the height where the probability of flame luminescence is 50%. Hydrogen addition strongly influences the stabilization position of the flame. The liftoff height is reduced by a factor of five for hydrogen addition of 10% as compared to the pure DNG flame at identical Reynolds number. The effect of carbon dioxide addition on the liftoff height is not as substantial as that of hydrogen addition. Increasing the carbon dioxide content in the fuel increases the liftoff height. However, for a carbon dioxide

addition of 30% the increase in liftoff height is only 10% (as compared to that for pure DNG at identical Reynolds number).

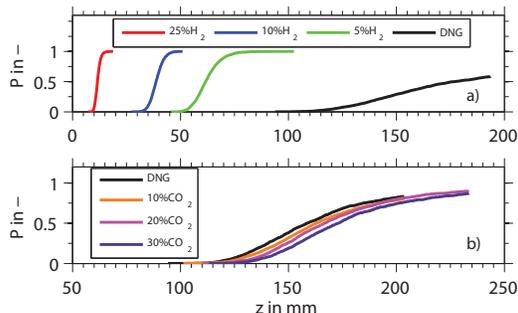


Fig. 3 Probability of flame luminescence as a function of the axial position. a) Results for H_2 /DNG fuel mixtures oxidized in hot coflow, b) Results for CO_2 /DNG fuel mixtures oxidized in hot coflow.

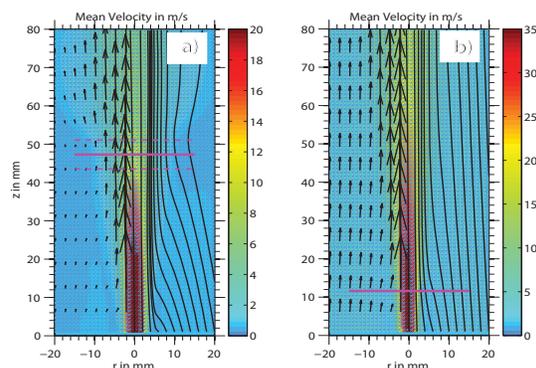


Fig. 4 Mean flow field for a 25/75 H_2 /DNG flame oxidized in a) cold coflow and b) hot coflow. The arrows indicate the velocity vectors and the solid lines denote streamlines. The solid magenta line marks the mean lift off height.

Figure 4 shows the mean flow field for a 25/75 H_2 /DNG flame oxidized in cold coflow (left) and hot coflow (right). In the lower region the coflow has a negative radial velocity component due to the entrainment of jet fluid. Near the liftoff height (horizontal magenta line in Fig. 4) the radial velocity changes sign due to sudden heat release and thermal expansion. Figure 5a shows the images of the seed particles when these are illuminated in the PIV laser light sheet. The boundary between the relatively cold reactants and the hot combustion products is marked by a green line. Figure 5b shows the corresponding instantaneous flow field with the above mentioned boundary superimposed. The stabilization point is located in the lean side of the shear layer between the jet and coflow fluid. Large turbulent structures interact with the reaction zone deforming it and changing its position.

The fuel composition has a substantial impact on the flame stability for flames in cold coflow. Hydrogen addition to the fuel will substantially increase the stability while carbon dioxide addition has the opposite effect. In flames oxidized in hot coflow, only hydrogen addition has a strong influence on the growth velocity of autoignition kernels and the stream wise extend of the region where the autoignition events occur while carbon dioxide addition to the fuel will slightly shift the reaction zone downstream.

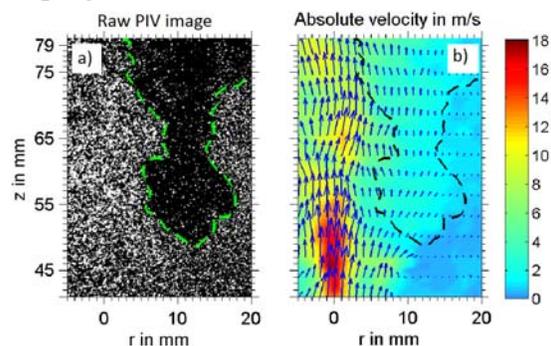


Fig. 5 a) Raw PIV image with green line marking the boundary between the reactants and the hot combustion products and b) the instantaneous flow field of a 25/75 H_2 /DNG flame in cold coflow.

Dependence of Localized Extinction and Thermal Dissipative Structures on Nozzle Diameter in Turbulent Non-Premixed Jet Flames

B. Coriton and J. H. Frank*

*Combustion Research Facility, Sandia National Laboratories
Livermore, California 94551 USA*

*corresponding author's email: jhfrank@sandia.gov

In the context of the TNF Workshop, studies of turbulence-chemistry interactions in benchmark turbulent jet flames have focused on sets of flames with different jet Reynolds numbers $Re_D = U_0 D / \nu_0$, where U_0 , ν_0 , and D are the mean bulk velocity, the kinematic viscosity of the fuel mixture, and the jet nozzle diameter, respectively. For practical convenience, Re_D has previously been varied by changing the jet exit velocity rather than the nozzle diameter. An increase in U_0 leads to smaller dissipative lengthscales, λ_D , and an increased probability of localized extinction. In the present study, we compare the effects of varying the jet exit velocity with those of varying the jet nozzle diameter. Measurements of the extinction and thermal dissipative structures are performed in a series of turbulent, non-premixed $CH_4/H_2/N_2$ jet flames using nozzle diameters ranging from 3 mm to 10.2 mm. The fuel mixture is the same as the DLR benchmark jet flames that have been studied previously in the TNF Workshop. We consider cases with different degrees of localized extinction, and each nozzle diameter provides a different range of thermal dissipative lengthscales. Following the same approach as in previous studies [1-3], simultaneous high-resolution Rayleigh scattering imaging and planar laser-induced fluorescence of OH are combined to measure the dissipative scales associated with thermal mixing and the scales of extinguished regions of the reaction zone. We investigate the distributions of lengthscales of thermal dissipative structures, as well as correlations between the dissipation field and localized extinction.

Figures 1 and 2 illustrate the dependence of the thermal dissipative lengthscales, λ_D , and the probability of localized extinction on the nozzle diameters, at an axial location of $x/D = 10$ above the nozzle exit. Probability Density functions (PDFs) are compared for three different nozzle diameters of 3.0 mm, 6.2 mm and 10.2 mm but for a same jet Reynolds number of 12000. In Fig.1, the size of the dissipative layers is found to systematically increase with the jet nozzle diameter. From $D = 3$ mm to 10.2 mm, the peak of the PDFs increases from 210 μm to 490 μm along the jet centerline ($R/D = 0$) and from 290 μm to nearly 800 μm at $R/D = 1$. The broadest distribution of lengthscales is observed in the largest nozzle of 10.2 mm. However, Fig.2 indicates that localized extinctions are more significant for the smallest nozzle diameter of 3 mm. Identical probabilities of localized extinctions are found for the 6.2 mm and 10.2 mm nozzles. Additional results at various axial positions in the flame will be presented in the poster.

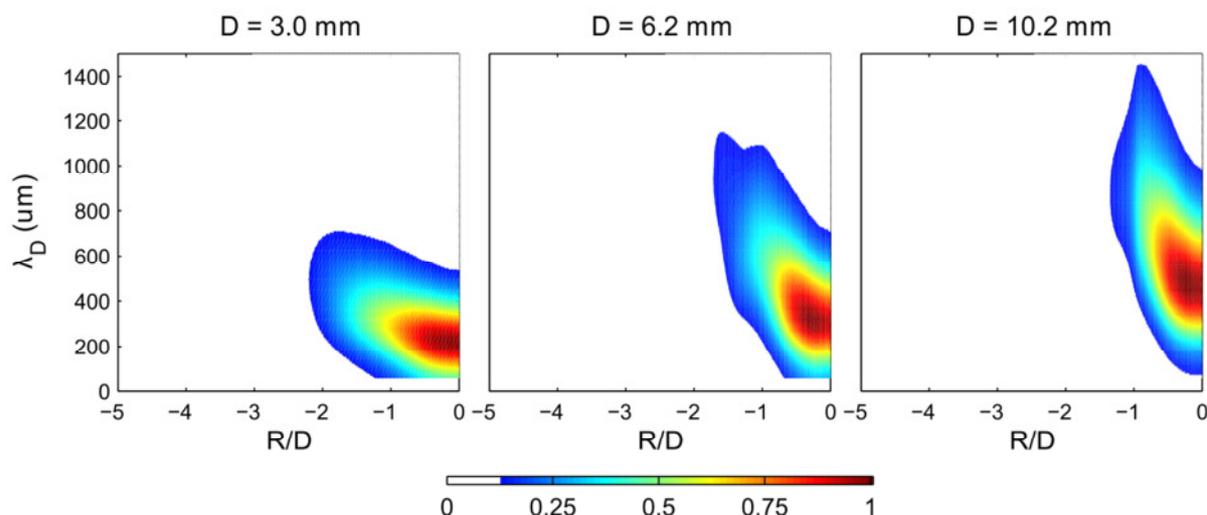


Fig.1 – PDFs of the dissipative lengthscales λ_D for different radial positions at an axial location of $x/D = 10$, for 3 different nozzle diameters $D = 3$ mm, 6.2 mm, and 10.2 mm, and at same jet Reynolds numbers $Re_D = 12000$.

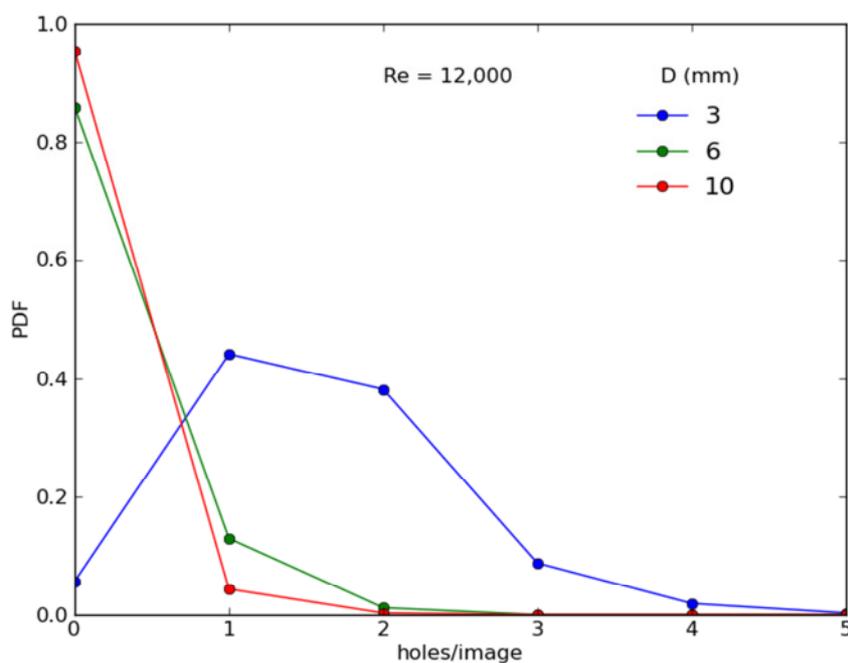


Fig.2 – PDFs of the number of holes in the OH layer per instantaneous OH-LIF image at an axial location of $x/D = 10$ for different nozzle diameters $D = 3$ mm, 6.2 mm and 10.2 mm and $Re_D = 12000$.

Reference(s)

- [1] S.A. Kaiser and J.H. Frank, *Proc. Combust. Inst.*, **31**, 1515 (2007)
- [2] S.A. Kaiser and J.H. Frank, *Proc. Combust. Inst.*, **32**, 1639 (2009)
- [3] J.H. Frank and S.A. Kaiser, *Exp. Fluids*, **49**, 823 (2010)

Simultaneous OH/CH₂O LIF Imaging and PIV Measurements in Turbulent Partially Premixed Dimethyl Ether/Air Jet Flames

Bruno Coriton¹, Mirko Gamba², Seong-kyun Im², Godfrey Mungal², Jonathan H. Frank¹

¹*Combustion Research Facility, Sandia National Laboratories, Livermore, CA 94551 USA*

²*Dept. of Mechanical Engineering, Stanford University, Stanford, CA 94305 USA*

jhfrank@sandia.gov

We present recent results from combined scalar-velocity imaging measurements in a series of partially premixed piloted dimethyl ether (DME)/air jet flames. These benchmark flames provide an opportunity to understand turbulence-flame interactions for oxygenated fuels and to develop predictive models for these interactions. The development of accurate models for DME/air flames would establish a foundation for studies of more complex oxygenated fuels. This series of jet flames spans jet exit Reynolds numbers, Re_d , from approximately 27,000 to 68,000 with the probability of localized extinction increasing with Re_d . The flames are stabilized on the same burner as the piloted CH₄/air jet flames that have been studied extensively within the context of the TNF Workshop. The fuel mixture consists of 20% DME and 80% air, by volume, resulting in a stoichiometric mixture fraction of $\xi_{st} = 0.353$, which is the same as that of the previous piloted CH₄/air flames. Simultaneous laser-induced fluorescence (LIF) imaging of OH and CH₂O provide insights into the distribution of these intermediate species in DME/air jet flames with and without localized extinction. The LIF measurements are combined with particle imaging velocimetry (PIV) to investigate interactions between the distributions of these intermediate species and the velocity field.

The sample single-shot measurement in Fig. 1 shows the superimposed LIF signals and velocity field in a turbulent piloted DME/air jet flame. The formaldehyde and hydroxyl LIF signals are shown in red/orange and blue color scales, respectively. The formaldehyde, which is formed during the decomposition of DME, is distributed over a wide region of the turbulent jet and is subject to significant turbulent mixing. In contrast, the structure of the OH field is considerably less turbulent. We are particularly interested in studying regions of localized extinction. The gap in the OH layer within the sub-region shown in Fig. 1c indicates localized extinction, and frequently we observe formaldehyde within the extinguished regions, as shown here. In this shot, we also capture a vortical structure that is centered on the lower boundary of the extinguished region. To show this structure more clearly, we have subtracted a constant velocity from the vectors in Fig. 1c. We will present a detailed statistical analysis of flames with different levels of localized extinction at the workshop. Experimental results are being coupled with simulations from groups within the TNF Workshop.

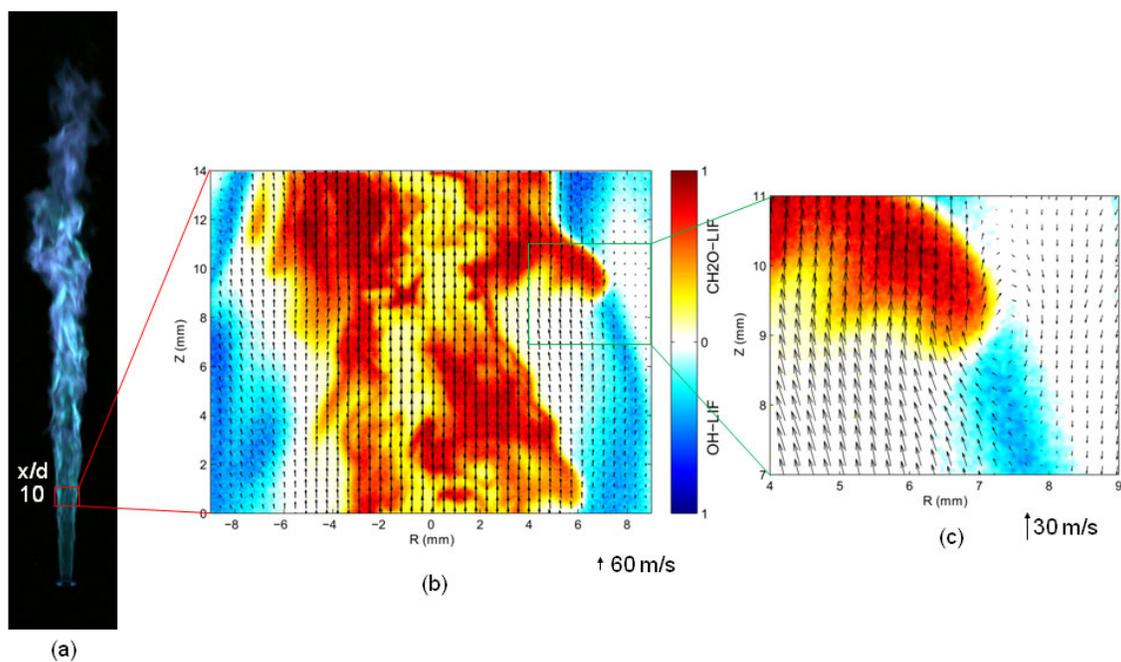


Fig. 1. (a) Chemiluminescence image of turbulent partially-premixed piloted DME/air jet flame. (b) Single-shot simultaneous OH-LIF, $\text{CH}_2\text{O-LIF}$, and PIV measurements. Velocity field and LIF signals are superimposed with the respective fluorescence signals displayed using different color scales. One out of every four vectors is plotted. Velocity field is shown in the laboratory frame of reference. (c) Sub-region shows a locally extinguished reaction zone with a vortical structure in the velocity field and formaldehyde within the extinguished region. All measured vectors are plotted, and a constant velocity is subtracted to show the velocity field relative to a convecting frame of reference.

Transported PDF Calculations of a Turbulent, Non-Premixed, Hydrogen-Air Flame (“H3-flame”)

A. Fiolitakis¹, P. R. Ess¹, P. Gerlinger², M. Aigner¹,

¹ Institute of Combustion Technology, German Aerospace Center (DLR),
70569 Stuttgart, Germany

² Institute of Combustion Technology for Aerospace Engineering,
University of Stuttgart, 70569 Stuttgart, Germany

Andreas.Fiolitakis@dlr.de

Transported PDF calculations of a turbulent, non-premixed, hydrogen-air flame (“H3-flame”) are presented here. To solve the PDF transport equation a hybrid finite-volume/Lagrangian Monte-Carlo method is implemented into the unstructured DLR-THETA code. In this hybrid approach turbulence is modeled by the standard $k - \varepsilon$ model [5], while the transported PDF method treats the evolution of enthalpy and composition [3]. A major difficulty of the transported PDF approach is the closure of conditional diffusive fluxes. In case of the presented flame these terms need to be modeled accurately since differential diffusion is known to play an important role for flame stabilization [6]. Therefore an approach is used which introduces an individual diffusion velocity in composition space to each stochastic particle. These diffusion velocities V_{Y_i} and V_h are defined as [3]

$$V_{Y_i}(\boldsymbol{\psi}) = \sum_{\alpha=1}^3 \left[D_i(\boldsymbol{\psi}) \frac{\partial^2 \tilde{Y}_i}{\partial x_\alpha \partial x_\alpha} - Y_i(\boldsymbol{\psi}) \sum_{j=1}^{N_s} D_j(\boldsymbol{\psi}) \frac{\partial^2 \tilde{Y}_j}{\partial x_\alpha \partial x_\alpha} \right], V_h(\boldsymbol{\psi}) = \sum_{\alpha=1}^3 \frac{\lambda(\boldsymbol{\psi})}{\rho(\boldsymbol{\psi})} \frac{\partial^2 \tilde{T}}{\partial x_\alpha \partial x_\alpha} + \sum_{i=1}^{N_s} h_i(\boldsymbol{\psi}) V_{Y_i}(\boldsymbol{\psi}),$$

where T is the temperature and Y_i are the species mass fractions. To evaluate V_{Y_i} and V_h the diffusion coefficients D_i , the thermal conductivity λ , the density ρ and the species enthalpies h_i are required. In the present approach these quantities are algebraic functions of $\boldsymbol{\psi}$, which is the sample space vector of the (random) thermochemical variables $\boldsymbol{\phi} = (h, Y_i)$. Using the diffusion velocities together with the “Linear Mean Square Estimate” (LMSE) model [10] the conditional diffusive fluxes are modeled as [3]

$$-\left\langle \frac{1}{\rho} \frac{\partial q_\alpha}{\partial x_\alpha} \middle| \boldsymbol{\psi} \right\rangle = V_h(\boldsymbol{\psi}) + \frac{1}{2} C_\phi \frac{\varepsilon}{k} (h - \tilde{h}), \quad -\left\langle \frac{1}{\rho} \frac{\partial j_{i\alpha}}{\partial x_\alpha} \middle| \boldsymbol{\psi} \right\rangle = V_{Y_i}(\boldsymbol{\psi}) + \frac{1}{2} C_\phi \frac{\varepsilon}{k} (Y_i - \tilde{Y}_i),$$

where C_ϕ equals 2. These drifts alter the Favre means of the thermochemical variables at a rate governed by mean diffusion, i.e. $\frac{\partial \tilde{\phi}_i}{\partial t} = \tilde{v}_{\phi_i}$ [3]. A similar approach is discussed by McDermott and Pope [4]. Using the presented model it is possible to avoid extinction of the flame and to predict super-equilibrium temperatures close to the flame root. To visualize this effect temperatures are shown in Fig. 1 close to the nozzle exit as a function of mixture fraction [3, 6]. As a reference the equilibrium temperature is included. Super-equilibrium temperatures are clearly visible on the lean side. Mesh size and particle numbers are varied to ensure the numerical independence of the solution from effects of discretization (see Table 1).

Case	No.-cells	Particles per cell
1	17250	64
2	17250	128
3	17250	256
4	35333	64

Table 1: Computational cases

Only a 10° azimuthal segment of the burner is computed. The results given in Fig. 3 prove that the solution is independent of discretization. In general, a good agreement between computation and experiment is found, except for a shift in the flame position upstream. This is explained in Ref. [3] by an overprediction of the jet spreading rate caused by the $k - \varepsilon$ model, where standard model constants are used [5]. The computations use the hydrogen mechanism developed by Peters and Rogg [8]

combined with the NO subset of San Diego mechanism [9]. In Ref. [2] it is demonstrated that this combination yields an acceptable accuracy in NO predictions. Corresponding results are shown in Fig. 2 (line “PRSD”). Additionally NO computations with the GRI 2.11 mechanism [1] (line “GRI2.11”) and with the thermal pathway as reference (line “PRW”, nitric oxide reaction rates from Ref. [11], hydrogen chemistry from Peters and Rogg [8]) are given. Large differences in NO are observed, which have been found in laminar flames [2], too. Therefore further improvements in NO chemistry are required to obtain accurate NO predictions.

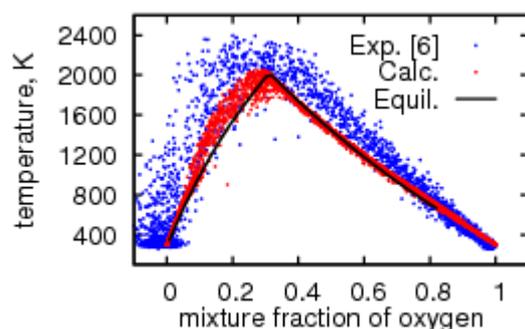


Fig. 1 Scatterplot of temperature (case 3) at 5 diameters distance from nozzle.

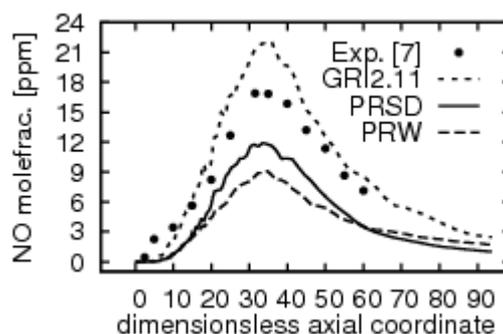


Fig. 2 Nitric oxides along flame axis (case 1).

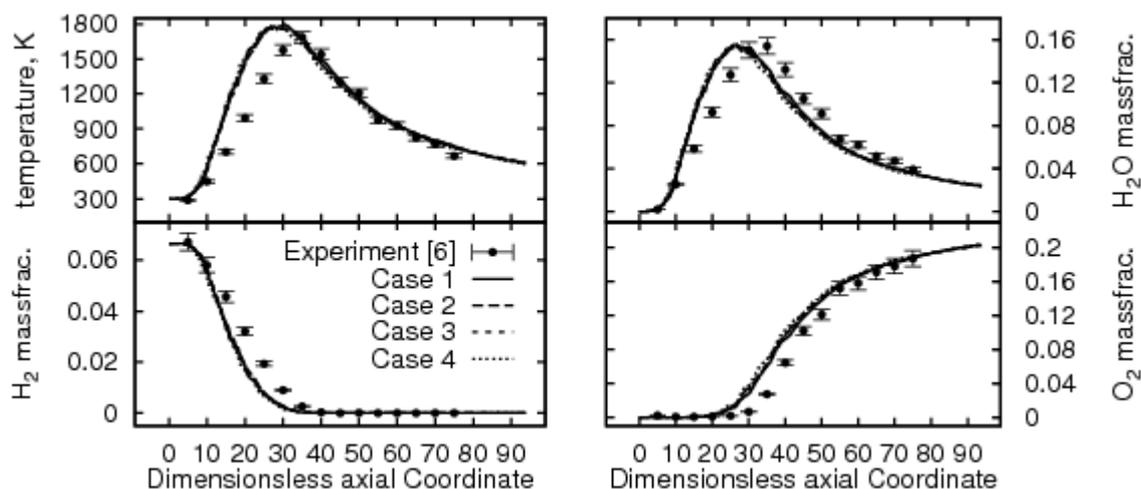


Fig. 3 Comparison of computed and measured Favre averages along the flame axis. Details of the test cases are given in Table 1.

References

- [1] C.T. Bowman, R.K. Hanson, D.F. Davidson, W.C. Gardiner Jr., V. Lissian, G.P. Smith, D.M. Golden, M. Frenklach, M. Goldenberg, http://www.me.berkeley.edu/gri_mech/
- [2] A. Fiolitakis, P. Gerlinger, B. Noll, M. Aigner, W. Krebs, B. Wegner, AIAA 2010-0608 (2010)
- [3] A. Fiolitakis, P. R. Ess, P. Gerlinger, M. Aigner, AIAA 2012-0179 (2012)
- [4] R. McDermott, S.B. Pope: *Journal of Computational Physics* 226:947-993 (2007)
- [5] B.E. Launder, B.I. Sharma *Letters of Heat and Mass Transfer* 1, 131-138 (1974)
- [6] W. Meier, S. Prucker, M.-H. Cao, W. Stricker *Comb. Sci.Tech.*, 118:293-312 (1996)
- [7] A. Neuber, G. Krieger, M. Tacke, E. Hassel, J. Janicka *11. TECFLAM Seminar*, 83-99 (1995)
- [8] N. Peters, B. Rogg: *Red. Kinetic Mech. for Applications in Combustion Systems* Springer, (1993)
- [9] San-Diego mech. <http://maeweb.ucsd.edu/~combustion/Mechanisms>, accessed Sep. 25th, 2008
- [10] J. Villiermaux, J.C. Devillon *Second Intern. Symp. on Chem. React. Eng.*, 1-13 (1972)
- [11] J. Warnatz, U. Maas, R.W. Dibble *Verbrennung: Physikalisch-Chemische Grundlagen, Modellierung und Simulation, Experimente, Schadstoffentstehung*. Springer, (1997)

The Effects of Diffusion Models, Turbulence, and Pressure on Autoignition Delay Time for a H₂/N₂ Jet Flame in a Vitiated Co-flow using a 1-D Laminar Mixing Model and the Linear Eddy Model

Frederick, D.¹; North, A.¹; Dibble, R.¹; Chen, J. Y.¹; Gruber, A.²

¹University of California – Berkeley, Berkeley, CA 94720

²SINTEF Energy Research, 7465 Trondheim, Norway

don.frederick@berkeley.edu

The autoignition of a fuel jet into a hot turbulent co-flow is a problem of theoretical and practical interest, because of the fundamental interactions among chemical reactions, molecular diffusion, and turbulent transport. The current study is based on the Berkeley Vitiated Co-flow Burner (VCB), which was designed to study lifted turbulent jet flames, having similar characteristics to the flames found in industrial combustion systems. The VCB consists of a high velocity fuel jet issuing into a surrounding co-flow of lean premixed hydrogen combustion products. The temperature of the co-flow is controlled by its stoichiometry. To encourage the flame to lift from the nozzle, nitrogen can be added to the jet while adjusting the hydrogen flow rate to increase jet momentum independent of jet velocity.

Mixing between the fuel jet and co-flow in the VCB is modeled only in the radial direction (e.g. 1-D) by marching downstream in time. At the nozzle exit, the gradient between the fuel concentration and co-flow is extremely sharp since the mixing width is small. This initial mixing layer is characterized by its width, d , as sketched in Figure 1. Downstream, the mixing width increases as molecular diffusion and/or turbulent transport can decrease the gradient between fuel and co-flow, creating conditions with low scalar dissipation rate where autoignition can occur.

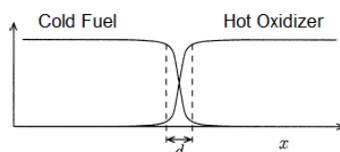


Figure 1 Definition of initial mixing width, d .

Simulations of laminar and turbulent flows are performed for two sets of jet/co-flow combinations and pressures of 1, 2, and 5 bar. We solve the species and energy equations for the laminar flows. For turbulent flows, we use the same underlying equations but the addition of turbulent stirring based on the concept of LEM. A simplified model for species diffusion is used in terms of Lewis number, Le . For equal diffusion calculations, all Le are set to unity. To account for differential diffusion, a constant value of Le is assigned to each species, where this set of Le are calculated a priori using the Chemkin transport package for the specific fuel and oxidizer. We study the impact of differential diffusion on the autoignition delay time, τ_{ign} , and mixture fraction at ignition in both laminar and turbulent flows. The computed results are compared to homogeneous mixture ignition (HMI) calculations of the minimum autoignition delay time ($\tau_{hmi-ref}$) and the most reactive mixture fraction at ignition, ξ_{mr} , which is defined at $\tau_{hmi-ref}$. As a range of mixtures can ignite near $\tau_{hmi-ref}$, we define a range of ξ_{mr} within 10% of the minimum ignition delay time from HMI simulations.

Figure 2 shows the computed τ_{ign} versus the initial mixing width for both equal and differential diffusion models in laminar flows. The co-flow represents the 1200 K burned products of a premixed flame at a 0.35 equivalence ratio at 2 bar. At very thin initial mixing widths, τ_{ign} differs greatly between the two diffusion models, where differential diffusion always leads to early ignition and at mixtures richer than equal diffusion. For thick initial mixing widths, both models approach each other and reach values determined by the homogeneous model. The same trend is found for all conditions simulated (not shown). When the initial mixing width decreases, the delay time approaches an asymptotic value. Using the

asymptotic values, we define auto ignition delay times, $\tau_{lam-ref}^{dd}$ and $\tau_{lam-ref}^{eq}$ where “dd” refers to differential diffusion and “eq” refers to equal diffusion.

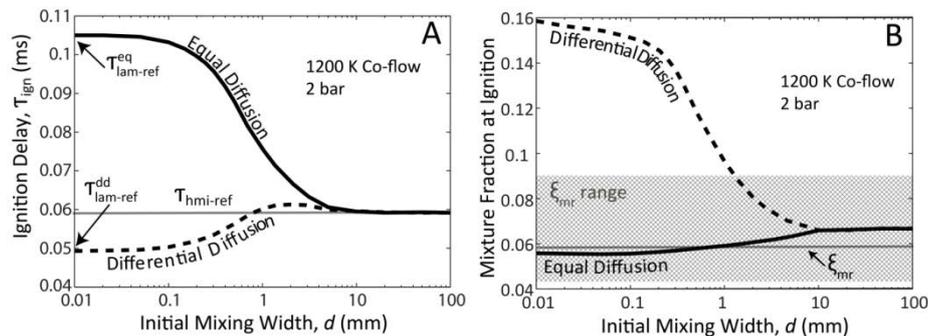


Figure 2: Laminar τ_{ign} and ξ for a 1200 K co-flow at a pressure of 2 bar. Differential diffusion always ignites sooner and richer than equal diffusion.

For a turbulent mixing process, species transport can be enhanced by turbulent stirring. The turbulence parameters needed in the LEM model are estimated from a PDF combustion model. The initial mixing width is fixed to 0.1 mm, roughly just before τ_{ign} begins to vary greatly with increasing d . Two regimes can be defined: regime I for $\tau_{turb} > \tau_{lam-ref}$ and regime II for $\tau_{turb} < \tau_{lam-ref}$, where τ_{turb} is the turbulence time scale and $\tau_{lam-ref}$ refers to the respective diffusion model reference time (i.e. $\tau_{lam-ref}^{dd}$ or $\tau_{lam-ref}^{eq}$). In regime I, the mixture ignites at roughly the same time as in the laminar simulations and turbulence has little effect on τ_{ign} . In regime II, at low turbulence Reynolds number, Re_t , the delay times with/without differential diffusion ignite at $\tau_{lam-ref}^{dd}$ and $\tau_{lam-ref}^{eq}$ respectively. As Re_t increases, τ_{ign} remains roughly constant for the equal diffusion model. On the other hand, τ_{ign} increases as turbulence intensity increases for the differential diffusion model.

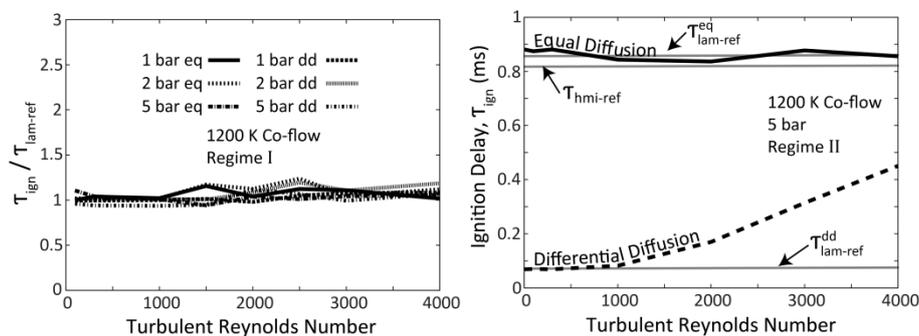


Figure 3: Turbulent ignition delay time for the two defined regimes. In regime I, turbulence does not impact τ_{ign} while in regime II, only the differential diffusion model is impacted by turbulence.

Thus for hydrogen autoignition, our results show a differential diffusion model ignites sooner and richer than an equal diffusion model for both laminar flows at thin initial mixing widths and turbulent flows at low Re_t . Additionally, using a homogeneously mixed model to find τ_{ign} and ξ_{mr} in non-premixed flows may yield incorrect estimates.

References:

- [1] J. Y. Chen, and W. Kollmann, *Symposium (International) on Combustion*, **22**, 645-653 (1989)
- [2] R. Hilbert, and D. Thévenin, *Combustion and Flame*, **128**, 22-37 (2002)
- [3] H. G. Im, J. H. Chen, and C. K. Law, *Symposium (International) on Combustion*, **27**, 1047-1056 (1998)
- [4] R. Knikker, A. Dauptain, B. Cuenot, and T. Poinsot, *Combustion Science and Technology*, **175**, 1783-1806 (2003)
- [5] J. Li, Z. Zhao, A. Kazakov, and F. Dryer, *International Journal of Chemical Kinetics*, **36**, 566-575 (2004)
- [6] E. Mastorakos, *Progress in Energy and Combustion Science*, **35**, 57-97 (2009)
- [7] P. McMurty, S. Menon, and A. Kerstein, *Energy and Fuels*, **7**, 817-826 (1993)
- [8] S. Sreedhara, and K. Lakshmisha, *Proceedings of the Combustion Institute*, **29**, 2051-2059 (2002)

Signal-to-noise and signal-to-background ratios in laminar and turbulent flames of ethylene and ethane in 1D Raman/Rayleigh scattering and CO-LIF measurements

F. Fuest¹, R. S. Barlow², J. A. Sutton¹, A. Dreizler³

1 *Department of Mechanical and Aerospace Engineering, The Ohio State University, Columbus, OH, USA*

2 *Sandia National Laboratories, Livermore, CA, USA*

3 *FG Reactive Flows and Diagnostics, Center of Smart Interfaces, TU Darmstadt, Germany*

fuest.1@osu.edu

Alternative fuels are becoming increasingly attractive in view of economic and environmental sustainability. To allow for accurate prediction of efficiency and pollutant formation in suitable combustion devices, the validation of computational models describing coupled turbulent flow and combustion phenomena is essential. An important tool for this purpose is one-dimensional Raman/Rayleigh scattering to provide the thermochemical state, i.e. all major species concentrations and temperature. Recently, collaborative efforts were made within the TNF Workshop to extend the focus on hydrogen- and methane-based flames to more complex fuels, such as dimethyl ether. Laminar and turbulent jet flames were used to investigate the feasibility of one-dimensional temperature and species measurements via Raman-/Rayleigh scattering and CO-LIF measurements [1,2]. A major difficulty in the application of Raman scattering to flames of higher hydrocarbon fuels is the higher level of laser excited fluorescence interference on the Raman signals. Figure 1 shows spectra taken in a rich laminar ethane jet flame. Very high interference levels on all Raman channels are apparent, exceeding the Raman signals by more than an order of magnitude. Clearly, this is causing limitations in the applicability of data processing methods developed for methane flames and lower interference. Here, these restrictions are discussed and pointed out using experimental data from laminar and turbulent jet flames of ethane and ethylene in the limit of very high levels of interference. Raman spectra, corresponding signal-to-noise ratios, here shown in Fig. 2 for the ethane jet, and signal-to-interference ratios in critical regions of these flames are presented and especially assessed in terms of measurements in corresponding turbulent flames.

References

- [1] F. Fuest, 1D Raman/Rayleigh-scattering and CO-LIF measurements in laminar and turbulent jet flames of dimethyl ether using a hybrid data reduction strategy. Technische Universität Darmstadt, Dissertation, <http://tuprints.ulb.tu-darmstadt.de/2773/>, (2011)
- [2] F. Fuest, R. S. Barlow, J.-Y. Chen, A. Dreizler, Raman/Rayleigh scattering and CO-LIF measurements in laminar and turbulent jet flames of dimethyl ether, *Combustion and Flame*, <http://dx.doi.org/10.1016/j.combustflame.2011.11.001>

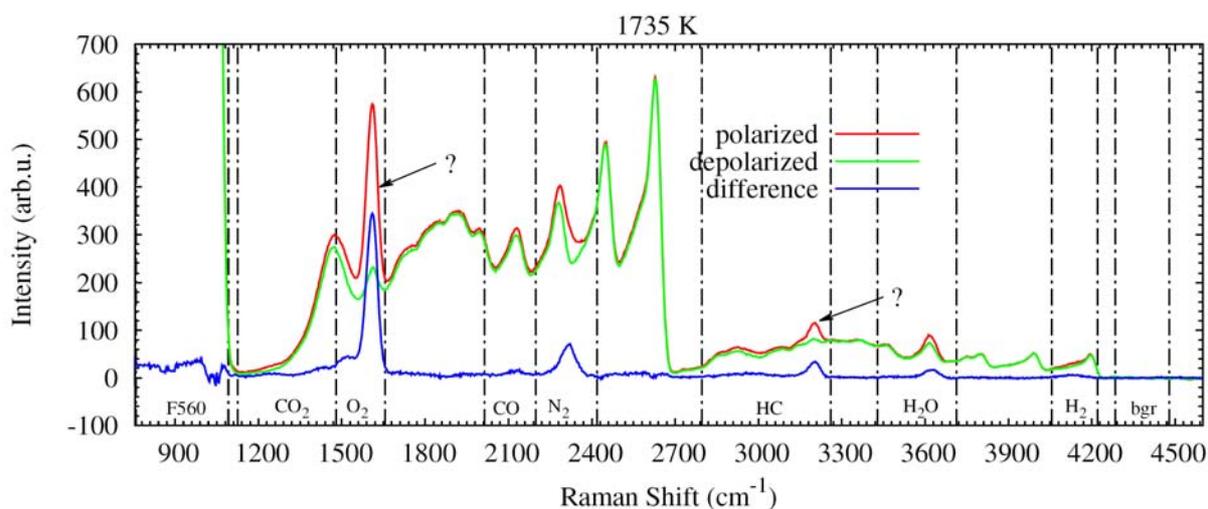


Figure 1: Strongest interference on Raman signals in a rich laminar ethane jet flame (23 vol.% ethane in air, 100 shot-avg) at a temperature of 1735 K. Two sets of data were taken subsequently by turning a thin-film polarizer in front of the spectrometer by 90° degree. Between 85-95% of the total Raman signal is polarized and thus can be discriminated from the usually depolarized interference by subtraction of the entire depolarized spectrum. Vertical dash-dotted lines mark the binning regions of the channels to detect the Raman scattering from particular molecules (HC: Hydrocarbons, bgr: background luminosity, F560: interference detection, used for the interference correction on all other channels, peaks at 3600). An unidentified, very strong and highly polarized feature appears on the O₂ channel causing heavy interference, another unidentified feature shows up on the hydrocarbon channel.

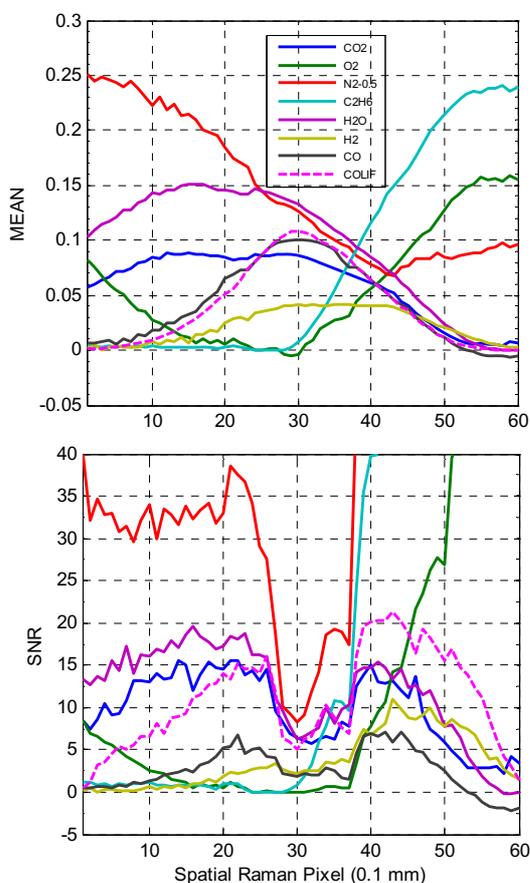


Figure 2: Species mean mole fractions (top) and SNR values (bottom) through the reaction zone of the ethane jet flame aligned along the 6-mm long Raman probe volume. All species are affected by the interference (shown in Fig. 1 for Raman pixel 30) at temperatures between 1100 K to 2000 K on the rich side of the flame (Raman pixels 40 to 23). In particular, a strong impact is observed on the SNR values of O₂, H₂ and CO-Raman. They drop below acceptable values, which should be greater than 5.

Quantification and Accuracy of a CMOS-Based Raman Scattering Imaging System for High-Speed Measurements in Flames

Kathryn N. Gabet, Frederik Fuest, Jeffrey A. Sutton

Department of Mechanical and Aerospace Engineering, The Ohio State University

Gabet.1@osu.edu

In this poster we will describe recent advances made in our laboratory towards the quantification of a combined 1D Raman-Rayleigh scattering imaging system utilizing a CMOS-based detection system for use in high-speed (> 10 kHz acquisition rate) imaging. As CMOS camera technology has not been studied in the same detail as CCD-based detectors, the quantification and accuracy of the CMOS acquisition systems is of particular importance [1,2], especially for low-signal applications such as Raman scattering. This poster will demonstrate progress on extending our previous efforts [3] of high-speed 1D imaging of Raman-accessible species in turbulent jets and flames at multi-kilohertz acquisition rates. Specifically, we will focus on quantifying the precision, accuracy, and detection limits in flames using a CMOS-based detection system, which is necessary for high-speed imaging. Raman scattering images acquired with the CMOS-based acquisition system are processed using a hybrid method for data evaluation derived from that described by Fuest et al. [4]. A key point of any high-speed measurement is to understand the accuracy (and limitations) of results acquired by CMOS detectors which are known to exhibit increased levels of non-uniformity, non-linearity, varying pixel response, and higher levels of noise. The ultimate goal of our work is to measure all major combustion species and deduce time-varying mixture fraction profiles in turbulent combustion environments that can be used to assess time-dependent turbulent combustion models.

Approach for High-Speed Raman Scattering Imaging

In recent years, advances in high-repetition-rate lasers and CMOS cameras have made it feasible for a subset of laser-based imaging techniques such as particle imaging velocimetry (PIV) and planar laser-induced fluorescence (PLIF) to be extended to high repetition rates [e.g., 5]. Recently, we have demonstrated the ability to extend high-speed imaging capabilities to include Rayleigh and Raman scattering [2,3]. In order to generate the high pulse energies necessary for Rayleigh and Raman scattering, we rely on a pulse burst laser system, which has been described in detail in Ref. 6. The work presented in this poster is quantifying the accuracy and precision of the detection system for a new set of high-speed measurements utilizing a new pulse-burst laser system (approx. 1J per pulse, 10 kHz repetition rate, > 100 pulses per train) developed at Ohio State.

A key component of making quantitative Raman scattering measurements is the detection system. For the majority of high-speed imaging experiments, CMOS cameras are used because conventional CCD cameras cannot operate at sufficiently high acquisition rates. Unlike CCD cameras, which have uniform pixel response, each pixel on CMOS cameras has a unique response which needs to be characterized individually. In addition, CMOS cameras exhibit higher levels of readout noise, which is of particular concern when performing Raman scattering measurements which exhibit very weak emission signals. In this poster, a CMOS-based acquisition system is being assessed for accuracy and the ability to derive quantitative species concentrations within flames.

Similar to the line imaging system at Sandia National Laboratories [e.g., 7], we have assembled a high-efficiency 1D imaging system that combines Rayleigh and Raman scattering to obtain quantitative measurements of temperature, major species, and mixture fraction in flames. A pair of 150-mm diameter achromats (Qioptic Linos Photonics) collects both Raman and Rayleigh scattered-light which is focused through the slit of a custom-built high-throughput transmission imaging spectrometer, similar to that described in Ref. 8. Two-high-speed CMOS cameras (Vision Research, Phantom v710) for both the Raman and Rayleigh scattering are integrated into one optical system, which consists of five commercially-available camera lenses, wavelength filtering optics, and one custom transmission holographic grating (Kaiser Optical) to disperse the species-specific Raman-shifted light. The collection system is shown in Fig. 1. Upon entering into the spectrometer, the Rayleigh-scattered (532-nm) portion of the collected light is split off using a dichroic beamsplitter and focused onto one of the CMOS cameras for 1D Rayleigh imaging. The remaining light (550-700 nm) is transmitted through the optical train of the Raman spectrometer. The four lenses used in conjunction with the Raman-portion of the optical system are 105-mm f/1.8, 50-mm f/1.4, 135-mm f/2, and 135-mm f/2. This combination of

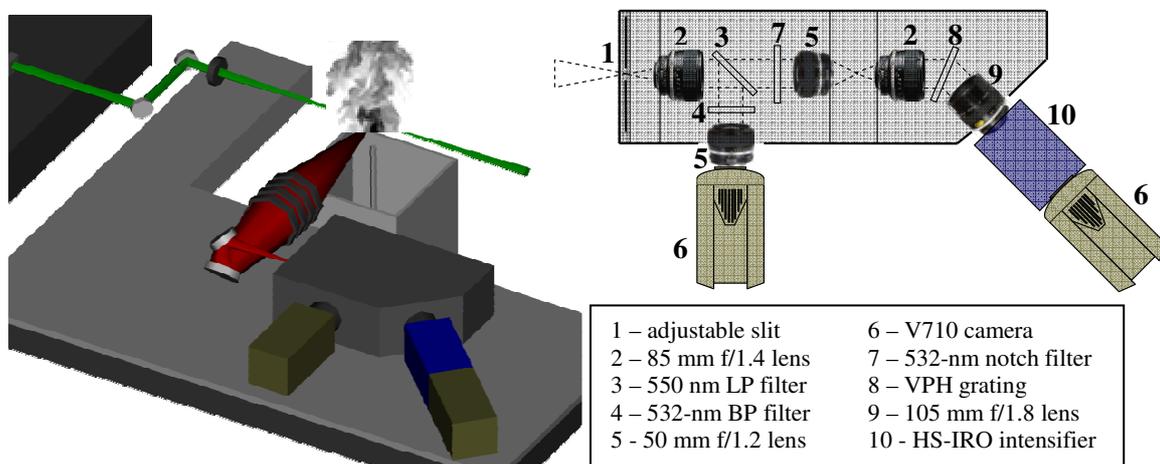


Figure 1. Raman/Rayleigh Experimental Setup. a) Overview of experimental setup for 1D Raman/Rayleigh scattering imaging. b) Detailed schematic and optical layout of the high-throughput, imaging spectrometer, which integrates the cameras for both Raman and Rayleigh scattering into one unit.

lenses (when coupled to the 150-mm diameter f/4 and f/2 collection achromats) results in an overall system magnification of ~ 1 for the Raman scattering. The Raman spectrum is dispersed through the custom transmission grating (1200 lines/mm, 22° incident/refracted angles, $>85\%$ efficiency from 550 to 680 nm) and onto one intensified-CMOS camera. A major emphasis of this poster is to assess the ability to convert the Raman signals to accurate, species concentrations.

References

- [1] V. Weber *et al.*, *Applied Physics B*, **103**(2), 421 (2011)
- [2] R. A. Patton *et al.*, *Applied Physics B*, **106**(2), 457 (2012)
- [3] K.N. Gabet *et al.*, *Applied Physics B*, **101**(1), 1 (2010)
- [4] F. Fuest *et al.*, *Proc. of the Comb. Inst.*, **33**, 815 (2010)
- [5] I. Boxx *et al.*, *Applied Physics* **95**(1), 23 (2009)
- [6] F. Fuest, M. Papageorge, W. R. Lempert, and J. A. Sutton, *Opt. Lett.* accepted (2012).
- [7] A. N. Karpetis *et al.*, *Proc. of the Comb. Inst.*, **29**, 1929 (2002)
- [8] R.S. Barlow *et al.*, *Proc. of the Comb. Inst.*, **32**, 945 (2009)

Localisation and convergence testing in sparse-Lagrangian MMC simulations

Y. Ge¹, B. Sundaram¹, M. J. Cleary², A. Y. Klimenko¹

1. *School of Mechanical and Mining Engineering, The University of Queensland, Queensland 4072, Australia*
2. *School of Aerospace, Mechanical and Mechatronic Engineering, The University of Sydney, New South Wales 2006, Australia*

yipeng.ge@uqconnect.edu.au, brruntha.sundaram@uqconnect.edu.au,
m.cleary@sydney.edu.au, a.klimenko@uq.edu.au

Multiple Mapping Conditioning (MMC) is a micro-mixing model that combines the Probability Density Function (PDF) and Conditional Moment Closure (CMC) models [1]. MMC has been applied in a sparse-Lagrangian scheme to model the methane Sandia Flame E, yielding high quality results with a thousand-fold reduction in computation cost [2]. A key feature of MMC is the use of reference variables to enforce localness in composition space. An Eulerian LES generates filtered turbulent flow field data including velocity, pressure and mixture fraction while a sparse ensemble of Pope particles (i.e. Lagrangian particles with properties and mixing) solves a Filtered Density Function (FDF) for reactive scalars. A gradient-fractal model [3] which improves control of localisation by linking characteristic inter-particle distances in the extended space with scalar gradients and the particle density is applied here. To further characterise the performance of MMC, the possibility of numerical convergence is tested for an idealised jet flame with a thin reaction zone [4]. Additionally, a lifted hydrogen flame in a vitiated coflow [5] is used to test the sensitivity of flame characteristics to the degree of localization in mixture fraction space.

For the idealised jet flame, numerical convergence is investigated by increasing the particle density (as much as allowed by our computational resources) while keeping the mixing model unchanged. The particle density is doubled but the distance between mixing particles in the extended space is set such that mixing still occurs under equivalent sparse conditions. Results are obtained for case A with one Lagrangian particle per 10 Eulerian cells (1L/10E) and for case B with 1 particle per 5 cells (1L/5E) but with the mixing distances corresponding to the 1L/10E case. The similarity in conditional means and fluctuations between both cases in Figure 1 indicates that stochastic errors, which are associated with a limited number of particles in the simulation, are relatively small. Note that this test is different to the one conducted by Cleary and Klimenko [3] where mixing distances were decreased with increased particle number density but adjusted to preserve the characteristic mixing distances in the mixture fraction space (although not in the physical space).

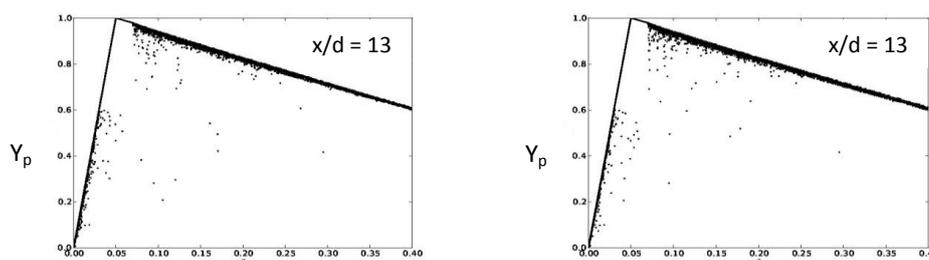


Fig. 1: Scatter plots of Y^p versus Z at $x/D = 13$ for the idealized jet. Cases A (left) and B (right).

In MMC simulations to date, localisation in mixture fraction space has been prioritised at the expense of localisation in physical space. This corresponds to the physics of non-premixed turbulent flames and significantly improves the simulations. The lifted flame is a case where lift-off and stabilisation are dominated by convective terms rather than by the details of mixing and is thus less sensitive to localisation of mixing in the mixture fraction space. It is therefore a particularly difficult case for sparse-Lagrangian MMC simulations, which is not expected to benefit from the MMC prioritisation of mixing distances. This case therefore is specifically selected to test treatment of convective terms in sparse-Lagrangian MMC simulations.

The effect of varying the localisation parameter with the Mueller reaction mechanism [6] for the 1L/8E case is investigated. Lift-off and flame characteristics are captured with certain localisation values, as demonstrated by Figure 2. Increasing localization in mixture fraction tend to have a limited effect on the simulations but only to a certain threshold. Excessive localisation in physical space results in a fully attached flame, which is contrary to physical observations.

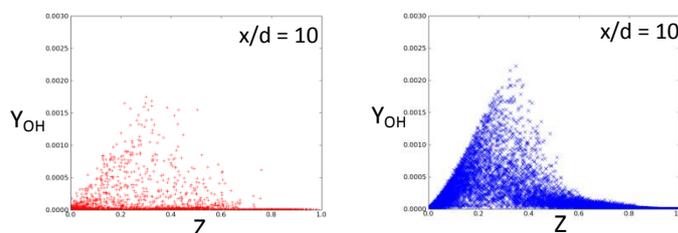


Fig. 2: Experimental (left) and simulation (right) scatter plots of Y_{OH} versus Z at $x/d = 10$ for the lifted hydrogen flame.

Work on advanced mixing models is ongoing. Mixing used in conventional models (e.g. IEM, Curl, EMST, MMC) preserves conservation properties and can therefore be termed ‘conservative mixing’. Recent important developments are associated with the introduction of ‘competitive mixing’ which treats mixing particles unequally. This type of mixing has been shown to be instrumental in modelling turbulent premixed combustion [7], although its applications are not restricted to this field. Competitive mixing appears to bring some clarity into emergence of complexity in competitive evolving systems and its consistency with the thermodynamic principles - this is one of the most fundamental questions of modern science [8]. The concept of Pope particles, which has now been extended to simulations of complex evolutions in competitive systems, represents a conceptual link between traditional modelling of combustion and these newest developments.

References

- [1] A. Y. Klimenko, S. B. Pope, *Phys. Fluids*, **15**, 1907-1925 (2003)
- [2] Y. Ge, M. J. Cleary, A. Y. Klimenko, *Proc. Combust. Inst.*, **33**, 1401-1409 (2011)
- [3] M. J. Cleary, A. Y. Klimenko, *Phys. Fluids*, **23**, 115102.1-115102.19 (2011)
- [4] S. Subramaniam, S. B. Pope, *Combust. Flame*, **115**, 487 (1998)
- [5] R. Cabra, T. Myhrvold, J. Y. Chen, R. W. Dibble, A. N. Karpetsis, R. S. Barlow, *Proc. Combust. Inst.*, **29**, 1881-1888 (2002)
- [6] M. A. Mueller, T. J. Kim, R. A. Yetter, F. L. Dryer, *Int. J. Chem. Kinet.*, **31**, 113-125 (1999)
- [7] A. Y. Klimenko, S. B. Pope, *Combust., Theory Mod.*, doi: 10.1080/13647830.2011.647091 (2012)
- [8] A. Y. Klimenko, *Phil. Trans. R. Soc.*, to appear, (2012)

Conditional Statistics, Length Scales and Energy Distribution in Fractal Generated Turbulence

P. Geipel^{1,2}, K. H. H. Goh¹, F. Hampf¹, R. P. Lindstedt¹

¹*Department of Mechanical Engineering, Imperial College, London SW7 2AZ, UK*

²*Siemens Industrial Turbomachinery, AB, SE-612 83 Finspong, Sweden*

p.lindstedt@imperial.ac.uk

Lean premixed methane and propane flames were investigated in an opposed jet configuration featuring fractal-generated turbulence [1]. First and second moments of conditional velocity-scalar statistics were obtained using Particle Image Velocimetry (PIV) and the density segregation method of Goh et al. [2].

Estimates of the conditional dissipation rate along the burner axis were derived using the method of George and Hussein [3] with values of kinematic viscosities obtained from laminar flame calculations [4]. Kolmogorov length scales were estimated to be ~ 0.1 mm and ~ 0.5 mm in the reactant and product streams respectively.

Conditional longitudinal energy spectra were obtained in the radial direction at the nozzle exit and at the nominal stagnation plane. Heat release causes an increase in the energy (E_{11}) across the wavenumber spectrum (k_{11}) with a more distinct impact at lower wave numbers as shown in Fig. 1 for spectra obtained along the stagnation point streamline.

Conditional Proper Orthogonal Decomposition (POD) was applied and the cumulative energy E , defined to be the sum of radial and axial kinetic energy in the modes, was resolved. Results in Fig. 1 show that unconditional POD is unable to segregate the relative turbulence kinetic energies of each stream. The impact of the flames on the energy distribution in reactant streams is negligible while causing a large increase in the turbulent kinetic energy in the product streams. A modest increase is observed when the equivalence ratio is increased from 0.80 to 0.90. Results from conditional spectra and conditional POD show qualitative agreement on the relative size of structures in relation to energy levels.

The relative structures for the first four modes are shown in Fig. 2 for conditional and unconditional POD obtained for methane flames at an equivalence ratio of 0.90. Results indicate that the POD modes in the unconditional case are 'hybrids' of the reactant and product streams. In addition, the normalised energy in each corresponding mode show distinct differences between each stream. The unconditional POD is unable to show such differences.

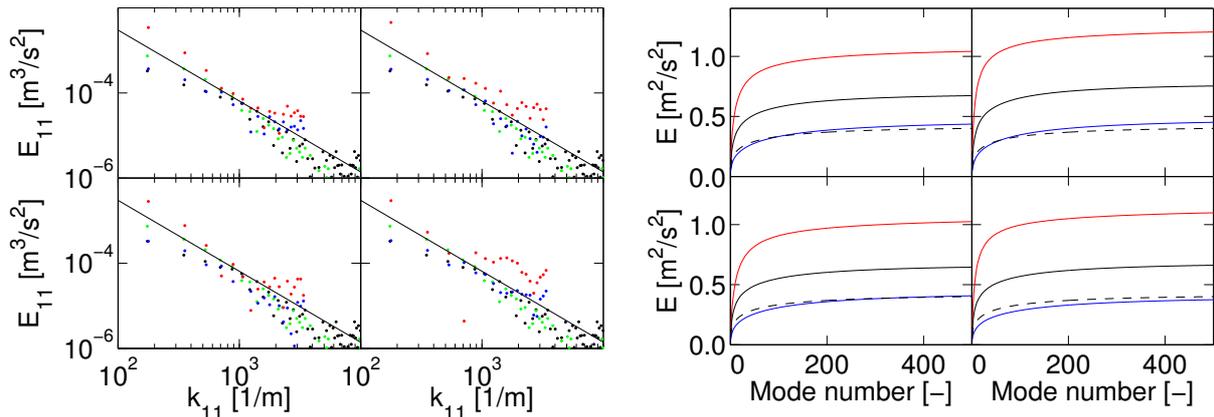


Fig. 1 Left set of plots: Conditional spectra with longitudinal energy (E_{11}) in wavenumber (k_{11}) space. Black and green dots – isothermal spectra from radial covariance profiles at 1 mm from nozzle exit and stagnation plane respectively. Blue and red dots – conditional spectra for reactants (nozzle exit) and products (stagnation plane). Black lines indicate the $-5/3$ spectra. Right set of plots: Cumulative energy (E) for each stream resolved using conditional POD. Dashed lines - isothermal case. Blue lines – reactant streams. Red lines – product streams. Black lines – unconditional POD. For each set of plots: methane (top row) and propane (bottom row) flames at equivalence ratios of 0.80 (left column) and 0.90 (right column).

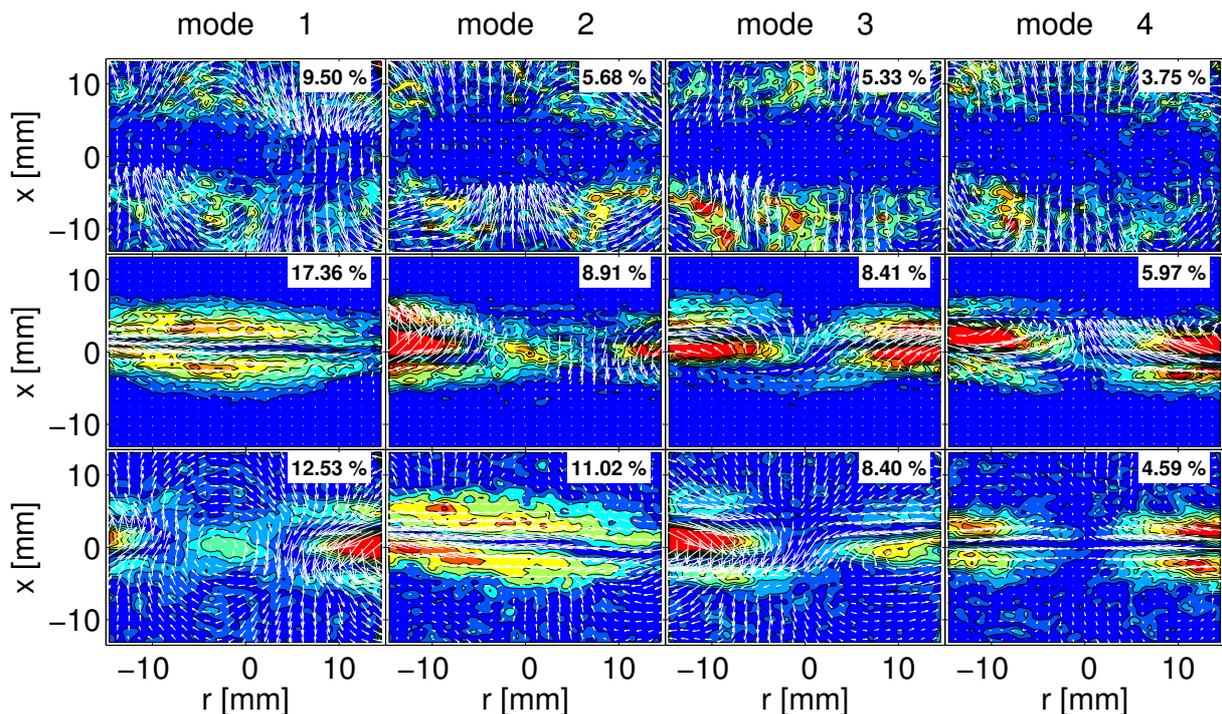


Fig. 2 First four POD modes for methane flames at an equivalence ratio of 0.90 overlaid with vorticity contours. Top to bottom rows represent reactant, product and unconditional cases respectively. The corresponding percentage contribution of each mode to the turbulent kinetic energy is indicated.

Reference(s)

- [1] P. Geipel, K. H. H. Goh, R. P. Lindstedt, *Flow Turbul. Combust.*, **85**, 397 (2010)
- [2] K. H. H. Goh, P. Geipel, R. P. Lindstedt, Conditional Statistics of Lean Premixed Turbulent Opposed Jet Flames Using Particle Image Velocimetry and Density Segregation, in : Proceedings of the European Combustion Meeting, 2011
- [3] W. K. George, H. J. Hussein, *J. Fluid Mech.* **233**, 1 (1991)
- [4] R. P. Lindstedt, V. D. Milosavljevic, M. Persson, *Proc. Combust. Inst.*, **33**, 1277 (2011)

DNS of boundary layer flashback in turbulent channel flow

A. Gruber¹, H. Kolla², D. Valiev³, J.H. Chen²

¹*SINTEF Energy Research, 7465 Trondheim, Norway*

²*Combustion Research Facility, Sandia National Laboratories, 94550 Livermore, California, USA*

³*Combustion Energy Frontier Research Center, Princeton University, Princeton, NJ 08544-5263, USA*

andrea.gruber@sintef.no

Direct numerical simulations are performed to investigate the transient upstream propagation (flashback) of premixed hydrogen-air flames in the boundary layer of a fully developed turbulent channel flow at two pressure levels (1 and 2 Atm) and for both fuel lean ($\phi=0.55$) and fuel rich ($\phi=1.5$) conditions. Initial results show that the near-wall streaky velocity fluctuations pattern of the turbulent boundary layer triggers wrinkling of the initially flat flame sheet as it starts propagating against the main flow direction, and that the structure of the characteristic boundary layer streaks ultimately has an important impact on the resulting flame shape and on its propagation mechanism [1]. Analysis of the instantaneous velocity fields clearly reveals the existence, on the reactant side of the flame sheet, of backflow pockets that, induced by the presence of the flame, extend well above the wall-quenching distance, see **Fig. 1** below.

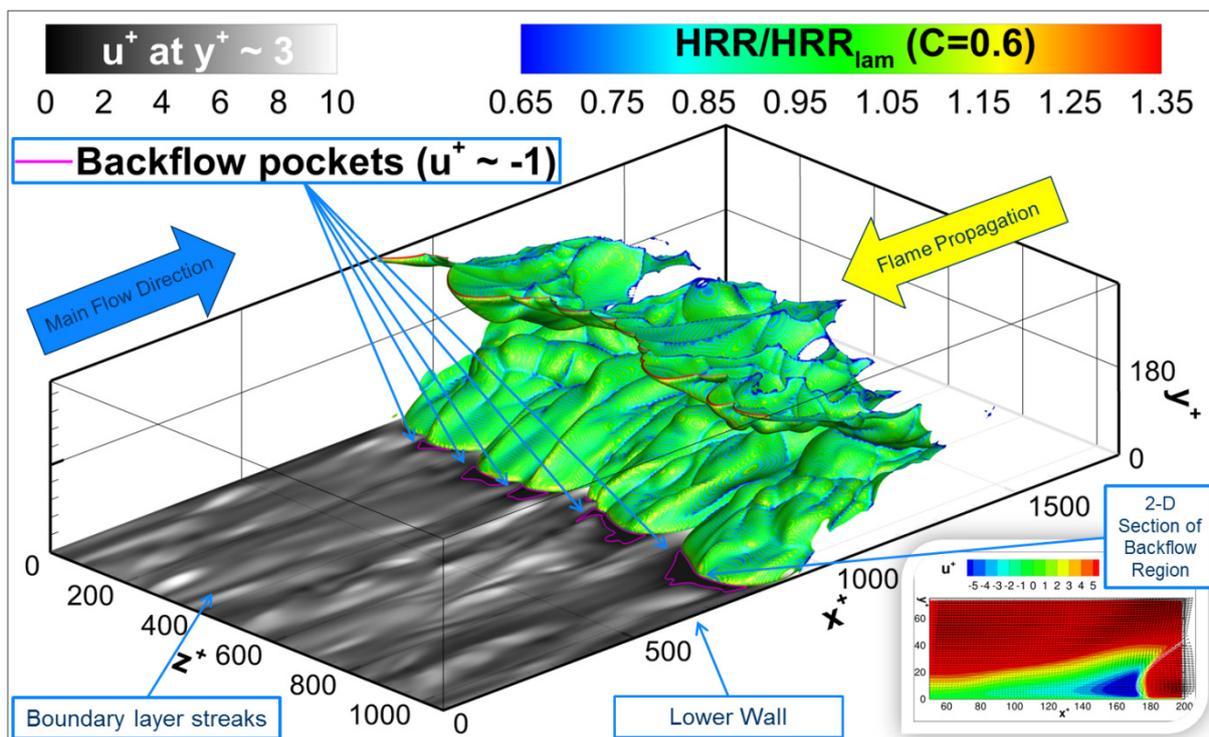


Fig.1 Instantaneous snapshot of turbulent flame sheet and near-wall velocity field ($P=2$ Atm & $\phi=0.55$).

There is a strong correspondence between each of the backflow pockets and the convex flame sheet bulges present on the leading edge of the flame. This finding is confirmed by recent experimental observations [2,3] and challenges the traditional near-wall flashback modeling approach that assumes negligible effect of the flame sheet on the approaching flow of the fresh reactants [4]. It is suggested that the origin of the formation of the backflow pockets, along with the subsequent mutual feedback mechanism, is due to the interaction of the approaching streaky turbulent flow pattern with the Darrieus-Landau hydrodynamic instability at first, and, subsequently, to its interaction with the fluctuating pressure field and the gas dilatation due to the heat release. Moreover, the presence of the backflow pockets, coupled to the associated hydrodynamic instability and pressure-flow field interaction, greatly facilitates flame propagation in turbulent boundary layers. This ultimately

leads to high flashback velocities, up to twice the unstrained laminar flame speed, at both lean and rich conditions. Also, the effect of pressure was investigated at fuel rich conditions, keeping the reactants bulk flow velocities equal, and resulted in even larger flashback speed at the higher pressure, see **Figs. 2(a)** and **2(b)**.

Fig. 2(a) – Reactants bulk flow velocities ($\phi=1.5$)

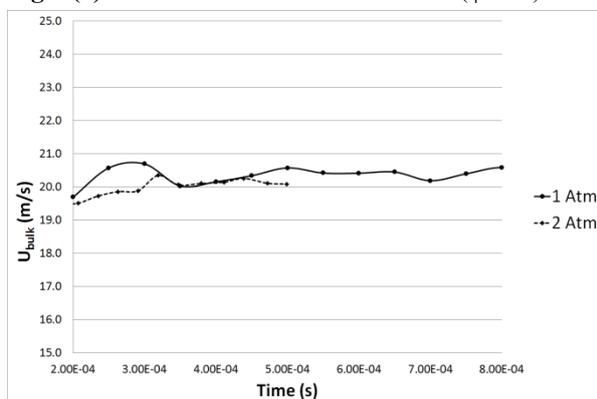


Fig. 2(b) – Flame front flashback velocities ($\phi=1.5$)

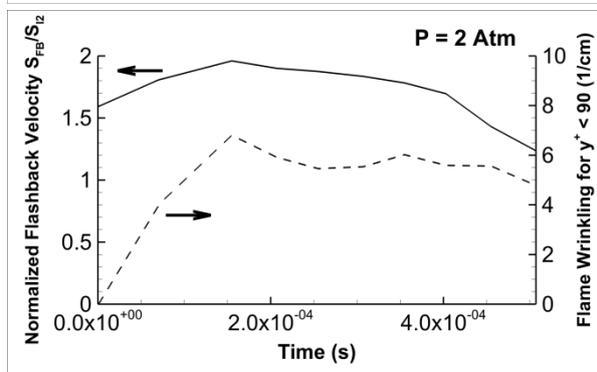
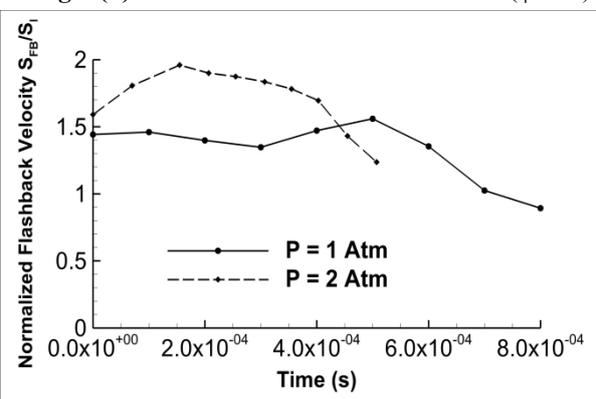


Fig. 2(c) – Flame speed and wrinkling ($\phi=1.5$)

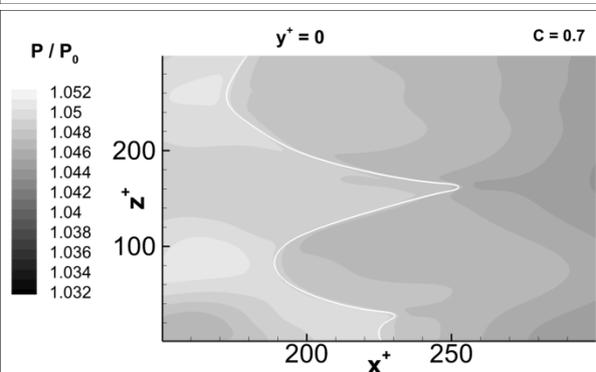


Fig. 2(d) – Wall pressure field across flame front

The observed flashback behavior can be summarized as follows:

- Initially, the flat flame accelerates after being wrinkled by the combined effect of the approaching turbulence and of the Darrieus-Landau hydrodynamic instability, see **Fig. 2(c)**.
- Once the effect of the DL instability becomes negligible due to the high flame sheet curvature, the flame wrinkling is slightly reduced (with larger perturbation wavelengths dominating), and the flashback velocity is also reduced slightly.
- The flame front propagates upstream in the channel, with a nearly stationary flashback speed, along the low velocity streaks of the approaching boundary layer turbulence where it induces the formation of adverse pressure gradients and backflow pockets, see **Fig. 2(d)**.
- As the flame approaches the upstream inlet of the domain, the imposed boundary conditions on the streamwise velocity component weaken the backflow regions induced by the flame, reducing their physical extent and ultimately leading to their disappearance, thereby negatively affecting the flashback speed, see solid line in **Fig. 2(c)** for $t > 4.0 \cdot 10^{-4}$ (s).
- The reduction in the flashback speed, initially due to the weakening and subsequently to the disappearance of the backflow regions, occurs upstream and independently of the reduction in flame wrinkling caused by the interaction of the flame with the upstream inlet boundary.
- At the very end of the simulation, flame wrinkling is also affected by the inlet boundary conditions that artificially flatten the most upstream flame portions (bulges), see dashed line in **Fig. 2(c)** for $t > 4.5 \cdot 10^{-4}$ (s).

References

- [1] Gruber, A., Chen, J. H., Valiev, D. & Law, C. K. Direct numerical simulation of premixed flame boundary layer flashback in turbulent channel flow. Accepted for publication on the Journal of Fluid Mechanics
- [2] Heeger, C., Gordon, R. L., Tummers, M. J., Sattelmayer, T. & Dreizler, A. Experimental analysis of flashback in lean premixed swirling flames: Upstream flame propagation. Experiments in Fluids 49 (4), 853-863 (2010)
- [3] Eichler, C. & Sattelmayer, T. Premixed flame flashback in wall boundary layers studied by long-distance micro-piv. Experiments in Fluids 52 (2), 347-360 (2012)
- [4] Lewis, B. & von Elbe, G. Stability and structure of burner flames. Journal of Chemical Physics 11, 75-97 (1943)

Combined Reduction-Tabulation based Strategies for Computationally-Efficient Implementation of Combustion Chemistry

Varun Hiremath and Stephen B. Pope

*Sibley School of Mechanical and Aerospace Engineering,
Cornell University, Ithaca, NY 14853, USA*

vh63@cornell.edu

Advances in experimental and theoretical studies (for example using *ab initio* quantum-chemical calculations) of real fuel chemistry have led to more accurate chemical mechanisms of real fuels involving hundreds to thousands of chemical species and reactions [1]. However, the direct use of such detailed chemistry in large-scale calculations of turbulent reacting flows still remains computationally prohibitive. Thus, a major challenge in the numerical study of turbulent combustion problems is to develop accurate and efficient methods for representing combustion chemistry.

We focus on the combined Large-Eddy Simulation (LES)/Probability Density Function (PDF) computations of turbulent reactive flows, in which the thermochemical composition of the fluid is represented by a large number of particles as seen in Fig.1. The main advantage of using PDF methods is that the chemical source term in the species evolution equation is represented exactly without any modeling [2]. This enables the use of detailed chemistry in computations, though the computations become expensive as the number of species involved increases. To reduce the cost of chemistry calculations in large-scale LES/PDF computations, we have developed a combined reduction-tabulation approach in which the dimension-reduction of combustion chemistry is performed using the Rate-Controlled Constrained Equilibrium (RCCE) [3] method followed by tabulation using *In Situ* Adaptive Tabulation (ISAT) [4,5]. A crucial component of this combined approach is selection of "good" represented species for performing the RCCE dimension reduction, and for this we have developed an automated Greedy Algorithm with Local Improvement (GALI) which is used for selecting "good" represented species [6]. We have extensively tested this combined ISAT-RCCE-GALI approach for methane and ethylene chemistry with chemical mechanisms involving 30-100 species and have shown that this approach (i) yields the same level of accuracy as other skeletal and reduced mechanism with relatively fewer represented species; and (ii) gives a speed-up by a factor of 2-15 relative to using ISAT alone with the detailed chemistry [6].

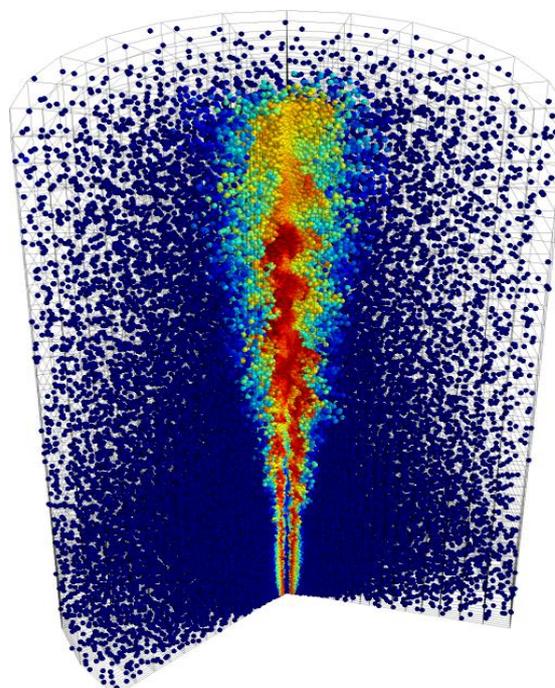


Figure 1. LES/PDF simulation of Sandia Flame D. 3D slice view of the particle temperature distribution.

For a chemical mechanism involving n_s -species with chemical composition denoted by an n_s -vector \mathbf{z} , in the classical RCCE approach [3] the rate-equations for the n_r (with typically $n_r \ll n_s$) constraints or the constrained-potentials are solved. This method has been further developed and applied in numerous chemistry computations [7, 8]. However, in our implementation of RCCE [6], we use a simpler though computationally more expensive approach of solving the rate-equations for all the n_s -species. In our implementation, as shown in Fig.2, given the initial constraints denoted by an

n_r -vector $\mathbf{r}(0)$, the constrained-equilibrium composition $\mathbf{z}^{\text{CE}}(0)$ is computed using CEQ [9]. Starting from this composition the rate-equations for all the n_s -species are solved to obtain the *reaction mapping* $\mathbf{z}(t)$ – the composition at the end of the reaction time step – from which we obtain $\mathbf{r}(t)$. We henceforth refer to our implementation of RCCE as RCCE/TIFS (Trajectory In Full Space). Recently we performed some tests to compare the relative accuracy and efficiency of these two approaches, and have found that our RCCE/TIFS implementation is significantly more accurate than the classical RCCE approach. In the classical RCCE approach, by solving the rate-equations for the n_r constrained-potentials, the reaction trajectory is implicitly assumed to stay on the constrained-equilibrium manifold (CEM). However, it is a known fact that the CEM is not an invariant manifold, and this non-invariance of the CEM introduces large errors in the RCCE approach at large reaction time steps as seen in Fig.3. Our recent studies have shown that using an alternative approach which we call the Reaction-mixing Attracting Manifold Projector (RAMP), the error introduced due to the non-invariance of the CEM can be reduced. The RAMP approach is an extension of the Close Parallel Inertial Manifold (CPIM) method [10]. In the RCCE/RAMP approach, the rate-equations for the n_r constraints are solved by evaluating the reaction source vector on an invariant attracting manifold close-and-parallel to the CEM and then projecting the source vector onto the CEM (as illustrated in Fig.2). This approach is shown to yield the same level of accuracy as our current RCCE/TIFS approach as seen in Fig.3. However, we do not see any significant improvement in the computational efficiency of the RCCE/RAMP approach over our current RCCE/TIFS approach due to the additional cost involved in computing the projector.

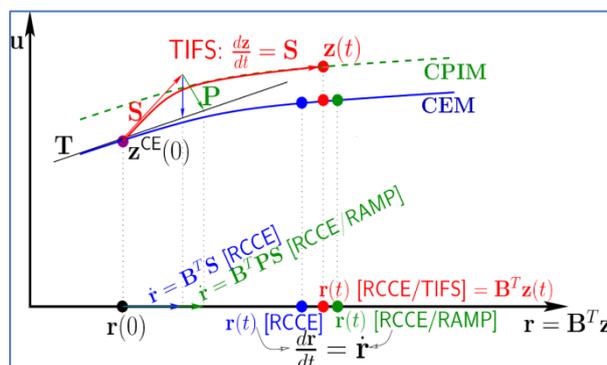


Figure 2: Illustration of reaction mapping computation using three different implementations of the RCCE method: RCCE, RCCE/TIFS and RCCE/RAMP.

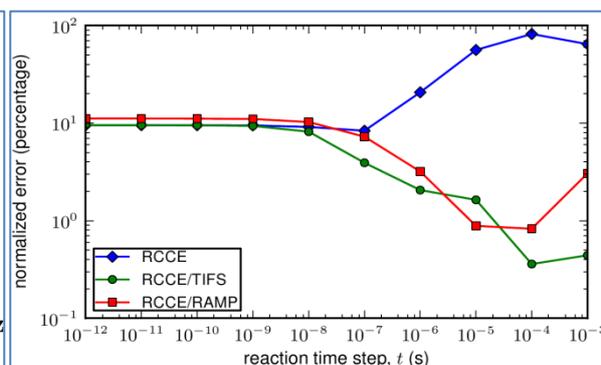


Figure 3: Comparison of normalized-error in the reaction mapping obtained using the three implementations of the RCCE method for methane/air premixed combustion using 12 represented species with the 31-species GRI Mech 1.2 mechanism.

We have used the combined ISAT-RCCE-GALI approach for performing large-scale LES/PDF computations of Sandia Flame D on over 1,000 cores (see Fig.1). We have shown that without losing much accuracy, this approach enables significant reduction in simulation time. These combined methodologies have also been demonstrated to achieve good parallel scaling for performing large scale LES/PDF computations using our Partitioned Uniform Random (P-URAN) strategy [11].

References

- [1] S. Sarathy, C. Westbrook, M. Mehl, W. Pitz, C. Togbe, P. Dagaut, H. Wang, M. Oehlschlaeger, U. Niemann, K. Seshadri, P. Veloo, C. Ji, F. Egolfopoulos, T. Lu, *Combustion and Flame* 158(12) (2011) 2338–2357.
- [2] S. B. Pope, *Progress in Energy and Combustion Science* 11 (1985) 119–192.
- [3] J. C. Keck, D. Gillespie, *Combust. Flame* 17 (1971) 237–241.
- [4] S. B. Pope, *Combust. Theory Model.* 1 (1997) 41–63.
- [5] L. Lu, S. B. Pope, *Journal of Computational Physics* 228(2) (2009) 361–386.
- [6] V. Hiremath, Z. Ren, S. B. Pope, *Combustion and Flame* 158(11) (2011) 2113–2127.
- [7] W. Jones, S. Rigopoulos, *Combustion and Flame* 142(3) (2005) 223 – 234.
- [8] M. Janbozorgi, S. Ugarte, H. Metghalchi, J. C. Keck, *Combustion and Flame* 156 (2009) 1871–1885.
- [9] S. B. Pope, *Combustion and Flame* 139 (2004) 222–226.
- [10] Q. Tang, S. B. Pope, *Combust. Theory Modelling* 8 (2004) 255–279.
- [11] V. Hiremath, S. R. Lantz, H. Wang, S. B. Pope, *Combustion and Flame* (accepted) (2012)

Scalar and Velocity Results in a Turbulent Stratified CH₄/Air Swirl Burner

S. Hochgreb¹, M. S. Sweeney¹, R. Zhou¹, M. J. Dunn², R. S. Barlow³

1 Department of Engineering, University of Cambridge, Cambridge, UK

2 University of Sydney, Sydney, Australia

3 Sandia National Laboratories, California, USA

simone.hochgreb@eng.cam.ac.uk

A series of flames in a turbulent methane/air stratified swirl burner is presented. The degree of stratification and swirl are systematically varied to generate a matrix of experimental conditions, allowing their separate and combined effects to be investigated. A mean equivalence ratio of $\bar{\phi} = 0.75$ is used, with ϕ for the highest level of stratification spanning 0.375 to 1.125. The burner features a central bluff-body to aid flame stabilization, and the influence of the induced recirculation zone is also considered.

The velocity field in the reacting and non-reacting flows are captured by two-component particle image velocimetry, while three-component velocity profiles are measured 2 mm from the burner exit using LDA. The results indicate that the flames lie in the thin-reaction zone regime, with levels of swirl comparable to commercial applications.

Scalar data are obtained from Rayleigh/Raman/CO laser induced fluorescence (CO-LIF) line measurements at 103 μm resolution, allowing the behavior of key combustion species – CH₄, CO₂, CO, H₂, H₂O and O₂ – to be probed within the instantaneous flame front. Simultaneous cross-planar OH-PLIF is used to determine the orientation of the instantaneous flame normal in the scalar measurement window, allowing gradients in temperature and progress variable to be angle corrected to their three dimensional values. The relationship between curvature and flame thickness is investigated using the OH-PLIF images, as well as the effect of stratification on curvature.

The main findings are that both hydrogen and carbon monoxide mass fractions are elevated throughout temperature space by stratification, while the behavior of the other key combustion species is well captured by laminar flame calculations regardless of the level of stratification. Values for surface density function and by extension thermal scalar dissipation rate are found to be substantially lower than laminar values, as the thickening of the flame due to turbulence dominates the effect of increased strain.

The findings in the scalar data hold for all flames surveyed, whether premixed, stratified, swirling or non-swirling. The current series of flames is proposed as an interesting if challenging set of test cases for existing and emerging turbulent flame models, and data are available on request [1-3].

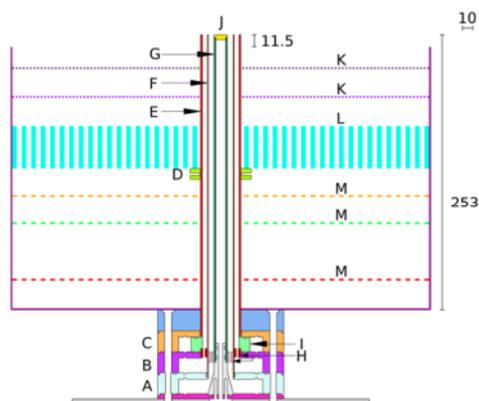


Fig. 1 Cross-section of Cambridge Stratified Swirl Burner. All dimensions in mm and to scale.

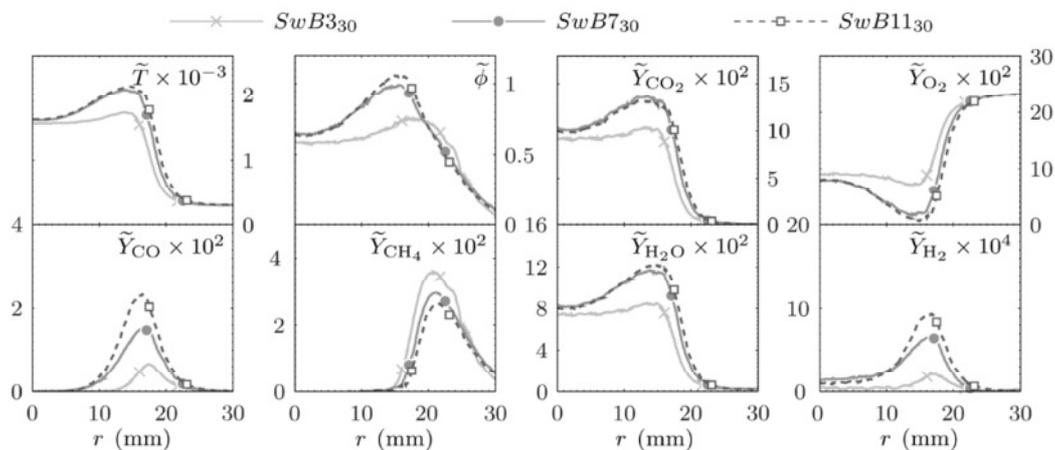


Fig. 2 Radial profiles of Favre-averaged scalar means in highly swirling premixed (SwB₃₀), moderately stratified (SwB₇₀) and highly stratified (SwB₁₁₀) flames

References

- [1] M. S. Sweeney, S. Hochgreb, M. J. Dunn, R. S. Barlow, *A comparative analysis of flame surface density metrics in premixed and stratified flames*. P. Combust. Inst., 33. pp. 1419-1427 (2011)
- [2] M. S. Sweeney, S. Hochgreb, M. J. Dunn, R. S. Barlow, *The Structure of Turbulent Stratified and Premixed Methane/Air Flames I: Non-Swirling Flows*. Combust. Flame, accepted (2012)
- [3] M. S. Sweeney, S. Hochgreb, M. J. Dunn, R. S. Barlow, *The Structure of Turbulent Stratified and Premixed Methane/Air Flames II: Swirling Flows*. Combust. Flame, accepted (2012)

Preferential Diffusion in Bluff-Body Stabilized Turbulent Premixed Flames

V. R. Katta¹ and W. M. Roquemore²

1 Innovative Scientific Solutions, Inc, Dayton, OH, USA

2 Air Force Research Laboratory, WPAFB, OH, USA

vrkatta@gmail.com

The primary zone of a gas-turbine engine typically consists of recirculation zones (RZs) that are established with bluff-bodies and swirling fuel and/or air jets. Experimental or numerical studies focusing on understanding the primary zones are limited due to the complexity in the combustor geometries and operating conditions such as pressure. Alternatively, researchers are obtaining detailed flowfields and chemical structures of the RZs in simple bluff-body burners with a hope that the fundamental understanding gained on these RZ-supported flames can be extrapolated to the primary zones of a gas-turbine engine. For example, Air Force centerbody burner [1] is designed to establish different sooting structures, Cambridge swirl burner [2] is designed to stabilize stratified flames over a range of flow rates and Sidney bluff-body burners [3] are designed to produce benchmark data for model validation. Recent experiments of Barlow et al. [4] in a bluff-body stabilized, turbulent lean premixed CH₄/air flames revealed that atom balances (atomic mass fractions) are not conserved across the flame brush going from reactants to products. Through the measurements of temperature and major species (CO₂, O₂, CO, N₂, CH₄, H₂O, and H₂) they computed C/H atom ratios at different locations in the flame and found that its values can exceed that of the original fuel by more than 10 percent. Conducting some well-planned experiments on laminar and turbulent burners they hypothesized that H₂ and H₂O diffuse preferentially ahead of CO₂ and CO toward the reactants and are subsequently transported (through advection) downstream and away from the local flame brush. They also concluded that RZ causing preferential transport effect to be amplified. In the present paper, reacting flows in Sandia bluff-body burner [4] are simulated using a detailed CFD code and investigated the reasons for increase in local C/H atom ratio.

A time-dependent, axisymmetric mathematical model UNICORN [5,6] is used for simulating combusting flows in the bluff-body burners. This model solves for u- and v-momentum equations, continuity, and enthalpy- and species-conservation equations on a staggered-grid system. A detailed chemical-kinetics model, GRI Version 3.0 [7] developed by Gas Research Institute (consisting of 53 species and 650 elementary-reaction steps), is incorporated into UNICORN. Thermo-physical properties such as enthalpy, viscosity, thermal conductivity, and binary molecular diffusion of all the species are calculated from the polynomial curve fits developed for the temperature range 300 - 5000 K. Mixture viscosity and thermal conductivity are then estimated using the Wilke and Kee expressions, respectively. Temperature-dependent molecular diffusion is assumed to be of the binary type, and the diffusion velocity of a species is calculated using Fick's law of mass diffusion and the effective-diffusion coefficient of that species in the mixture. While the thermal diffusion (Soret effect) is ignored, the final diffusion velocity of each species is obtained by adding a constant (independent of species) correction velocity that is obtained from the mass-conservation equation [8]. Turbulence is modeled using the standard k- ϵ model. The finite-difference forms of the momentum equations are obtained using an implicit QUICKEST scheme [5], and those of the species, energy and turbulence equations are obtained using a hybrid scheme of upwind and central differencing.

Calculations for the Sandia bluff-body burner are made using a nonuniform mesh system of 301X501 points distributed over a physical domain of 50-mm x 200-mm in the radial and axial directions, respectively. This gave a 40- μ m resolution in the neighborhood of the reaction zone. Premixed mixture of methane and air at an equivalence ratio of 0.77 is used as fuel. Velocities for the fuel jet and coflowing air are set equal to 15.0 m/s and 0.4 m/s, respectively. Flame computed for this high fuel-jet velocity became unsteady with vortices shedding along outer surface of the RZ. Instantaneous and time-averaged flames are shown in Fig. 1. Flame is stably anchored to the outer edge of the bluff-body. A pseudo RZ is evident in the time-averaged visualization of the flow field (Fig.

1b). Distributions of the C/H atom ratio are shown on the right halves using rainbow color scheme. The C/H atom ratio increased significantly near the flame surface close to the bluff-body. This confirms the findings of Barlow et al. [4]. Variations in the C/H atom ratio with respect to temperature at 2 and 6.5 mm above the bluff-body are shown in Figs. 2a and 2b, respectively. Distributions of the simulation at two instants and that of the time-averaged data are shown in these figures. Note that temperature is nearly uniform within the RZ (Fig. 1). Data obtained for an unstrained laminar 1D flame at an equivalence ratio of 0.77 (from Ref. 13) are also included in Figs. 2a and 2b for comparison purpose. The C/H atom ratio increased significantly from its stoichiometric value of 0.25, especially near the bluff body. These profiles also qualitatively match with those measured by Barlow et al [4].

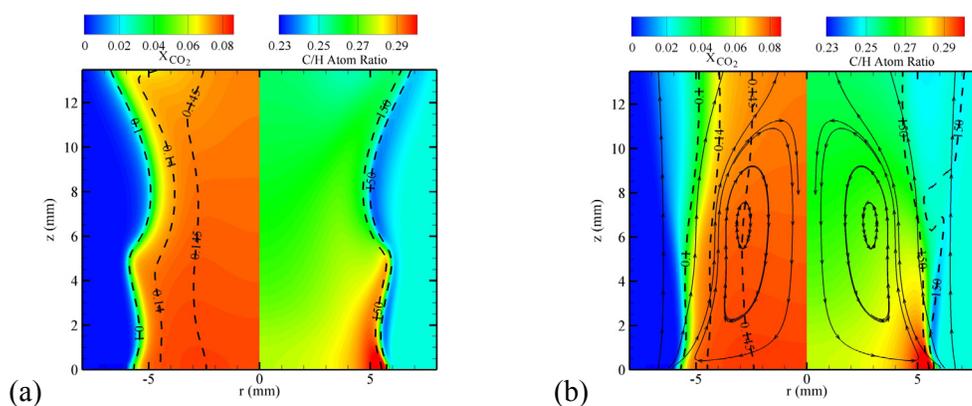


Fig. 1. Premixed flame stabilized on a 12.7-mm diameter bluff-body burner. Iso-concentration contours of H_2O (broken lines) are superimposed on CO_2 distribution in the left halves. Heat-release-rate contour (broken lines) of 150-w/cm^3 are superimposed on C/H-atom-ratio distribution in the right halves. (a) Instantaneous, (b) time-averaged flames. Streamlines are superimposed on time-averaged image.

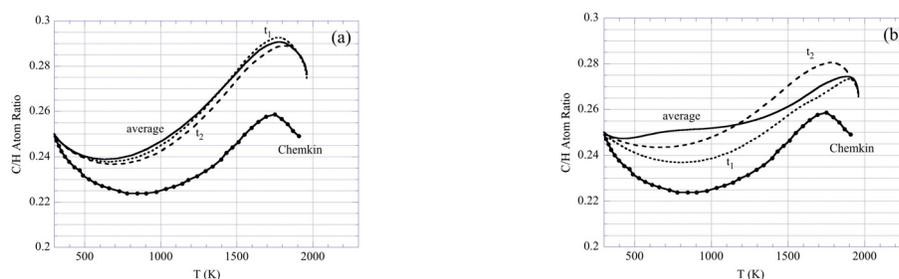


Fig. 2. Distributions of C/H atom ratio with respect to temperature (along a radial line) at (a) 2 mm and (b) 6.5 mm above the burner surface. Results for an unstrained laminar 1D flame obtained with Chemkin (Ref. 4) are included.

References

- [1] W.M. Roquemore, V.R. Katta, S.D. Stouffer, V. Belovich, R. Pawlik, M. Arstingstall, G. Justinger, J.R. Gord, A. Lynch, J. Zelina, S. Roy, *Proc. Combust. Inst.* 32 (2009) 729-736.
- [2] M. S. Sweeney, S. Hochgreb, M. J. Dunn, R. S. Barlow, *Proc. Combust. Inst.* 33 (2011) 1419-1427.
- [3] A. R. Masri, P. A. M. Kalt, R. S. Barlow, *Combust. Flame* 137 (2004) 1-37.
- [4] R. S. Barlow, M. J. Dunn, M. S. Sweeney, S. Hochgreb, in press doi:10.1016/j.combstflame.2011.11.013
- [5] V.R. Katta, L.P. Goss, W.M. Roquemore, *AIAA J.* 32 (1994) 84-94.
- [6] V.R. Katta, W.M. Roquemore, *AIAA J.* 46 (2008) 1640-1650.
- [7] G. P. Smith et al., GRI-Mech 3.0, available at http://me.berkeley.edu/gri_mech
- [8] T. P. Coffee and J. M. Heimerl, *Combust. Flame* 43 (1981) 273-289.

Fundamental insight into flame stabilization in transverse jets in cross-flow using direct numerical simulations (DNS)

H. Kolla¹, A. Gruber², R.W. Grout³, J.H.Chen¹

¹Combustion Research Facility, Sandia, National Laboratories, Livermore, CA, USA

²SINTEF Energy Research, Trondheim, Norway

³National Renewable Energy Laboratory, Golden, CO, USA

jhchen@sandia.gov

Compressible three-dimensional DNS of reactive transverse jets in turbulent cross-flow (JICF) are performed with detailed chemical kinetics and transport properties to gain fundamental insight into the flame stabilization mechanism. Conditions typical of the premixer section of a stationary gas turbines are chosen: cross-flow of preheated air at 750 K and free stream velocity of 55 m/s, hydrogen enriched fuel jet at 420 K issuing from a nozzle flush with the wall and a bulk velocity of 250 m/s, with a jet-to-cross flow momentum flux ratio of 3.4. The ultimate objective is to aid the design of premixers for enhanced mixing and intrinsic flashback safety. A comprehensive database is generated by systematically varying the parameters that are most likely to influence the flow field, mixing field and flame propagation in the JICF near field: jet nozzle geometry, jet transverse injection angle and fuel composition.

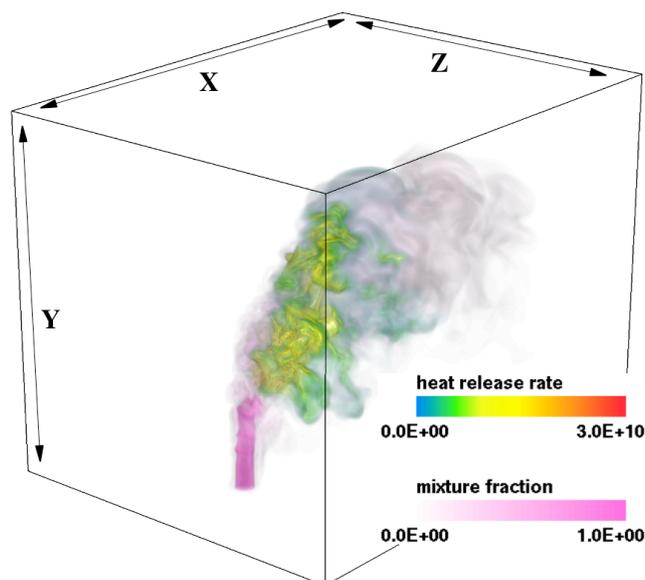


Fig. 1 Instantaneous volume rendering of heat release rate and mixture fraction in the JICF DNS.

The broad findings of the parametric studies are as follows:

Jet nozzle geometry: Three nozzle geometries are investigated: square [1], circular [2] and elliptic, and the nozzle area was kept constant at $\pi/4 \text{ mm}^2$, which corresponds to a nozzle diameter of 1 mm for the circular nozzle. In all the cases a stable flame was observed with the flame anchoring by premixed flame propagation in a region of low velocity magnitudes on the jet leeward side [1]. The flame stabilization is not very sensitive to the nozzle geometry and the mean flame anchoring location is roughly the same in the square and circular nozzle cases.

In the elliptic case it is displaced marginally downstream due to higher jet penetration (see Fig. 2).

Fuel composition: Three syngas fuel compositions are considered with varying amounts of $H_2:CO$ by volume: 1:0 (pure H_2), 1:0.06 (CO lean) and 1:1 (CO rich). In all cases the fuel was diluted by 30% nitrogen by volume. The laminar flame speeds for the three mixtures at nominal conditions (stoichiometric mixture, unburnt temperature of 420 K) are in the ratio 1:0.93:0.49 respectively. In spite of a considerable difference in the laminar propagation speeds, the mean flame stabilization characteristics are largely the same with the flame anchoring at roughly the same location in all three cases.

Injection angle: The flame stabilization is found to be most sensitive to the jet transverse injection angle. While a stable flame was observed for at least two cross-flow through times in the cases with 90 degree injection, a transient flame blowout is observed in the 75 degrees case [3]. Non-reacting simulations show that the low velocity region on the jet leeward side where the flame anchors in the 90 degree case, is significantly reduced in the 75 degree case. Two stages of the transient flame blowout were identified and reported earlier [3].

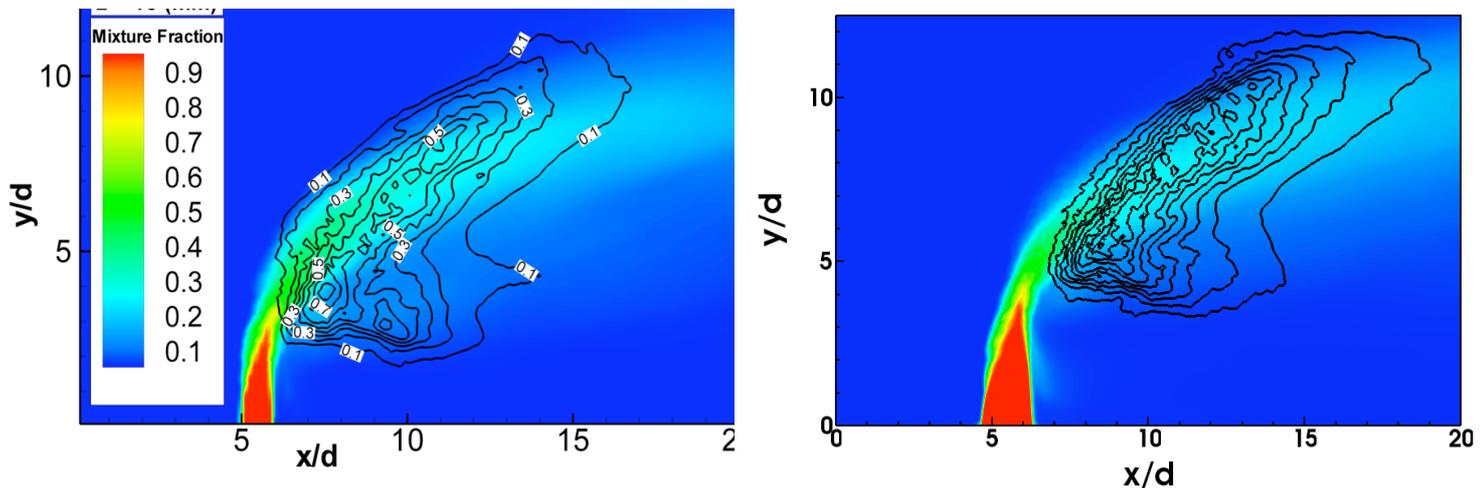


Fig.2 Time averaged mixture fraction (color contours) and heat release rate normalized by its maximum value (black lines) are shown for the square nozzle (left) and elliptic nozzle (right) JICF cases. The flame anchoring location in the square case is at $x/d = 6.5$ and $y/d = 2.5$, while in the elliptic case it is marginally downstream at $x/d = 7.0$ and $y/d = 4.0$.

References

- [1] R.W. Grout *et al.*, *Proc. Comb. Inst.*, **33**, 1629 (2011)
- [2] R.W. Grout *et al.*, *Jou. Fluid Mech.*, (**provisionally accepted**), (2012)
- [3] H. Kolla *et al.*, *Comb. Flame*, (**online**), (2012)

Bluff-body flame blowoff dynamics under stratified fueling and thermoacoustic coupling

Kristin M. Kopp-Vaughan, Steven G. Tuttle, Trevor R. Jensen,
Baki M. Cetegen and Michael W. Renfro

*Department of Mechanical Engineering, 191 Auditorium Rd, U-3139
University of Connecticut
Storrs, CT 06269-3139 USA*

renfro@engr.uconn.edu

The impact of fuel stratification and thermoacoustics on flame stability were examined for turbulent, bluff-body flames near blowoff. Three fuel injectors (shown in Fig. 1) were used to control stratification just upstream of a bluff-body stabilized flame [1]. The local equivalence ratio was characterized by probe measurements as shown in Fig. 2 and five levels of fuel gradients (G) were considered. Acoustic damping in the combustor was separately adjusted to affect the level of thermoacoustic coupling. High speed chemiluminescence imaging and particle imaging velocimetry (PIV) was performed through blowoff for each condition. For globally lean flames, fuel stratification delayed blowoff due to the enhanced stability of the richer side of the flame. Proper orthogonal decomposition (POD) was applied to the high speed chemiluminescence images to quantitatively track the flame front dynamics through blowoff. POD modes for stratified but acoustically uncoupled flames are shown in Fig. 3a while POD modes for acoustically coupled flames are shown in Fig. 3b. For stratified cases, the leanest side of the flame was found to extinguish first near blowoff and the dynamics of the flame were controlled by the richer side which continued to burn for around 20 ms. An example of the time constants for the most important POD modes near blow is shown in Fig. 4a for the stratified case. Just prior to blowoff both sides of the flame extinguish and a residual flame burns in the recirculation zone. The POD time constants demonstrate that a strong fuel gradient decreases the time it takes for the flame to transition from fully burning to burning only on the rich side and then to blowoff [2]. For uniform fueling and for small gradients, the flame periodically transitions back to a fully burning flame after forming a residual flame in the recirculation zone. For strong fuel gradients, the time scale for blowoff is sufficiently fast that no relighting events are observed.

The blow off process in the acoustically coupled cases was dominated by symmetric large scale fluctuations of the flame as it coupled to a longitudinal mode in the combustor rig. These symmetric modes are clear in the POD mode shapes shown in Fig. 3b. The time constants for these POD modes near blowoff, shown in Fig. 4b, are consistent with the large scale periodic fluctuations observed in the chemiluminescence images. In particular, the most important mode (mode 1) oscillates periodically as compared to the non-acoustically coupled case in Fig. 4a. These large scale fluctuations lead to sudden blowoff and repeated measurements show this always occurs during the oscillation when the acoustic velocity at the end of the recirculation zone is negative. Enhanced straining of the flame near the stagnation point behind the recirculation zone was found using PIV to lead to local extinction that triggered blowoff [3]. Extinction and rapid entrainment of reactants into the recirculation zone was characterized using POD time constants.

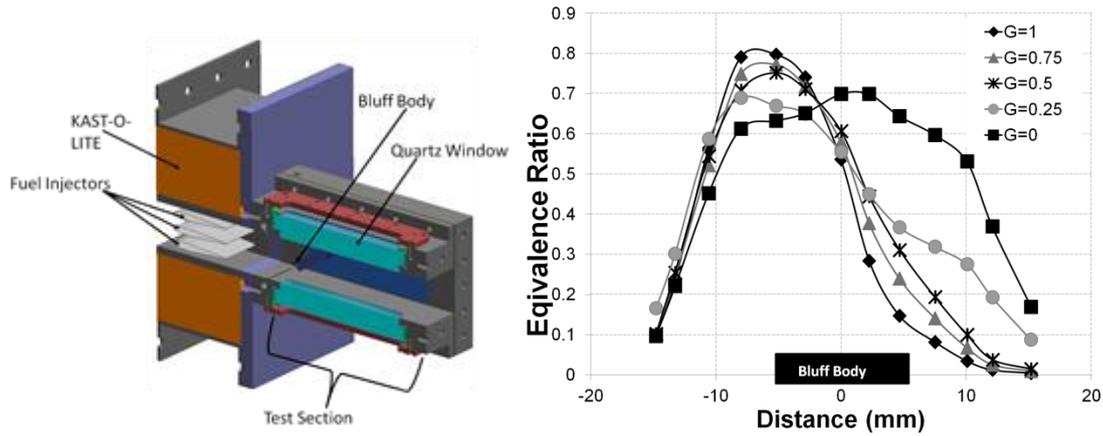


Fig. 1 (left): Experimental facility for bluff body flame measurements with stratified fueling.

Fig. 2 (right): Equivalence ratio profiles for five stratified cases.

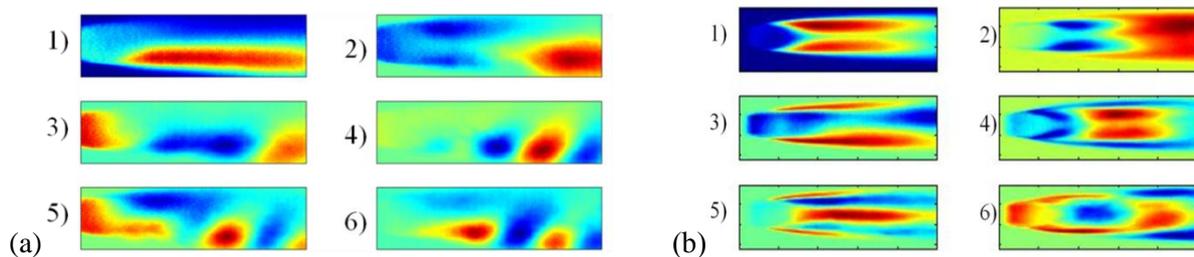


Fig. 3: The first six POD modes for (a) stratified fueling and (b) acoustically coupled cases.

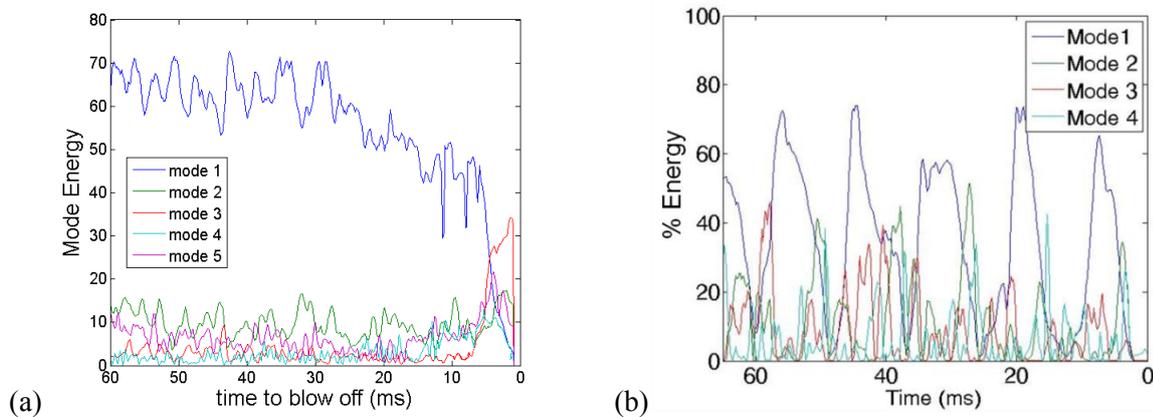


Fig. 4: POD mode time constants through blowoff for (a) stratified fueling with no acoustic coupling and (b) strong acoustic coupling.

References

- [1] S. Chaudhuri *et al.*, *Combustion and Flame*, **158**, 1358 (2011)
- [2] K.M. Kopp-Vaughan *et al.*, Analysis of blowoff dynamics from flames with stratified fueling, *Proceedings of the Combustion Institute*, **34**, in review.
- [3] S.G. Tuttle *et al.*, Lean blow off behavior of asymmetrically-fueled bluff body-stabilized flames, *Combustion and Flame*, in review.

Evaluating mixing models for transported probability density function simulations of nonpremixed turbulent flames

A. Krisman¹, E. R. Hawkes^{1,2}, J. C. K. Tang², J. E. C. Chan¹, S. Kook¹, J. H. Chen³

1. *Mechanical and Manufacturing Engineering, UNSW, Sydney Australia 2052*
2. *Photovoltaic and Renewable Energy Engineering, UNSW, Sydney Australia 2052*
3. *Sandia National Laboratories, Livermore CA USA 96551-0969*

a.krisman@unsw.edu.au

Transported probability density function (TPDF) methods [1, 2] are well suited to modelling computationally difficult phenomena such as turbulent, reacting, variable density flows. One of the main challenges to the successful deployment of TPDF methods is accurately modelling the unclosed molecular mixing term [3, 4]. This study examines three of the most widely used mixing models: Interaction by Exchange with the Mean (IEM) [5], Modified Curl (MC) [6, 7] and the Euclidean Minimum Spanning Tree (EMST) [8].

A parallel code was implemented to evaluate the performance of the three models. This code solves transport equations which model the governing equation for the compositional-TPDF (C-TPDF) [9].

The TPDF was used to model a nonpremixed plane jet flame previously simulated by Hawkes *et al* using DNS [10]. The DNS was used to provide initial conditions, the mean velocity field, turbulent diffusivity, and mixing frequency. Moreover the identical chemical kinetic and thermodynamic models were used in the modelling and DNS. The simulation scenario was a one-dimensional, non-premixed, turbulent jet flame burning a syn-gas fuel stream that featured extinction and re-ignition. This test scenario was selected because extinction and re-ignition phenomena are sensitive to the mixing model. Three DNS cases were considered with different Reynolds numbers (Lower, Medium, and Higher). The cases feature increasing extinction with Reynolds number.

The simulation results indicate that first and second order moments for: mixture fraction, temperature, and minor species concentrations, are well predicted in the Lower and Medium cases in terms of both their spatial and conditional profiles by the IEM, MC, and EMST mixing models. However the Higher case is poorly predicted by all mixing models, *e.g.* see Figures (1), (2), (3), and (4). One interesting feature was that although the EMST model performed slightly better in the prediction of conditional means, the model had difficulty correctly matching the conditional PDFs, with very narrow distributions predicted.

The results from these simulations allow us to draw the following conclusions:

1. A RANS-based C-TPDF model is successful in simulating the given syn-gas fueled non-premixed jet flame for the lower and moderate Reynolds number cases.
2. The IEM, MC and EMST mixing models are all successful in cases L and M in terms of spatial and conditional means and spatial RMS information.
3. The EMST model significantly under-predicts the variance of flow properties conditioned upon mixture fraction. This results in narrow conditional PDFs that do not resemble the DNS simulation. The IEM and MC models provide a closer match in case M, but all mixing models fail in case H.
4. The C-TPDF method is unable to match the DNS results for case H. All mixing models greatly under-predict the degree of re-ignition during the simulation.

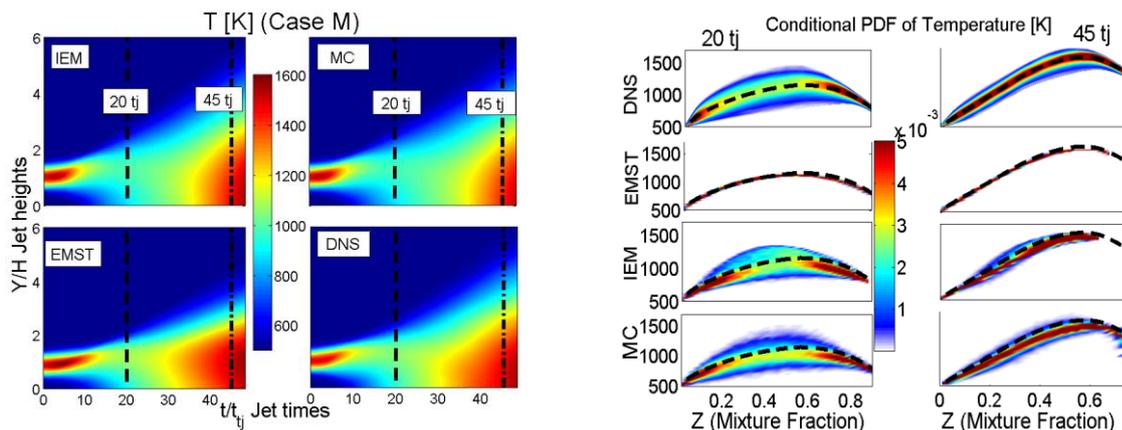


Figure 1: (Left) Extinction and re-ignition for case M. Domain coloured by temperature shows the one-dimensional spatial profile's progression over time. The DNS (bottom right) shows that extinction should occur by 20 jet times and re-ignition should be established by 45 jet times.

Figure 2: (Right) Probability density function of temperature conditioned on mixture fraction for case M at 20 and 45 jet times for the DNS and EMST, IEM, and MC mixing models. The black dashed line represents the conditional mean of the DNS for reference purposes.

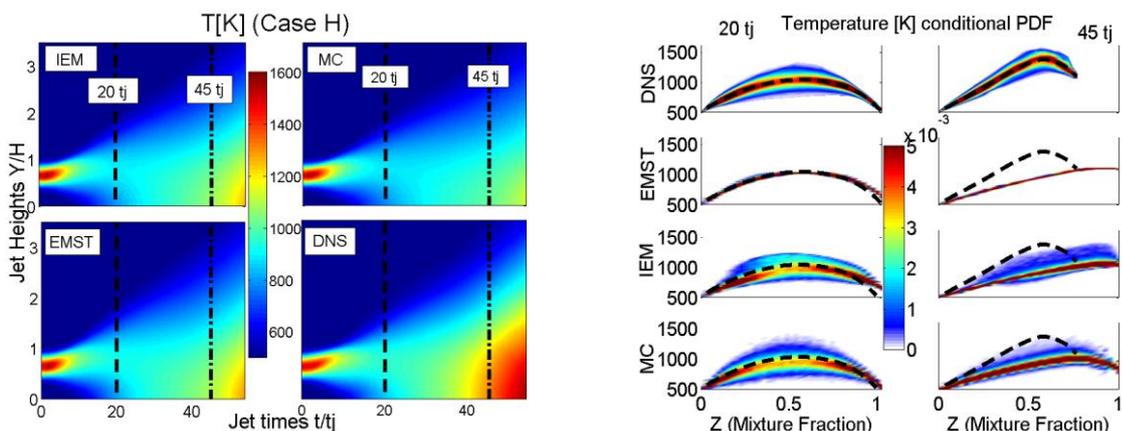


Figure 3: (Left) Extinction and re-ignition for case H. Domain coloured by temperature shows the one-dimensional spatial profile's progression over time. The DNS (bottom right) shows that extinction should occur by 20 jet times and re-ignition should be initiated by 45 jet times

Figure 4: (Right) Probability density function of temperature conditioned on mixture fraction for case H at 20 and 45 jet times for the DNS and EMST, IEM, and MC mixing models. The black dashed line represents the conditional mean of the DNS for reference purposes.

References

- [1] S.B. Pope, Progress in Energy and Combustion Science, **11**, 119-192 (1985)
- [2] S.B. Pope, Physics of Fluids, **23**, 011301 (2011)
- [3] R.R. Cao, S.B. Pope, Combustion and Flame, **143**, 450-470 (2005)
- [4] S. Mitarai, J. Riley, G. Kosály, Physics of Fluids, **17**, 047101 (2005)
- [5] J. Villermaux, J.C. Devillon, Proceedings of the Second International Symposium on Chemical Reaction Engineering, 1-13 (1972)
- [6] R.L. Curl, American Institute of Chemical Engineering, **9**, 175-181 (1963)
- [7] J. Janicka, W. Kolbe, W. Kollmann, Non-Equilibrium Thermodynamics, **4**, 47-66 (1979)
- [8] S. Subramaniam, S.B. Pope, Combustion and Flame, **117**, 732-754 (1999)
- [9] S. Viswanathan, H. Wang, S.B. Pope, Journal of Computational Physics, **230**, 6916-6957 (2011)
- [10] E.R. Hawkes, R. Sankaran, J.C. Sutherland, J. H. Chen, Proceedings of the Combustion Institute, **31**, 1633-1640 (2007)

Investigation of heat loss effects within the Darmstadt Stratified Burner by means of Large Eddy Simulation and a joint ATF-FGM approach

Guido Kuenne^{1,a}, Anja Ketelheun¹, Amer Avdic^{1,b}, Amsini Sadiki¹, Johannes Janicka¹

¹Institute of Energy and Power Plant Technology
TU Darmstadt, Petersenstr. 30, 64287 Darmstadt, Germany

^akuenne@ekt.tu-darmstadt.de, ^bavdic@ekt.tu-darmstadt.de

In order to reduce the pollutant formation, lean premixed combustions is of increasing importance where stratification is often found either intentionally or due to incomplete mixing. This poster presents the continuation of our work dealing with the simulation of these flames as initiated at the previous TNF workshop where the purpose is on both, the assessment of the numerical method as well as on insight into physical processes [1]. These first simulations conducted back then already showed reasonable success but also revealed deviations from the measurements which are assumed to be partially caused by the neglect of heat transfer – a deficiency intrinsic to the state description by the mixture fraction and progress variable only [2]. From the subsequent discussions this was one of the main uncertainties for the TSF-A-r configuration.

Therefore, to allow a more physical description at non-adiabatic walls which influence the flow field, species concentration and temperature distribution, we extended our modeling approach making it capable to account for heat loss and preheating effects. Based on the previously used method of artificial flame thickening and FGM (flamelet generated manifolds) - tabulated chemistry [3], the enthalpy has been added as a third table access parameter [4]. As illustrated in Fig. 1 this enables the simulation to capture the modification of the chemistry by enthalpy input or removal.

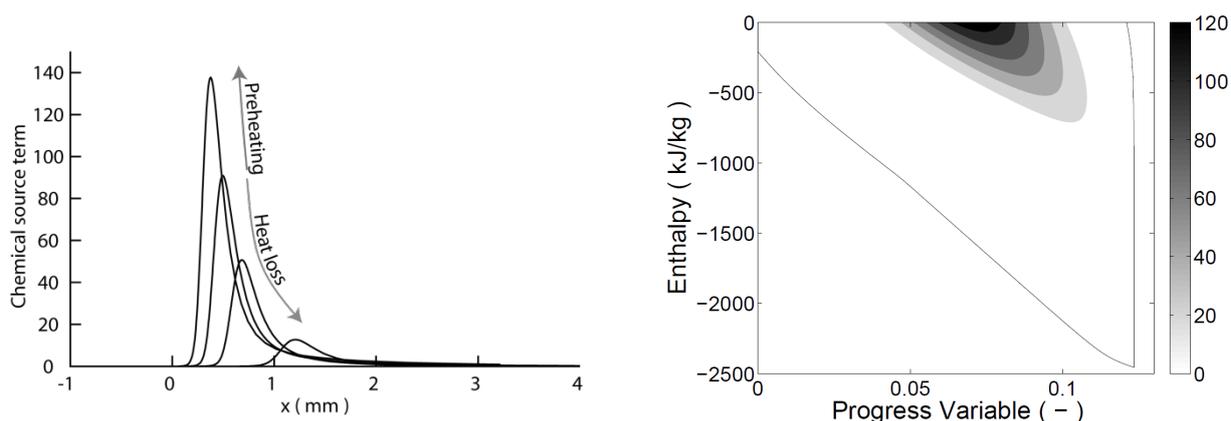


Fig. 1: Representation of the chemical source term (kg/m³/s) in physical space (left) and as stored in the table (right) for one equivalence ratio and different enthalpy levels.

Figure 2 shows first results from the simulation to be presented on the poster where the wall temperature is currently set according to a Nusselt-number estimation since no experimental data is available for this boundary condition yet. Furthermore radiation has been neglected in this first study. In comparison to the adiabatic simulation shown on the left a significant difference is visible. While – as expected from theory – the adiabatic simulation predicts the flame to be attached to the wall, the low enthalpy region originating from the ceramic tube suppresses the chemical reaction in this region leading to a lift-off which is in qualitative agreement with the lower flame luminosity observed on flame photographs. The simulation will be finished until the TNF and a detailed evaluation including a comparison of statistical quantities amongst the two simulations and experimental data will be given.

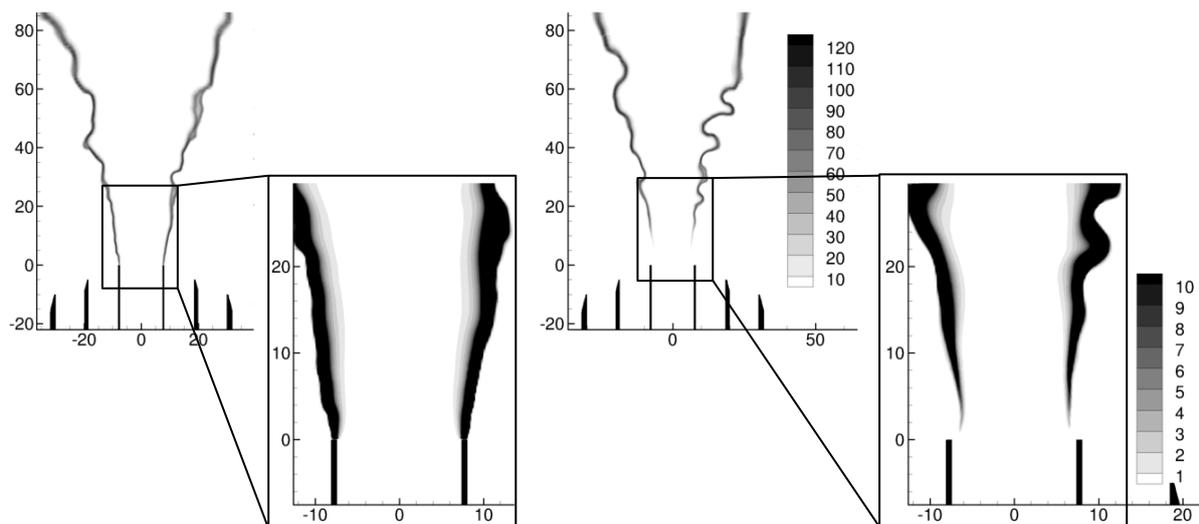


Fig. 2: Snapshot of the simulation showing the chemical source term ($\text{kg/m}^3/\text{s}$) with heat transfer (right) and in the adiabatic simulation (left). Lower two plots show a magnified region of the flame attachment point and the color map covers lower values.

References

- [1] TNF 10 Proceedings (2010)
- [2] G. Kuenne, F. Seffrin, F. Fuest, T. Stahler, A. Ketelheun, D. Geyer, J. Janicka, A. Dreizler, *Combust. Flame*, In press, online access doi:10.1016/j.combustflame.2012.02.010 (2012).
- [3] G. Kuenne, A. Ketelheun, J. Janicka, *Combust. Flame* 158 (2011) 1750–1767.
- [4] A. Ketelheun, G. Kuenne, J. Janicka, *Flow Turb. Combust.*, submitted (2012)

Investigations of DME jet flames with emphasis on stabilization, transport and turbulence-chemistry interactions

Guilhem Lacaze* and Joseph C. Oefelein[♦]

*Sandia National Laboratories, Combustion Research Facility
7011 East Avenue, Livermore, CA 94550, USA*

*gnlacaz@sandia.gov

[♦]oefelei@sandia.gov

Energy security and environmental concerns motivate significant efforts in research on alternative fuels. Aspects such as emissions, availability, cost, safety and versatility are key selection criteria. Compared to existing alternative fuel candidates (i.e. Fischer–Tropsch fuels, ethanol, methanol, syngas), dimethyl ether (DME) appears to have promising potential. Replacing conventional diesel fuel by DME may reduce NO_x emission by 70% and its combustion is almost smokeless. In addition, DME is attractive since its production can be achieved at low cost from a large variety of resources such as coal, natural gas, biomass [1]. To optimize the development of future DME combustion system, some fundamental aspects have to be investigated in detail. The turbulent flame structure and stability must be described more accurately. The engine community is also very interested in understanding emission mechanisms and their interaction with turbulence. DME flames have the particularity to produce a significant amount of formaldehyde (CH₂O). Turbulent diffusive transport of CH₂O is very efficient, and it is present in relatively high concentration in re-ignition regions. A major question is to understand the role of formaldehyde in the re-ignition processes as well as transport phenomena. To address these points, quantitative experiments are required as well as simulations. Experimental measurements give access to a certain level of insights about the physics as well as validation data for numerical investigations. On the other hand, simulations may be used to calibrate experimental diagnostics, decrease uncertainties, and be combined with measurements to provide complementary data.

The objective of our research is to provide a set of high-fidelity simulations that provide insights that are not accessible by measurements in key experiments. One aspect is to understand how simulations can be used to improve experimental diagnostics accuracy. Temperature can be quantitatively measured in flames using Coherent anti-Stokes Raman Spectroscopy (CARS), which is a well-established point-wise technique [2].

This method is sensitive to change in the mixture composition and its accuracy depends on how well species distribution is known. Such data can be provided by simulations of laminar counter-flow flames at relevant conditions. Here we show how our numerical data are used by Barlow et al. to reconstruct the temperature field in turbulent DME jet flames. Similarly, a new experimental technique has been developed by Frank et al. [3] to quantitatively measure mixture fraction in non-premixed gaseous flames. Using this technique, Frank and Coriton utilize Krypton as an inert tracer in DME flames to study mixing processes. Two-photon laser-induced fluorescence (LIF) is employed to detect the spatial distribution of the tracer. Contrary to conventional techniques, this approach guarantees that the tracer is a conserved scalar that is only subject to passive mixing. This eliminates ambiguities on the definition of mixture fraction. Quantitative krypton LIF measurements require knowledge of the temperature and species-dependent collisional quenching rates. Detailed numerical

simulations are carried out to provide the missing information at experimental conditions. Turbulent DME jet flames are experimentally studied by Frank and Coriton. Stereo Particle Image Velocimetry (PIV) and LIF of OH and formaldehyde are simultaneously obtained to study flame dynamics. Three-dimensional high-fidelity LES are examined along with the experimental measurements to describe the effect of turbulence on mixing and flame stabilization. As mentioned above, formaldehyde is believed to play a significant role in flame stabilization. The complementary analysis of numerical and experimental data will provide fundamental insights in the path to control emission and efficiency of DME future combustion systems.

References

- [1] GREENHALGH, D., Quantitative CARS spectroscopy. *John Wiley and Sons*, (1988).
- [2] HANSEN, J., VOSS, B., JOENSEN, F., AND SIGUROARDOTTIR, I. Large scale manufacture of dimethyl ether: A new alternative diesel fuel from natural gas. *SAE paper 950063* 104, 4 (1995), 70–79.
- [3] HSU, A. G., NARAYANAS WAMY, V., CLEMENS, N. T., AND FRANK, J. H. Mixture fraction imaging in turbulent non-premixed flames with two-photon LIF of krypton. *Proceedings of the Combustion Institute* 33, 1 (2011), 759–766.

DQMOM-based PDF Transport Modeling for Turbulent Lifted Flame with Vitiated Co-flow

J. Lee , S. Park , Y. Kim

Hanyang University, Seoul, Korea

ymkim@hanyang.ac.kr

The Direct-Quadrature Method of Moment (DQMOM) based PDF transport approach [1-3] has been adopted to simulate turbulent H_2/N_2 lifted jet flame [4] in vitiated co-flow. In this study, the joint composition PDF is approximated using the multi-environment PDF consisting the combination of weights and abscissas on composition and physical space. The micromixing is represented by the IEM model. To numerically simulate the auto-ignition process and conditional fluctuations on composition space, all composition vector including species mass fraction and enthalpy are directly integrated with stiff ode solver.

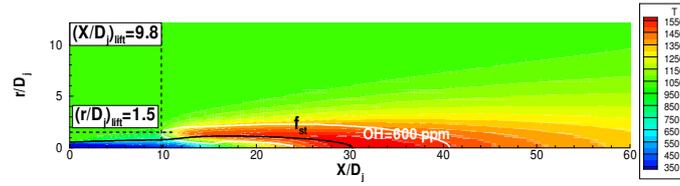
Numerical results displayed in Figures 1 and 2 clearly indicate that the present DQMOM based PDF transport model has the capability to predict the auto-ignition, flame lift-off, and stabilization process in the turbulent H_2/N_2 lifted jet flame [4]. In terms of the lifted-off height, mean and rms of temperature and species mass fractions, the predicted axial and radial profiles for both mean and rms of temperature and mass fraction of H_2 , O_2 , N_2 , H_2O and OH reasonably agree with experimental data.

Fig. 3 shows the predicted and measured conditional data on mixture fraction space for temperature and mass fraction of OH at $x/D=8, 11, 14$. At the upstream location, it can be clearly seen that only mixing process on composition space is dominant. When the mixture reaches to the slight downstream region($x/D_j=11$) of the flame anchoring zone, the mixing process interacts with the reaction process. At this region, for the certain conditions of reactivity, flow and scalar fluctuations, the auto-ignition and local extinction take place. At the downstream flame region ($x/D_j=14$), the turbulent combustion processes are nearly mixing controlled and the resulting conditional fluctuations are substantially reduced. Each environment corresponds to the upper and lower bound of the flame structure on the mixture fraction space. These upper and lower limits have the essential information to describe the unconditional and conditional mean, and conditional fluctuations on physical and mixture fraction space, respectively.

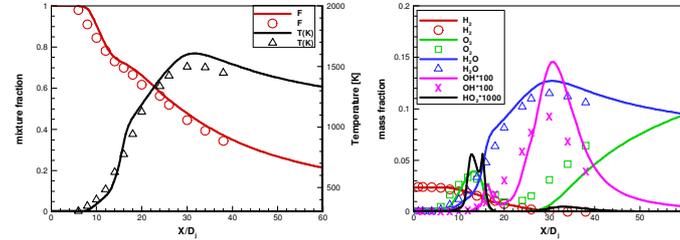
In order to investigate the stabilization mechanism around the flame base, the energy budget analysis of DQMOM transport equation is presented in Fig.4. The chemical reaction term is greater than the convection and diffusion terms in environment 2. This implies that environment 2 mainly controls to initiate and sustain the turbulent lifted flame at the flame base. On the other hand, when the mixture of environment 1 is sufficiently heated by the micro mixing process with environment 2, the chemical reaction is occurred at the downstream of flame base. In this region, the diffusion term and chemical reaction term are balanced and the diffusion-mode burning processes are mainly influenced by environment 1.

References

- [1] R. O. Fox, Computational Models for Turbulent Reacting Flows, Cambridge Universe Press, 2003.
- [2] J. Akroyd, A. J. Smith, L. R. McGlashan, M. Kraft, Chem. Eng. Sci. 65 (2010) 1915-1924.
- [3] H. Koo, P. Donde, V. Raman, Proc. Combust. Inst. 33 (2011) 2203-2210.
- [4] R. Cabra, T. Myhrvold, J. Y. Chen, R. W. Dibble, A. N. Karpetis, R. S. Barlow, Proc. Combust. Inst. 29 (2002) 1881-1887.

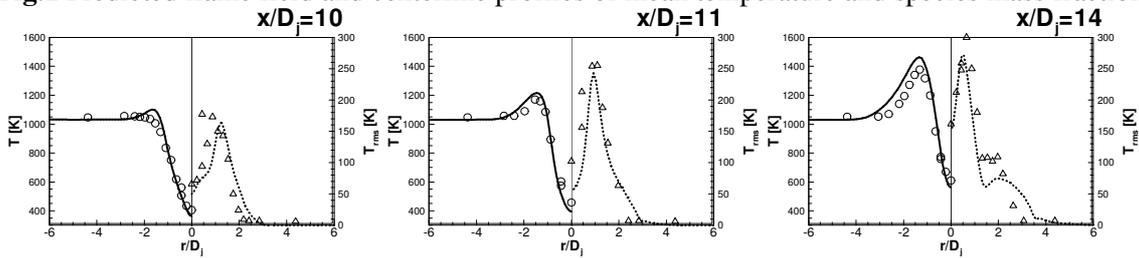


(a) Temperature

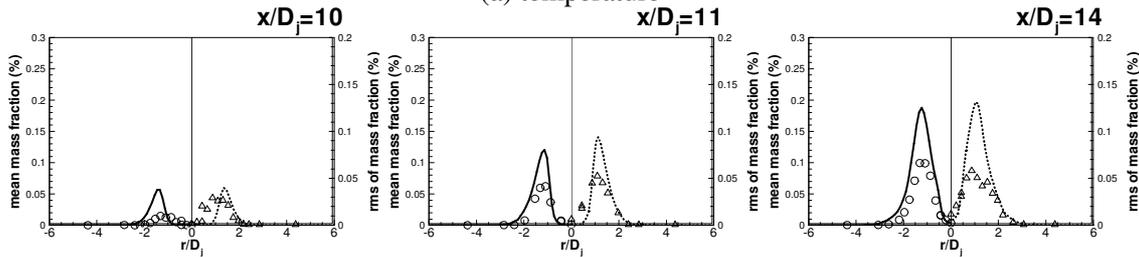


(b) centerline profiles of mixture fraction, temperature and species mass fraction

Fig.1 Predicted flame field and centerline profiles of mean temperature and species mass fraction



(a) temperature



(b) OH mass fraction

Fig.2 Radial profiles for mean and r.m.s. of temperature and OH mass fraction at three axial stations

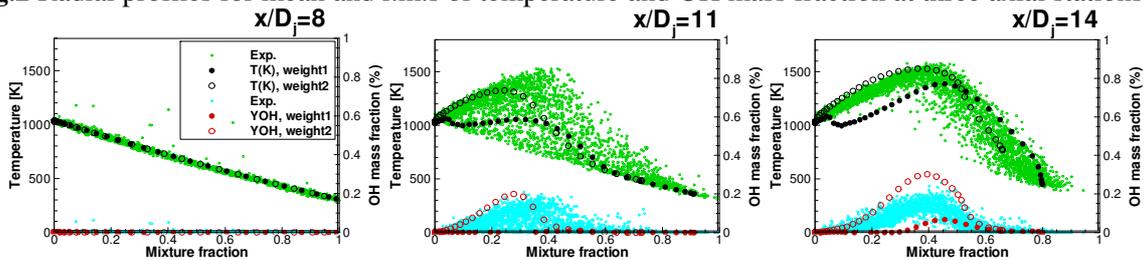


Fig.3 Predicted and measured data conditioned on mixture fraction space for temperature and OH mass fraction at three axial stations under each environment

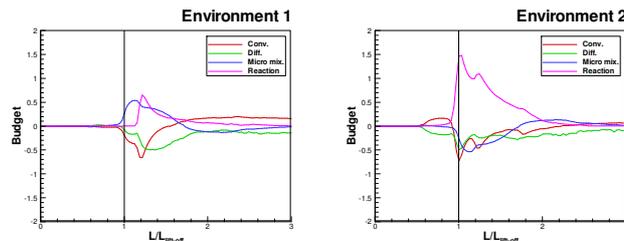


Fig.4 Budget analysis for convection, diffusion, micro mixing and reaction of DQMOM transport equations along the axial direction at $r/D_j=1.5$

Dual Pump CARS Measurements in a Supersonic Combusting Free-Jet

G. Magnotti¹, A. D. Cutler²

¹ Combustion Research Facility, Sandia National Laboratories, Livermore, CA 94551, USA

² Mechanical and Aerospace Engineering Department, The George Washington University, Newport News, VA 23602, USA

gmagnot@sandia.gov

Large experimental databases are needed to develop and calibrate new computational fluid dynamics (CFD) models for turbulence and turbulence-chemistry interaction in supersonic combustion. Available experimental data are limited, due to difficulties in taking measurements in such a harsh environment.

Dual-pump coherent anti-Stokes Raman spectroscopy (CARS) is a non-intrusive, non-linear, laser-based technique that provides temporally and spatially resolved measurements of temperature and absolute mole fractions of N_2 , O_2 and H_2 in H_2 -air flames. A dual-pump CARS instrument has been developed to obtain measurements in supersonic combustion and generate databases for the CFD community. [1]

A laboratory scale, axis-symmetric, supersonic combusting coaxial jet facility has been developed to provide a simple, yet suitable flow to CFD modelers.[2] The facility provides a center jet of "vitiated" air, reproducing the sensible enthalpy of air entering the engine of a hypersonic vehicle flying at Mach numbers (M_f) between 5 and 7. The vitiated air is the product of combustion of O_2 -enriched air with H_2 that has the same O_2 mass fraction of air, but high temperature and water. Nozzles with exit Mach number (M_e) 1, 1.6, and 2 are available to provide flows with different effects of compressibility. Hydrogen is available in order to generate a supersonic combusting free-jet. As an alternative, N_2 can be used as co-flow for non-reacting (mixing) studies. Figure 1 shows an infrared picture of the jet for a combustion case with exit Mach number $M_e=1.6$ and flight Mach number $M_f=7$.

About 800,000 dual-pump CARS single-shots measurements have been collected for various values of the center-jet flight and exit Mach number, for mixing and combustion test cases. Averages, standard deviations and co-variances have been computed and selected results are shown.

Figure 2 shows at each location the mole fraction of gases originated in the center-jet, the co-flow and the ambient air. The left side of Figure 2 shows that the increased compressibility reduces the mixing of the center-jet with the co-flow and the ambient air, in agreement with what previously observed by Papamoschou. [3] Similarly the right side of Fig. 2 shows that the heat released from the combustion limits the growth of the co-flow shear layer, and the mixing of the center jet, as observed by Hermanson [4] in incompressible flows.

Figure 3 shows the shear layer growth rate normalized by the incompressible growth rate, and plotted versus the compressibility parameter Π introduced by Slessor. [5] The continuous curve represents a fitting of several experimental results.

Figure 4 shows that increased compressibility reduced the

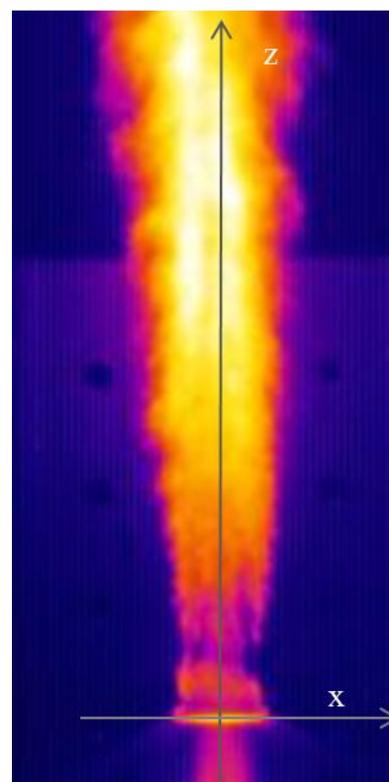


Figure 1. Infra-red picture of the supersonic combusting jet.

standard deviation, consistently with the reduction in turbulence production predicted by Pantano using DNS simulations. [6]

The experimental results are in agreement with what was previously observed or predicted, but the relevance of the acquired data-set lays in providing accurate quantitative measurements of the distributions of mean and fluctuation parameters (i.e. variances covariances, pdfs).

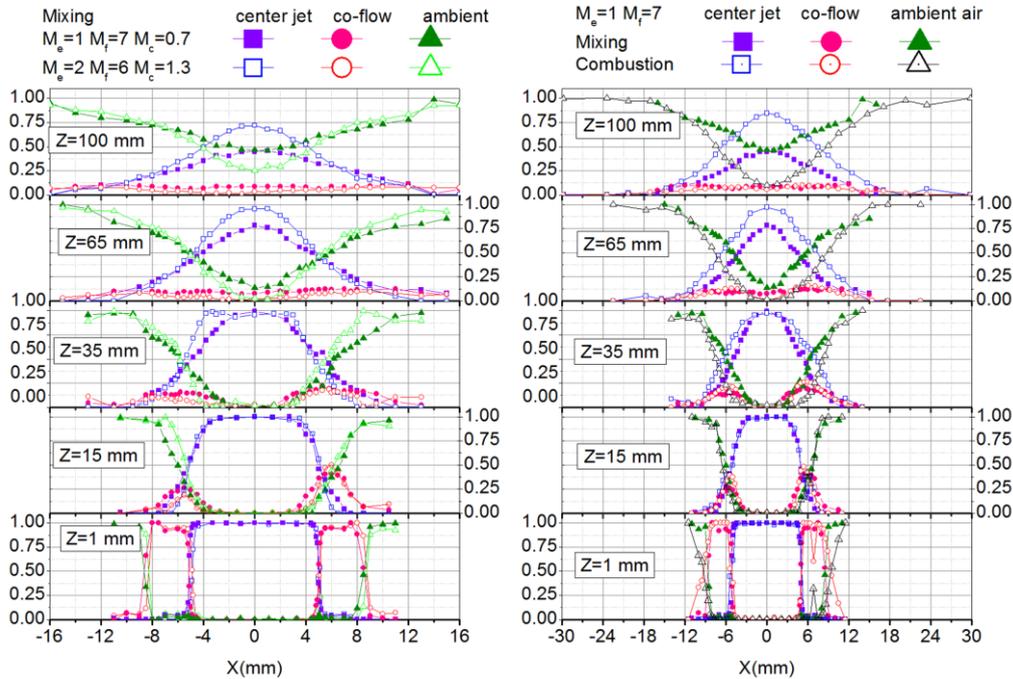


Figure 2. Average mole fraction of gases based on their provenance. Left) Effect of the compressibility; right) effect of the heat release.

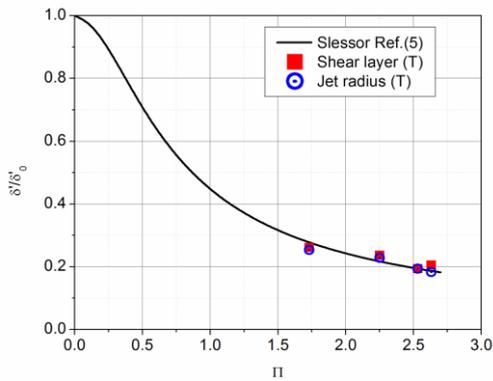


Figure 3. Normalized growth rates as function of the compressibility parameter Π , compared to Slessor’s fitting curve.

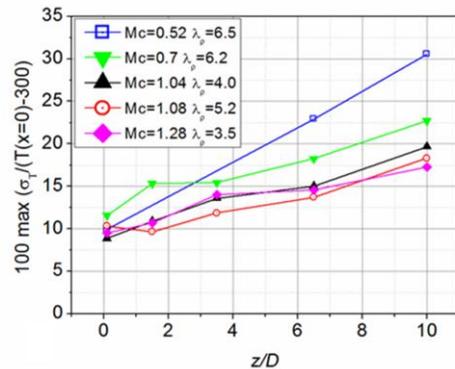


Figure 4. Normalized peak standard deviation as function of the distance from the nozzle exit, expressed in nozzle diameters.

References

[1] G. Magnotti *et al.*, AIAA 2012-1193 (2012)
 [2] A. D. Cutler *et al.*, AIAA 2007-0978 (2007)
 [3] M. D. Slessor *et al.* *J. Fluid Mech.* **414**, 35 (2000)
 [4] J. C. Hermanson *et al.*, *J. Fluid Mech.* **199**, 333 (1989)
 [5] M. D. Slessor *et al.* *J. Fluid Mech.* **414**, 35 (2000)
 [6] C. Pantano, *et al.*, *J. Fluid Mech.* **481**, 291 (2003)

Experimental Observation of Lifted Flames in a Heated and Diluted Coflow

Paul R. Medwell and Bassam B. Dally

School of Mechanical Engineering, The University of Adelaide, AUSTRALIA

paul.medwell@adelaide.edu.au

Lifted flames in a hot coflow have recently been used to investigate autoignition properties of jet flames. A fuel jet issuing in a heated and diluted oxidant stream is also the fundamental operating principle of MILD combustion. This study investigates similarities and differences of the liftoff behaviour of jet flames under a wide variety of coflow oxidant conditions, ranging from the autoignitive conditions to MILD combustion.

The burner used in this study is the Jet in Hot Coflow (JHC) burner from The University of Adelaide [1–4]. The JHC burner consists of a central fuel jet that issues into a coflowing stream of hot combustion products from a premixed secondary burner mounted upstream of the jet exit plane. This configuration may be used to emulate MILD combustion in a simplified geometry with well-controlled conditions. The JHC configuration is also very similar to the vitiated coflow burner of Cabra *et al.* [5,6] used to investigate autoignition.

In the heated oxidant stream configuration, autoignition is the dominant stabilisation mechanism of the lifted flames. With the exception of an extreme sensitivity of the liftoff height with small changes in coflow temperature, many features of the flames with the Cabra burner are similar to conventional flames. In contrast, under MILD combustion conditions using the JHC burner the OH radical has been measured all the way to the jet exit plane, including in the "lifted" region [3]. Due to the fundamental difference in this region, these flames are described as 'transitional' rather than lifted. Furthermore, in the JHC burner a reduction in the liftoff/transition height with an increase in jet Reynolds number has been observed [3,7,8]. Therefore, although the general configuration of the JHC and Cabra burners are similar, there are some significant differences in the flame behaviour. It is important to note that the operating conditions of the previous experiments have been quite different. The present results aim to provide an initial investigation on the flame behaviour that occurs in the transition between the existing disparate experiments.

The flame liftoff height is estimate using a combination of visual observation, photographs (with a range of exposure times) and CH* chemiluminescence imaged with an intensified CCD camera. An example of the flame images is presented in Figure 1. The liftoff height is based on visual observation and analysis of the photographs and CH* chemiluminescence, rather than an absolute threshold. Since different methods are used to estimate the liftoff height, and there is some degree of uncertainty in interpretation of the images, the results presented show a range of liftoff heights (presented as errorbars).

Figure 2 shows the estimated liftoff height for natural gas flames, over a range of Reynolds numbers and coflow temperatures (1300-1600K) with 3% O₂ in the coflow. Below 1300K no flame could be sustained. At 1300K coflow temperature the flame luminosity is very low, and is considered to be in the MILD combustion regime. A faint reaction zone can be identified to extend to the jet exit plane, though a definite flame is not apparent until approximately 20mm. Interestingly, increasing the temperature of the coflow from 1300K to 1400K leads to an increase in the liftoff height. It could be expected that increasing the temperature of the oxidant stream would increase the reactivity, and hence reduce the liftoff height. Despite the

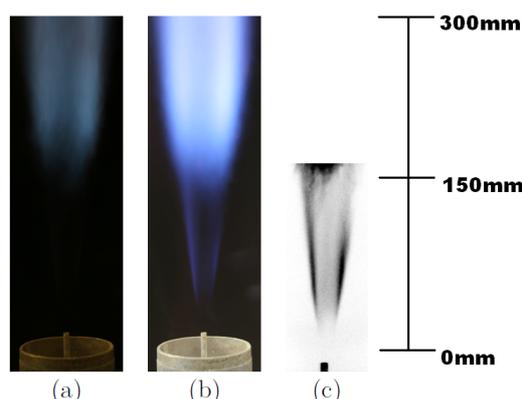


Fig. 1: Flame photographs for (a) short exposure time, and (b) long exposure time. (c) CH^* chemiluminescence image (inverse-intensity). Approximate image height shown in millimetres.

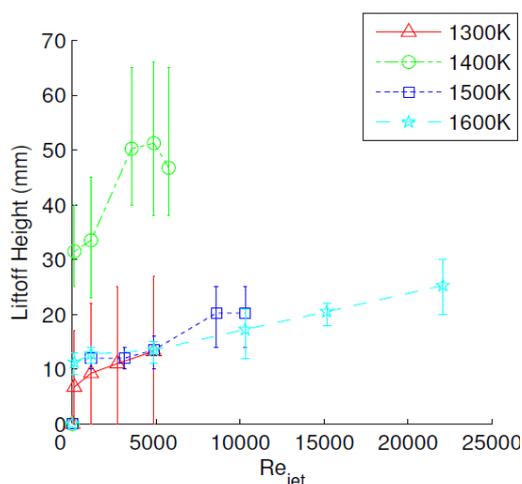


Fig. 2: Liftoff height over a range of jet Reynolds numbers for natural gas flames issuing into a coflow containing 3% O_2 (vol/vol) at various temperatures.

range of uncertainty in the data due to the low luminosity of these flames, there is a clear trend seen in flames presented in Figure 2. As the temperature is increased from the minimum required to sustain a visible flame (*i.e.* 1300K) to 1400K the flame liftoff height increases. A subsequent increase in coflow temperature leads to a reduction in the liftoff height, but never back to the attached flame of the 1300K case. It seems that impact of the temperature change on the chemical kinetics or the mixing rate between the coflow and the fuel becomes critical at these conditions. Measuring the mixture fraction will shed more light on this phenomenon.

Beyond the results presented, the liftoff behaviour is observed to not be monotonic with either coflow temperature or oxygen content. The results clearly indicate that there is a fundamental transition in the stabilisation mechanism, depending on the oxidant stream properties. There is significant scope for further investigation of the stabilisation mechanisms in these flames.

References

- [1] Dally, Karpetis, Barlow, *Proc. Combust. Inst.*, **29**, 1147–1154 (2002)
- [2] Medwell, Kalt, Dally, *Combust. Flame*, **148**, 48–61 (2007)
- [3] Medwell, Kalt, Dally, *Combust. Flame*, **152**, 100–113 (2008)
- [4] Medwell, Kalt, Dally, *Combust. Sci. Tech.*, **181**, 937–953 (2009)
- [5] Cabra, Myhrvold, Chen, Dibble, Karpetis, Barlow, *Proc. Combust. Inst.*, **29**, 1881–1888 (2002)
- [6] Cabra, Chen, Dibble, Karpetis, Barlow, *Combust. Flame*, **143**, 491–506 (2005)
- [7] Oldenhof, Tummer, van Veen, Roekaerts, *Combust. Flame*, **158**, 1553–1563 (2011)
- [8] De, Oldenhof, Sathiak, Roekaerts, *Flow Turb. Combust.*, **87**, 537–567 (2011)

Modeling flame stabilization by heat losses using Filtered Tabulated Chemistry for Large Eddy Simulation

R. Mercier^{1,2}, P. Auzillon^{1,2}, V. Moureau³, N. Darabiha^{1,2}, O. Gicquel^{1,2},
D. Veynante^{1,2}, B. Fiorina^{1,2}

1 Ecole Centrale Paris, Grande Voie des Vignes, 92290 Châtenay-Malabry, France

2 CNRS, UPR 288, Laboratoire d’Energétique Moléculaire et Macroscopique,
Combustion (EM2C), Grande Voie des Vignes, 92290 Châtenay-Malabry, France

3 CORIA - CNRS, Université et INSA de Rouen, Technopole du Madrillet, BP 8, 76801
Saint-Etienne-du-Rouvray, France

renaud.mercier@ecp.fr

Novel combustion chambers mainly operate in premixed regimes to control the flame temperature and the pollutant emissions. For safety reasons, fuel and oxidizer are injected separately in the combustion chamber leading to complex “stratified flames” propagating in partially premixed flows, where characteristic spatial scales of equivalence ratio variations are of the order of the reaction zone thickness [1, 2, 3].

In order to predict the stabilization of stratified flames, it is crucial to accurately model the impact of the unsteady mixing process on the flame chemistry. In this context, an attractive approach is to combine large eddy simulations (LES) and tabulated chemistry methods [4, 5, 6]. The model Filtered Tabulated Chemistry for LES (F-TACLES) has been proposed to include detailed chemistry in LES [7, 8]. This approach has been derived to capture the correct flame propagation speed when the flame wrinkling is fully resolved, a situation oftenly encountered for practical grid meshes. Recently, Auzillon *et al.* [9] extended this model to stratified combustion regimes accounting for mixture fraction heterogeneities at the subgrid scale level.

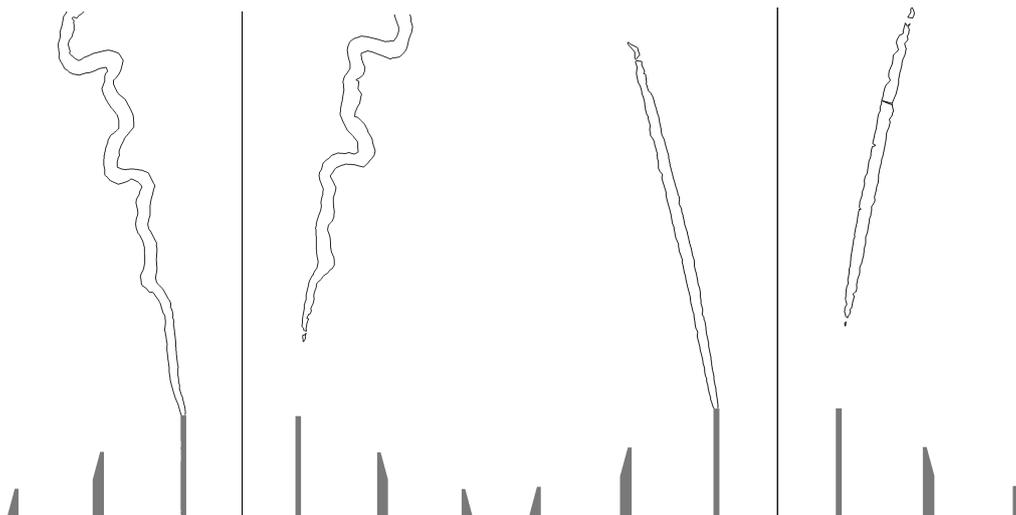


Fig. 1 Iso-line of instantaneous (left) and mean (right) progress variable source term at a value of $\bar{\omega}_{Y_c} = 0.5 \max(\bar{\omega}_{Y_c})$. Burner left part: Adiabatic burner. Burner right part: Isothermal burner.

The flame stabilisation mechanism may be more complex in other situations such as jet flames because reactive zones develop close to the burner lips and may be affected by thermal

wall heat losses. As suggested by Roux and Pitsch [10] and Kuenne *et al.* [1], this phenomenon is of importance in the TSF (Turbulent Stratified Flame) configuration designed for turbulent lean premixed or stratified jet flames at high Reynolds number [2, 3]. In the present study, we have extended the F-TACLES formulation to account for heat losses.

The proposed approach is validated through the simulation of TSF-A flame lifted by heat losses. The computation has been realized under both adiabatic and non-adiabatic flow assumptions. The reaction zone predicted by the adiabatic F-TACLES simulation is anchored at the burner lip causing a mismatch between the predicted and the measured mean flame front positions (See Fig. 1). The non-adiabatic simulation exhibits local extinction due to heat losses near the burner exit. The flame is then lifted in the non-adiabatic simulation improving the comparison with experiments (See Fig. 2). This approach allows tackling the right flame position when stabilization process is governed by heat loss.

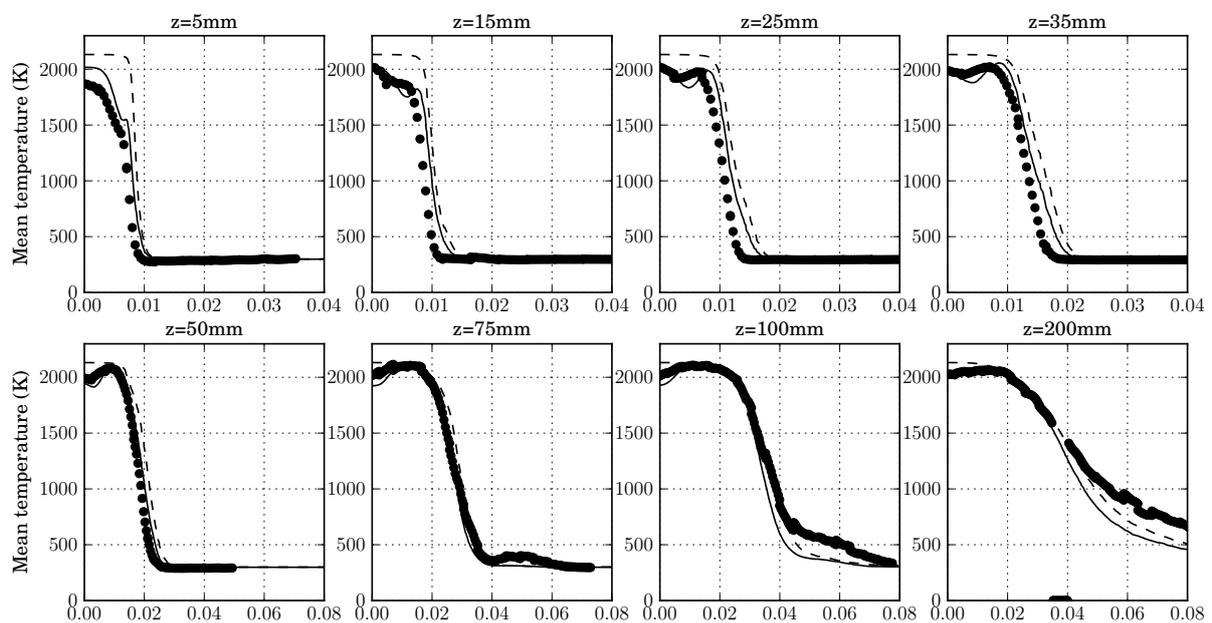


Fig. 2 Mean temperature at eight distances from the pilot tube exit. – – Adiabatic burner. — Isothermal burner. • • Experiments. Non-adiabatic effects close to the burner are highlighted by important gaps between mean temperature measurement and adiabatic simulation. These gaps are recovered in the non-adiabatic simulation.

Reference(s)

- [1] G. Kuenne, F. Seffrin, F. Fuest, T. Stahler, A. Ketelheun, D. Geyer, J. Janicka, A. Dreizler, *Combustion and Flame*. In press.
- [2] B. Böhm, J.H. Frank, A. Dreizler, *Proceedings of the Combustion Institute* 33 (2011) 1583–1590.
- [3] F. Seffrin, F. Fuest, D. Geyer, A. Dreizler, *Combustion and Flame* 157 (2009) 384–396.
- [4] U. Maas, S. Pope, *Combust. Flame* 88 (1992) 239–264.
- [5] O. Gicquel, N. Darabiha, D. Thévenin, *Proceedings of the Combustion Institute* 28 (2) (2000) 1901–1908.
- [6] J.A. van Oijen, F.A. Lammers, L.P.H. de Goeij, *Combustion and Flame* 127 (3) (2001) 2124–2134.
- [7] B. Fiorina, R. Vicquelin, P. Auzillon, N. Darabiha, O. Gicquel, D. Veynante, *Combustion and Flame* 157 (2010) 465–475.
- [8] P. Auzillon, B. Fiorina, R. Vicquelin, N. Darabiha, O. Gicquel, D. Veynante, *Proceedings of the Combustion Institute* 33 (1) (2011) 1331–1338.
- [9] P. Auzillon, O. Gicquel, N. Darabiha, D. Veynante, B. Fiorina, *Combustion and Flame*. In press.
- [10] A. Roux, H. Pitsch, *Annual research briefs, Center for Turbulence Research* (2010).

Modeling of laminar partially premixed dimethyl ether flames

D. Messig^{a)}, J. Keller^{b)}, C. Hasse^{a)}

^{a)} Numerical Thermo-Fluid Dynamics, University of Technology Freiberg, Germany

^{b)} Engler-Bunte-Institute, KIT, Karlsruhe, Germany

Danny.Messig@iec.tu-freiberg.de

Dimethyl ether (DME) is a promising candidate as a diesel replacement especially in the context of bio-fuels. Despite the importance, only a limited number of investigations with detailed experimental data on DME flames is currently available. Recently, Fuest et al. [1] investigated laminar and turbulent DME jet flames using Raman/Rayleigh scattering and CO-LIF and preliminary results were shown at the TNF10 workshop. They obtained detailed species profiles in radial direction. They especially emphasized the complexity in interpreting the experimental data compared to methane flames due to the non-negligible amount of intermediate hydrocarbons. The authors used laminar 1D flame calculations and used the results for postprocessing the experimental data.

The current work investigates numerically the L1 flame in an axisymmetric 2D configuration using detailed transport formulations and complex chemistry with 55 species among 290 reactions [2] using the solver diffusionFoam. Such an approach provides additional and potentially more accurate information compared to 1D calculations since the scalar dissipation rate is a part of the CFD solution itself and it is not required to be chosen a priori. Different diffusion models were used in this study ranging from unity Lewis-number to detailed multicomponent flux modeling based on the Curtis-Hirschfelder approach. The results obtained considering differential diffusion can be seen in Fig. 1. The results are plotted after reaching steady state conditions in the measured area by F. Fuest et al. [1]. The fluctuations of the laminar flame above a fuel nozzle distance $z \geq 0.1$ m always occur but do not effect the results below $z = 0.1$ m. The strongest mixing occurs in the vicinity of the fuel nozzle exit, shown by the radial velocity U_y in Fig. 1.

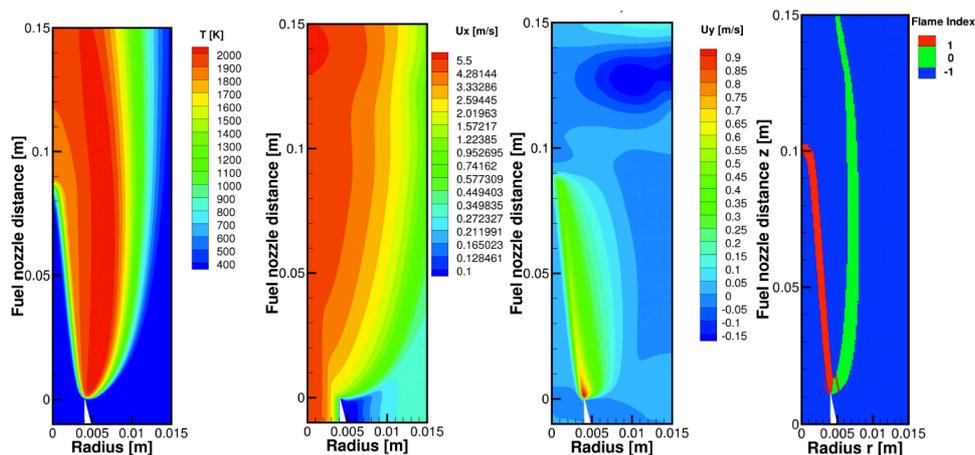


Fig. 1: L1 Simulation results from left to right: temperature, axial and radial velocity, flame index. The comparison of the experimental and numerical results confirms that differential diffusion effects are non-negligible for the investigated setup and must be considered to accurately describe the flame structure. Using the $Le = 1$ model does not reproduce the experimental tip height from F. Fuest et al. [1]. On the other hand, both Soret and Dufour effect do not effect the central premixed cone of the Flame L1 significantly (not shown here). The partially premixed flame structure with an inner rich premixed flame and the outer diffusion flame is also shown in Fig. 1 using a slightly modified normalized flame index by Domingo et al. [3].

Further details on the flame structure are plotted in Fig. 2 showing a comparison of numerical and experimental results in a radial slice at a height of 0.02 m both in physical and in mixture fraction space. Two different sets of numerical results are included. The standard setting using the experimentally reported boundary condition for the coflow (Curtis standard) as well as a modified boundary condition further discussed below (Curtis). In general, good agreement is obtained for the inner flame region, whereas in the outer flame region for $r \geq 6$ mm larger differences can be observed. However, comparing the experimental and the numerical data conditioned on the mixture fraction F using the definition by Barlow and Frank [4], only small differences can be found near the fuel rich zone $0.8 \leq F \leq 1$, whereas in the lean part, which showed larger differences in physical space, is very well described. Thus, the differences can be attributed to the mixture fraction field itself, which is directly influenced by the co-flow velocity. An increase of the air co-flow velocity to $u = 1.3$ m/s as compared to $u = 0.3$ m/s leads to different radial distributions at the outer flame zone as seen in Fig. 2 (Curtis). A much closer agreement of numerical results to the experimental values can be achieved for $r \geq 6$ mm. Except for very small differences for the temperature, the inner flame zone results are unchanged. Plotting the results conditioned on mixture fraction, similar results are obtained compared to the standard boundary conditions (Curtis Standard).

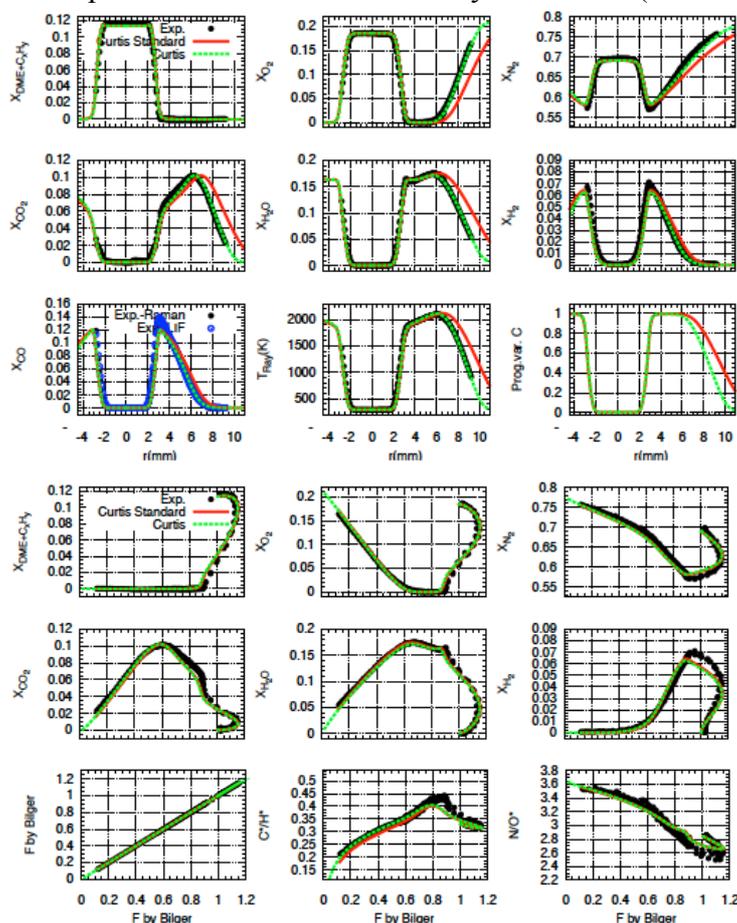


Fig. 2: Comparison numerical and experimental data at a height of 0.02 m Top: physical space; Bottom: mixture fraction space. For the numerical results both standard boundary conditions (Curtis standard) and modified boundary conditions (Curtis) are shown.

References

- [1] F. Fuest *et al.*, Combustion and Flames, (2012)
- [2] Z. Zhao *et al.*, International Journal of Chemical Kinetics, (2008)
- [3] P. Domingo *et al.*, Combustion and Flame, (2005)
- [4] R.S. Barlow *et al.*, Proc. Combust. Inst. (1998)

Modeling differential diffusion in Large Eddy Simulation of a bluff body stabilized premixed weakly turbulent flame

S. Nambully, P. Domingo, V. Moureau, L. Vervisch

CORIA - CNRS & INSA Rouen, BP 8, 76801 Saint-Etienne-du-Rouvray, France

suresh.nambully@coria.fr

In the Cambridge premixed swirl burner experiment, Barlow et al. [1] reported a net increase exceeding 10% in the equivalence ratio occurring across the turbulent flame brush. This was attributed to effects of preferential transport by molecular diffusion acting in the lean premixed methane/air turbulent flame resulting in the accumulation of carbon species in the re-circulation zone behind the bluff body.

To simulate this differential diffusion effect from resolved scales and thus to capture the anomalous equivalence ratio behaviour, the following procedure is adopted:

First, using Bilger's definition [2] the mixture fraction profiles $Z(\xi)$ are collected for several laminar premixed flames using the GRI-3 mechanism and a complex transport in CANTERA solver. A globalized differential diffusion source can then be constructed from $Z(\xi)$ as

$$\dot{\omega}_Z(\xi) = \rho_o S_L \frac{dZ(\xi)}{d\xi} - \frac{d}{d\xi} \left(\frac{\mu}{S_c} \frac{dZ(\xi)}{d\xi} \right)$$

Here μ and S_c take the values they have in the LES solver. ρ_o is the density in fresh gases, S_L the premixed laminar flame speed and ξ is the physical space coordinate. Introduced into a three-dimensional Z balance equation, $\dot{\omega}_Z(\xi)$ ensures that the Z profile computed in the normal direction to reaction zones, with μ/S_c as diffusion coefficient, would match exactly the one observed with detailed chemistry in the laminar flame.

Secondly, the flame is remapped onto a progress-variable space defined as $Y_c = Y_{CO} + Y_{CO_2}$, and then filtered and tabulated as:

$$\tilde{\omega}_Z(\underline{x}, t) = \int_0^1 \dot{\omega}_Z(Y_c) \tilde{P}_\Delta(Y_c; \underline{x}, t) dY_c$$

with $\tilde{P}_\Delta(Y_c; \underline{x}, t)$ the Filtered-Laminar-Flame PDF (FLF-PDF) discussed in [3]. Figure 1(a) shows the source term $\dot{\omega}_Z(Y_c)$ with a positive value in the burnt gas side representing the fast diffusion of lighter species towards fresh gases and hence the consequent increase of Z in burnt gases.

Finally, the source of SGS differential diffusion is added to the LES space filtered mixture fraction $\tilde{Z}(\underline{x}, t)$ transport equation:

$$\frac{\partial \bar{\rho} \tilde{Z}}{\partial t} + \nabla \cdot (\bar{\rho} \tilde{\mathbf{u}} \tilde{Z}) = \nabla \cdot \left(\left[\frac{\mu}{S_c} + \frac{\mu_T}{S_{cT}} \right] \nabla \tilde{Z} \right) + \tilde{\omega}_Z$$

In Fig. 1(b), the non-passive mixture fraction (bold line) captures the experimental values properly whereas the passive Z (dashed line) misses the equivalence ratio increase completely.

It was found that this differential diffusion effect generated at micro scales appear at larger length scales when there exists a gradient of residence time across the reaction zone. Therefore, to determine the possible existence of this phenomenon in other burners qualitatively, a differential diffusion number (NB_{diff}) defined as

$$NB_{diff} = \frac{\tau_{res}^b - \tau_{res}^f}{\tau_z} = (\tau_{res}^b - \tau_{res}^f) \dot{\omega}_Z$$

is proposed where τ_{res}^f and τ_{res}^b denote the residence time in the fresh and burnt gas respectively. A high value of NB_{diff} indicates a higher probability of the differential diffusion effect appearing at larger length scales.

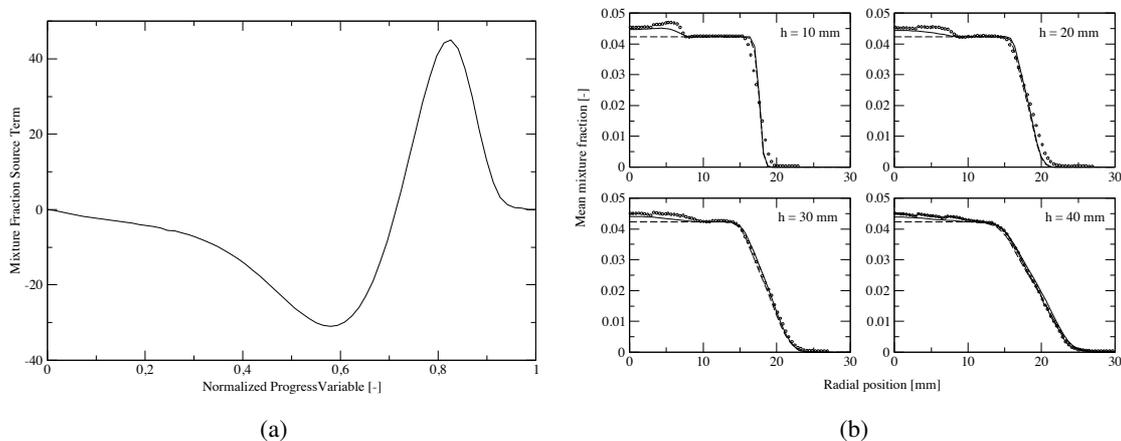


Figure 1: (a) Mixture fraction source term across the reference flame (s^{-1}). (b) Mean mixture fraction distribution at different heights from burner exit.

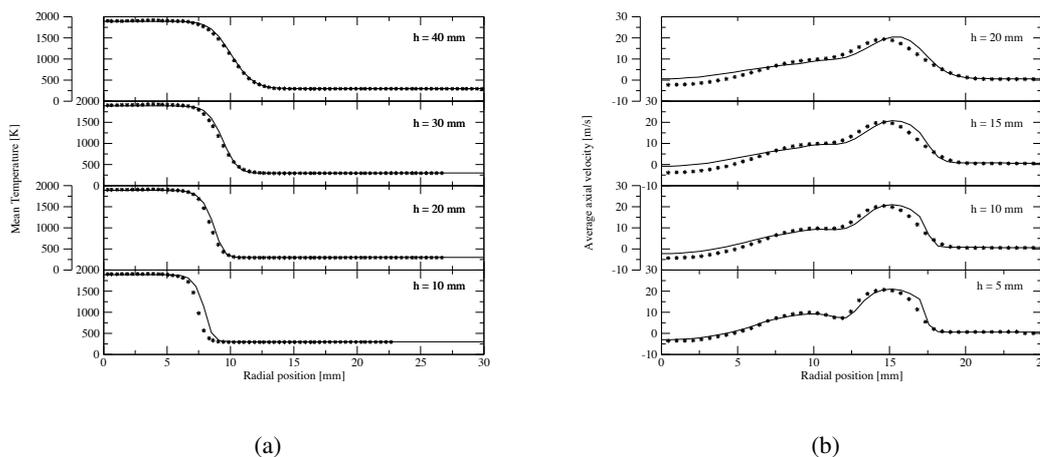


Figure 2: Radial profiles. Symbol: measurements. (a): Temperature, streamwise position from 10 to 40 mm. (b): axial velocity, streamwise position from 5 to 20 mm.

References

- [1] Robert S. Barlow, Matthew J. Dunn, Mark S. Sweeney and Simone Hochgreb. Effects of preferential transport in turbulent bluff-body-stabilized lean premixed CH₄/air flames. *Combustion and Flame*, **159**(8): 2563–2575, 8 2012.
- [2] R. W. Bilger, S. H. Starner, and R. J. Kee. On reduced mechanisms for methane-air combustion in non-premixed flames. *Combustion and Flame*, **80**(2): 135–149, 1990.
- [3] V. Moureau, P. Domingo, and L. Vervisch. From large-eddy simulation to direct numerical simulation of a lean premixed swirl flame: Filtered laminar flame-pdf modeling. *Combustion and Flame*, **158**(7): 1340–1357, 2011.

The Effect of Pressure, Environment Temperature, Jet Velocity and Nitrogen Dilution on the Liftoff Characteristics of a Hydrogen Jet Flame in a Vitiated Co-flow

North, A.¹, Frederick, D.¹, Dibble, R. W.¹, Chen, J. Y.¹, Gruber, A.²

¹University of California – Berkeley, Berkeley, CA 94720

²SINTEF Energy Research, 7465 Trondheim, Norway

anorth@berkeley.edu

Hydrogen has been identified as a potential fuel for stationary gas turbine combustors for reducing carbon dioxide emissions. H₂ may be produced through pre-combustion Carbon Capture and Sequestration (CCS), where H₂ is extracted from fossil fuels and separated from CO₂ before combustion. In achieving low nitric oxide emissions, H₂ is burned in a Lean-Premixed (LP) mode. A diluent, such as nitrogen, can be added to the H₂ fuel encouraging flame detachment from the nozzle, which facilitates partially premixed combustion. An improved understanding of the mixing and subsequent ignition behavior of N₂-in-H₂ flames will aid in the design of combustors for H₂ operation as well as determining stable operating conditions for such combustors. Lifted flames are a convenient and useful problem for understanding the influence of the many independent parameters which affect combustion stability. In this study, the impact of pressure (P_{chamb}), temperature, fuel jet nitrogen dilution mole fraction (y_{N_2}), and fuel jet velocity (V_{jet}) on the liftoff height of lifted H₂ jet flames in a vitiated co-flow is characterized. Figure 1 shows the sensitivity of liftoff height to P_{chamb} (with jet momentum or jet Reynolds number, Re_{jet} , held constant), P_{chamb} (with V_{jet} held constant), co-flow equivalence ratio ($\phi_{\text{co-flow}}$), y_{N_2} , and V_{jet} for a selected set of condition of $P_{\text{chamb}} = 1.5$ bar, $V_{\text{jet}} = 400$ m/s, $\phi_{\text{co-flow}} = 0.15$, and $y_{\text{N}_2} = 0.33$. Liftoff height is found strongly dependent on P_{chamb} , y_{N_2} , and $\phi_{\text{co-flow}}$, and weakly dependent on V_{jet} in the region studied.

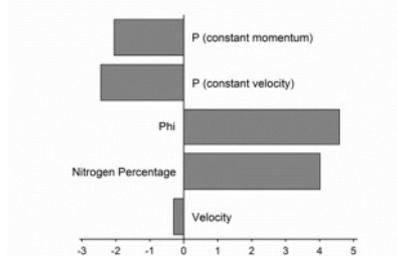


Figure 1: Sensitivity of liftoff height of a N₂-in-H₂ jet flame in a vitiated co-flow to P_{chamb} (with constant Re_{jet}), P_{chamb} (with constant V_{jet}), $\phi_{\text{co-flow}}$, y_{N_2} , and V_{jet} at a base case of $P_{\text{chamb}} = 1.5$ bar, $V_{\text{jet}} = 400$ m/s, $\phi_{\text{co-flow}} = 0.15$, and $y_{\text{N}_2} = 0.33$.

The influence of P_{chamb} on liftoff height is characterized extensively for liftoff height correlation development that includes P_{chamb} as a parameter. The resulting correlation will lend insights in describing the fundamental impacts that pressure has on liftoff height and H₂ ignition behavior. In determining liftoff height pressure dependence, it is prudent to first decide whether to hold V_{jet} constant or Re_{jet} constant. The constant V_{jet} assumption is logical if ignition behavior is dominated by ignition delay time, while the constant Re_{jet} assumption is more appropriate if turbulent mixing rates dominate liftoff behavior. Figure 2 shows normalized liftoff heights for cases where V_{jet} is held constant for one data set and Re_{jet} is held constant for the other at 400 m/s and 41500, respectively, and with $y_{\text{N}_2} = 0.33$, and

$\phi_{\text{co-flow}} = 0.15$. Re_{jet} is held constant by fixing the product of jet density by V_{jet} , leaving jet diameter constant.

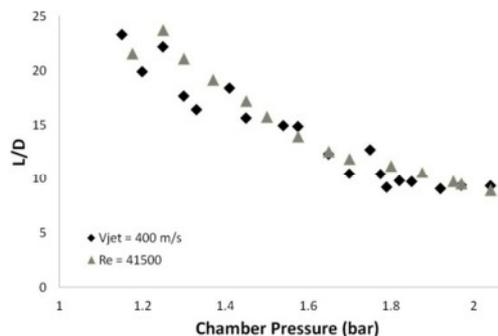


Figure 2: Liftoff height versus P_{chamb} for $\phi_{\text{co-flow}} = 0.15$, $y_{\text{N}_2} = 0.33$, and (a) $V_{\text{jet}} = 400$ m/s; (b) $Re_{\text{jet}} = 41500$.

The measured liftoff heights for both cases decrease with P_{chamb} . For constant Re_{jet} , V_{jet} is inversely proportional to P_{chamb} . The reduction in V_{jet} as P_{chamb} increases for constant $Re_{\text{jet}} = 41500$ does not seem to affect the resulting liftoff height, which is supported by the sensitivity analysis. When y_{N_2} is reduced to 0.20, however, the constant V_{jet} or constant Re_{jet} choice becomes important, as shown in Figure 3.

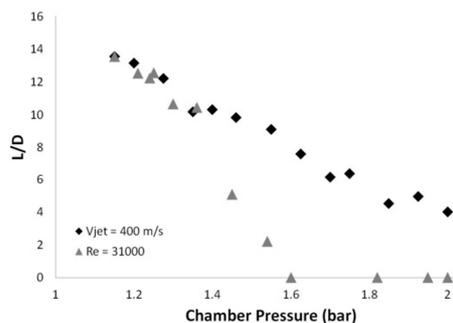


Figure 3: Liftoff height versus P_{chamb} for $\phi_{\text{co-flow}} = 0.15$, $y_{\text{N}_2} = 0.20$, and (a) $V_{\text{jet}} = 400$ m/s; (b) $Re_{\text{jet}} = 31000$.

Here, the dependence of liftoff height on P_{chamb} is stronger for constant Re_{jet} than for constant V_{jet} . When Re_{jet} is held constant, the jet attaches when P_{chamb} exceeds 1.6 bar. The increased sensitivity to V_{jet} at lower y_{N_2} values is presumably due to the reduction in Re_{jet} (31000 for $y_{\text{N}_2} = 0.20$ versus 41500 for $y_{\text{N}_2} = 0.33$). Consequently, the appropriate choice between constant V_{jet} and constant Re_{jet} becomes relevant for lower Re_{jet} values. This result may be caused by insufficient turbulence when $Re_{\text{jet}} = 31000$ for turbulent diffusivity to increase linearly with jet velocity. The theory that turbulent diffusivity increases linearly with V_{jet} for fully turbulent jet flames is used to explain the observation that flame height remains constant with increasing V_{jet} for attached turbulent jet flames [8]. Similar arguments can be used in explaining the independence of liftoff height to V_{jet} observed in Figure 1 and Figure 2 for fully turbulent flames when Re_{jet} exceeds a “fully turbulent” value. Additional experiments are necessary for determining the “fully turbulent” Re_{jet} value which results in liftoff height insensitivity to V_{jet} , though the present study suggests that the threshold Re_{jet} value lies between 31000 and 41500.

References

- [1] R Cabra, J Y Chen, R W Dibble, *Combustion and Flame*, **143**, 491-506 (2005)
- [2] M J Dunn, *et al.*, *Proceedings of the Combustion Institute*, **32**, 1779-1786 (2009)
- [3] S McAllister, J Y Chen, A C Fernandez-Pello, *Fundamentals of Combustion Processes*, Springer, (2011)

***A priori* assessment of SGS models for non-premixed turbulent flames close to wall**

Z. Pouransari¹, L. Vervisch² and A. V. Johansson¹

¹ *Linné FLOW Centre, Department of Mechanics, KTH, SE-100 44 Stockholm, Sweden*

² *CORIA - CNRS and INSA de Rouen, Technopole du Madrillet, BP 8, 76801, France*

zeinab@mech.kth.se

Direct numerical simulations of non-premixed reacting turbulent wall-jet flows are carried out using a higher order compact finite difference scheme. A priori analyses of the DNS data are performed to evaluate variable density subgrid-scale (SGS) models for Large Eddy Simulation (LES). The SGS dissipation of the kinetic energy and scalar variance are examples of the key quantities in the evaluation of SGS stress and scalar flux models, which are essential in turbulent combustion simulations[1]. The filtered DNS data are used to evaluate some of the models and to discuss their ranges of validity. In addition, the filter size effects are considered and the relative importance of resolution effects for the dynamic procedure in LES are examined [2]. Comparisons with the statistics of an isothermal simulation are performed in order to draw conclusions on how heat release will affect the predictive capability of different SGS models [3].

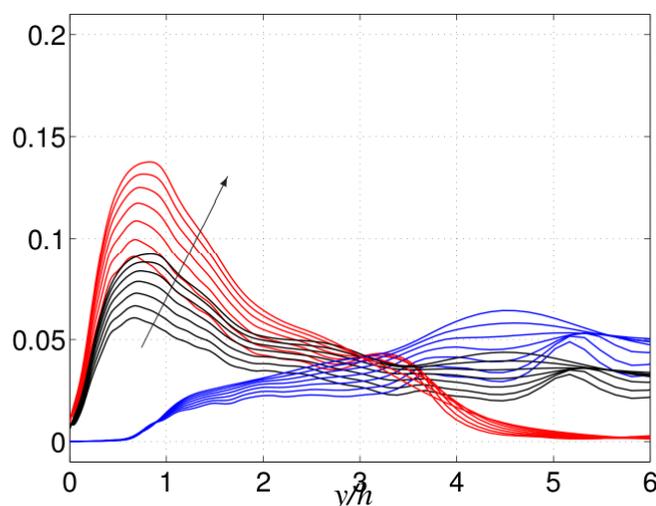


Fig. The scaling parameters $\langle \bar{\rho}(\tilde{\theta}^2 - \tilde{\theta}^2) \rangle / \langle \bar{\rho}(\Delta|\nabla\tilde{\theta}|)^2 \rangle$ for the SGS scalar variance model of passive and reacting species. Color code for different scalars as follows, passive: (black), fuel: (red) and oxidizer: (blue). Different filter size, (4, 6, 8, 10, 12, 14, 16) are shown and the arrow shows the direction of increase of the filter size.

References

- [1] Vervisch et al., *Combust. Flame* 157, 778 (2010)
- [2] Rasam et al., *J. Turb.* 12 10 (2011)
- [3] Pouransari et al., *Phys. Fluids* 23, 085104 (2011)

Notes

LES of the Cambridge Stratified Flame Series

F. Proch¹, F. Cavallo Marincola², A.M. Kempf¹

*1 Institute for Combustion and Gasdynamics (IVG), Simulation of Reactive Flows,
University of Duisburg-Essen, Duisburg, 47048, Germany*

*2 Department of Mechanical Engineering, Imperial College London, London, SW7 2AZ,
UK*

fabian.proch@uni-due.de

Large-Eddy simulation results are presented for the Cambridge Stratified Flame Series. The turbulent methane/air burner features a variable swirl flow ratio and a central bluff body for flame stabilization. Experimental investigations and measurements were performed by Sweeney, Hochgreb, Dunn and Barlow at the University of Cambridge and the Sandia National Laboratories [1].

The simulations are performed with the in-house code PsiPhi [2, 3]. The Favre-filtered governing equations for density, momentum, mixture fraction and progress variable are solved in 3D. The equations are discretized by the finite-volume method on a structured Cartesian grid consisting of cubic cells. Spatial discretization is achieved by a 2nd-order central-difference scheme for the momentum-equations and TVD-scheme for density and scalars. A 3rd-order Runge-Kutta scheme is used for time integration. The momentum equations are closed by adding turbulent viscosity ν_t , which is computed using the model of Smagorinsky [4]. As the computations show only a minimal sensitivity of the results to the Smagorinsky constant, it is set to a fixed value of 0.173 [5]. For the description of the unclosed reaction rate, a flame surface density (FSD) method is used, which was applied successfully to the very similar Darmstadt turbulent stratified flame series [6]. The laminar flame speed is evaluated as a function of the equivalence ratio using a higher order interpolation polynomial for the experimental data from [7], as shown in figure 1.

The computational domain is a cuboid with a length of 100 mm and a height and depth of 120 mm. The grid has a resolution of 0.5 mm, which leads to a domain size of 11.52 million cells. Finer computations with a resolution of 0.25 mm and 92.16 million cells will be presented on the poster. Computations are performed for three different cases without swirl and different rates of stratification and for a non-reactive case. The corresponding boundary conditions at the inflow (burner exit) are listed in table 1. Pseudo-turbulent fluctuations, which are generated by filtering of a random field [8], are added at the inflow; zero gradient conditions are applied at the outflow.

The simulations performed yet show good agreement with the experimental results, as shown in figures 2 and 3, the poster will present further results.

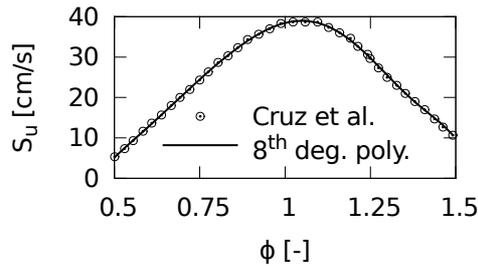


Fig. 1: Laminar flame speed polynomial

Case	ϕ_i [-]	ϕ_o [-]	U_i [$\frac{m}{s}$]	U_o [$\frac{m}{s}$]	U_{co} [$\frac{m}{s}$]
NonReac	-	-	8.31	18.7	0.4
SwB1	0.75	0.75	8.31	18.7	0.4
SwB5	1.0	0.5	8.31	18.7	0.4
SwB9	1.125	0.375	8.31	18.7	0.4

Tab. 1: Boundary conditions

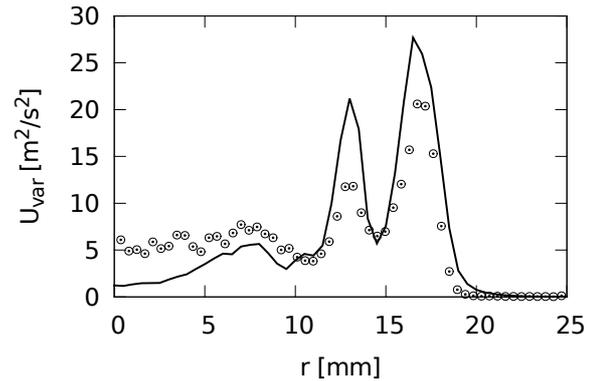
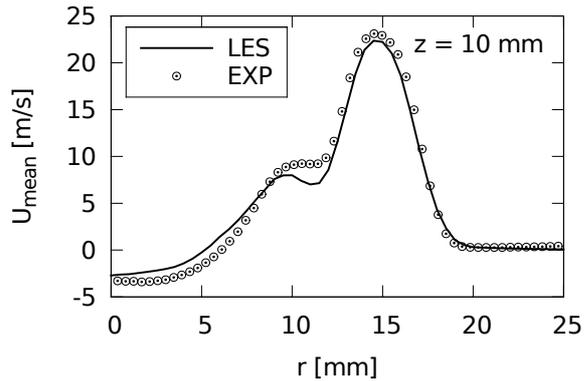


Fig. 2: Mean and variance of axial velocity for the non-reactive case (NonReac)

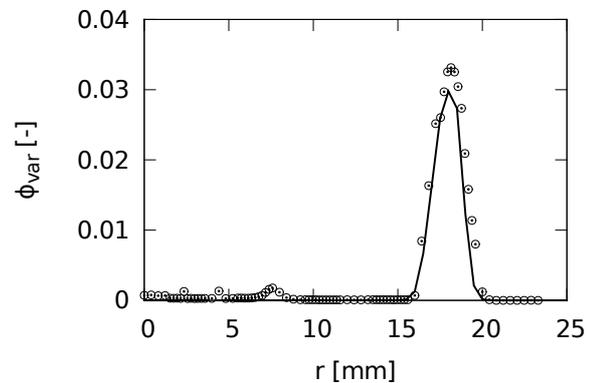
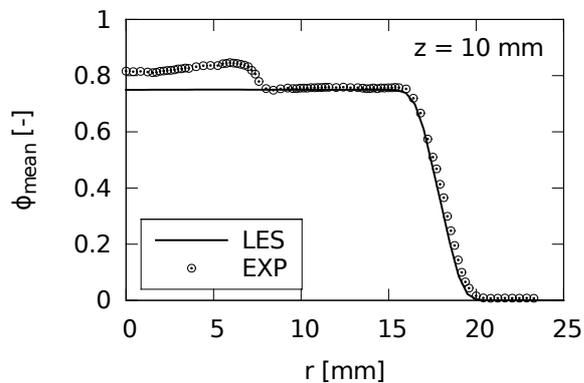


Fig. 3: Mean and variance of equivalence ratio for the reactive case without stratification (SwB1)

References

- [1] M.S. Sweeney, S. Hochgreb, M.J. Dunn, R.S. Barlow, *The Structure of Turbulent Stratified and Premixed Methane/Air Flames I: Non-Swirling Flows*, Combust. Flame, 2012. (under review)
- [2] M.W. Pettit, B. Coriton, A. Gomez, A.M. Kempf, Proc. Combust. Inst., 33 (2011) 1391-1399.
- [3] A.M. Kempf, B.J. Geurts, J. Oefelein, Combust. Flame 158 (2011) 2408-2419.
- [4] J. Smagorinsky, Mon. Wea. Rev., 91 (1963), 99–164.
- [5] D. Lilly, Proc. of the IBM Scientific Comp. Symp. on Environmental Sciences 1 (1967) 195–210.
- [6] F. Cavallo Marincola, T. Ma, A.M. Kempf, *Large Eddy Simulations of the Darmstadt Turbulent Stratified Flame Series*, Accepted for oral presentation at the 34th International Symposium on Combustion, 2012.
- [7] A. Pires Da Cruz, A. M. Dean, J. M. Grenda, Proc. Combust. Inst. 28 (2000) 1925–1932.
- [8] M. Kempf, S. Wysocki, M. Pettit, Computers & Fluids, Volume 60, 2012, 58-60.

Dynamic Adaptive Chemistry for Turbulent Flame Simulations

Zhuyin Ren, Tianfeng Lu

Department of Mechanical Engineering, University of Connecticut, Storrs, CT 06269, USA

Graham M. Goldin

ANSYS, Inc., 10 Cavendish Court, Lebanon, NH, 03766, USA

Zhuyin.Ren@enr.uconn.edu

The direct use of large chemical mechanisms in flame simulations is computationally expensive due to the large number of chemical species and the wide range of chemical time scales involved. This study investigates the use of dynamic adaptive chemistry (DAC) for efficient chemistry calculations. DAC is achieved through the directed relation graph (DRG) method, which is invoked for each CFD cell to obtain a small skeletal mechanism that is valid for the local thermochemical condition. Consequently, one needs to solve a much smaller set of ordinary differential equations governing chemical kinetics during reaction fractional steps. Test calculations are performed in a partially-stirred reactor involving both premixed and nonpremixed methane/air combustion with GRI-Mech 3.0 and USC-Mech II with updated NO_x pathways, respectively. Results show that DAC achieves a speedup factor of up to three for GRI-Mech 3.0 and up to six for USC-Mech II with good accuracy, respectively.

Introduction

Incorporation of detailed chemical kinetics in computational fluid dynamics (CFD) is important though challenging for reliable flame and emission predictions, with the major difficulty being the time-intensive nature of solving large sets of chemical kinetic equations. In most reactive flow solvers, the operator splitting scheme is employed to separate chemical reactions from other physical processes such as diffusion into a single reaction fractional step, which is governed by a large system of nonlinear stiff ordinary differential equations (ODEs) resulting from detailed chemical kinetics. The task in this reaction fractional step is to determine the thermo-chemical composition (species mass fractions, enthalpy and pressure) due to chemical reactions over a time step Δt . The time step, typically determined by the flow field, may be either a constant or a variable with a typical range spanning several orders of magnitude. During the reaction step, the composition of each computational cell evolves according to,

$$\frac{d\phi}{dt} = S(\phi) \quad (1)$$

where ϕ is the vector of cell thermochemical compositions and S is its rate of change due to chemical reactions. The CFD solver loops over all computational cells and calculates the reaction step, typically using stiff ODE solvers. The numerical integration of the large number of such ODEs is computationally expensive. In this study, we explore the dynamic adaptive chemistry (DAC) involving on-the-fly kinetic mechanism reduction to accelerate the ODE integrations.

Methodology and Results

The DAC is achieved through the directed relation graph (DRG) based method [1], which is invoked for each CFD cell/particle to obtain a small skeletal mechanism that is valid for the local thermochemical condition. More specifically, given a specific thermochemical state ϕ , DRG is invoked to eliminate unimportant species and corresponding reactions in the mechanism that have a negligible effect on quantities of interest. The ODE system in Eq. (1) is simplified by eliminating the ODEs for the unimportant species, and consequently a smaller set of ODEs are obtained. The unimportant species concentrations are treated as frozen during the integration time step. As a result of the elimination of unimportant species, a reaction is included in the local skeletal mechanism only if it involves an important species. The DAC scheme does this reduction on-the-fly for each set of local and instantaneous CFD composition.

Test calculations are performed in a partially-stirred reactor (PaSR) involving both methane/air premixed and nonpremixed combustion with GRI-Mech 3.0 and USC-Mech II with updated NO_x pathways, respectively. For the premixed cases, the PaSR involves two inflowing streams: a stoichiometric premixed stream of fuel/air mixture at 600 K; and a pilot stream consisting of the adiabatic equilibrium products of the stoichiometric fuel/air mixture (corresponding to unburned temperature of 600 K). The mass flow rates of these streams are in the ratio 0.95:0.05. For the

non-premixed cases, the PaSR involves three inflowing streams: a stream of pure CH_4 at 300 K; a stream of air at 300K, and a pilot stream consisting of the adiabatic equilibrium products of the stoichiometric fuel/air mixture (corresponding to unburned temperature of 300 K). The mass flow rates of these streams are in the ratio 0.10:0.85:0.05. The three time scales in PaSR are chosen such that a good range of non-equilibrium temperature and species compositions are present. In this study, we measure the incurred errors in the species and temperature, which are defined as the relative errors between the descriptions with and without DAC.

As shown in Fig. 1, the DRG tolerance effectively controls the incurred errors in the predicted temperature and species concentrations. With a specified allowed incurred error, the required reduction error tolerance depends on the quantities of interest. With USC-Mech II, for the nonpremixed case, DAC achieves a speedup factor ranging from 2 to 4, depending on the tolerance. With a tolerance of 0.01, DAC achieves a speedup factor of about 2 with about 1%, 0.6% and 0.04% incurred errors in NO, CO, and temperature, respectively. For the premixed case, DAC achieves a speedup factor ranging from 2 to 6 depending on the tolerance. With a tolerance of 0.2, DAC achieves a speedup factor of 6 with about 6%, 0.3% and 0.04% incurred errors in NO, CO, and temperature, respectively. For GRI-Mech 3.0, DAC achieves a speedup factor up to 3 (not shown). The DAC approach can be used to further accelerate chemistry calculation in cell agglomeration methods or dimension-reduction/tabulation methods via facilitating the integration of ODEs governing chemical kinetics.

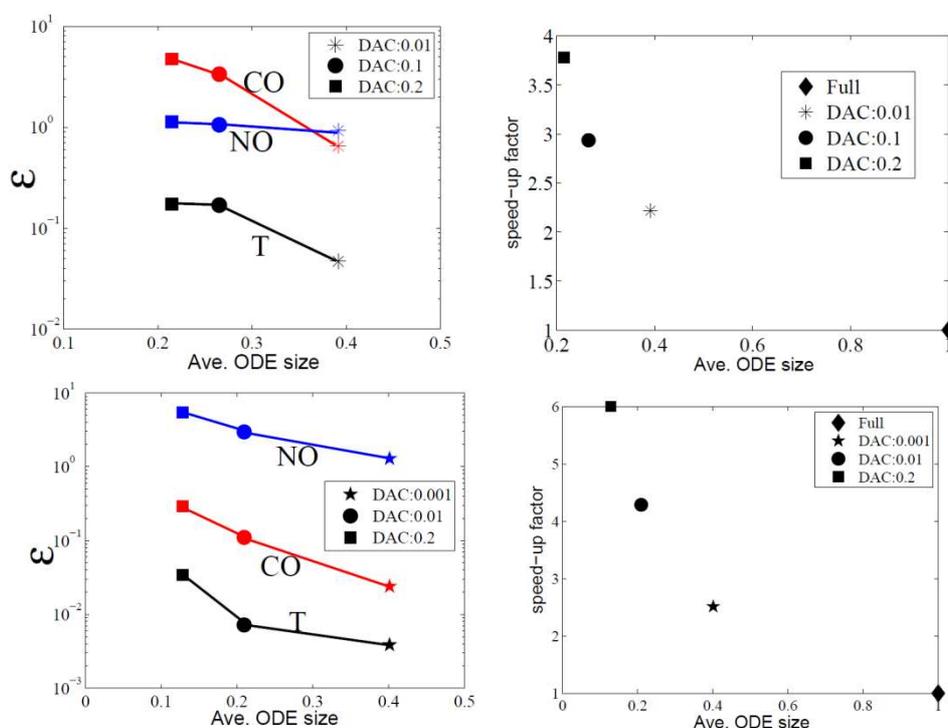


Figure 1: Left: the incurred error in temperature, CO, and NO, respectively, against the scaled average ODE sizes; right: the speed-up factor against the scaled average ODE sizes. The results are from different DRG error tolerances for nonpremixed (top row) and premixed (bottom row) combustion with the 129-species USC-Mech II mechanism.

References

- [1] Lu, T. and Law, C.K., A directed relation graph method for mechanism reduction, Proceedings of the Combustion Institute 30 (2005) 1333-1341.
- [2] Yang, H., Ren, Z., Lu, T. and Goldin G.M., Dynamic Adaptive chemistry for turbulent flame simulations, Combustion Theory and Modelling, to be submitted, 2012.

Simulation of the Delft-jet-in-hot-coflow burner using transported PDF methods and FGM tabulated chemistry

G. Sarras¹, M. K. Stöllinger², D. J. E. M. Roekaerts^{1,2}

1 *Process and Energy, Delft University of Technology, Leeghwaterstraat 44, 2628 CA Delft, The Netherlands*

2 *Multi-Scale Physics, Delft University of Technology, Leeghwaterstraat 44, 2628 CB Delft, The Netherlands*

g.sarras@tudelft.nl

1. Motivation

Flameless combustion is a clean combustion technique where the oxidizer and/or fuel are diluted with hot combustion products before entering the main reaction zone. This technique relies on exhaust gas heat recovery and high recirculation ratios. In order to mimic the important characteristics of flameless combustion without the complications of a real furnace, a simplified laboratory scale configuration has been realized in the Delft-Jet-in-Hot-Coflow (DJHC) burner. The DJHC burner creates a turbulent diffusion flame of a gaseous fuel in a coflowing oxidiser stream of high temperature with low oxygen concentration. In this conditions the reaction rates are lower due to oxygen dilution as compared to conventional diffusion flames. The Reynolds numbers in all experimentally studied DJHC flames are not very high ($Re_{jet} < 10^4$). To handle adequately the influence of turbulent fluctuations on mean reaction rates is a modeling challenge.

Transported probability density function (PDF) method allows to include the effects of turbulence-chemistry interaction in the Reynolds Averaged Navier Stokes (RANS) framework. The distinct advantage of this method is that the mean reaction rate is treated exactly for complex finite rate chemistry. However, the high computational costs related to the integration of the reaction rates can result in prohibitive computational time. A promising method of simplified chemistry is based on the so called Flamelet Generated Manifold (FGM) [1].

2. Modeling approach

A hybrid finite-volume transported PDF method is used. It combines an underlying Reynolds stress model with the Monte Carlo simulation of velocity and scalar statistics. The joint velocity-composition PDF or the joint composition PDF is represented by a number of particles and stochastic differential equations are solved for particles properties. Statistics of averaged quantities are estimated simply by an ensemble averaging. The local thermochemical state of the mixture is assumed to evolve on a FGM table.

To construct the FGM that is suitable to describe the chemistry in the DJHC two main issues have to be considered. First, the spatial non-uniformity of the coflow composition and temperature requires two mixture fractions to describe the mixing in the DJHC. A suitable FGM has to be at least three dimensional (two mixture fractions and a progress variable). At

any point of the flow field, the 3-stream mixing is represented by two mixture fractions Z_1 and Z_2 . Z_1 describes the mixing between the fuel and the coflow stream, while Z_2 the entrainment of the surrounding air and the radial variation of oxygen concentration at the coflow inlet. The radial variation of the enthalpy at the coflow inlet is implicitly accounted through the second mixture fraction Z_2 . Second, to adequately describe the auto-ignition effects which have been observed experimentally in the DJHC, unsteady non-premixed flamelet solutions are used to construct the FGM. The FGM is based on 1D, unsteady, non-premixed flamelets between the fuel ($Z_1=1$) and a certain coflow composition. The unsteady flamelet solutions are obtained with the CHEM1D code [2].

A suitable progress variable Y is defined and the time coordinate is then transformed into the reaction progress variable e.g. $T(Z_1,t) \rightarrow T(Z_1,Y)$ [3] and all relevant thermo-chemical variables are stored in a 2D FGM table. Several 2D FGM tables are created corresponding to different values of Z_2 . A total of eight 2D FGM tables are used to construct a 3D FGM. A single strain rate $a=100\text{s}^{-1}$ was used in all the flamelet calculations. This value corresponds to an estimated average of the mean scalar dissipation rate at the stoichiometric mixture fraction observed in the DJHC simulations. Using the 3D FGM all thermo-chemical variables are given by e.g. $Y_i=Y_i(Z_1, Y, Z_2)$. To improve the memory efficiency, the 3D FGM is tabulated using the Delft FLAME code [4].

Every Monte-Carlo particle carries two mixture fractions Z_1, Z_2 and a progress variable Y . This means that every particle now evolves in composition space according to the general equation:

$$d\phi_{\alpha,mix}^* = \theta_{\alpha,mix}^* dt + S_{\alpha}(\vec{\phi}) dt,$$

where $\alpha = 1,2,3$. Also, $\theta_{\alpha,mix}$ represents the IEM or EMST micro-mixing model, $S_{\alpha}(\vec{\phi})$ the chemical source term of the progress variable, ν the molecular viscosity. The mixture fractions are not affected by chemical reactions ($S_{\alpha}(\vec{\phi})=0$) and their values only change according to the chosen micro-mixing model.

3. Conclusions

A comparison of joint composition PDF and joint velocity-composition PDF approaches was conducted with IEM and EMST micro-mixing models. The radial profiles of the mean temperature for JCPDF are closer to the experimental data comparing to the JVCPDF, where a consistent overprediction is observed in the shear layer. The differences observed employing the two micro-mixing models for both PDF approaches are insignificant. To fully describe the radial profile of the coflow oxygen concentration and temperature, the enthalpy deficit will be introduced as an additional independent variable and a 4D-FGM table will be constructed.

References

- [1] J. A. van Oijen *et al.*, *Comb. Flame*, **127**(3): 2124-2134 (2001)
- [2] CHEM1D, *A one-dimensional laminar flame code*, Eindhoven University of Technology
- [3] W. J. S. Ramaekers *et al.*, *Flow, Turb. Combustion* **84**: 439-458 (2010)
- [4] T. W. J. Peeters, *Numerical modeling of turbulent natural-gas diffusion flames*. PhD Thesis, Technische Universiteit Delft.

ADVANCES IN RAMAN SPECTROSCOPY FOR MODEL VALIDATION ON TURBULENT FLAMES

T. Stahler¹, S. Schneider¹, G. Kuenne¹, D. Geyer², A. Dreizler^{1*}

¹Technische Universität Darmstadt, Germany; ²Hochschule Darmstadt, Germany
dreizler@csi.tu-darmstadt.de

Stratification of the (partially) premixed fuel is rather the norm than the exception in technical combustion processes. The stratification can be caused unintentionally by incomplete mixing of fuel and oxidizer or by transient inlet conditions provoked by combustion instabilities. It may also be created intentionally to reduce fuel consumption and pollutant formation as in lean stratified direct injection IC engines or gas turbine combustors. Within the scope of numerical simulations as Large Eddy Simulation (LES) comprehensive data sets for model validation are required. There is a lack of suitable test cases for premixed and especially stratified flames at higher turbulence levels. Thus, the aim of the current series of studies is to provide flow and scalar field data of a broad series of this type of flames, so called *turbulent stratified flame* (TSF) cases [1].

The axisymmetric burner consists of three staged concentric tubes, see Figure 1, with inner diameters of 16, 37, and 60 mm, respectively, resulting in almost constant hydraulic diameters for the inner tube and the two annular slots. The flame is stabilized by a premixed pilot flame in the ceramic center tube, burning 40 mm upstream the exit plane on a centered flame holder ring. Flow fields were characterized with Laser Doppler Velocimetry (LDV) and Particle Image Velocimetry (PIV). Profiles of the radial and axial velocity components, integral time and length scales, and vorticity maps were provided [1].

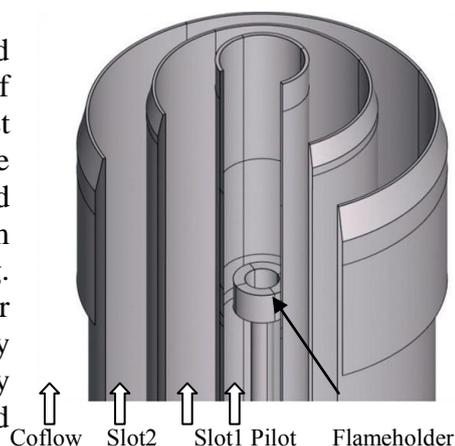


Figure 1: Illustration of the burner geometry and flame stabilization

Scalars of the TSF_A case flame were recently quantified using 1D-Raman/Rayleigh scattering [2]. Since these investigations, the setup has been substantially improved by a custom made laser system (532 nm, 1.5 J/pulse) which was designed with a particular focus on its application

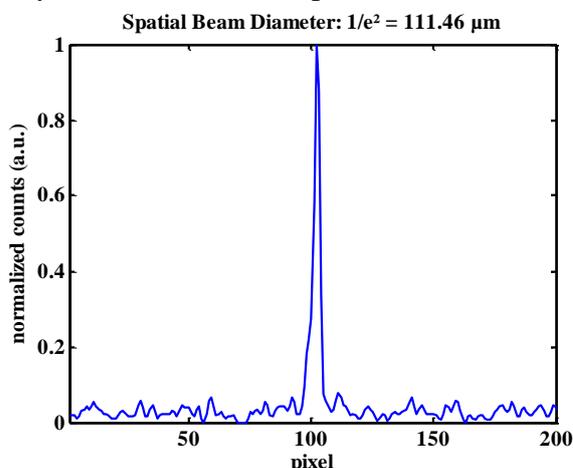


Figure 2: Spatial beam diameter measured using a TaperCamD20-15 UCD23

as light source for Raman/Rayleigh scattering. To prevent optical breakdowns, the pulse duration is stretched to approximately 650 ns at full width at half maximum using pockels cells. This laser allows for measurements with an improved spatial resolution and, at the same time, for an improved signal-to-noise ratio. As shown in Figure 2 the spatial beam diameter is reduced to approximately 112 μm at $1/e^2$ compared to the beam diameter of 520 μm $1/e^2$ pointed out in [2].

The detection side of the experimental setup is only slightly modified and described in the following. Scattered light from a section of the focused laser beam is collected by an achromatic lens system. A dichroic long pass filter separates the Rayleigh from Raman scattered light. The latter is dispersed by an imaging spectrometer mounted with a specially developed fast mechanical shutter with short gating times of only 10.5 μs full width half max to suppress background. Due to high flame luminosity and reflections of laser light at the test bench an additional polarizing filter is mounted inside the spectrometer to further suppress background radiation. Finally, the scattered light is imaged by two low noise backside illuminated CCD cameras with high quantum efficiencies. Thus, a line of 6 mm length can be probed with a projected resolution of 150 μm , thereby improving the spatial resolution of the system. The negative impact of beam steering on signal matching and spatial resolution was reduced by the 'same side' detection of Raman and Rayleigh signals. Instantaneous temperature and the main species concentrations (fuel, N_2 , O_2 , CO_2 , H_2O) are inferred using this technique. Thus, the full thermo-kinetic state is probed. Derived quantities such as equivalence ratio and scalar correlations may be calculated and (multi-) conditioning can be accomplished.

The poster will discuss the differences of the results obtained in the current study to the ones presented in [2] as a consequence of the improvements of the experimental setup. Additionally, an improved treatment of the background in the data evaluation process which has been applied to the current data set will be presented. The poster will emphasize on the not yet published scalar data from Raman/Rayleigh scattering with the improved experimental setup which allows for deeper understanding of the chemistry-turbulence interaction of the turbulent stratified flames. For instance, double conditioned statistics pointing out the flame propagation will be shown.

- [1] F. Seffrin et al., *Flow field studies of a new series of turbulent premixed stratified flames*, Combust. Flame 157 (2010) 384–396
- [2] G. Kuenne et al., *Experimental and numerical analysis of a lean premixed stratified burner using 1D Raman/Rayleigh scattering and large eddy simulation*, Combust. Flame (2012), doi:10.1016/j.combustflame.2012.02.010

Empirical low-dimensional manifolds in composition space

Yue Yang^{1,2}, Stephen B. Pope¹ and Jacqueline H. Chen²

1 Sibley School of Mechanical and Aerospace Engineering, Cornell University, Ithaca, NY 14853, USA

2 Combustion Research Facility, Sandia National Laboratories, Livermore, CA 94551, USA

yy463@cornell.edu

To reduce the computational cost of turbulent combustion simulations with a detailed chemical mechanism, it is useful to find a low-dimensional manifold in composition space that can approximate the full system dynamics. Most previous low-dimensional manifolds in turbulent combustion are based on the governing conservation equations or thermochemistry and their application involves certain assumptions. On the other hand, empirical low-dimensional manifolds (ELDMs) are constructed based on samples of the compositions observed in experiments or in direct numerical simulation (DNS).

We assume that compositions occurring in turbulent combustion lie close to a low-dimensional manifold. An ELDM Φ^M can be constructed from an ensemble of N observations of $\Phi = \{T, \mathbf{Y}\}$ by minimizing some measure of the departures of the observations from the manifold, where T is the temperature and \mathbf{Y} is the vector of species mass fractions. Using principal component analysis (PCA) and multivariate adaptive spline regression (MARS), plane and curved ELDMs can be obtained respectively [1,2]. Both PCA and MARS are applied to a DNS database of a non-premixed CO/H₂ temporally evolving jet flame with a low Damkohler number $Da = 0.011$ and two Reynolds numbers $Re = 2510$ and $Re = 9017$ [3] at a series of timesteps $t = \{0, 10t_j, 20t_j, 40t_j\}$, where t_j is a characteristic jet time scale and the maximum local extinction occurs near $t = 20t_j$.

To examine the root-mean-squares (r.m.s.) distance of the data from the manifold, for species i we define ε_i as the r.m.s. departure $\Phi_i - \Phi_i^M$ normalized by the r.m.s. of Φ_i . In Fig. 1, this normalized error is shown for different species as a function of the dimension n_r of the manifold. As may be seen from the figure, for the data from the high- Re DNS at the final time, about five dimensions are needed to reduce these departures from the PCA ELDM $\Phi^M(\boldsymbol{\eta})$ to below 5%, where $\boldsymbol{\eta}$ is the n_r -vector of principal components. The number of dimensions for the prescribed 5% error remains the same for the DNS data at both low and high Re after $t = 10t_j$ with different scaling methods used in PCA [2]. Furthermore, the represented species \mathbf{Y}^r can be determined from the PCA results by minimizing the distance between subspaces [4] and then they could be used in *posteriori* tests.

Although representing and determining "best-fit" curved manifolds is much more challenging than PCA, better accuracy can be achieved by curved MARS ELDMs with lower dimensions. As shown in Fig. 1, for a given dimension n_r , the departures are smaller for MARS than for PCA. In order to reduce the normalized r.m.s. to below 5%, on average three dimensions are required for MARS compared to five dimensions for PCA. It is noted that the curved ELDM obtained from MARS is an estimate of the conditional manifold. Another purpose of MARS is that it can be used to approximate non-linear functions such as the chemical source term \mathbf{S} . Two different approaches of the *posteriori* test based on the ELDMs Φ^M and \mathbf{S}^M are discussed.

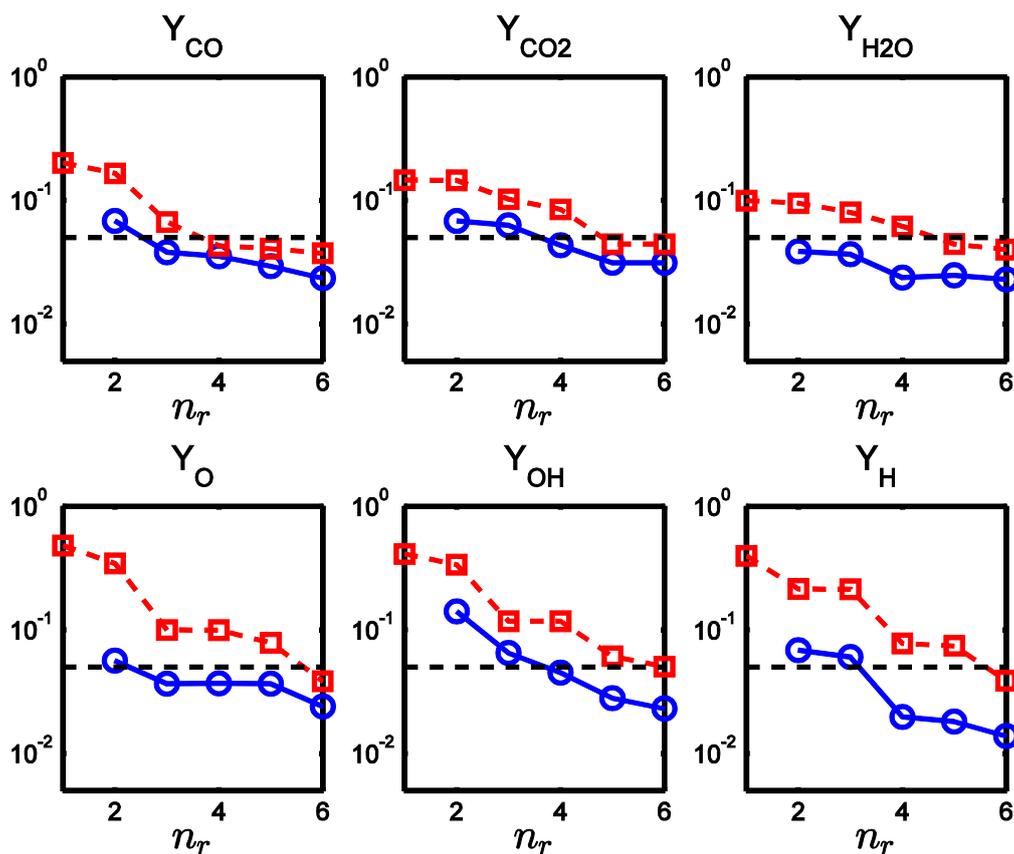


Fig. 1 Normalized r.m.s. departures of different species from PCA with the STD scaling and MARS for the high- Re DNS database at $t=40t$ (\square : PCA; \circ : MARS), where n_r denotes the number of dimensions. The dashed line shows the 5% level.

In addition, the effect of differential diffusion on ELDMs is examined in large-eddy simulations with PDF modeling [5]. It shows that differential diffusion effects contribute to producing larger departures of mass fractions from the ELDM.

References

- [1] J. C. Sutherland and A. Parente, *Proc. Combust. Inst.*, **32**, 563 (2009)
- [2] A. Biglari and J. C. Sutherland, *Combust. Flame*, **159**, 1960 (2012)
- [3] E. R. Hawkes *et al.*, *Proc. Combust. Inst.*, **31**, 1633 (2007)
- [4] G. H. Golub and C. F. Van Loan, *Matrix computations*, The Johns Hopkins University Press, 3rd version (1996)
- [5] Y. Yang *et al.*, *Proc. Combust. Inst.*, submitted (2012)

LES-CMC predictions of turbulent piloted DME jet flames

M. Zendeudel, S. Ukai, O.T. Stein, A. Kronenburg

Institut für Technische Verbrennung, Stuttgart University, Herdweg 51, 70174 Germany

o.stein@itv.uni-stuttgart.de

Dimethyl Ether (DME) from biomass synthesis is considered as a potential renewable replacement for fossil Diesel fuel. In this study, a combination of large eddy simulation (LES) and a conditional moment closure (CMC) combustion model in conservative form is used for predicting DME combustion in a turbulent, piloted jet flame. LES-CMC modelling has shown improved predictions of turbulent methane/air jet flames in previous studies [1]. The geometrical data of the burner, the bulk velocity of the fuel jet and the co-flow velocity are identical to existing conditions of the experimental set-up of the Sandia Flame series A-F [2], while the new fuel jet consists of DME/air (1:4 by vol.) and the bulk velocity and composition of the pilot differ from the previous experiment. A prior experimental study of laminar and turbulent DME flames by Fuest et al. [3] comprised a turbulent flame configuration ("T2") that was comparable to the conditions considered here. Flame T2 was found to be diffusion-controlled, which motivates classical non-premixed CMC modelling. A new experimental campaign is currently underway [4], which will provide additional PIV and LIF measurements and its results will be used to validate LES-CMC.

The LES-CMC study is carried out with the in-house code BOFFIN. To trigger turbulent jet break up, sinusoidal perturbations are superimposed on the mean inlet velocity. To accurately represent the kinetics of DME/air combustion, two detailed chemical mechanisms are used, the mechanism by Kaiser/Fischer et al. [5,6] considering 78 species and 351 reactions, and an updated mechanism by Zhao et al. [7], including 55 species and 290 reactions. Fuest et al. [3] have found the latter mechanism to yield better predictions of laminar burning velocities and we are comparing results from both mechanisms to investigate the sensitivity of turbulent DME/air predictions to combustion chemistry.

An impression of the flame structure can be gained from an instantaneous temperature field, Fig. 1, which illustrates the similarity of the DME/air flame to the previously investigated non-premixed CH₄/air flames. In Fig. 2 conditional mean profiles of the temperature and the fuel at $z/D=10$ are presented. Both chemical mechanisms give similar predictions with very similar temperature profiles and somewhat more fuel depletion on the rich side for the Zhao mechanism.

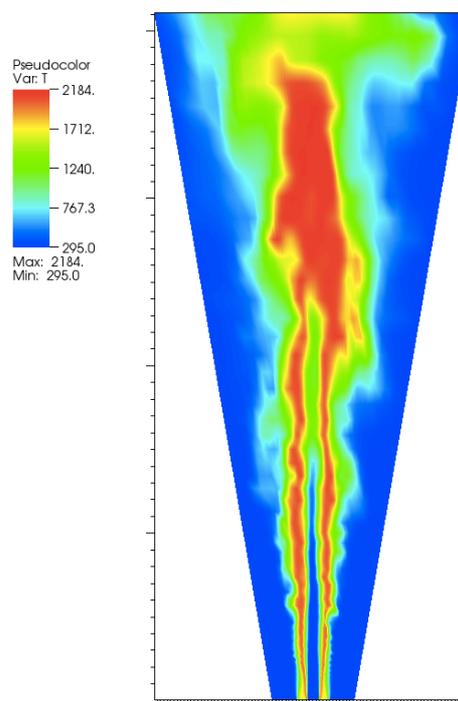


Fig. 1: Snapshot of the instantaneous LES temperature field using the mechanism by Kaiser/Fischer et al. [5,6]

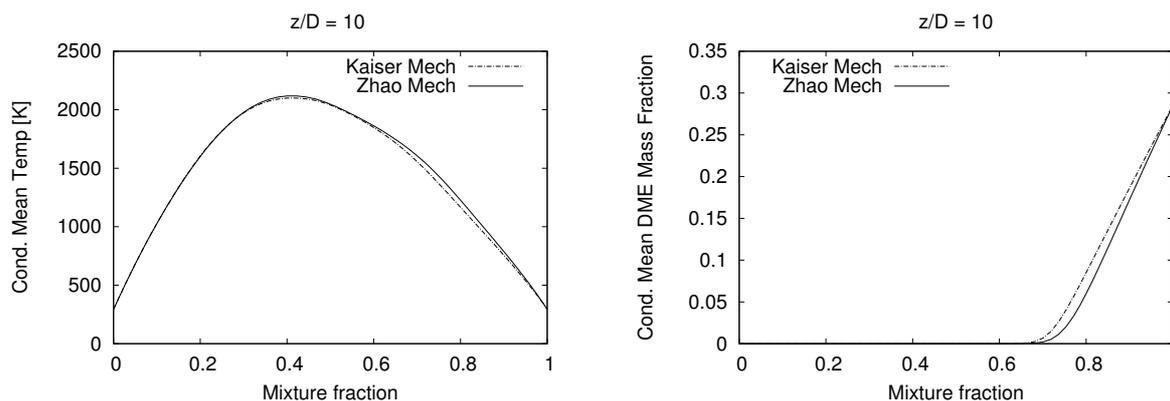


Fig. 2: Conditional mean temperature profile (left) and DME (right) at $z/D=10$.

Figure 3 presents conditional mean profiles of the mass fractions of H_2 and OH from CMC-LES.

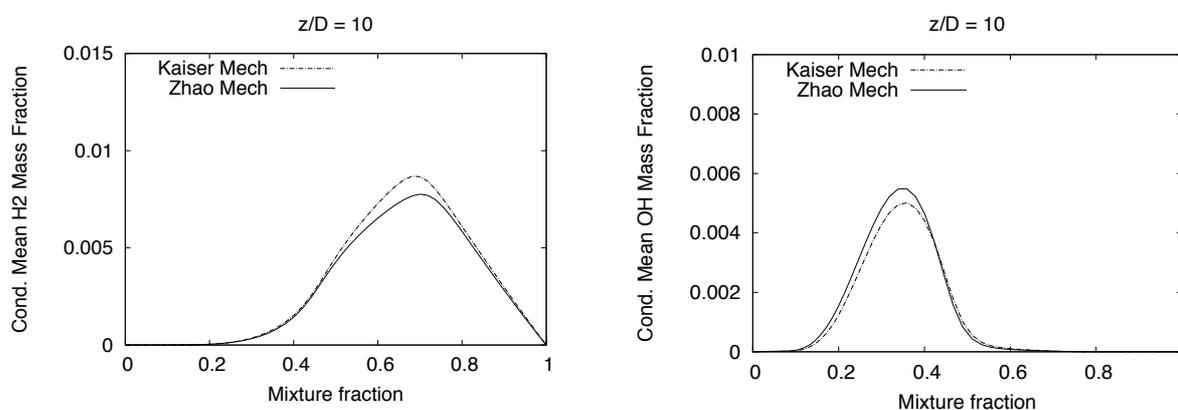


Fig. 3: Conditional mean species profiles at $z/D=10$, H_2 (left) and OH (right) mass fraction.

Small differences between the two chemical mechanisms can also be observed for the intermediates and the radicals. The conditionally averaged mass fraction of hydrogen is slightly higher for the Kaiser mechanism, while the radical concentration is somewhat lower (cf. Fig. 3). The current results are considered preliminary, as coarse LES and CMC grids have been used. Further studies that will be presented at the workshop will include a comparison of our computations with species measurements by Frank [4] and a more detailed analysis of the influence of the oxidation pathways of the two different chemical mechanisms on turbulent flame structure.

References

- [1] S. Navarro-Martinez, A. Kronenburg, F. Di Mare, *Flow, Turbul. Combust.*, **75**, 245 (2005)
- [2] R. Barlow, J. Frank, *Proc. Combust. Inst.*, **27**: 1087 (1998)
- [3] F. Fuest, R.S. Barlow, J.-Y. Chen, A. Dreizler, *Combust. Flame*,
DOI:10.1016/j.combustflame.2011.11.001
- [4] J. Frank, *Person. Commun.* (2012)
- [5] E.W. Kaiser, T.J. Wallington, M.D. Hurley, J. Platz, H.J. Curran, W.J. Pitz, C.K. Westbrook, *J. Phys. Chem. A*, **104**(35), 8194 (2000)
- [6] S.L. Fischer, F.L. Dryer, H.J. Curran, *Int. J. Chem. Kinet.*, **32**(12), 713 (2000)
- [7] Z. Zhao, M. Chaos, A. Kazakov, F.L. Dryer, *Int. J. Chem. Kinet.*, **40**, 1 (2008)

Flow Field Studies of Cambridge Stratified Swirl Burner

R. Zhou¹, M. S. Sweeney¹, S. Hochgreb¹, R. S. Barlow²

1 Department of Engineering, University of Cambridge, UK

2 Sandia National Laboratories, California, USA

rz242@cam.ac.uk

Many practical combustion applications encounter or intentionally use stratification and swirl to achieve improved performance. The fundamental physics of such flames remain an area of interest to the combustion research community. A novel co-annular turbulent methane-air burner designed by Cambridge and Sandia has been studied extensively in terms of scalar fields [1-3]. The flow field results for a selection of interesting operating conditions of the burner are presented here.

The burner was designed to provide simple geometry (see Fig. 1) and well defined boundary conditions to assist modelling. The inner annulus was run as a non-swirling flow, at a richer equivalence ratio than the outer annulus flow. The outer annulus was run with two CH₄/air flows split between an axial flow plenum and a swirl plenum depending on the degree of swirl required. The annuli are approximately 25 hydraulic diameters in length to ensure fully developed flow at exit from the tube. A low velocity co-flow is used to prevent entrainment of ambient air. This flow system allowed for a range of premixed, stratified, and swirling operating conditions.

Flow fields of the burner were investigated using two-component laser Doppler anemometry (LDA), and low speed two-component particle image velocimetry (PIV). The flow fields correspond to non-reacting and reacting operating conditions investigated in previous publications on this burner.

For PIV measurements, a double-pulsed 532 nm laser (Litron Nano PIV) was used to illuminate calcined aluminium oxide seed particles with mean diameter of 1 µm. The resulting scattered light was captured using a CCD camera in double-frame mode (LaVision Imager ProX 4M). The field of view was approximately 60 x 60 mm and the frame resolution was 2048 x 2048 pixels. The mean velocity field for the premixed non-swirling case SwB1 and highly swirling case SwB3 as well as stratified non-swirling case SwB9 and highly swirling case SwB11 are shown in Fig. 2.

For LDA measurements, the axial, radial and tangential velocity components were obtained by rotating the experimental set up. An Ar-ion laser operating at 514.5 and 488 nm was used to illuminate the particles; the signals were collected by Dantec colour separators and photodetectors. The data covers the locations of interest corresponding to the previous line scalar measurements, with measuring volume dimensions around 0.15 mm along each direction. High temporal resolutions (>10 kHz) were obtained, which allowed assessment of the power spectral density of the turbulence as shown in Fig. 3.

Excellent agreement between flow field results of LDA and PIV was obtained. The flow field profiles show significant differences between non-reacting and reacting conditions, premixed and stratified flames, non-swirling and swirling flames. Selective results are shown in Fig. 2. A comprehensive flow field data set of the burner is available upon request.

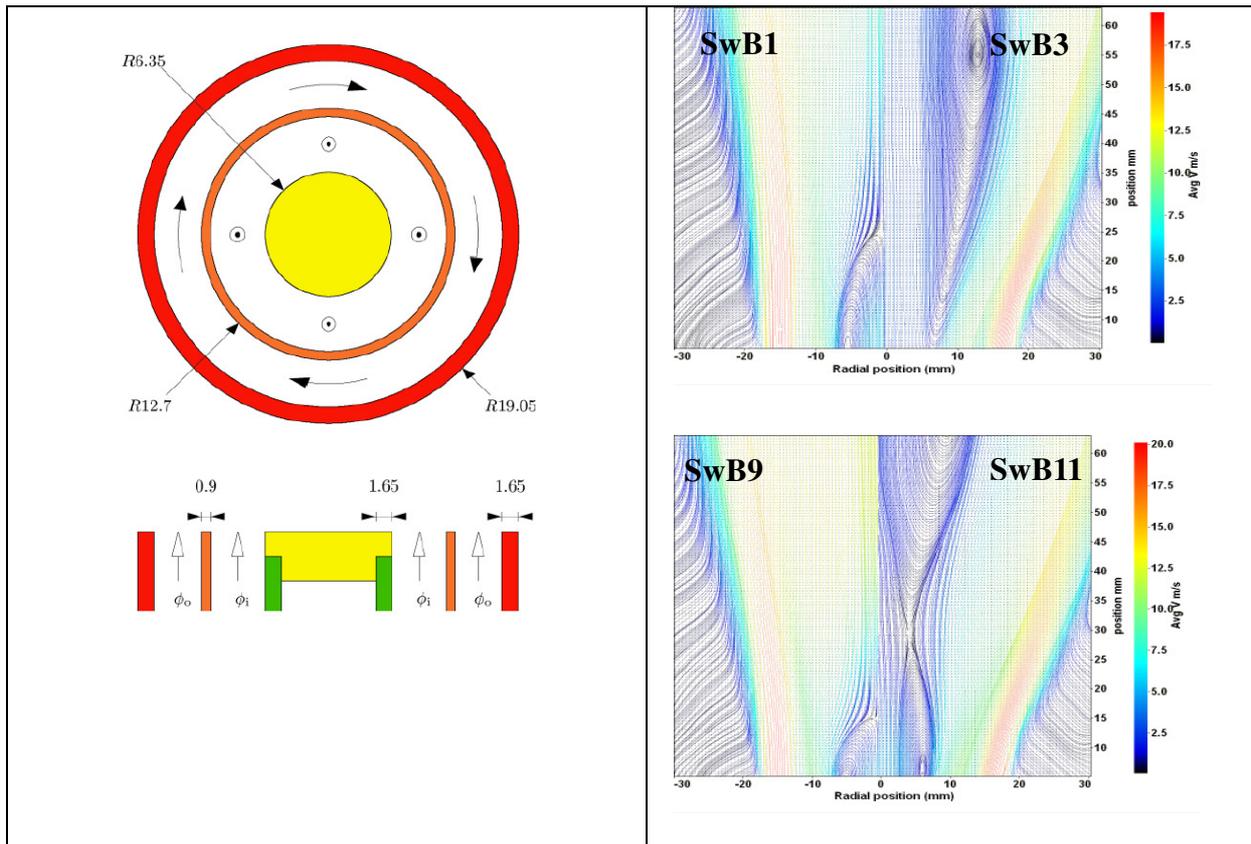


Fig. 1: Schematic of swirl burner. All dimensions in mm. Direction of swirl flows in outer annulus shown by curved arrows.

Fig. 2: Streamlines coloured by velocity for cases with same swirl, but increasing stratification from premixed (SwB1) to stratification level of $\phi_i / \phi_o = 3$ (SwB11)

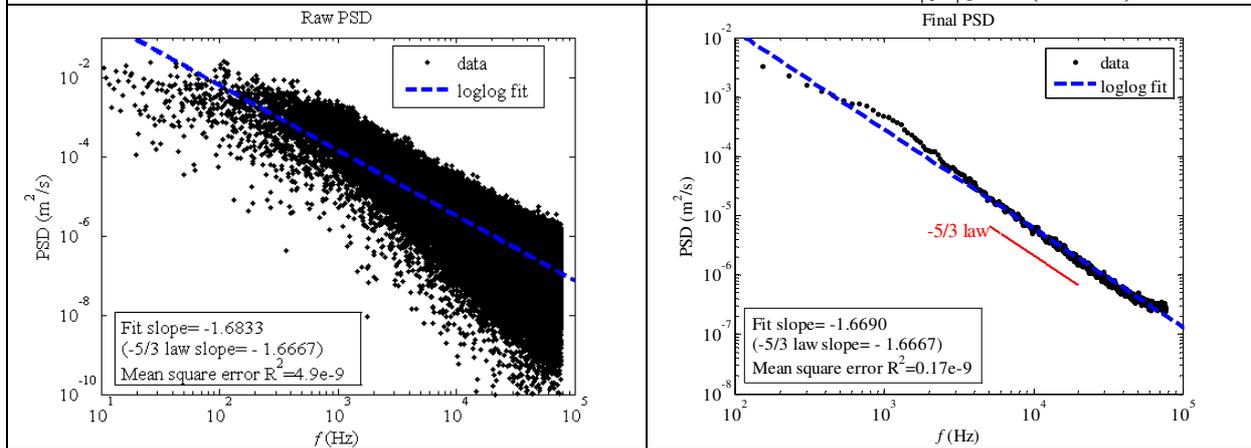


Fig. 3a: Raw power spectral density of the flow field without optimization.

Fig. 3b: Power spectral density of the flow field with denoising and block averaging.

References

- [1] M. S. Sweeney, S. Hochgreb, M. J. Dunn, R. S. Barlow, *A comparative analysis of flame surface density metrics in premixed and stratified flames*. P. Combust. Inst., 33, pp. 1419-1427 (2011)
- [2] M. S. Sweeney, S. Hochgreb, M. J. Dunn, R. S. Barlow, *The Structure of Turbulent Stratified and Premixed Methane/Air Flames I: Non-Swirling Flows*. Combust. Flame, accepted (2012)
- [3] M. S. Sweeney, S. Hochgreb, M. J. Dunn, R. S. Barlow, *The Structure of Turbulent Stratified and Premixed Methane/Air Flames II: Swirling Flows*. Combust. Flame, accepted (2012)